# METABOLOMICS
AND **LIPIDOMICS**

## Waters
**THE SCIENCE OF WHAT'S POSSIBLE.®**

# TABLE OF CONTENTS

## CHAPTER 3: TARGETED METABOLOMICS AND LIPIDOMICS

## CHAPTER 4: MS IMAGING AND AMBIENT IONIZATION-MS FOR METABOLOMICS AND LIPIDOMICS

## CHAPTER 5: SELECTED PEER-REVIEWED PUBLICATIONS

# INTRODUCTION

Metabolomics and lipidomics are powerful tools in systems biology that aim to understand metabolites and lipids present in samples of biological origins (animals, plants, and microorganisms). Differences in the species or amounts of metabolites and lipids can be used to characterize phenotypes and biological responses to perturbations (diseases, genetic modifications, or nutritional and pharmacological treatments). This information allows scientists to understand how a specific organism works, or to understand the underlying mechanism of a given disease. Metabolomics and lipidomics solutions will help the medical community realize the promise of personalized medicine and help translate biomarker discovery and clinical research from bench to bedside. Similar analytical tools have also been applied to food and nutrition research. The molecular fingerprint of food components can be used for investigations into origin, authenticity, and to evaluate their impact on the human metabolism.

A number of important technology advancements have become increasingly important to enhance metabolomics and lipidomics experiments. Multidimensional UPLC® solutions and new chromatographic tools further improve the separations of complex mixtures of metabolites and lipids. Atmospheric pressure gas chromatography (APGC) is a soft ionization technique which results in an increased abundance of the parent ion and therefore enhanced sensitivity and specificity. Ultra performance convergence chromatography (UPC$^{2}$®), which uses liquid $CO_2$ as the mobile phase, represents an evolution of supercritical fluid chromatography, in terms of speed and reproducibility of analysis. UPC$^{2}$ is enabling new ways of separating lipids. A novel integrated microfluidics device, the ionKey/MS™ System, for omics applications, offers the advantages of increased sensitivity, ease of use, decreased solvent consumption, and lower injection volume over traditional UPLC.

In addition to chromatography, Ion Mobility-MS can support traditional MS-based metabolomic and lipidomic protocols. Ion mobility separates gas-phase ions according to their physical size and shape, that is, the ion-collision cross section (CCS) and occurs on a timescale of milliseconds. Ion mobility disperses mass signals across drift time, an additional dimension of information and therefore delivers an enhanced peak capacity and signal-to-noise ratio, as compared with a conventional, single dimension of MS analysis.
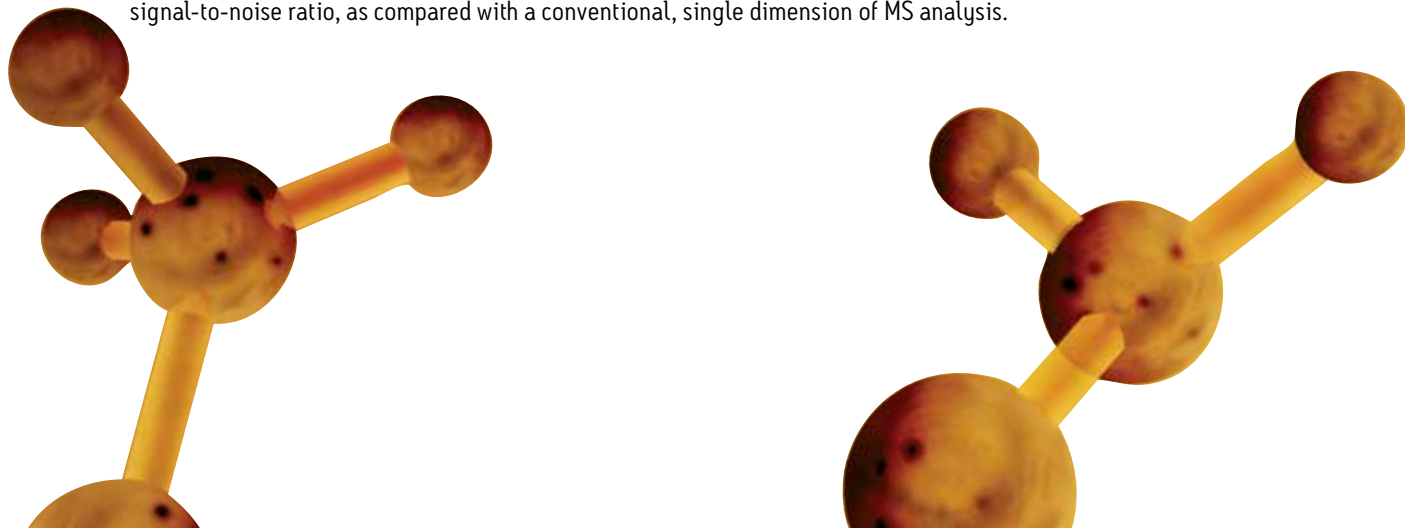
The use of data-independent acquisition (DIA) capabilities further helps to elucidate the chemical structures of unexpected or unknown analytes in biological samples. $MS^E$ is a DIA operating mode that utilizes alternating low and elevated collision energies, independently, from the previous scan. In this type of acquisition, the quadrupole mass analyzer does not pre-select precursor ions. The low-collision-energy acquisition generates accurate mass information about the intact precursor ions, and the elevated-collision-energy acquisition provides accurate mass information about fragments. Both precursor and fragment-ion information are collected in a single analytical run, eliminating the need to rerun the samples to obtain further tandem MS spectra. This method of acquisition results in minimal loss of information from poor duty cycle limitations. In Waters' Q-Tof™ instruments, operated in MSE mode, the collision energy can be varied or ramped. The simultaneous generation of high-resolution, full scan, and fragmentation spectra could serve as a repository of biological information that can be re-interrogated as new insights are revealed.

Waters® state-of-the-art chromatography, ionization sources, and MS technology combined with simple, scalable, yet powerful informatics solutions provide a set of tools to unlock biological information like never before. In this notebook, we will cover applications with Waters solutions for metabolomics and lipidomics, including untargeted and targeted analyses, structural elucidation, MS imaging, and ambient ionization-MS applications.
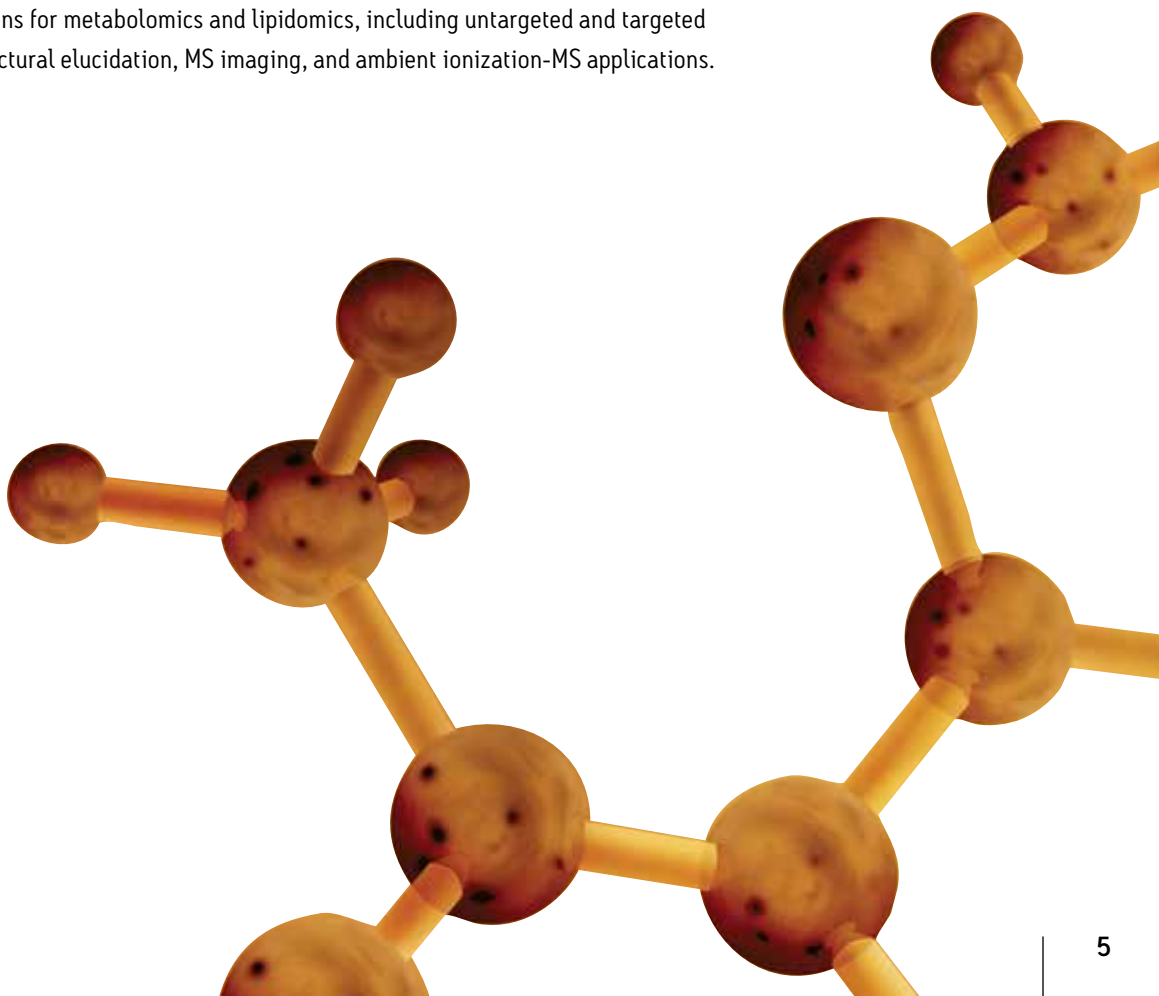
# CHAPTER 1 UNTARGETED METABOLOMICS AND LIPIDOMICS
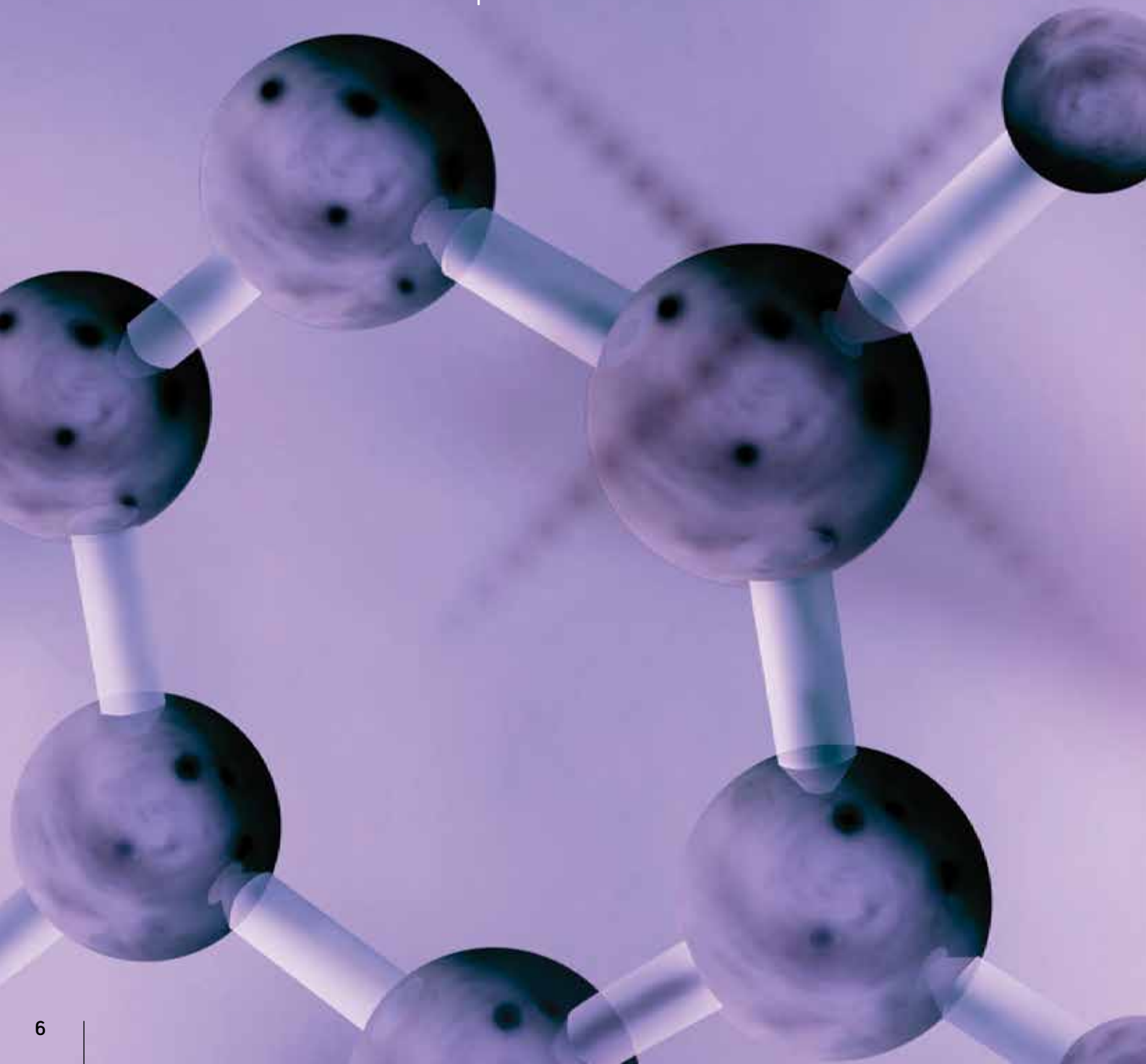
# UNTARGETED METABOLOMICS AND LIPIDOMICS

Untargeted metabolomics and lipidomics are hypothesis-generating and exploratory in nature, their purpose is to perform an unbiased screening of metabolites and lipids in biological samples. By comparing metabolite and lipid profiles, we can thus determine patterns of variations between different groups: healthy versus diseased, control versus treated, or wild-type versus genetically modified. Dealing with variations in thousands of molecular species, untargeted metabolomic and lipidomic strategies apply statistical tools, such as multivariate and pattern-recognition analyses to group and identify the observed changes in metabolite and lipid species.

Powerful LC-MS data analysis software is critical to the quantification and identification of metabolites and lipids that are significantly changing in biological samples. Progenesis® QI Software offers the capability to handle the large sample sets typical of today's experiments. With support for all common vendor data formats and a highly intuitive, visually guided workflow, Progenesis QI Software helps to rapidly, objectively, and reliably discover metabolites and lipids of interest using multi-group experimental designs. As well as conventional data-dependent analysis (DDA), Progenesis QI supports Waters MS$^E$ and HDMS$^E$ DIA. Uniquely, the software also takes advantage of the additional dimension of resolution offered by ion-mobility separations to give improvements in the accuracy and precision of compound identification and quantification. Progenesis QI Software is developed by Nonlinear Dynamics, a Waters Company.

Central to Waters solutions for untargeted metabolomics and lipidomics are the use of novel and unique chromatographic tools, high-resolution exact mass time-of-flight (TOF) mass spectrometers and specialized software for statistical analysis.

■ Advanced chromatographic separations of lipids and metabolites coupled to the widest range of ionization capabilities (UPLC, ionKey™, UPC$^2$, APGC)

■ Powerful data dependant and data independent technology (MS$^E$) for both qualitative and quantitative routine applications

■ Simple data processing and easy identification of statistically significant quantitative changes with Progenesis QI

Waters
THE SCIENCE OF WHAT'S POSSIBLE.®
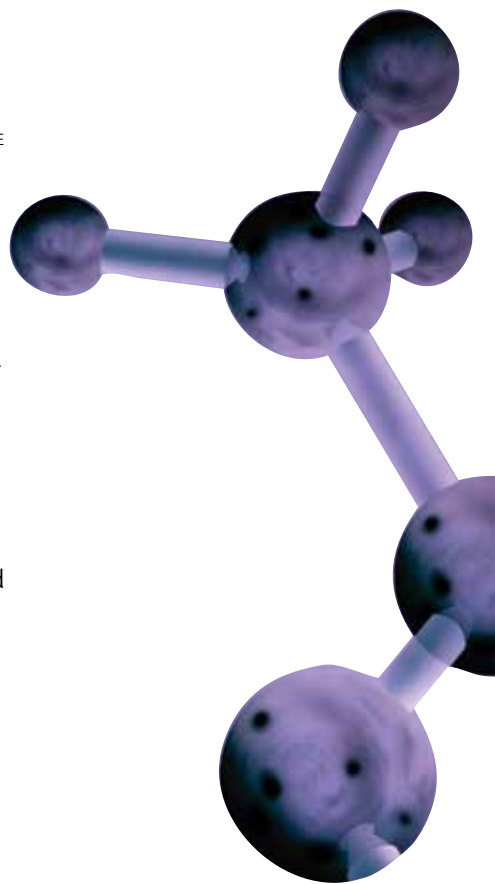
# Development of a Metabolomic Assay for the Analysis of Polar Metabolites Using HILIC UPLC/QTof MS

Giuseppe Paglia,[1] James Langridge,[2] and Giuseppe Astarita[3]
[1]Center for Systems Biology, University of Iceland, Iceland;  [2-3]Waters Corporation, Manchester, UK and Milford, MA, USA

## APPLICATION BENEFITS

The combination of UPLC-based hydrophilic interaction liquid chromatography (HILIC) and a hybrid quadrupole time-of-flight (Q-Tof™) mass spectrometer allows the comprehensive analysis of small polar metabolites including sugars, phosphorylated compounds, purines and pyrimidines, nucleotides, nucleosides, acylcarnitines, organic acids, hydrophilic vitamins, and amino acids. Retention times and accurate masses of metabolites involved in key metabolic pathways were annotated for routine high-throughput screening in both untargeted and targeted metabolomics analyses.

## WATERS SOLUTIONS

ACQUITY UPLC® System

ACQUITY UPLC BEH Amide Column

SYNAPT® G2 System

TransOmics™ Informatics

## KEY WORDS

HILIC, UPLC®, small polar metabolites, QTof MS, metabolomics

## INTRODUCTION

Metabolomics, a powerful tool in systems biology, aims to screen small metabolites present in biological samples. Differences in the species or amounts of metabolites can be used to characterize phenotypes and biological responses to perturbations (diseases, genetic modifications, or nutritional and pharmacological treatments).

Small metabolites can be mainly divided into hydrophilic and hydrophobic compounds. Because water is the major constituent of cells, a high number of hydrophilic metabolites are present in their intracellular content including sugars, phosphorylated compounds, nucleobases, nucleotides, nucleosides, acylcarnitines, organic acids, hydrophilic vitamins, and amino acids, as shown in Figure 1. Such polar metabolites are the building blocks of large macromolecules such as nucleic acids (DNA and RNA), proteins, and oligosaccharides. Furthermore, they are involved in central pathways (glycolysis, pentose-phosphate pathway and citric acid cycle), which are essential for energy metabolism.



Figure 1. Representative classes of polar metabolites present in biological samples.

## EXPERIMENTAL

### LC conditions, acidic

| | |
|---|---|
| System: | ACQUITY UPLC |
| Column: | BEH Amide<br>2.1 x 150 mm, 1.7 µm |
| Mobile phase A: | ACN + 0.1% formic acid |
| Mobile phase B: | $H_2O$ + 0.1% formic acid |
| Flow rate: | 0.4 mL/min |
| Column temp.: | 45 °C |
| Injection volume: | 3.5 µL |
| Sample loop option: | Partial loop with needle overfill |
| ESI mode: | Positive and negative |

| Elution gradient: | min | A% | B% | Curve |
|---|---|---|---|---|
| | 0.0 | 99 | 1 | |
| | 0.1 | 99 | 1 | 6 |
| | 7.0 | 30 | 70 | 6 |
| | 7.1 | 99 | 1 | 6 |
| | 10.0 | 99 | 1 | 6 |

### LC conditions, basic

| | |
|---|---|
| System: | ACQUITY UPLC |
| Column: | BEH Amide<br>2.1 x 150 mm, 1.7 µm |
| Mobile phase A: | ACN 95% - ammonium bicarbonate 10 mM 5% (pH 9) |
| Mobile phase B: | ACN 5% - ammonium bicarbonate 10 mM 95% (pH 9) |
| Flow rate: | 0.4 mL/min |
| Column temp.: | 45 °C |
| Injection volume: | 3.5 µL |
| Sample loop option: | Partial loop with needle overfill |
| ESI mode: | negative |

| Elution gradient: | min | A% | B% | Curve |
|---|---|---|---|---|
| | 0.0 | 99 | 1 | |
| | 0.1 | 99 | 1 | 6 |
| | 6.0 | 30 | 70 | 6 |
| | 6.5 | 99 | 1 | 6 |
| | 10.0 | 99 | 1 | 6 |

### MS conditions

Analytical column to ESI probe: PEEK Tubing, 1/16 inch (1.6 mm) O.D. x 0.005 inches (0.127 mm) I.D. x 5 ft (1.5 m) length , cut to 450 mm in length; (p/n WAT022995)

| | |
|---|---|
| Mass spectrometer: | SYNAPT G2 |
| Acquisition mode: | Sensitivity mode (centroid) |
| Capillary: | 1.5 kV |
| Sampling cone: | 30 V |
| Extraction cone: | 5 V |
| Source temp.: | 120 °C |
| Desolvation gas temp.: | 500 °C |
| Desolvation gas flow: | 800 L/h |
| Cone gas flow: | 50 L/h |
| Lock spray: | Leukine enkephalin (3 ng/L) 556.2771 *m/z* |
| Scan range: | 50 to 1000 *m/z* |
| Scan time: | 0.3 s |
| Calibration: | Sodium formate |

The analysis of hydrophilic compounds using traditional reversed-phase LC/MS presents some challenges due to the fact that these metabolites are poorly retained and usually eluted in the void volume.[1] On the other hand, it has been demonstrated that HILIC-MS methods easily resolve polar metabolites for better identification and quantification.[1,2] A HILIC-UPLC/MS strategy for the routine high-throughput screening of polar metabolites in biological samples is presented here. Such a strategy could be used for both targeted and untargeted metabolomics.

## Sample description

All materials were purchased from Sigma-Aldrich (Germany). All chemicals and solvents were analytical grade or higher purity. Human platelets were obtained from the Blood Bank of Reykjavik.

Polar metabolites were extracted from platelets (0.5 mL of platelets concentrate) by adding 1 mL of 7:3 MeOH/$H_2$O containing a 30-μL mixture of chemical homologous internal standards, as shown in Table 1. Two freeze-and-thaw steps were applied, then samples were passed to vortex. After centrifugation (5 min 10,000 x g) the supernatant was recovered, filtered (cutoff: 0.2 μm), dried using speed vacuum, and reconstituted in 0.3 mL of 50:50 $H_2$O/$CH_3$CN. A typical sample list included water-based blank samples, quality control samples containing commercially available metabolites at two concentration levels, a five-point serial dilution of calibrators, and pooled quality control samples in which small aliquots of each biological sample are pooled and mixed together.

| Metabolites | Molecular formula | MW | [M+H]+ | [M-H]- | Retention time (min) | | | Concentration ng/L |
| --- | --- | --- | --- | --- | --- | --- | --- | --- |
| | | | | | BASIC | NEG | POS | |
| Phenylalanine $d_2$ | $C_9D_2H_9NO_2$ | 167.0915 | 168.0994 | 166.0837 | 3.15 | 3.7 | 3.7 | 50 |
| Succinate $d_4$ | $C_4D_4H_2O_4$ | 122.0517 | 123.0595 | 121.0439 | 2.5 | 2.3 | – | 50 |
| Glucose $^{13}C_6$ | $^{13}C_6H_{12}O_6$ | 186.0835 | 209.073 | 185.0757 | – | 4.2 | 4.2 | 2000 |
| Carnitine $d_9$ | $C_7D_9H_6NO_3$ | 170.1617 | 171.1695 | 169.1678 | – | – | 3.6 | 5 |
| Glutamic Acid $d_5$ | $C_5D_5H_4NO_4$ | 152.0845 | 153.0924 | 151.0767 | 3.2 | 4.4 | 4.4 | 40 |
| AMP $^{13}C_{10}$, $^{15}N_5$ | $^{13}C_{10}H_{14}{}^{15}N_5O_7P$ | 362.0818 | 363.0896 | 361.074 | 3.15 | 5.2 | 5.2 | 50 |
| Octanoic Acid $d_{15}$ | $C_8D_{15}H_1O_2$ | 159.2092 | 160.217 | 158.2014 | 1.2 | 1.2 | – | 180 |
| Lysine $d_4$ | $C_6D_4H_{10}N_2O_2$ | 150.1306 | 151.1385 | 149.1228 | 6.6 | 5.6 | 5.6 | 50 |

*Table 1. Internal standard mixture.*

## Cleaning procedures

For practical consideration, to remove residues that can reduce column lifetime and instrument sensitivity, the samples were filtered before the UPLC/MS analysis (cutoff: 2 μm). Furthermore, a routine cleaning procedure was applied at the end of each analytical batch of approximately 80 samples, including both column and ion source cleaning. The column was flushed first with 50% of solvent A (acetonitrile) and 50% of solvent B (50:50 water/methanol) for 30 min at a flow rate of 0.25 mL/min, then for 20 min with 100% of solvent A at a flow rate of 0.25 mL/min. When a new column was used, at least 30 injections were required for system equilibration; whereas, 15 injections were sufficient after each cleaning procedure using the same column. The sample cone was sonicated in a 50:50 (vol/vol) methanol/water solution containing 1% (vol/vol) formic acid for 15 min, and dried with nitrogen b efore replacing.

## RESULTS AND DISCUSSION

The primary focus of this work was to provide a high-throughput solution to screen for unknown metabolites and to simultaneously quantify selected polar metabolites in biological samples.

In order to optimize the separation conditions, the initial analysis focused on a mixture of commercially available polar metabolites, representative of the major cellular biochemical pathways including amino acids, sugars, acylcarnitines, organic acids, nucleobases, nucleotides, and nucleosides, as shown in Figure 1.

To allow a comprehensive separation of the different chemical classes of metabolites, two different HILIC-UPLC conditions (acidic and basic) were selected, as shown in Figure 2.
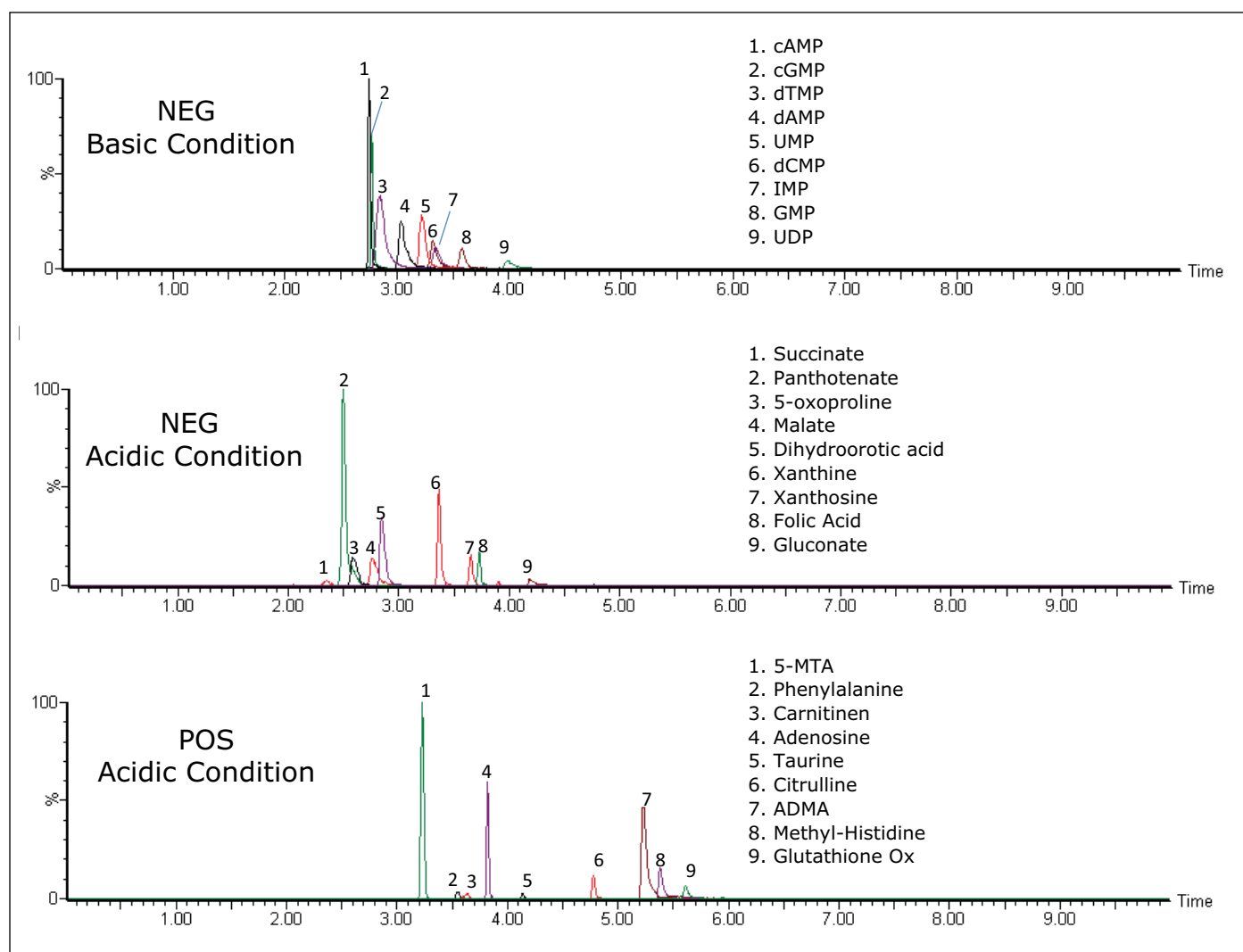


*Figure 2. Representative UPLC/MS separation of selected polar metabolites using both basic and acidic chromatographic conditions.*

In fact, the analysis of polar metabolites was strongly influenced by pH of the mobile phase, as shown in Figures 3A and 3B. In particular, many phosphorylated compounds, such as nucleotides, could be well separated using basic conditions; whereas, they were strongly retained using acidic conditions resulting in poor chromatographic peak shape, as shown in Figures 3A and 3B. Notably, the analysis of similar compounds using traditional reversed-phase LC/MS presented some challenges due to the fact that these metabolites were poorly retained and usually eluted in the void volume, as shown in Figure 3C.[1] Using HILIC conditions, the set of polar metabolites eluted in order of increasing polarity. Retention times were annotated, as well as with the accurate masses of precursor, adducts, and fragment ions using both ES+ and ES-, as shown in Table 2.



Figure 3. Basic chromatographic conditions allow for better separation of nucleoside phosphates compared to acidic conditions (Panels A and B); for method details please see Experimental section. Similarly, columns based on 150 mm HILIC amide chemistry improve the analysis of nucleoside phosphates compared to 150 mm reversed-phase HSS T3 C$_{18}$ chemistry (Panel C; for method details please see reference 1).

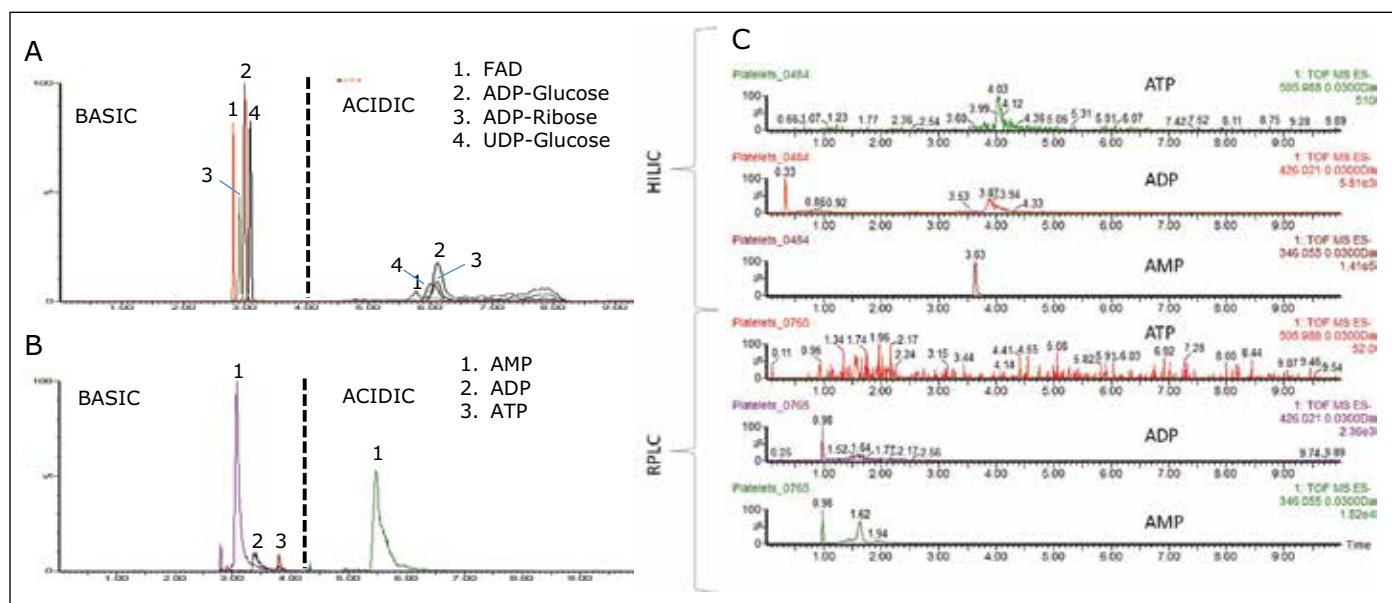| # | Class | HMDB ID | Metabolites | Molecular Formula | MW | [M+H]+ | [M-H]- | Retention time (min) BASIC | NEG | POS | Suggested Condition | Quantification Ions | Internal Standard |
|---|---|---|---|---|---|---|---|---|---|---|---|---|---|
| 1 | Aminoacid | HMDB00929 | Tryptophan | C11H12N2O2 | 204.0899 | 205.0977 | 203.0821 | 3.2 | 3.6 | 3.6 | ACID POS | 205.098+188.070 | Phenylalanine d2 |
| 2 | Aminoacid | HMDB00517 | Arginine | C6H14N4O2 | 174.1117 | 175.1195 | 173.1039 | 6.6 | 5.6 | 5.6 | ACID POS | 158.093+175.12 | Lysine d4 |
| 3 | Aminoacid | HMDB00904 | Citrulline | C6H13N3O3 | 175.0957 | 176.1035 | 174.0879 | 4.2 | 4.8 | 4.8 | ACID POS | 176.104+159.076 | Lysine d4 |
| 4 | Aminoacid | HMDB00574 | Cysteine | C3H7NO2S | 121.0198 | 122.0276 | 120.0120 | – | – | 5.7 | ACID POS | 120.012 | Lysine d4 |
| 5 | Aminoacid | HMDB00177 | Histidine | C6H9N3O2 | 155.0695 | 156.0773 | 154.0617 | – | 5.6 | 5.6 | ACID POS | 156.077+110.071 | Lysine d4 |
| 6 | Aminoacid | HMDB00182 | Lysine | C6H14N2O2 | 146.1055 | 147.1133 | 145.0977 | 6.6 | 5.7 | 5.7 | ACID POS | 147.113+84.081 | Lysine d4 |
| 7 | Aminoacid | HMDB00159 | Phenylalanine | C9H11NO2 | 165.0790 | 166.0868 | 164.0712 | 3.2 | 3.6 | 3.6 | ACID POS | 120.081+166.087 | Phenylalanine d2 |
| 8 | Aminoacid | HMDB00162 | Proline | C5H9NO2 | 115.0633 | 116.0711 | 114.0555 | 3.7 | 4.1 | 4.1 | ACID POS | 116.071+160.035 | Glutamic Acid d5 |
| 9 | Aminoacid | HMDB00172 | Isoleucine | C6H13NO2 | 131.0946 | 132.1024 | 130.0868 | 3.3 | 3.3 | 3.6 | ACID POS | 132.102+86.097 | Phenylalanine d2 |
| 10 | Aminoacid | HMDB00168 | Asparagine | C4H8N2O3 | 132.0535 | 133.0613 | 131.0457 | 4.0 | 4.8 | 4.8 | ACID POS | 133.061 | Phenylalanine d2 |
| 11 | Aminoacid | HMDB00725 | Hydroxyproline | C5H9NO3 | 131.0582 | 132.0660 | 130.0504 | – | – | 4.3 | ACID POS | 132.066+86.061 | Glutamic Acid d5 |
| 12 | Aminoacid | HMDB00696 | Methionine | C5H11NO2S | 149.0511 | 150.0589 | 148.0433 | 2.6 | 3.8 | 3.8 | ACID POS | 104.053+150.059 | Phenylalanine d2 |
| 13 | Aminoacid derivative | HMDB11745 | Acetyl-methionine | C7H13NO3S | 191.0616 | 192.0694 | 190.0538 | 2.6 | – | 2.2 | ACID POS | 192.069 | Phenylalanine d2 |
| 14 | Aminoacid derivative | HMDB03337 | Glutathione Oxidized | C20H32N6O12S2 | 612.1520 | 613.1598 | 611.1442 | 3.9 | 5.6 | 5.6 | ACID POS | 613.16+355.073 | Lysine d4 |
| 15 | Aminoacid derivative | HMDB00125 | Glutathione Reduced | C10H17N3O6S | 307.0838 | 308.0916 | 306.0760 | 4.0 | 5.5 | 5.5 | ACID POS | 308.092+179.05 | Lysine d4 |
| 16 | Aminoacid derivative | HMDB00092 | Dimethylglycine | C4H9NO2 | 103.0630 | 104.0708 | 102.0552 | 3.2 | – | 4.1 | ACID POS | 104.071 | Glutamic Acid d5 |
| 17 | Aminoacid derivative | HMDB01539 | ADMA | C8H18N4O2 | 202.1430 | 203.1508 | 201.1352 | – | – | 5.2 | ACID POS | 203.150+158.129 | Lysine d4 |
| 18 | Aminoacid derivative | HMDB00192 | Cystine | C6H12N2O4S2 | 240.0239 | 241.0317 | 239.0161 | 4.2 | – | 5.7 | ACID POS | 239.016 | Lysine d4 |
| 19 | Aminoacid derivative | HMDB00001 | 1-Methylhistidine | C7H11N3O2 | 169.0851 | 170.0929 | 168.0773 | – | 5.4 | 5.4 | ACID POS | 170.093+109.076 | Lysine d4 |
| 20 | Aminoacid derivative | HMDB00064 | Creatine | C4H9N3O2 | 131.0690 | 132.0768 | 130.0612 | 3.9 | 4.1 | 4.1 | ACID POS | 90.056+132.077 | Phenylalanine d2 |
| 21 | Biogenic Amine | HMDB00259 | Serotonin | C10H12N2O | 176.0950 | 177.1028 | 175.0872 | – | – | 3.5 | ACID POS | 160.076+177.103 | Phenylalanine d2 |
| 22 | Biogenic Amine | HMDB00068 | Epinephrine | C9H13NO3 | 183.0895 | 184.0973 | 182.0817 | – | 3.7 | 3.7 | ACID POS | 166.086+184.097 | Phenylalanine d2 |
| 23 | Carnitine | HMDB00201 | Acetylcarnitine | C9H17NO4 | 203.1158 | 204.1236 | 202.1080 | – | – | 3.2 | ACID POS | 204.124+145.051 | Carnitine d9 |
| 24 | Carnitine | HMDB00062 | Carnitine | C7H15NO3 | 161.1052 | 162.1130 | 160.0974 | – | – | 3.6 | ACID POS | 162.113+103.039 | Carnitine d9 |
| 25 | Carnitine | HMDB00222 | Palmitoylcarnitine | C23H45NO4 | 399.3350 | 400.3428 | 398.3272 | – | – | 2.5 | ACID POS | 400.343 | Carnitine d9 |
| 26 | Nucleobase | HMDB00262 | Thymine | C5H6N2O2 | 126.0429 | 127.0507 | 125.0351 | 1.8 | 2.4 | 2.4 | ACID POS | 127.051 | Phenylalanine d2 |
| 27 | Nucleobase | HMDB00034 | Adenine | C5H5N5 | 135.0540 | 136.0618 | 134.0462 | 2.6 | 3.7 | 3.7 | ACID POS | 136.062 | Phenylalanine d2 |
| 28 | Nucleobase | HMDB00132 | Guanine | C5H5N5O | 151.0490 | 152.0568 | 150.0412 | 2.6 | 3.9 | 3.9 | ACID POS | 152.057+135.03 | Phenylalanine d2 |
| 29 | Nucleobase | HMDB00157 | Hypoxanthine | C5H4N4O | 136.0390 | 137.0468 | 135.0312 | 2.6 | 3.2 | 3.2 | ACID POS | 137.047+119.035 | Phenylalanine d2 |
| 30 | Nucleobase | HMDB00300 | Uracil | C4H4N2O2 | 112.0273 | 113.0345 | 111.0195 | – | – | 3.2 | ACID POS | 113.035+96.008 | Phenylalanine d2 |
| 31 | Nucleoside | HMDB00050 | Adenosine | C10H13N5O4 | 267.0970 | 268.1048 | 266.0892 | – | – | 3.8 | ACID POS | 136.062+268.105 | Phenylalanine d2 |
| 32 | Nucleoside | HMDB00089 | Cytidine | C9H13N3O5 | 243.0855 | 244.0933 | 242.0777 | 3.2 | 4.1 | 4.1 | ACID POS | 244.093+266.075 | Phenylalanine d2 |
| 33 | Nucleoside derivative | HMDB01173 | 5-MTA | C11H15N5O3S | 297.0896 | 298.0974 | 296.0818 | - | - | 3.2 | ACID POS | 298.097+136.062 | Phenylalanine d2 |
| 34 | Nucleoside derivative | HMDB00939 | SAH | C14H20N6O5S | 384.1216 | 385.1294 | 383.1138 | 4 .1 | 5.2 | 5.2 | ACID POS | 134.027+385.129 | Lysine d4 |
| 35 | Nucleoside derivative | HMDB14266 | SAMe | C15H22N6O5S | 398.1372 | 399.1450 | 397.1294 | – | – | 6.0 | ACID POS | 298.094+399.145 | Lysine d4 |
| 36 | Nucleoside derivative | HMDB01517 | AICAR | C9H14N4O5 | 258.0964 | 259.1042 | 257.0886 | 2.9 | 3.8 | 3.8 | ACID POS | 259.104+127.062 | Phenylalanine d2 |
| 37 | Phosphorilated compound | HMDB01565 | Phosphorylcholine | C5H14NO4P | 183.0660 | 184.0738 | 182.0582 | Nd | – | 5.1 | ACID POS | 184.074+124.999 | AMP 13C10, 15N5 |
| 38 | Sugar | HMDB00660 | Fructose | C6H12O6 | 180.0634 | 181.0712 | 179.0556 | – | – | 4.0 | ACID POS | 203.054* | Glucose 13C6 |
| 39 | Sugar | HMDB01514 | Glucosamine | C6H13NO5 | 179.0794 | 180.0872 | 178.0716 | – | – | 4.5 | ACID POS | 180.087 | Glucose 13C6 |
| 40 | Sugar | HMDB00122 | Glucose | C6H12O6 | 180.0634 | 181.0712 | 179.0556 | – | 4.2 | 4.2 | ACID POS | 203.054* | Glucose 13C6 |
| 41 | Sugar | HMDB41627 | Lactose | C12H22O11 | 342.1162 | 343.1240 | 341.1084 | – | 4.8 | – | ACID POS | 365.106* | Glucose 13C6 |
| 42 | Sugar | HMDB00765 | Mannitol | C6H14O6 | 182.0790 | 183.0868 | 181.0712 | 3.6 | 4.1 | 4.1 | ACID POS | 205.069* | Glucose 13C6 |
| 43 | Sugar | HMDB00169 | Mannose | C6H12O6 | 180.0634 | 181.0712 | 179.0556 | – | 4.0 | 4.0 | ACID POS | 203.054* | Glucose 13C6 |
| 44 | Sugar | HMDB00215 | Acetyl-Glucosamine | C8H15NO6 | 221.0899 | 222.0977 | 220.0821 | – | – | 3.8 | ACID POS | 222.098+204.086 | Glucose 13C6 |
| 45 | Sugar | HMDB00258 | Sucrose | C12H22O11 | 342.1162 | 343.1240 | 341.1084 | 4.1 | 4.7 | 4.7 | ACID POS | 365.106* | Glucose 13C6 |
| 46 | Sugar | HMDB03213 | Raffinose | C18H32O16 | 504.1690 | 505.1768 | 503.1612 | 4.6 | 5.3 | 5.3 | ACID POS | 527.167* | Glucose 13C6 |
| 47 | Vitamin | HMDB00121 | Folic acid | C19H19N7O6 | 441.1397 | 442.1475 | 440.1319 | 2.9 | 3.7 | 3.7 | ACID POS | 442.148+295.094 | Phenylalanine d2 |
| 48 | Vitamin | HMDB01396 | 5-Me-THF | C20H25N7O6 | 459.1866 | 460.1944 | 458.1788 | – | – | 4.5 | ACID POS | 460.194+313.142 | Glutamic Acid d5 |
| 49 | Vitamin | HMDB01406 | Niacinamide | C6H6N2O | 122.0480 | 123.0558 | 121.0402 | – | – | 2.5 | ACID POS | 123.056 | Carnitine d9 |
| 50 | Vitamin | HMDB01488 | Nicotinic acid | C6H5NO2 | 123.0320 | 124.0398 | 122.0242 | – | – | 2.3 | ACID POS | 124.04 | Carnitine d9 |
| 51 | Vitamin | HMDB01392 | PABA | C7H7NO2 | 137.0480 | 138.0558 | 136.0402 | – | – | 1.4 | ACID POS | 138.056+94.065 | Carnitine d9 |
| 52 | Vitamin | HMDB00607 | Vitamin B12 | C63H88CoN14O14P | 1354.5674 | 1355.5752 | 1353.5596 | – | – | 4.6 | ACID POS | 679.292** | Glutamic Acid d5 |
| 53 | Vitamin | HMDB00030 | Biotin | C10H16N2O3S | 244.0882 | 245.0960 | 243.0803 | – | 2.6 | 2.6 | ACID POS | 245.096+227.085 | Carnitine d9 |
| 54 | Vitamin | HMDB00244 | Riboflavin | C17H20N4O6 | 376.1383 | 377.1461 | 375.1305 | – | 3.4 | 3.4 | ACID POS | 377.146 | Phenylalanine d2 |
| 55 | Vitamin | HMDB00239 | Pyridoxine | C8H11NO3 | 169.0739 | 170.0817 | 168.0661 | – | 3.5 | 3.5 | ACID POS | 170.0812 | Phenylalanine d2 |
| 56 | Vitamin | HMDB00235 | Thiamine | C12H16N4OS | 264.1045 | 263.0967 | 265.1123 | – | – | 5.2 | ACID POS | 265.112+122.071 | Lysine d4 |
| 57 | Vitamin | HMDB00097 | Choline | C5H14NO | 104.1075 | 104.1075 | 103.0997 | – | – | 2.7 | ACID POS | 104.107 | Lysine d4 |
| 58 | Aminoacid | HMDB00191 | Aspartic Acid | C4H7NO4 | 133.0375 | 134.0453 | 132.0297 | 3.3 | 4.6 | 4.6 | ACID NEG | 132.03 | Glutamic Acid d5 |
| 59 | Aminoacid | HMDB00641 | Glutamine | C5H10N2O3 | 146.0691 | 147.0769 | 145.0613 | 4.1 | 4.7 | 4.7 | ACID NEG | 145.061+127.05 | Glutamic Acid d5 |
| 60 | Aminoacid | HMDB00187 | Serine | C3H7NO3 | 105.0426 | 106.0504 | 104.0348 | – | 4.6 | – | ACID NEG | 104.035 | Glutamic Acid d5 |
| 61 | Aminoacid | HMDB00167 | Threonine | C4H9NO3 | 119.0582 | 120.0660 | 118.0504 | – | 4.6 | 4.6 | ACID NEG | 118.051 | Glutamic Acid d5 |
| 62 | Aminoacid | HMDB00161 | Alanine | C3H7NO2 | 89.0477 | 90.0555 | 88.0399 | 3.9 | 4.3 | – | ACID NEG | 88.04 | Glutamic Acid d5 |
| 63 | Aminoacid | HMDB00158 | Tyrosine | C9H11NO3 | 181.0739 | 182.0817 | 180.0661 | 3.5 | 4.1 | 4.1 | ACID NEG | 180.066+163.04 | Phenylalanine d2 |
| 64 | Aminoacid | HMDB00883 | Valine | C5H11NO2 | 117.0790 | 118.0868 | 116.0712 | – | 3.9 | – | ACID NEG | 116.071 | Phenylalanine d2 |
| 65 | Aminoacid derivative | HMDB00267 | 5-Oxoproline | C5H7NO3 | 129.0426 | 130.0504 | 128.0348 | 2.7 | 2.6 | 2.6 | ACID NEG | 128.035 | Succinate d4 |
| 66 | Nucleobase | HMDB00292 | Xanthine | C5H4N4O2 | 152.0334 | 153.0412 | 151.0256 | 2.8 | 3.3 | 3.3 | ACID NEG | 151.026 | Phenylalanine d2 |
| 67 | Nucleobase | HMDB00289 | Uric acid | C5H4N4O3 | 168.0283 | 169.0361 | 167.0205 | 2.7 | 4.0 | 4.0 | ACID NEG | 167.021 | Phenylalanine d2 |
| 68 | Nucleoside | HMDB00296 | Uridine | C9H12N2O6 | 244.0695 | 245.0773 | 243.0617 | 2.6 | 3.1 | 3.1 | ACID NEG | 243.062+110.024 | Phenylalanine d2 |
| 69 | Nucleoside | HMDB00299 | Xanthosine | C10H12N4O6 | 284.0757 | 285.0835 | 283.0679 | 2.8 | 3.7 | 3.6 | ACID NEG | 283.068 | Phenylalanine d2 |
| 70 | Nucleoside | HMDB00133 | Guanosine | C10H13N5O5 | 283.0917 | 284.0995 | 282.0839 | – | 3.9 | 3.9 | ACID NEG | 282.084 | Phenylalanine d2 |
| 71 | Nucleoside | HMDB00195 | Inosine | C10H12N4O5 | 268.0808 | 269.0886 | 267.0730 | 3.0 | 3.5 | 3.5 | ACID NEG | 267.073 | Phenylalanine d2 |
| 72 | Organic Acid | HMDB00072 | Aconitic Acid | C6H6O6 | 174.0164 | 175.0242 | 173.0086 | 2.8 | 2.5 | – | ACID NEG | 173.009+85.029 | Succinate d4 |
| 73 | Organic Acid | HMDB03349 | Dihydroorotic Acid | C5H6N2O4 | 158.0328 | 159.0406 | 157.0250 | 2.8 | 2.8 | – | ACID NEG | 157.025+113.036 | Succinate d4 |
| 74 | Organic Acid | HMDB00139 | Glyceric Acid | C3H6O4 | 106.0270 | 107.0348 | 105.0192 | 2.7 | 2.7 | – | ACID NEG | 105.0192 | Succinate d4 |
| 75 | Organic Acid | HMDB00156 | Malic Acid | C4H6O5 | 134.0215 | 135.0293 | 133.0137 | 3.1 | 2.8 | – | ACID NEG | 133.014+115.003 | Succinate d4 |
| 76 | Organic Acid | HMDB00134 | Fumaric Acid | C4H4O4 | 116.0110 | 117.0188 | 115.0032 | – | 2.3 | – | ACID NEG | 115.003 | Succinate d4 |
| 77 | Organic Acid | HMDB00094 | Citric Acid | C6H8O7 | 192.0270 | 193.0348 | 191.0192 | 4.0 | 3.7 | – | ACID NEG | 191.019 | Phenylalanine d2 |
| 78 | Organic Acid | HMDB00227 | Mevalonic Acid | C6H12O4 | 148.0736 | 149.0814 | 147.0658 | 2.7 | 2.2 | – | ACID NEG | 147.066 | Succinate d4 |
| 79 | Organic Acid | HMDB00226 | Orotic Acid | C5H4N2O4 | 156.0171 | 157.0249 | 155.0093 | 2.6 | – | 3.2 | ACID NEG | 155.009+111.0192 | Succinate d4 |
| 80 | Organic Acid | HMDB01895 | Salicylic Acid | C7H6O3 | 138.0320 | 139.0398 | 137.0242 | 0.6 | 1.4 | – | ACID NEG | 137.024+93.035 | Octanoic Acid d15 |
| 81 | Organic Acid | HMDB00254 | Succinic Acid | C4H6O4 | 118.0266 | 119.0344 | 117.0188 | 2.7 | 2.3 | – | ACID NEG | 117.019 | Succinate d4 |
| 82 | Sugar | HMDB00625 | Gluconic Acid | C6H12O7 | 196.0583 | 197.0661 | 195.0505 | 2.9 | 4.2 | 4.2 | ACID NEG | 195.051 | Glucose 13C6 |
| 83 | Sugar | HMDB00127 | Glucuronic Acid | C6H10O7 | 194.0426 | 195.0504 | 193.0348 | 3.0 | 4.2 | – | ACID NEG | 193.035 | Glutamic Acid d5 |
| 84 | Vitamin | HMDB00017 | Pyridoxal Acid | C8H9NO4 | 183.0532 | 184.0610 | 182.0454 | 0.6 | 2.9 | 2.9 | ACID NEG | 138.055+182.045 | Succinate d4 |
| 85 | Vitamin | HMDB00044 | Ascorbic Acid | C6H8O6 | 176.0321 | 177.0399 | 175.0243 | – | 3.0 | – | ACID NEG | 175.024 | Succinate d4 |
| 86 | Vitamin | – | Panthotenic Acid | C9H17NO5 | 219.1107 | 220.1185 | 218.1028 | – | 2.5 | 2.5 | ACID NEG | 146.082+218.103 | Succinate d4 |
| 87 | Aminoacid | HMDB00148 | Glutamic Acid | C5H9NO4 | 147.0532 | 148.0610 | 146.0454 | 3.3 | 4.5 | 4.5 | BASIC NEG | 146.045+102.056 | Glutamic Acid d5 |
| 88 | Aminoacid derivative | HMDB00766 | Acetylalanine | C5H9NO3 | 131.0582 | 132.0660 | 130.0504 | 2.7 | 2.5 | – | BASIC NEG | 130.05+88.04 | Phenylalanine d2 |
| 89 | Aminoacid derivative | HMDB00251 | Taurine | C2H7NO3S | 125.0147 | 126.0225 | 124.0069 | 3.4 | 4.2 | 4.2 | BASIC NEG | 79.957+124.007 | Glutamic Acid d5 |
| 90 | Coenzyme | HMDB01423 | CoA | C21H36N7O16P3S | 767.1152 | 768.1230 | 766.1074 | 3.7 | – | – | BASIC NEG | 766.107 | "AMP 13C10, 15N5" |
| 91 | Coenzyme | HMDB00902 | NAD | C21H27N7O14P2 | 663.1091 | 664.1169 | 662.1013 | 3.7 | – | – | BASIC NEG | 540.053+662.101 | AMP 13C10, 15N5 |
| 92 | Coenzyme | HMDB00217 | NADP | C21H28N7O17P3 | 743.0755 | 744.0833 | 742.0676 | 3.8 | – | – | BASIC NEG | 620.023+742.068 | AMP 13C10, 15N5 |
| 93 | Coenzyme | HMDB01248 | FAD | C27H33N9O15P2 | 785.1571 | 786.1649 | 784.1493 | 2.8 | – | – | BASIC NEG | 784.149+528.053 | AMP 13C10, 15N5 |
| 94 | dNucleotide | HMDB00058 | cAMP | C10H12N5O6P | 329.0525 | 330.0603 | 328.0447 | 2.7 | – | – | BASIC NEG | 328.045 | AMP 13C10, 15N5 |
| 95 | dNucleotide | HMDB01314 | cGMP | C10H12N5O7P | 345.0474 | 346.0552 | 344.0396 | 2.7 | – | 5.1 | BASIC NEG | 344.040 | AMP 13C10, 15N5 |
| 96 | dNucleotide | HMDB00905 | dAMP | C10H14N5O6P | 331.0682 | 332.0760 | 330.0604 | 3.0 | 5.2 | – | BASIC NEG | 330.060 | AMP 13C10, 15N5 |
| 97 | dNucleotide | HMDB01202 | dCMP | C9H14N3O7P | 307.0569 | 308.0647 | 306.0491 | 3.3 | 5.3 | – | BASIC NEG | 306.049 | AMP 13C10, 15N5 |
| 98 | dNucleotide | HMDB01227 | dTMP | C10H15N2O8P | 322.0566 | 323.0644 | 321.0488 | 2.9 | – | – | BASIC NEG | 321.049 | AMP 13C10, 15N5 |
| 99 | Nucleoside derivative | HMDB00536 | Adenylosuccinic Acid | C14H18N5O11P | 463.0740 | 464.0818 | 462.0662 | 3.6 | – | – | BASIC NEG | 462.066 | Glutamic Acid d5 |
| 100 | Nucleoside diphosphate | HMDB00295 | UDP | C9H14N2O12P2 | 404.0022 | 405.0100 | 402.9944 | 4.0 | – | – | BASIC NEG | 402.994 | AMP 13C10, 15N5 |
| 101 | Nucleoside diP derivative | HMDB06557 | ADP-Glucose | C16H25N5O15P2 | 589.0822 | 590.0900 | 588.0744 | 3.0 | – | – | BASIC NEG | 588.074 | AMP 13C10, 15N5 |
| 102 | Nucleoside diP derivative | HMDB01178 | ADP-Ribose | C15H23N5O14P2 | 559.0717 | 560.0795 | 558.0639 | 2.9 | – | – | BASIC NEG | 558.064 | AMP 13C10, 15N5 |
| 103 | Nucleoside diphosphate | HMDB00286 | UDP-Glucose | C15H24N2O17P2 | 566.0550 | 567.0628 | 565.0472 | 3.2 | – | – | BASIC NEG | 565.047 | AMP 13C10, 15N5 |
| 104 | Nucleoside diphsphate | HMDB01341 | ADP | C10H15N5O10P2 | 427.0294 | 428.0372 | 426.0216 | 3.9 | – | – | BASIC NEG | 426.022 | AMP 13C10, 15N5 |
| 105 | Nucleoside diphsphate | HMDB01201 | GDP | C10H15N5O11P2 | 443.0243 | 444.0321 | 442.0165 | 4.3 | – | – | BASIC NEG | 442.016 | AMP 13C10, 15N5 |
| 106 | Nucleoside Triphosphate | HMDB01273 | GTP | C10H16N5O14P3 | 522.9907 | 523.9985 | 521.9829 | 4.3 | – | – | BASIC NEG | 521.983 | AMP 13C10, 15N5 |
| 107 | Nucleoside Triphosphate | HMDB00538 | ATP | C10H16N5O13P3 | 506.9958 | 508.0036 | 505.9879 | 3.9 | – | – | BASIC NEG | 505.988+408.009 | AMP 13C10, 15N5 |
| 108 | Nucleotide | HMDB00045 | AMP | C10H14N5O7P | 347.0631 | 348.0709 | 346.0553 | 3.2 | – | 5.6 | BASIC NEG | 346.055 | AMP 13C10, 15N5 |
| 109 | Nucleotide | HMDB00095 | CMP | C9H14N3O8P | 323.0519 | 324.0597 | 322.0441 | 3.5 | – | – | BASIC NEG | 322.044 | AMP 13C10, 15N5 |
| 110 | Nucleotide | HMDB01397 | GMP | C10H14N5O8P | 363.0580 | 364.0658 | 362.0502 | 3.6 | – | – | BASIC NEG | 362.050 | AMP 13C10, 15N5 |
| 111 | Nucleotide | HMDB00175 | IMP | C10H13N4O8P | 348.0471 | 349.0549 | 347.0393 | 3.3 | – | – | BASIC NEG | 347.039 | AMP 13C10, 15N5 |
| 112 | Nucleotide | HMDB00288 | UMP | C9H13N2O9P | 324.0359 | 325.0437 | 323.0281 | 3.2 | – | – | BASIC NEG | 323.028 | AMP 13C10, 15N5 |
| 113 | Organic Acid | HMDB00357 | 3-Hydroxybutyric Acid | C4H8O3 | 104.0473 | 105.0551 | 103.0395 | 3.1 | – | – | BASIC NEG | 103.040 | Phenylalanine d2 |
| 114 | Organic Acid | - | 4-Methyl-2-Oxopentanoic Acid | C6H10O3 | 130.0630 | 131.0708 | 129.0552 | 0.7 | 1.3 | – | BASIC NEG | 129.055 | Octanoic Acid d15 |
| 115 | Organic Acid | HMDB00190 | Lactic acid | C3H6O3 | 90.0317 | 91.0395 | 89.0239 | 2.0 | 2.7 | – | BASIC NEG | 89.024 | Succinate d4 |
| 116 | Phosphorilated compound | HMDB00362 | 2-Phosphoglyceric Acid | C3H7O7P | 185.9929 | 187.0007 | 184.9851 | 3.4 | – | – | BASIC NEG | 184.985 | AMP 13C10, 15N5 |
| 117 | Phosphorilated compound | - | Glycerol Monophosphate | C3H9O6P | 172.0137 | 173.0215 | 171.0059 | 3.2 | – | – | BASIC NEG | 171.006 | AMP 13C10, 15N5 |
| 118 | Phosphorilated compound | HMDB01511 | Phosphocreatine | C4H10N3O5P | 211.0360 | 212.0438 | 210.0282 | 3.3 | – | – | BASIC NEG | 210.028 | AMP 13C10, 15N5 |
| 119 | Phosphorilated compound | HMDB00263 | Phosphoenolpyruvic Acid | C3H5O6P | 167.9820 | 168.9898 | 166.9742 | 3.4 | – | – | BASIC NEG | 166.974 | AMP 13C10, 15N5 |
| 120 | Phosphorilated Sugar | HMDB01316 | 6-Phosphogluconic Acid | C6H13O10P | 276.0246 | 277.0324 | 275.0168 | 3.6 | – | – | BASIC NEG | 275.017+257.006 | AMP 13C10, 15N5 |
| 121 | Phosphorilated Sugar | HMDB00124 | Fructose 6-Phosphate | C6H13O9P | 260.0297 | 261.0375 | 259.0219 | 3.5 | – | – | BASIC NEG | 259.022 | AMP 13C10, 15N5 |
| 122 | Phosphorilated sugar | HMDB01058 | "Fructose-1,6-Diphosphate" | C6H14O12P2 | 339.9961 | 341.0039 | 338.9883 | 4.1 | – | – | BASIC NEG | 338.988 | "AMP 13C10, 15N5" |
| 123 | Phosphorilated Sugar | HMDB01254 | Glucosamine-6-Phosphate | C6H14NO8P | 259.0457 | 260.0535 | 258.0379 | 4.0 | – | – | BASIC NEG | 258.038 | "AMP 13C10, 15N5" |
| 124 | Phosphorilated Sugar | HMDB01401 | Glucose 6-Phosphate | C6H13O9P | 260.0297 | 261.0375 | 259.0219 | 3.7 | – | – | BASIC NEG | 259.022 | "AMP 13C10, 15N5" |
| 125 | Phosphorilated Sugar | HMDB01548 | Ribose 5-Phosphate | C5H11O8P | 230.0192 | 231.0270 | 229.0114 | 3.4 | – | – | BASIC NEG | 229.011 | "AMP 13C10, 15N5" |

\*    [M+Na]+

\*\*    [M+2H]2+

Calibration curves were obtained for various chemical classes of the metabolites, shown in Figure 4, which displayed a linear coefficient (Pearson's correlation, $R^2$) higher than 0.99. The LOD was lower than 100 ng/mL for most of the analytes reported in Table 2.
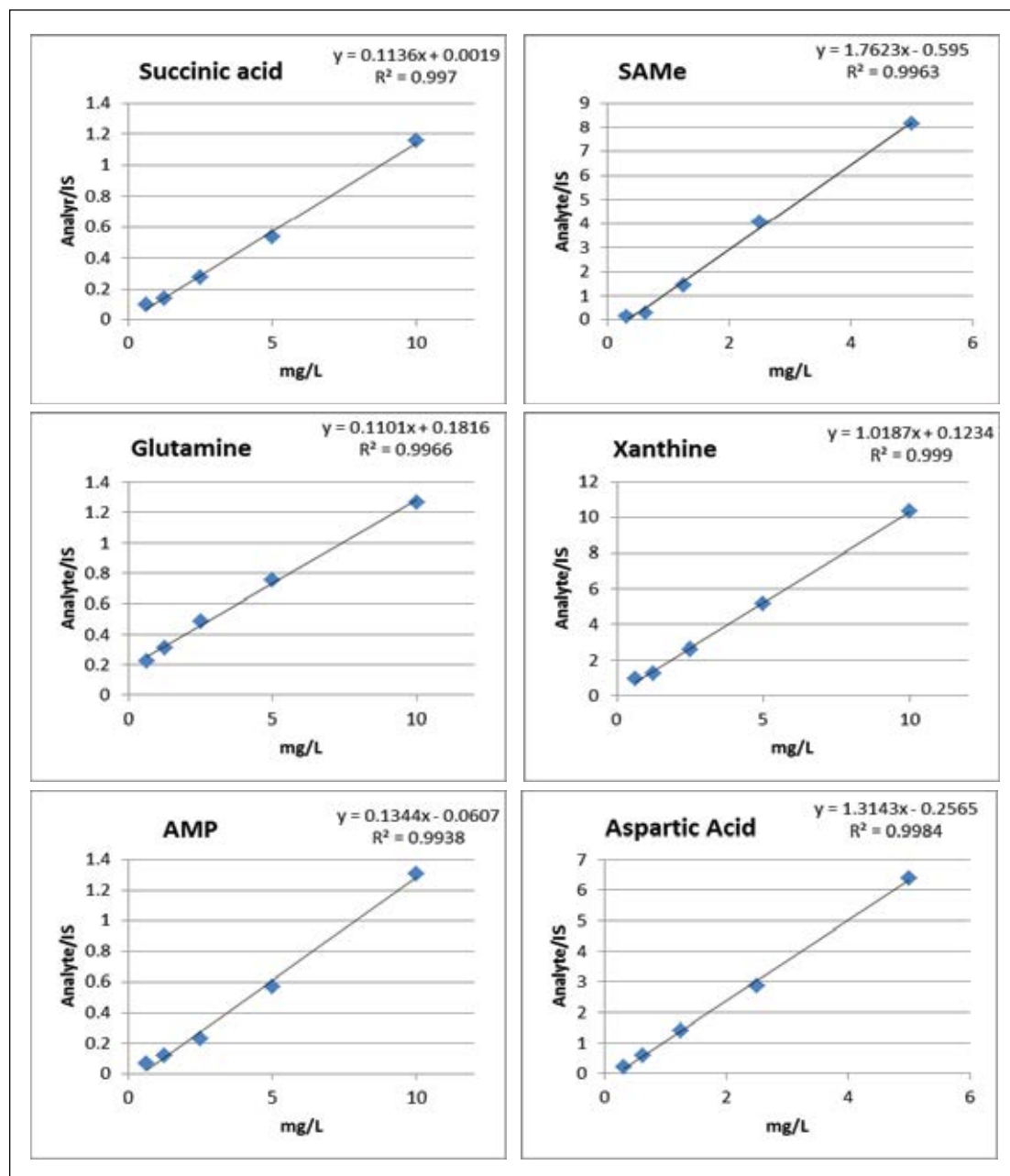


Figure 4. Calibration curves from selected small polar metabolites.

To test the applicability of this HILIC-UPLC/MS strategy in real biological samples, polar metabolites extracted from human platelets were analyzed. Polar metabolites were separated with excellent retention time reproducibility, shown in Figure 5, acquiring accurate mass information from *m/z* 50 to *m/z* 1000. As general workflow, untargeted analyses were performed on this dataset using TransOmics Informatics tools for the visualization, processing, and interpretation of MS data, allowing the discovery and identification of unexpected alterations among sample groups (data not shown).
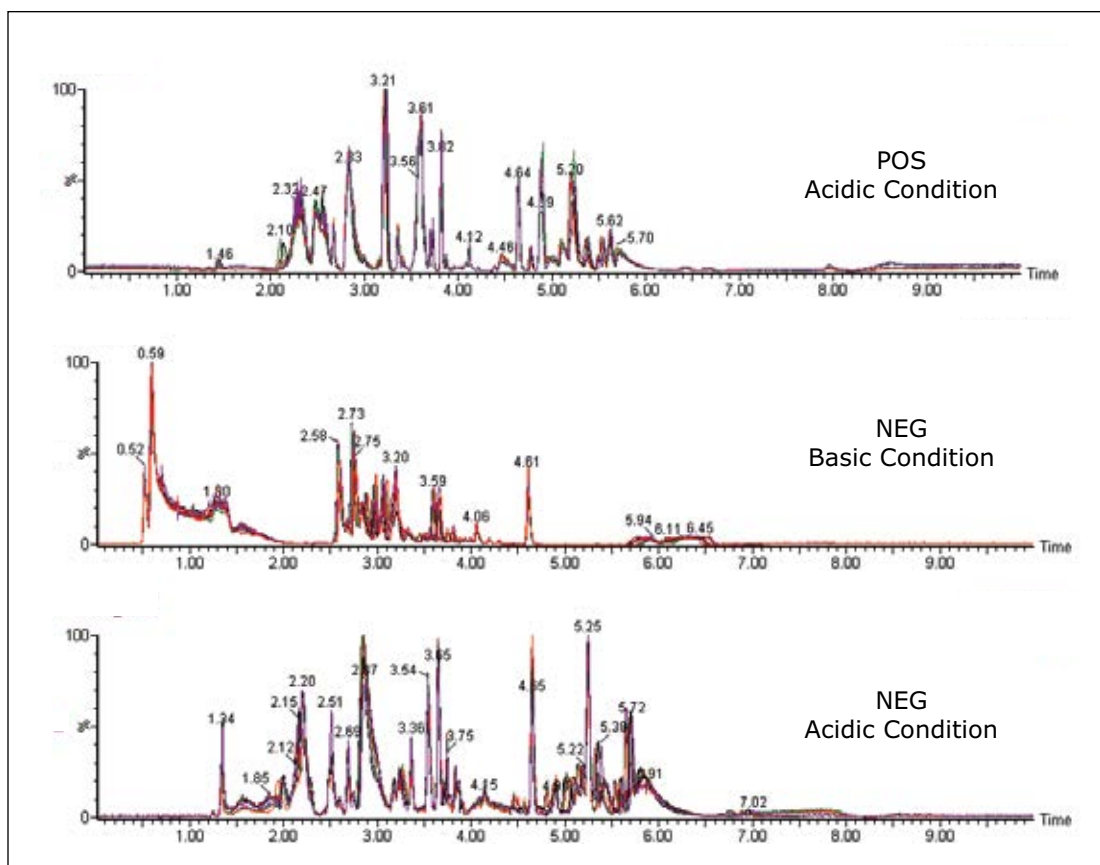


*Figure 5. Overlaid chromatographic trace of multiple injections of polar metabolites exctracted from platelets. Each polar metabolite extract was injected eight times during two different batches (80 injections) in two different days of analysis.*

Additionally, targeted analyses were conducted using the list of retention times and masses information reported in Table 2, allowing the identification and quantification of the most common metabolites present in biological samples, as shown in Figures 6A and 6B.
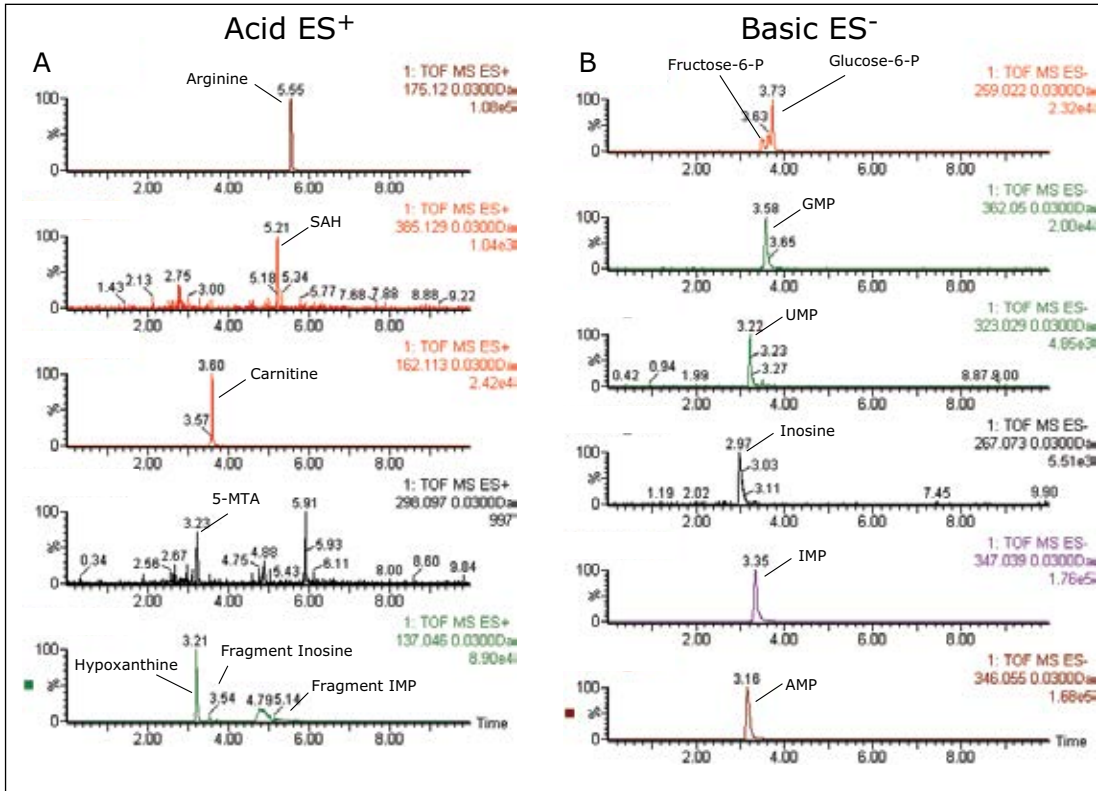


Figure 6. Representative UPLC/MS chromatograms of polar metabolites extracted from platelets and analyzed using acidic conditions for positive ES (A) and basic conditions for negative ES (B).

## CONCLUSIONS

A HILIC UPLC/TOF-MS strategy was developed for the analysis of polar metabolites, which could not be easily analyzed using reversed-phase chromatography. Such a method is suitable for routine high-throughput screening of polar metabolites for both untargeted and targeted metabolomics applications.

### References

1. Paglia G, Magnusdottir M, Thorlacius S, Sigurjonsson OE, Guethmundsson S, Palsson BO, Thiele I. Intracellular metabolite profiling of platelets: evaluation of extraction processes and chromatographic strategies. *J Chromatogr B Analyt Technol Biomed Life Sci.* 2012; 898:111-120. doi:10.1016/j.jchromb.2012.04.026.

2. Paglia G, Hrafnsdottir S, Magnusdottir M, Fleming RM, Thorlacius S, Palsson BO, Thiele I. Monitoring metabolites consumption and secretion in cultured cells using ultra-performance liquid chromatography quadrupole-time of flight mass spectrometry (UPLC-Q-ToF-MS). *Anal Bioanal Chem.* 2012;402(3):1183-1198. doi:10.1007/s00216-011-5556-4.

## Waters
### THE SCIENCE OF WHAT'S POSSIBLE.®

**Waters Corporation**
34 Maple Street
Milford, MA 01757 U.S.A.
T: 1 508 478 2000
F: 1 508 872 1990
www.waters.com

Waters
THE SCIENCE OF WHAT'S POSSIBLE.®

# Lipid Separation using UPLC with Charged Surface Hybrid Technology

Giorgis Isaac, Stephen McDonald, and Giuseppe Astarita
Waters Corporation, Milford, MA, USA

## APPLICATION BENEFITS

The chromatographic separation performed using Ultra Performance Liquid Chromatography (UPLC®) with Charged Surface Hybrid (CSH™) $C_{18}$ Technology shows superior performance over traditional reversed-phase techniques to give fast, sensitive separation of lipids based upon their acyl chain length, and the number, position, and geometry of double bonds. The resolving power of the CSH $C_{18}$ UPLC System provides an attractive solution for analyzing complex lipid mixtures in biological samples and comparative lipidomic analysis.

## WATERS SOLUTIONS

ACQUITY UPLC®

UPLC

SYNAPT® G2 HDMS™

## KEY WORDS

Separation of lipids, Charged Surface Hybrid, CSH, reversed-phase, lipids, time-of-flight mass spectrometry

## INTRODUCTION

Lipids play key roles in human health. Alterations in lipid levels have been associated with the occurrence of various diseases, including cardiovascular diseases, diabetes, cancer, and neurodegenerative diseases.[1] Advances in LC/MS have allowed lipids to be studied with greater sensitivity and specificity, alleviating the effects of co-eluting compounds and isobaric interference, and allowing low abundance lipids to be more readily detected.[1]

Conventional mass spectrometric analysis of lipids is often performed by direct infusion, or reversed-phase (RP) / normal-phase (NP) HPLC.[2-5] However, each of these methods faces its own challenges.

With direct infusion, chromatographic separation of lipids is not performed prior to injection into the mass spectrometer. This method of sample introduction gives rise to ion suppression and it does not allow for separation of isobaric lipids, which can complicate the resultant analysis, necessitating deconvolution, and compromising the sensitivity of the method. In order to fully explore the lipidome, a technique of sample introduction into the mass spectrometer that minimizes these issues is needed.

NP chromatography allows separation of lipids by class but often suffers from long elution times, is difficult to handle due to the volatility and toxicity of the mobile phase, and proves challenging for ionization and introduction into mass spectrometry.[6] Recent work in HILIC chromatography overcomes many of these issues.[7]

Traditional RP methods similarly suffer from extensive elution times and the quality of the resulting chromatography is relatively poor. Peak capacity and resolution are compromised in a typical analysis and it is not unusual to see peaks widths > 30 seconds,[5] which ultimately results in poor sensitivity and difficulty in characterization.

In this application note, novel RP-UPLC separations are performed using a Waters® ACQUITY UPLC System with Charged Surface Hybrid (CSH™) $C_{18}$ chemistry. The combination of sub-2-μm particle size with an optimized liquid chromatography system and novel chemistry allows for a significantly improved RP method that maximizes the performance of these particles and is optimized for the analysis of complex lipid mixtures.

## EXPERIMENTAL

### LC conditions

| | |
|---|---|
| LC system: | ACQUITY UPLC |
| Column: | ACQUITY UPLC CSH $C_{18}$ 2.1 x 100 mm, 1.7 µm |
| Column temp.: | 55 °C |
| Flow rate: | 400 µL/min |
| Mobile phase A: | Acetonitrile/water (60:40) with 10 mM ammonium formate and 0.1% formic acid |
| Mobile phase B: | Isopropanol/acetonitrile (90:10) with 10 mM ammonium formate and 0.1% formic acid |
| Injection volume: | 5 µL |

Gradient

| Time (min) | % A | % B | Curve |
|---|---|---|---|
| Initial | 60 | 40 | Initial |
| 2.0 | 57 | 43 | 6 |
| 2.1 | 50 | 50 | 1 |
| 12.0 | 46 | 54 | 6 |
| 12.1 | 30 | 70 | 1 |
| 18.0 | 1 | 99 | 6 |
| 18.1 | 60 | 40 | 6 |
| 20.0 | 60 | 40 | 1 |

### MS conditions

| | |
|---|---|
| Mass spectrometer: | SYNAPT G2 HDMS |
| Acquisition mode: | MS$^E$ |
| Ionization mode: | ESI positive/negative |
| Capillary voltage: | 2.0 KV (for positive) 1.0 KV (for negative) |
| Cone voltage: | 30 V |
| Desolvation temp.: | 550 °C |
| Desolvation gas: | 900 L/Hr |
| Source temp.: | 120 °C |
| Acquisition range: | 100 to 2000 *m/z* |

## Sample preparation

### Standard lipid mixtures

Lipid standards were purchased from Avanti Polar Lipids and Nu-Chek Prep. The standards were diluted prior to analysis in isopropanol/acetonitrile/ water (2:1:1, 250 µL). The list of lipid standards analyzed and other detailed information is provided in Table 1.

### Total liver extract

A total lipid extract from bovine liver was purchased from Avanti Polar Lipids. The extract was prepared by making a 5 mg/mL stock solution in chloroform/methanol (2:1). A working 0.1 mg/mL solution was then prepared by diluting the stock solution with isopropanol/acetonitrile/water (2:1:1).

### Total plasma extract

Rat plasma (25 µL) from Equitech-Bio, Inc. was extracted with 100 µL of chloroform/methanol (2:1); this solution was then allowed to stand for 5 min at room temperature, followed by vortexing for 30 s. After centrifuging (12,000 g, for 5 min at 4 °C) the lower organic phase was collected in a new vial and evaporated to dryness under vacuum. Immediately prior to analysis the lipid extract was diluted with isopropanol/acetonitrile/water (2:1:1, 250 µL ).

## RESULTS AND DISCUSSION

The UPLC RP method employed for this analysis showed improved separation of both inter and intra class lipids over traditional HPLC RP methods. Figures 1 and 2 show the lipid classes based on Lipid MAPS classification and representative structures for major lipid categories respectively. Highlighted in yellow are the classes that are included in the standard mix, which reflect the most abundant lipids present in animal tissues.
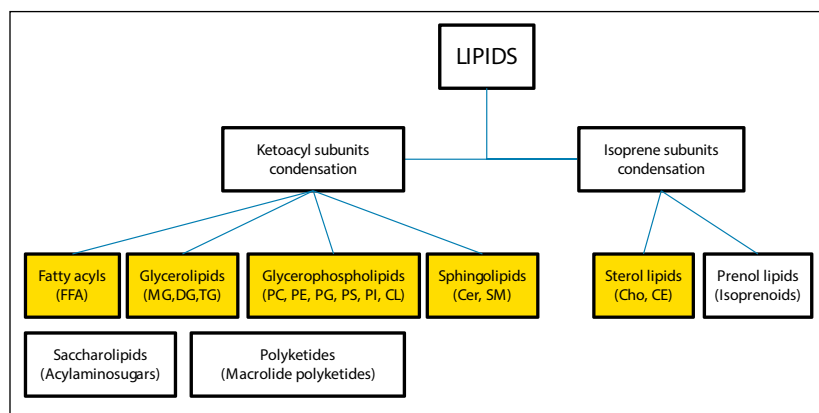


Figure 1. Lipid categories and examples of common lipids analyzed in this application. Abbreviations: FFA, free fatty acids; MG, monoacylglycerols; DG, diacylglycerols; TG, triacylglycerols; PC, phosphatidylcholines; PE, phosphatidylethanolamines; PG, phosphatidylglycerols; PS, phosphatidylserines; PI, phosphatidylinositols; CL, cardiolipins; Cer, ceramides; SM, sphingomyelins; Cho, cholesterol; CE, cholesterol esters.
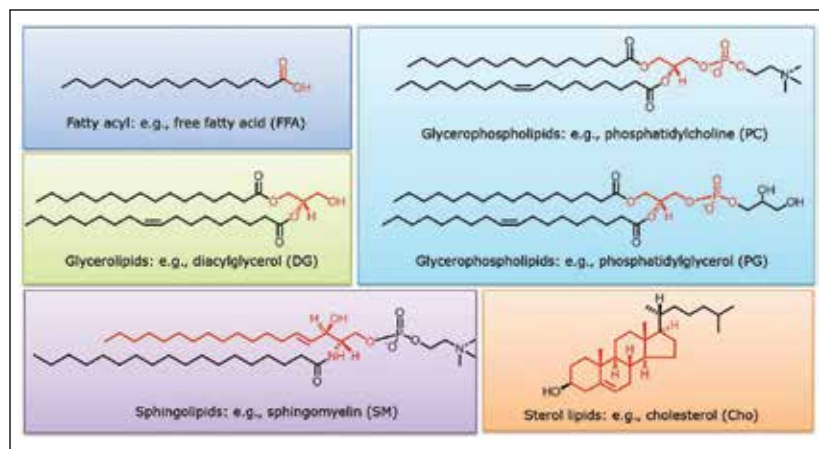


Figure 2. Representative structures for major lipid categories and examples of core structures in red.

The resolution, sensitivity, and speed of analysis were significantly increased compared with HPLC. The CSH chemistry's charged surface is believed to interact with the lipids on column in a unique manner. Due to the diverse chemical nature of lipids, from highly polar to highly non-polar, a different mechanism of retention from traditional RP columns was observed.

The additional speed allows for large sample sets to be analyzed efficiently, while the added resolution and sensitivity increase peak purity. This provides added confidence in the assignment of a lipid or class of lipids while allowing identification to be made at lower concentrations.

Our initial analysis focused on the separation of a mixture of 67 lipid standards, as shown in Table 1.

The resulting base peak intensity chromatogram can be seen in Figure 3.
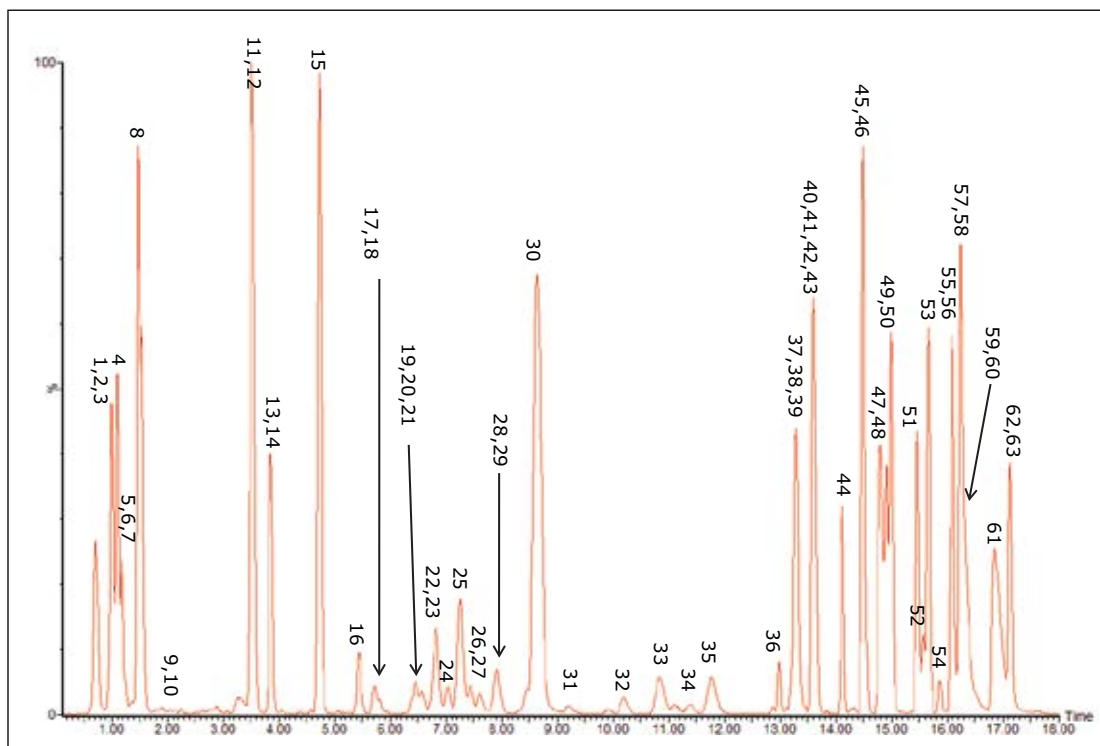


Figure 3. CSH C$_{18}$ separation of 67 standard lipid mixtures.

As can be seen in Figure 3, several interesting observations were made during the course of developing this method. First, we have shown previously that the phophatidylcholines (PC) typically co-elute with sphingomyelins (SM) during a RP separation.[8] Using CSH Technology C$_{18}$, an enhanced separation of these classes was observed. This is especially useful when coupling with mass spectral detection as both classes fragment to give a phosphocholine ion at *m/z* 184.074, the common head group. Also, in complex biological matricies, SM are less abundant than PC species, leading to ion suppression effects that affect the efficiency of detection of minor species. Figures 4 and 5 show the analysis of total lipid extracts from bovine liver and rat plasma respectively.

| Lipid sub class | Lipid molecular species | Concentration (pmol/uL) | Rt* (min) | Peak ID |
|---|---|---|---|---|
| FA | C13:1 (12Z) | 4 | 1.24 | ** |
| | C17:1 (10Z) | 4 | 2.3 | ** |
| | C23:1 (14Z) | 4 | 5.44 | ** |
| MG | 14:1 (9Z) | 4 | 1.11 | 5 |
| | 17:1 (10Z) | 4 | 1.7 | 9 |
| | 19:2 (10Z, 13Z) | 4 | 1.87 | 10 |
| D5-DG Mix I | 1,3-14:0/14:0 | 2 | 7.6 | 27 |
| | 1,3-15:0/15:0 | 2 | 10.17 | 32 |
| | 1,3-16:0/16:0 | 2 | 12.98 | 36 |
| | 1,3-17:0/17:0 | 2 | 13.6 | 40 |
| | 1,3-19:0/19:0 | 2 | 14.55 | 46 |
| | 1,3-20:5 (5Z, 8Z, 11Z, 14Z, 17Z)/20:5 (5Z, 8Z,11Z, 14Z, 17Z) | 2 | 5.41 | 16 |
| | 1,3-20:4 (5Z, 8Z, 11Z, 14Z)/20:4 (5Z, 8Z, 11Z, 14Z) | 2 | 7.88 | 28 |
| | 1,3-20:2 (11Z, 14Z)/20:2 (11Z, 14Z) | 2 | 13.23 | 38 |
| | 1,3-20:0/20:0 | 2 | 14.95 | 49 |
| DG | 19:1/19:1 (10Z) | 4 | 13.65 | 42 |
| | 19:1/19:1 (10Z) 1,3 isomer | 4 | 13.65 | 43 |
| D5-TG Mix I | 14:0/16:1 (9Z)/14:0 | 2 | 14.99 | 50 |
| | 15:0/18:1 (9Z)/15:0 | 2 | 15.65 | 53 |
| | 16:0/18:0/16:0 | 2 | 16.24 | 57 |
| | 19:0/12:0/19:0 | 2 | 16.24 | 58 |
| | 17:0/17:1 (10Z)/17:0 | 2 | 16.08 | 55 |
| | 20:4 (5Z, 8Z, 11Z, 14Z)/18:2 (9Z, 12Z)/20:4 (5Z, 8Z, 11Z, 14Z) | 2 | 14.9 | 48 |
| | 20:2 (11Z, 14Z)/18:3 (6Z, 9Z, 12Z)/20:2 (11Z, 14Z) | 2 | 15.46 | 51 |
| | 20:5 (5Z, 8Z, 11Z, 14Z, 17Z)/22:6 (4Z, 7Z, 10Z, 13Z, 16Z, 19Z)/20:5 (5Z , 8Z, 11Z, 14Z, 17Z) | 2 | 14.1 | 44 |
| | 20:0/20:1 (11Z)/20:0 | 2 | 17.13 | 62 |
| TG | 19:2 (10Z, 13Z)/19:2 (10Z, 13Z)/19:2 (10Z, 13Z) | 4 | 15.57 | 52 |
| PC | 17:0/20:4 (5Z, 8Z, 11Z, 14Z) | 2.18 | 7.25 | 25 |
| | 18:1 (9Z)/18:0 | 4 | 10.84 | 33 |
| | 19:0/19:0 | 4 | 13.6 | 41 |
| | 21:0/22:6 (4Z, 7Z, 10Z, 13Z, 16Z, 19Z) | 2.28 | 11.74 | 35 |
| Lyso PC | 17:0 | 4 | 1.5 | 8 |
| PA | 16:0/18:1 | 4 | 7.92 | 29 |
| PE | 15:0/15:0 | 4 | 6.46 | 20 |
| | 17:0/17:0 | 4 | 11.38 | 34 |
| | 18:0/18:0 | 4 | 13.2 | 37 |
| Lyso PE | 17:1 (10Z) | 4 | 1.25 | 7 |
| PS | 16:0/18:1 (9Z) | 4 | 6.38 | 19 |
| | 17:0/20:4 (5Z, 8Z, 11Z, 14Z) | 2.61 | 5.7 | 17 |
| | 18:1 (9Z)/18:1 (9Z) | 4 | 6.54 | 21 |
| | 21:0/22:6 (4Z, 7Z, 10Z, 13Z, 16Z, 19Z) | 2.28 | 9.2 | 31 |
| Lyso PS | 17:1 (10Z) | 4 | 1 | 2 |
| PG | 14:0/14:0 | 4 | 3.81 | 13 |
| | 17:0/17:0 | 4 | 8.36 | 30 |
| | 18:1 (9Z)/18:1 (9Z) | 4 | 6.71 | 22 |
| | 18:1 (9E)/18:1 (9E) | 4 | 7.36 | 26 |
| | 18:0/18:2 (9Z, 12Z) | 4 | 6.97 | 24 |
| Lyso PG | 17:1 (10Z) | 4 | 1 | 3 |
| Lyso PI | 17:1 (10Z) | 25 | 1 | 1 |
| CL Mix I | 14:1 (9Z)/14:1 (9Z)/14:1 (9Z)/15:1 (10Z) | 4 | 13.29 | 39 |
| | 15:0/15:0/15:0/16:1 (9Z) | 4 | 14.82 | 47 |
| | 22:1 (13Z)/22:1(13Z)/22:1(13Z)/14:1 (9Z) | 4 | 16.32 | 59 |
| | 24:1 (15Z)/24:1 (15Z)/24:1 (15Z)/14:1 (9Z) | 4 | 16.89 | 61 |
| Sphingolipid Mix | d17:1 | 5 | 1.08 | 4 |
| | d17:0 | 5 | 1.16 | 6 |
| | d18:1/12:0 SM | 5 | 3.49 | 11 |
| | d18:1/12:0 Cer | 5 | 4.72 | 15 |
| | d18:1/25:0 Cer | 5 | 14.49 | 45 |
| | d18:1/12:0 Glucosylceramide | 5 | 3.84 | 14 |
| | d18:1/12:0 Lactosylceramide | 5 | 3.56 | 12 |
| | d18:1/17:0 SM | 4 | 6.83 | 23 |
| Cho | Cho | 4 | 5.84 | 18 |
| CE | 17:0 | 4 | 16.33 | 60 |
| | 18:2 (TT) | 4 | 15.86 | 54 |
| | 18:1 | 4 | 16.16 | 56 |
| | 23:0 | 4 | 17.19 | 63 |

Table 1. A list of analyzed 67 lipid standard mixtures with corresponding concentration (pmol/µL), retention time (min) and peak ID.
For lipid abbreviation refer to the legend in Figure 1. *Rt, retention time in minutes;
**Peak ID not shown in Figure 3. Retention time values are identified from negative mode.
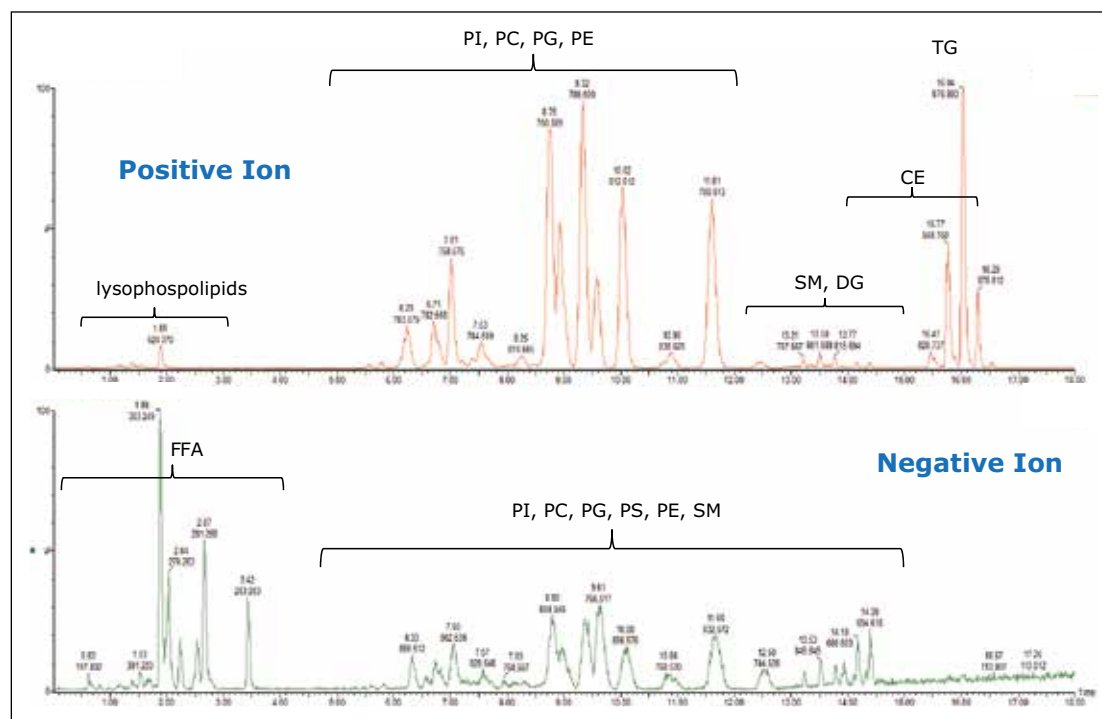
Figure 4. Total bovine liver lipid extract acquired in both positive and negative ionization modes. For lipid abbreviation refer to the legend in Figure 1.
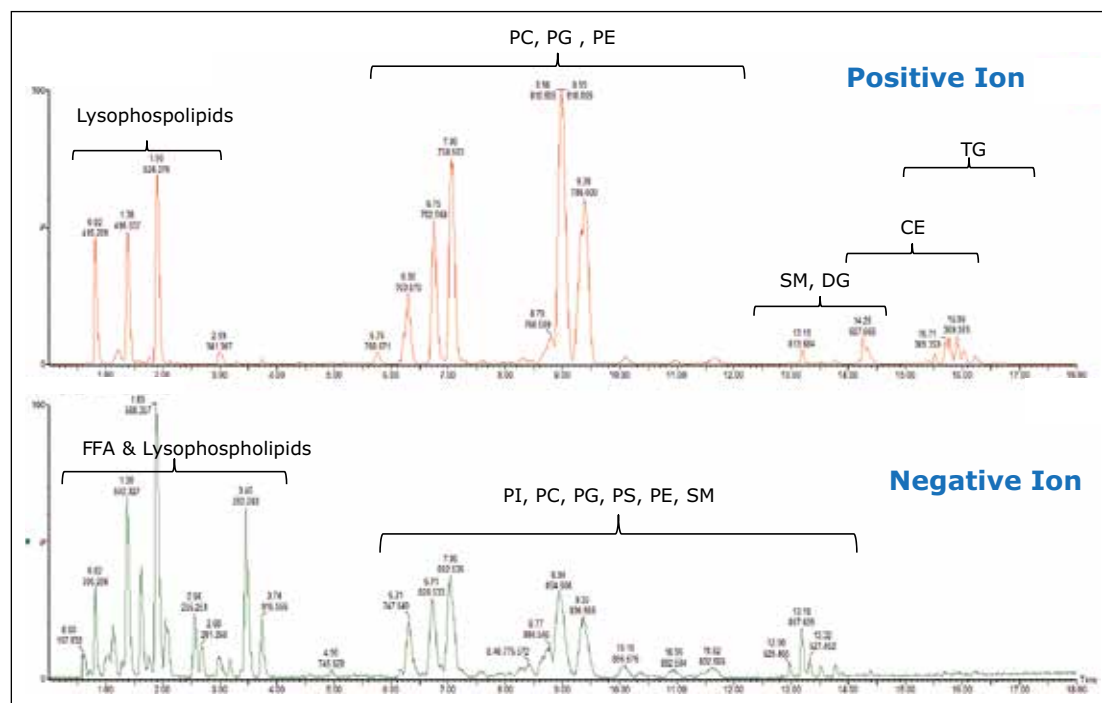


Figure 5. Total rat plasma lipid extract acquired in both positive and negative ionization modes. For lipid abbreviation refer to the legend in Figure 1.

In this analysis the ability of UPLC and CSH Technology to differentiate between structural cis (Z) and trans (E) isomers was also observed. The separation of cis and trans isobaric phosphatidylglycerol (PG) species, such as PG 18:1(9Z)/18:1(9Z) and PG 18:1(9E)/18:1(9E) were easily separated. In addition, structural isomers such as PG 18:1(9Z)/18:1(9Z) versus PG 18:0/18:2(9Z, 12Z) were resolved, as shown in Figure 6. This information would typically not be available using an infusion or traditional HPLC methods.

To test the applicability of this novel chromatographic method in real biological samples, we analyzed total lipid extracts from bovine liver and rat plasma. Using the CSH $C_{18}$ ACQUITY UPLC System, we were able to separate the major lipid classes with high resolution and sensitivity, which improved the detection of low abundant lipid species, as shown in Figures 4 and 5. Notably, the CSH $C_{18}$ ACQUITY UPLC System presented excellent retention time reproducibility from multiple injections of a bovine liver extract (%RSD < 0.136; n=20), as shown in Figure 7. This is especially useful for lipidomic analysis, which requires the comparison of a large number of LC/MS chromatograms deriving from multiple sample sets.
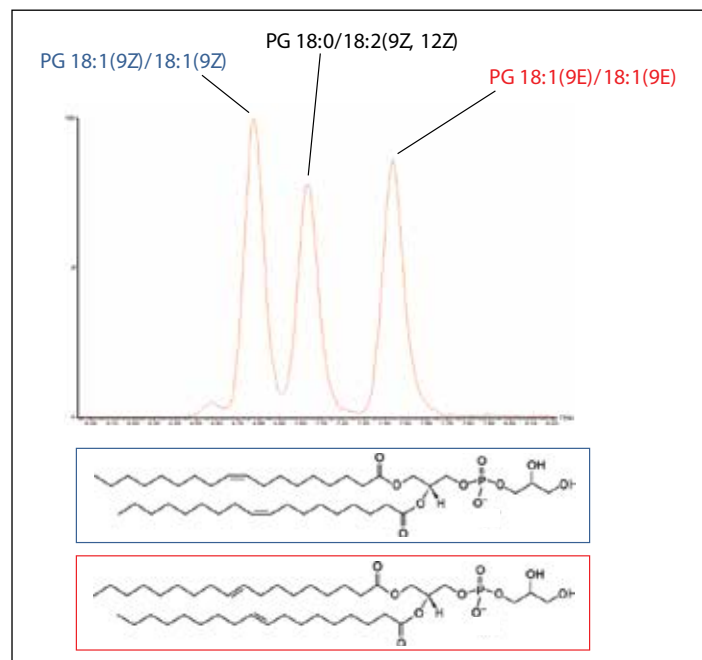


Figure 6. Separation of PG 18:1(9Z)/18:1(9Z) and PG 18:1(9E)/18:1(9E) as well as PG 18:0/18:2(9Z, 12Z).
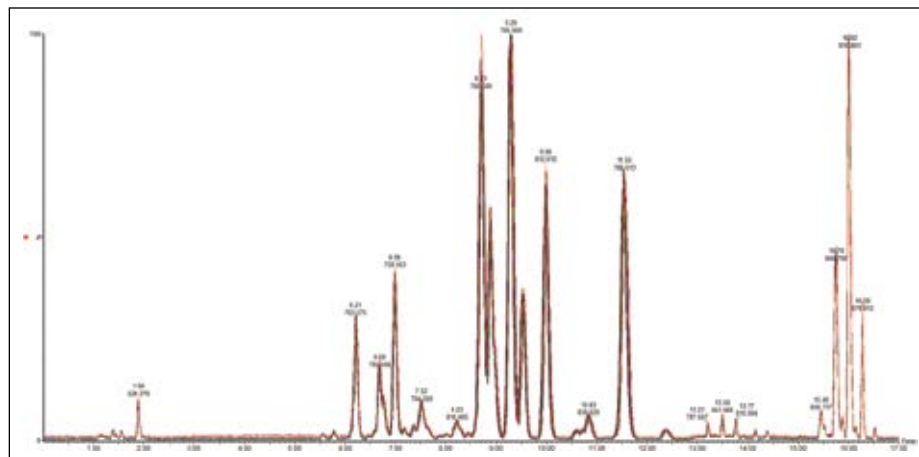


Figure 7. Overlaid chromatographic trace of 20 injections with < 0.136% RSD for retention time.

## CONCLUSIONS

The use of UPLC with CSH $C_{18}$ column described in this method provides clear improvements over other NP and RP traditional HPLC methods. It also marks an improvement over the UPLC methods highlighted in previous application notes for lipid analysis.[8] This method offers a robust and reliable approach for lipid analysis.

## References

1.  Shui G, *et. al.* Sensitive profiling of chemically diverse bioactive lipids. J. Lipid Res. 2007, 48; 1976-1984.

2.  Han X, Gross RW. Shotgun lipidomics: electrospray ionization mass spectrometric analysis and quantitation of the cellular lipidomes directly from crude extracts of biological samples. Mass Spectr. Rev. 2005, 24; 367-412.

3.  Sommer U, *et. al.* LC-MS based method for the qualitative and quantitative analysis of complex lipid mixtures. J. Lipid Res. 2006, 47; 804-814.

4.  Castro-Perez JM, *et. al.* Comprehensive LC MS[E] lipidomic analysis using a shotgun approach and its application to biomarker detection and identification in osteoarthritis patients. J. Proteome Res. 2010, 9; 2377-2389.

5.  Camera E, *et. al.* Comprehensive analysis of the major lipid classes in serum by rapid resolution-high performance liquid chromatography and electrospray mass spectrometry. J. Lipid Res. 2010.

6.  Henderson MA and McIndoe JS. Ionic liquids enable electrospray ionisation mass spectrometry in hexane. chem. Commun. 2006, 2872-2874.

7.  Mal M and Wong S. A HILIC-based UPLC/MS method for the separation of lipid classes from plasma. 2011, 720004048en.

8.  Shockor J, *et. al.* Analysis of intact lipids from biological Matrices by UPLC/High Definition MS. 2010, 720003349en.

## Waters

### THE SCIENCE OF WHAT'S POSSIBLE.®

**Waters Corporation**
34 Maple Street
Milford, MA 01757 U.S.A.
T: 1 508 478 2000
F: 1 508 872 1990
www.waters.com

Waters
THE SCIENCE OF WHAT'S POSSIBLE.®

# High Resolution Separation of Phospholipids Using a Novel Orthogonal Two-Dimensional UPLC/QTof MS System Configuration

Jeremy Dietrich Netto, Stephen Wong, Mark Ritchie
Waters Pacific Private Limited, Singapore

## APPLICATION BENEFITS

■ Improved peak capacity by using multiple columns for better characterization of complex mixtures such as lipids

■ Low abundance components are chromatographically separated from high abundance components allowing high confidence in identification and accurate quantification due to the removal of isotopic interferences

■ Ability to use combinations of different chemistries, such as IEX and SEC, for truly orthogonal 2D LC separations

## WATERS SOLUTIONS

ACQUITY UPLC® System with 2D Technology

Xevo® G2 QTof Mass Spectrometer

Ostro™ Sample Preparation Plates

## KEY WORDS

2D UPLC®/MS, phospholipids, lipidomics, HILIC, CSH™ C$_{18}$, Ostro

## INTRODUCTION

Lipids play many important roles in maintaining homeostasis of living organisms. These include energy storage, maintaining structural integrity of cell membranes, and acting as signaling molecules. Understanding these lipids may provide insights into mechanisms of disease, including the identification of biomarkers and potential drug targets. Lipids can be either hydrophobic or amphiphilic in nature, with phospholipids being the latter comprised of a hydrophilic phosphate head group and a lipophilic diglyceride tail.

The chemical behavior of amphiphilic lipids has led to the adoption of three main techniques for analysis by liquid chromatography including reversed phase, normal phase, and HILIC separation sciences. While reversed phase chromatography separates these lipids based on their lipophilicity (alkyl chain length and/or degree of saturation), it does not show class distinction especially between classes such as the phosphotidylcholines and sphingomyelins. Normal phase and HILIC chromatography, on the other hand, provide a separation based on the lipid's head group polarity but provides little separation within the given class.

In this application note, we present a novel configuration of the Waters® ACQUITY UPLC System with 2D Technology. This minimally modified system is able to utilize the advantages of both HILIC and reversed phase methods in tandem to provide a truly orthogonal and high resolution separation of amphiphilic lipids. We demonstrate the application of 2D UPLC/MS for the analysis of lipids in human plasma as this biofluid is a highly complex matrix with large lipid diversity covering many orders of concentration, thus presenting an analytical challenge when analyzed using traditional single-dimensional liquid chromatography.

## EXPERIMENTAL

### UPLC conditions

System:                         ACQUITY UPLC with
                                2D Technology

First dimension
column:                         ACQUITY® BEH HILIC
                                2.1 x 100 mm, 1.7 µm

Second dimension
column:                         ACQUITY CSH $C_{18}$
                                2.1 x 100 mm, 1.7 µm

Trap column:                    ACQUITY UPLC BEH
                                $C_8$ VanGuard 130Å
                                2.1 x 5 mm, 1.7 µm

### Alpha pump

Mobile phase A:                 95% ACN 5% $H_2O$
                                10 mM $NH_4Ac$ (pH 5.0)

Mobile phase B:                 50% ACN 50% $H_2O$
                                10 mM $NH_4Ac$ (pH 5.0)

UPLC flow rate:                 0.5 mL/min

Gradient:

| Time (min) | %A | %B |
|------------|-----|----|
| Initial | 100 | 0 |
| 10.0 | 80 | 20 |
| 10.1 | 20 | 80 |
| 13.0 | 20 | 80 |
| 13.1 | 100 | 0 |
| 16.0 | 100 | 0 |

### Beta pump

Mobile phase A:                 40% ACN 60% $H_2O$
                                10 mM $NH_4Ac$ (pH 5.0)

Mobile phase B:                 10% ACN 90% IPA
                                10 mM $NH_4Ac$ (pH 5.0)

UPLC flow rate:                 0.5 mL/min

Gradient:

| Time (min) | %A | %B |
|------------|-----|----|
| Initial | 100 | 0 |
| Fraction Elute (FE)* | 100 | 0 |
| FE + 0.10 | 60 | 40 |
| FE + 20.0 | 0 | 100 |
| FE + 23.0 | 0 | 100 |
| FE + 23.1 | 100 | 0 |
| FE + 25 | 100 | 0 |

*Fraction Elute (FE) time will vary according to the
 RT of the lipid class of interest.

### Column Manager (CM-A)

First dimension column temp.:          30 °C

Second dimension column temp.:         65 °C

Valve Events Table:

| Time (min) | Left valve | Right valve |
|------------|------------|-------------|
| 0 | Position 2 | Position 2 |
| Fraction Trap | Position 1 | Position 1 |
| Fraction Elute (FE) | Position 2 | Position 2 |
| FE + 25 | Position 1 | Position 1 |

### MS conditions

Mass spectrometer:              Waters Xevo G2 QTof

Acquisition mode:               ESI +ve / -ve, $MS^E$

Capillary voltage:              2.0 kV (+ve) /
                                1.00 kV (-ve)

Sampling cone:                  35.0 V

Extraction cone:                4.0 kV

MS collision energy:            4.0 V

$MS^E$ energy ramp:             20 to 45 V

Source temp.:                   120 °C

Desolvation temp.:              500 °C

Desolvation gas flow:           1000 L/h

Cone gas flow:                  10 L/h

Acquisition range:              *m/z* 50 to 1200

Lock mass (LeuEnk):             +ve, *m/z* 556.2771
                                and 278.1141

                                -ve, *m/z* 554.2615
                                and 236.1035

## Sample description

Lipids were extracted from human plasma using the Waters Ostro sample preparation method.[1]

## 2D UPLC flow diagram
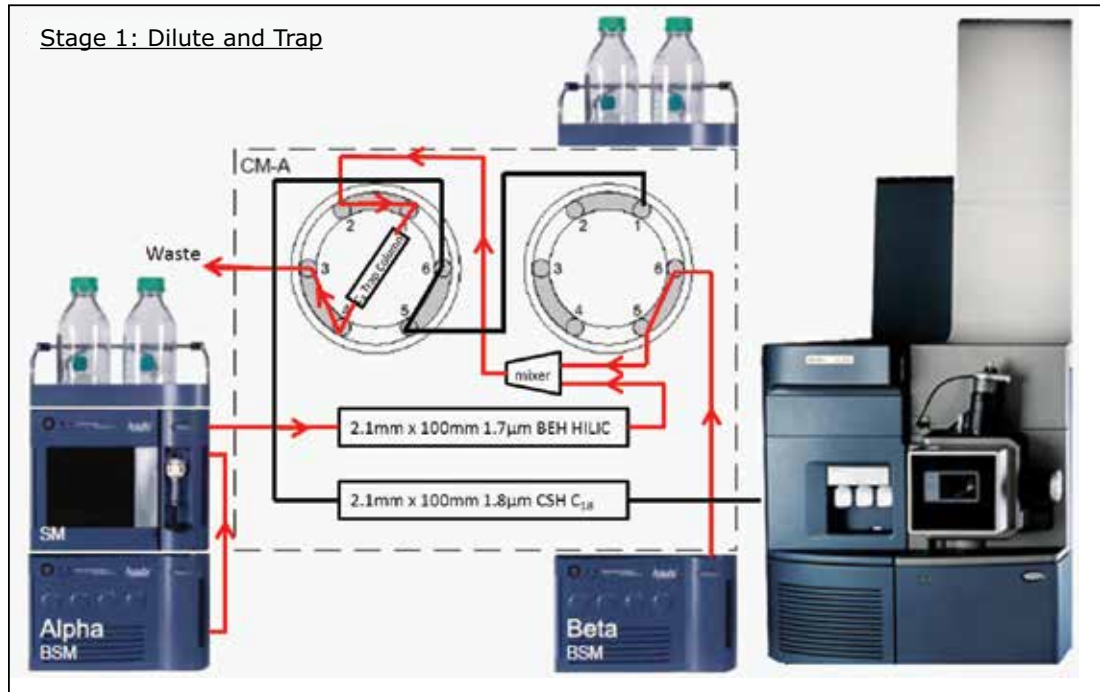


*Figure 1. Flow diagram of the 2D UPLC/MS system showing stage 1 where the left and right valves are both in position 1, and trapping analytes eluting off the HILIC column is performed.*
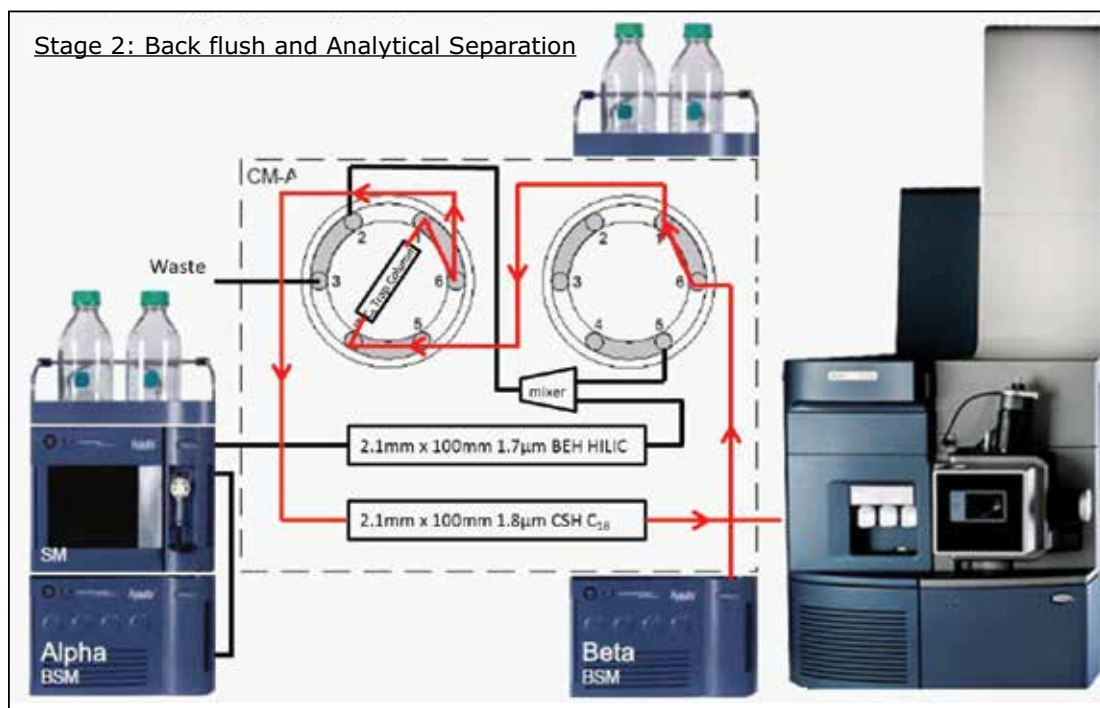


*Figure 2. Flow diagram of the 2D UPLC/MS system showing stage 2 where the left and right valves are both in position 2 when the trapped analytes are back-flushed off the trapping column, and sent to the $C_{18}$ column for reversed phase separation.*

## RESULTS AND DISCUSSION

### Comparison of separation between 1D and 2D UPLC/MS

By combining the orthogonality of the HILIC and reversed phase separations into a single tandem 2D UPLC/MS method, we overcame the challenges of inter-class co-elution posed by reversed phase liquid chromatography, as shown in Figure 3, between the PC and SM classes. The coelution of these two classes are particularly problematic, as they have only a single dalton difference between them, and co-elution makes identification and accurate quantification difficult due to isotopic interferences.
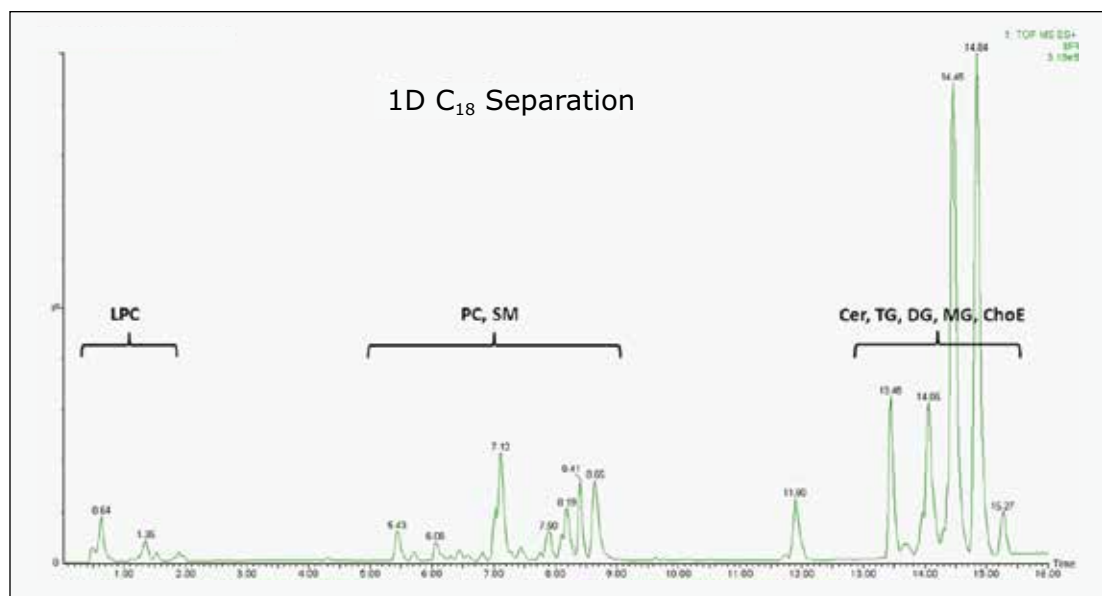


*Figure 3. Chromatogram showing single-dimensional reversed phase separation of plasma lipids. SMs co-elute with PCs making identification and quantification difficult due to 1Da difference between species of the two classes.*
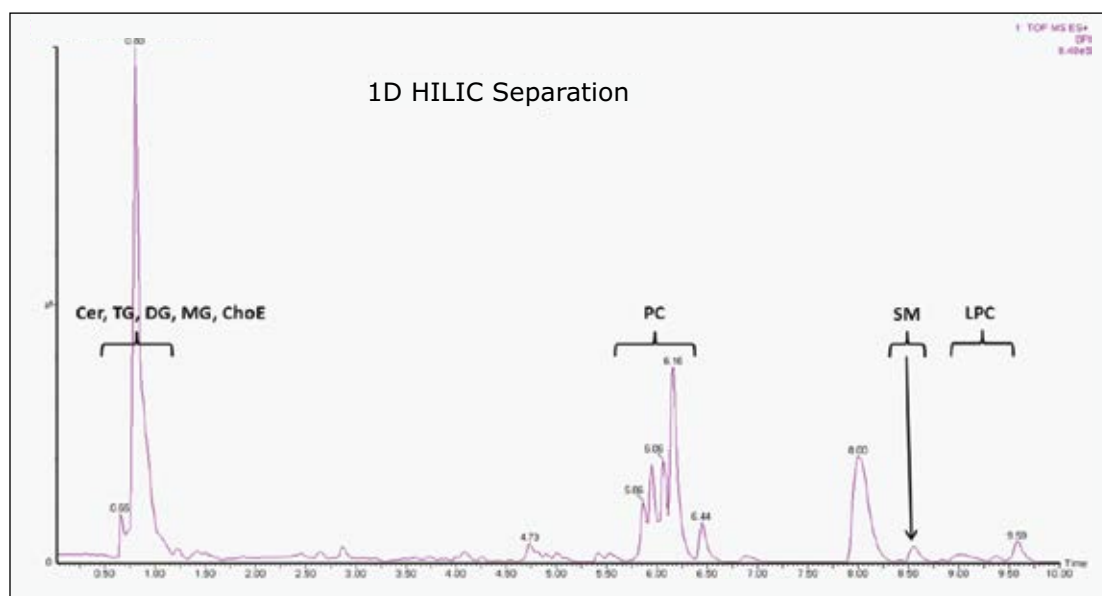


*Figure 4. Chromatogram showing single-dimensional HILIC separation of plasma lipids. SMs are separated from PCs but individual species within each class co-elute, leading to poor resolution and dynamic range.*
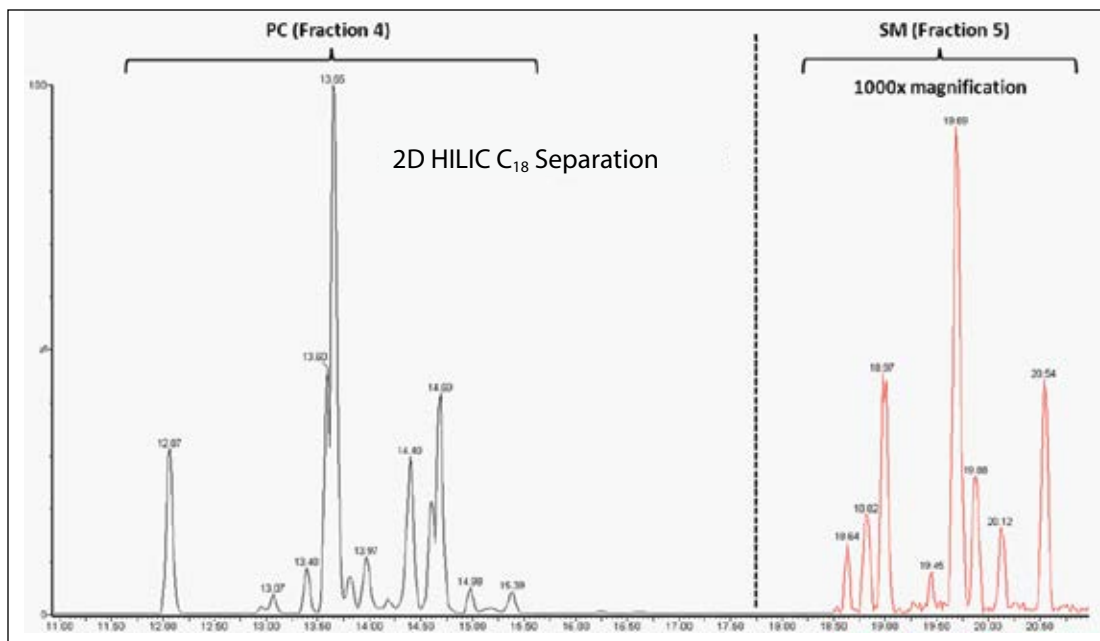
*Figure 5. Overlay of fractions from two-dimensional separation of plasma lipids. SMs are now class separated from the PCs by HILIC, and the individual lipids within each class are separated further by reversed phase.*

In the HILIC method, inter-class separation is eliminated, as shown in Figure 4, with the PCs and SMs well separated. However, there is now intra-class co-elution which affects the peak capacity and, hence, the sensitivity of the method. In the 2D UPLC/MS method there was improved resolution of the individual lipids of each class using the PC and SM classes as examples, as shown in Figure 5.

The increased peak capacity from the use of combined columns improved both the resolution, shown in Figure 5, as well as the dynamic range of the individual lipids within each class. Using the PC class as an example, the SimLipid (Premier Biosoft) lipid identification software was able to detect and identify 37% more PCs than the HILIC method, and 40% more PCs than the reversed phase $C_{18}$ method. Generally, the ion intensities for the 2D UPLC/MS method were higher than the HILIC or $C_{18}$ methods for the same samples run, which could be attributed to the removal of isotopic interferences.

**Predictable separation of the 2D UPLC/MS method**
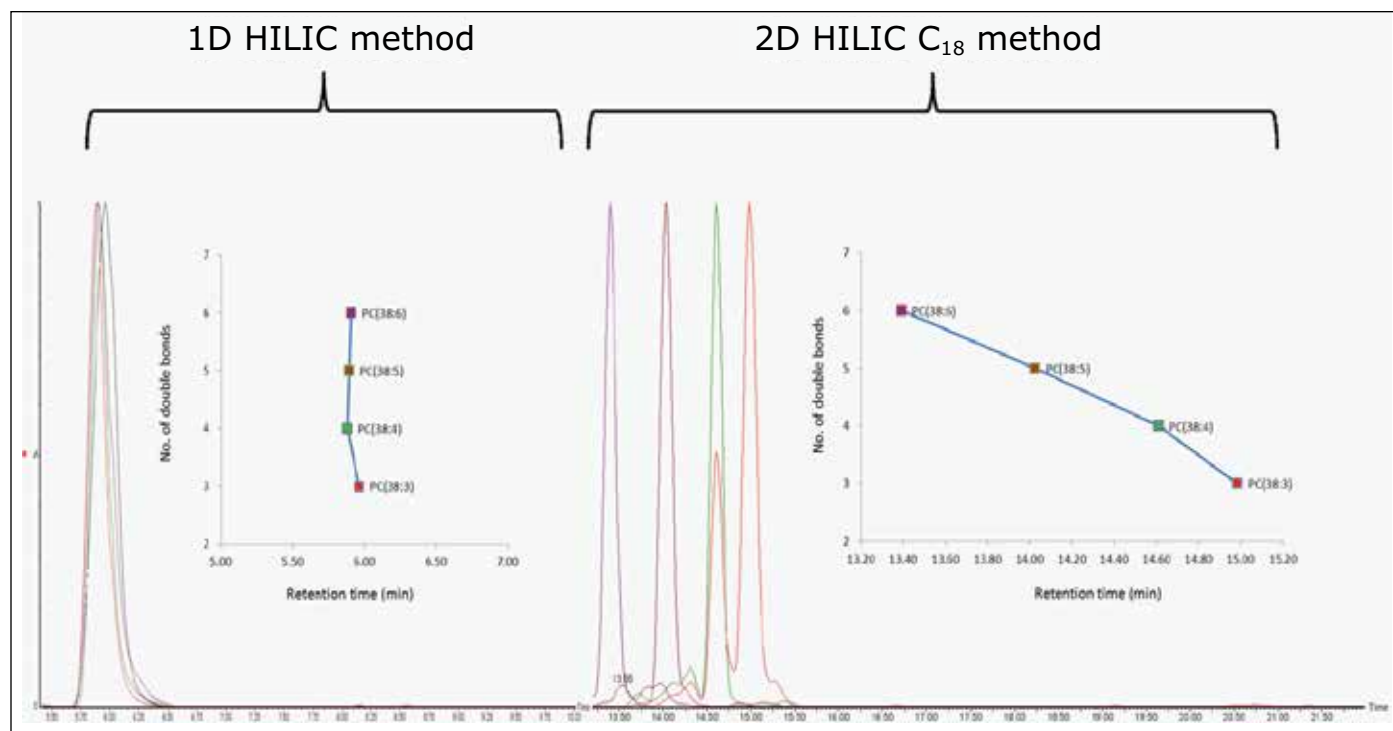


*Figure 6. Comparison between 1D HILIC and 2D HILIC C$_{18}$ of the degree of PC alkyl chain saturation (number of double bonds) against retention time.*

Since the second dimension of separation is reversed phase, the lipids were able to be further separated chromatographically, according to their hydrophobicity (alkyl chain length and degree of saturation), as shown in Figure 6. This was more advantageous than the HILIC method; whereby, residual isotopic interferences due to the co-elution could affect the confidence level for positive identification and quantification of these lipids.

**Improved specificity of the 2D UPLC/MS method**
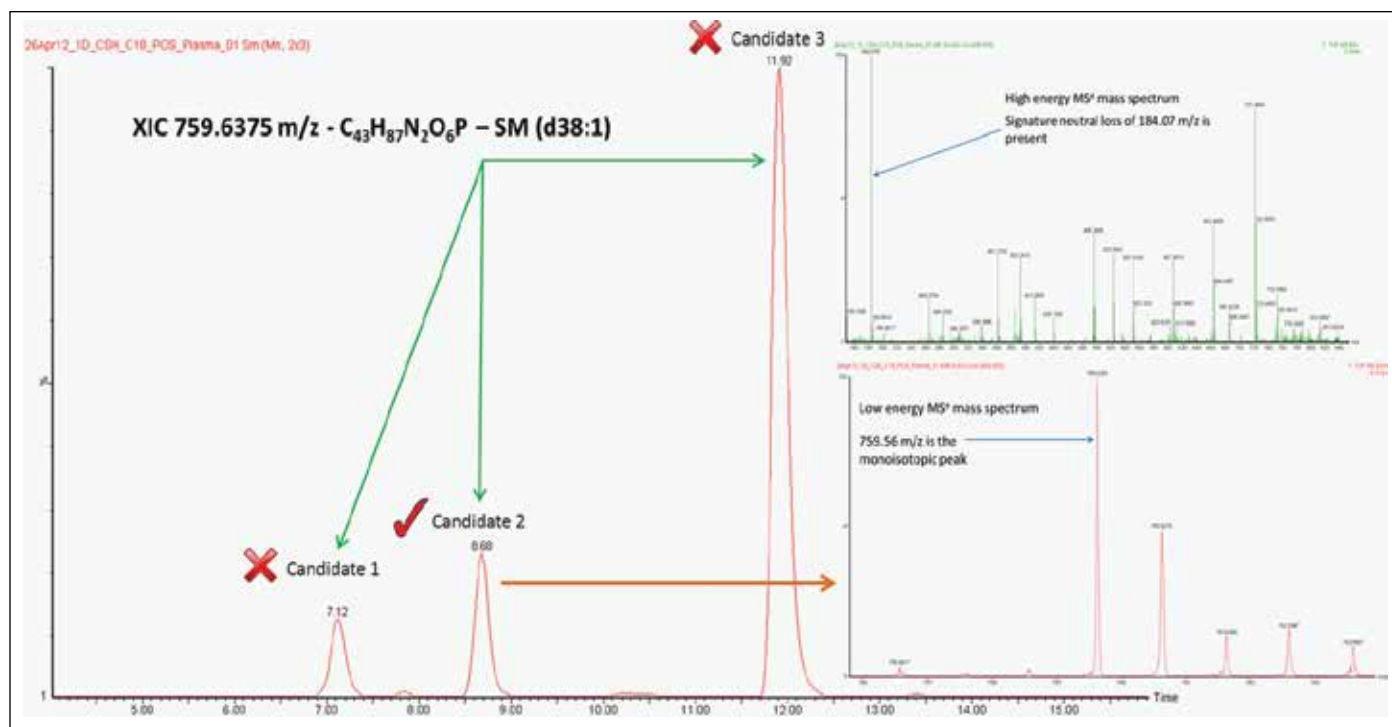


*Figure 7. XIC of 759.6375 m/z from the 1D C$_{18}$ TIC reveals three potential candidates for an SM. Further analysis of both the MS and MS$^E$ data reveals candidate two to be the correct one.*
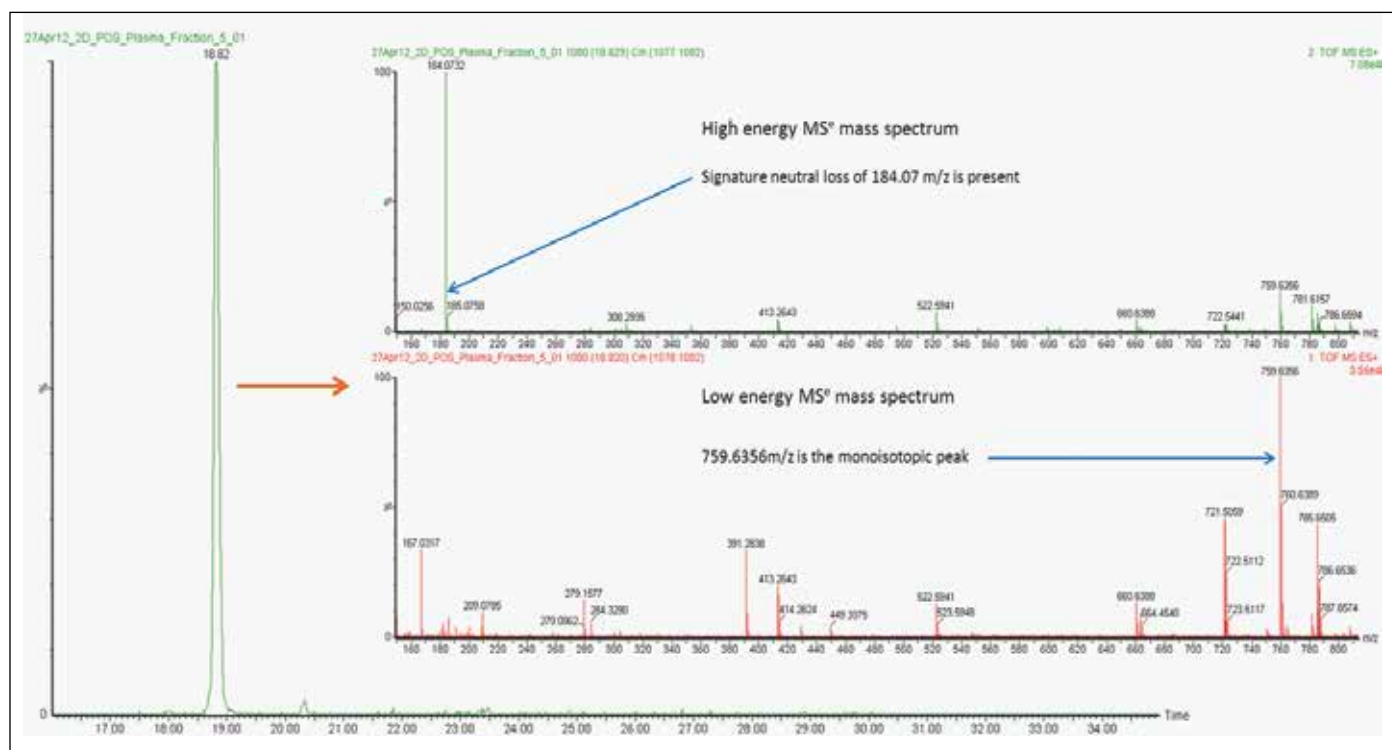


*Figure 8. XIC of 759.6375 m/z from the 2D HILIC C$_{18}$ TIC reveals only one potential candidate for the SM. Further analysis of both the MS and MS/MS data confirms this candidate is the correct one.*

"Heart cutting" a pure fraction of each lipid class using the HILIC column as the first dimension, followed by further separation using reversed phase in the second dimension eliminates errors in identification due to isotopic interferences from co-eluting peaks. This is especially true for the PC and SM classes which differ by 1Da, as shown in Figures 7 and 8.

## CONCLUSIONS

The limitations posed by traditional single-dimensional separations of HILIC or reversed phase were overcome by the introduction of this novel 2D UPLC/MS configured system which leverages the advantages of both types of methods. This resulted in improved chromatographic resolution, peak capacity, and specificity. In addition, the system is completely automated and UPLC technology provides the capability of high throughput, high resolution analyses compared to traditional HPLCs.

In this application note, we show the orthogonality of this system by pairing the HILIC and $C_{18}$ chemistries; however, the system can also be easily adapted for other two-dimensional applications such as IEX-RP and SEC-RP. The 2D UPLC/MS system configuration described here uses commercially available components with little modification needed and can easily be switched to other UPLC with 2D technology modes, such as parallel column regeneration or conventional single-dimensional separation.

### References

1. Ritchie M, Mal M, Wong S. Extraction of Phospholipids from Plasma using Ostro Sample Preparation. Waters Application Note 720004201en. 2012 Jan.

2. Mal M, Wong S. A HILIC-Based UPLC/MS Method for the Separation of Lipid Classes from Plasma. Waters Application Note 720004048en. 2011 July.

3. Ritchie M, Mal M, Wong S. UPLC BEH HILIC: The Preferred Separation Chemistry for Targeted Analysis of Phospholipids. Waters Application Note 720004219en. 2012 Jan.

4. Isaac G, McDonald S, Astarita G. Lipid Separation using UPLC with Charged Surface Hybrid Technology. Waters Application Note 720004107en. 2011 Sept.

5. Isaac G, McDonald S, Astarita G. Automated Lipid Identification Using UPLC/HDMS[E] in Combination with SimLipid. Waters Application Note 720004169en. 2011 Dec.

## Waters
### THE SCIENCE OF WHAT'S POSSIBLE.®

Waters Corporation
34 Maple Street
Milford, MA 01757 U.S.A.
T: 1 508 478 2000
F: 1 508 872 1990
www.waters.com

Waters
THE SCIENCE OF WHAT'S POSSIBLE.®

# A Multidimensional Lipidomics Method: HILIC Coupled with Ion Mobility Enabled Time-of-Flight Mass Spectrometry

Giuseppe Astarita,[1] Jeremy Netto,[2] Giorgis Isaac,[1] Marc V. Gorenstein,[1] Mark Ritchie,[2] James Langridge[3]
[1] Waters Corporation, Milford, MA, USA
[2] Waters Pacific, Singapore
[3] Waters Corporation, Manchester, UK

## APPLICATION BENEFITS

Combining HILIC-UPLC® liquid phase separation with gas phase ion mobility mass spectrometry to achieve a multi-dimensional characterization of lipids in complex mixtures enhances profiling of lipids in biological samples.

## WATERS SOLUTIONS

Omics Research Platform
with TransOmics™ Informatics

ACQUITY UPLC® System

SYNAPT® G2-S HDMS

## KEY WORDS

Lipids, lipidome, metabolomics, lipidomics, ion mobility spectrometry, Hydrophilic interaction chromatography (HILIC), HDMS Compare, T-Wave™ Technology

## INTRODUCTION

One of the main challenges for a global lipid analysis (lipidomics) is the separation of the wide array of lipid species present in biological samples (Figure 1). Such a separation is not achievable using a single chromatographic dimension such as reversed- or normal-phase separation methods.[1-5] Normal-phase UPLC separates lipid classes based on their polar head group, whereas reversed-phase separates lipids according to their acyl chain length and number of double bonds.[1-6] Hydrophilic interaction chromatography (HILIC) separation has been proposed as an alternative to normal-phase separation, offering better MS compatibility and using less toxic solvents.[4-6] Recently, a two-dimensional separation using HILIC and reversed-phase has been proposed to maximize the separation of the lipidome before MS detection.[5,6]

In addition to chromatography, ion mobility can be used to separate lipid ions in the gas phase according to their size and molecular shape.[7,8] In this study, we apply the Waters® Omics Research Platform with TransOmics Informatics. A HILIC-UPLC separation with ion mobility-Tof MS (SYNAPT G2-S HDMS) enables a multi-dimensional separation of complex biological mixtures, enhancing the information obtained from profiling lipids. HDMS Compare Software and TransOmics Informatics facilitate the comparison of the biological samples.
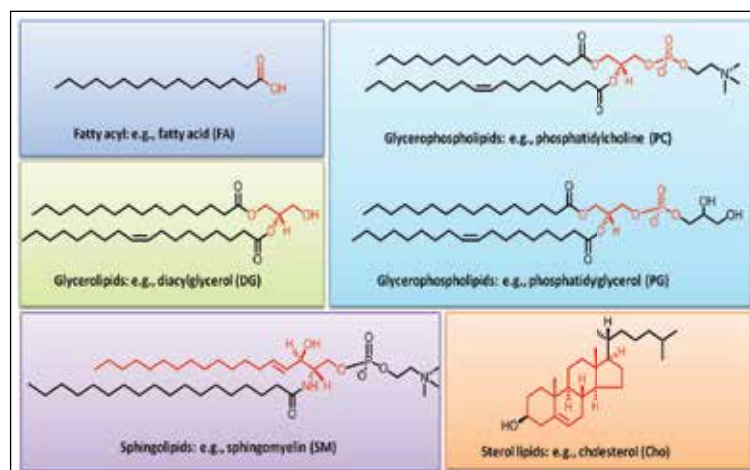


Figure 1. Lipid diversity. Lipids are divided into classes according to common structural moieties (in red), which may give rise to different chromatographic behaviors during HILIC.

## EXPERIMENTAL

### Sample description

Lipid standards and total lipid extracts from bovine brain, heart, and liver were purchased from Avanti Polar Lipids. Non-natural lipids were spiked in the biological extracts and used as internal standards (Table 2).

### UPLC conditions

| | |
|---|---|
| System: | ACQUITY UPLC |
| Column: | ACQUITY UPLC BEH HILIC 2.1 x 100 mm |
| Column temp.: | 30 °C |
| Mobile phase A: | 10 mM ammonium acetate (pH 8.0) in 95% ACN |
| Mobile phase B: | 10 mM ammonium acetate (pH 8.0) in 50% ACN |

| Gradient: | Time/min | %A | %B |
|---|---|---|---|
| | 0.00 | 99.9 | 0.1 |
| | 10.00 | 80.0 | 20.0 |
| | 13.00 | 20.0 | 80.0 |
| | 13.01 | 99.9 | 0.1 |
| | 16.00 | 99.9 | 0.1 |

| | |
|---|---|
| Flow rate: | 0.5 mL/min |
| Injection volume: | 5 µL |

### MS conditions

MS analyses were performed on a SYNAPT G2-S HDMS (Figure 2) with a conventional ESI source in LC/HDMS$^E$ mode. Capillary voltages were optimized separately for positive (2.8 kV) and negative (1.9 kV) ion modes. Data were collected in two channels all of the time; low collision energy (6.0 V) for the molecular ions and high collision energy (20 to 35 V) for product ions. IMS gas: nitrogen; IMS T-Wave velocity: 900 m/s; IMS T-Wave height: 40 V.

### Data acquisition and processing

TransOmics Informatics and HDMS Compare Software

## RESULTS AND DISCUSSION

To separate lipids, we used hydrophilic interaction chromatography (HILIC) with an ACQUITY UPLC BEH HILIC 2.1 x 100 mm, 1.7 µm Column, and a reversed-phase solvent system (organic/aqueous) characterized by high organic mobile phase (>80% acetonitrile). This UPLC method was highly compatible with ESI, and separated lipids by classes, according to their polar properties (Figure 3 and Table 1).

In addition to HILIC chromatography, the ion mobility capability of the SYNAPT G2-S HDMS Mass Spectrometer (Figures 2A-C and 3) was used to further discriminate lipid classes into their constituent components, based upon the different size and shape, that is, the ions collision cross section ($\Omega$).[7,8] Lipid ions with different degrees of unsaturation and acyl length migrate with characteristic mobility times, due to their unique shape in the gas phase as they migrate through the ion mobility cell, which is filled with nitrogen gas at relatively high pressure (Figures 3 and 5). Ion mobility separations occur in the millisecond timeframe, making it ideal for situating between LC and MS, where LC separations upstream typically work in the second timeframe and Tof MS downstream works in the nanosecond timeframe (Figures 2A and 3). The addition of ion mobility to the LC/MS provides enhanced peak capacity and improved signal-to-noise ratio (Figure 3).

To gain more structural information, we analyzed lipids employing LC/MS$^E$, which uses an alternating low and elevated collision energy in separate scans to acquire both precursor and product ion information in a single analytical run (Figures 2B and 4A). Ion mobility separation coupled with LC/MS$^E$ (HDMS$^E$) improves the specificity for coeluting lipids by fragmenting ions after IMS separation (Figures 2C and 4B). Due to the complexity of the lipidome, the addition of ion mobility drift time as an orthogonal measurement to retention times provides complementary information regarding the lipid species, adding further specificity to lipid identification and data interpretation (Figure 4B).

Using this novel technological approach, multidimensional molecular maps of lipids present in various animal tissues were generated. In these maps, each lipid is characterized by a combination of molecular coordinates including retention time, drift time, exact mass, fragment ions, and intensity (Figure 5). Such features highlighted the capacity of ion mobility to separate isobaric lipid species (i.e., species with the same mass). The molecular landscape visualized using multidimensional molecular maps also allows the detection of lipid species that could otherwise go unnoticed (Figures 3 and 5).
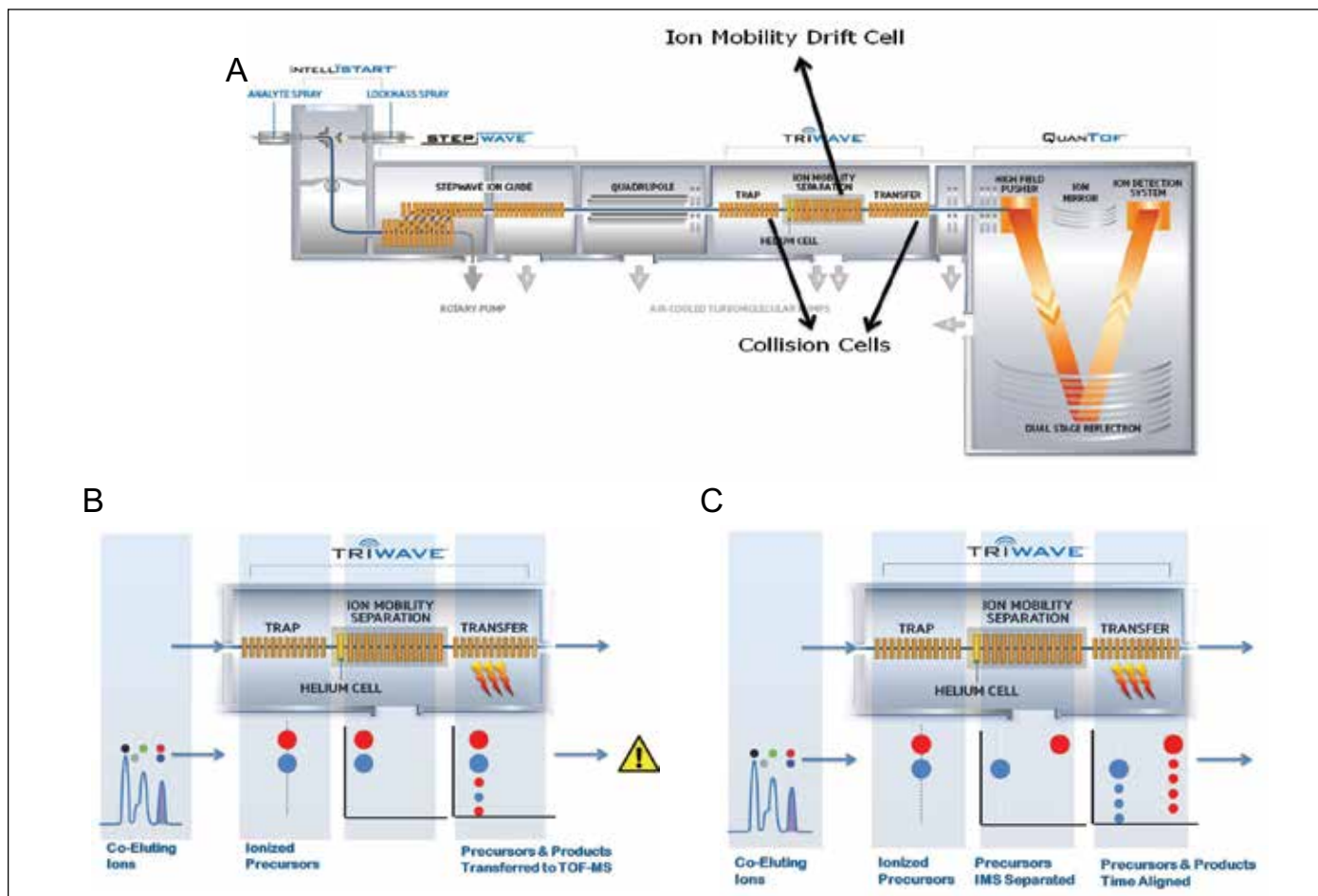
Figure 2. Ion mobility separation and fragmentation. A) Schematic of the SYNAPT G2-S HDMS System. B) MS$^E$ can be extremely useful by itself, however when we consider a complex mixture of metabolites present in biological samples, they often co-elute. By fragmenting them, we only obtain a mixture of fragments which derive from various co-eluting precursors in this example. C) Ions can be separated in the ion mobility cell and subsequently fragmented in the transfer collision cell. The product ions generated in the collision cell have the same mobility drift time as their parent ions. Using this acquisition condition namely high-definition MS$^E$ (HDMS$^E$), product ions can be aligned with their parent ions on the basis of mobility drift time as well as chromatographic retention time using the Waters® proprietary Apex4D algorithm.

| Lipid class | ES polarity | RT window |
|-------------|-------------|-----------|
| FA | Neg | 0-1 |
| Cer | Pos | 0-2 |
| HexCer | Neg | 0-2 |
| ST | Neg | 0-2 |
| DiHexCer | Neg | 2-4 |
| PG | Neg | 1-3 |
| PE | Neg/Pos | 5-7 |
| PI | Neg | 3-5 |
| PS | Neg | 4-6 |
| PC | Pos | 5-7 |
| LPE | Neg/Pos | 6-8 |
| SM | Pos | 7-9 |
| LPC | Pos | 8-10 |

Abbreviations: FA, fatty acids; Cer, ceramides; HeXCer, HexosylCeramides; ST, sulfatides; DiHexCer, DihexosylCeramides; PG, phosphatidylglycerols; PE, phosphatidylethanolamines; PI, phosphatidylinositols; PS, phosphatidylserines; PC, phosphatidylcholines; LPE, lysophosphatidylethanolamines; SM, sphingomyelins; LPC, lysophosphatidylcholines.

Table 1. Lipid classes are separated by retention time (RT) windows in HILIC conditions.

The comparison of molecular maps is facilitated by the use of HDMS Compare and TransOmics (Figures 6 and 7). HDMS Compare Software was used for a rapid comparison of different drift versus *m/z* plots at selected windows of retention times (Table 1). The drift time and spectral information associated with the components responsible for the differentiation can be extracted from the dataset and further analyzed (Figure 6). The use of TransOmics Informatics allows feature detection, alignment, and comparisons across multiple samples using multivariate statistical approaches (PCA, dendrogram analysis) and database searching of discriminating features for the identification of the lipids alternating between samples. TransOmics uses ion mobility information to separate co-eluting isobaric lipids in the drift time dimension, increasing the specificity of identification and quantification (Figure 7). Lipid quantification was performed using appropriate internal standards for each lipid class (Table 2).

| Lipid class | Internal standard | Abbreviation | Vendor | Catalog # |
|---|---|---|---|---|
| **Sphigolipids** | | | | |
| Ceramides | N-Lauroyl-D-erythro-sphingosine | Cer(d18:1/12:0) | Avanti Polar Lipids | 860512P |
| Sphingomyelin | N-(dodecanoyl)-sphing-4-enine-1-phosphocholine | SM (d18:1/12:0) | Avanti Polar Lipids | 860583P |
| **Glycerophospholipids** | | | | |
| Phosphatidylethanolamines | 1,2- Dimyristoyl-sn-glycero-3-phosphoethanolamine | PE (14:0-14:0) | Avanti Polar Lipids | 850745 |
| | Avanti Polar Lipids | | | |
| Phosphatidylcholines | 1,2- Dimyristoyl-sn-glycero-3-phosphocholine | PC (14:0/14:0) | Avanti Polar Lipids | 850345 |
| | Avanti Polar Lipids | | | |
| Phosphatidylserine | 1,2- Dimyristoyl-sn-glycero-3-phosphoserine | PS (14:0/14:0) | Avanti Polar Lipids | 840033 |
| | Avanti Polar Lipids | | | |
| Phosphatidylglycerol | 1,2- Dimyristoyl-sn-glycero-3-phosphoglycerol | PG (14:0/14:0) | Avanti Polar Lipids | 840445 |
| | Avanti Polar Lipids | | | |
| Phosphatidylinositol | 1,2-DiHexanoyl-sn-glycero-3-phospho-(1'-myo-inositol) | 16:0 PI | Avanti Polar Lipids | 850141 |
| | Avanti Polar Lipids | | | |
| Lysophosphatidylcholine | 1-Heptadecenoyl-2-hydroxy-sn-glycero-3-phosphocholine | LPC (17:1) | Avanti Polar Lipids | LM-1601 |
| **Fatty acyl** | | | | |
| Fatty acids | 10-heptadecenoic acid | FA (17:1) | Nu-Chek Prep | U-42-A |

*Table 2. List of lipids used as internal standards for selected lipid classes.*
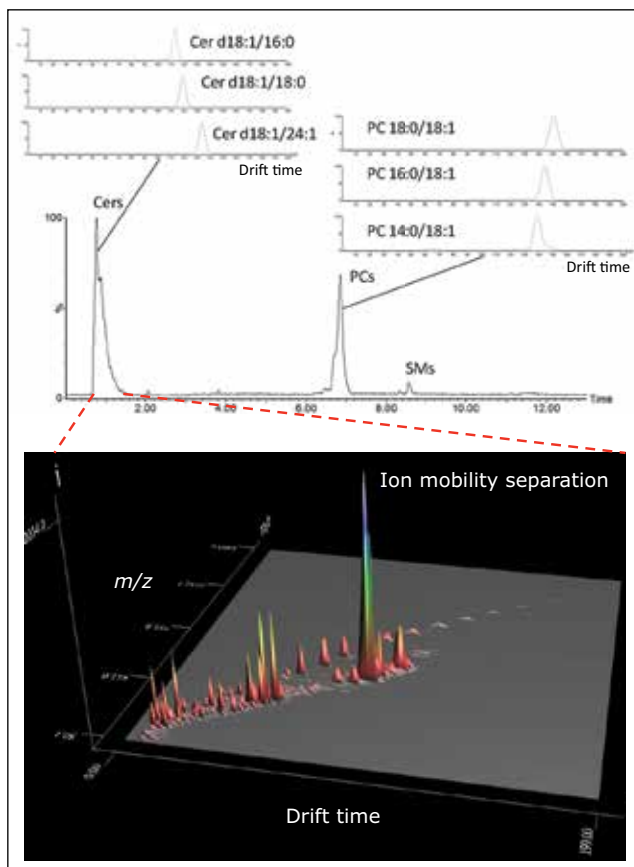
Figure 3. 2D separation by HILIC-ion mobility. Representative analysis of lipid standards using a combination of HILIC separation and ion mobility (IM) separation (inserts) in positive ion mode. HILIC-IM analysis provides an additional degree of separation beyond chromatography, which is ideal for the analysis of complex lipid mixtures extracted from biological samples. After HILIC separation, ion mobility further separates ceramide species according to their molecular shapes. The molecular landscape visualized using an unbiased 3D representation (drift time, m/z, intensity) of a selected interval of retention time (0.5 to 1.5 minutes) allows the detection of many isobaric ceramide species. Such an approach highlights the power of ion mobility for the discovery of many low abundance molecular species that could otherwise be undetected.
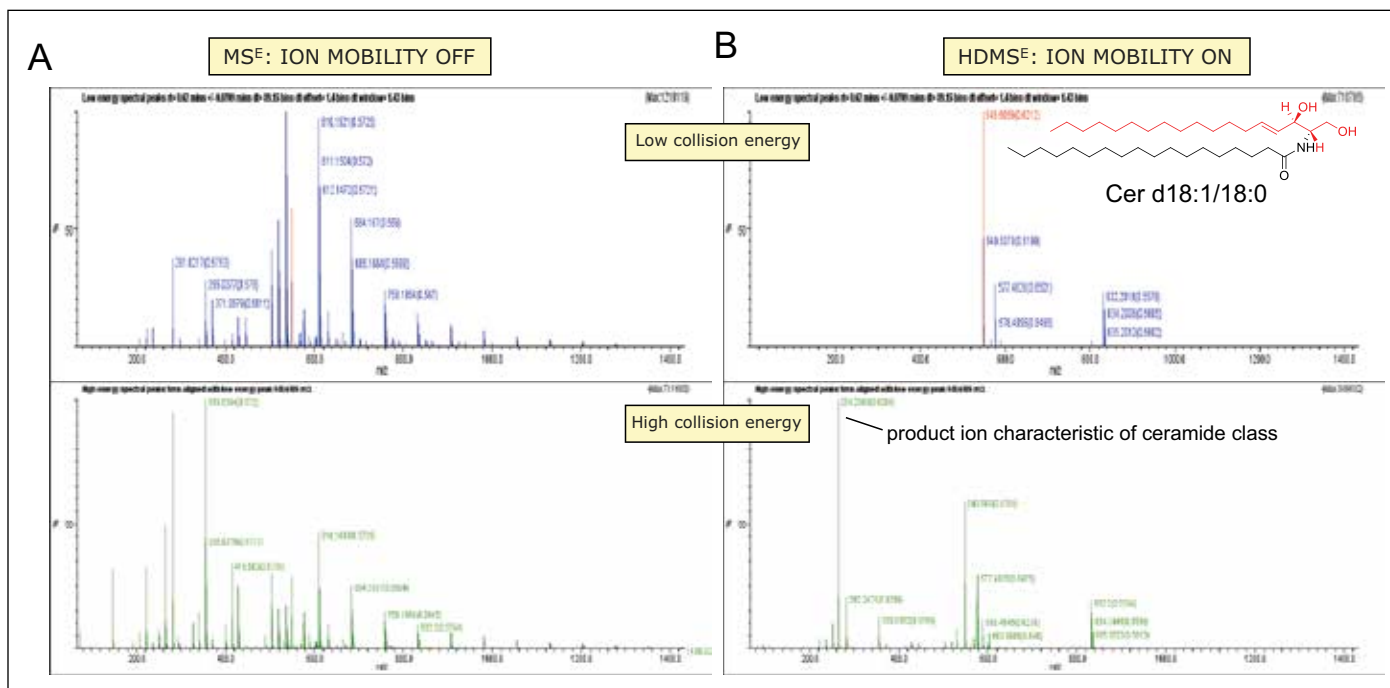


Figure 4. Structural characterization of lipid classes. Lipid classes generate characteristic fragments (product ions) upon collision-induced dissociation (CID). In positive ionization mode, ceramides are usually detected as dehydrated molecular ions using low collision energy; however, high collision energy generates all ceramide species with a common characteristic product ion. A) Waters instruments enable alternating low and high collision energy (MS$^E$), allowing to acquire precursor and product ion information in a single chromatographic run. The presence of co-eluting lipids, however, makes the interpretation of the high collision energy spectra difficult. B) By applying ion mobility separation, co-eluting lipids are separated based on their molecular size and shape before fragmentation in the transfer cell. This mode of acquisition (HDMS$^E$) results in cleaner fragmentation spectra and a more confident identification of lipid classes.
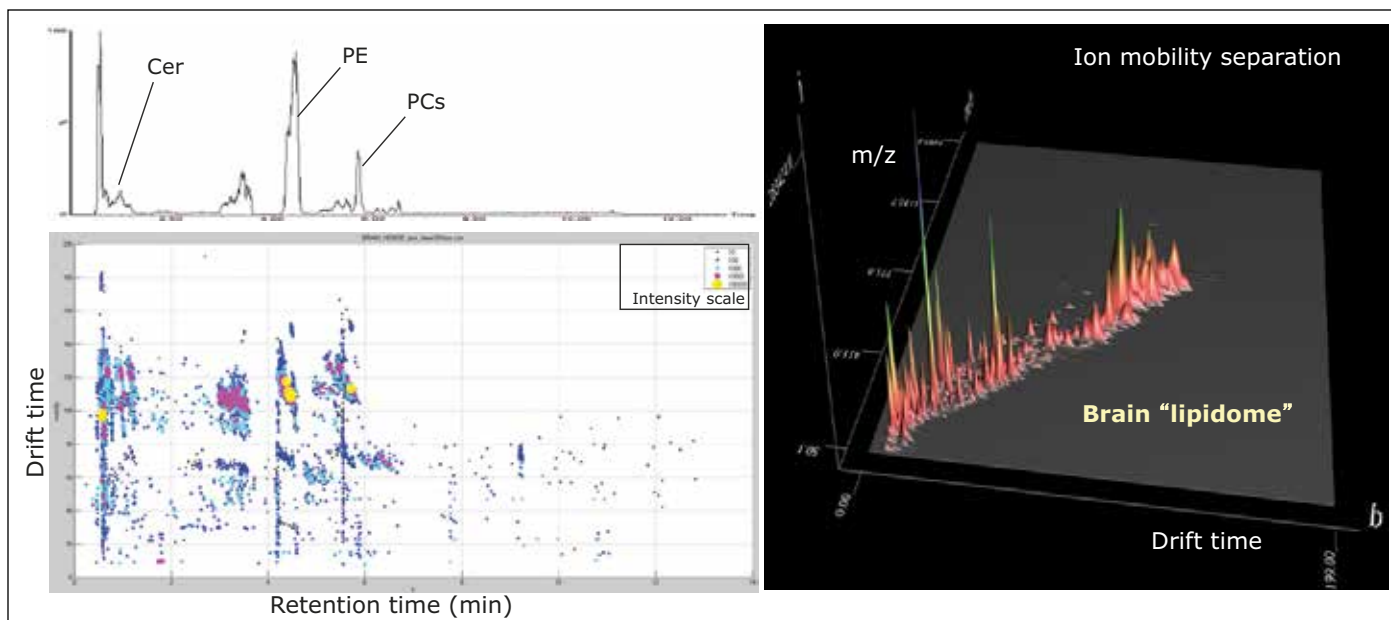
Figure 5. Mapping the brain lipidome using HILIC-ion mobility. Representative HILIC-ion mobility Tof analysis of total lipid extract from bovine brain. Lipids are separated by both retention time and mobility time (drift time). A multi-dimensional molecular map could be generated using unique coordinates such as retention times, mobility times, accurate masses, and intensities.
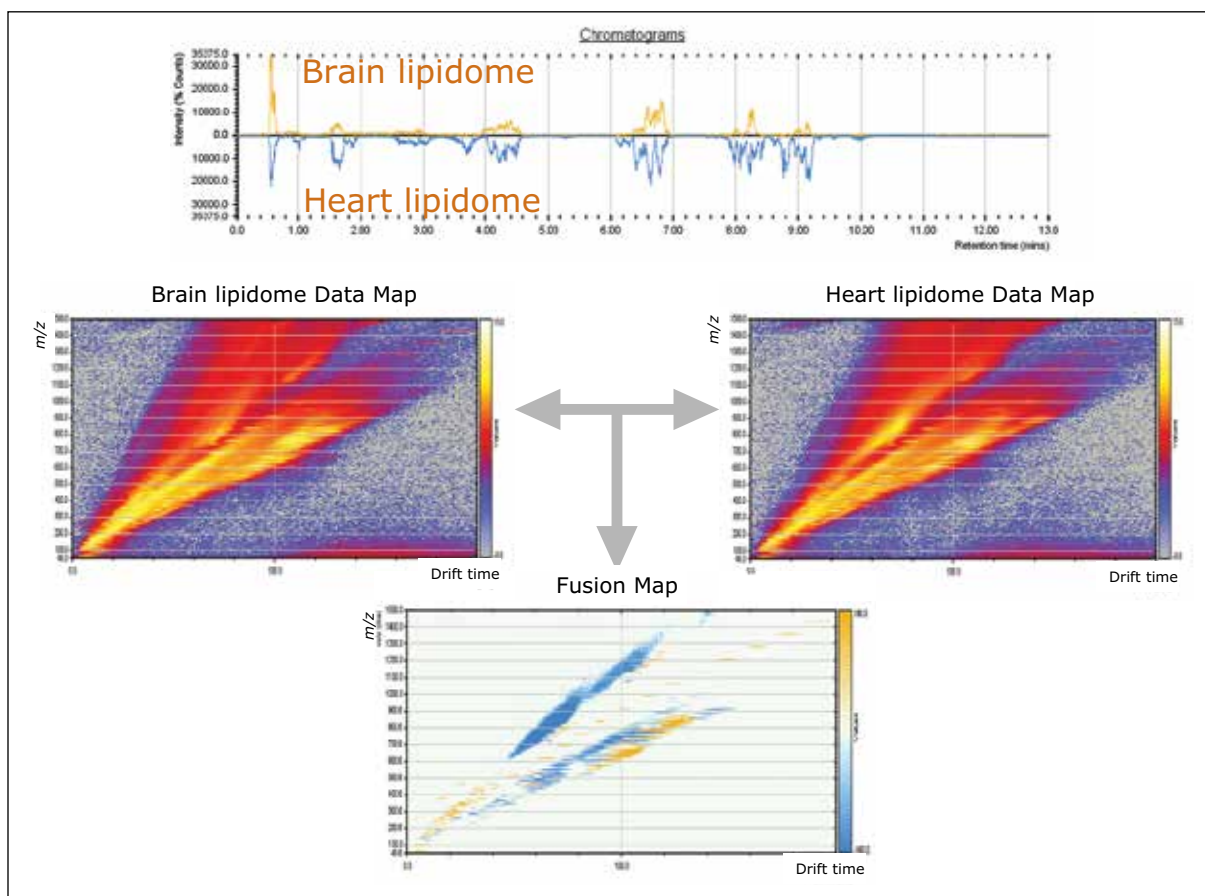


Figure 6. HDMS Compare Software for the comparison of lipid extracted from brain and heart tissues. HDMS Compare Software was used to overlay tissue-specific molecular maps. Key areas of significant differences between two samples were clearly visualized and identified with two different colors. Retention times, drift time, and mass information can be used for database searches and further identification of such molecular differences.
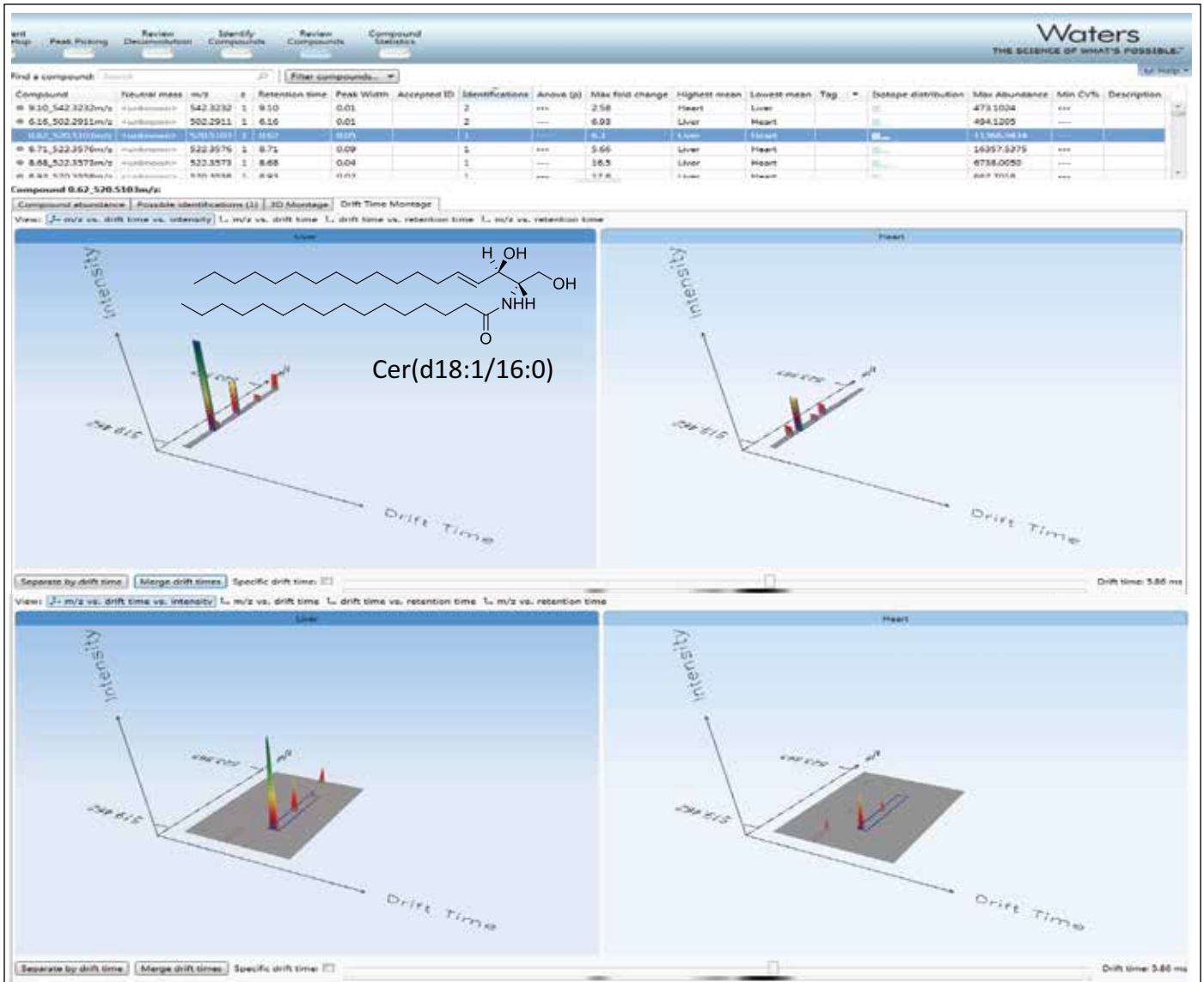
*Figure 7. TransOmics for the comparison of lipid extracted from heart and liver tissues. TransOmics uses ion mobility information to separate co-eluting isobaric lipids in the drift time dimension, increasing the specificity of identification and quantification.*

## CONCLUSIONS

The combination of liquid chromatography, ion mobility, and oa-Tof mass spectrometry is a multidimensional separation strategy capable of analyzing complex biological mixtures to a depth not previously possible, enhancing the detail obtained from lipidomic profiling.

■ HILIC separates lipid classes according to their polarity, providing stable retention time coordinates.

■ Ion mobility separates lipids according to their difference in size and molecular shapes, providing $\Omega$ values (drift time coordinates).

■ LC/MS$^E$ coupled with ion mobility separation (HDMS$^E$) allows the simultaneous collection of exact mass precursor and fragment ion information, providing structural information and improving the experimental specificity.

■ HILIC coupled with LC/HDMS$^E$ generates molecular maps with unique coordinates, including retention times, drift times, accurate precursor and fragment ion masses, as well as intensities.

■ HDMS Compare and TransOmics provide informatics solutions to compare large numbers of molecular maps in a scalable fashion using multi-variate statistical approaches, adding further specificity and confidence to lipid identification and biological interpretation.

## References

1. Rainville PD, Stumpf CL, Shockcor JP, Plumb RS, Nicholson JK. Novel Application of Reversed-Phase UPLC-oaTOF-MS for Lipid Analysis in Complex Biological Mixtures: A New Tool for Lipidomics. *J Proteome Res.* 2007 Feb; 6(2):552-8.

2. Lísa M, Cífková E, Holčapek M. Lipidomic profiling of biological tissues using off-line two-dimensional high-performance liquid chromatography-mass spectrometry. *J Chromatogr A.* 2011 Aug 5; 1218(31):5146-56. Epub 2011 May 30.

3. Isaac G, McDonald S, Astarita G. Lipid Separation: UPLC System for the Separation of Complex Biological Total Lipid Extracts. Waters Application Note 720004107en. 2011 Sept.

4. Netto J, Wong S, Ritchie M, Torta F, Narayanaswamy P. A Definitive Lipidomics Workflow for Human Plasma Utilizing Off-line Enrichment and Class Specific Separation of Phospholipids. Waters Application Note 720004521en. 2012 Dec.

5. Nie H, Liu R, Yang Y, Bai Y, Guan Y, Qian D, Wang T, Liu H. Lipid profiling of rat peritoneal surface layers by online normal- and reversed-phase 2D LC QToF-MS. *J Lipid Res.* 2010 Sep; 51(9):2833-44.

6. Netto JD, Wong S, Ritchie M. High Resolution Separation of Phospholipids Using a Novel Orthogonal Two-Dimensional UPLC/QTof MS System Configuration. Waters Application Note 720004546en. 2013 Jan.

7. Shvartsburg AA, Isaac G, Leveque N, Smith RD, Metz TO. Separation and classification of lipids using differential ion mobility spectrometry. *J Am Soc Mass Spectrom.* 2011 Jul;22(7):1146-55. Epub 2011 Apr 12. Erratum in: *J Am Soc Mass Spectrom.* 2011 Jul; 22(7):1156.

8. Kliman M, May JC, McLean JA. Lipid analysis and lipidomics by structurally selective ion mobility-mass spectrometry. *Biochim Biophys Acta.* 2011 Nov; 1811(11):935-45.

## Waters
### THE SCIENCE OF WHAT'S POSSIBLE.®

Waters
THE SCIENCE OF WHAT'S POSSIBLE.®

# Lipid Class Separation Using UPC²/MS

Michael D. Jones,[1,3] Giorgis Isaac,[1] Giuseppe Astarita,[1] Andrew Aubin,[1] John Shockcor,[1] Vladimir Shulaev,[2]
Cristina Legido-Quigley,[3] and Norman Smith[3]
[1]Waters Corporation, Milford, MA, USA
[2]Department of Biological Sciences, Center for Plant Lipid Research, University of North Texas, Denton, Texas, USA
[3]Pharmaceutical Science Division, School of Biomedical and Health Sciences, King's College, London, UK

## APPLICATION BENEFITS

■ Provides ACQUITY UPC²™ methodology conditions for comprehensive lipid intra- and inter-class analysis

■ Highlights the method parameters that aid as method development tools for comprehensive lipid profiling

■ Provides a single separation technique and a single instrumentation approach for rapid lipids analyses

## WATERS SOLUTIONS

ACQUITY UPC² System with MS detection

Empower 3® Software

ACQUITY UPC² columns

## KEY WORDS

UPC², MS, UPC²/MSE, lipidomics, metabolomics, method development, convergence chromatography

## INTRODUCTION

The analysis of complex lipids has historically been a challenging task and may require a variety of analytical techniques. Lipids are generally recognized as hydrophobic compounds, but the properties of complex lipids containing phosphorus, sulfur, sugar, and nitrogen have a wide polarity range. Developing separation-based methodology utilizing a single technique is recognized as a common challenge for scientists researching lipidomic and metabolomic applications.

Recent advances in technology have revived the exploration of supercritical fluid chromatography (SFC) as a viable analytical technique. Research and development focused on improvements of SFC instrumentation has provided a holistically designed chromatographic system that utilizes liquid $CO_2$ as a mobile phase to leverage the chromatographic principles and selectivity of normal phase chromatography while providing the ease-of-use of reversed phase LC (RPLC). This new separation technique is referred to as UltraPerformance Convergence Chromatography™ (UPC²™).

In this application note, UPC² technology is implemented for the analysis of lipid class separation. Method variables influencing the peak integrity and chromatographic separation for a mixture of lipids with different degrees of polarity are explored. The experiments were designed to understand the chromatographic behavior of lipids in a controlled setting using a variety of lipid extracts. Acyl chain length and a number of double bond influences were investigated using single moiety standards. The methodology parameters were tested using lipid extracts composed of intra-class components. The method conditions are applied to biological lipid extracts, whereas method adjustments are investigated to manipulate the chromatography based on the goal of the analyst. Insights from these method variable manipulations help to scope the development of targeted lipid profiling and screening protocols.

## EXPERIMENTAL

### Lipid abbreviations

| | |
|---|---|
| CER | Ceramides |
| SM | Sphingomyelin |
| PG | Phosphatidylglycerol |
| PE | Phosphatidylethanolamine |
| PC | Phosphatidylcholine |
| LPC | Lyso-Phosphatidylcholine |
| LPE | Lyso-Phosphatidylethanolamine |

### Sample description

Samples and standards were purchased from Avanti Polar Lipids. Mix 1 and Mix 2 were brain (porcine) extracts except LPC and PG which were egg (chicken) extracts. Stocks were prepared in 50:50 chloroform/methanol. Working lipid mixtures were prepared to the specified concentration.

| | |
|---|---|
| Mix 1: | Ceramide, SM, (0.05 mg/mL) PG, PE, PC, (0.1 mg/mL) |
| Mix 2: | LPC, LPE, (0.05 mg/mL) |
| Mix 3: | 1:1 of [mix 1] and [mix 2] |

### UPC$^2$ conditions

| | |
|---|---|
| System: | ACQUITY UPC$^2$ |
| Columns: | ACQUITY UPC$^2$ BEH and HSS C$_{18}$ SB |
| Column temp.: | 60 °C |
| Sample temp.: | 10 °C |
| Injection volume: | 1 µL |
| Flow rate: | 1.85 mL/min |
| Back pressure: | 1500 psi |
| Mobile phase A: | CO$_2$ |
| Mobile phase B: | 50:50 methanol/acetonitrile with 1 g/L ammonium formate |
| Gradient: | Refer to figures for detailed information |

### MS conditions

| | |
|---|---|
| Mass spectrometers: | ACQUITY® SQD and SYNAPT® G2 MS |
| Ionization mode: | ESI positive |
| Acquisition range : | 100 to 1500 Da |
| Capillary voltage : | 3.5 kV |
| Cone voltage : | 30 V |
| Informatics: | Empower 3 and MassLynx® Software |

## RESULTS AND DISCUSSION

### MS optimization

The ACQUITY UPC$^2$ System was configured with an ACQUITY single quadrupole detector (SQD) for this preliminary investigation of chromatographic parameters. Injections of [Mix 3] were screened with different cone and capillary voltages to determine the best operating conditions. Based on the cone voltage screening results, 30 V was chosen for controlling overall in-source fragmentation of the optimal signal for the spectra of L-α-phosphatidylglycerol (egg PG) to provide precursor ion and valuable fragmentation information, as shown in Figure 1A. The optimal capillary voltage observed for all the peaks in the [Mix 3] was 3.5 to 4.0 kV, as shown in Figure 1B. The final MS conditions used 3.5 kV capillary voltage and 30 V cone voltage.
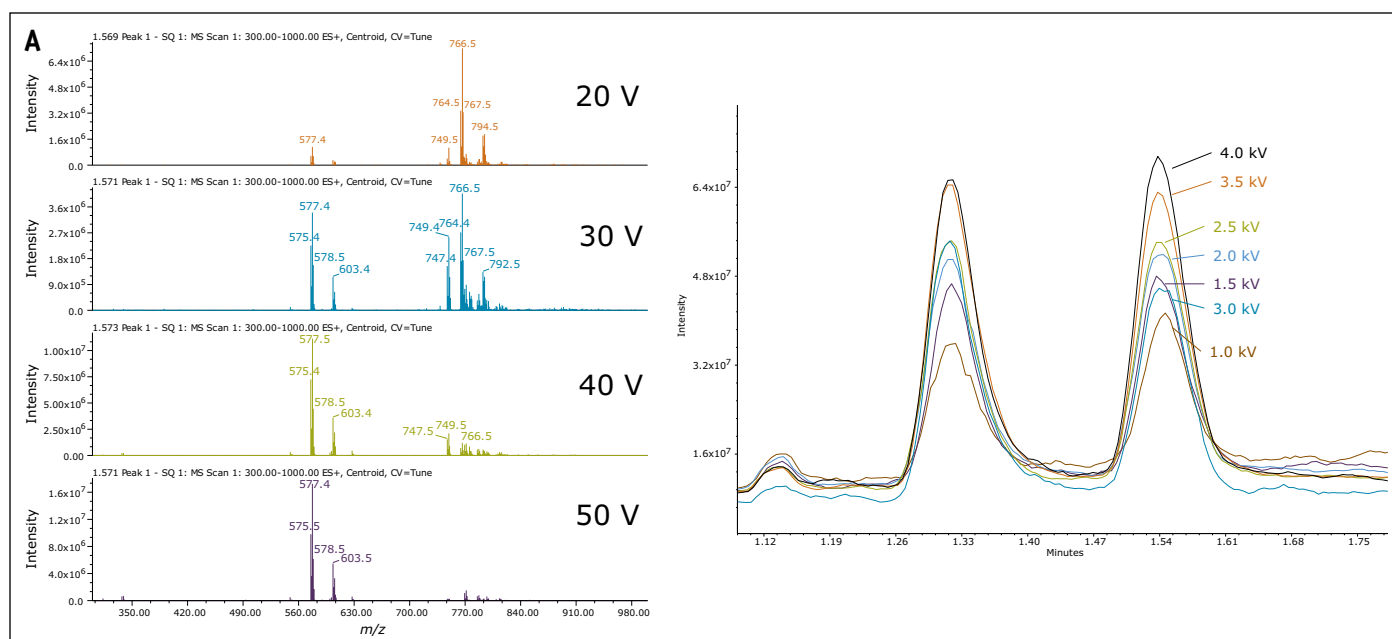


Figure 1. (A) Cone voltage screening results for L-α-phosphatidylglycerol; and (B) capillary voltage screening results for L-α-phosphatidylglycerol.

## Chromatographic method development

The sample preparation workflow was very convenient for use with the ACQUITY UPC[2] System. The chloroform/methanol diluent provided good solubility without any noticeable adverse effects on peak shape. In a typical RPLC lipid analysis, the organic extract containing the lipids would have to be evaporated and re-constituted in a more compatible solvent. When using UPC[2], however, the organic extract containing the lipids can be directly injected onto the system, thereby saving time and costs when analyzing hundreds of biological samples. Screening different column stationary phases typically changes selectivity during method development. Therefore, our initial approach was to screen three stationary phases including UPC[2] CSH Flouro-Phenyl, UPC[2] BEH 2-EP, and UPC[2] BEH. Optimal peak shape and selectivity was achieved on the UPC[2] BEH stationary phase for the inter-class separation of the lipid mixture, as shown in Figure 2.
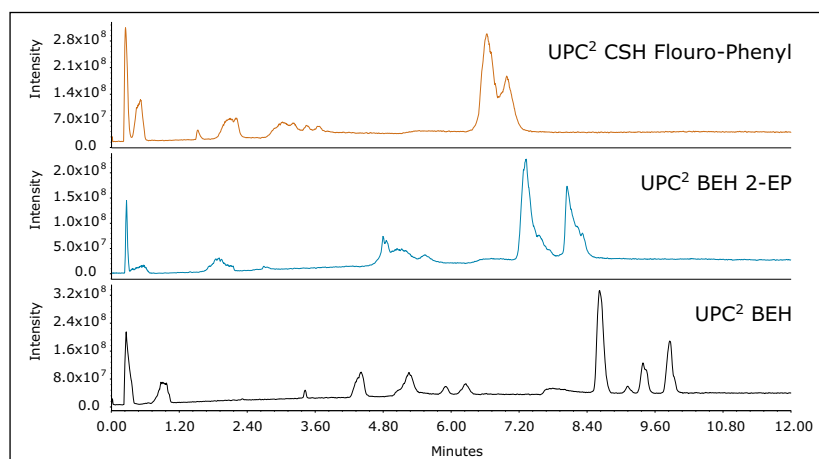


*Figure 2. Column screening of the [metdev] mixture of neutral and polar lipids. A 12-minute 10% to 50% B screening method was used. Due to less retentivity of the BEH 2-EP and CSH Flouro-Phenyl columns, the gradients were modified (10% to 30% B) to adjust for comparative use of the separation space. The mobile phase co-solvent was 1 g/L ammonium formate in MeOH derived from previously published reports.[1]*

Method development screening columns and modifier indicated the bridged ethylene hybrid (BEH) silica columns provided the best selectivity and peak shape. The lipid classes were identified by MS ESI+ utilizing the parameters determined by the MS optimization experiments. Injections of the individual lipid mixtures verified current peak assignments. The method used for screening the columns was optimized to focus on the inter-class separation of analytes in [Mix 3]. The previous 12-minute method was reduced and completed in 5 minutes, as shown in Figure 3.
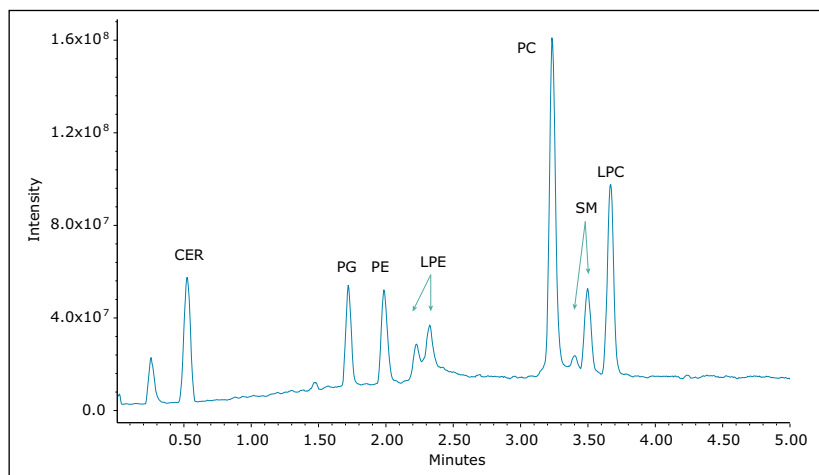


*Figure 3. Injection of [Mix 3] mixture using the ACQUITY UPC[2] BEH column. The original gradient was 5% to 50% at 1.85 mL/min over 10 min with a 2 min hold at 50% B and 1-min re-equilibration at initial conditions before the next injection. The gradient was modified to 15% to 50% B at 1.85 mL/min over 3 min, held at 50% B for 2 min. The column was re-equilibrated at initial conditions before the next injection.*

The lipid extracts purchased from Avanti provide documentation indicating various ratios of lipid intra-class constituents present within a respective standard extract. This was further confirmed when evaluating the mass spectral data for the two LPE peaks observed in chromatographic trace, as shown in Figure 4. It was found that the elution order of the molecular species within each lipid class depended on the number of double bonds on the acyl chain. Thus, the more saturated the acyl chain, the shorter the retention time. The acyl chain length has no effect on the elution order with each lipid class. Interestingly, the intra-class separation of LPE and SM standard extracts is observed when using the UPC$^2$ BEH stationary phase. The other stationary phases that provided broader peaks may offer a better intra-class separation of the Avanti extract standards. This hypothesis will be explored in future studies.
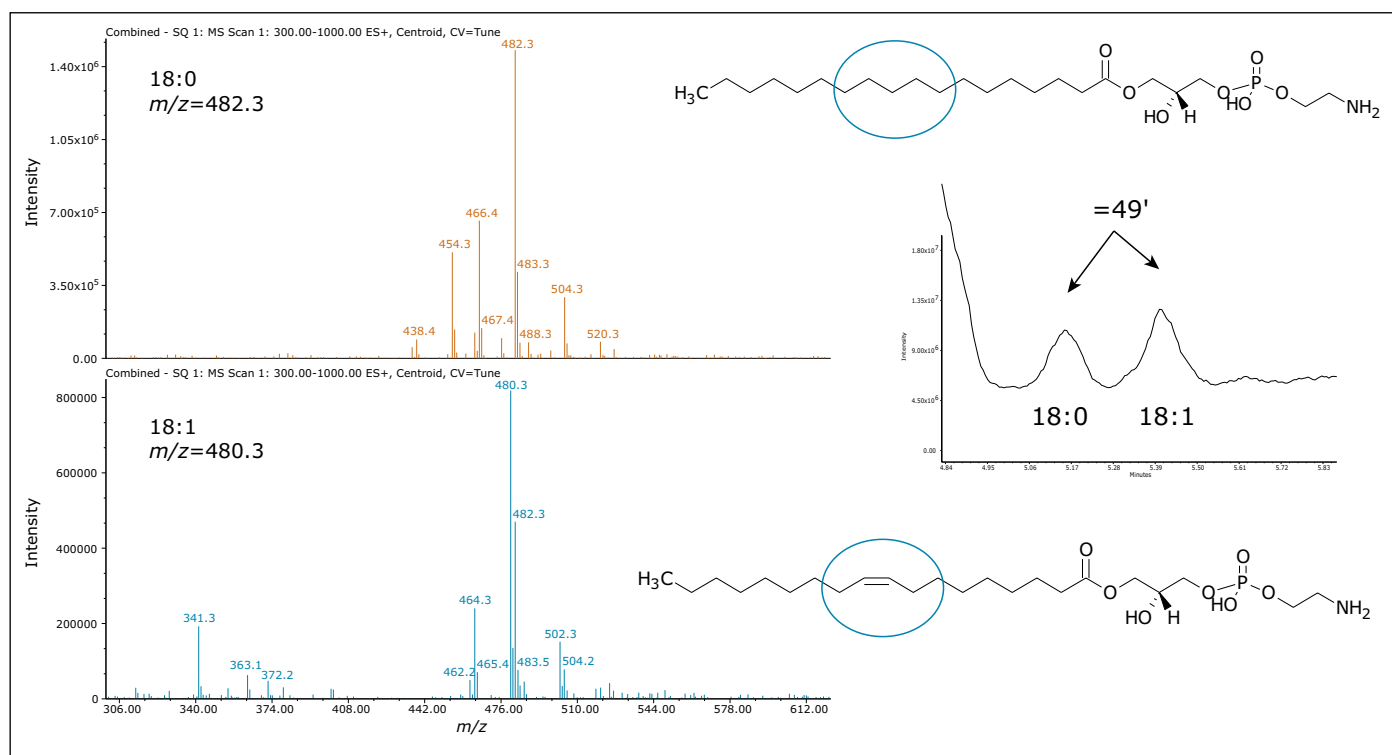


Figure 4. Interrogation of MS spectra for the two LPE peaks.

## Manipulating retentivity

The method development process explored changes in gradient slope; however, changes in resolution were not significant. Experiments to manipulate retentivity were investigated. The variable which resulted in the greatest retentivity changes included the addition of a less polar solvent, such as acetonitrile, to the modifier. Two experiments were performed. The first was conducted with the original modifier composition of 100% methanol. The second experiment was conducted with modifier composition of 80% methanol and 20% acetonitrile. Both modifiers were doped with 1 g/L ammonium formate. In general, using acetonitrile in the modifier improved resolution, as shown in Table 1.

| Peak ID | 100% MeOH (RS) | 80:20 MeOH:ACN (RS) | % Difference |
|---------|----------------|---------------------|--------------|
| PG | – | – | – |
| PE | 2.69 | 3.54 | +31.6 |
| LPE 1 | 1.96 | 2.74 | +39.8 |
| LPE 2 | 1.67 | 2.17 | +29.9 |
| PC | 10.81 | 8.56 | -20.8 |
| SM (1) | 2.24 | 2.07 | -7.6 |
| SM (2) | 1.10 | 1.06 | +45.5 |
| LPC | 1.33 | 1.05 | +12.8 |

Table 1. Impact of modifier composition on lipid resolution. Ceramide was excluded due to the large amount of resolution from the other peaks of interest.

## Analysis of biological samples

The methodology was used to investigate two biological samples, each for distinctly different purposes.
The first example examines a mouse heart extract using the six-minute method for the rapid inter-class targeted
screening of lipids with different polarity. The objective was to determine if the methodology could detect the
presence of specific lipids within the hundreds of samples collected from the diabetic treatment study. This
proof of concept approach will be used for further studies utilizing MS/MS quantification assessing increases
of phospholipids and sphingolipids during treatment. As seen in Figure 5, many of the phospholipids and
sphingolipids were easily identified in the mouse heart extract by using this targeted UPC$^2$/MS method.
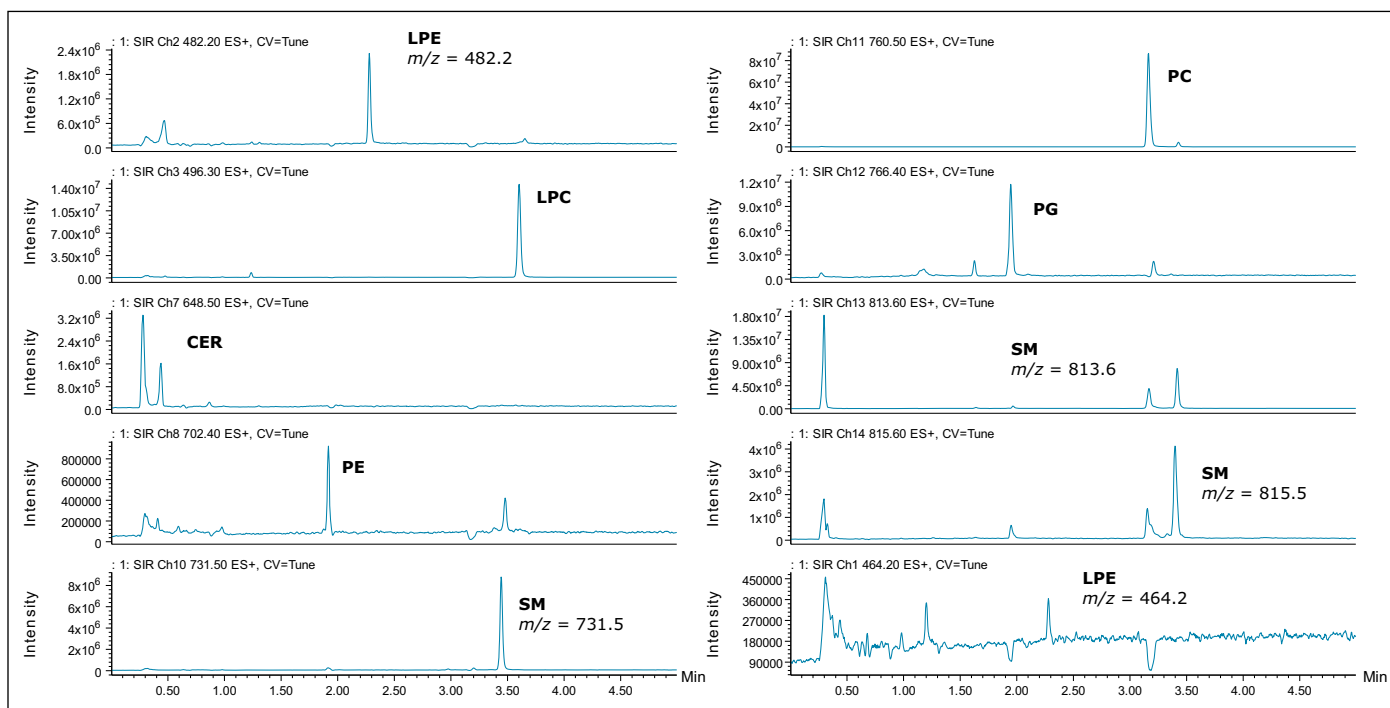


*Figure 5. Targeted SIR analysis of a mouse heart extract. The gradient was 15% to 50% B at 1.85 mL/min over 3 min, held at 50% B for 2 min. The column was re-equilibrated at initial conditions for 1 min before the next injection.*

Neutral lipids, such as acylglyceride and cholesterol esters, are characteristically non-polar. Typically, plant metabolomic profiling distinguishes heterogeneous distribution of neutral lipids, such as triacylglycerols and diacylgylcerols[2] at different conditions. The example in Figure 6 investigates lipids present in a cotton seed oil extract. The data was collected using MS[E] on a SYNAPT G2 Mass Spectrometer allowing for the characterization of the neutral lipids by precursor and product ion alignment. During the method development process, many neutral lipids eluted near the chromatographic void when starting the compositional gradient above 5% modifier using methanol (or methanol/acetonitrile). In this example, the UPC[2]/MS method was modified to retain the neutral lipids by reducing the starting percentage of modifier. The modifier was ramped to elute the polar lipids, known to be present as membrane lipid classes in cotton embryos.[2] By using this approach, the chromatography can be altered to provide greater retention, and often greater specificity for the neutral lipids. From an analytical technique perspective, the elution mechanisms are conceptually similar to performing a mobile phase gradient elution profile by liquid chromatography.
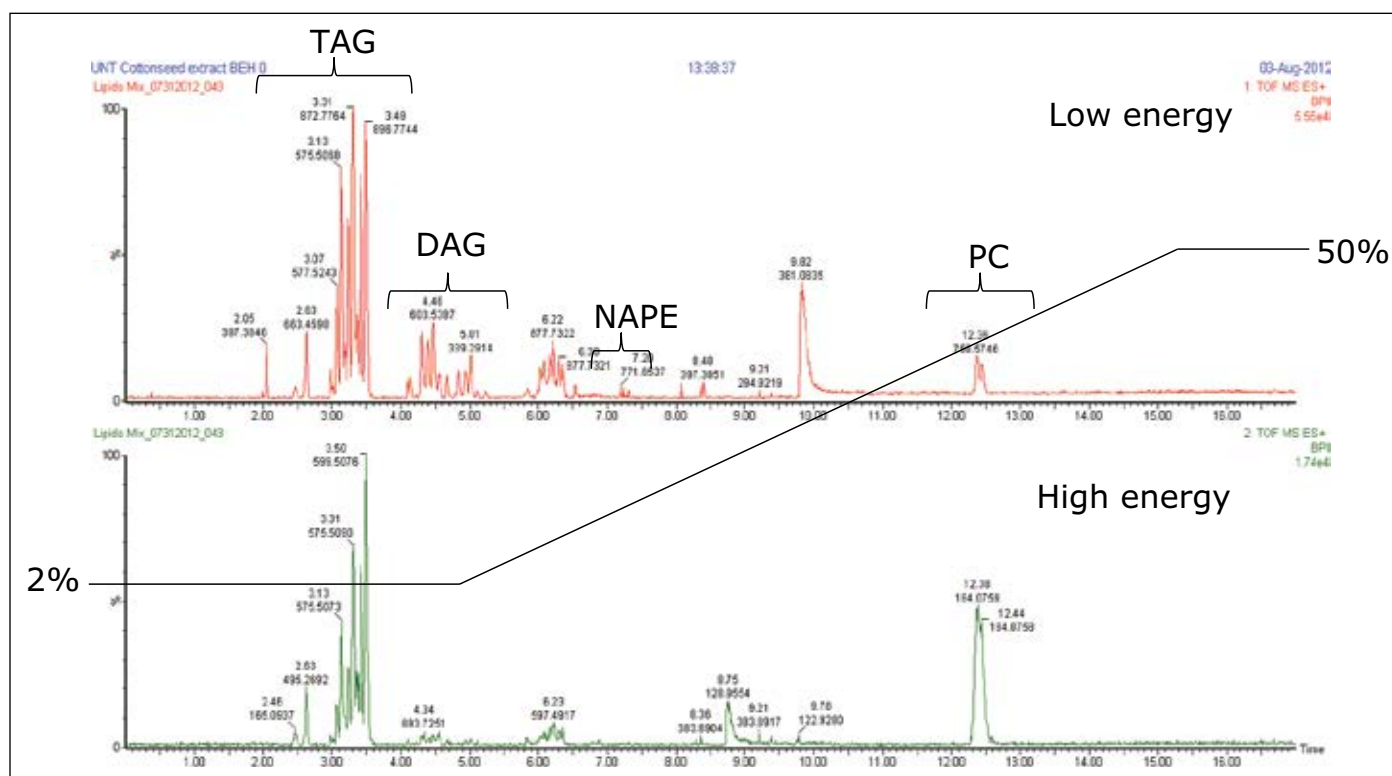


Figure 6. Comprehensive profiling of a cotton seed oil extract. The gradient was 2% to 5% B over 5 min, increased to 50% B over 10 min, and held at 50% B for 2 min using a flow rate of 1.85 mL/min. The column was re-equilibrated at initial conditions for 1 min before the next injection.

## CONCLUSIONS

A flexible universal method was developed for the analysis of inter-class separations of neutral and amphipathetic lipids. Since the goal of the experiment was to achieve flexible parameters providing the separation of lipids by class, the core methodology using the ACQUITY UPC$^2$ BEH column, methanol/acetonitrile modifier with ammonium formate as an additive provided the best results. The gradient methodology and run time was adjustable to focus on rapid screening or comprehensive profiling of lipids in biological samples. The lipid sample preparation workflow is suitable for UPC$^2$. The organic phase of the biological lipid extract can be directly injected onto the ACQUITY UPC$^2$ System with MS detection, thereby saving time and operating costs.

The rapid inter-class screening provided an analysis within seven minutes including re-equilibration. The MS spectral information confirmed instances of intra-class separation by distinguishing between the degrees of saturation, as demonstrated for the Lyso- Phosphatidylethanolamine separation on the ACQUITY UPC$^2$ BEH column. Resolution can be increased within the chromatographic space by the addition of acetonitrile. For this methodology, an increase of 30% to 40% resolution can be observed between lipid classes for the majority of the analytes. The method development knowledge gained from these experiments build a foundation for the applicability of lipid analysis by convergence chromatography.

### References

1. Bamba T, Shimonishi N, *et al.* High throughput and exhaustive analysis of diverse lipids by using supercritical fluid chromatography-mass spectrometry for metabolomics. *J Biosci Bioengin.* 2008 May; 105(5): 460-469.

2. Horn PJ, Korte AR, Neogi PB, *et al.* Spatial Mapping of Lipids at Cellular Resolution in Embryos of Cotton. *Plant Cell.* 2012 Feb; 24(2): 622-636.

## Waters

### THE SCIENCE OF WHAT'S POSSIBLE.®

**Waters Corporation**
34 Maple Street
Milford, MA 01757 U.S.A.
T: 1 508 478 2000
F: 1 508 872 1990
www.waters.com

Waters
THE SCIENCE OF WHAT'S POSSIBLE.®

# A Facile Database Search Engine for Metabolite Identification and Biomarker Discovery in Metabolomics

Panagiotis Arapitsas,[1] James Langridge,[2] Fulvio Mattivi,[1] Giuseppe Astarita[2]
[1]Department of Food Quality and Nutrition, Research and Innovation Centre, Fondazione Edmund Mach, San Michele all'Adige, Italy
[2]Waters Corporation, Milford, MA, USA

## APPLICATION BENEFITS

Progenesis™ QI Informatics simplifies the process of metabolite identification and biomarker discovery. Potential biomarkers can be searched in both publicly available and in-house databases for accurate mass, retention time, collision cross section, and fragmentation information. Such an approach is fast and it increases the confidence of metabolite identification in metabolomics experiments.

## WATERS SOLUTIONS

SYNAPT HDMS® System

ACQUITY UPLC® System

Progenesis QI Informatics

## KEY WORDS

Metabolomics, lipidomics, natural products, food, nutrition, wine

## INTRODUCTION

Metabolomics experiments offer a promising strategy for biomarker discovery. In a metabolomics workflow, however, the major bottleneck still remains metabolite identification. Currently, there are four levels of annotation for metabolite identification: 1) Confidently identified compound (two orthogonal properties based in authentic chemical standard analysis under the same condition); 2) Putative identified compounds (one or two orthogonal properties based in public database); 3) Putative identified compound class; and 4) Unknown compound.[1] A typical database search that relies only on one property *(i.e.,* accurate mass) usually leads to an extensive number of false positive and negative identifications. To increase the confidence of identification, a search engine should be able to use of in-house databases containing orthogonal molecular descriptors for each metabolite.[2]

Progenesis QI Informatics is a novel software platform that is able to perform alignment, peak-picking, and mining of metabolomics data to quantify and then identify significant molecular alterations between groups of samples. The software uses a search engine (MetaScope) for metabolite identification, with user-definable search parameters to probe both in-house and publicly available databases. With an easy-to-use interface, the user can combine information for metabolite identification, including accurate mass, retention time, collision cross section, and theoretical and/or experimental fragment ions. These physiochemical properties can increase the confidence of metabolite identification while concurrently decreasing the number of false positives.

In this study, we show the Progenesis QI workflow for metabolite identification using, as an example, a study on the effect of different bottling conditions on the nutritional composition of Italian wines.

## EXPERIMENTAL

### UPLC conditions

| | |
|---|---|
| System: | ACQUITY UPLC |
| Column: | ACQUITY UPLC HSS $C_{18}$ SB 1.8 µm 2.1 x 150 mm (p/n 186004120) |
| Pre column: | ACQUITY UPLC HSS T3 VanGuard™ 1.8 µm, 2.1 x 5 mm (p/n 186003976) |
| Mobile phase A: | Water + 0.1% formic acid |
| Mobile phase B: | Methanol + 0.1% formic acid |
| Flow rate: | 0.28 mL/min |
| Column temp.: | 40 °C |
| Injection volume: | 10.0 µL |

Elution gradient:

| Min | A% | B% | Curve |
|---|---|---|---|
| Initial | 100.0 | 0.0 | Initial |
| 1.0 | 100.0 | 0.0 | 6.0 |
| 3.0 | 90.0 | 10.0 | 6.0 |
| 18.0 | 60.0 | 40.0 | 6.0 |
| 21.0 | 0.0 | 100.0 | 6.0 |
| 25.5 | 0.0 | 100.0 | 6.0 |
| 25.6 | 100.0 | 0.0 | 6.0 |
| 28.0 | 100.0 | 0.0 | 6.0 |

### MS conditions

| | |
|---|---|
| MS system: | SYNAPT HDMS |
| Mode of operation: | Tof MS$^E$ |
| Ionization: | ESI +/- |
| Capillary voltage: | 2.5 kV (+) and 2.5 kV (-) |
| Cone voltage: | 25 V |
| Transfer CE: | Ramp 15 to 45 V |
| Source temp.: | 150.0 °C |
| Desolvation gas flow: | 1000 L/h |
| Desolvation temp.: | 500.0 °C |
| Cone gas: | 50 L/h |
| MS gas: | Nitrogen |
| Acquisition range: | 50 to 1200 |

### Data processing and mining:

Progenesis QI Informatics

### Sample collection and preparation

Mezzacorona winery (Trentino, Italy) provided the wines, which were bottled in typical 750-mL wine bottles with the filling industrial machine of the winery. The sample set included two types of wines bottled with nitrogen addition ($N_2$) and without nitrogen addition ($O_2$). Under nitrogen atmosphere, every wine was uncorked, 2 mL were transferred into a 5-mL amber vial, 2 mL Milli-Q water was added, and finally each sample was filtrated with 0.2-µm PTFE filters into a 2-mL Waters LCMS Certified Amber Glass Vial prior to LC/MS analysis.[3]

## RESULTS AND DISCUSSION

Wine is one of the most complex foods as far as its metabolomic profile is concerned, since grapes, yeasts, bacteria, fungi, exogenous antioxidants, fining agents, and other oenological materials, packaging, and aging are involved in its preparation. This great number of different primary and secondary metabolites, most of which are unknowns, highly affects wine quality and the important role it plays in human diet, health, and enjoyment. Different bottling and storage conditions may affect the molecular composition of wines, and thus value and quality.

In this study, we used Progenesis QI to identify the metabolites that were altered between wines bottled under two different levels of oxygen: high level ($O_2$) versus low level ($N_2$). Data were acquired in LC/MS$^E$ mode (Figure 1A) and pre-processed using retention time alignment and peak picking (Figure 1B). A composite ion map was built, which contained more than 3,000 compounds after isotopic and adduct deconvolution (Figure 1B). Metabolites of interest were filtered according to the ANOVA P value <0.01 and fold change >2, which decreased the number of metabolites of interest (markers) to less than 200 (Figure 2A). This data reduction strategy allowed us to focus on the metabolites that clearly discriminate the two groups of samples as shown by principal component analysis (Figure 2B).
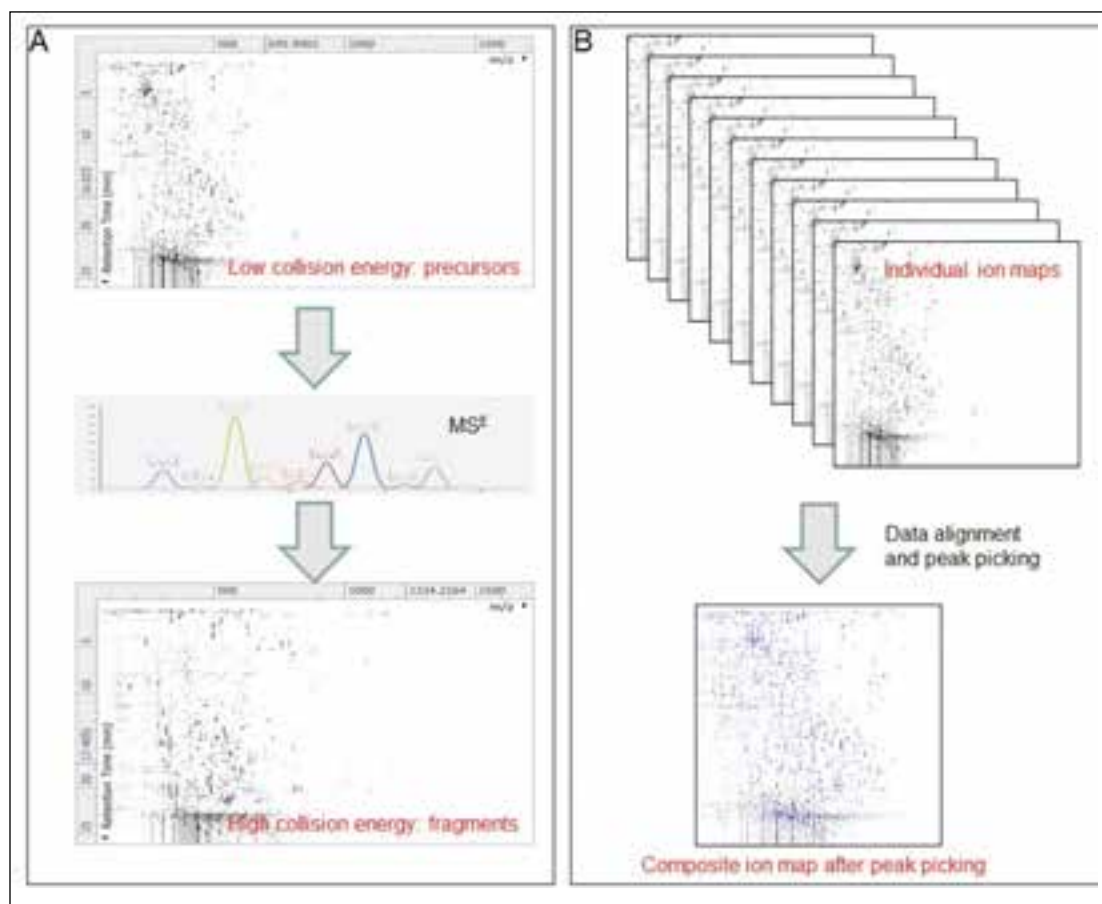


*Figure 1. A: Samples were acquired using data independent analysis (MS$^E$), which provided information for both the intact precursor ions (at low collision energy, upper panel) and the fragment ions (high collision energy, bottom panel). B: From the aligned runs, Progenesis QI produces an aggregate run that is representative of the compounds in all samples, and uses this aggregate run for peak picking. The peak picking from this aggregate is then propagated to all runs, so that the same ions are detected in every run.*
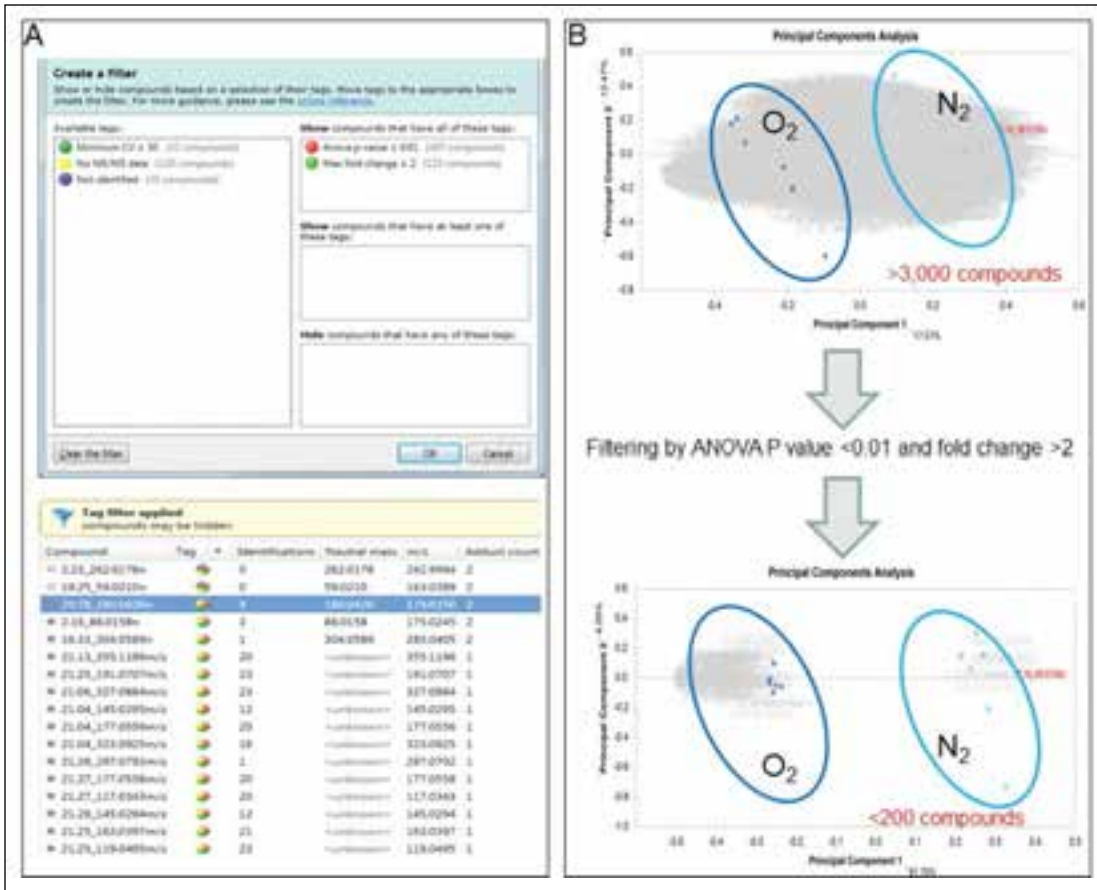
Figure 2. A: Progenesis QI allows tagging data according to various criteria, including ANOVA P values and fold changes. B: Principal component analysis (PCA) containing the entire dataset showed that the wines samples clustered according to the different amount of oxygen in which they were stored, suggesting that the two groups of wine contained a diverse set of metabolites (upper panel). After data reduction, PCA showed the discriminatory power of the selected compounds by filtering only those compounds that had ANOVA p values <0.01 and fold changes >2 (bottom panel).

Initial identification of metabolites was performed using the Human Metabolome Database (HMDB), leading to multiple ambiguous identifications for each compound of interest (Figure 3A and 3B). To decrease the number of false positives, we used in-house metabolite databases, which contain accurate mass, retention time, and fragment information.[2] (Figure 3A-C). We customized the search engine parameters for these orthogonal measures (Figure 3A), allowing a more balanced set of tolerance criteria, which significantly decreased the number of false positives and false negatives (Figure 3B). Experimental fragments were matched against those derived from theoretical fragmentation to further increase the confidence in metabolite identification (Figure 3C). The entire metabolomics workflow for data processing, mining, and identification was completed in just a few hours.
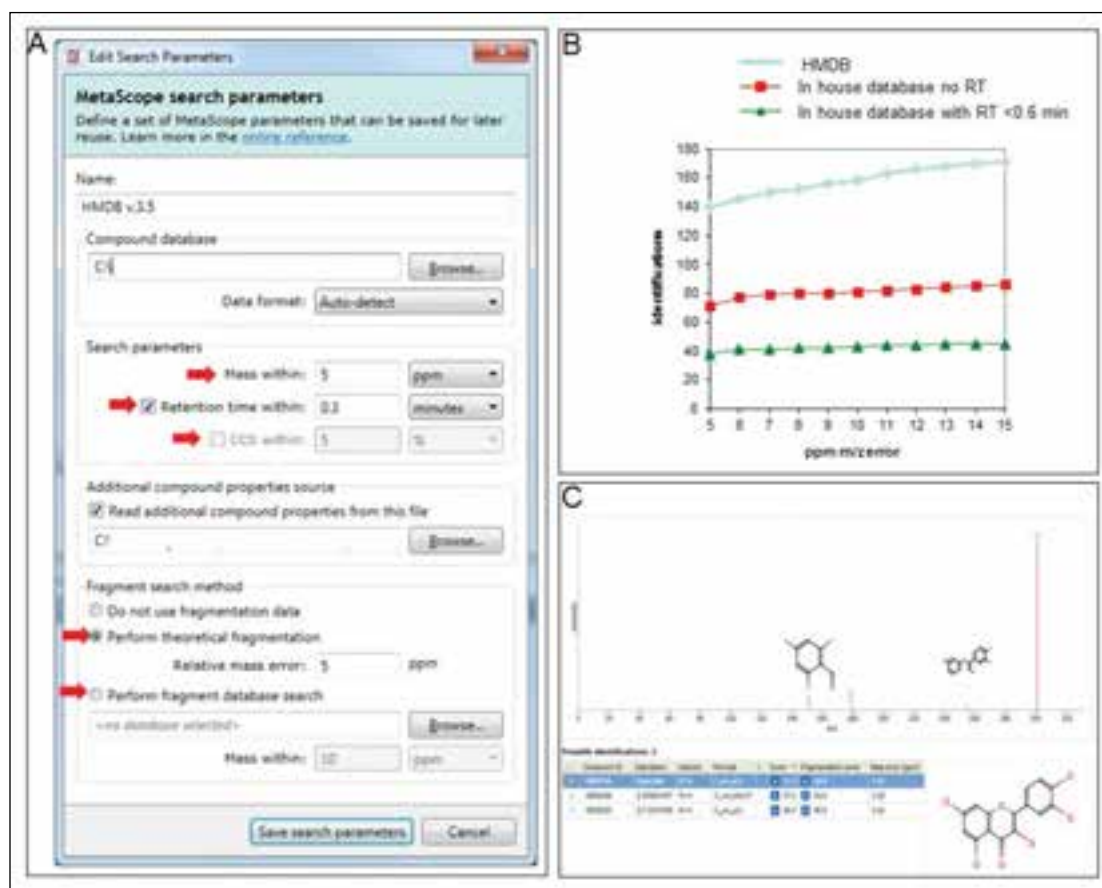


Figure 3. A: The Progenesis QI search engine allows users to query both publicly available databases (e.g., HMDB) and in-house databases, customizing the search parameters for the metabolite identification according to multiple orthogonal measures: mass accuracy, retention time, collision cross section and fragmentation matching. B: Metabolite identification using in-house database allows to filter the results by mass accuracy and retention time tolerance reducing significantly the number of false positives. C: Representative identification of the metabolite Quercetin using mass accuracy, retention time, isotopic distribution and four $MS^E$ fragments, which were matched against theoretically-generated fragments.

## CONCLUSIONS

Progenesis QI effectively streamlines and simplifies complicated metabolomics workflows and makes metabolite identification faster, easier, and more robust. User-definable search parameters dramatically decrease the number of false positive and false negative results in the identification workflow, improving the confidence of identification.

### References

1. Dunn WB, Erban A, Weber RJM, Creek DJ, *et al.* Mass appeal: metabolite identification in mass spectrometry-focused untargeted metabolomics. *Metabolomics*. 2013 March; 9 (1 Supplement): 44-66. doi:10.1007/s11306-012-0434-4.

2. Shahaf N, Franceschi P, Arapitsas P, Rogachev I, Vrhovsek U, Wehrens R. Constructing a mass measurement error surface to improve automatic annotations in liquid chromatography/mass spectrometry based metabolomics. *Rapid Commun Mass Spectrom.* 2013 Nov 15;27(21):2425-31. doi: 10.1002/rcm.6705.

3. Arapitsas P, Speri G, Angeli A, Perenzoni D, Mattivi F. (2014). The influence of storage on the "chemical age" of red wine. *Metabolomics*. 2014 February; online. doi: 10.1007/s11306-014-0638-x.

## Waters

### THE SCIENCE OF WHAT'S POSSIBLE.®

**Waters Corporation**
34 Maple Street
Milford, MA 01757 U.S.A.
T: 1 508 478 2000
F: 1 508 872 1990
www.waters.com

Waters
THE SCIENCE OF WHAT'S POSSIBLE.®

# Xevo G2-S QTof and TransOmics: A Multi-Omics System for the Differential LC/MS Analysis of Proteins, Metabolites, and Lipids

Ian Edwards, Jayne Kirk, and Joanne Williams
Waters Corporation, Manchester, UK

## APPLICATION BENEFITS

■ Simplified workflow, validation, and data interpretation

■ Designed for large-scale metabolomics and proteomics data sets

■ Integrated Omics platform for versatile and comprehensive qualitative and quantitative profiling

■ Statistically validated results across Omics sample sets

## WATERS SOLUTIONS

Omics Research Platform Solutions with TransOmics™ Informatics

ACQUITY UPLC® I-Class System

nanoACQUITY® UPLC® System

Xevo® G2-S QTof

TransOmics Informatics

MassPREP™ Protein Digestion Standard

## KEY WORDS

Omics, metabolomics, lipidomics, proteomics, MS$^E$, principal components analysis, label-free LC/MS

## INTRODUCTION

Recent advances in omics technologies, including LC/MS-based metabolomics, lipidomics, and proteomics instrumentation, enable the quantitative monitoring of the abundance of various biological molecules in a high-throughput manner, thus allowing for determination of their variation between different biological states.

The ultimate aim is to improve the understanding of biological processes, leading to improved disease treatment efficacy, more efficient drug development, or maintaining optimal agricultural growth conditions for crop growth while minimizing infection and other negative effects. In this regard, the results provided from different analytical disciplines are often seen as complementary since they afford orthogonal insights.

The development and application of flexible informatics solutions that are capable of integrating the results from multiple discovery areas is of key importance. This study describes a multi-omics solution for the large-scale analysis of MS data from metabolomics and proteomics data sets. The Waters® Omics Research Platform Solutions with TransOmics Informatics, featuring the Xevo G2-S QTof System, was utilized in a study comprised of both technical and biological replicates.

## RESULTS AND DISCUSSION

A metabolomics experiment was conducted involving the identification of low- and high-dosed samples versus a control/pool sample. According to the experimental design, the samples should be classified into three different groups and the marker ions responsible for the group separation identified. The TransOmics for metabolomics and lipidomics (TOIML) procedure involves the following steps:

1. Importing the raw $MS^E$ continuum data set (six technical replicates/group)

2. Peak alignment to correct retention time drift between analytical runs

3. Chromatographic peak normalization to allow comparison across different sample runs

4. Chromatographic peak detection (peak picking)

5. Ion deconvolution to group ions by compound

6. Compound identification against an available custom built database

7. Perform data analysis to find the ions (features) responsible for the separation of the groups into QC (pool), blank (matrix), and analyte (high dose)

The matrix background comprised System Evaluation Matrix to which Analgesic Standard Mixture A was differentially added, creating a low- (QC) and high-dose (blank) sample. A pool sample (QC) was created by combing equal volumes of the low- and high-dose sample.

The metabolites were separated and analyzed using the ACQUITY UPLC I-Class System coupled with a Xevo G2-S QTof, operated in positive electrospray mode at a mass resolution of >30k FWHM. Data were acquired in LC/$MS^E$ mode, an unbiased Tof acquisition method in which the mass spectrometer switches between low and elevated energy on alternate scans. Processing, searching, and quantification were conducted with TOIML using a compound database.

Steps one, two, and three of the TOMIL procedure are detailed elsewhere (TransOmics Informatics Powered by Nonlinear Dynamics). The grouping by means of principal component analysis (PCA) of the detected ions prior to identification, as shown in Figure 1, represents a composite scores and loadings plot. Primary clustering at the technical replicate level and clear separation of the samples were achieved.
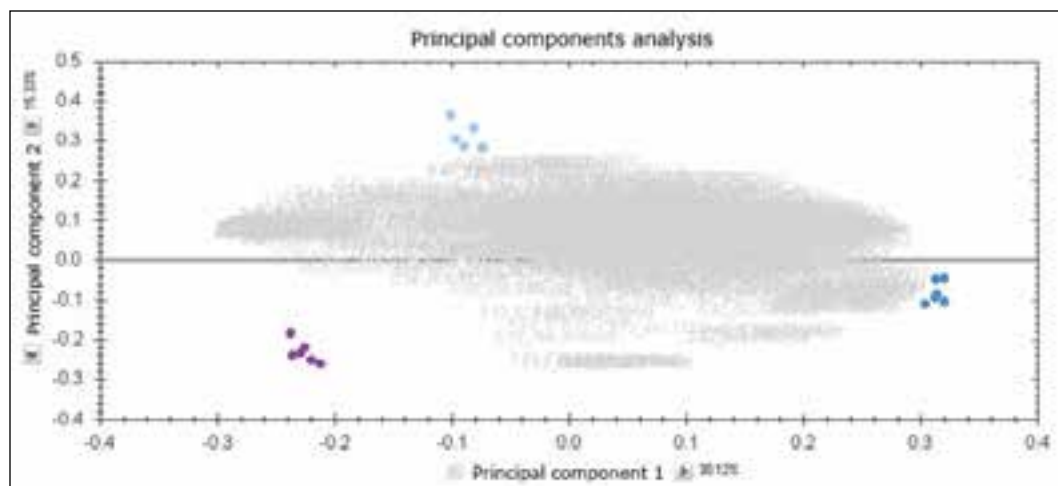


Figure 1. Principal component analysis of analyte (Analgesic Standard Mixture A high dose; purple), Blank (System Evaluation Matrix; light blue) and QC (pooled sample; dark blue).
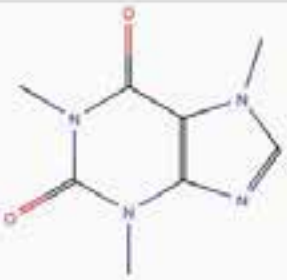
Next, compound identification was conducted using an integrated search tool, leading to the correct identification of the four Analgesic Standard Mixture standards that can be detected in positive ion electrospray mode. An overview of the TOIML compound search results page is shown in Figure 2, highlighting the identification of caffeine based on accurate mass, retention time (optional), and theoretical isotopic pattern distribution.

In addition to the previously described PCA, additional multivariate statistical tools are integrated within TOIML, including correlation and trend analysis. An example is shown in Figure 3, representing normalized trend plots for the four spiked standards, illustrating good agreement between the six technical replicates of each of the standards, as well as relative abundances that are in agreement with the experimental design.

Moreover, TOIML enables the scientist to link the analysis results with other omics data or provide input into separate statistical software packages such as EZinfo. Results from downstream bioinformatics (i.e., Umetrics software) can be imported back into an analyzed experiment, combining all compound data into a single table to review or share.



*Figure 2. Compound identification page TOIML.*

*Figure 3. Normalized abundance profiles analgesic standards.*

For the proteomics experiment, three replicates of two 10-ng *E.coli* samples differentially spiked with bovine serum albumin (BSA), alcohol dehydrogenase (ADH), enolase, and glycogen phosphorylase B were analyzed. The injected on-column amounts for the spiked protein in the first sample (Mixture 1) were one femtomoles each and 8, 1, 2, and 0.5 femtomoles for the second sample (Mixture 2), respectively. The nominal expected ratios (Mixture 2:Mixture 1) were therefore 8:1, 1:1, 2:1, and 0.5:1. Here, the peptides were separated and analyzed using a nanoACQUITY UPLC System coupled to a Xevo G2-S QTof and operated in LC/MS$^E$ acquisition mode. Processing, searching, and quantification were conducted with TransOmics for Proteomics (TOIP) using a species specific database to which sequence information of the spiked proteins was appended.

The TOIP procedure involves the following steps:

1. Importing the raw MS$^E$ continuum data set (three technical replicates per sample)

2. Peak alignment to correct retention time drift between analytical runs

3. Chromatographic peak normalization to allow comparison across different sample runs

4. Chromatographic peak detection (peak picking)

5. Protein and peptide identification utilizing integrated database search algorithms

6. Multivariate statistical analysis

7. Absolute and relative quantitation

TOIP offers the same multivariate analysis tools as TOIML. Figure 4 illustrates an example of PCA of the detected features, i.e. charge state groups. Primary clustering at the technical replicate level can be readily observed. A qualitative peptide identification result for one of the spiked protein digest is shown in Figure 5, and the normalized expression profiles of all peptides identified to this protein are shown in Figure 6. The latter is demonstrative for the type of quantitation precision that can be obtained by means of label-free MS studies using and LC/MS$^E$- based acquisition strategy.

Figure 5 shows the qualitative results overview for an LC/MS$^E$ acquisition of one of the analyses of the differentially spiked samples. In this particular instance, the on-column amount of highlighted BSA was 8 fmol and the amount of *E.coli* digest equal to 10 ng. The results, shown in Figure 6, demonstrate the corresponding relative quantification result.
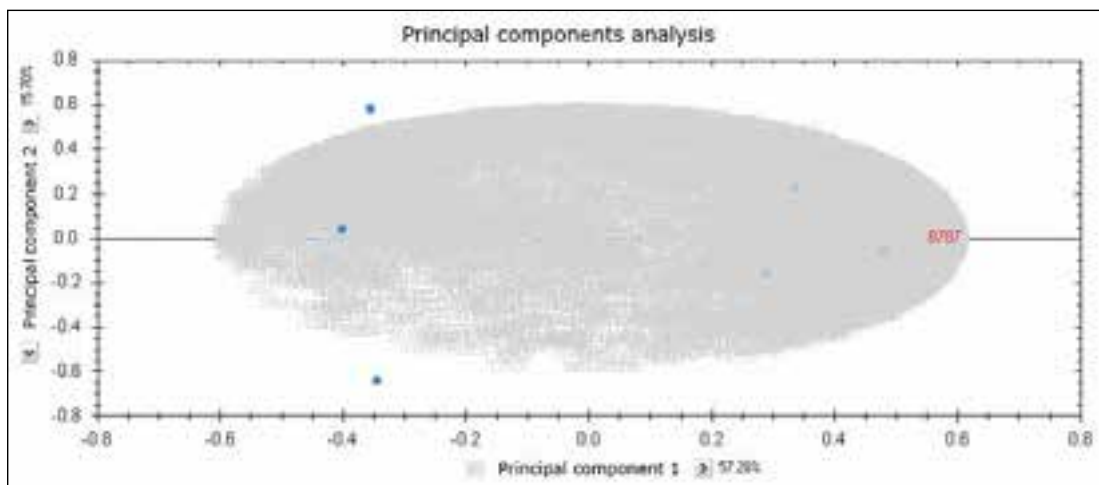


Figure 4. PCA of Mixture 1 spiked into E.coli (dark blue) and Mixture 2 spiked into E.coli (light blue) features (charge state groups).
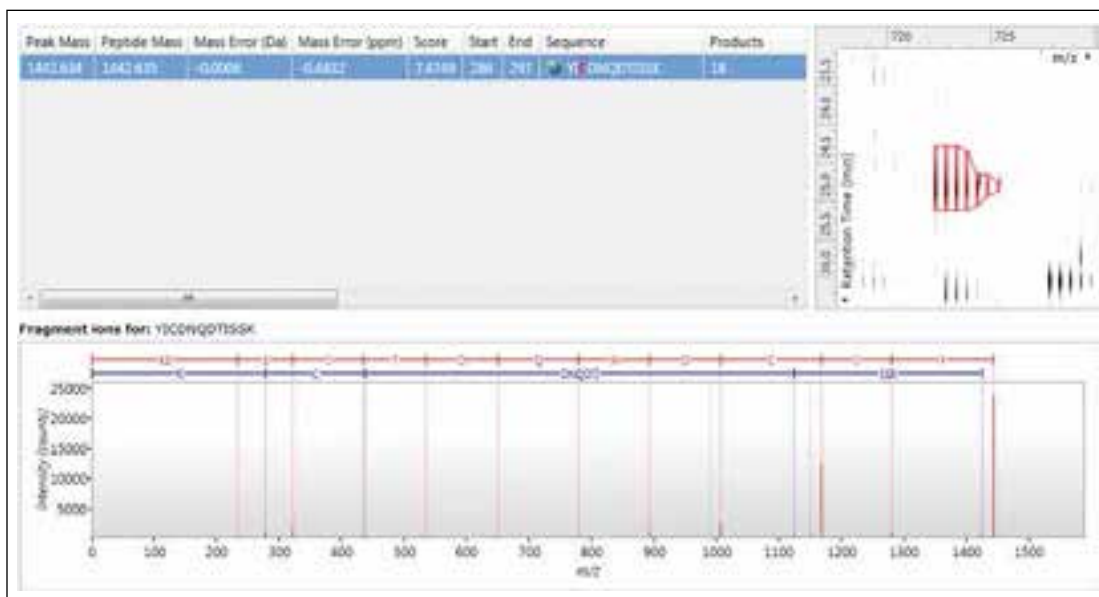


Figure 5. Qualitative LC/MS$^E$ identification for a bovine serum albumin peptide that was differentially spiked into E.coli. Shown clock-wise are the identification associated metrics (score and error), a detail of the contour plot, and the annotated product ion spectrum.
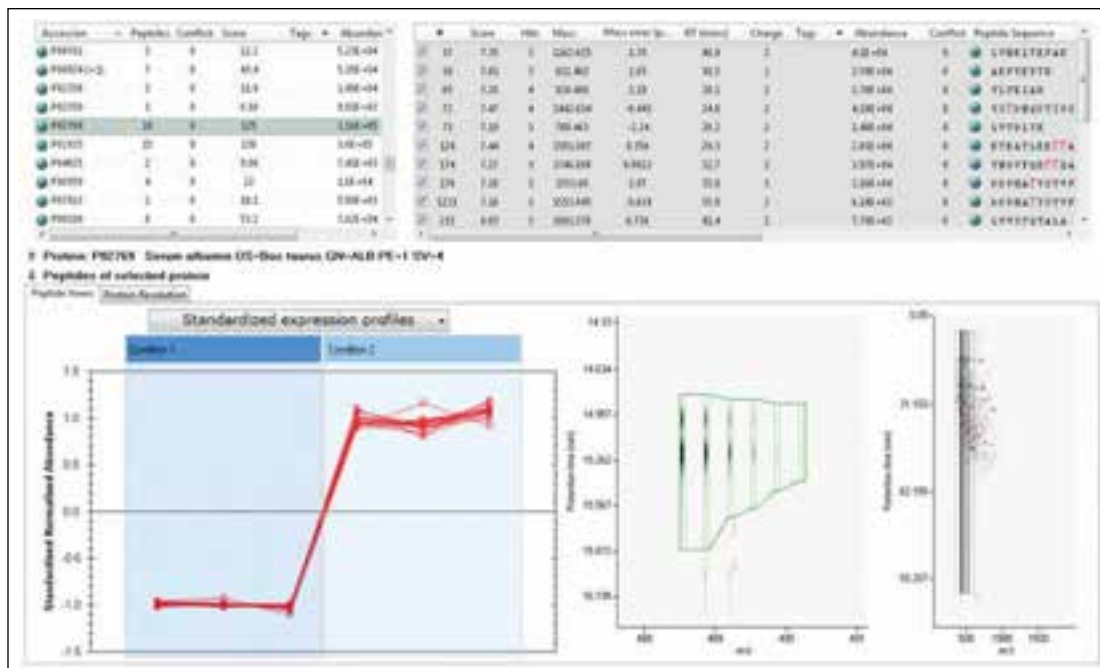
*Figure 6. Quantitative profiling of the peptides identified to bovine serum albumin.*

## CONCLUSIONS

- TransOmics Informatics provides an easy-to-use, scalable system for multi-omics studies.

- LC/MS$^E$ (LC with Data Independent Acquisition MS) provides a comprehensive qualitative and quantitative data set from a single experiment.

- Complementary information can be rapidly obtained and linked from metabolite, lipid, and protein analysis.

## Waters
### THE SCIENCE OF WHAT'S POSSIBLE.®

Waters
THE SCIENCE OF WHAT'S POSSIBLE.®

# An Ion Mobility-Enabled Data Independent Multi-Omics Approach to Quantitatively Characterize Urine From Children Diagnosed With Idiopathic Nephrotic Syndrome

Lee Gethings[1]; Sandra Kraljević Pavelić[2]; Mirela Sedic[2]; John Shockcor[3]; Stephen McDonald[3]; Johannes Vissers[1]; Maja Lemac[4]; Danica Batinić[4]; James Langridge[1]

[1]Waters Corporation, Manchester, UK; [2]Department of Biotechnology, University of Rijeka, Rijeka, Croatia; [3]Waters Corporation, Milford, MA, USA; [4]Zagreb Univerisity Hospital Centre, Zagreb, Croatia

## APPLICATION BENEFITS

A label-free multi-omics approach for the analysis of the urine of Idiopathic Nephrotic Syndrome (INS) patients that provides both qualitative and quantitative information in a single experiment. This enables possible diagnostic and therapeutic solutions for patients with INS.

## WATERS SOLUTIONS

ACQUITY UPLC® System

nanoACQUITY® UPLC® System

SYNAPT® G2 Mass Spectrometer

Oasis® HLB Extraction Cartridges

ProteinLynx GlobalSERVER™

Markerlynx™ XS

TransOmics™ Platform and Informatics

MS$^E$/HDMS$^E$

TriWave™ technology

## KEY WORDS

Idiopathic Nephrotic Syndrome (INS), metabolomics, clinical proteomics, multi-omics

## INTRODUCTION

Idiopathic Nephrotic Syndrome (INS) results from the malfunction of the glomerular filter and it is the most prevalent glomerular disease in children. In spite of some progress, its pathogenesis is still unknown and therapy options are confined to gross immune modulation. A variety of methods for diagnostic and treatment purposes are available for patients; however, the lack of understanding regarding the pathogenic mechanisms underlying INS can lead to poor therapeutic response and adverse side-effects. In this application note, we describe a multi-omic approach to reveal new molecular factors involved in pathogenesis of INS with potential diagnostic and therapeutic significance.
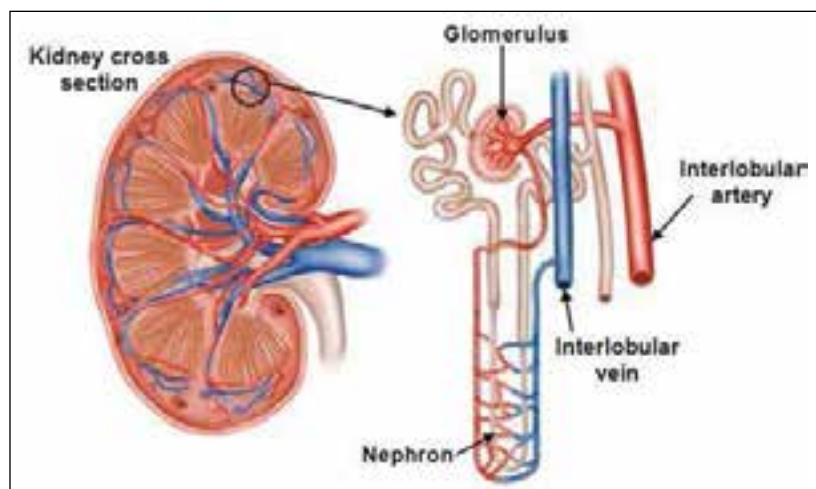


Figure 1. Kidney section highlighting a single nephron. A malfunctioning glomerulus is where INS occurs (courtesy of Wellcome Images).

## EXPERIMENTAL

### Sample preparation

Pediatric urine samples intended for peptide analysis were prepared for LC/MS analysis as previously described.[1] Samples were treated with 1% RapiGest™ SF prior to reduction and alkylation. Aliquots were incubated with anti-HSA resin and centrifuged using Vivaspin 5,000 MWCO filters. A series of washes using water were implemented to ensure adequate recovery. The resulting supernatant was digested using trypsin overnight as shown in Figure 2. Metabolite analysis samples were purified using Oasis HLB Extraction Cartridges. Water/methanol (90/10) washes were performed, followed by analyte elution using methanol. The resulting residue was reconstituted in 200 µL mobile phase and vortexed prior to LC/MS.

### LC/MS conditions

Label-free LC/MS was used for qualitative and quantitative peptide analyses. Experiments were conducted using a 90 min gradient from 5% to 40% acetonitrile (0.1% formic acid) at 300 nL/min using a nanoACQUITY UPLC System and a BEH 1.7 µm $C_{18}$ reversed phase 75 µm x 20 cm nanoscale LC Column.

For metabolite identification, the LC/MS experiments consisted of a 10 min gradient from 0% to 50% acetonitrile (0.1% formic acid) at 500 µL/min using an ACQUITY UPLC System. Here, a BEH 1.7 µm $C_{18}$ reversed phase 2.1 x 10 cm LC column was used.

Data were acquired in data independent analysis (DIA) mode that utilized a nanoACQUITY UPLC or ACQUITY UPLC system directly interfaced to a hybrid IM-oaTof SYNAPT G2 Mass Spectrometer. Ion mobility (IM) was used in conjunction with both acquisition schemes, as illustrated in Figure 3.

### Bioinformatics

The LC/MS peptide data were processed and searched with ProteinLynx GlobalSERVER. Normalized label-free quantification was achieved using TransOmics Software. The resulting metabolomic data were processed using MassLynx™ Software, and additional statistical analysis conducted with EZ Info.
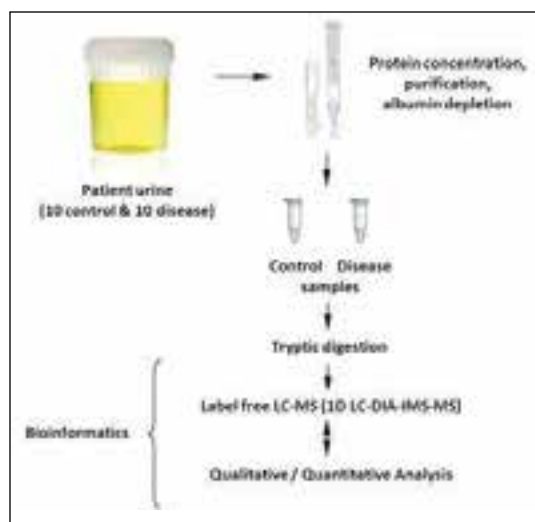


Figure 2. Experimental design study for urinary proteins.
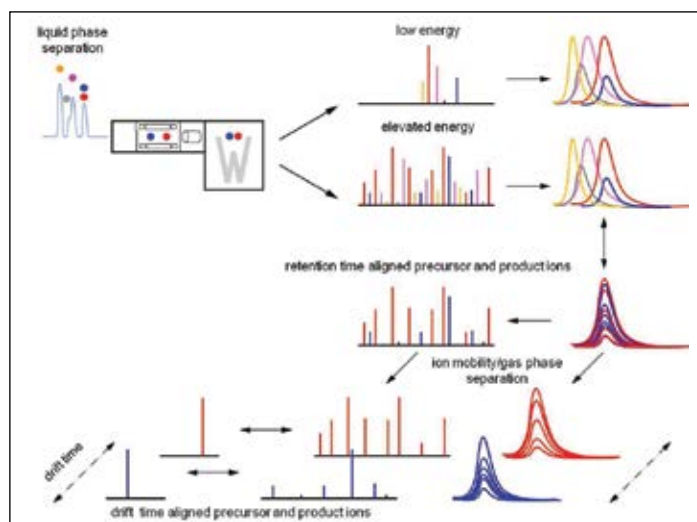


Figure 3. Retention and drift time principle ion mobility enabled data-independent analysis (IM-DIA-MS/HDMS[E]).

## RESULTS AND DISCUSSION

Small amounts of the purified urine were analyzed to identify, quantify, and investigate the proteomic and metabolomic variance between control and disease pre-treated subjects.

Principal Component Analysis (PCA) was used to identify and highlight significant changes between the control and disease pre-treated samples, as shown in Figure 4. Similar clustering patterns were observed for both the protein and metabolite datasets.
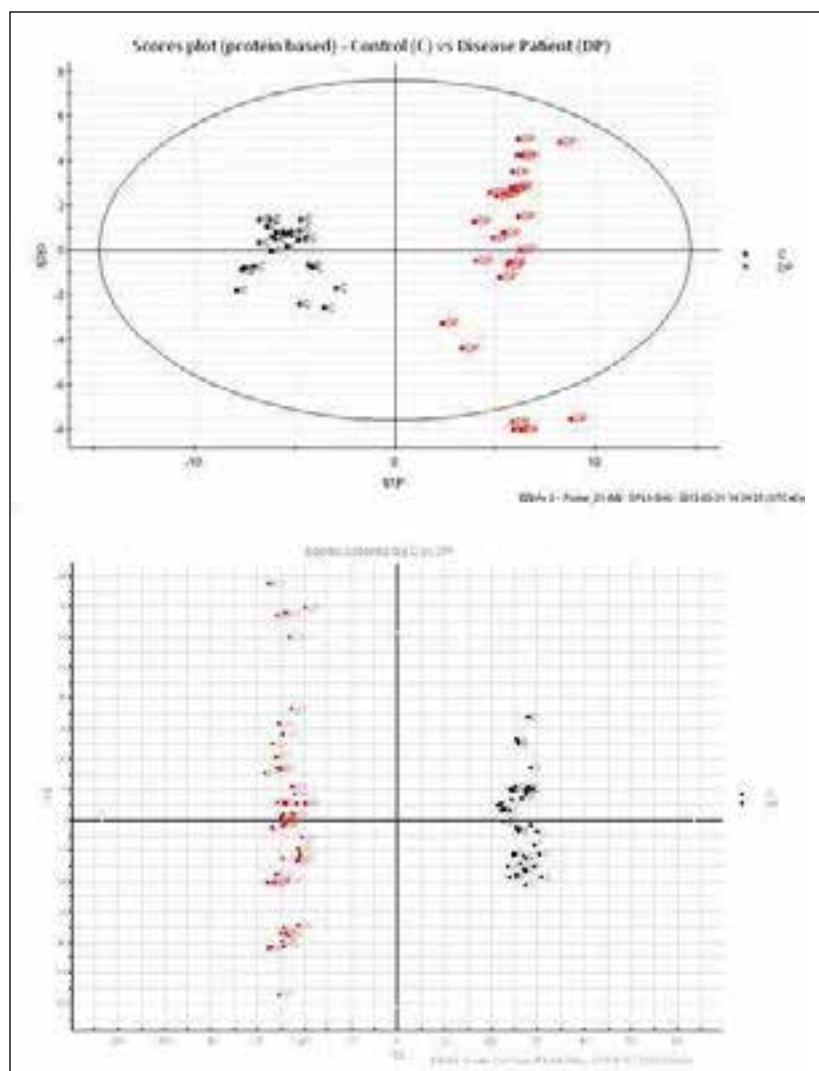


*Figure 4. Scores plot from OPLS-DA analysis of disease pre-treated (red) vs. control (black).*

Proteomic data were aligned, normalized, and quantified. A large proportion of the identified proteins are glycosylated and over 80% of the total number of proteins identified and exhibited a significant expression fold change. Figure 5 highlights the proteins, which have greater than a two-fold change between sample sets. The fold change at the peptide level can be visually displayed using 3D montage images. A charge state feature of one of the peptides of interest is shown in Figure 5.

The metabolomics workflow results are summarized in Figure 6. Using the metabolite contrasting loadings plot, significant metabolite identifications can be found at the extremes and are shaded in blue. Example compounds, which were found to contribute most significantly to the variance, are also shown.

A common pathway is shown in Figure 7, which illustrates a glutamate [NMDA] receptor subunit as one such example. NMDA belongs to the glutamate-gated ion channel family of proteins and is used in neuronal system pathways. Glutamate can also be located within the same pathway. Postsynaptic Ca(2+) is thought to increase through the NMDA receptors, which activate several signal transduction pathways including Erk/MAP kinase and cAMP regulatory pathways.
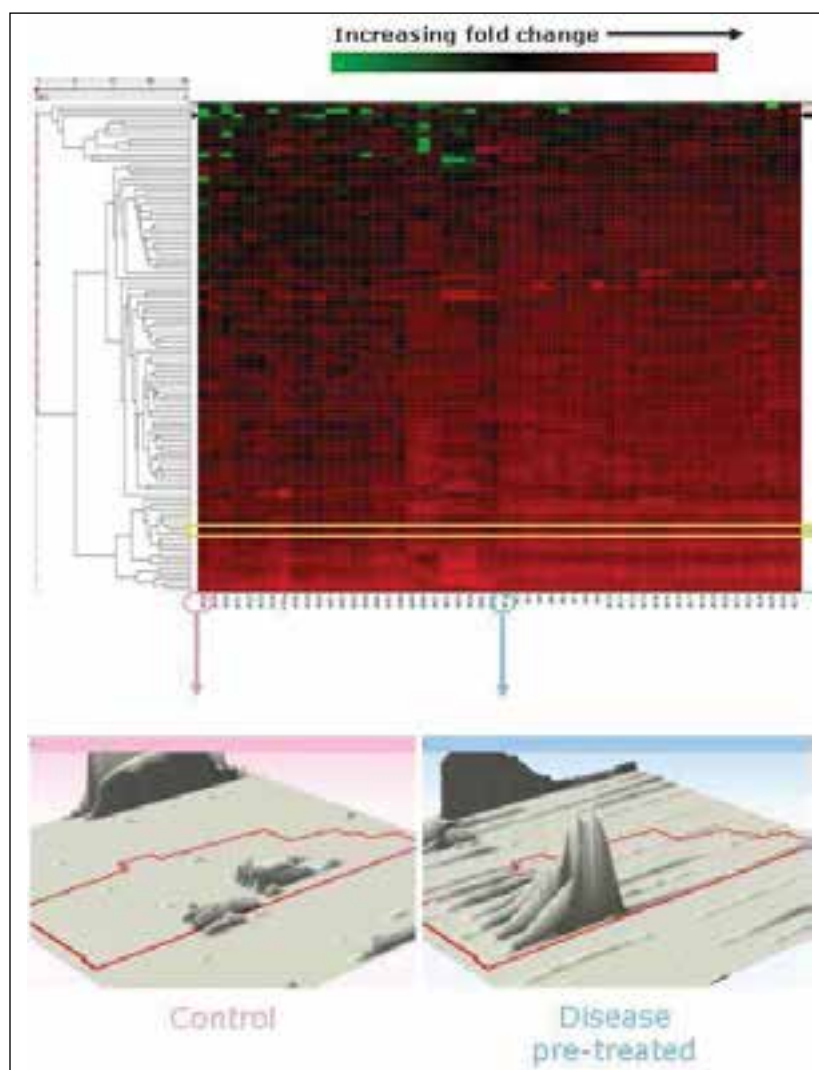


Figure 5. Hierarchal cluster analysis regulated proteins with a minimum of three identified peptides and a fold change greater than two. The highlighted region represents prostaglandin with associated 3D montage images for TMLLQPAGSLGSYSYR.
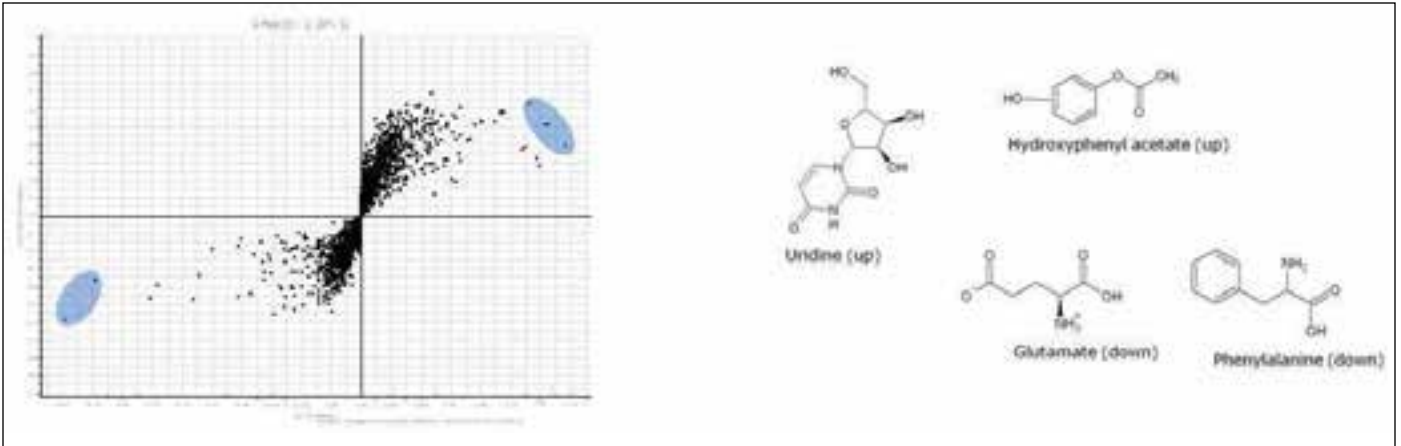
*Figure 6. Metabolite loadings plot from OPLS-DA analysis of disease pre-treated versus control subjects based in positive ion mode. Metabolites contributing the greatest variance are represented within the blue shaded areas with examples provided.*
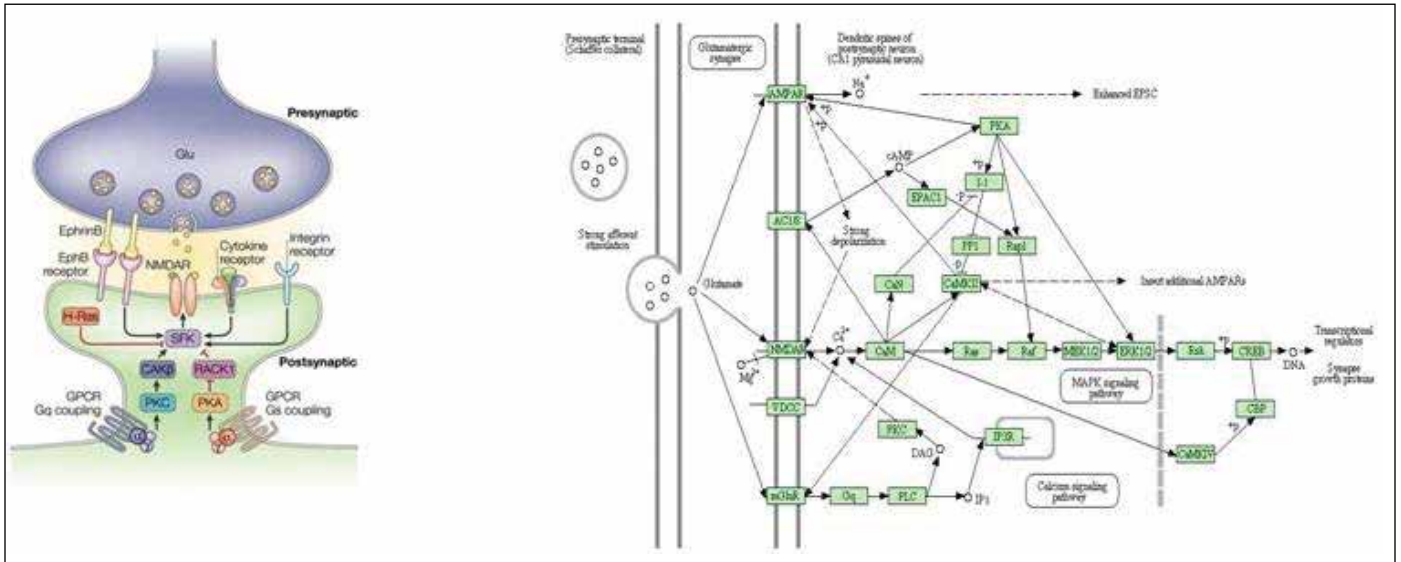


*Figure 7. Neuronal system pathway, specifically highlighting the role of the glutamate [NMDA] receptor subunit and glutamate for downstream transmission in the postsynaptic cell.*

## CONCLUSIONS

- 80% of the proteins identified were expressed, with 30% of proteins having a maximum fold change ≥ 2 and ANOVA (p) value ≤ 0.05.

- The majority of identified proteins were glycosylated, of which many showed changes in relative abundance.

- PCA analysis shows both protein and metabolite data to be complimentary.

- A variety of analytes were identified as contributing towards the metabolite variance.

- Complementary information obtained from metabolite and protein analysis has been shown through the use of glutamate and NMDA within the neuronal system pathway.

- A label-free multi-omics approach has been applied for the analysis of the urine of INS patients by implementing HDMS$^E$, which provides both qualitative and quantitative information in a single experiment.

### References

1. Vaezzadeh AR, Briscoe AC, Steen H, Lee RS. One-step sample concentration, purification and albumin depletion method for urinary proteomics. J Proteome Res. 2010;9(11):6082-89.

2. Li GZ, Vissers JP, Silva JC, Golick D, Gorenstein MV, Geromanos SJ. Database searching and accounting of multiplexed precursor and product ion spectra from the data independent analysis of simple and complex peptide mixtures. Proteomics. 2009 Mar;9(6):1696-719.

3. Han CL, Chien CW, Chen WC, Chen YR, Wu CP, Li H, Chen YJ. A multiplexed quantitative strategy for membrane proteomics: opportunities for mining therapeutic targets for autosomal dominant polycystic kidney disease. Mol Cell Proteomics. 2008 Oct;7(10):1983-97.

4. Salter MW, Kalia, LV. Src kinases: a hub for NMDA receptor regulation. Nature Reviews Neuroscience, 2004 April; 5: 317-328.

## Waters
### THE SCIENCE OF WHAT'S POSSIBLE.®

**Waters Corporation**
34 Maple Street
Milford, MA 01757 U.S.A.
T: 1 508 478 2000
F: 1 508 872 1990
www.waters.com

Waters
THE SCIENCE OF WHAT'S POSSIBLE.®

# Metabolomics of Broccoli Sprouts Using UPLC with Ion Mobility Enabled LC/MSE and TransOmics Informatics

Mariateresa Maldini[1], Simona Baima[1], Fausta Natella[1], Cristina Scaccini[1], James Langridge[2], and Giuseppe Astarita[2]
[1]National Research Institute on Food and Nutrition, Rome, Italy; [2]Waters Corporation, Milford, MA, USA

## APPLICATION BENEFITS

Use of the Waters Omics Research Platform, which combines UPLC® with ion mobility LC/MSE and TransOmics™ Informatics, allows for the rapid characterization of molecular phenotypes of plants that are exposed to different environmental stimuli.

## WATERS SOLUTIONS

Omics Research Platform
with TransOmics Informatics

ACQUITY UPLC® System

SYNAPT® G2-S HDMS®

## KEY WORDS

Lipid, metabolomics, lipidomics, natural products, food, nutrition, HDMS Compare

## INTRODUCTION

Cruciferous vegetables, such as broccoli, cabbage, kale, and brussels sprouts, are known to be anti-carcinogenic and possess antioxidant effects. They are widely consumed in the world, and represent a rich source of bioactive metabolites[1] Young broccoli plants are an especially good source of chemoprotective metabolites, with levels several times greater than mature plants. Growth conditions and environmental stresses exert a significant influence on the metabolism of broccoli sprouts[2]

The aim of this work is to study how the complete set of small-molecule metabolites, the "metabolome," of broccoli sprouts is modulated under different growth conditions. As the metabolome reflects both genetic and environmental components (e.g., light conditions and nutrients), comprehensive metabolite profiles can describe a biological system in sufficient depth to closely reflect the ultimate phenotypes, as shown in Figure 1.
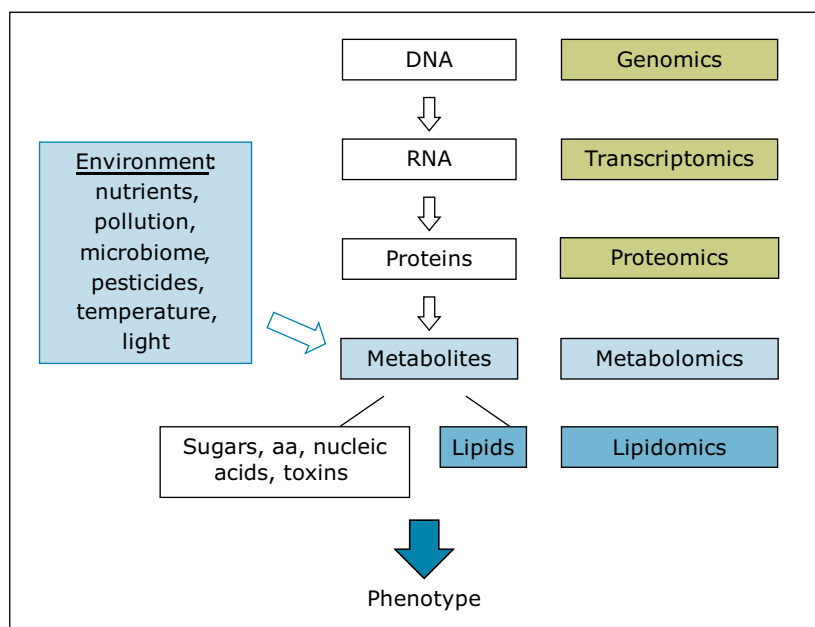


Figure 1. Metabolomics aims to screen all the metabolites present in biological samples. Metabolites can derive from both the generic imprint and from the environment (e.g., different growth conditions). Metabolites are counted in the order of thousands and have a wide range of chemical complexity and concentration. The profiling of the entire set of metabolites, or metabolome, characterizes the molecular phenotype of the biological system.

## EXPERIMENTAL

### Sample description

Broccoli seeds (*Brassica oleracea* L. var. *botrytis* subvar. *cymosa*) were germinated in the germination cylinder of Vitaseed sprouter, and grown hydroponically for five days at 21 °C in a plant growth chamber (Clf Plant Climatics, Wertingen, Germany) equipped with PHILIPS Master TL-D 36W/840 cool-white fluorescent tubes providing a photosynthetic photon flux density of 110 mmol m-2 s-1, under three different light regimes: a) dark (achieved by covering the sprouting device with a cardboard box), b) continuous light, and c) continuous light plus two days of treatment with sucrose 176 mM.

Sprout samples, collected from the germination cylinder, were immediately frozen in liquid nitrogen and stored at -80 °C. Frozen sprouts were ground to a fine powder in a Waring blendor cooled with liquid nitrogen. Each sample of broccoli sprouts was extracted with 100% methanol (sample to solvent ratio 1:25 w/v) at 70 °C for 30 minutes under vortex mixing to facilitate the extraction. The samples were successively centrifuged (4000 rpm, 30 minutes, 4 °C), the supernatants were collected, and the solvent was completely removed using a rotary evaporator under vacuum at 40 °C. The dried samples were dissolved in methanol with the same volume of extraction, and filtered through 0.20-μm syringe PVDF filters.[3]

### UPLC conditions

| | |
|---|---|
| System: | ACQUITY UPLC |
| Column: | ACQUITY CSH $C_{18}$ 2.1 x 100 mm, 1.7 μm |
| Mobile phase A: | 60:40 10 mM $NH_4HCO_2$ in $ACN/H_2O$ |
| Mobile phase B: | 90:10 10 mM $NH_4HCO_2$ in IPA/ACN |
| Flow rate: | 0.4 mL/min |
| Column temp.: | 55 °C |
| Injection volume: | 5.0 μL |

Elution gradient:

| Min | A% | B% | Curve |
|---|---|---|---|
| Initial | 60.0 | 40.0 | Initial |
| 2.0 | 57.0 | 43.0 | 6 |
| 2.1 | 50.0 | 50.0 | 1 |
| 12.0 | 46.0 | 54.0 | 6 |
| 12.1 | 30.0 | 70.0 | 1 |
| 18.0 | 1.0 | 99.0 | 6 |
| 18.1 | 60.0 | 40.0 | 6 |
| 20.0 | 60.0 | 40.0 | 1 |

### MS conditions

UPLC analytical column was connected to the ESI probe using PEEK Tubing, 1/16 inch, (1.6 mm) O.D. x 0.004 inch. (0.100 mm) I.D. x 5 ft (1.5 m) length, cut to 400 mm in length.

| | |
|---|---|
| Mass spectrometer: | SYNAPT G2-S HDMS |
| Mode of operation: | Tof HDMS[E] |
| Ionization: | ESI +ve and -ve |
| Capillary voltage: | 2.0 KV (+ve) and 1.0 KV (-ve) |
| Cone voltage: | 30.0 V |
| Transfer CE: | Ramp 20 to 50 V |
| Source temp.: | 120 °C |
| Desolvation temp.: | 550 °C |
| Cone gas: | 50 L/h |
| MS gas: | Nitrogen |
| IMS T-Wave™ velocity: | 900 m/s |
| IMS T-Wave height: | 40 V |
| Acquisition range: | 50 to 1200 |

### Data acquisition and processing:

TransOmics Informatics and HDMS Compare for SYNAPT Systems

## RESULTS AND DISCUSSION

We applied an untargeted metabolomics approach (Figure 1) to identify molecular alterations induced by different growth conditions in broccoli sprouts (Figure 2). Metabolites were extracted from the sprouts, and analyzed using UltraPerformance LC® (UPLC) coupled with an ion mobility enabled QTof mass spectrometer, the SYNAPT G2-S HDMS (Figure 3), as reported in the Experimental conditions.
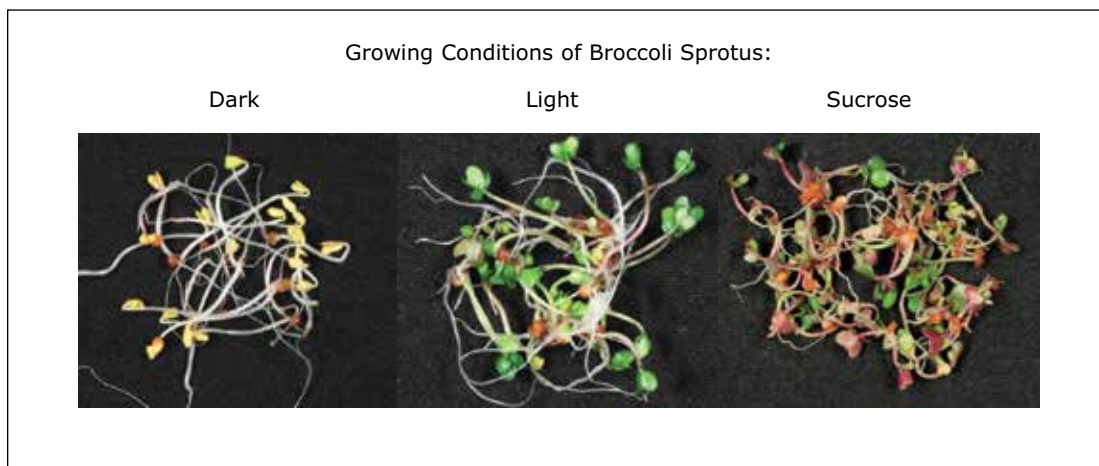


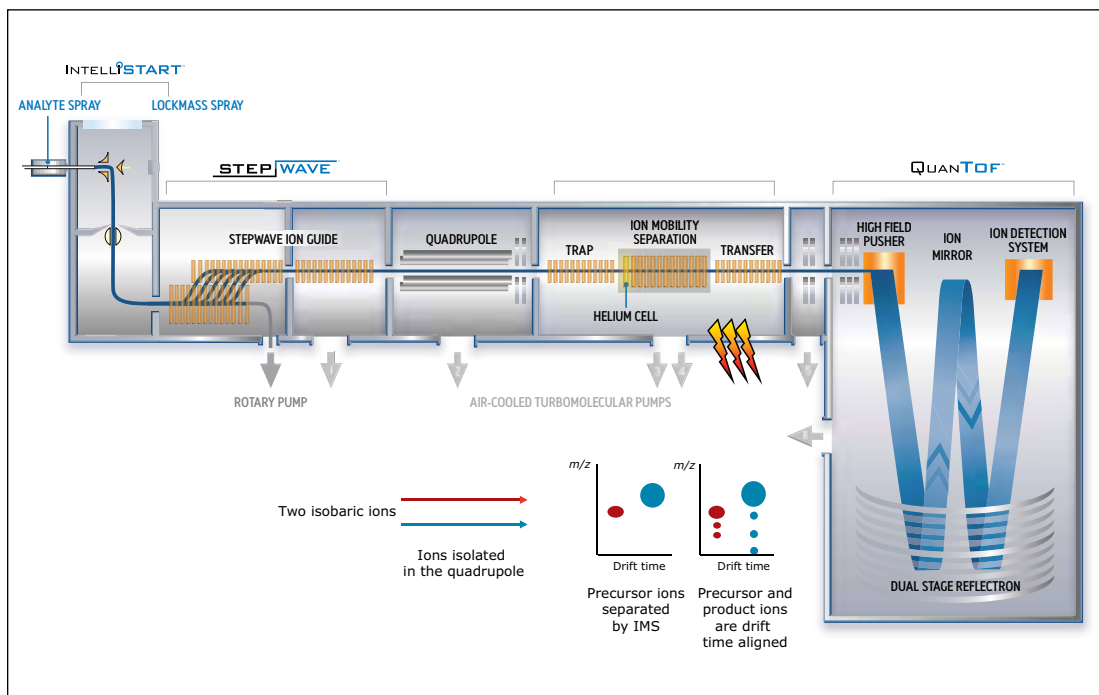Figure 2. Broccoli sprout samples grown under different conditions.



Figure 3. Schematic of the SYNAPT G2-S HDMS System configuration showing the ion mobility cell and the collision cell used to fragment the metabolites in HDMS[E] mode.

UPLC maximized the separation of a wide range of chemical complexity present in the broccoli sprouts (Figure 4). Metabolites were ionized using ESI and, subsequently entered into the vacuum region of the MS system where they passed through the tri-wave ion mobility separation (IMS) cell (Figures 3, 4, and 5).
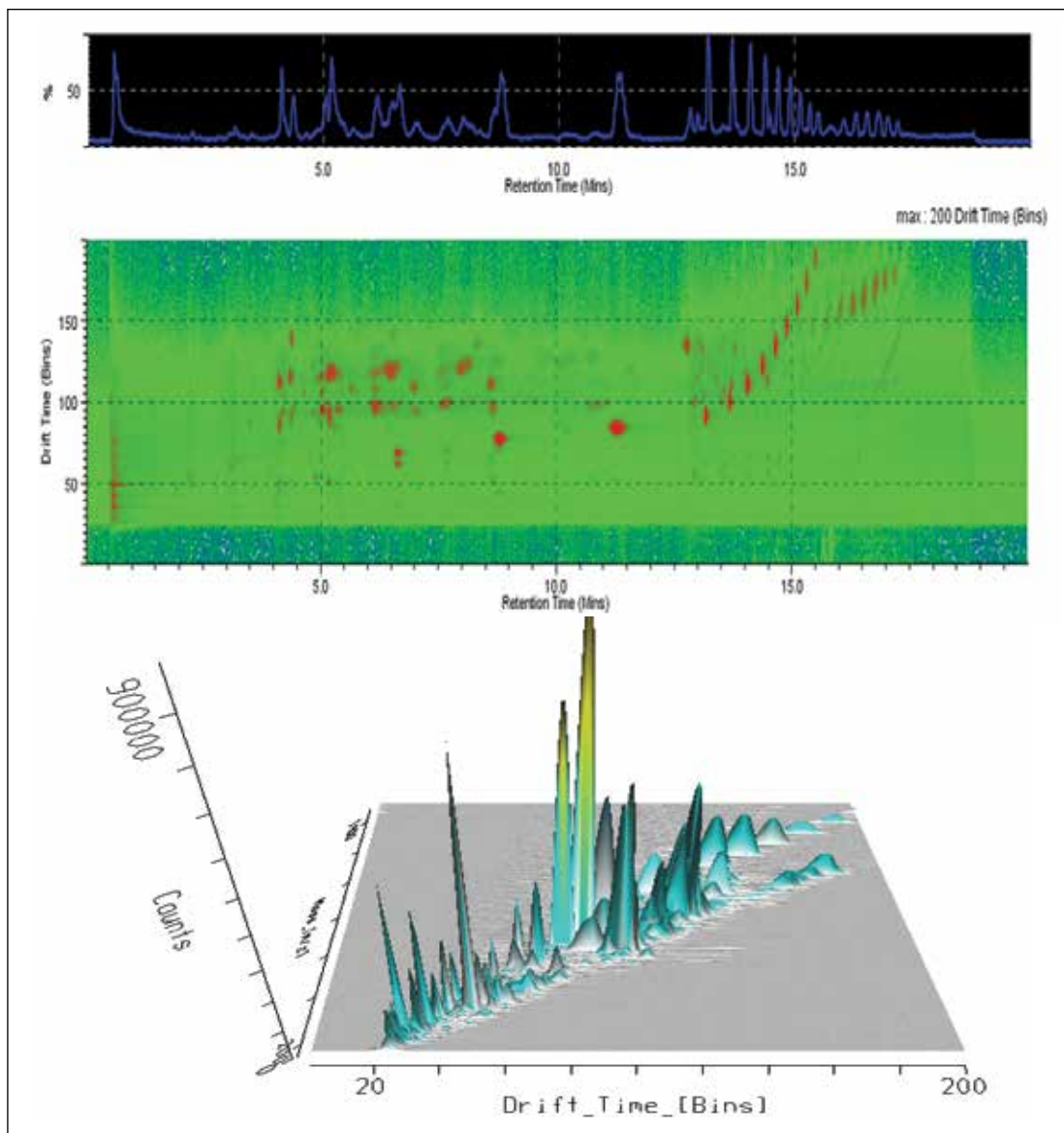


Figure 4. After UPLC separation, metabolites can be further separated in another dimension using ion mobility cell before MS detection This mode of acquisition is named High Definition Mass Spectrometry® (HDMS). Metabolites show characteristic drift times according to their size, shape and charge. The combination of UPLC and ion mobility increase peak capacity and specificity in the quantification and identification process.

The T-Wave IMS device uses RF-confining fields to constrain the ions in the radial direction, while a super-imposed repeating DC voltage wave propels ions in the axial direction through the dense gas-filled cell. The height and speed of the wave can be used to separate ions by their ion mobility[1]. As such, metabolites migrate with characteristic mobility times (drift times) according to their size and shape (Figures 3, 4, and 5). Therefore, IMS provides an additional degree of separation to chromatography, improving peak capacity over conventional UPLC/MS techniques (Figure 5).
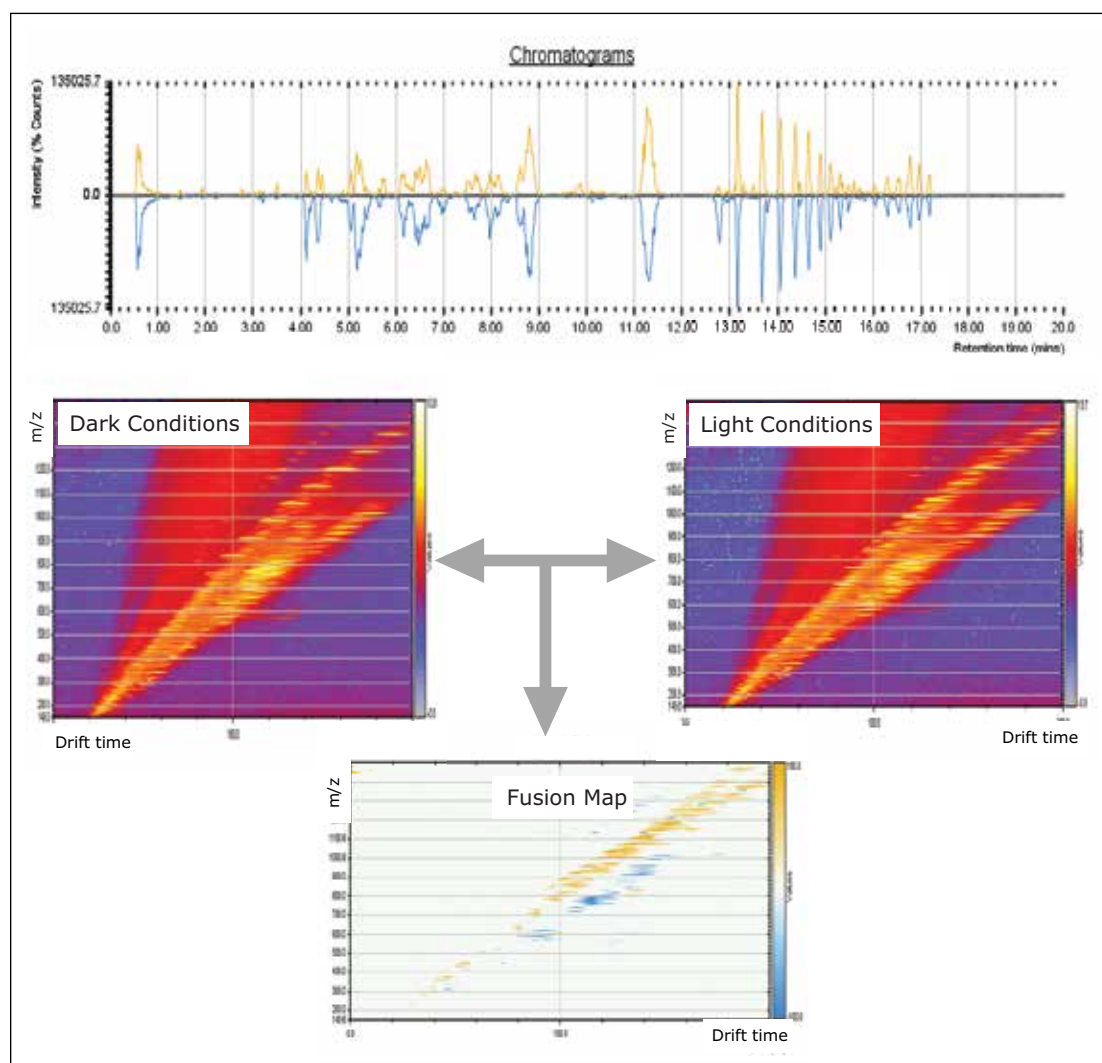


*Figure 5. Representative UPLC/UPLC/MS chromatograms showing qualitative differences between broccoli sprout samples grown under light or dark conditions (upper panel). HDMS Compare Software was used to compare condition-specific molecular maps, highlighting key areas of significant differences between two samples with two different colors (bottom panel).*

To aid in the identification and structural elucidation of metabolites, collision induced dissociation (CID) of metabolite precursor ions after IMS separation is performed using a particular mode of operation named HDMS[E]. This approach utilizes alternating low and elevated collision energy in the transfer cell, thus recording all of the precursor and fragment ions in a parallel and continuous manner (Figure 6). The alternating scans acquire low collision energy data, generating information about the intact precursor ions, and elevated collision energy data, that provides information about associated fragment ions (Figure 6). The incorporation of ion mobility separation of coeluting precursor ions before CID fragmentation produces a cleaner MS/MS product ion spectra, facilitating easier metabolite identification, as shown in the bottom panel of Figure 6.
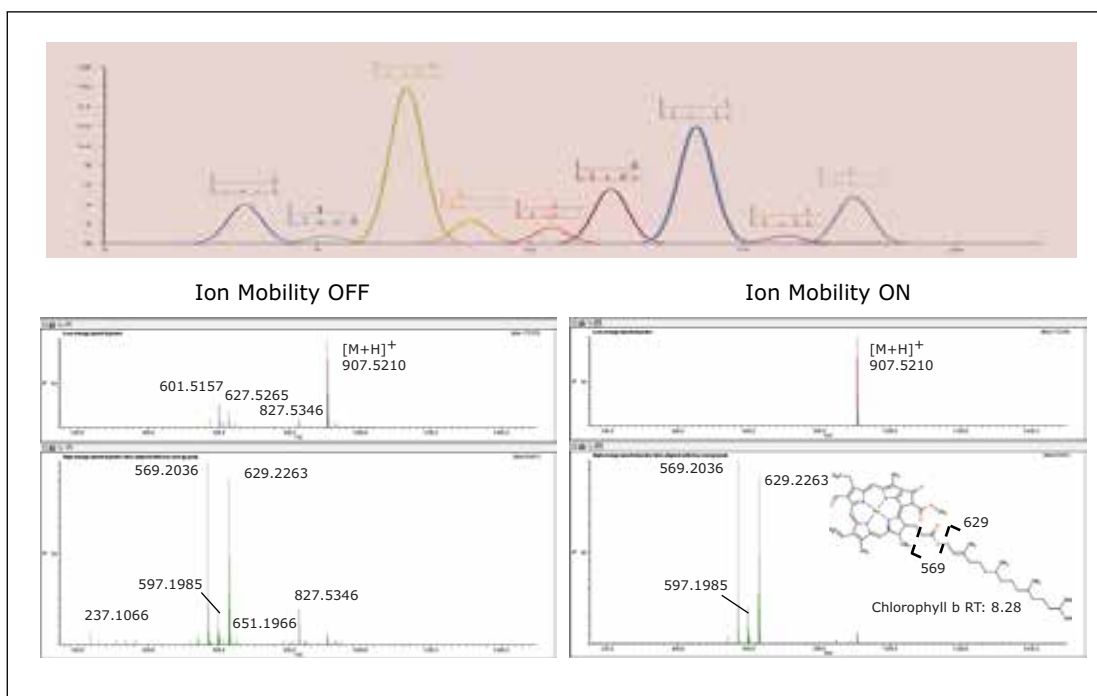


Figure 6. Representative UPLC/HDMS[E] chromatogram showing the acquisition of both precursors and fragment spectra information along one single chromatographic run (upper panel). Applying high collision energy in the transfer collision cell, precursor molecules can be broken down into constituent parts, to deduce the original structure (bottom panel). In this example, the identification of the chlorophyll structure is based on the observation of characteristic fragments generated with high energy, using MS[E] which matched with a compound search (Figure 8) and previously published results.[4]

The analysis provided a metabolite profile, which represents a biochemical snapshot of the metabolite inventory for each sample analyzed. Differences at the metabolite level between groups were analyzed using TransOmics Informatics which provided multivariate statistical analyses tools, including principal component analysis (PCA) (Figure 7A), correlation analysis (Figure 7B), review compound (Figure 8A), and database search functionalities (Figure 8B) for metabolite identification.

Preliminary results suggest that growth conditions induce specific alterations in the "metabolome" of broccoli sprouts, some of which are strictly related to photosynthetic processes.
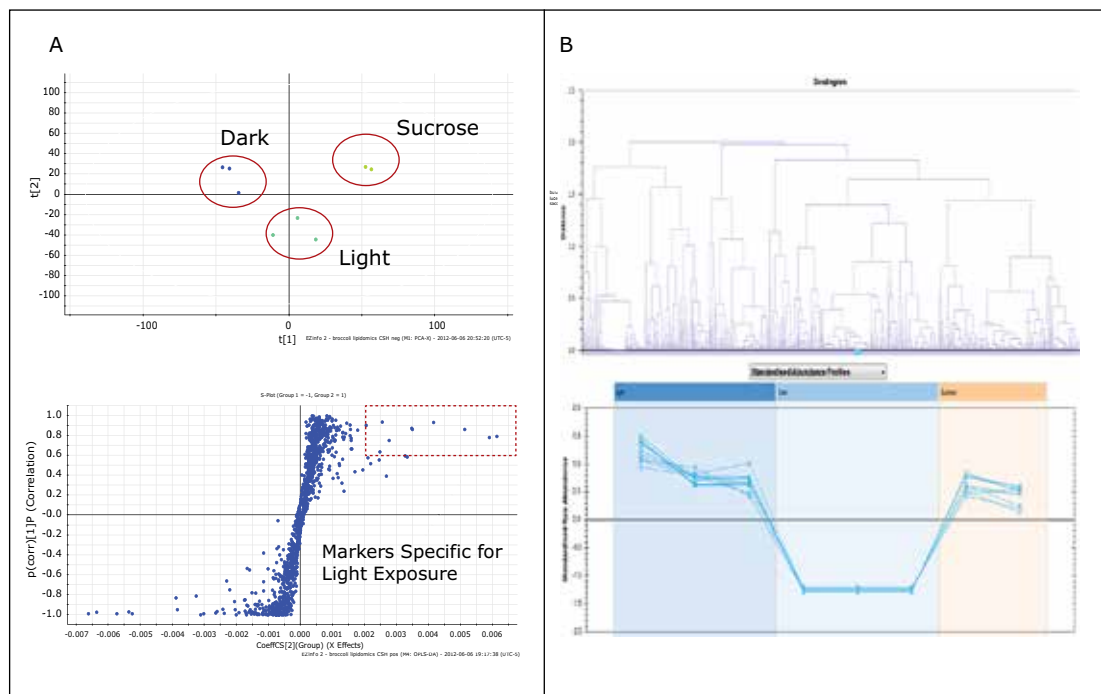


Figure 7. TransOmics multi-variate statistical analysis of the UPLC/HDMS$^E$ runs (A) allowed to separate samples into clusters, isolating the metabolites that contributed most to the variance among groups. Correlation analysis (B) helped to identify similar patterns of alterations among metabolites.
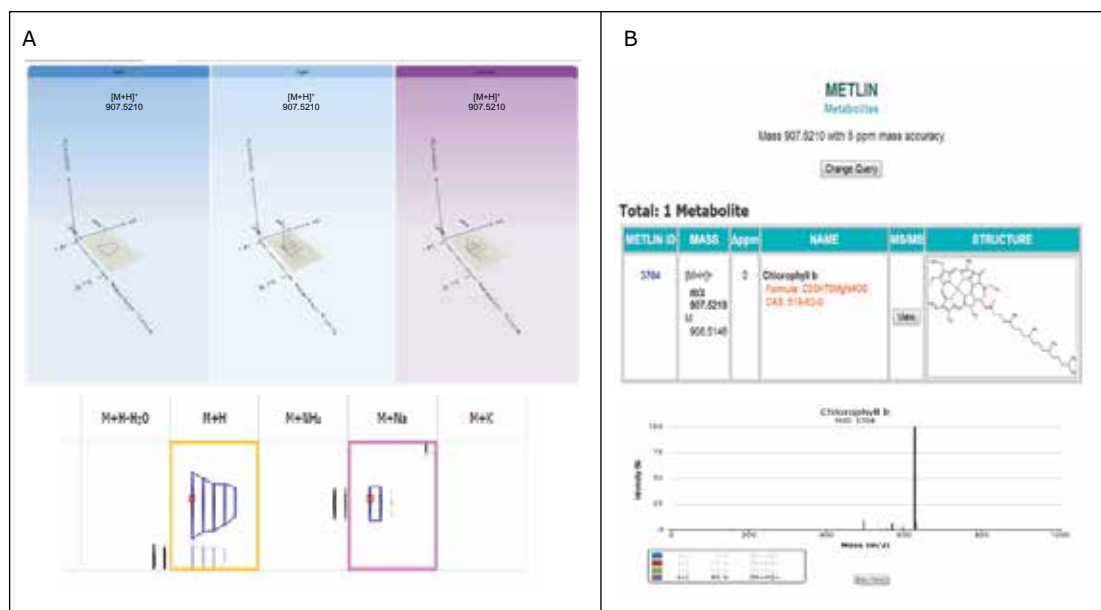


Figure 8. The statistical identification of metabolic alterations was followed by a review of the measurements (e.g., 3D montage and adducts deconvolution, (A) and a search on local or online databases (e.g., METLIN, (B)) for structural identification. In this example, a database search lead to a putative structure of a chlorophyll metabolite, which was only detected in broccoli sprouts grown in light conditions (A).

## CONCLUSIONS

The Waters Omics Research Platform with TransOmics Informatics, featuring UPLC and HDMS$^E$ technologies, enables researchers to improve how they screen and differentiate molecular phenotypes of plants exposed to different environmental stimuli. This high-throughput approach has applications in agricultural, food, and nutritional, as well as natural product research.

**References**

1. Jahangir M, Abdel-Farid IB, Kim HK, Choi YH, Verpoorte R. Metal ion-inducing metabolite accumulation in *Brassica rapa*. *Environmental and Experimental Botany.* 2009; 67: 23-33.

2. Pérez-Balibrea S, Moreno D, Garcìa-Viguera C. Glucosinolates in broccoli sprouts (*Brassica oleracea var. italica*) as conditioned by sulphate supply during germination. *Journal of the Science of Food and Agriculture.* 2008; 88: 904-910.

3. Maldini M, Baima S, Morelli G, Scaccini C, Natella F. A liquid chromatography-mass spectrometry approach to study "glucosinoloma" in broccoli sprouts. *Journal of Mass Spectrometry.* 2012; 47: 1198-1206.

4. Fu W, Magnúsdóttir M, Brynjólfson S, Palsson BØ, Paglia G. UPLC-UV MS(E) analysis for quantification and identification of major carotenoid and chlorophyll species in algae. *Anal Bioanal Chem.* 2012 Dec; 404(10): 3145-54.

## Waters
**THE SCIENCE OF WHAT'S POSSIBLE.®**

**Waters Corporation**
34 Maple Street
Milford, MA 01757 U.S.A.
T: 1 508 478 2000
F: 1 508 872 1990
www.waters.com

Waters

THE SCIENCE OF WHAT'S POSSIBLE.®

# Qualitative and Quantitative Characterization of the Metabolome, Lipidome, and Proteome of Human Hepatocytes Stably Transfected with Cytochrome P450 2E1 Using Data Independent LC/MS

Suzanne Geenen,[1] Cristian Cojocariu,[2] Lee Gethings,[2] Janet Hammond,[2] Giorgis Isaac,[3] Lucy Fernandes,[2] Robert Tonge,[2] Johannes Vissers,[2] James Langrige,[2] Ian Wilson[1]

[1] AstraZeneca, Macclesfield, UK; [2] Waters Corporation, Manchester, UK; [3] Waters Corporation, Milford, MA, US

## APPLICATION BENEFITS

A label-free multi-omics approach has been applied for the analysis of the transfected human hepatocyte cells by implementing LC/HDMS[E] (LC-DIA-IM-MS), providing both qualitative and quantitative information within a single experiment.

## WATERS SOLUTIONS

ACQUITY UPLC® System

nanoACQUITY® UPLC® System

SYNAPT® G2 HDMS™

CSH™ Technology

ProteinLynx GlobalSERVER™

MarkerLynx™ Application Manager

TransOmics™ Informatics Software

MS[E]/HDMS[E]

Triwave® Technology

## KEY WORDS

Omics, metabolomics, lipidomics, proteomics, THLE cells

## INTRODUCTION

Drug toxicity is a major reason for the failure of candidate pharmaceuticals during their development. Therefore, it is important to realize the potential for toxicity in a timely fashion. Many xenobiotics are bioactivated into toxic metabolites by cytochromes P450 (CYP), as shown in Figure 1. However, the activity of these enzymes typically falls in *in vitro* systems. Recently, a transformed human hepatocyte cell line (THLE) became available, where the metabolic activity of specific CYP isoforms is maintained. THLE cells could be an ideal system to examine the potential toxicity of candidate pharmaceuticals. The baseline effect of the addition of CYP2E1 gene, which encodes a member of the cytochrome P450 superfamily of enzymes into THLE hepatocytes, has been characterized to better understand the biochemistry of this model system. In this application note, a label-free multi-omics approach has been applied for the analysis of the transfected human hepatocyte cell by implementing LC/HDMS[E] (LC-DIA-IM-MS), providing both qualitative and quantitative information within a single experiment.
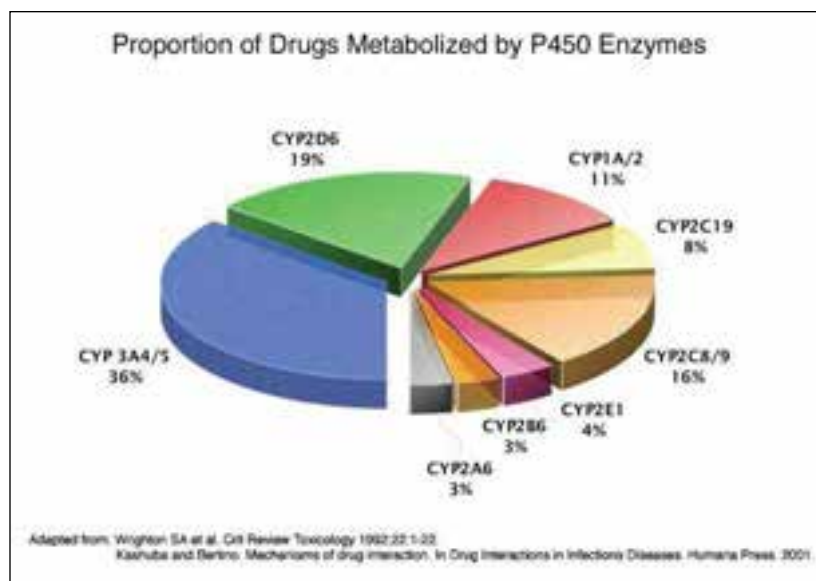


Figure 1. CYPs are the major enzymes involved in drug metabolism, accounting for about 75% of the total metabolism. Most drugs undergo deactivation by CYPs, either directly, or by facilitated excretion from the body.

## EXPERIMENTAL

### Sample preparation

Dedicated and independent sample preparation protocols were applied in order to isolate metabolites, lipids, or proteins, as shown in Figure 2. Three independent replicates of THLE null or THLE+2E1 cells were investigated for all analyte classes. Proteins were recovered and digested with trypsin overnight.
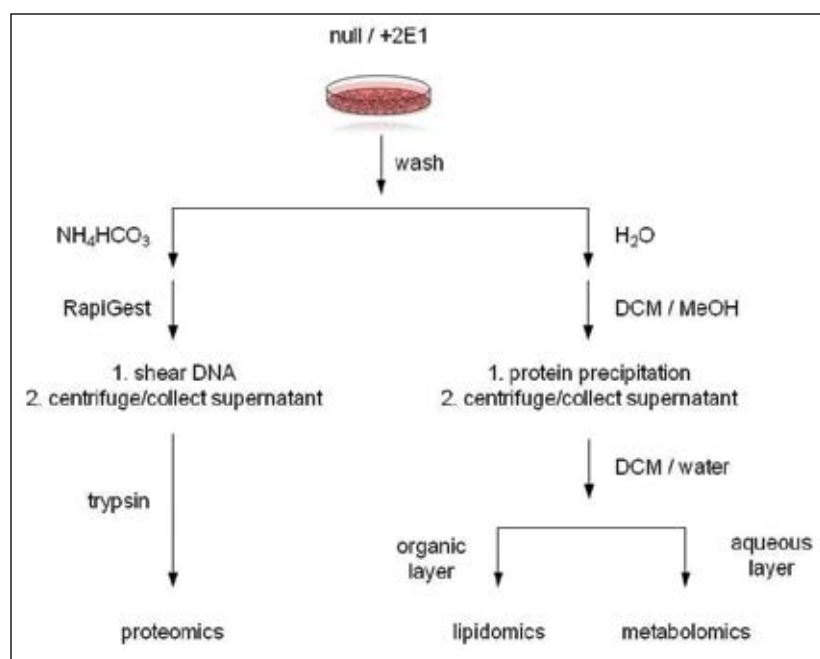


*Figure 2. Sample preparation protocol cytochrome P450 2E1 THLE cells for integrated proteomics, lipidomics, and metabolomics LC/MS experiments/studies.*

### LC/MS conditions

Waters® Omics Research Platform Solution with TransOmics Informatics powered by Nonlinear Dynamics was used for all experiments; generic application-dependent LC conditions were applied throughout. In all instances, MS data were acquired using a data independent analysis (DIA) approach, MS[E], where the energy applied to the collision cell was switched between a low and elevated energy state during alternate scans. For the proteomics experiments, ion mobility separation (IM) was incorporated into the analytical schema (IM-DIA), HDMS[E]. The principle of an HDMS[E] acquisition is shown in Figure 3. Precursor and product ions were associated using dedicated algorithms by retention and/or drift time alignment. For structural elucidation, supplementary MS/MS experiments were conducted for the metabolomics and lipidomics studies.

Label-free LC/MS was used for qualitative and quantitative peptide/protein analyses. Experiments were conducted using a 90 min gradient from 5% to 40% acetonitrile (0.1% formic acid) at 300 nL/min, using a nanoACQUITY UPLC System and an ACQUITY UPLC BEH 1.7 μm $C_{18}$ reversed phase 75 μm x 20 cm nanoscale LC Column.

For metabolite identification, the LC/MS experiments consisted of a 10 min gradient from 0% to 50% acetonitrile (0.1% formic acid) at 500 μL/min, using an ACQUITY UPLC System. Here, an ACQUITY UPLC BEH 1.7 μm $C_{18}$ reversed phase 2.1 x 10 cm LC Column was used.

The lipid separations were conducted with a CSH (Charged Surface Hybrid) $C_{18}$, 1.7 μm, 2.1 x 100 mm Column, also connected to an ACQUITY UPLC System. Mobile phase A consisted of 10 mM $NH_4HCO_2$ in ACN/$H_2O$ (60/40); and mobile phase B of 10 mM $NH_4HCO_2$ in IPA/ACN (90/10). The initial composition of the gradient was 40% B, which was stepped from 43% to 54% B from 2 to 12 min, followed by an additional gradient step from 70% to 99% from 12.1 to 18.0 min. The column flow rate was 400 μL/min and the column temperature maintained at 55 °C.

## Data acquisition

Data were acquired through data independent analysis (DIA) that utilized a nanoACQUITY UPLC or ACQUITY UPLC System directly interfaced to a hybrid IM-oaToF SYNAPT G2 Mass Spectrometer.

## Bioinformatics

The LC/MS peptide data were processed and searched with ProteinLynx GlobalSERVER v.3.0. Normalized label-free quantification was achieved using TransOmics Informatics Software and additional statistical analysis conducted with Spotfire and EZinfo. The resulting metabolomic and lipidomic data were processed using either MarkerLynx Application Manager or TransOmics Informatics Software, and complementary statistical analysis was conducted with EZinfo.
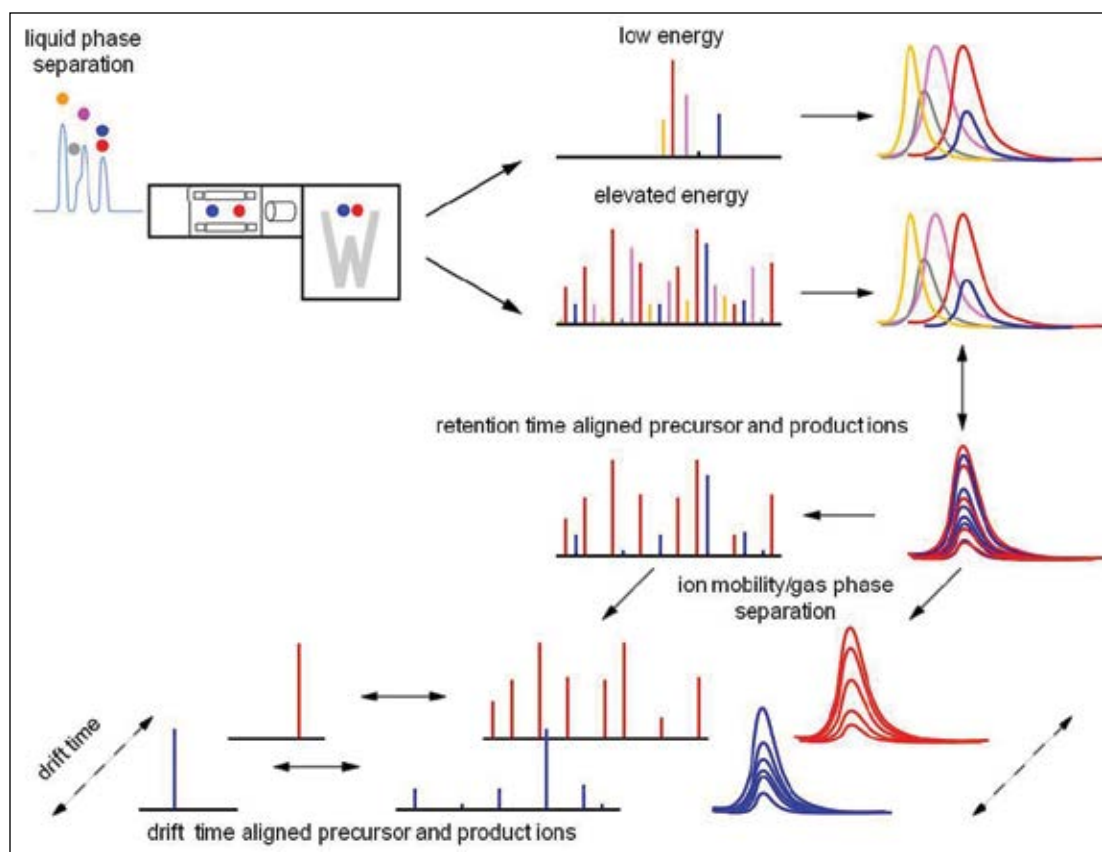


Figure 3. Retention and drift time principle ion mobility enabled data-independent LC/HDMSE analysis (LC-DIA-IM-MS).

## RESULTS AND DISCUSSION

Small amounts of the isolated and purified samples were LC/MS analyzed to identify, quantify, and investigate the metabolomic, lipidomic, and proteomic variances between THLE null (CYP2E1 gene absent) and THLE+2E1 cells. Figure 4 shows the type of chromatographic profiles that were typically obtained for the samples, providing chromatographic definition for downstream analysis of the various data streams. In a similar fashion, spectral profiles were obtained for all sample types and in the instance of the proteomics datasets, ion mobility profiles were obtained as well.
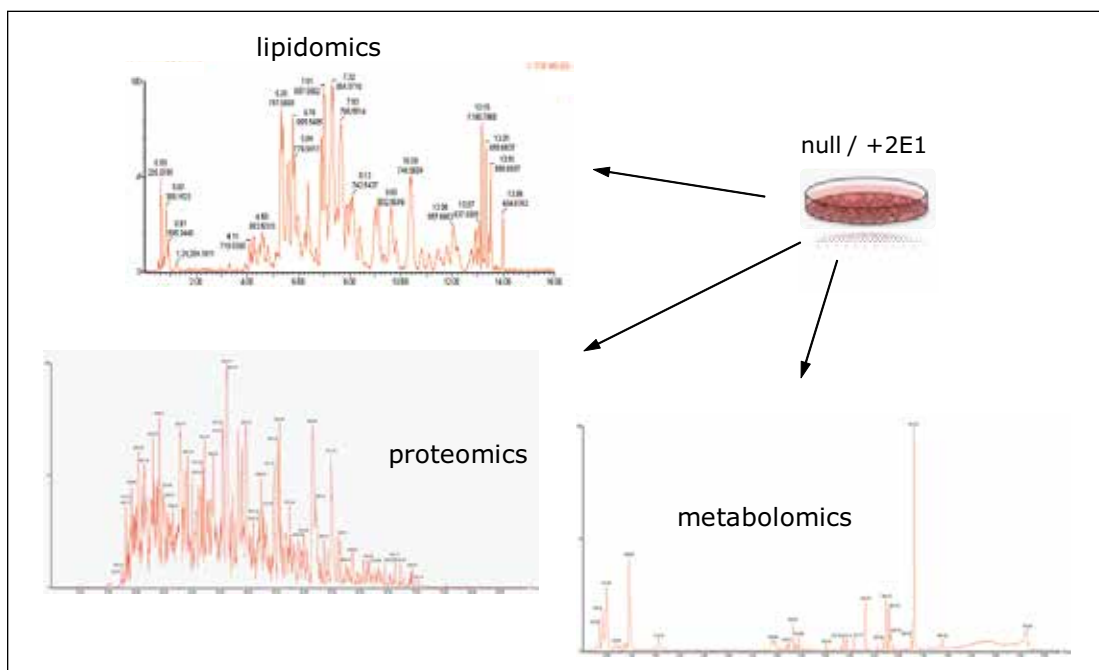


*Figure 4. Chromatographic example profiles THLE+2E1 cells. The lipidomics experiments were conducted in ESI(-) mode, whereas the metabolomics and proteomics experiments were carried out in ESI(+) mode.*

Principal component analysis (PCA) was used in the first instance to identify and highlight significant differences between THLE null and THLE+2E1 cells; an example is shown in Figure 4. For all experiments, good technical LC/MS measurement replication was observed, with slightly greater biological and/or sample preparation variation. The top pane of Figure 4 illustrates group level analysis of the metabolomics data using TransOmics Informatics Software, whereas the bottom pane of Figure 4 demonstrates analysis at the sample level using EZinfo. Further analysis of the data using MarkerLynx Application Manager indicates significant variance in the metabolic expression of guanine and heteropyrithiamine (data not shown). Similar clustering patterns were observed for the lipid, metabolite, and protein datasets.
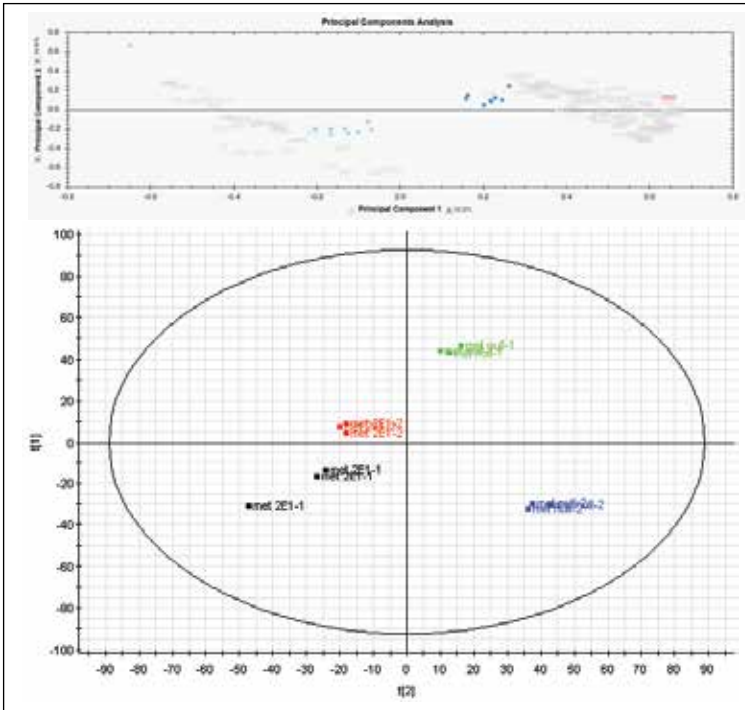
*Figure 5. TransOmics Informatics Software (top) and EZinfo (bottom) principal component analysis of the metabolism data, illustrating THLE null versus THLE+2E1 group and sample level differences, respectively.*

The estimated protein amounts were normalized and exported to facilitate additional statistical analysis at the protein level. First, hierarchical clustering was conducted, which revealed primary grouping at the technical level and secondary grouping at the sample level, as shown in Figure 6. Next, protein regulation values were calculated as a function of sample group level regulation probability. Only the proteins that were identified for which a regulation probability value could be expressed and found to be common to both samples; *i.e.* THLE null and THLE+2E1 were considered for protein/gene pathway analysis using Ingenuity IPA. The most significantly enriched canonical signalling pathways were EIF2, regulation of EIF4 and p70S6K, mTOR, Actin cytoskeleton, and ILK.
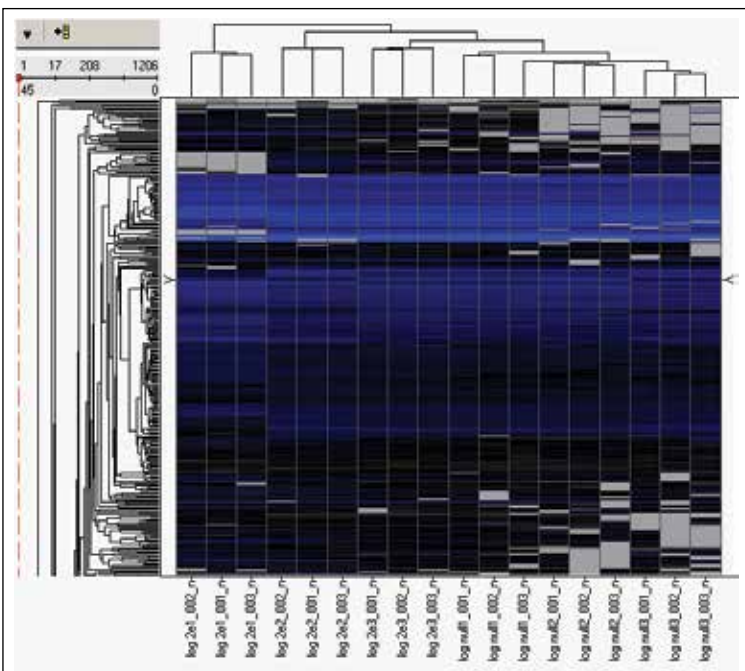


*Figure 6. Unsupervised hierarchical clustering protein data using TransOmics Informatics Software normalized, log-scaled estimated protein amounts as input values.*

The previously mentioned metabolites interplay with the proteins/genes in the EIF2 (eukaryotic initiation factor 2) signalling pathway, as shown in Figure 7. For example, EIF2B is a guanine nucleotide releasing factor required to release Guanosine diphosphate (GDP), so that a new Guanosine-5'-triphosphate (GTP) molecule can bind and activate EIF2. Moreover, the presence of thiamines is known to inhibit the synthesis of 40S ribosomal subunits. These observations are not unexpected since CYPS readily induce oxidative stress when no substrate is available. Moreover, the EIF2 signalling pathway is one of the primary responders to cellular stress.



eIF2B is a guanine nucleotide releasing factor

presence inhibits 40S ribosomal subunit synthesis

Figure 7. EIF2 signalling pathway, which illustrates up-regulated genes/protein (groups) in green and down-regulated components in red. The size and direction (angle) of the arrows is a measure of the regulation value. The pathway is annotated with two components that were identified as part of the metabolomics track of the experiment/analysis.

## CONCLUSIONS

- A label-free multi-omics approach has been applied for the analysis of the transfected human hepatocyte cells by implementing LC/HDMS$^E$ (LC-DIA-IM-MS), providing both qualitative and quantitative information within a single experiment.

- Various clustering, statistical, and data analysis approaches show protein, lipid, and metabolite data to be complimentary.

- A variety of compounds were identified as contributing towards the metabolite and lipid variance.

- Approximately 20% of the proteins identified were significantly expressed with 10% of the proteins illustrating a p value ≤0.05 when common to both samples.

- Complementary information obtained from metabolite/lipid and protein analysis has been shown through the use of guanine and heteropyrithiamine within the EIF2 signaling pathway.

**References**

1. Liu H, Jones BE, Bradham C, Czaja MJ. Increased cytochrome P-450 2E1 expression sensitizes hepatocytes to c-Jun-mediated cell death from TNF-alpha. Am J Physiol Gastrointest Liver Physiol. 2002 Feb;282(2):G257-66.

2. Pavitt GD, Ron D. New Insights into Translational Regulation in the Endoplasmic Reticulum Unfolded Protein Response. Cold Spring Harb Perspect Biol. 2012 Apr 25; doi: 10.1101/cshperspect.a012278. [Epub ahead of print]

3. Silva JC, Gorenstein MV, Li GZ, Vissers JP, Geromanos SJ. Absolute quantification of proteins by LCMS$^E$: a virtue of parallel MS acquisition. Mol Cell Proteomics. 2006 Jan;5(1):144-56.

4. Rodríguez-Suárez E, Hughes C, Gethings L, Giles K, Wildgoose J, Stapels M, Fadgen KE, Geromanos SJ, Vissers JP, Elortza F, Langridge JI. An Ion Mobility Assisted Data Independent LC-MS Strategy for the Analysis of Complex Biological Samples. Current. Anal. Chem. special issue: Ion Mobility Spectrometry: Using Size and Shape to Understand Real-World Systems at the Molecular Level, HT-SBJ-CAC-0005.

## Waters
### THE SCIENCE OF WHAT'S POSSIBLE.®

**Waters Corporation**
34 Maple Street
Milford, MA 01757 U.S.A.
T: 1 508 478 2000
F: 1 508 872 1990
www.waters.com

Waters
THE SCIENCE OF WHAT'S POSSIBLE.®

# Metabolic Phenotyping Using Atmospheric Pressure Gas Chromatography-MS

Vladimir Shulaev,[2] Ghaste Manoj,[2,3] Steven Lai,[1] Carolina Salazar,[2] Nobuhiro Suzuki,[2] Janna Crossley,[2] Feroza Kaneez Coudhury,[2] Khadiza Zaman,[2] Ron Mittler,[2] James Langridge,[1] Robert Plumb,[1] Fulvio Mattivi,[3] Giuseppe Astarita[1]

[1] Waters Corporation, Milford, MA, USA
[2] Department of Biological Sciences, College of Arts and Sciences, University of North Texas, Denton, TX, USA
[3] Department of Food Quality and Nutrition, Research and Innovation Centre, Fondazione Edmund Mach,
   San Michele all'Adige, Italy

## APPLICATION BENEFITS

Atmospheric pressure gas chromatography mass spectrometry (APGC-MS) provides molecular ion information, which is typically absent when traditional vacuum source (i.e., electron ionization) gas chromatography mass spectrometry (GC-MS) is employed. This application note highlights the use of APGC-MS[E] for analysis in metabolomics.

## WATERS SOLUTIONS

SYNAPT® G2-S HDMS®
Mass Spectrometer

APGC System

Progenesis® QI Software

MassLynx® Software v4.1 SCN870

## KEY WORDS

Metabolomics, GC, atmospheric
pressure gas chromatography

## INTRODUCTION

Gas chromatography coupled with mass spectrometry is a well established analytical approach to metabolomics. The most widely used ionization technique is electron ionization (EI), which produces highly fragmented spectra that are library searchable. The molecular ion in an EI spectrum is often absent or of very low abundance. The lack of molecular ion information, especially for derivatized compounds in complex mixtures, can lead to incorrect identification when using spectral matching alone.

Atmospheric pressure GC (APGC) is a soft chemical ionization technique that generates a mass spectrum in which there is minimal fragmentation and conservation of the molecular ion (Figure 1). Additionally, when APGC is combined with a time of flight mass spectrometer (TOF-MS) for exact mass MS[E] analysis, comprehensive precursor and fragment ion spectral data is obtained for every detectable component in a complex sample. GC-MS[E] offers a simple route to providing high selectivity and confidence for simultaneous identification and quantitation in a single analysis.

Here we report an APGC-TOF MS[E] profiling approach and its application to metabolic fingerprinting of Arabidopsis.

## EXPERIMENTAL

### GC conditions

| | |
|---|---|
| GC system: | 7890A GC |
| Column: | HP-5MS column, 30 m length, 0.25 mm I.D., and 0.25 µm film thickness (Agilent Technologies) |
| Carrier gas: | Helium 1 mL/min |
| Temp. gradient: | Initial 70 °C, 5 °C/min to 310 °C, hold 1 min |
| Injection type: | split mode (split 4:1) |
| Injector temp.: | 230 °C |
| Injection vol.: | 1 µL |
| Make-up gas: | Nitrogen 400 mL/min |
| Transfer line temp.: | 310 °C |

### MS conditions

| | |
|---|---|
| MS system: | SYNAPT G2-S HDMS |
| Mode of operation: | TOF-MS$^E$ |
| Ionization: | APGC |
| Corona current: | 3 µA |
| Cone voltage: | 20 V |
| Source temp.: | 150 °C |
| Cone gas: | 10 L/h |
| Auxiliary gas flow: | 500 L/h |
| MS gas: | Nitrogen |
| Acquisition range: | 50 to 1200 |
| Transfer CE: | Ramp 20 to 40 V |

### Data management

Progenesis QI Software v1.0

MassLynx Software v4.1 SCN870

## Sample preparation

Arabidopsis thaliana seeds were grown under controlled conditions. Seedlings were harvested and polar metabolites were extracted and derivatized. The dried polar phase was methoximated for 90 minutes at 45 °C and trimethylsilylated for 30 minutes at 37 °C.
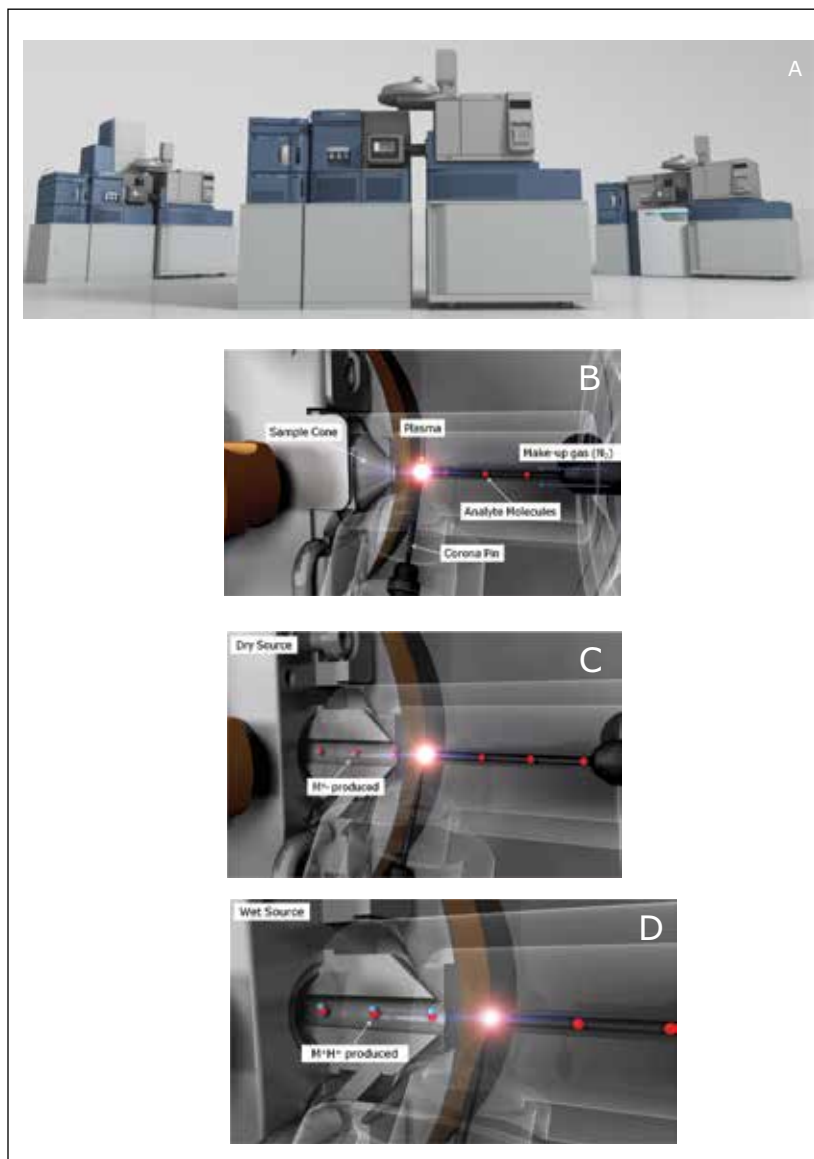


Figure 1. A) An APGC System can be coupled to various Waters MS instruments, including the Xevo® TQ-S and the SYNAPT G2-S. The changeover from UPLC® to APGC takes less than five minutes. B) The APGC source consists of an ion chamber with a corona pin inside. The GC column enters the source via a heated transfer line. Corona discharge creates nitrogen plasma within this region. Radical cations generated in this plasma interact and ionize the analyte molecules. The ions created are then transferred to the mass analyzer. C) Under dry source conditions the predominant method of ionization is charge transfer, generating molecular radical cations [M$^{+\bullet}$]. This method favours relatively non-polar molecules. D) When a protic solvent, such as water or methanol, is added to the source, the predominant ionisation is proton transfer, generating [M+H]$^+$ ions. This method favors relatively polar molecules.

## RESULTS AND DISCUSSION

APGC-MS analysis of commercially available pure reference compounds of known plant metabolites was performed. Following the analysis, an in-house APGC reference database was created containing retention times, and accurate mass-to-charge ratio (*m/z*) for precursor and fragment ions (Figure 2). APGC provided abundant molecular ions with minimal fragmentation at low collision energy (Figure 2A). To add confidence to compound identification, collision energy was ramped from 20 to 40 eV in the high energy function to generate maximum information from fragment ions (Figure 2A). Due to the use of charge exchange chemical ionization, elevated collision energy data resulted in a spectrum similar to the traditional EI data (Figure 2B).
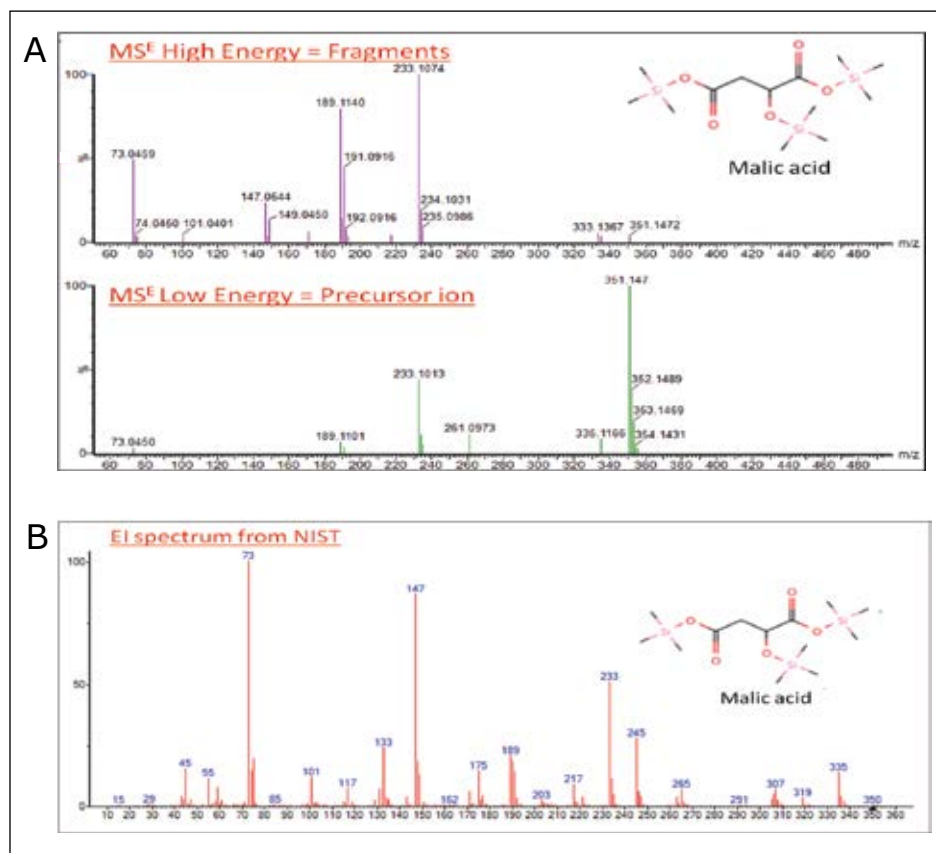


Figure 2. A) Synthetic reference standards were derivatized and analyzed by APGC-SYNAPT HDMS using MS$^E$ acquisition mode. This mode alternates between low and elevated collision energy to acquire both precursor and product ion information in a single analytical run. Advanced software algorithms align precursor and fragment spectra according to retention time and links them together. An in-house database of derivatized precursors and fragments, and retention times was created. B) EI spectrum of derivatized malic acid, obtained from the NIST library, was comparable with the MS$^E$ spectrum obtained by ramping up the collision energy from 20 to 40 eV in the high energy function.

Plant extracts were analyzed using APGC-TOF MS$^E$ and raw data were imported to Progenesis QI Software for processing and analysis (Figure 3A and B). Multivariate statistical analysis highlighted the molecular differences between groups of samples (Figure 4A and B). The Progenesis QI search engine Metascope allowed us to query experimentally-derived or in-house databases. We were able to customize the search parameters for the metabolite identification according to multiple orthogonal measures such as mass accuracy, retention time and fragmentation matching (Figure 4C). Additionally, if ion mobility is activated, collision cross-section (CCS) data, which reflect the ionic shape of the metabolites in the gas phase, can also be mined for identification.
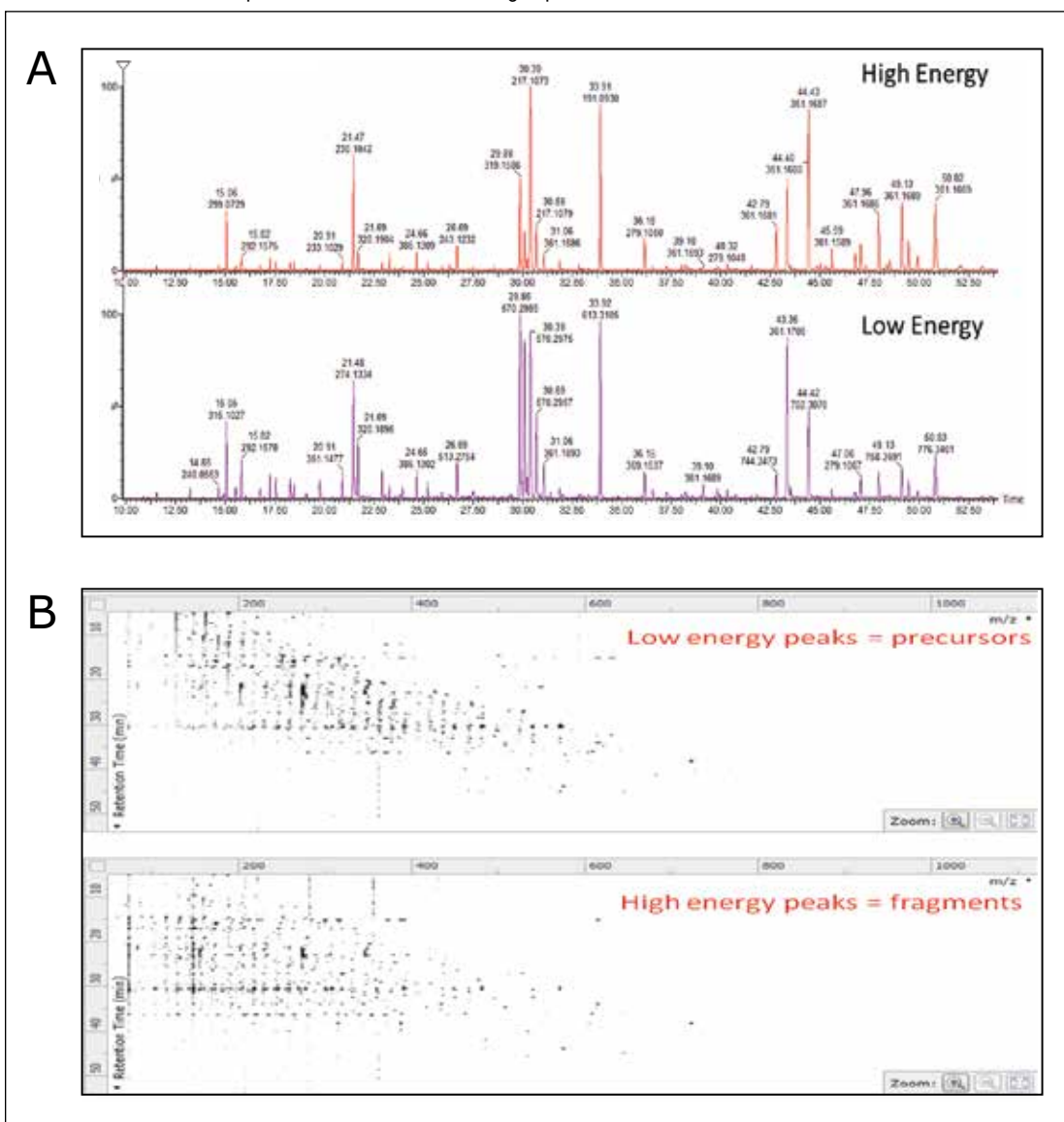


Figure 3. Biological samples were analyzed using APGC-MS$^E$ which provided information for both the intact precursor ions (at low collision energy) and the fragment ions (high collision energy). A) APGC-MS$^E$ chromatogram of the Col-O Arabidopsis leaf extract. B) Data were imported as bidimentional maps (retention times versus m/z) and processed using Progenesis QI.
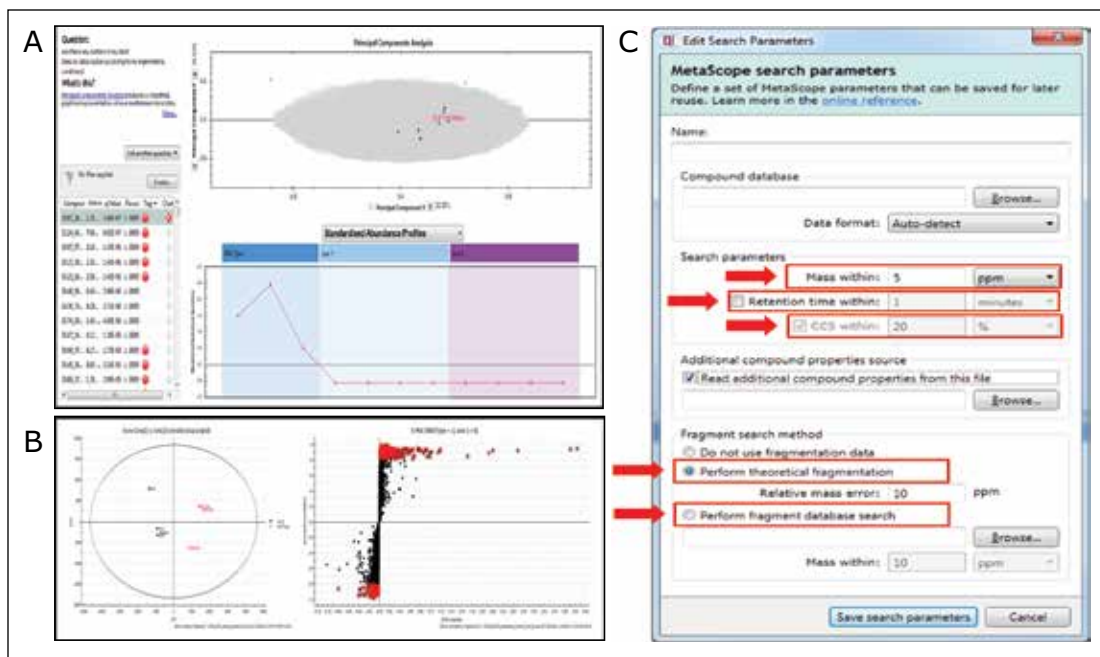
Figure 4. A) PCA model for wild type and mutant lines. B) OPLS-DA model for Arabidopsis Col-O wild type plants and mutant line. C) The Progenesis QI search engine allowed us to query experimentally-derived or in-house databases.

Sample data, generated with the low energy (precursor ion) spectrum and high energy (fragment ion) spectrum of each component, was searched against both the in-house and commercial mass spectrum libraries (Figure 5A and B). The identification score described the level of confidence obtained for each library hit based on accurate mass for precursor and fragment matching, retention time, and isotope ratios (Figure 5A and B).
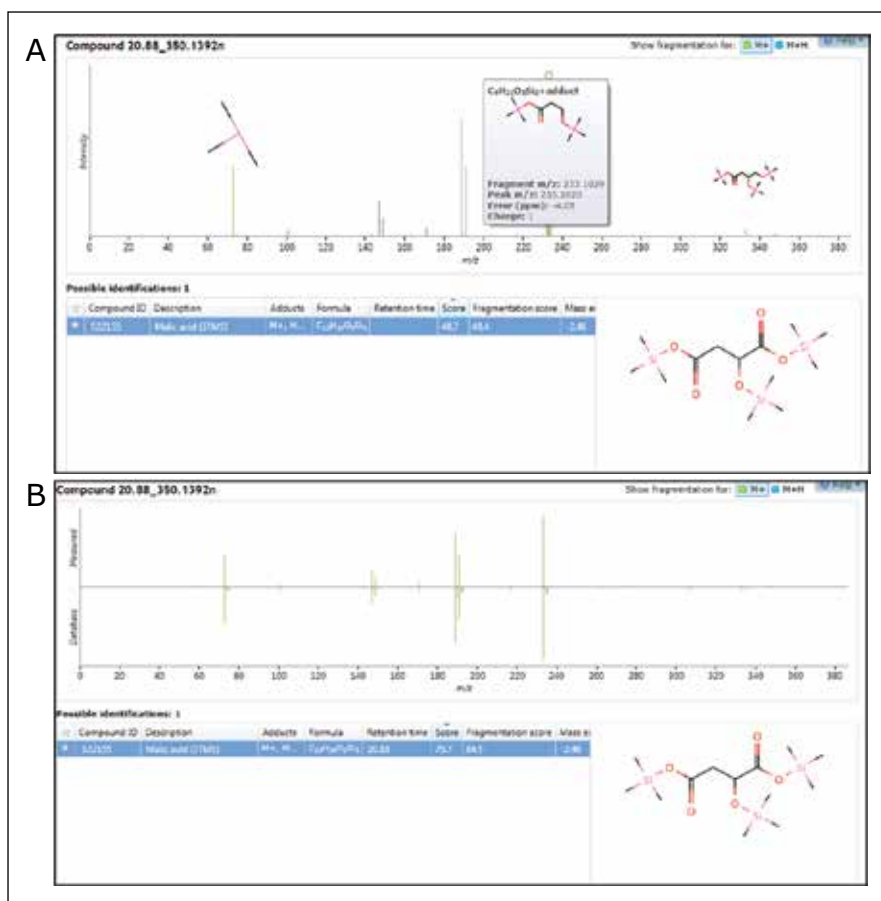


Figure 5. A) APGC-MS$^E$ allowed the identification of malic acid extracted from a biological matrix, using theoretical fragmentation within Progenesis QI. The spectra of fragment ions were aligned with co-eluting precursor ions and matched against theoretically generated spectra (green signals). B) The identification score improved when identification of malic acid was conducted using an in-house database within Progenesis QI. The spectra of fragment ions were aligned with co-eluting precursor ions and matched against experimentally generated spectra (green signals).

As structurally similar metabolites often co-elute, the concurrent acquisition of an intact molecular ion, along with fragmentation data for sub-structural determination, was particularly useful. In combination with accurate mass measurement, the molecular ion helps determine the limits of chemical composition, which can subsequently be used along with the fragmentation data for more detailed and specific structural elucidation of both known and unknown metabolites.

A summary workflow for the APGC-TOF-MS$^E$ approach:

1. An in-house database of derivatized metabolites was generated using APGC-MS$^E$

2. APGC provided abundant molecular ions with minimal fragmentation at low collision energy, which are typically missing when traditional vacuum source GC-MS is employed.

3. Due to the use of charge exchange chemical ionization, the elevated collision energy data resulted in a spectrum similar to the traditional EI data.

4. APGC-MS approach was used for metabolic fingerprinting of a set of Arabidopsis mutants.

5. Sample data generated with the low and high energy function (MS$^E$) were searched against the in-house database using the search engine within Progenesis QI.

## CONCLUSIONS

APGC-TOF MS$^E$ with Progenesis QI is a valuable solution for metabolomics applications. The use of orthogonal information for the metabolite identification, including accurate mass, retention time, and theoretical or measured fragmentation, increased the confidence of metabolite identification while decreasing the number of false positive identifications.

## Waters

### THE SCIENCE OF WHAT'S POSSIBLE.®

**Waters Corporation**
34 Maple Street
Milford, MA 01757 U.S.A.
T: 1 508 478 2000
F: 1 508 872 1990
www.waters.com

Waters
THE SCIENCE OF WHAT'S POSSIBLE.®

# The Use of HRMS and Statistical Analysis in the Investigation of Basmati Rice Authenticity and Potential Food Fraud

Gareth Cleland,[1] Adam Ladak,[2] Steven Lai,[2] and Jennifer Burgess[1]
[1]Waters Corporation, Milford, MA, USA
[2]Waters Corporation, Beverly, MA, USA

## APPLICATION BENEFITS

■ Authenticity of food

■ Detecting food fraud

■ Metabolomics

## WATERS SOLUTIONS

MassLynx® Software

Atmospheric Pressure Gas Chromatography (APGC)

SYNAPT® G2-Si High Definition Mass Spectrometry® (HDMS®)

Progenesis® QI Software

## KEY WORDS

HDMS[E], APGC, Multivariate Analysis, MVA, spectral cleanup, ion mobility, data alignment, CCS, food fraud, food authenticity, food safety, food research

## INTRODUCTION

There is increased concern regarding the authenticity of basmati rice throughout the world. For years, traders have been passing off a lesser quality rice as the world's finest long-grained, aromatic rice, basmati, in key markets like the US, Canada, and the EU. A DNA rice authenticity verification service in India has concluded that more than 30% of the basmati rice sold in the retail markets of the US and Canada is adulterated with inferior quality grains.[1] In Britain, the Food Standard Agency found in 2005 that about half of all basmati rice sold was adulterated with other strains of long-grain rice.[2]

Genuine basmati rice is grown in the foothills of the Himalayas. What external factors play a part in the growth of the rice? Can a basmati strain grown elsewhere in the world can be classed as basmati rice?

A proof of principle method has been established to assess the authenticity of basmati rice using off the shelf supermarket samples with the latest advancements in high resolution GC-MS hardware and informatics. Volatile compounds of interest were extracted from heated dry rice via SPME and headspace. Following a generic GC separation, detection was performed using a Waters® SYNAPT G2-Si MS run in HDMS[E] mode.[3] Collection of an HDMS[E] dataset offers a high level of specificity as a result of an ion mobility separation of compounds based on size, shape, and charge, performed after and orthogonal to a GC or UPLC separation.

Progenesis QI, the latest OMICS informatics package from Waters, is designed to utilize the 4-dimensional data produced during a SYNAPT G2-Si HDMS[E] acquisition. Initially, alignment of all injections is performed followed by the unique peak co-detection process resulting in the same number of analyte measurements in every sample and no missing values. Data from all isotopes and adducts of a parent compound are then deconvoluted giving a single robust and accurate measurement for that parent compound. Compounds of interest were highlighted using various Multi Variate Analysis (MVA) techniques and identified using elucidation tools and relevant database searches within the software platform.

## EXPERIMENTAL

### Autosampler conditions

| | |
|---|---|
| System: | CTC PAL |
| Incubation temp.: | 120 °C |
| Extraction time: | 300 s |
| Desorption time: | 600 s |
| SPME Fiber: | Supelco SPME fiber assembly (DVB/CAR/PDMS) 50/30 µm coating |

### GC conditions

| | |
|---|---|
| GC system: | 7890A GC |
| Column: | DB5-MS 30 m x 0.25 mm x 0.25 µm film |
| Carrier gas: | He 2 mL/min |
| Temp. gradient: | Initial 40 °C for 2 minutes, 30 °C/min to 130 °C, 10 °C to 270 °C, 30 °C to 320 °C, hold 2 min |
| Injection type: | Pulsed splitless |
| Injector temp.: | 250 °C |
| Pulse time: | 2.00 min |
| Pulse pressure: | 550 KPa |
| Injection volume: | 2 mL |
| Make up gas: | $N_2$ at 200 mL/min |
| Transfer line temp.: | 330 °C |

### Data processing

Principle Component Analysis (PCA), Orthogonal Projections to Latent Structures Discriminent Analysis (OPLS-DA), and Correlation Analysis were statistical analysis algorithms utilized within EZ Info and Progenesis QI.

### MS conditions

| | |
|---|---|
| MS system: | SYNAPT G2-S*i* |
| Mode: | API |
| Corona: | 2.2 µA |
| Cone gas: | 220 L/h |
| Aux gas: | 200 L/h |
| Source temp.: | 150 °C |
| Low energy CE: | 4 V |
| High energy CE ramp: | 10 to 45 V |

### Sample preparation

Several varieties of rice from different producers, shown in Table 1, were obtained from local supermarkets. Sample IDs were given to avoid brand disclosure. 10 g of dried rice was weighed out in a 20 mL amber headspace vial. Rice samples were prepared in triplicate as to provide three replicate injections for each sample without returning to the same vial. A pooled, composite sample was prepared by mixing 100 g of each rice sample together prior to weighing out 10 g vials. All samples were placed in the autosampler tray and data collected with a randomized sample list.

| Sample | Description | Sample ID |
|---|---|---|
| 1 | Basmati Manufacturer 1 | BAS M1 |
| 2 | Basmati Manufacturer 2 | BAS M2 |
| 3 | Long Grain Manufacturer 3 | LG M3 |
| 4 | Basmati Manufacturer 4 | BAS M4 |
| 5 | Jasmine Manufacturer 5 | JAS M5 |
| 6 | Basmati Manufacturer 3 | BAS M3 |
| 7 | Jasmine Manufacturer 4 | JAS M4 |
| 8 | Composite Sample | Pool |

*Table 1. Off the shelf rice samples used during the study.*

## RESULTS AND DISCUSSION

Collection and interrogation of a comprehensive APGC/HDMS[E] non-targeted dataset was performed following the analysis workflow shown in Figure 1. Atmospheric Pressure Gas Chromatography (APGC) is a 'soft' ionization technique resulting in less compound fragmentation when compared to conventional electron ionization (EI).[4]

Increased abundance of precursor ion enhances sensitivity for compounds of interest. Precursor ion fragmentation can now be controlled via a high definition MS[E] (HDMS[E]) acquisition, which also leads to an increase in specificity.

HDMS[E] collects accurate mass precursor ion and accurate mass fragment ion data (at elevated collision energy) in alternate MS functions in combination with ion mobility separations to provide time aligned, drift aligned accurate mass precursor and accurate mass product ion information in a single injection.[2] Ion mobility provides an additional degree of separation to the chromatography used, which improves the overall peak capacity over conventional GC-MS techniques.



Figure 1. Analysis workflow for rice samples in this study.

Data processing was performed using Progenesis QI, the latest Omics software package from Waters fully able to utilize the information afforded in HDMS[E] datasets. Progenesis QI  is a novel software platform that is able to perform alignment, peak picking and mining of data to quantify then identify significant molecular differences between groups of samples.

Following alignment, peak detection and deconvolution, 3885 compound ions were investigated. Initially, Principle Component Analysis (PCA) was performed yielding the scores plot in Figure 2. Tight pooling of injections from replicate samples and a centralized composite/pool sample indicated a statistically relevant dataset. Some of the basmati rice samples fell in the upper left quadrant, jasmine rice samples fell in the lower right quadrant and a long grain rice in the upper right quadrant. Exceptions to the pooling of the rice types were observed for two basmati rice samples. One originated from the same producer as a jasmine rice and pooled with other jasmine rice samples (BAS M4). The second basmati outlier (BAS M3) came  from the same producer as the long grain rice and pooled alongside this long grain rice sample (LGM3).

Since the origin of these stored purchased samples is essentially unknown, it is not possible to draw conclusions about the origin or purity of the samples. The aim of this work was to devise a proof-of-principle method for the investigation of basmati rice authenticity and potential food fraud. A study with a larger number of well characterized samples, including both authentic and non-authentic basmati rice samples, is required. Finding unique markers of interest in this new study may then make it possible for a pass/fail method to be established on a more routinely used instrument in a quality control laboratory, such as a single or tandem quadrupole.
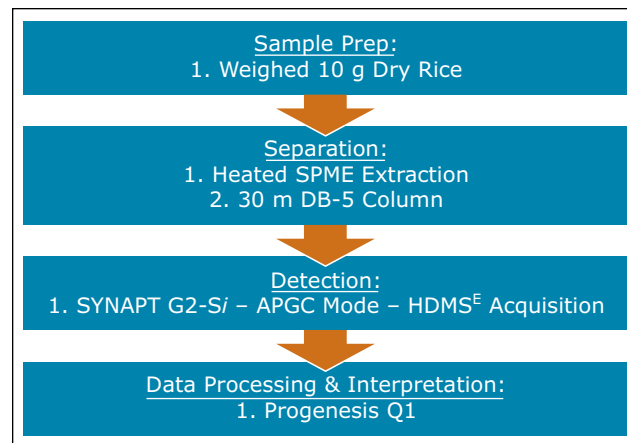
Further investigation into the data was performed using a supervised Orthogonal Projections to Latent Structures Discriminant Analysis (OPLS-DA) model. For this, the markers comprising the injections for the basmati rice samples (BAS M1 and BAS M2), highlighted with blue squares in Figure 2, were compared to the markers comprising the long grain rice sample (LG M3), highlighted with red squares in Figure 2. The S-plot from this analysis is shown in Figure 3 where the x-axis shows the measure of the magnitude of change in a particular analyte, and the y-axis shows a measure of analyte significance in the two-group comparison. Significant markers or ions of interest, highlighted with red squares in Figure 3, are the ions representing the significant markers with the biggest difference between the two rice types. Once highlighted, a set of markers can be tagged with a simple right mouse click. This subset of analytes can then be assigned a 'tag' within Progenesis QI for further consideration.
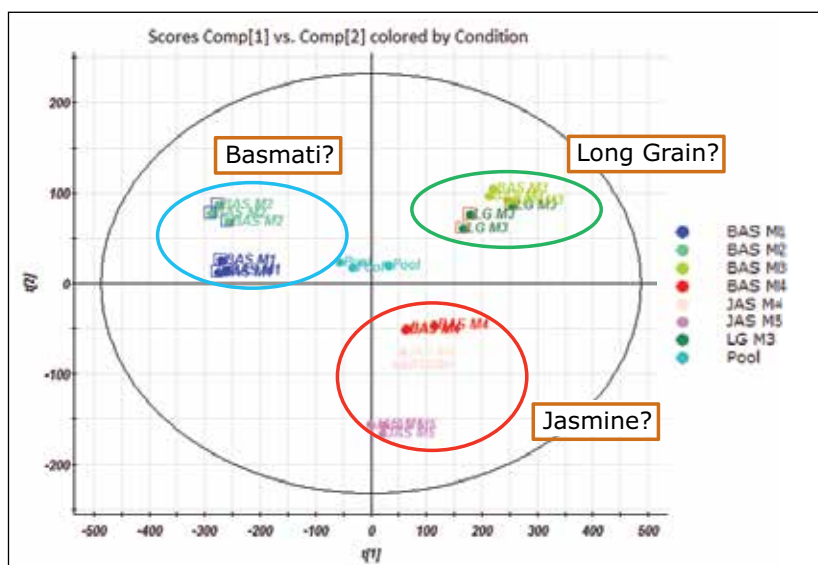


Figure 2. Scores plot from the PCA performed on rice samples.
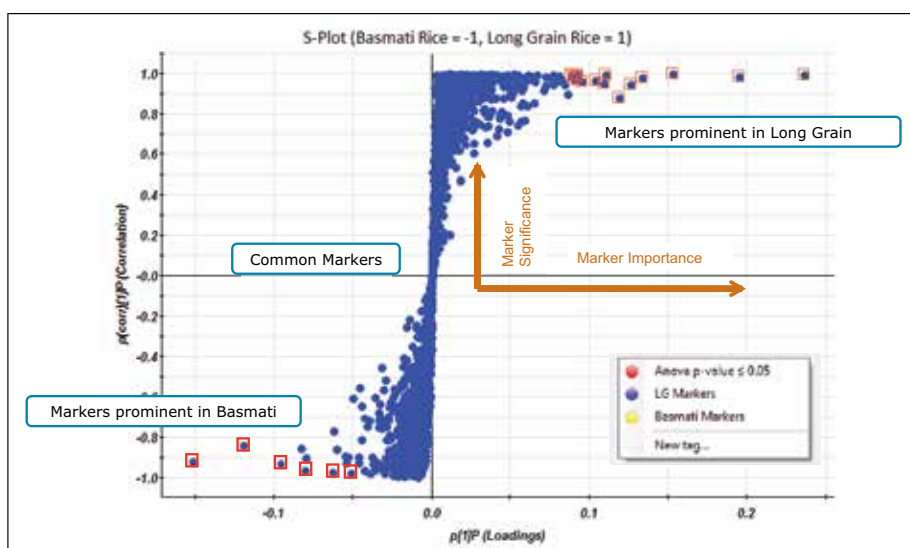


Figure 3. OPLS-DA model showing differences between basmati rice and long grain rice samples.

Figure 4 shows the standardized abundance profile for the six markers tagged in basmati rice. The standardized abundance profile (also known as a trend plot) shows the normalized intensity of the six markers of interest that were highest in basmati M1 and M2 samples compared to all other injections. Their presence in the composite sample (pool) is expected owing to the contribution of the M1 and M2 samples.



*Figure 4. Standardized abundance profiles for six basmati rice-related markers.*

Further interrogation of the 3885 compounds ions was performed using default quick tag filters and the Correlation Analysis, available within Progenesis QI. Applying the quick tag filter for ANOVA P value (p<0.05), resulted in a focus on 2907 statistically significant ions from the 3885 originally generated. Figure 5 shows the table of markers satisfying the ANOVA P value filter (A). The standardized abundance profile for a marker of interest previously obtained from the S-Plot in Figure 3, is also displayed (B). Selecting Correlation Analysis from the highlighted dropdown menu (C) results in a Dendrogram of markers. The correlation analysis groups compounds according to how similar their abundance profiles are across all samples. Our marker of interest is shown as the red line highlighted by the circle (D). Markers showing a similar abundance profile are found within the same Dendrogram branch.



*Figure 5. Accessing and using the correlation analysis within Progenesis QI (C) enables the user to extract further ions of interest that follow a similar profile to a selected marker (B).*

These markers of a similar profile to the one highlighted are easily isolated, viewed and tagged using the Dendrogram within the Correlation Analysis, as shown in Figure 6. Over 50 markers of interest in basmati rice, showing a similar trend across all injections, have now been isolated and tagged.
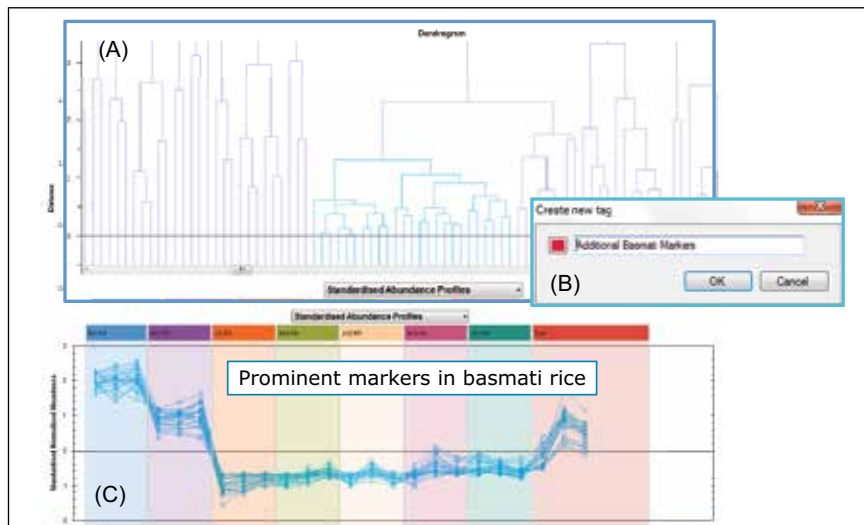


*Figure 6. (A) Further markers of interest in basmati rice, isolated using the Correlation Analysis in Progenesis QI. (B) A right click allows easy tagging of these markers for elucidation. (C) Standardized abundance profiles of all 57 isolated markers are shown across all injections.*

The same steps were followed for selection of the key markers in the long grain rice sample (LGM3). The standardized abundance profile of 26 markers of interest, extracted using the correlation analysis within Progenesis QI, in long grain rice are displayed in Figure 7. As can be seen from Figure 7, the basmati rice from the same producer as the long grain rice showed very similar abundance profiles on the same markers of interest; yet none of these markers were observed in other basmati rice samples. This could imply that is very little difference between the basmati rice and the long grain rice samples from this producer. This could also imply that packaging material is having an impact on our profiling.

A study with a larger number of well characterized samples, including both authentic and non–authentic basmati rice samples, is required to test this proof-of-principle method, as previously mentioned.
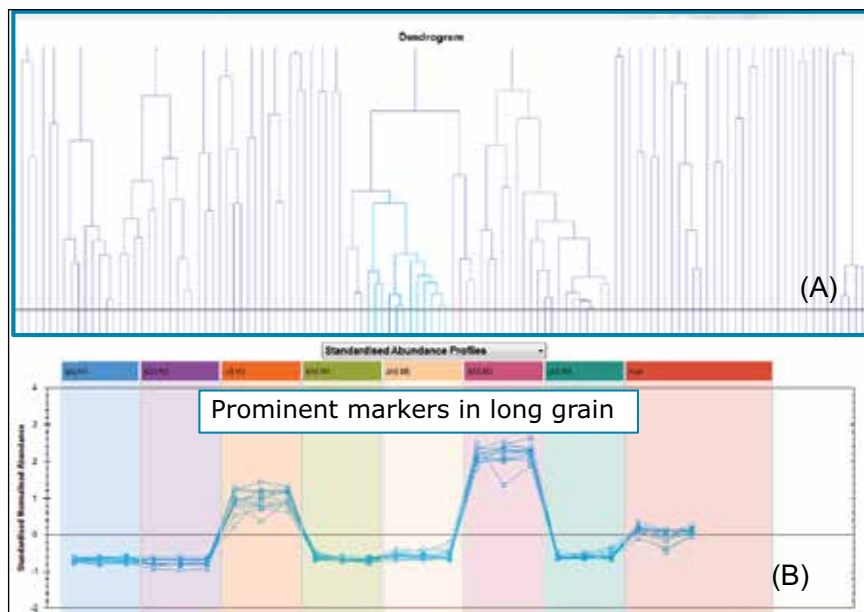


*Figure 7. (A) Markers of interest in long grain rice isolated using Correlation Analysis. (B) Standardized abundance profiles of all 26 isolated markers across all injections.*

Once markers of interest have been isolated there are several options for elucidation and identification:

1. Structural elucidation within MassLynx Software.

2. Batch database searching within Progenesis QI.

3. Batch database searching outside of Progenesis QI.

**Structural elucidation**

To determine the structure of an ion of interest the mass, or formula (from elemental composition calculation) is submitted to a chemical structure database, such as ChemSpider. A selected structure resulting from the search is checked for matching high energy accurate mass fragment ions using the MassFragment™ tool. Figure 8 summarizes the steps involved in structural elucidation for the marker 271.2644 Da at 10.79 minutes (10.79_271.2644) obtained from the OPLS-DA analysis. To confirm the proposed structure, a purchased or synthesized standard would have to be analyzed using GC-MS/MS.

Note: Progenesis QI V2.0, available end 2014, will have Elemental Composition and ChemSpider search functionality embedded within the software. These functions were not available for use when this project was completed.



Figure 8. MassLynx Software's structural elucidation workflow for isolated markers of interest.

**Database searching within Progenesis QI**

Progenesis QI's search engine (Progenesis Metascope) allows users to query in-house and publicly available databases. Search parameters can be customized to maximize all aspects of the data acquired to the database being searched. A list of potential identifications is generated and scored using criteria such as mass accuracy, isotope distribution, retention time, drift time, and fragment matching. If the chosen database contains structures, theoretical fragmentation of the molecule is performed and a fragmentation score is used to rank potential identifications of high energy accurate mass fragment ions to the theoretical dissociation of the molecule.

Figure 9 highlights these customizable database searching parameters in Progenesis QI software (A). An example identification of the marker elucidated earlier is shown (B) when searching several downloaded publically available databases (NIST, ChEBI, and HMDB), and the search settings used in Figure 9A. High spectral specificity (spectral cleanup) is observed due to the ability of the software to time align and drift align spectra from the four-dimensional HDMS$^E$ acquisition. All fragments in the high energy spectrum of Figure 9 (B) have been assigned to the theoretical dissociation of the molecule proposed in the database search, which increases confidence in the identification made. Identification of the same molecule via elucidation within MassLynx and via database searching within Progenesis QI also increases confidence in the identifications made.
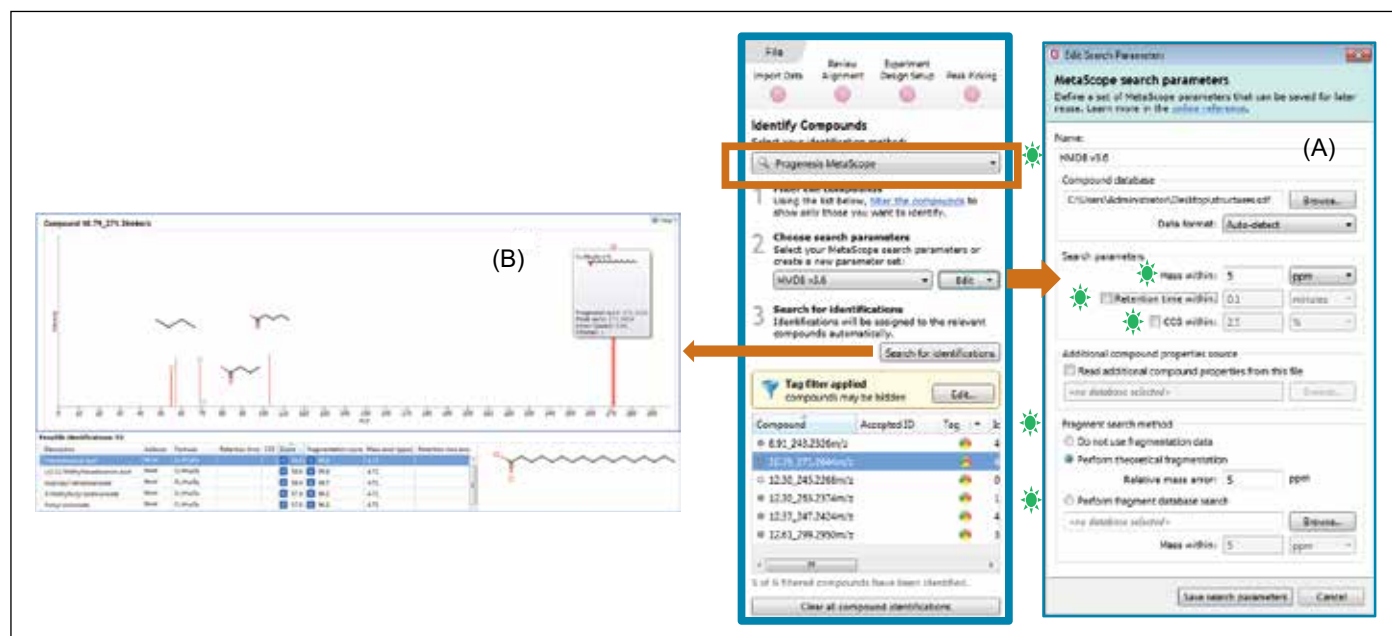


*Figure 9. Database and search settings available in Progenesis QI (A). An example of a typical identification is also shown (B).*

**Database searching outside of Progenesis QI**

Batch submission to the METLIN (Metabolite and Tandem MS Database) is also possible using a clipboard copied list of masses from Progenesis QI, Figure 10. The Scripts Center for Metabolomics web page is automatically launched when the user copies a list of tag filtered markers of interest to the clipboard. MS/MS spectra within the METLIN database can be used to compare to the drift and time aligned high energy spectra obtained from a HDMS$^E$ acquisition.



*Figure 10. Screen capture of the compound identification page in Progenesis QI. Highlighted areas show the ease of batch submission for markers of interest to an external (METLIN) database.*

**References**

1. The Economic Times, "Basmati Export Adulteration Leaves Bad Taste in Mouth", Prabha Jagannathan, Jul 6, 2007. http://articles.economictimes.indiatimes.com/2007-07-06/news/28467196_1_basmati-rice-india-s-basmati-basmati-export

2. Contamination concerns force new Basmati regulations, Fletcher A, August 2005. http://www.foodnavigator.com/Legislation/Contamination-concerns-force-new-Basmati-regulations

3. Waters SYNAPT G2-Si product brochure, Part. No. 720004681EN.

4. Waters APGC White Paper, Part No. 720004771EN.

## Waters
THE SCIENCE OF WHAT'S POSSIBLE.®

**Waters Corporation**
34 Maple Street
Milford, MA 01757 U.S.A.
T: 1 508 478 2000
F: 1 508 872 1990
www.waters.com

# CHAPTER 2 STRUCTURAL ELUCIDATION
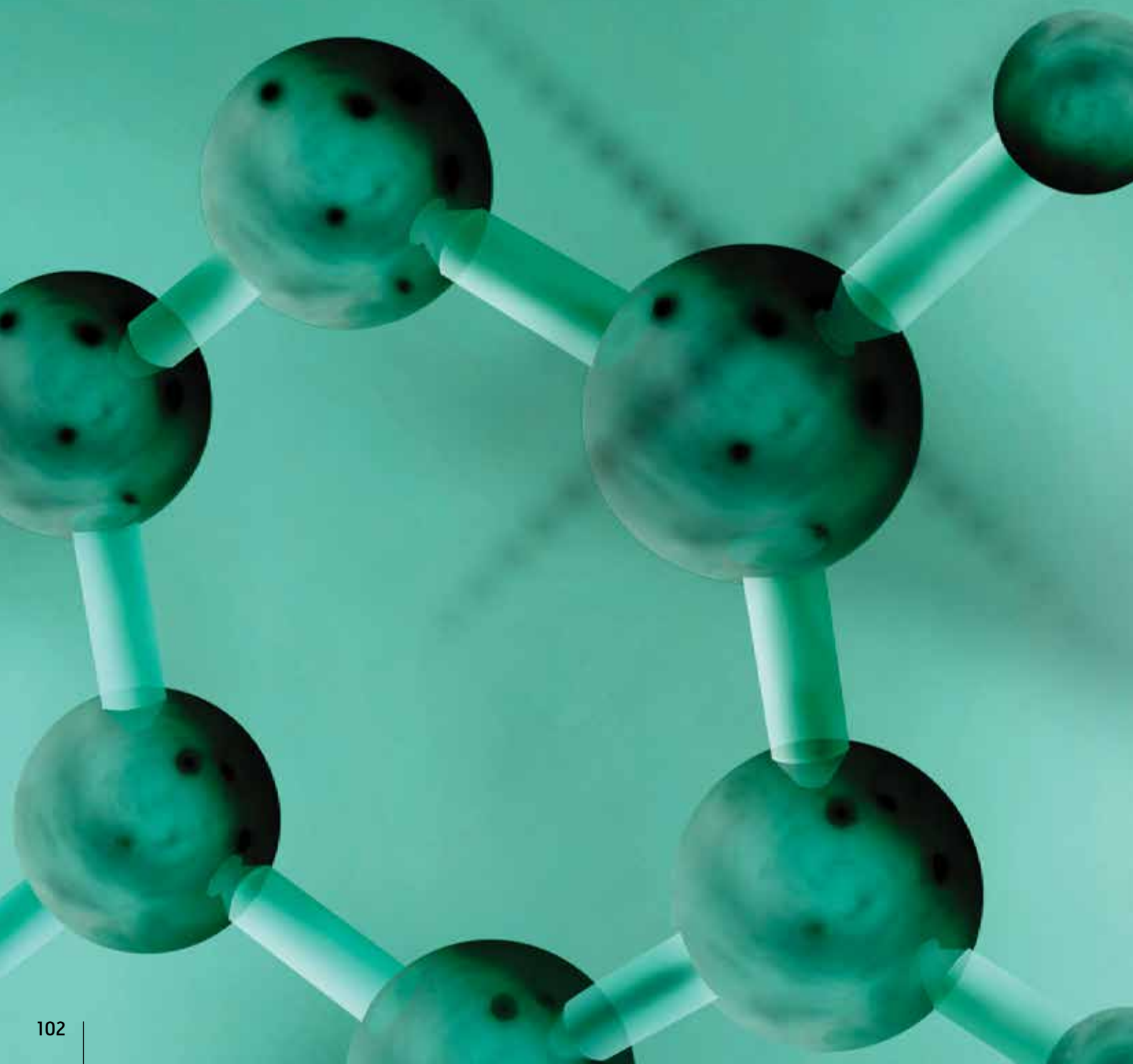
# STRUCTURAL ELUCIDATION

There are significant challenges when detecting and characterizing metabolites and lipids from biological matrices due to the large number of potential interferences on the mass scale. Ion Mobility-MS can provide an opportunity to better detect ions in the absence of interferences and subsequently deliver cleaner, more reliable spectral tandem MS data. Because of the complexity of the biological metabolome and lipidome, the addition of mobility times as an orthogonal measurement to mass, retention times and MS-MS fragmentation provides complementary information regarding the analyte, which adds further specificity to the identification of metabolites and lipids.

Thousands of metabolites and lipids exist in biological samples, many of which can co-elute at the same retention time or appear in similar regions of the *m/z* scale. Applying data-independent (DIA) or data dependant acquisition (DDA) to these samples would lead to product ion spectra, containing a mixture of fragments deriving from multiple co-eluting or co-isolated precursors, which may complicate the interpretation of spectra. To aid the identification of complex mixtures of analytes, DIA fragmentation of precursor ions can be performed following the ion mobility separation. The incorporation of ion mobility separation of co-eluting precursor ions before fragmentation produces cleaner, product-ion spectra, which improves identification and reduces false-positive assignments. In the Waters' SYNAPT® Mass Spectrometer, such a mode of operation is referred to as HDMS$^E$ (High Definition® MS$^E$).

The elucidation of the chemical structure of complex lipids and metabolites often requires multiple fragmentation techniques and/or methods. Time-aligned parallel (TAP) fragmentation is a particular mode of acquisition typical of the Waters' SYNAPT, which contains an ion-mobility separation cell between two collision cells (C1, C2). In this mode of operation, the precursor ion of interest is selected with the quadrupole mass filter and subjected to fragmentation in the first collision cell, C1. Next, the packet of fragment ions produced are subjected to ion mobility separation followed by secondary fragmentation in the second collision cell, C2 (pseudo-MS3). This process results in a driftogram, showing the different drift regions for each of the first-generation fragment ions aligned with the second generation fragment ions. This mode of acquisition has been used for fine, structural characterization of complex structures in a single analytical step.

- Unique gas phase separation of isobaric species by ion mobility (HDMS®)
- CID and ETD fragmentation capabilities
- Confirmation of metabolite/lipid identity by CID fragmentation in conjunction with ion mobility separation (HDMS$^E$, TAP)

Waters
THE SCIENCE OF WHAT'S POSSIBLE.®

# Traditional Herbal Medicine Structural Elucidation using SYNAPT HDMS with Time-Aligned Parallel (TAP) Fragmentation

Kate Yu, Jose Castro-Perez, and John Shockcor,
Waters Corporation, Milford, MA, USA

## INTRODUCTION

The challenges in analyzing Traditional Herbal Medicine (THM) or Traditional Chinese Medicine (TCM) samples arise from the complexity of the matrix as well as variability from sample to sample. We have reported a generic intelligent work flow[1-2] that allows fast sample analysis while obtaining maximum information by effectively utilizing UPLC®/HDMS™ analysis in time-of-flight (TOF) mode with a variety of advanced profiling software tools (MetaboLynx™ and MarkerLynx™ Application Managers).

In this application note, we demonstrate a strategy that provides an effective means of confirming known components and elucidating structures of unknown components.

Ion mobility mass spectrometry (IMS) allows the separation of ionic species as they drift through a gas phase under the influence of an electric field. The rate of an ion's drift depends on the mass of the ion, the charge state of the ion, as well as the average collisional cross-section of the ion. With IMS, it is possible to separate ions with the same nominal mass if they have different charge states or different collisional cross-sections.

The strategy reported here comprises of an initial sample screening using the Waters® ACQUITY UPLC® System with the SYNAPT™ HDMS System in full-scan IMS mode. Once a compound or class of compounds are identified, a targeted fraction collection is performed in analytical scale and the fraction collected can be infused into the mass spectrometer at a nano-scale flow rate so that structural elucidation can be performed for the compound of interest. The nano-scale flow rate allows infusion to be carried out over an extended time period, making it possible to conduct multiple MS/MS experiments, including time-aligned parallel (TAP) fragmentation experiments.

TAP, which is CID-IMS-CID, allows users to take the advantage of the Triwave(tm) configuration on the SYNAPT HDMS (Figure 1). This configuration allows pre-IMS T-Wave™ and post-IMS T-Wave to operate as two separate collision cells.

The fragment ions produced in the Trap T-Wave (pre-IMS) can be separated based on their charge states and sizes as they move through the IMS cell. Ions separated by drift time can be fragmented further in the Transfer T-Wave (post-IMS). As a result, the fragment ions generated in the Transfer T-Wave are drift time-aligned with their respective precursor ions, resulting in Time Aligned Parallel (TAP) fragmentation patterns. When these fragmentation results are combined with tools such as MassFragment™ Software, structural elucidation for small molecule is simplified.

Here, a Chinese Ginseng extract was analyzed by utilizing the ACQUITY UPLC/SYNAPT HDMS systems operating in IMS mode. Fraction collection was performed using a TriVersa NanoMate (Advion). The fractions collected were directly infused into the SYNAPT HDMS for analysis, providing more in-depth information about the compounds of interest. The example analyte discussed in this application note is the Ginsenoside Rb1.



*Figure 1. Schematic of the SYNAPT HDMS System's Triwave design.*

## EXPERIMENTAL

A Chinese Ginseng extract was used for this work. The sample was filtered prior to injection. A chip-based nano-electrospray device (TriVersa NanoMate, Advion) was used as the mass spectrometer interface.

### LC conditions

| | | | |
|---|---|---|---|
| LC system: | Waters ACQUITY UPLC System | | |
| Column: | ACQUITY UPLC HSS T3 Column | | |
| | 2.1 x 100 mm, 1.7 µm, 65 °C | | |
| Flow rate: | 600 µL/min | | |
| Mobile phase A: | Water + 0.1% Formic Acid | | |
| Mobile phase B: | MeOH | | |
| Gradient: | Time | Composition | Curve |
| | 0 min. | 95%A | |
| | 10 min. | 30%A | Curve 6 |
| | 17 min. | 0%A | Curve 6 |
| | 20 min. | 95%A | Curve 1 |

### Fraction collection (FC) conditions

| | |
|---|---|
| FC system: | Advion TriVersa NanoMate |
| Flow split: | 300 nL/min flow to the MS and the rest of the flow to the waste or the collection plate when triggered |
| Collection plate: | 96-well plate |
| Collection time: | 7 sec per well |
| Trigger: | Time-based |

### MS conditions

| | |
|---|---|
| MS system: | Waters SYNAPT HDMS System |
| Ionization mode: | ESI Negative |
| Capillary voltage: | 3000 V |
| Cone voltage: | 35 V |
| Desolvation temp: | 450 °C |
| Desolvation gas: | 800 L/Hr |
| Source temp: | 120 °C |

| | |
|---|---|
| Acquisition range: | 50 to 1500 $m/z$ |
| Collision gas: | Argon |
| IMS carrier gas: | Helium |
| He gas flow: | 80 L/min |

## RESULTS

For THM studies, it is typically desirable to have the compound of interest physically separated from the raw extract so that it can be analyzed in detail and to enhance structural elucidation. Even though preparative-scale chromatography is a common practice for fraction collection in the THM field, it is often desirable to determine a component's structure prior to rigorous isolation of a pure compound in preparative scale.

In this work, we have connected the ACQUITY UPLC/SYNAPT HDMS systems with a TriVersa NanoMate[3-4] such that fraction collection can be performed in the analytical scale. For this sample analysis, we have set the NanoMate for the collection of the major peak at $m/z$ 1107, which corresponds to the Ginsenoside Rb1.

The NanoMate utilizes a chip-based nano-electrospray as the LC/MS interface.[3] This allows samples to be analyzed in the nL/min flow range. As a result, fractions collected can be analyzed by direct infusion. The low flow rate allows small volume of sample to be infused for a considerable amount of time (about 30 to 40 minutes) such that compounds at low concentration levels can be analyzed utilizing various full-scan MS, and MS/MS acquisition modes including TAP (Figure 2).
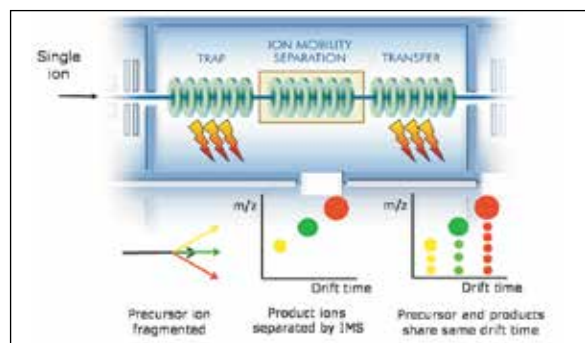


Figure 2. TAP fragmentation for m/z 1077 by direct infusion of fraction collected for the 10.02 minute peak.

The chemical structure and the possible major fragment ions for the Ginsenoside Rb1 are shown in Figure 3. The fragmentation is described left to right. As Ginsenoside Rb1 losses the sugar moiety in sequence, it generates fragment ions corresponding to $m/z$ 945, $m/z$ 783, and $m/z$ 621. The $m/z$ 459 is from the core ring structure of Rb1.
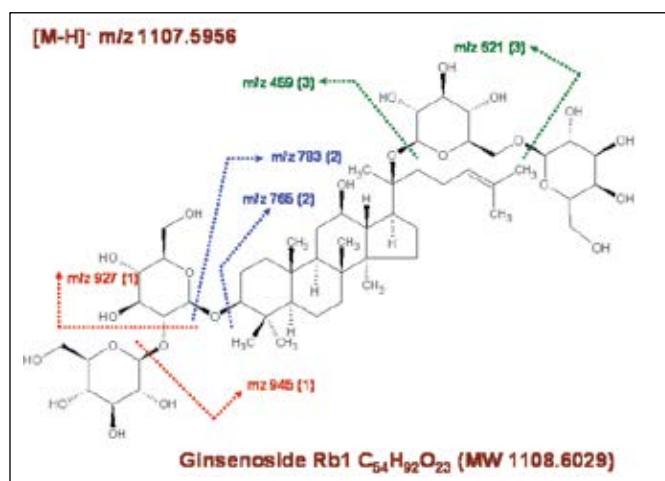


Figure 3. Chemical structure for Ginsenoside Rb1.

To demonstrate the TAP behavior, Figure 4 shows a DriftScope™ Plot comparison from two separate experiments. In Figure 4a, fragmentation was conducted in the T-Wave Trap region only. The fragment ions with a different numbers of sugar moieties migrated through the drift tube at different rates.

Drift time 1 in Figure 4a shows mainly the deprotonated molecule and the major fragment ion at $m/z$ 945, which is the loss of one sugar moiety. Major ions in drift time 2 are $m/z$ 945 and $m/z$ 783 (loss of two sugar moieties). And drift time 3 mainly contains fragment ions generated from the sugars and from the fragmentation of core structures rings.

Figure 4b shows the TAP fragmentation data. At each drift time region, the precursor ions or first-generation ions were further fragmented, producing second-generation fragment ions. These ions are drift time aligned with the first-generation product ions and obtained in parallel. This produces a fragmentation tree that allows the user to account for the source of the second-generation fragments within the proposed structure. The true advantage of this experiment is that the entire second-generation fragment ions can be generated on the fly, i.e., in parallel with the generation of the first-generation product ions.

Typically a single ion-mobility experiment is carried out every 10 milliseconds. For nanoflow-scale infusion, it is possible to average many spectra across the infusion experiment to obtain a good signal-to-noise. Moreover, this approach allows the user to conduct multiple stages of fragmentation for compounds of interest that may exist in extremely low levels.

Figure 5 shows a combined TAP spectrum of the three regions that correlates to Figure 4b. Figure 6 shows the individual MS spectrum for each region (1, 2, and 3) with a few of the proposed structures shown therein. This provides valuable information for the study of the fragmentation mechanisms. For example, it should be noted that the fragment ion at $m/z$ 323, which consists two sugars, is observed in drift times 1 and 2, but not 3. This indicates that the precursor ions for region 3 do not have the di-sugar side chain.
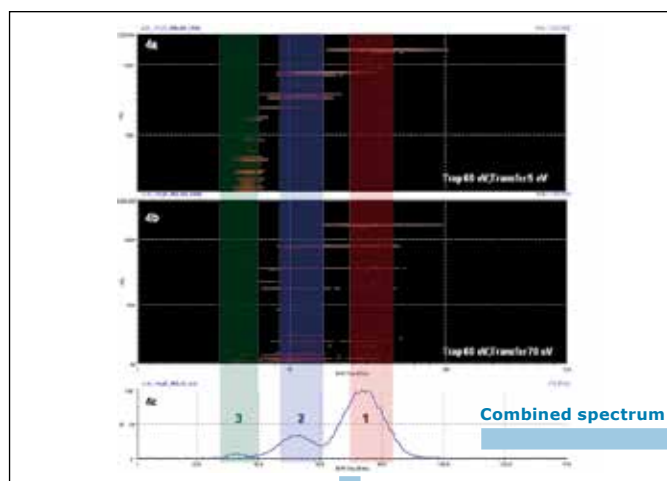
Figure 4. Fragmentation results obtained for Ginsenoside Rb1 using different fragmentation strategies.
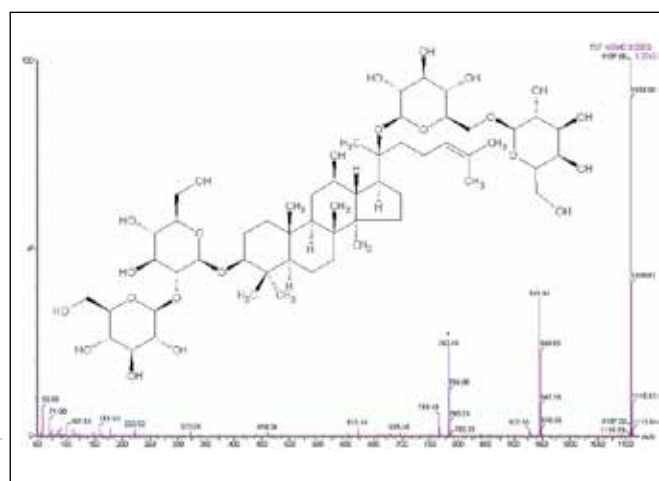
Combined spectrum



Figure 5. The MS spectrum of Ginsenoside Rb1 by combining the three driftogram peaks from 4c.

Spectrum for each peak
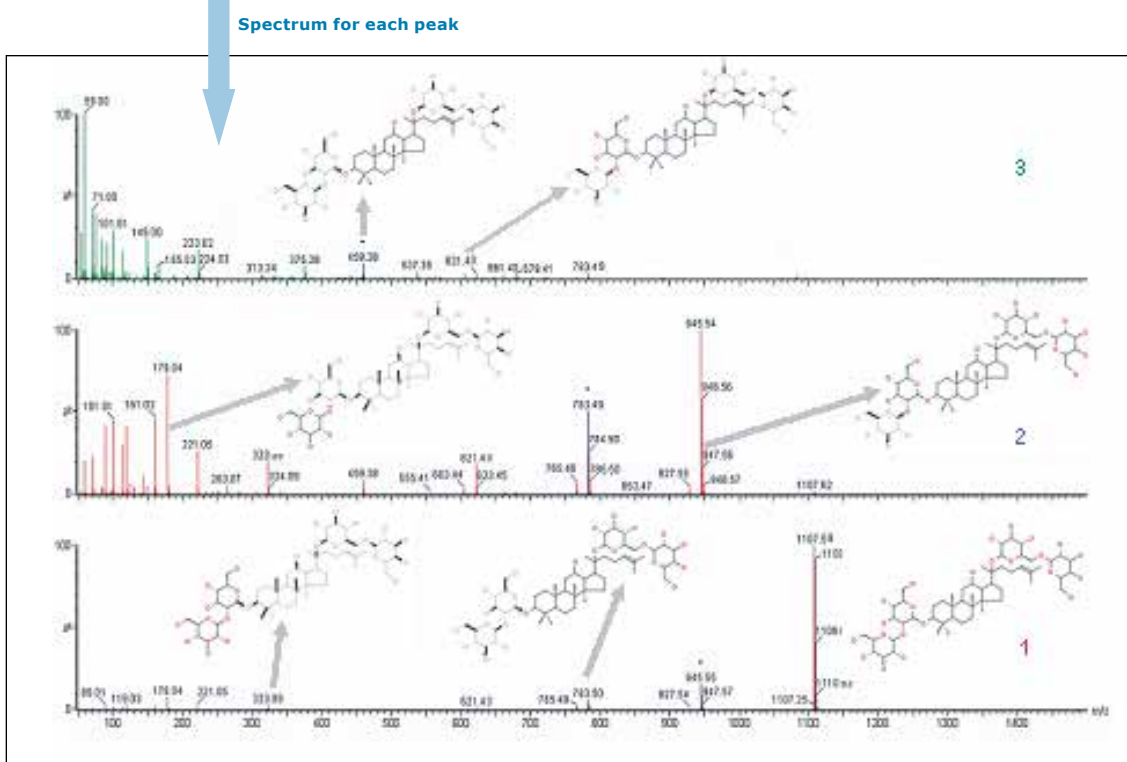


Figure 6. The individual spectrum for each region corresponds to driftogram peak 1, 2, and 3.

## CONCLUSION

UPLC/HDMS and analytical-scale fraction collection combined with TAP fragmentation is complementary to the UPLC/TOF MS workflow. As a result, Traditional Herbal Medicine (THM) samples can be analyzed with high resolution, high sensitivity and fast turnaround time.

This technique enhances the user's ability to perform structural elucidation for individual components from a complex matrix. TAP fragmentation, used in combination with the MassFragment structure elucidation software tool, provides a fast and accurate approach to solving complex elucidation problems.

### References

1.  An Intelligent Workflow for Traditional Herbal Medicine Compound Identification by UPLC/TOF-MS. Yu K, Castro-Perez J, Shockor J. Waters Application Note. 2008; 720002486EN.

2.  A Multivariate Statistical Approach using UPLC/TOF-MS for Traditional Herbal Medicine Analysis to Compare Different Sample Classes. Yu K, Castro-Perez J, Shockor J. Waters Application Note. 2008; 720002541EN.

3.  Automated Nanofluidic System for Real-Time Monitoring of Enzymatic Assay. Corso R, Almeida R, et al., ASMS 2007 Poster.

4.  Optimized Trap and Elute Strategies Using nano-LC-MS/MS for the Identification of Sypro Ruby Stained Proteins Separated by 2-Dimensional Gel Electrophoresis. Prosser S, Eilel D, et al. ASMS 2007 Poster.

## Waters

### THE SCIENCE OF WHAT'S POSSIBLE.®

**Waters Corporation**
34 Maple Street
Milford, MA 01757 U.S.A.
T: 1 508 478 2000
F: 1 508 872 1990
www.waters.com

# THE BENEFITS OF GAS-PHASE COLLISION CROSS-SECTION (CCS) MEASUREMENTS IN HIGH-RESOLUTION, ACCURATE-MASS UPLC/MS ANALYSES

The rotationally-averaged collision cross-section (CCS) represents the effective area for the interaction between an individual ion and the neutral gas through which it is travelling. CCS is an important distinguishing characteristic of an ion in the gas phase, being related to its chemical structure and three-dimensional conformation. CCS affects the mobility of an ion as it moves through a neutral gas under the influence of an electric field and ions may be separated accordingly using ion mobility spectrometry (IMS).[1] CCS values may be measured experimentally using IMS. CCS values may also be estimated computationally if the 3D structure of the molecule is known.[2]

Waters
THE SCIENCE OF WHAT'S POSSIBLE.®

Figure 1 illustrates the separation of ionic species achieved by IMS. In this example, two ions of equal mass and charge, but different three-dimensional conformation, will travel through an IMS device at rates dependent on their mobilities and emerge at different times (drift times). The ion with a more compact three-dimensional conformation has a shorter drift time through the IMS device because its smaller CCS value gives it a higher mobility than its neighbour with a more open three-dimensional conformation.
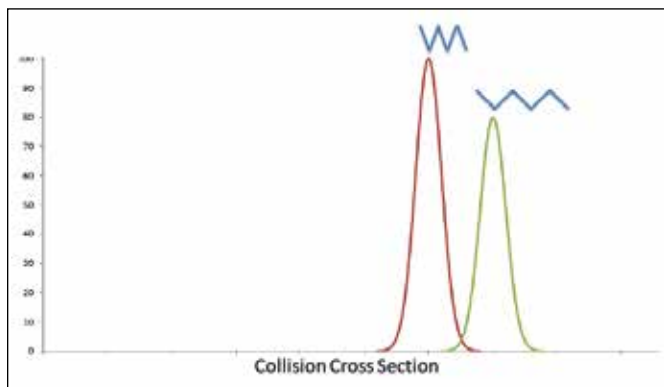


*Figure 1. The CCS value of an ion may be determined using its drift time through an IMS device.*

By calibrating the IMS device using ions of known CCS, the drift times measured during subsequent analyses of unknown species may be converted directly to CCS values.

The Waters® SYNAPT® G2-S*i* HDMS™ Mass Spectrometer incorporates high-efficiency T-Wave™ ion mobility separations and enables CCS values to be measured routinely as an integral part of high-resolution, accurate-mass LC/MS experiments.[3] This allows CCS to be used alongside the traditional molecular identifiers of precursor ion accurate mass, fragment ion accurate masses, isotope pattern, and chromatographic retention time as a confirmation of compound identity or as an indicator of compound structure.

## CCS FOR MAXIMIZING ANALYTICAL PEAK CAPACITY AND SELECTIVITY

The selectivity of an analytical method depends on the ability of the analytical system to resolve sample constituents from each other. Often, a sample may contain many thousands of individual components.

Chromatography and mass spectrometry are techniques typically used to resolve sample constituents. The resolving power of modern UltraPerformance LC® (UPLC®) instruments and high resolution mass spectrometers, when combined, deliver very high levels of analytical selectivity but many analyses either cannot make full use of chromatographic separations (MALDI[4] or direct analysis techniques such as DART, DESI, and ASAP[5]) or demand levels of selectivity that cannot be provided even by the combination of state of the art LC/MS systems.

In such cases T-Wave ion mobility separation provides an additional dimension of resolution that works orthogonally to both chromatography and mass spectrometry to multiply the peak capacity and selectivity of an analytical method.[6] By incorporating CCS based separations into an analytical method it is possible to distinguish analyte from matrix interferences or even resolve structural isomers[7], conformers, and protomers.[8] For MALDI Imaging experiments, where samples may be complex and chromatographic separation is not possible, CCS based separation provides the selectivity required to accurately and confidently determine the spatial distribution of important molecular species.[9]

## CCS FOR CONFIRMING COMPOUND IDENTITY

Because CCS measurements are undertaken in the gas phase, remotely from the ion source, CCS values are unaffected by sample matrix and are consistent between instruments and across a range of experimental conditions. The precision of CCS measurements obtained with T-Wave IMS can be used in combination with other molecular identifiers to increase the confidence of compound identifications.

As an example, Figure 2 shows the average measured CCS values from a range of pesticides analysed in a variety of different sample extracts, compared with the values measured in solvent standards. The results show that CCS may be measured within 2% of the expected value regardless of the nature and complexity of the analytical sample.
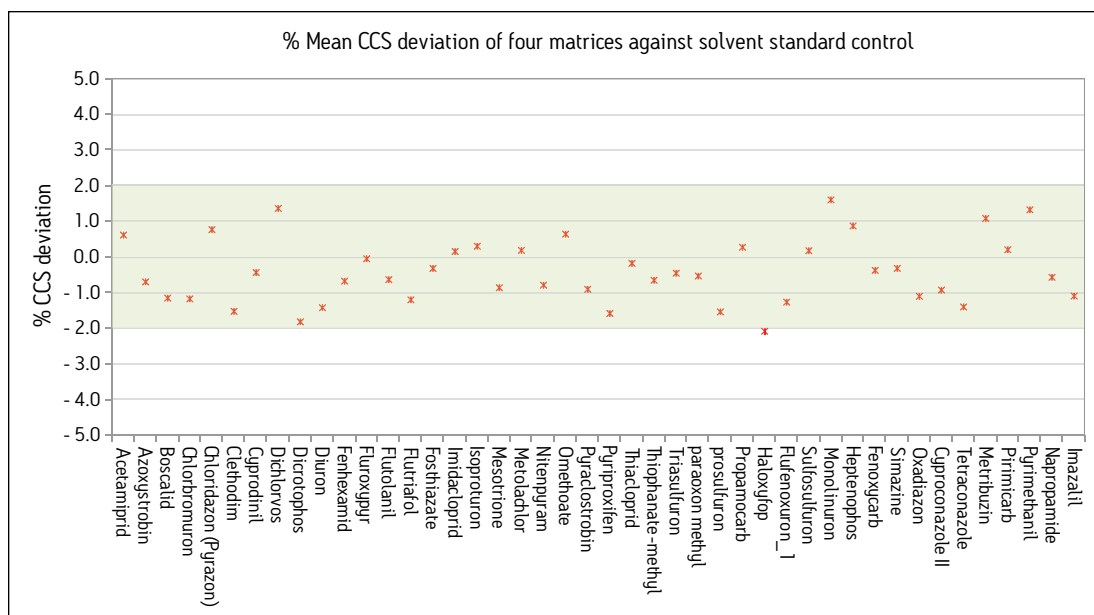
Figure 2. Average measured CCS values for a wide range of pesticide compound classes over a range of sample matrices deviate by less than 2% from CCS values measured using solvent standards.

Large numbers of pesticides can be screened for in high-resolution, accurate-mass LC/MS experiments but often, components in the sample matrix give rise to signals that can obscure the signal from a residue present in the sample (false negative detection) or can be mistaken for pesticide residues not present in the sample (false positive detections). The number of false negative and false positive detections can be minimised by choosing appropriate mass accuracy and retention time tolerance windows and by filtering the results based on the presence of expected fragment, adduct or isotope confirmatory ions. The CCS values of pesticides may be used as an additional, orthogonal means of filtering the data to significantly reduce the proportion of false positive and false negative detections.

A spiked extract of mandarin fruit, produced for a European Union Reference Laboratories (EURL) proficiency test, was analysed in a blind study using a Waters SYNAPT mass spectrometer. The data were searched against a library of approximately 480 pesticide compounds. Approximately 50,000 sample components were observed and filtering these components according to chromatographic retention time, the presence of expected fragment ions and a 5 ppm mass tolerance gave 9 identifications, with 1 false negative and 2 false positive results. Increasing the mass tolerance to 10 ppm gave 10 identifications with 2 false positive results. Applying a CCS tolerance of ± 2%, as a further filter to the results reduced the number of identifications to 8 as shown in Figure 3. The 8 identifications obtained using CCS as an extra, orthogonal data filter were all correct and,

in this particular case, the false positive and false negative identifications were removed.

|  | Without CCS | Without CCS | With CCS |
|---|---|---|---|
| *m/z* tolerance (+/-) | 5 ppm | 10 ppm | 10 ppm |
| rt tolerance (+/-) | 2.5% | 2.5% | 2.5% |
| CCS tolerance (+/-) | – | – | 2% |
| Correct IDs | 7 | 8 | 8 |
| False Negatives | 1 | 0 | 0 |
| False Positives | 2 | 2 | 0 |

Figure 3. EURL proficiency test sample results: Pesticide screening without using CCS shows a number of false positive and false negative identifications. For this study, using CCS information removes false positive and false negative identifications.

The use of CCS as an additional, orthogonal means of filtering the data effectively allows a more balanced set of tolerance criteria to be applied to compound screening experiments, which results in more confident compound identifications.

## CCS AS AN INDICATOR OF MOLECULAR CONFORMATION

Theoretical CCS values determined by molecular modelling may be compared directly with experimentally derived CCS values obtained by T-Wave ion mobility separations, in order to yield useful information on the structures and shapes of large proteins/protein complexes, peptides, organometallic complexes and small

molecules; information that can provide unique insights into important biological and chemical processes.

The use of T-Wave IMS has enhanced knowledge in diverse areas of scientific research, from mapping the size distribution in oil and petroleum samples[10] to revealing the molecular architecture of multi protein complexes[11,12] and to rapidly determining sites of biotransformation in drug metabolism studies.[13,14]

These types of studies are able to provide useful scientific information far more rapidly and efficiently than by more traditional techniques. Often, using CCS to probe molecular structure can yielded scientific advances not possible by other means.

## CONCLUSION

The ability to separate ions by T-Wave IMS and measure their CCS values as an integral part of high-resolution, accurate-mass LC/MS experiments allows significant increases in the peak capacity and resolution of analytical methods. It enables the separation of isomers, conformers and protomers that cannot be separated by other means. It also provides a unique, orthogonal identifier for target analytes in screening experiments and can be used to probe the structures and conformations of diverse types of molecule. All these experiments can be carried out on the Waters SYNAPT G2-S*i* HDMS Mass Spectrometer, enabling significant increases in the performance of analytical methods and delivering unique capabilities not available on conventional mass spectrometers.

### References

1.  Ion mobility-mass spectrometry, Abu B. Kanu, Prabha Dwivedi, Maggie Tam, Laura Matz and Herbert H. Hill Jr., *J. Mass Spectrom.* 2008; 43: 1–22.

2.  Factors Contributing to the Collision Cross Section of Polyatomic Ions in the Kilodalton to Gigadalton Range: Application to Ion Mobility Measurements, Thomas Wyttenbach, Christian Bleiholder, and Michael T. Bowers; *Anal. Chem.*, 2013, 85 (4), pp 2191–2199.

3.  Waters TriWave white paper (www.waters.com) Literature No. 720004176en.

4.  Waters Application Note, Unparalleled Specificity Using HDMS Technology in a MALDI Imaging Experiment, (www.waters.com) Literature No. 720004259en.

5.  Waters Application Note, Investigating the Applicability of Direct Analysis and Ion Mobility TOF MS for Environmental Analysis, (www.waters.com) Literature No. 720004465en.

6.  Resolving the microcosmos of complex samples: UPLC/travelling wave ion mobility separation high resolution mass spectrometry for the analysis of *in vivo* drug metabolism studies, Stefan Blech and Ralf Lau, *Int. J. Ion Mobil. Spec.* (2013) 16:5–17.

7.  Separation of isomeric disaccharides by travelling wave ion mobility mass spectrometry using $CO_2$ as drift gas, Maíra Fasciotti, Gustavo B. Sanvido, Vanessa G. Santos, Priscila M. Lalli, Michael McCullagh, Gilberto F. de Sá, Romeu J. Daroda, Martin G. Petera, and Marcos N. Eberlin, *J. Mass Spectrom.* 2012, 47, 1643–1647.

8.  Protomers: formation, separation and characterization via travelling wave ion mobility mass spectrometry, Priscila M. Lalli, Bernardo A. Iglesias, Henrique E. Toma, Gilberto F. de Sa,c,d Romeu J. Daroda, Juvenal C. Silva Filho, Jan E. Szulejko, Koiti Arakib and Marcos N. Eberlin, *J. Mass. Spectrom.* 2012, 47, 712–719.

9.  On-Tissue Protein Identification and Imaging by MALDI-Ion Mobility Mass Spectrometry, Jonathan Stauber, Luke MacAleesea, Julien Franck, Emmanuelle Claude, Marten Snel, Basak Kükrer Kaletas, Ingrid M.V.D. Wiel, Maxence Wisztorski, Isabelle Fournier, Ron M.A. Heeren, *J Am Soc Mass Spectrom* 2010, 21, 338–347.

10. Evaluating the multiple benefits offered by ion mobility-mass spectrometry in oil and petroleum analysis, Jérémie Ponthus, Eleanor Riches, *Int. J. Ion Mobil. Spec.* (2013) 16:95–103.

11. Integrating Ion Mobility Mass Spectrometry with Molecular Modelling to Determine the Architecture of Multiprotein Complexes, Argyris Politis, Ah Young Park, Suk-Joon Hyung, Daniel Barsky, Brandon T. Ruotolo, Carol V. Robinson, PLoS ONE | www.plosone.org, August 2010 | Volume 5 | Issue 8 | e12080.

12. Evidence for Macromolecular Protein Rings in the Absence of Bulk Water, Brandon T. Ruotolo, Kevin Giles, Iain Campuzano, Alan M. Sandercock, Robert H. Bateman, Carol V. Robinson, *Science* 2005: vol. 310 no. 5754 pp. 1658-1661.

13. Sites of metabolic substitution: investigating metabolite structures utilising ion mobility and molecular modelling, Gordon J. Dear, Jordi Munoz-Muriedas, Claire Beaumont, Andrew Roberts, Jayne Kirk, Jonathan P. Williams, and Iain Campuzano, *Rapid Commun. Mass Spectrom.* 2010; 24: 3157–3162.

14. Product ion mobility as a promising tool for assignment of positional isomers of drug metabolites, Filip Cuyckens, Carola Wassvik, Russell J. Mortishire-Smith, Gary Tresadern, Iain Campuzano and Jan Claereboudt, *Rapid Commun. Mass Spectrom.* 2011, 25, 3497–3503.

## Waters
### THE SCIENCE OF WHAT'S POSSIBLE.®

Waters
THE SCIENCE OF WHAT'S POSSIBLE.®

# SYNAPT G2 High-Defintion Mass Spectrometry: Separation and COLLISION CROSS-SECTION Determination of Leucine and Isoleucine by Travelling Wave Ion Mobility Mass Spectrometry

Iain Campuzano, Kevin Giles, Kieran Neeson, and Keith Richardson
Waters Corporation, Manchester, UK

## INTRODUCTION

Here we demonstrate the use of travelling wave ion mobility mass spectrometry with the SYNAPT™ G2 High Definition Mass Spectrometry™ (HDMS™) platform to separate the two amino acid structural isomers isoleucine and leucine, which differ in a collision cross-section (CCS; ($\Omega$)) by less than 3 $Å^2$.

Distinguishing between isoleucine and leucine has only previously been demonstrated on instruments such as magnetic sectors or MALDI Tof-Tof mass spectrometers that are capable of performing high energy Collision Induced Dissociation (CID).

Following separation of these isomers, the T-Wave™ collision cross-section values were automatically generated with DriftScope™ Informatics (v2.1). This new capability allows one to automatically generate a T-Wave ion mobility calibration function, and derive CCS values for such compounds.



*Figure 2. T-Wave ion mobility drift time (msec) chromatograms for isoleucine and leucine and their respective T-Wave derived collision cross-sections ($\Omega$).*

## EXPERIMENTAL

SYNAPT G2 is an innovative hybrid quadrupole IMS oa-Tof mass spectrometer incorporating second-generation Triwave Technology (Figure 1), which provides significantly enhanced ion mobility resolution (over 40 ($\Omega/\Delta\Omega$)). The increased pressures of the drift gas (e.g. $N_2$) and overall length of the IMS T-Wave provide an ion mobility resolution increase of up to a factor of 4 compared to traditional Triwave Technology, while maintaining high transmission efficiency via the novel Helium-filled entry cell. The T-Wave ion mobility calibration was carried out using previously determined collision cross-section values for polyglycine (from www.indiana.edu/~clemmer).



*Figure 1. Schematic of the second-generation Triwave™ Technology of SYNAPT G2. The enhanced IM resolution is achieved through both the increased length and pressure of the IMS T-Wave region.*
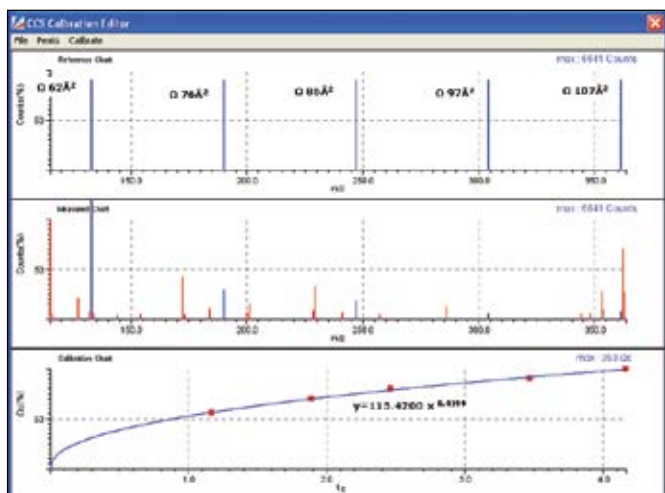
*Figure 3. DriftScope Software's (v2.1) automated T-Wave ion mobility collision cross-section calibration editor. Data displayed are polyglycine.*

An automated T-Wave ion mobility calibration can be carried out using DriftScope Software (v2.1) (Figure 3). The top panel shows the ion mobility calibration compound (polyglycine) with annotated collision cross-sections. The second panel shows a polyglycine mass spectra with automated peak selection. The third panel shows a charge and reduced-mass corrected collision cross-section vs. drift time plot, fitted with a power relationship, which can be used to derive CCS values for unknown compounds.

## CONCLUSIONS

It is possible to distinguish between the structural isomers of leucine and isoleucine by travelling wave ion mobility MS where the absolute collision cross-section measurements of structural isomers differ by less than 3 $Å^2$.

DriftScope Informatics enable routine collision cross-section determination of such compounds with the use of an automated T-Wave ion mobility calibration editor.

SYNAPT G2 with HDMS now enables such structural studies to be performed with enhanced specificity (enhanced IM resolution (over 40 ($\Omega/\Delta\Omega$)) and speed (DriftScope Informatics).

### Reference

1. The travelling wave device described here is similar to that described by Kirchner in US Patent 5,206,506 (1993).

## Waters
### THE SCIENCE OF WHAT'S POSSIBLE.®

**Waters Corporation**
34 Maple Street
Milford, MA 01757 U.S.A.
T: 1 508 478 2000
F: 1 508 872 1990
www.waters.com

Waters
THE SCIENCE OF WHAT'S POSSIBLE.®

# Flavonoids Identification in Complex Plant Extracts using Ion Mobility TOF MS and MS[E]

Melvin Gay, Evelyn Goh, Mark Ritchie
Waters Pacific Pte Ltd., Singapore

## APPLICATION BENEFITS

■ Screening of flavonoids in complex plant extract (*Ficus* sp.) using ACQUITY UPLC®/SYNAPT® G2 HDMS.™

■ Identification of isomers using ion mobility and MS[E] acquisition functionality.

■ HDMS[E] provides another dimension of orthogonal separation, delivering unprecedented peak capacity for increased confidence in isomers identification of complex mixtures.

## WATERS SOLUTIONS

ACQUITY UPLC System

SYNAPT G2 High Definition Mass Spectrometry™ (HDMS)

DriftScope™

MS[E] Data Viewer

ACQUITY UPLC HSS
(High Strength Silica) Technology

## KEY WORDS

Flavonoids, isomers, ion mobility,
TOF, HDMS

## INTRODUCTION

Flavonoids are a remarkable group of plant metabolites that ubiquitously exist in natural products that have been considered as an active ingredient of many medicinal plants.[1] Generally, the backbone of flavonoids consists of two phenyl rings and a heterocyclic ring, but they are often conjugated to a carbohydrate moiety with individual differences arising from various chemical processes, such as hydroxylation, methoxylation, glycosylation, and acylation.[2]

Plants containing flavonoids have been used for thousands of years in traditional Eastern medicine. In recent years, plant flavonoids have been shown to be of vital significance to humans. They have been linked as active contributors of health benefits, including its antioxidant properties in beverages such tea and wine, and in foods such as fruits and vegetables.

Waters® SYNAPT G2 High Definition Mass Spectrometry (HDMS), a combination of high-efficiency ion mobility separation (IMS) and time-of-flight (TOF) mass spectrometry, has been used to effectively separate and identify natural product structural isomers.[3] The rapid orthogonal gas separation technique in the IMS T-Wave™ allows another dimension of separation via their mass and shape without compromising MS data quality or sensitivity.

MS[E] is an acquisition technique that provides a simple, unbiased, and parallel route to deliver exact mass, low energy precursor (MS) and high energy fragment ion (MS[E]) information from every detectable component, without the need for multiple injections.

This application note describes the analysis of *Ficus* sp. extract using Waters ACQUITY UPLC System combined with the SYNAPT G2 HDMS System with IMS and MS[E] functionality to provide chromatographic and isobaric separation for a more comprehensive structural characterization of flavonoids.

## EXPERIMENTAL

### LC conditions

| | |
|---|---|
| LC system: | ACQUITY UPLC |
| Column: | ACQUITY HSS T3 2.1 x 100 mm, 1.8 µm |
| Column temp.: | 40 °C |
| Mobile phase A: | Water + 0.1% formic acid |
| Mobile phase B: | Acetonitrile + 0.1% formic acid |
| Injection volume: | 5.0 µL PLNO |
| Total run time: | 10.0 min |

### MS conditions

| | |
|---|---|
| MS System: | SYNAPT G2 HDMS |
| Ionization: | ESI negative |
| Capillary voltage: | 1.7 kV |
| Sampling cone: | 30 V |
| Extraction cone: | 4.0 V |
| Source temp.: | 120 °C |
| Desolvation temp.: | 500 °C |
| Desolvation gas: | 1000 L/hr |
| Cone gas: | 50 L/hr |
| Trap CE: | 4 V |
| Transfer CE: | 0 V |
| Trap/transfer gas: | Ar |
| IMS gas: | $N_2$ (~3.4 mbar) |
| IMS T-Wave speed: | 650 m/sec |
| IMS T-Wave height: | 40 V |
| Mass range: | 50 to 1200 $m/z$ |

### Sample preparation

Plant samples (*Ficus* sp.) were extracted in 50% methanol/water solution. The extract was then centrifuged and the supernatant was collected for further analysis.

Mobile phase gradient is detailed in Table 1.

| Time (min) | Flow rate (mL/min) | %A | %B | Curve |
|---|---|---|---|---|
| Initial | 0.4 | 99 | 1 | – |
| 1.0 | 0.4 | 95 | 5 | 6 |
| 6.5 | 0.4 | 50 | 50 | 6 |
| 7.5 | 0.4 | 5 | 95 | 6 |
| 8.0 | 0.4 | 99 | 1 | 6 |
| 10.0 | 0.4 | 99 | 1 | 6 |

Table 1. ACQUITY UPLC System mobile phase gradient.

## RESULTS AND DISCUSSION

In this profiling study, the base peak ion chromatograms of the extracted *Ficus* sp. samples showed a high degree of complexity, with numerous co-eluting components and also the presence of isomers. The advantages of ACQUITY UPLC not only produces highly reproducible chromatograms between injections, as shown in Figure 1, but also high throughput with a rapid analysis time of 10 mins. When coupled together with IMS and MS$^E$ functionality of the SYNAPT G2 HDMS, another dimension for the separation of isomers/isobaric compounds is attained. With this system, comprehensive structural information can be acquired without compromising sensitivity and analysis time.
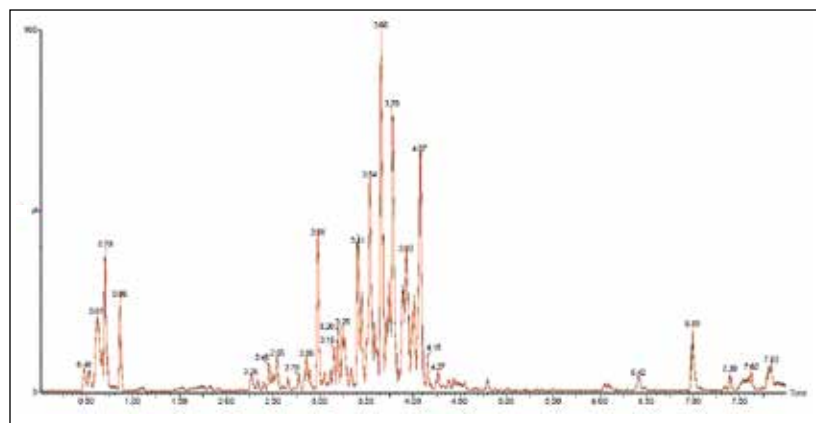


Figure 1. Overlay BPI chromatograms of extracted Ficus sample (six injections).

The flavone C-glycosides are an important subclass of the flavonoids family. Flavone C-glycosides are present in foodstuffs and nutraceuticals and they include orientin (luteolin-8-C-glucoside), isoorientin (luteolin-6-C-glucoside), vitexin (apigenin-8-C-glucoside), and isovitexin (apigenin-6-C-glucoside). They are also reported to exhibit anti-inflammatory and anti-nociceptive properties.[4,5]

Both vitexin and isovitexin have the same chemical formula of $C_{21}H_{20}O_{10}$ with an exact mass of $m/z$ 431.0978 $[M-H]^-$. Using the above UPLC® method, the extracted ion chromatogram showed two peaks with a baseline chromatographic separation at 4.07 min and 4.66 min, as shown in Figure 2A. As both compounds are isobaric, the assignment of vitexin and isovitexin to these peaks (4.07 min and 4.66 min) are not possible with only high resolution spectra alone. The identities of these two peaks were further confirmed using $MS^E$ and IMS.
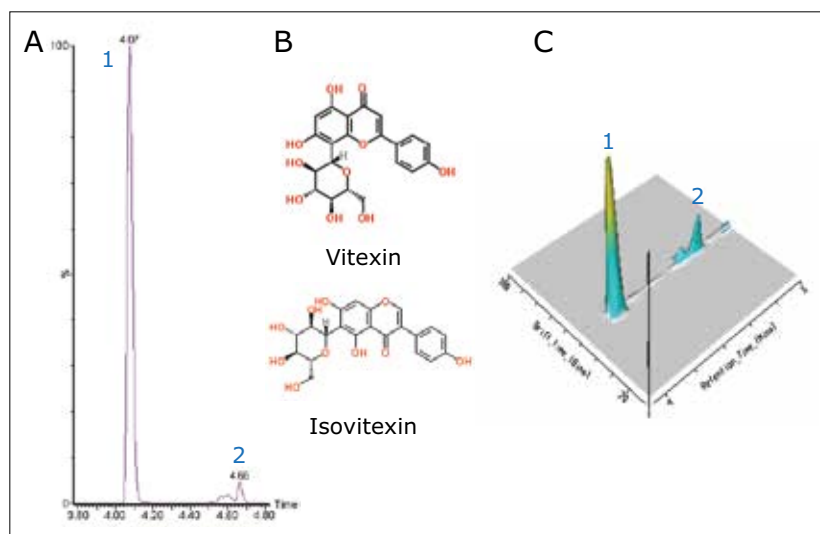


Figure 2. UPLC/SYNAPT G2 HDMS of Ficus sp. extract. 2A. XIC of Ficus sp. extract at 431.0978 m/z. 2B. Molecular structure of vitexin and isovitexin. 2C. 3D illustration of Ficus sp. extract from 4 to 5 min. The 3D plot shows the components were separated by chromatographic retention time. Vitexin and isovitexin are labeled as 1 and 2 respectively.

Baseline chromatographic separation of vitexin and isovitexin via retention time was achieved. However the fragmentation patterns observed in the $MS^E$ spectra for both vitexin and isovitexin were identical. The predicted product ions of vitexin and isovitexin, were then cross-checked against the $MS^E$ spectra of the *Ficus sp.* extract samples using MassFragment™ Software to provide added confidence. The MS and $MS^E$ spectra of isovitexin are shown in Figure 3.

Using HDMS, both compounds were further separated via ion mobility based on their structural configuration and a 3D plot was generated, as shown in Figure 2C. From Figure 2C, it can be observed that vitexin and isovitexin have drift times of 81.78 bins (4.45 ms) and 83.44 bins (4.53 ms) respectively. Thus using retention times, $MS^E$ and HDMS, the identity of vitexin and isovitexin can be determined.
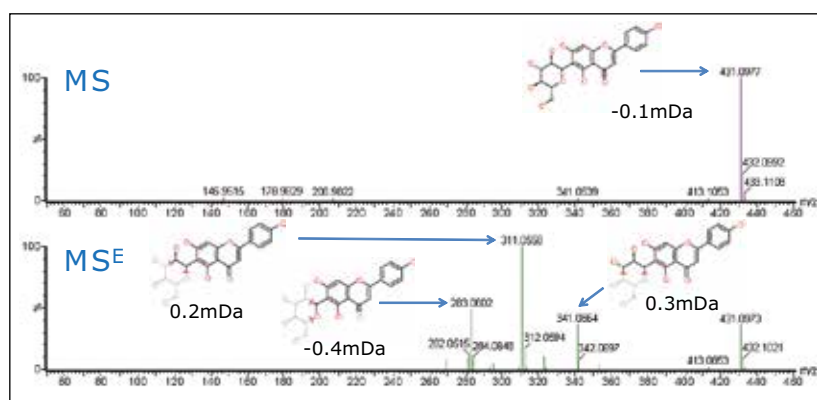


Figure 3. MS and $MS^E$ spectra of isovitexin (with mass error) at 4.66 min.

Two additional important C-glycoside flavonoids are orientin and isoorientin. They have a chemical formula of $C_{21}H_{20}O_{11}$ with an exact mass of *m/z* 447.0927 [M-H]⁻. The extracted ion chromatogram in Figure 4 shows two major peaks at 3.72 min and 3.83 min.

Baseline chromatographic separation of isoorientin and orientin via retention time was achieved. However upon further interrogation of these peaks using ion mobility and DriftScope Data Viewer, when a 3D plot was generated, shown in Figure 4C, it was observed that an unknown peak (*m/z* 635.1767) co-eluted with the orientin peak (marked with an asterisk in Figure 4C).
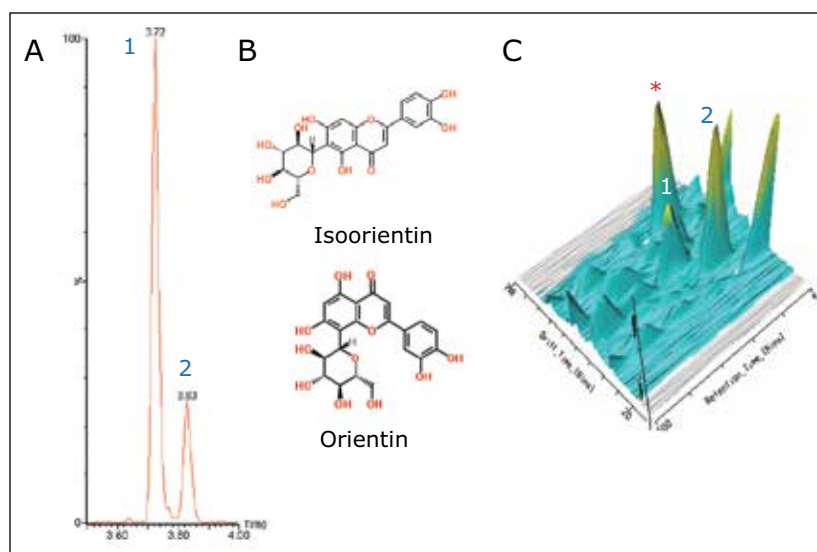


Figure 4: UPLC/SYNAPT G2 HDMS of Ficus sp. extract. 4A. XIC of Ficus sp. extract at 447.0927 m/z. 4B. Molecular structure of orientin and isoorientin. 4C. 3D illustration of Ficus sp. extract from 3.5 to 4.0 min. The 3D model shows the components were separated by chromatographic retention time and ion mobility drift time. Isoorientin and orientin are labeled as 1 and 2 respectively. An unknown co-eluting compound is marked with an asterisk.

The 2D DriftScope plot in Figure 5 illustrates the IMS separation of isobaric orientin and isoorientin (447.0927 *m/z*), showing two isomers with drift times of 76.83 bins (4.16 ms) and 84.33 bins (4.54 ms) respectively. Thus by estimating the cross-sectional structure of orientin and isoorientin , shown in Figure 4B, it can be proposed that the more compact orientin is the species with the drift time of 4.16 ms and the more extended structure of isoorientin has a longer drift time of 4.54 ms. Using the HDMS$^E$ available on the SYNAPT G2 HDMS, the product ions of orientin and isoorientin were easily visualized by their drift times and mass-to-charge ratios, as shown in the insert in Figure 5.
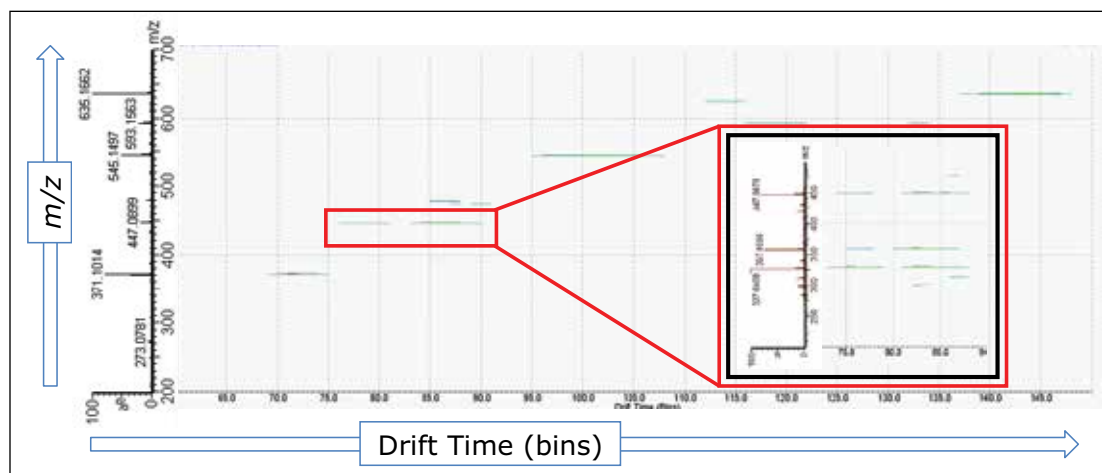


Figure 5. Visualization (drift time versus m/z) of compounds eluting between 3.7 and 3.9 min. Note the separation of orientin and isoorientin with drift times of 4.16 and 4.54 ms respectively. Inset: Product ions of orientin and isoorientin via post-IMS collision-induced dissociation.

Using the MS$^E$ Data Viewer, with the selection of *m/z* 447.0927, the BPI chromatogram window showed two prominent peaks at 3.73 and 3.84 min, as shown in Figure 6A. However upon further data interrogation of the peak at 3.84 min, it was observed that there were several co-eluting compounds, which were of higher intensity than the peak of interest, as shown in Figure 6B. Thus due to the high complexity of the sample and the vast amount of product ions present in the MS$^E$ spectra. It is impossible to accurately determine the fragmentation pattern of orientin, see Figures 6C and 6D.
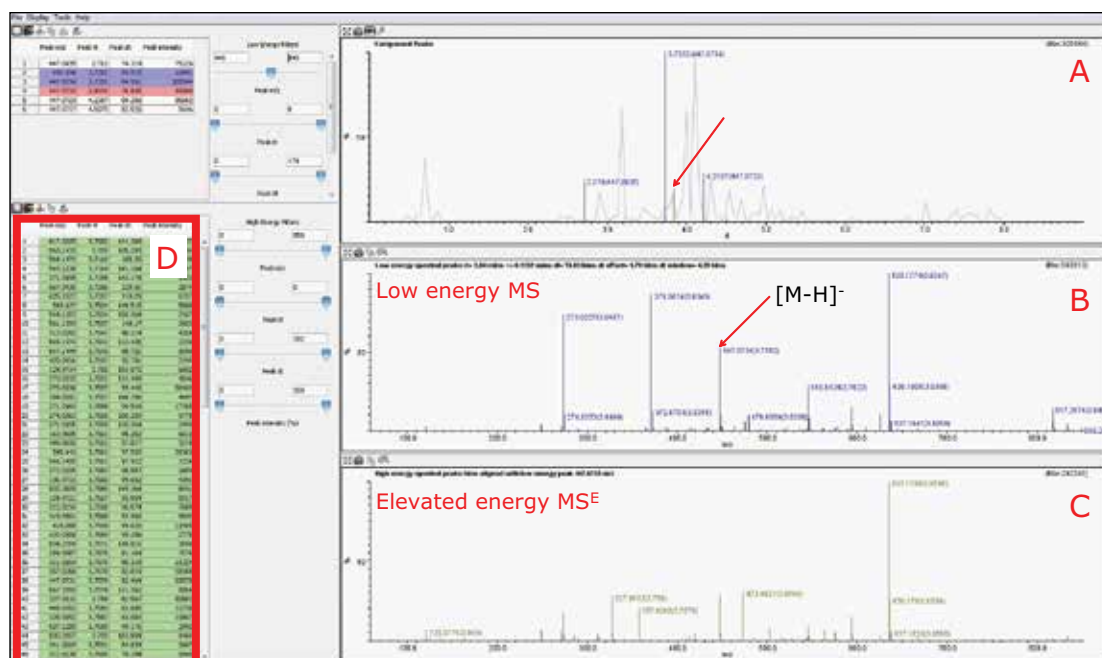


Figure 6. Orientin peak at 3.84 min using MS$^E$ Data Viewer software. 6A. Chromatogram of peaks with m/z 447.0927. Orientin peak with retention time of 3.84 min was selected (highlighted in red with an arrow). 6B. Low energy mass spectrum (MS) of peak at 3.84 min. Molecular mass of orientin [M-H]$^-$ is indicated (arrow). 6C. High-energy mass spectrum (MS$^E$) of peak at 3.84 min. 6D. List of product ions present in the MS$^E$ spectrum. HDMS function is not activated.

However, by activating the HDMS function of the MS$^E$ Data Viewer, the co-eluting components in the same peak at 3.84 min could be mobility resolved. As shown in Figure 7B, the precursor ion of orientin has a drift time of 4.16 ms. With the HDMS functionality activated, the product ions were easily resolved and the list of product ions were also greatly reduced, as shown in Figures 7C and 7D, thus increasing the confidence level of identifying orientin. HDMS$^E$ is an essential tool for separating compounds in complex mixtures containing numerous co-eluting compounds as it provides another dimension of orthogonal separation for increased confidence in isomer identification.

For isoorientin with a retention time at 3.73 min, a drift time of 4.54 ms with similar HDMS$^E$ fragmentation pattern as orientin was observed, as shown in Figure 8.
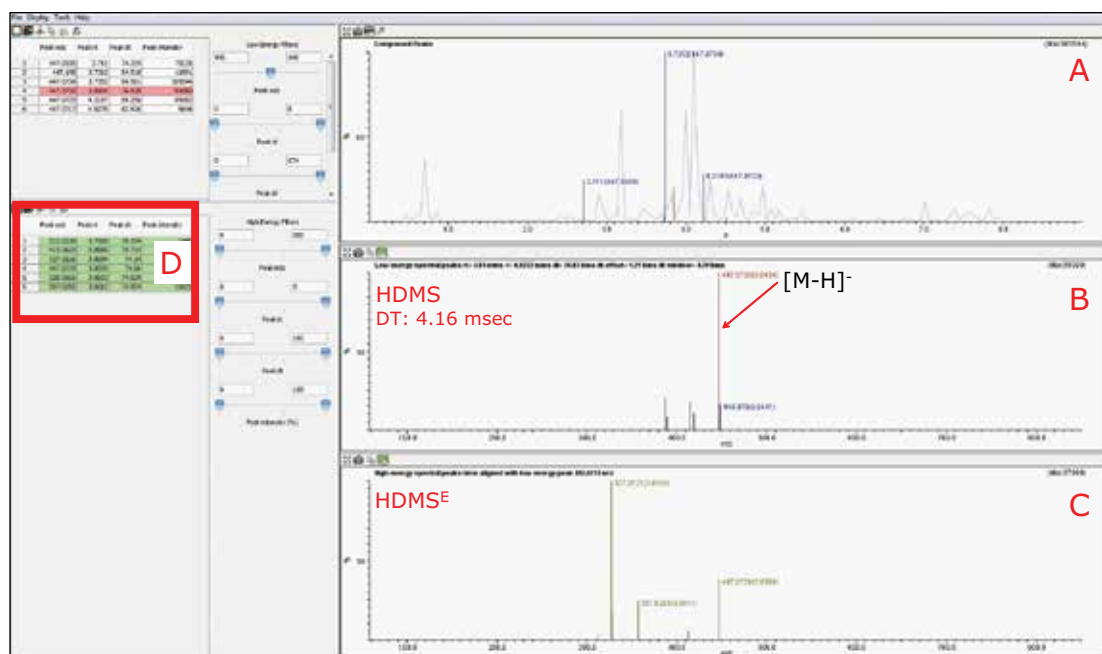


Figure 7. Orientin peak at 3.84 min with HDMS function activated. 7A. Chromatogram of peaks with 447.0927 m/z. 7B. Low energy mass spectrum (HDMS) with orientin peak selected (highlighted in red). 7C. High-energy mass spectrum (HDMS$^E$) of orientin peak. 7D. List of product ions present in the HDMS$^E$ spectrum.
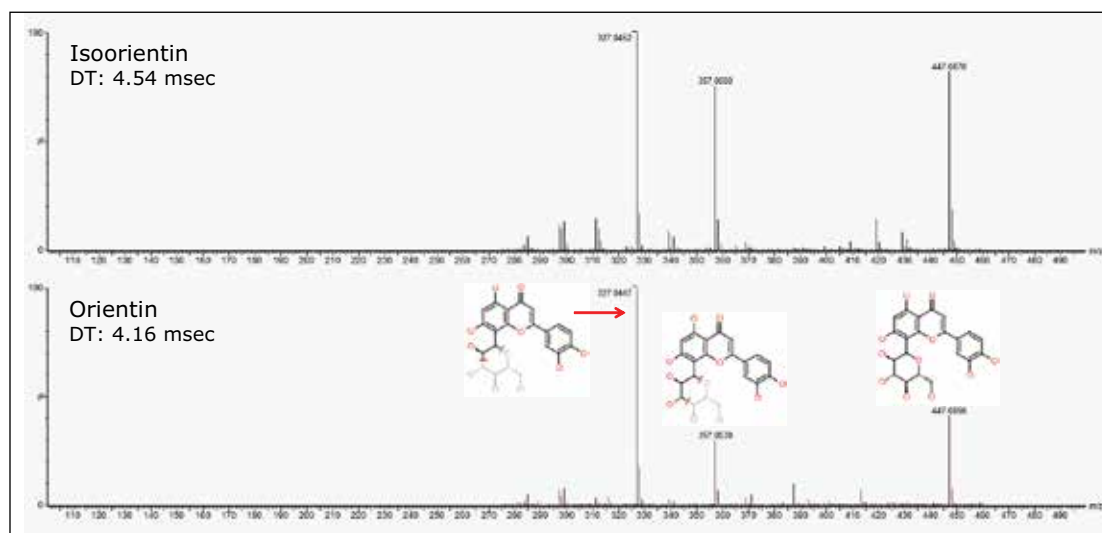


Figure 8. HDMS fragmentation pattern of orientin and isoorientin. Inset: Product ions of orientin generated using MassFragment Software.

## CONCLUSIONS

- The ACQUITY UPLC System combined with SYNAPT G2 HDMS is an effective system solution for rapid screening and identification of flavonoids in *Ficus* sp. extract.

- Plant extracts are complex matrices that contain many co-eluting compounds and isomers. HDMS provides an extra dimension of separation via ion mobility, which allows the separation of orientin from other co-eluting compounds. Together with the MS$^E$ functionality, where both low energy (precursor) and high energy (product ion) data can be acquired within a single analysis, provides greater confidence in the identification of flavonoids in *Ficus* sp. extract.

- The co-eluting interference peak with orientin are easily visualized using 3D models and drift-time plots generated using DriftScope. While further spectra cleanup for accurate product ions fingerprint for qualitative analysis is achieved using MS$^E$ Data Viewer.

### References

1. K Robards, M Antolovich. Analytical chemistry of fruit bioflavonoids. *Analyst.* 122: 11R-34R, 1997.

2. J Zhang, J Yang, J Duan, Z Liang, L Zhang, Y Huo, Y Zhang. Quantitative and qualitative analysis of flavonoids in leaves of *Adinandra nitida* by high performance liquid chromatography with UV and electrospray ionization tandem mass spectrometry detection. *Analytica Chimica Acta.* 532: 97-104, 2005.

3. I Campuzano, K Giles. SYNAPT G2 high definition mass spectrometry: ion mobility separation and structural elucidation of natural product structural isomers. Waters Application Note no. 720003041EN, 2009.

4. R Z Da Silva, R A Yunes, M M de Souza, F D Monache, and V Cechinel-Filho. Antinociceptive properties of conocarpan and orientin obtained from *Piper solmsianum* C. DC. var. *solmsianum* (Piperaceae). *J Nat Med.* 64: 402-408, 2010.

5. Y Zhang, J Jian, C Liu, X Wu, Y Zhang. Isolation and purification of four flavones C-glycosides from antioxidant of bamboo leaves by macroporous resin column chromatography and preparative high-performance liquid chromatography. *Food Chemistry.* 107: 1326-1336, 2008.

## Waters
### THE SCIENCE OF WHAT'S POSSIBLE.®

**Waters Corporation**
34 Maple Street
Milford, MA 01757 U.S.A.
T: 1 508 478 2000
F: 1 508 872 1990
www.waters.com

# An Added Dimension for Metabolite ID Studies Using Ion Mobility Combined with MS$^E$

## GOAL

To use HDMS$^E$ data to generate cleaner, more precise data sets and to resolve isobaric species. When LC/MS and LC/MS/MS just isn't enough, using DriftScope™ Software allows you to interrogate your data in an extra dimension, RT, *m/z*, and now drift time (ion mobility separation).

**HDMS$^E$ (Ion Mobility Mass Spectrometry) provides researchers with added orthogonal separation and peak capacity to differentiate small changes in closely eluting isobaric metabolites.**

## BACKGROUND

When performing metabolite identification it is common to observe multiple biotransformations that give the same isobaric mass. These compounds are often nearly indistinguishable and can be very difficult to resolve by chromatography alone. Extremely high levels of matrix, as is often the case with *in vivo* studies compound the problem. Although re-optimized chromatography, improved instrument sensitivity and careful

interpretation of data can lead to resolution of these species, they are time consuming steps and often require large data sets to be reacquired with modified conditions. Additional orthogonal separation such as ion mobility introduces selectivity that can often quickly resolve these differences and further improve spectral quality, leading to higher quality data sets and interpretations. This combination of Ion Mobility Separation (IMS) and MS$^E$ creates High Definition Mass Spectrometry,™ HDMS$^E$, and gives the researcher another powerful tool to understand and probe their datasets. In this technology brief we will study the applicability of HDMS$^E$ to complex datasets.
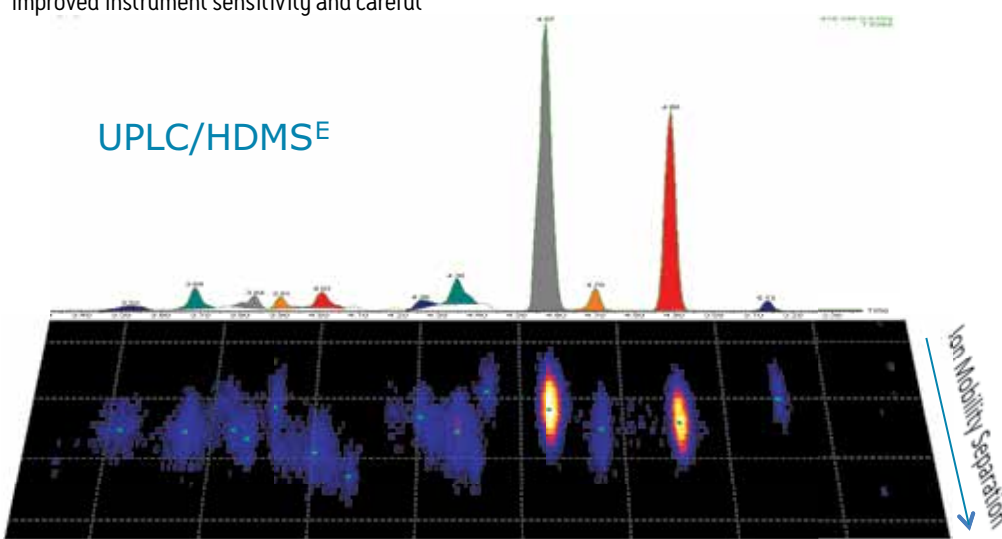


Figure 1. An additional three +32 Da metabolites of buspirone are clearly identified with the added dimension of separation generated by HDMS$^E$.

## THE SOLUTION

Rat liver microsomes spiked with 10 µM buspirone were incubated for 0 and 20 min at 37 °C. Samples were quenched with one volume of cold acetonitrile + 0.1% formic acid and centrifuged. In order to evaluate the application of HDMS$^E$ to *in vivo* metabolite identification studies, the above *in vitro* samples were diluted 10-fold with SD (Sprague Dawley) rat urine containing 0.1 % PEG400 by volume. Samples were analyzed using a Waters® SYNAPT® G2 coupled with an ACQUITY UPLC® System. Data acquisition was performed with HDMS$^E$ in positive ion, sensitivity mode. 5 µL of sample were injected onto an ACQUITY UPLC HSS T3, 1.8 µm, 2.1 x 100 mm Column and run with a 20 min gradient using a flowrate of 0.7 mL/min. The mobile phase consisted of 0.1% formic acid (A) and acetonitrile + 0.1% formic acid (B). Data was processed and visualized using DriftScope Software.

Figure 1 illustrates the added dimension of separation generated by HDMS,™ the additional peak capacity introduced by IMS clearly elucidates an additional three metabolites versus UPLC® alone.

Figure 2 shows a comparison between MS$^E$ data for a dealkylation metabolite generated with and without IMS separation enabled. Precursor and fragment ions that co-elute perfectly with the compound of interest can be quickly resolved using IMS techniques alone. Dedicated software using patented MS$^E$ and IMS peak peaking algorithms (Apex 4D) leads to clear resolution of all relevant peaks. The power of peak picking in four dimensions (RT, *m/z*, ion mobility, and intensity) allows for a thorough cleanup of background noise and artifact peaks.
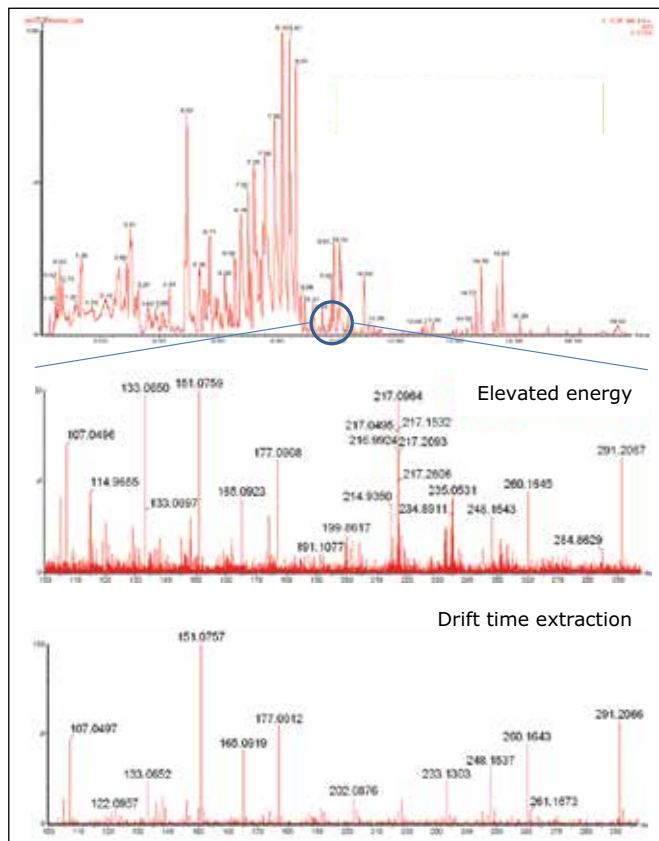


*Figure 2. An illustration of the use of HDMS$^E$ to remove background ions from a fragment ion spectrum in an in vivo sample.*

## SUMMARY

The advances presented in this technology brief facilitate the identification of metabolites, not only with better sensitivity and resolution, but through the unique properties of ion mobility. This allows the user to view data with less interference from matrix and other nominal mass interfering ions not separable through other methods.

Having an entirely unique mode of separation at your fingertips as an additional rich layer of information may mean the difference between an easy analysis and a costly, time-consuming revisiting of already worked out LC and MS methodology.

The benefits of UPLC coupled with SYNAPT G2 HDMS described in this technology brief are now available from Waters. As an additional weapon in your analytical toolkit, ion mobility separation can help you make insightful scientific discoveries and more keenly interpret and understand your experiments.

## Waters
### THE SCIENCE OF WHAT'S POSSIBLE.®

# CHAPTER 3
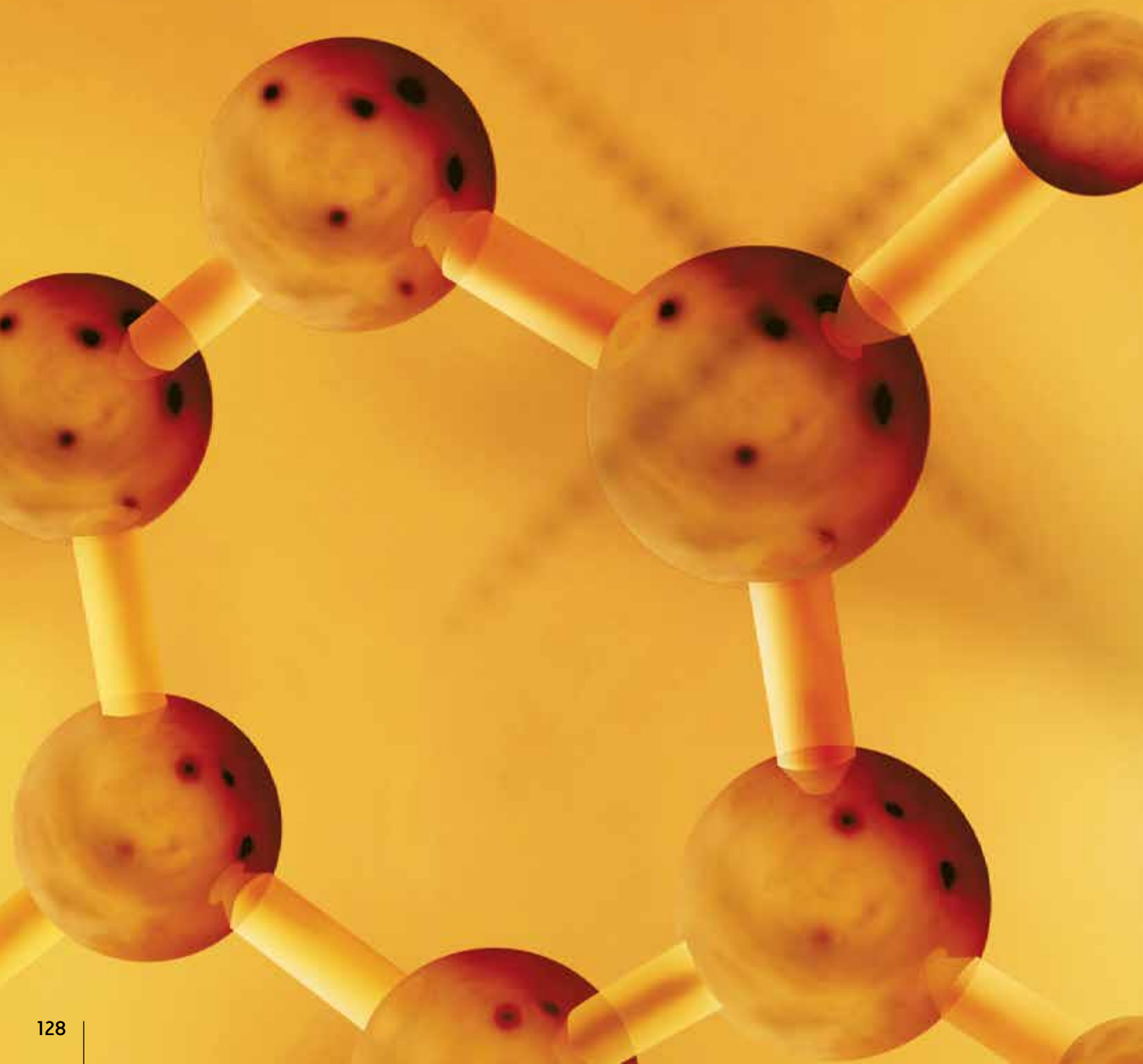
# TARGETED METABOLOMICS AND LIPIDOMICS

Targeted metabolomics and lipidomics are hypothesis-driven approaches that focus on analyzing a selected group of metabolites or lipids. Such approaches are generally used either for validation of initial discoveries or routine analysis for clinical research. The specific metabolites/lipids that will undergo analysis are selected according to the questions asked, and ad hoc analytical methods are developed for their quantification.

Waters innovative chromatographic solutions together with multiple-reaction monitoring (MRM) transitions on the MS instruments help to increase the number of analytes that can be simultaneously quantified in a single acquisition without losses in sensitivity.

- Advanced chromatographic separations of lipids and metabolites coupled with a range of ionization capabilities (UPLC, ionKey, UPC$^2$, APGC)
- High sensitivity and robustness enabling reproducible detection of metabolites and lipids at low levels in complex biological matrices
- Multiple analyses on limited sample volumes and reduced solvent consumption.
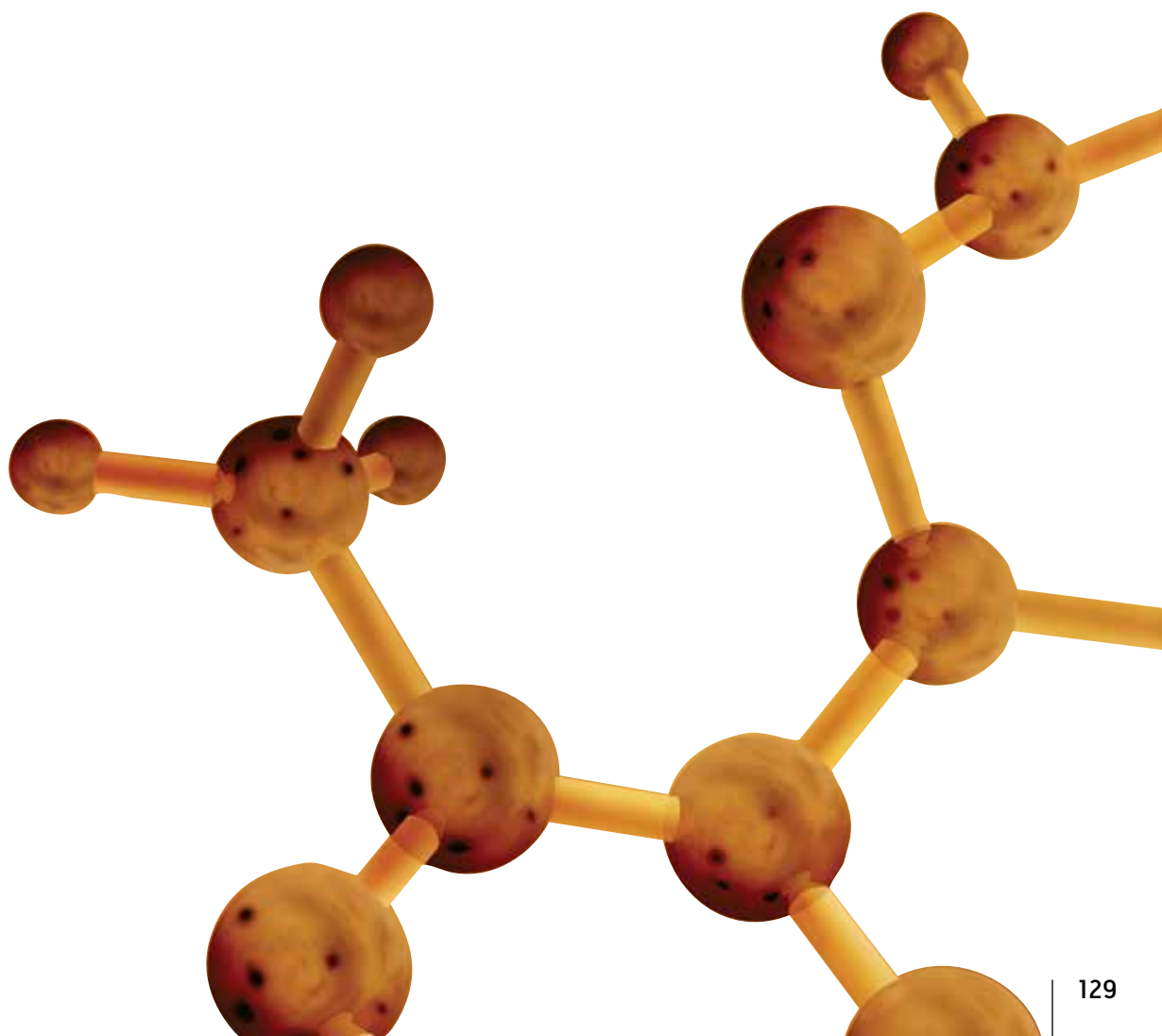
# A Validated Assay for the Quantification of Amino Acids in Mammalian Urine

Nicola Gray and Robert Plumb
Waters Corporation, Milford, MA, USA

## APPLICATION BENEFITS

■ A simple, robust, LC/MS/MS assay for the absolute quantification of 20 amino acids in human urine has been developed over the range of 0.2–200.0 µMol.

■ Fast analytical throughput: two, microtiter plates (192 samples) per day.

## WATERS SOLUTIONS

Xevo® TQ-S micro

ACQUITY® HSS Columns

ACQUITY UPLC® I-Class

AccQ•Tag™ Ultra

MassLynx® Software

TargetLynx™ Application Manager

StepWave™ ion guide

## KEY WORDS

TQS micro, amino acid, quantification, urine, LC/MS

## INTRODUCTION

Amino acids play a critical role in mammalian biochemistry, forming the simple building blocks of proteins, acting as neurotransmitters in biosynthesis and are essential in lipid transports, to name but a few. The rapid and accurate quantification of amino acids is critical to understanding the underlying biochemistry of multiple physiological and disease states. Previous methodologies have employed either ion exchange chromatography followed by derivatization with fluorescence detection or sample derivatization followed by analysis by LC/UV or LC-Fluorescence. However, both of these approaches are time consuming and require complete chromatographic resolution of the amino acids from other amine-containing compounds, so are not always suitable for the analysis of biological fluids. Here we present a method for the rapid, simple, quantification of amino acids by UPLC/MS/MS.
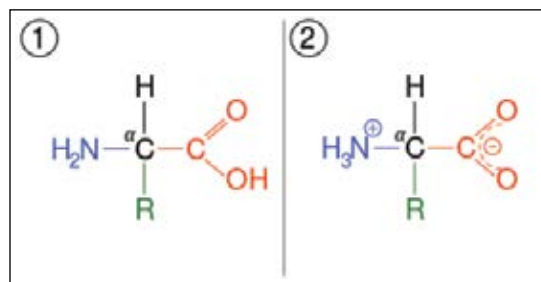


Figure 1. Amino acid structure.

## EXPERIMENTAL

### LC conditions

| | |
|---|---|
| LC system: | ACQUITY UPLC I-Class |
| Detector: | Xevo TQ-S micro |
| Vials: | Maximum Recovery vials |
| Column: | ACQUITY UPLC HSS T3 1.8 µm, 150 x 2.1 mm |
| Column temp.: | 45 °C |
| Sample temp.: | Room temperature |
| Injection vol.: | 2-µL |
| Flow rate: | 0.6 mL/min |
| Mobile phase A: | water + 0.1% formic acid |
| Mobile phase B: | acetonitrile + 0.1 % formic acid |
| Gradient: | Maintained at 4% B for 0.5 min; increasing to 10% B at 2.5 min; increasing to 28% B at 5 min, increasing to 95% B at 5 .1 min; reverting to 4% B at 6.2 min for a 1.3 min re-equilibration see Table 1 |

### MS conditions

| | |
|---|---|
| MS system: | Xevo TQ-S micro |
| Ionization mode: | Positive |
| Acquisition range: | MRM mode |
| Capillary voltage: | 1.5 kV |
| Collision energy: | Compound specific see Table 2 |
| Cone voltage: | Compound specific see Table 2 |

## Sample preparation

The sample preparation procedure employed for the analysis of the amino acids is shown below in Figure 2. A 50-µL aliquot of the samples and standards was vortex mixed with 150-µL of methanol, to precipitate protein. A 10-µL aliquot of the resultant sample was then transferred to a sample tube for derivatization according to the process defined in Figure 2.

**Sample – urine, plasma, serum**
- Protein precipitation using $CH_3OH$ + 0.1% formic acid
- Addition of isotope labeled internal standards

**Derivatization**
- 10 µL sample + 70 µL borate buffer (pH 8.6)
- Derivatization with 20 µL AccQ•Tag Ultra at 55 °C for 10 min

**Chromatography**
- Reversed-phase HSS T3 2.1 x 150 mm, 1.8 µm at 45 °C
- Gradient elution with $H_2O$ and $CH_3CN$ + 0.1% formic acid

**Xevo TQ-S micro**
- Electrospray ionization (positive mode)
- Selected reaction monitoring

*Figure 2. Sample preparation scheme for amino acid analysis.*

| Time (min) | Flow rate (mL/min) | %B |
|---|---|---|
| 0.0 | 0.6 | 4 |
| 0.5 | 0.6 | 4 |
| 2.5 | 0.6 | 10 |
| 5.0 | 0.6 | 28 |
| 5.1 | 0.6 | 95 |
| 6.1 | 0.6 | 95 |
| 6.2 | 0.6 | 4 |
| 7.5 | 0.6 | 4 |

*Table 1. Chromatographic gradient table.*

| Compound | Parent | Fragment | Window (min) | Dwell time (s) | CV (V) | CE (eV) | RT (min) |
|---|---|---|---|---|---|---|---|
| Histidine-d3 | 329.1 | 159.1 | 0.0–2.0 | 0.026 | 20 | 10 | 1.51 |
| Histidine | 326.1 | 156.1 | 0.0–2.0 | 0.026 | 20 | 10 | 1.52 |
| 1-methylhistidine | 340.1 | 170.1 | 0.0–2.0 | 0.026 | 30 | 18 | 1.70 |
| 4-hydroxyproline | 302.0 | 171.1 | 1.5–2.0 | 0.026 | 10 | 22 | 1.78 |
| 3-methylhistidine | 340.1 | 124.2 | 0.0–2.0 | 0.026 | 30 | 28 | 1.78 |
| Carnosine | 397.1 | 227.2 | 1.8–2.2 | 0.026 | 30 | 14 | 1.99 |
| Asparagine | 303.1 | 171.1 | 1.8–2.1 | 0.026 | 30 | 22 | 2.00 |
| Arginine | 345.1 | 70.1 | 1.8–2.2 | 0.026 | 30 | 36 | 2.01 |
| Taurine | 296.1 | 116.3 | 2.0–2.5 | 0.026 | 30 | 60 | 2.22 |
| Glutamine-d5 | 322.1 | 171.1 | 2.0–2.5 | 0.026 | 30 | 24 | 2.27 |
| Glutamine | 317.1 | 171.1 | 2.0–2.5 | 0.026 | 30 | 24 | 2.29 |
| Serine-d3 | 279.1 | 171.1 | 2.0–2.5 | 0.026 | 30 | 20 | 2.30 |
| Serine | 276.1 | 171.1 | 2.0–2.5 | 0.026 | 30 | 20 | 2.32 |
| Homoserine | 290.1 | 171.1 | 2.2–2.6 | 0.030 | 10 | 18 | 2.46 |
| Ethanolamine | 232.1 | 171.1 | 2.2–2.7 | 0.030 | 10 | 20 | 2.47 |
| Glycine | 246.1 | 116.1 | 2.2–2.8 | 0.013 | 30 | 14 | 2.54 |
| Aspartic acid-d3 | 307.0 | 171.1 | 2.5–2.8 | 0.030 | 30 | 20 | 2.67 |
| Aspartic acid | 304.1 | 171.1 | 2.5–2.8 | 0.030 | 30 | 22 | 2.69 |
| Citrulline | 346.2 | 171.1 | 2.5–2.9 | 0.030 | 30 | 26 | 2.77 |
| Sarcosine | 260.1 | 116.1 | 2.6–3.6 | 0.024 | 30 | 44 | 2.85 |
| Glutamic acid-d3 | 321.0 | 171.0 | 2.5–3.2 | 0.030 | 30 | 20 | 2.90 |
| Glutamic acid | 318.1 | 171.1 | 2.5–3.2 | 0.030 | 30 | 22 | 2.91 |
| β-alanine | 260.1 | 116.1 | 2.6–3.6 | 0.024 | 30 | 44 | 3.06 |
| Threonine | 290.1 | 171.1 | 2.9–3.2 | 0.062 | 30 | 20 | 3.11 |
| Threonine-13C4 15N | 295.1 | 171.0 | 2.9–3.2 | 0.062 | 30 | 26 | 3.11 |
| Alanine-d3 | 263.1 | 171.0 | 3.2–3.6 | 0.024 | 30 | 16 | 3.45 |
| Alanine | 260.1 | 116.1 | 2.6–3.6 | 0.024 | 30 | 44 | 3.47 |
| γ-amino-n-butyric acid | 274.1 | 171.1 | 3.2–4.2 | 0.013 | 10 | 20 | 3.51 |
| Hydroxylysine | 333.2 | 171.1 | 3.4–4.0 | 0.013 | 16 | 16 | 3.56 |
| Aminoadipic acid | 332.1 | 171.1 | 3.2–3.8 | 0.024 | 30 | 18 | 3.61 |
| Proline-d7 | 293.0 | 171.1 | 3.5–4.0 | 0.013 | 30 | 24 | 3.74 |
| Proline | 286.1 | 116.1 | 3.5–4.0 | 0.013 | 30 | 50 | 3.77 |
| β-aminoisobutyric acid | 274.1 | 171.1 | 3.2–4.2 | 0.013 | 10 | 20 | 3.78 |
| Ornithine | 303.1 | 171.1 | 3.6–4.2 | 0.013 | 54 | 22 | 3.85 |
| Cystathionine | 393.2 | 171.1 | 3.5–4.1 | 0.013 | 66 | 18 | 3.86 |
| Phosphoserine | 356.1 | 171.1 | 3.8–4.2 | 0.013 | 20 | 18 | 4.05 |
| Lysine 224-d4 | 246.1 | 171.1 | 3.8–4.3 | 0.013 | 30 | 14 | 4.07 |
| Cystine 291 | 291.1 | 171.1 | 3.8–4.2 | 0.013 | 10 | 12 | 4.07 |
| Cystine 411 | 411.0 | 171.1 | 3.8–4.2 | 0.013 | 60 | 18 | 4.07 |
| Cystine 581 | 581.0 | 171.1 | 3.8–4.2 | 0.013 | 34 | 26 | 4.07 |
| Lysine 487-d4 | 491.2 | 171.0 | 3.8–4.3 | 0.013 | 30 | 32 | 4.07 |
| Lysine 317-d4 | 321.1 | 171.0 | 3.8–4.3 | 0.013 | 50 | 24 | 4.07 |
| Lysine 244 | 244.2 | 171.1 | 3.8–4.3 | 0.030 | 30 | 12 | 4.08 |
| Lysine 317 | 317.1 | 171.1 | 3.8–4.3 | 0.013 | 56 | 16 | 4.08 |
| Lysine 487 | 487.1 | 171.0 | 3.8–4.3 | 0.013 | 18 | 34 | 4.08 |
| α-amino-n-butyric acid | 274.1 | 171.1 | 3.2–4.2 | 0.013 | 10 | 20 | 4.09 |
| Tyrosine | 352.1 | 171.1 | 4.2–4.8 | 0.046 | 30 | 24 | 4.45 |
| Methionine | 320.1 | 171.1 | 4.3–4.8 | 0.046 | 30 | 22 | 4.58 |
| Valine-d8 | 296.1 | 171.1 | 4.4–4.8 | 0.046 | 30 | 20 | 4.61 |
| Valine | 288.1 | 171.1 | 4.4–4.8 | 0.046 | 30 | 16 | 4.64 |
| Isoleucine-d10 | 312.1 | 171.0 | 5.0–5.5 | 0.048 | 30 | 20 | 5.21 |
| Isoleucine | 302.1 | 171.1 | 5.0–5.5 | 0.048 | 30 | 20 | 5.24 |
| Leucine-d10 | 312.1 | 171.0 | 5.0–5.5 | 0.048 | 30 | 20 | 5.27 |
| Leucine | 302.1 | 171.1 | 5.0–5.5 | 0.048 | 30 | 20 | 5.31 |
| Phenylalanine-d5 | 341.1 | 171.1 | 5.2–5.7 | 0.048 | 30 | 22 | 5.43 |
| Phenylalanine | 336.1 | 171.1 | 5.2–5.7 | 0.048 | 30 | 22 | 5.45 |
| Tryptophan-d3 | 378.1 | 171.1 | 5.2–5.8 | 0.048 | 6 | 24 | 5.54 |
| Tryptophan | 375.1 | 171.1 | 5.2–5.8 | 0.048 | 30 | 26 | 5.55 |

*Table 2. Mass spectrometric analysis conditions for amino acids.*

## Data management

■ MassLynx Mass Spectrometry Software

■ TargetLynx Application Manager

## One day validation

The assay was subjected to a one day validation according to the FDA guidelines for bioanalytical assay validation. The samples employed are shown below:

■ Double blank (with no analyte or internal standard)

■ Single blank (with analyte but no internal standard)

■ Eight point calibration curve (performed at the beginning and end of run)

■ Six replicates of:
  ■ LLOQQC (0.2 μM)
  ■ LQC (0.6 μM)
  ■ MQC (30 μM)
  ■ HQC (160 μM)
  ■ ULOQQC (20 μM)

■ Twenty rat urine samples from a toxicology study ([4-chloro-6-(2, 3-xylidino)-2-pyrimidinylthio]acetic acid) were used to test the robustness of the assay.

## Amino acids quantified in this assay

The amino acids analyzed in this study are listed in Table 3. The twenty proteinogenic amino acids were subjected to validation for absolute quantification using stable isotope labeled internal standards. Those additional eighteen amino acids, for which no stable isotope labeled internal standard was used, were subjected to relative quantification. The stable isotopes employed for each amino acid is listed in Table 4.

| Validated For Absolute Quantification | Monitored For Relative Quantification |
|---|---|
| L-Alanine | 3-Methyl-L-histidine |
| L-Arginine | 1-Methyl-L-histidine |
| L-Asparagine | Cystathionine |
| L-Aspartic acid | DL-β-Aminoisobutryic acid |
| L-Cystine | Ethanolamine |
| L-Glutamic acid | Homoserine |
| L-Glutamine | Hydroxy-L-proline |
| Glycine | Hydroxylysine |
| L-Histidine | L-Carnosine |
| L-Isoleucine | L-Citrulline |
| L-Leucine | L-Ornithine |
| L-Lysine | L-α-aminoadipic acid |
| L-Methionine | L-α-Amino-n-butyric acid |
| L-Phenylalanine | Phosphoserine |
| L-Proline | Sarcosine |
| L-Serine | Taurine |
| L-Threonine | β-Alanine |
| L-Tryptophan | γ-Amino-n-butyric acid |
| L-Tyrosine | |
| L-Valine | |

Table 3. Amino acids subjected to absolute and relative quantification.

| Compound | Labeled internal standard |
|---|---|
| L-Alanine | Alanine-d3 |
| L-Arginine | Serine-d3 |
| L-Asparagine | Serine-d3 |
| L-Aspartic acid | Aspartic acid-d3 |
| L-Cystine | Proline-d7 |
| L-Glutamic acid | Glutamic acid-d3 |
| L-Glutamine | Glutamine-d5 |
| Glycine | Serine-d3 |
| L-Histidine | Histidine-d3 |
| L-Isoleucine | Isoleucine-d10 |
| L-Leucine | Leucine-d10 |
| L-Lysine | Lysine-d4 |
| L-Methionine | Valine-d8 |
| L-Phenylalanine | Phenylalanine-d5 |
| L-Proline | Proline-d7 |
| L-Serine | Serine-d3 |
| L-Threonine | Threonine-13C4 |
| L-Tryptophan | Tryptophan-d5 |
| L-Tyrosine | Tyrosine-d7 |
| L-Valine | Valine-d8 |

Table 4. Amino acids quantified using stable isotope labeled internal standards.

## Calibration Curves

The calibration line was prepared from a Sigma Aldrich physiological, amino acid standard (acidics, basics, neutrals) by spiking into 50/50 $CH_3OH/H_2O$. The calibration curve was generated over three orders of magnitude, covering the physiological range of 0.2-200.0 µM. The QC samples were prepared from a separate Sigma Aldrich physiological amino acid standard.

## RESULTS AND DISCUSSION

A typical separation obtained from the amino acid standard mix is shown in Figure 3. The data displayed illustrates the separation obtained for the amino acids and the throughput of the assay. The peak shape obtained from the chromatography was excellent with a peak width at the base of approximately 3 seconds. The assay was shown to be reproducible and reliable with no retention time drift. The Xevo TQ-S micro is equipped with a new novel, state of the art, ion transfer optics which allows more ions to be sampled from the source and transferred to the analyser. The StepWave ion guide in the Xevo TQ-S micro is designed to cope with the challenges of the modern laboratory that are produced by high sample throughput and difficult matrices. Neutrals and gas load are passively removed for enhanced transmission with the ions actively transferred into the mass analyzer, improving sensitivity and robustness.
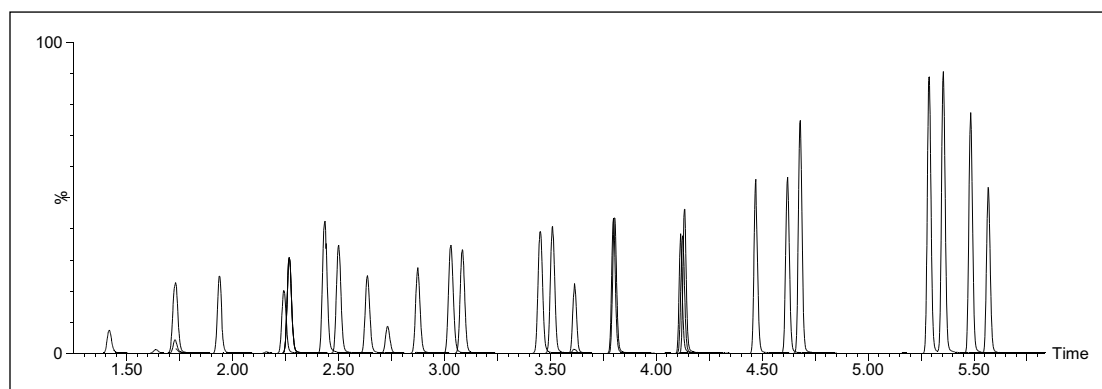


Figure 3. Amino acid LC/MS QC chromatogram 200 µM.

## Validation results

The assay validation was carried out according to FDA guidelines. The resulting amino acid data was processed and quantified using Waters® MassLynx Software with TargetLynx Application Manager employing internal standard calibration and 1/x weighting. A summary of the QC data for each amino acid is listed below in Table 5. The data obtained for the quantification of each amino acid was acceptable for routine quantification.

| Amino Acid | 0.2 µM | 0.6 µM | 6 µM | 30 µM | 160 µM | 200 µM |
|---|---|---|---|---|---|---|
| Aspartic Acid | 7.26 | 3.40 | 2.02 | 0.91 | 0.80 | 0.83 |
| Asparagine | 6.30 | 4.13 | 1.01 | 1.71 | 1.74 | 2.58 |
| Cystine | 5.73 | 3.17 | 3.00 | 4.72 | 2.13 | 1.70 |
| Glutamic Acid | 9.81 | 3.02 | 1.28 | 0.88 | 0.88 | 3.31 |
| Glutamine | 3.23 | 3.86 | 0.49 | 1.18 | 0.73 | 1.11 |
| Glycine | 17.92 | 8.48 | 2.32 | 2.31 | 2.27 | 3.21 |
| Histidine | 2.68 | 5.30 | 3.26 | 3.95 | 2.06 | 3.37 |
| Isoleucine | 5.29 | 0.57 | 3.06 | 1.57 | 0.63 | 0.75 |
| Leucine | 5.09 | 1.19 | 1.09 | 3.07 | 0.31 | 0.38 |
| Lysine | 7.46 | 3.11 | 2.48 | 1.10 | 1.07 | 1.29 |
| Methionine | 0.91 | 2.25 | 1.59 | 1.16 | 2.12 | 1.40 |
| Phenylalanine | 4.85 | 1.15 | 0.95 | 0.77 | 5.13 | 0.83 |
| Proline | 8.56 | 3.31 | 1.68 | 1.58 | 0.95 | 1.09 |
| Serine | 23.57 | 6.47 | 2.46 | 1.85 | 1.61 | 2.33 |
| Threonine | 4.30 | 2.45 | 1.25 | 1.24 | 1.06 | 0.68 |
| Tryptophan | 1.88 | 2.14 | 1.74 | 1.00 | 5.86 | 1.38 |
| Tyrosine | 5.32 | 2.52 | 2.96 | 2.32 | 4.43 | 2.79 |
| Valine | 3.55 | 1.12 | 1.65 | 0.44 | 1.01 | 0.84 |

Table 5. Coefficient of variation (%) for QCs at various concentrations.

The validation results as well as example chromatograms and calibration lines for the amino acids glutamic acid and aspartic acid are shown in Figures 4–7 and Tables 6 and 7. Here we can see that the methodology demonstrated acceptable peak shape and signal to noise ratio at the lowest level of quantification. The assay demonstrated excellent bias and precision for every amino acid.



Compound name: Glutamic acid
Correlation coefficient: r = 0.999953, r$^2$ = 0.999907
Calibration curve: 0.0907391 * x + 0.000270687
Response type: Internal Std ( Ref 9 ), Area * ( IS Conc. / IS Area )
Curve type: Linear, Origin: Exclude, Weighting: 1/x, Axis trans: None
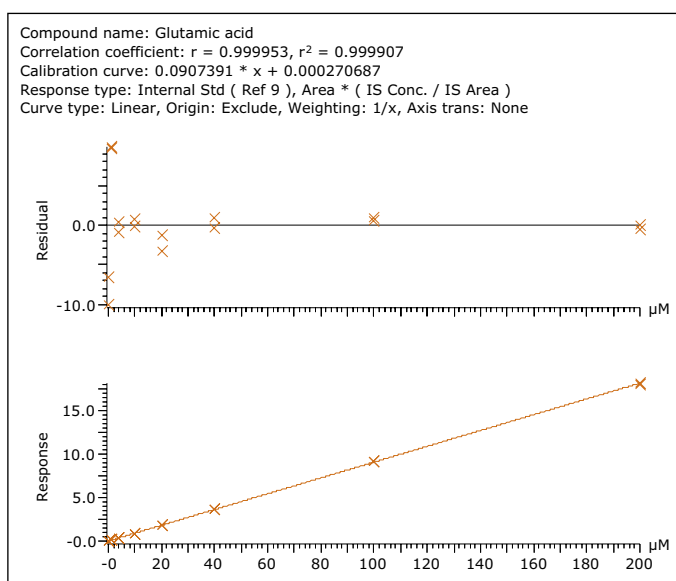
Figure 4. Calibration line for glutamic acid.
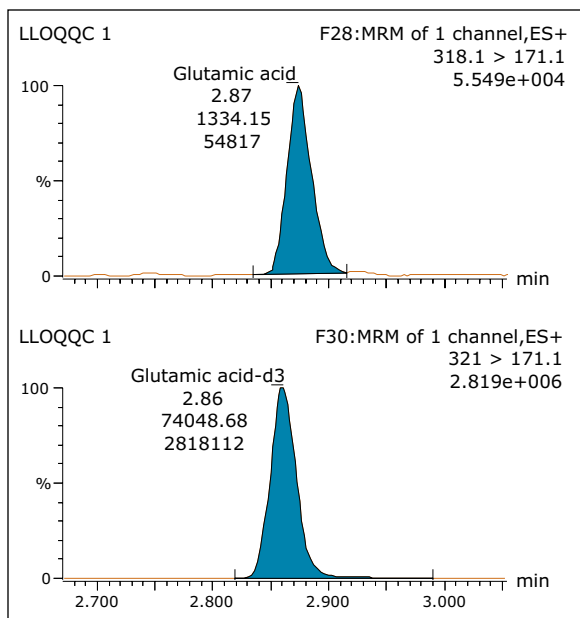
Figure 5. Lower limit of quantification QC (0.2 µM) LC/MS chromatogram for glutamic acid.
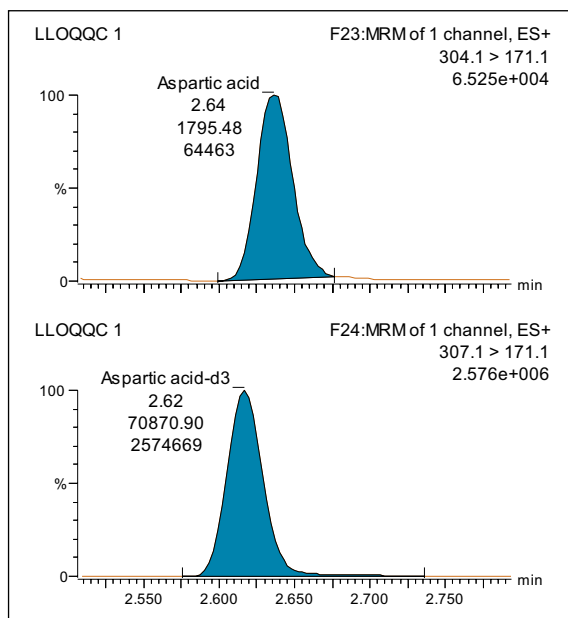


Figure 6. Lower limit of quantification QC (0.2 µM) LC/MS chromatogram for aspartic acid.



Compound name: Aspartic acid
Correlation coefficient: r = 0.999880, r² = 0.999761
Calibration curve: 0.0871411 * x + 0.00714136
Response type: Internal Std (Ref 5), Area * (IS Conc. / IS Area)
Curve type: Linear, Origin: Exclude, Weighting: 1/x, Axis trans: None
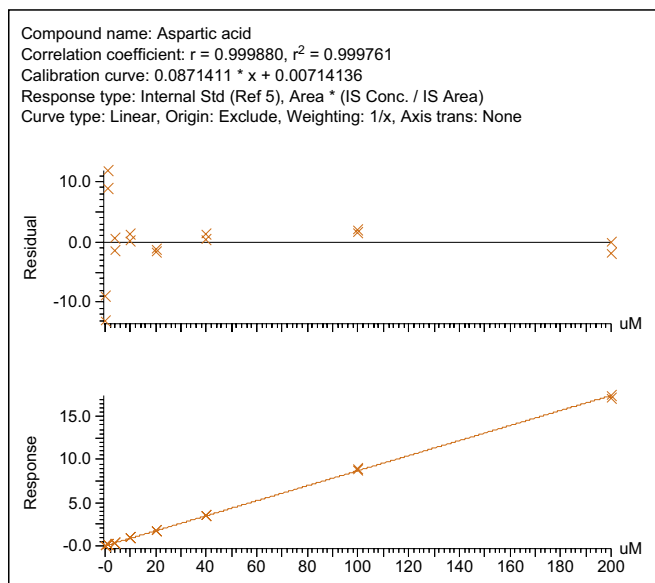
Figure 7. Calibration line for aspartic acid.

| Occasion | QC Nominal Concentration (µM) Glutamic acid | | | | |
|---|---|---|---|---|---|
| | 0.2 | 0.6 | 30 | 160 | 200 |
| 1 | 0.20 | 0.58 | 28.6 | 154 | 211 |
| 2 | 0.22 | 0.58 | 29.3 | 158 | 194 |
| 3 | 0.20 | 0.58 | 29.2 | 155 | 198 |
| 4 | 0.20 | 0.58 | 28.8 | 156 | 194 |
| 5 | 0.25 | 0.62 | 28.9 | 156 | 197 |
| 6 | 0.19 | 0.57 | 29.0 | 158 | 194 |
| Mean | 0.21 | 0.58 | 29.0 | 156 | 198 |
| STDEV | 0.02 | 0.02 | 0.25 | 1.37 | 6.56 |
| %CV | 9.81 | 3.02 | 0.88 | 0.88 | 3.31 |
| Bias | 4.08 | -2.56 | -3.36 | -2.37 | -1.05 |

Table 6. QC validation data for glutamic acid.

| Occasion | QC Nominal Concentration (µM) Aspartic acid | | | | |
|---|---|---|---|---|---|
| | 0.2 | 0.6 | 30 | 160 | 200 |
| 1 | 0.21 | 0.58 | 28.7 | 154 | 194 |
| 2 | 0.24 | 0.60 | 29.3 | 157 | 191 |
| 3 | 0.21 | 0.62 | 29.4 | 157 | 192 |
| 4 | 0.21 | 0.56 | 29.2 | 155 | 195 |
| 5 | 0.24 | 0.59 | 29.3 | 155 | 195 |
| 6 | 0.20 | 0.60 | 29.2 | 158 | 195 |
| Mean | 0.22 | 0.59 | 29.2 | 156 | 194 |
| STDEV | 0.02 | 0.02 | 0.27 | 1.24 | 1.61 |
| %CV | 7.26 | 3.40 | 0.91 | 0.80 | 0.83 |
| Bias | 9.17 | -1.22 | -2.66 | -2.50 | -3.19 |

Table 7. QC validation data for aspartic acid.

## CONCLUSION

A robust, reliable method for the absolute quantification of twenty amino acids and the relative quantification of a further eighteen amino acids in human urine has been developed and evaluated. The assay had an analysis time of 7.5 minutes per sample. This allows the analysis of two, 96-well, microtitre plates of samples in a 24 hour time period. The assay was found to be valid over the physiologically important range of 0.2–200.0 µMol. The chromatography was reproducible and reliable with no retention time drift detected for any of the amino acids. This data demonstrates that LC/MS/MS provides an attractive and viable alternative to traditional modes of amino acid analysis, providing fast and accurate quantification.

## Waters

**THE SCIENCE OF WHAT'S POSSIBLE.**®

**Waters Corporation**
34 Maple Street
Milford, MA 01757 U.S.A.
T: 1 508 478 2000
F: 1 508 872 1990
www.waters.com

# Targeted Metabolomics Using the UPLC/MS-based Absolute*IDQ* p180 Kit

Evagelia C. Laiakis,[1] Ralf Bogumil,[2] Cornelia Roehring,[2] Michael Daxboeck,[2] Steven Lai,[3] Marc Breit,[2] John Shockcor,[3] Steven Cohen,[3] James Langridge,[4] Albert J. Fornace Jr.,[1] and Giuseppe Astarita[1,3]

[1] Department of Biochemistry and Molecular and Cellular Biology, Georgetown University, Washington DC, USA
[2] BIOCRATES Life Sciences AG, Innsbruck, Austria
[3] Waters Corporation, Milford and Beverly, MA, USA
[4] Waters Corporation, Manchester, UK

## APPLICATION BENEFITS

Waters® ACQUITY UPLC® System with Xevo® TQ and Xevo TQ-S mass spectrometers combines with the commercially available Absolute*IDQ* p180 Kit (BIOCRATES Life Sciences AG, Innsbruck, Austria) to allow for the rapid identification and highly sensitive quantitative analyses of more than 180 endogenous metabolites from six different biochemical classes (biogenic amines, amino acids, glycerophospholipids, sphingolipids, sugars, and acylcarnitines). The assay is performed using MS-based flow injection and liquid chromatography analyses, which were validated on Waters' tandem quadrupole instruments.

## WATERS SOLUTIONS

ACQUITY UPLC System

ACQUITY UPLC BEH Columns

Xevo TQ Mass Spectrometer

Xevo TQ-S Mass Spectrometer

TargetLynx™ Application Manager

## KEY WORDS

Absolute*IDQ* p180 Kit, flow injection analysis (shotgun), targeted metabolomics, targeted lipidomics, MetIDQ software

## INTRODUCTION

Global metabolic profiling (untargeted metabolomics) is used for the identification of metabolic pathways that are altered following perturbations of biological systems, as shown in Figure 1. The analysis, however, encompasses significant statistical processing that leads to a low rate of successful identification of biomarkers. Additionally, a tedious marker validation process using pure standards is often required for the identification of a particular metabolite, unless an in-house database has been previously generated. Furthermore, the sample preparation required for the extraction of metabolites is a multi-step process that, without a standardization of the operating procedures, likely contributes to the intra- and inter-laboratory variations in the measurements.
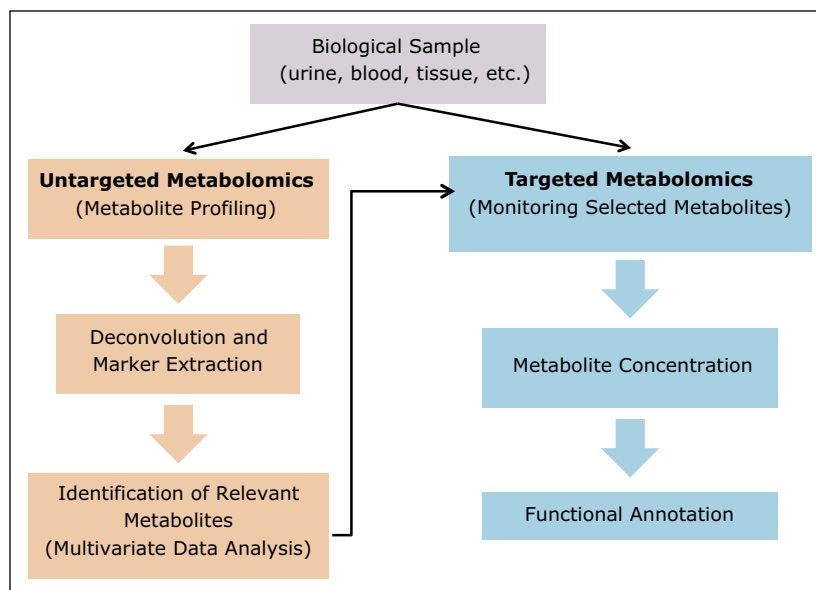


Figure 1. Workflows illustrating both untargeted and targeted metabolomics approaches.

To alleviate many of these limiting issues, another approach involves the application of targeted metabolomics assay, seen in Figure 1. The Absolute*IDQ* p180 (BIOCRATES Life Sciences AG) Kit is an MS-based assay for targeted metabolomics allowing the simultaneous identification and quantification of over 180 endogenous metabolites in biological samples.[1-2] MS-based flow injection analysis (FIA) for acylcarnitines, hexoses, glycerophospholipids, and sphingolipids as well as an MS-based LC method for amino acids and biogenic amines are used to provide a robust, high-throughput identification of preselected metabolites, as shown in Figure 2. Here, we applied this targeted metabolomics strategy to identify biochemical alterations and potential biomarkers in serum from mice exposed to 8 Gy of gamma radiation. Significant differences allowed for the identification of metabolites that could be used to develop a signature of radiation exposure in mice.

| Metabolite group | No. of metabolites | FIA-MS/MS | LC-MS/MS |
|---|---|---|---|
| Amino acids and biogenic amines | 40 | | X |
| Acylcarnitines | 40 | X | |
| Lyso-phosphatidylcholines | 14 | X | |
| Phosphatidylcholines | 74 | X | |
| Sphingomyelins | 14 | X | |
| Hexose | 1 | X | |
| Total | 183 | | |

Figure 2. List of metabolite classes and total metabolites covered by the kit.

## EXPERIMENTAL

### Mouse irradiation and sample collection

Male C57Bl/6 mice (8 to 10 weeks old) were irradiated at Georgetown University with 8 Gy of gamma rays (^{137}Cs source, 1.67 Gy/min). Blood was obtained by cardiac puncture 24 h post-irradiation, and serum was collected with serum separators (BD Biosciences, CA). All experimental conditions and animal handling were in accordance with animal protocols approved by the Georgetown University Animal Care and Use Committee (GUACUC).

### Sample preparation and data analysis

Metabolites were extracted from mouse sera using a specific 96-well plate system for protein-removal, internal standard normalization and derivatization (Absolute*IDQ* p180 Kit). The preparation was performed according to the Kit User Manual. Briefly, 10 samples (n=5 sham irradiated group and n=5 irradiated group) were added to the center of the filter on the upper 96-well plate kit at 10 μL per well, and dried using a nitrogen evaporator. Subsequently, 50 μL of a 5% solution of phenylisothiocyanate was added for derivatization of the amino acids and biogenic amines. After incubation, the filter spots were dried again using a nitrogen evaporator. The metabolites were extracted using 300 μL of a 5-mM ammonium acetate solution in methanol, and transferred by centrifugation into the lower 96-deep well plate. The extracts were diluted with 600 μL of the MS running solvent for further MS analysis using Waters tandem quadrupole mass spectrometers. One blank sample (no internal standards and no sample added), three water-based zero samples (phosphate buffered saline), and three quality control samples were also added to the Kit plate. The quality controls were comprised of human plasma samples containing metabolites, at several concentration

levels, used to verify the performance of the assay and mass spectrometer. A seven-points serial dilution of calibrators was added to the kit's 96-well plate to generate calibration curves for the quantification of biogenic amines and amino acids. The kit included a mixture of internal standards for the quantification of the natural metabolites as follows: chemical homologous internal standards were used for the quantification of glycerophospholipid and sphingomyelin species; whereas, stable isotopes-labeled internal standards were used to quantify the other compound classes. The amount of internal standards was identical in each well, and the internal standard intensities of zero sample and sample wells were compared to allow conclusions on ion suppression effects.

Acylcarnitines, glycerophospholipids, and sphingolipids were analyzed using the Waters tandem quadrupole mass spectrometers (Xevo TQ and Xevo TQ-S MS) by flow injection analysis (FIA) in positive mode, as shown in Figure 3. Hexose was analyzed using a subsequent FIA acquisition in negative mode. Amino acids and biogenic amines were analyzed using an ACQUITY UPLC System connected to the Xevo tandem quadrupole and Xevo TQ-S mass spectrometers in positive mode, as shown in Figure 4.

Identification and quantification of the metabolites was achieved using internal standards and multiple reaction monitoring (MRM) detection. Data analysis and calculation of the metabolite concentrations analyzed by FIA (acylcarnitines, glycerophospholipids, sphingolipids, and hexoses) is automated using Met*IDQ* software (BIOCRATES Life Sciences AG), an integral part of the kit that imports Waters' raw data files. Analysis of peaks obtained by HPLC/UPLC® (amino acids and biogenic amines) was performed using TargetLynx Application Manager, and the results were imported into Met*IDQ* software for further processing and statistical analysis.
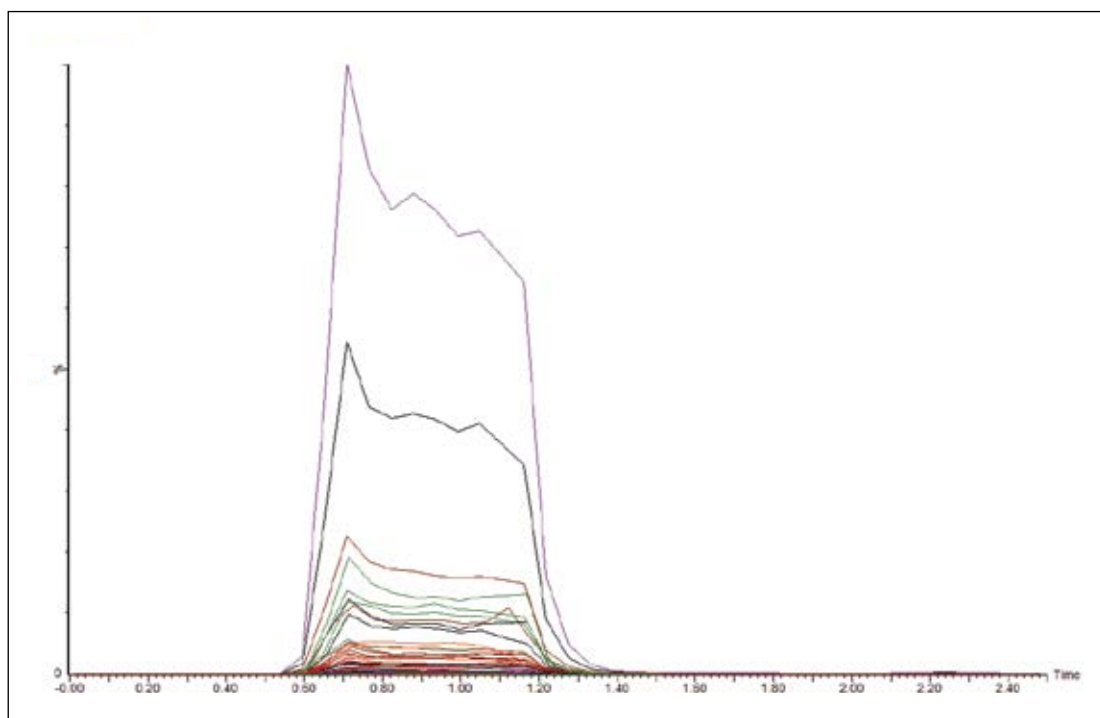


Figure 3. Representative FIA chromatogram.

## LC pump settings

Mobile phase A: water and 0.2% formic acid

Mobile phase B: ACN and 0.2% formic acid

## HPLC column

Column: Agilent Zorbax Eclipse XDB C$_{18}$, 3.0 x 100 mm, 3.5 µm

Pre-Column: SecurityGuard, Phenomenex, C$_{18}$, 4 x 3 mm

| Step | Time (min) | Flow (mL/min) | % A | % B | Curve |
|------|-----------|---------------|-------|------|---------|
| 0 | 0.00 | 0.5 | 100.0 | 0.0 | Initial |
| 1 | 0.50 | 0.5 | 100.0 | 0.0 | 6 |
| 2 | 4.00 | 0.5 | 30.0 | 70.0 | 6 |
| 3 | 5.30 | 0.5 | 30.0 | 70.0 | 6 |
| 4 | 5.40 | 0.5 | 100.0 | 0.0 | 6 |
| 5 | 7.30 | 0.5 | 100.0 | 0.0 | 6 |

## UPLC column

Column: Waters ACQUITY UPLC BEH C$_{18}$ 2.1 x 50 mm, 1.7 µm

Pre-Column: Waters ACQUITY UPLC BEH C$_{18}$ VanGuard,™ 1.7 µm

| Step | Time (min) | Flow (mL/min) | % A | % B | Curve |
|------|-----------|---------------|-------|------|---------|
| 0 | Initial | 0.9 | 100.0 | 0.0 | Initial |
| 1 | 0.25 | 0.9 | 100.0 | 0.0 | 6 |
| 2 | 3.75 | 0.9 | 40.0 | 60.0 | 6 |
| 3 | 3.95 | 0.9 | 40.0 | 60.0 | 6 |
| 4 | 4.25 | 0.9 | 100.0 | 0.0 | 6 |
| 5 | 4.35 | 0.9 | 100.0 | 0.0 | 6 |

## Flow injection analysis (FIA) pump settings

| Step | Time (min) | Flow (µL/min) | % A | % B |
|------|-----------|---------------|------|-------|
| 0 | Initial | 30 | 0.0 | 100.0 |
| 1 | 1.60 | 30 | 0.0 | 100.0 |
| 2 | 2.40 | 200 | 0.0 | 100.0 |
| 3 | 2.80 | 200 | 0.0 | 100.0 |
| 4 | 3.00 | 30 | 0.0 | 100.0 |

## Other systems settings

| Instrument | Parameter | Method | | |
|------------|-----------|--------|------|------|
| | | HPLC | UPLC | FIA |
| Autosampler | Injection volume | 10 | 5 | 20 |
| Column Oven | Temp. | 50 °C | 50 °C | No column |
| MS | Capillary voltage | 3.2 | 3.2 | 3.9 |
| | Cone voltage | 27 | 27 | 22 |
| | Source temp. | 150 °C | 150 °C | 150 °C |
| | Desolvation temp. | 600 °C | 600 °C | 350 °C |
| | Cone gas | 50 | 250 | 0 |
| | Desolvation gas | 720 | 1000 | 650 |
| | Collision gas | 0.15 | 0.15 | 0.15 |
| | Collision | 2 | 2 | 2 |

## RESULTS AND DISCUSSION

The extraction of metabolites from biological samples is a key delicate step for an accurate MS analysis. A multi-step sample preparation procedure could contribute to the variation and errors in the measurements of the natural metabolites. In order to minimize these issues, step-by-step operating procedures were followed as described in the Kit User Manual and detailed in the Experimental section of this application note.

The Absolute*IDQ* p180 Kit was tested with both HPLC (Agilent Zorbax Eclipse XDB C$_{18}$, 3.0 x 100 mm, 3.5 µm) and UPLC (Waters ACQUITY UPLC BEH C$_{18}$ 2.1 x 50 mm, 1.7 µm) columns coupled with Xevo TQ and Xevo TQ-S mass spectrometers, as shown in Figure 4. The UPLC-based assay at a flow rate of 0.9 mL/min allowed for a high-throughput separation of the selected metabolites in less than 5 min, which was considerably shorter than the HPLC-based assay at a flow rate of 0.5 mL/min, as shown in Figure 4.
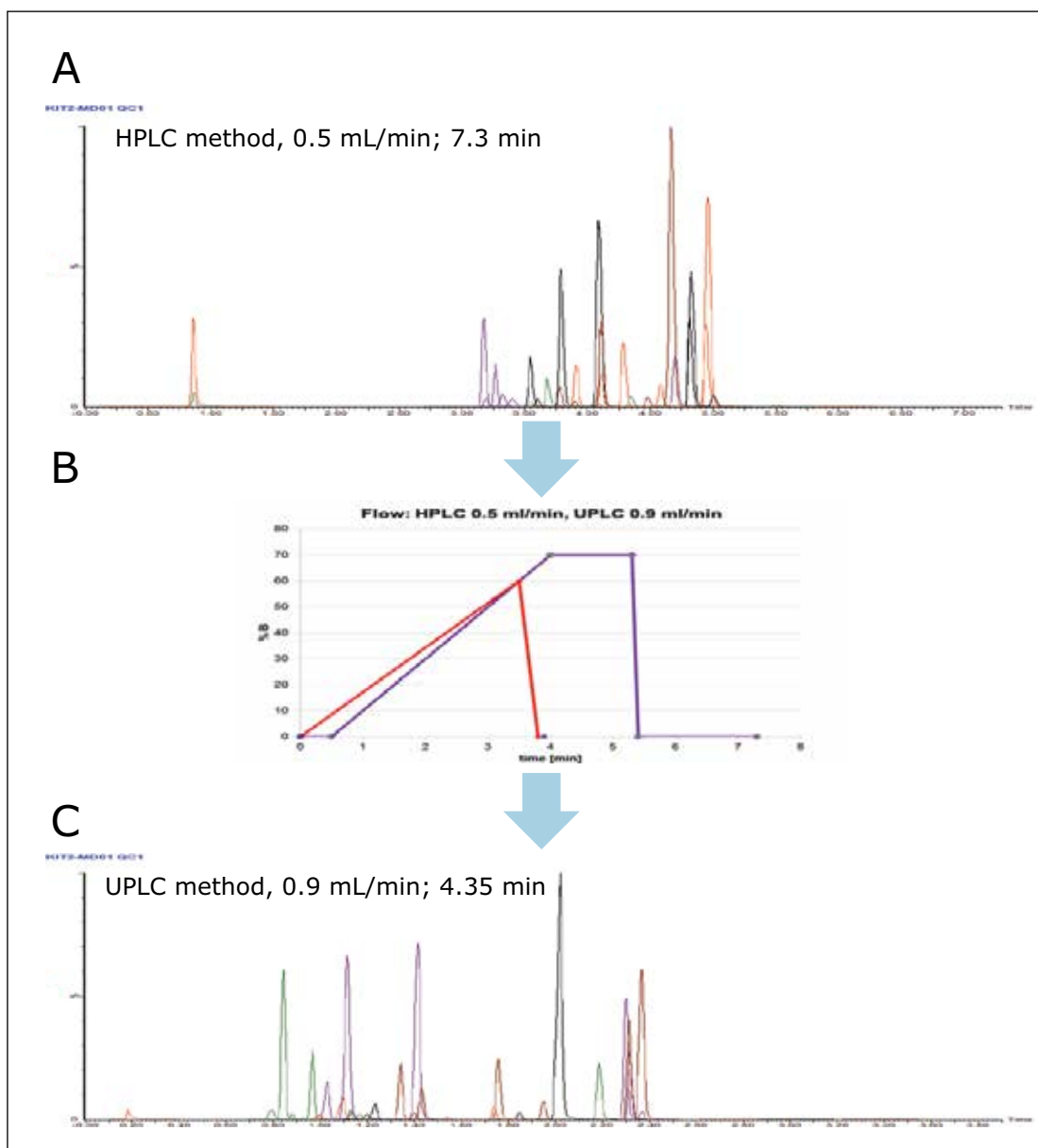


*Figure 4. A.) Representative HPLC/MS chromatogram illustrating the total run time of 7.3 min. B.) Optimization of the chromatographic gradient from HPLC-based method (violet) to UPLC-based method (red). C.) Representative UPLC/MS chromatogram showing a total run time of 4.3 min, which represents a significant gain in speed compared to HPLC/MS.*

The Absolute*IDQ* p180 Kit was utilized to determine differences in the serum metabolome between irradiated and non-irradiated mice. The identification of potential alterations in the levels of metabolites in the serum of mice exposed to gamma radiation is particularly significant because it could lead to the following: 1) a better understanding of the biochemical pathways involved in the response to gamma radiation; and 2) the discovery of biochemical indicators (biomarkers) of acute exposure to ionizing radiation. Rapid identification of biomarkers will be of particular importance in the case of accidental exposures and terrorist acts,[3,4] as classic cytogenetic methods available for biodosimetry are laborious and time-consuming. Using the Absolute*IDQ* p180 Kit, we were able to rapidly measure the serum levels of both polar and non-polar metabolites belonging to major biochemical pathways, as shown in Table 1.

| Acylcarnitines (40) | | | |
|---|---|---|---|
| C0 Carnitine | C10:1 Decenoylcarnitine | C5:1-DC Glutaconylcarnitine | C16 Hexadecanoylcarnitine |
| C2 Acetylcarnitine | C10:2 Decadienylcarnitine | C5-DC (C6-OH) Glutarylcarnitine* (Hydroxyhexanoylcarnitine) | C16:1 Hexadecenoylcarnitine |
| C3 Propionylcarnitine | C12 Dodecanoylcarnitine | C5-M-DC Methylglutarylcarnitine | C16:1-OH Hydroxyhexadecenoylcarnitine |
| C3:1 Propenoylcarnitine | C12:1 Dodecenoylcarnitine | C5-OH (C3-DC-M) Hydroxyvalerylcarnitine (Methylmalonylcarnitine) | C16:2 Hexadecadienylcarnitine |
| C3-OH Hydroxypropionylcarnitine | C12-DC Dodecanedioylcarnitine | C6 (C4:1-DC) Hexanoylcarnitine (Fumarylcarnitine) | C16:2-OH Hydroxyhexadecadienylcarnitine |
| C4 Butyrylcarnitine | C14 Tetradecanoylcarnitine | C6:1 Hexenoylcarnitine | C16-OH Hydroxyhexadecanoylcarnitine |
| C4:1 Butenylcarnitine | C14:1 Tetradecenoylcarnitine | C7-DC Pimelylcarnitine | C18 Octadecanoylcarnitine |
| C4-OH (C3-DC) Hydroxybutyrylcarnitine | C14:1-OH Hydroxytetradecenoylcarnitine | C8 Octanoylcarnitine | C18:1 Octadecenoylcarnitine |
| C5 Valerylcarnitine | C14:2 Tetradecadienylcarnitine | C9 Nonaylcarnitine | C18:1-OH Hydroxyoctadecenoylcarnitine |
| C5:1 Tiglylcarnitine | C14:2-OH Hydroxytetradecadienylcarnitine | C10 Decanoylcarnitine | C18:2 Octadecadienylcarnitine |
| Amino Acids and Biogenic Amines (40) | | | |
| Alanine | Leucine | Valine | Methioninesulfoxide |
| Arginine | Lysine | Acetylyornithine | Nitrotyrosine |
| Asparagine | Methionine | Asymmetric dimethylarginine | Hydroxyproline |
| Aspartate | Ornithine | Symmetric dimethylarginine | Phenylethylamine |
| Citrulline | Phenylalanine | Total dimethylarginine | Putrescine |
| Glutamine | Proline | alpha-Aminoadipic acid | Sarcosine |
| Glutamate | Serine | Carnosine | Serotonin |
| Glycine | Threonine | Creatinine | Spermidine |
| Histidine | Tryptophan | Histamine | Spermine |
| Isoleucine | Tyrosine | Kynurenine | Taurine |
| Sphingolipids (14) | | | |
| SM (OH) C14:1 | SM C18:0 | SM (OH) C22:2 | SM C26:0 |
| SM C16:0 | SM C18:1 | SM C24:0 | SM C26:1 |
| SM C16:1 | SM C20:2 | SM C24:1 | |
| SM (OH) C16:1 | SM (OH) C22:1 | SM (OH) C24:1 | |

*Table 1. List of metabolites analyzed using the kit.*

Principal Component Analysis showed that the gamma irradiated group was well separated from the control group (data not shown). The signal intensities of the MRM pairs of the internal standards in the murine serum samples were compared to the values obtained for human plasma and to the values of the zero samples. Median and standard deviation values of the coefficient of variation (CV) were calculated for the different metabolite classes for all sample preparation conditions used in this study, as shown in Figure 5. Only levels of analytes with values above the limit of detection (LOD, defined as three times the median value of the zero samples) were considered. Exposure to gamma radiation induced significant changes in the levels of specific amino acids, such as arginine and serine, lyso-phosphatidylcholines (lyso-PC), phosphatidylcholines (PC), and acylcarnitines in mouse serum, as shown in Figure 6.
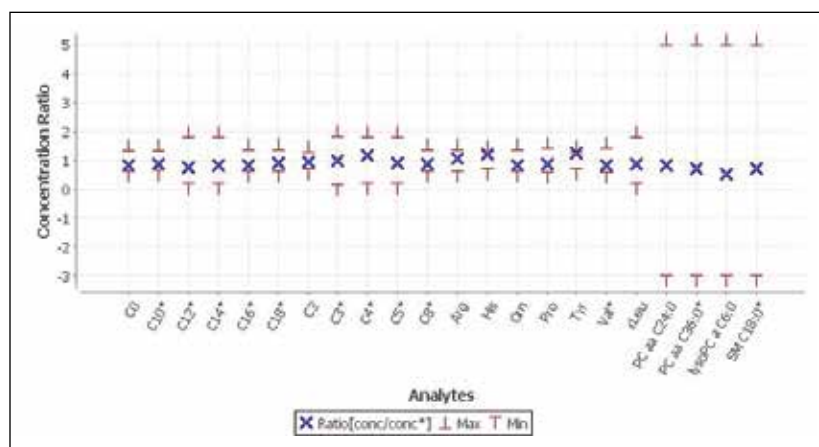


*Figure 5. Quality control samples. Measured concentration/expected concentration ratios are displayed in the MetIDQ software, which is an integral part of the kit. Representative values for acylcarnitines (CO-C$_{18}$), amino acids, and lipids.*
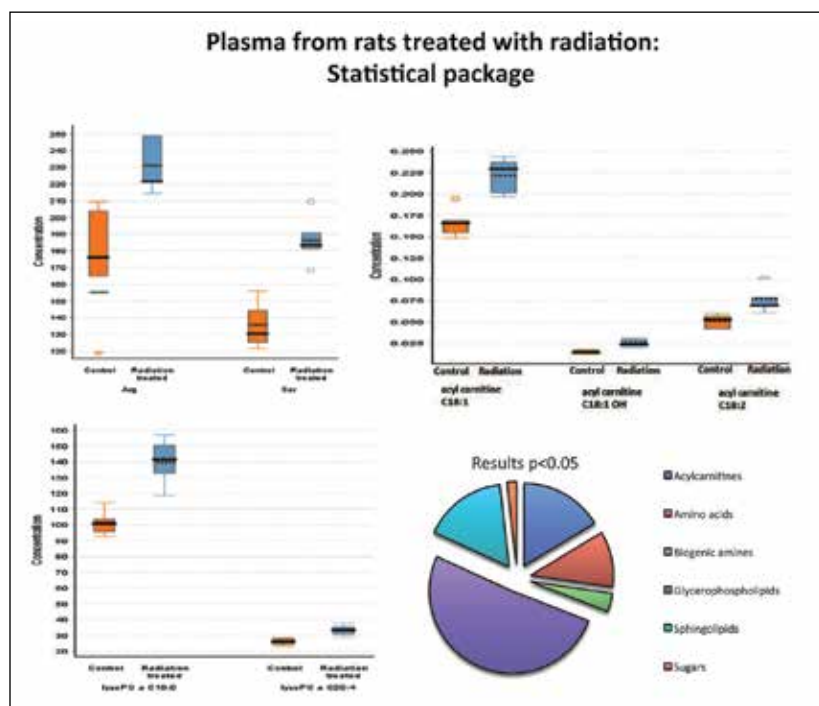


*Figure 6. The box plots show examples of altered metabolites in the serum samples of gamma irradiated mice. The pie chart illustrates the kit metabolite panel separated into metabolite classes. Results of the statistically significant ions are presented as a percentage in each metabolic class.*

## CONCLUSIONS

By combining the ACQUITY UPLC System with the Xevo TQ or Xevo TQ-S Mass Spectrometers and the commercially available Absolute*IDQ* p180 Kit, rapid identification and quantification of more than 180 metabolites in murine serum were successfully attained. Similar applications could lead to novel mechanistic insight and biomarker discovery in drug development, diagnostics, and systems biology research.

### References

1. Wang-Sattler R, Yu Z, Herder C, Messias AC, Floegel A, He Y, Heim K, Campillos M, Holzapfel C, Thorand B, *et al*. Novel biomarkers for pre-diabetes identified by metabolomics. *Mol Syst Biol.* 2012 Sep;8:615. DOI: 10.1038/msb.2012.43.

2. Schmerler D, Neugebauer S, Ludewig K, Bremer-Streck S, Brunkhorst FM, Kiehntopf M. Targeted metabolomics for discrimination of systemic inflammatory disorders in critically ill patients. *J Lipid Res.* 2012 Jul;53(7):1369-75.

3. Coy S, Cheema A, Tyburski J, Laiakis E, Collins S, Fornace AJ. Radiation metabolomics and its potential in biodosimetry. *Int J Radiat Biol.* 2011 Aug;87(8):802-23.

4. Laiakis E, Hyduke D, Fornace A. Comparison of mouse urinary metabolic profiles after exposure to the inflammatory stressors gamma radiation and lipopolysaccharide. *Radiat Res.* 2012 Feb; 177(2):187-99.

## Waters
### THE SCIENCE OF WHAT'S POSSIBLE.®

Waters
THE SCIENCE OF WHAT'S POSSIBLE.®

# Targeted Lipidomics of Oxylipins (Oxygenated Fatty Acids)

Katrin Strassburg,[1,2] Billy Joe Molloy,[5] Claude Mallet,[3] André Duesterloh,[4] Igor Bendik,[4] Thomas Hankemeier,[1,2] James Langridge,[5] Rob J. Vreeken,[1,2] Giuseppe Astarita[3]

[1]Analytical Biosciences, LACDR, Leiden University, Leiden, The Netherlands; [2]Netherlands Metabolomics Centre, Leiden University, Leiden, The Netherlands; [3]Waters Corporation, Milford, MA, USA; [4]DSM Nutritional Products Europe Ltd., Switzerland; [5]Waters Corporation, Wilmslow, UK

## APPLICATION BENEFITS

Here, we present a high-throughput approach for profiling bioactive oxylipins (oxidized fatty acids) in plasma. The combination of mixed mode solid-phase extraction (Oasis® MAX SPE) and UPLC®-ESI-MRM mass spectrometry (Xevo® TQ-S) provides a comprehensive analysis of oxylipins in a targeted analytical workflow. Retention times and transitions of 107 oxylipins (including prostaglandins, prostacyclines, thromboxanes, dihydroprostaglandins, and isoprostanes) were annotated for routine high-throughput analysis of plasma samples. Considering the prominent roles played by oxylipins in health and disease (*e.g.*, inflammation), such a UPLC-based assay could become important in nutritional research, clinical research, and drug discovery and development.

## WATERS SOLUTIONS

Xevo TQ-S Mass Spectrometer

Oasis MAX SPE Cartridges

TargetLynx™ Application Manager

## KEY WORDS

UPLC-MS/MS, fatty acids, metabolomics, lipidomics, triple quadrupole, oxylipins, multiple reaction monitoring, MRM, Xevo TQ-S

## INTRODUCTION

Oxylipins are signaling lipids that play prominent roles in the physiological regulation of many key biological processes, such as the relaxation and contraction of smooth muscle tissue, blood coagulation, and most notably inflammation. Alterations in oxylipin pathways have been associated with response to cardiovascular diseases, host defense, tissue injury and surgical intervention. The ability to semi-quantitatively profile a wide range of oxylipin in plasma samples could help our understanding of their roles in health and disease, as well as serve as biomarkers for disease diagnosis or prognosis.

Oxylipins are produced via enzymatic (e.g., mono- or dioxygenase-catalyzed) or non enzymatic oxygenation of an array of both omega-6 polyunsaturated fatty acid substrates (e.g., linoleic acid, dihomo-γ-linolenic acid, adrenic acid and arachidonic acid) and omega-3 polyunsaturated fatty acid substrates (α-linolenic acid, acid, eicosapentaenoic acid, and docosahexaenoic acid) (Figure 1A and 1B). Three major enzymatic pathways are involved in their generation: cyclooxygenase (COX), lipoxygenase (LOX), and cytochrome P450 (CYP). These pathways are important drug targets for multiple diseases (Figure 1A and 1B).

The main challenge for the measurement of oxylipins is the extremely low endogenous concentration of such lipid species and their limited stability. Furthermore, oxylipins are not stored in tissues but are formed on demand by liberation of precursor fatty acids from esterified forms. Lastly, the same fatty acid can be oxidized in different positions of its acyl chain leading to many isomeric species, each with specific metabolic actions. As a consequence, this requires a rapid, highly-sensitive, and specific analytical method.

Historically, measurements of oxylipins have been performed using radiometric and enzymatic immunoassays, which often lacked specificity and targeted only few compounds. GC-MS methodology has also been used, but this still requires multi-step procedures involving derivatization of the oxylipins to increase their volatility and stability.

Recently, various LC-MS methodologies have been described to monitor a broad range of low abundance oxylipins.[1-5] In particular the method by Strassburg et al.[2] reports on a wide range of oxylipins produced both enzymatically and non-enzymatically in human plasma. Although such methods are both sensitive and specific, there is an increasing demand for a comprehensive and high-throughput screening method to enable wide-ranging lipidomic studies.

Here we report a high-throughput assay for the profiling of over 100 oxylipins, including prostaglandins, prostacyclines, thromboxanes, dihydroprostaglandins, and isoprostanes, in plasma samples.

| Internal standard | Cayman #number | MRM transition | RT (min) | Cone voltage (V) | Collision energy (eV) |
|---|---|---|---|---|---|
| d4-6-Keto PGF1α | 315210 | 373.20 >167.20 | 2.28 | 35 | 15 |
| d4-TBX2 | 319030 | 373.20 >173.10 | 2.86 | 35 | 15 |
| d4-PGF2α | 316010 | 357.30 >197.20 | 3.12 | 35 | 20 |
| d4-PGE2 | 314010 | 355.20 >275.20 | 3.19 | 40 | 16 |
| d4-PGD2 | 312010 | 355.20 >275.20 | 3.31 | 10 | 16 |
| d5-LTE4 | 10007858 | 443.10 >338.00 | 4.11 | 35 | 20 |
| d4-LTB4 | 320110 | 339.20 >197.10 | 4.48 | 35 | 15 |
| d4-12,13-DiHOME | 10009994 | 317.30 >185.20 | 4.56 | 35 | 15 |
| d4-9,10-DiHOME | 10009993 | 317.30 >203.20 | 4.69 | 35 | 15 |
| d11-14,15-DiHETrE | 10008040 | 348.30 >207.10 | 4.77 | 35 | 15 |
| d4-15-deoxy-Δ12,14-PGJ2 | 318570 | 319.20 >275.30 | 5.20 | 35 | 15 |
| d6-20-HETE | 390030 | 325.20 >281.10 | 5.24 | 20 | 18 |
| d4-9-HODE | 338410 | 299.20 >172.10 | 5.53 | 35 | 20 |
| d8-12-HETE | 334570 | 327.30 >184.20 | 5.78 | 35 | 20 |
| d8-5-HETE | 334230 | 327.30 >116.10 | 5.97 | 35 | 20 |

*Table 1. Internal standards used for profiling natural oxylipins in plasma and optimal UPLC-ESI-MS settings.*

## EXPERIMENTAL

### Sample preparation

### Materials

All chemicals were purchased from Sigma-Aldrich (Germany) and were of analytical grade or higher purity. Oxylipins standards were purchased from Cayman Chemicals (Ann Arbor, MI), Biomol (Plymouth Meeting, PA), and Larodan (Malmö, Sweden). For mixed mode solid phase extraction we used Waters Oasis MAX 3 cc Vac Cartridge, 60 mg Sorbent per Cartridge, 30 µm Particle Size (p/n 186000367). An internal standard mixture containing 16 isotopically labeled compounds was used (Table 1).

### Sample pre-treatment

### (dilution, performed in borosilicate glass tubes 13 x 100 mm):

1. Add 200 µL of 10% glycerol in water to a glass tube

2. Add 50 – 250 µL of plasma (maximum sample volume available) sample to the tube and mix thoroughly

3. Add 5 µL of 10 mg/mL BHT in ethanol and mix thoroughly

4. Add 5 µL of internal standard solution (400 ng/mL) and mix

5. Make up the total sample volume to 3 mL with 25% MeCN(aq) and mix thoroughly

### MAX mixed mode solid phase extraction

1. Condition Oasis MAX SPE Cartridge with 3 mL of MeCN

2. Condition Oasis MAX SPE Cartridge with 3 mL of 25% MeCN(aq)

3. Load the entire pre-treated sample onto the Oasis MAX SPE Cartridge

4. Wash Oasis MAX SPE Cartridge with 3 mL of 25% MeCN(aq)

5. Wash Oasis MAX SPE Cartridge with 3 mL of MeCN

6. Elute analytes with 1.3 mL of 1% Formic in MeCN8*

7. Transfer eluate to a glass HPLC vial (TruView™ Max Recovery Vial)

8. Evaporate eluate down until only the glycerol remains (under nitrogen at 40 °C)

9. Add 60 µL of 50/50 MeOH/MeCN and mix thoroughly

10. Inject 3 µL onto the UPLC-MS/MS System

*Sample eluted into a glass tube containing 200 µL of 10% glycerol in methanol*

### UPLC conditions

| System: | ACQUITY UPLC® System in negative ESI mode |
| Column: | ACQUITY UPLC BEH C$_{18}$, 1.7 µm, 2.1 x 100 mm |
| Mobile phase A: | H$_2$O + 0.1% acetic acid |
| Mobile phase B: | ACN/IPA (90/10 v/v) |
| Flow rate: | 0.6 mL/min |
| Column temp.: | 40 °C |
| Volume: | 3.0 µL |

Elution gradient:

| Min | A% | B% | Curve |
|---|---|---|---|
| 0.0 | 75 | 25 | |
| 1.0 | 75 | 25 | 6 |
| 8.0 | 5 | 95 | 6 |
| 8.50 | 5 | 95 | 6 |
| 8.51 | 75 | 25 | 6 |
| 10.00 | 75 | 25 | 6 |

### MS conditions

For optimum reproducibility of retention times we recommend the following tubing to connect UPLC analytical column to ESI probe: PEEK Tubing, 1/16 in. (1.6 mm) O.D. X 0.004 in. (0.100 mm) I.D. X 5 ft (1.5 m) length, cut to 400 mm in length.

| MS system: | Xevo TQ-S in negative ESI mode |
| Acquisition mode: | MRM |
| Capillary voltage: | 2.5 kV |
| Cone voltage: | 10-40 V (compound Specific, default = 35 V) |
| Source temp.: | 150 °C |
| Desolvation gas temp.: | 600 °C |
| Desolvation gas flow: | 1000 L/h |
| Cone gas flow: | 150 L/h |
| Collision energy: | 15-20 V (compound Specific, default = 15 V) |

### Data management

TargetLynx Application Manager

## RESULTS AND DISCUSSION

The primary focus of this work was to provide a high-throughput method to profile bioactive oxylipins in plasma samples.
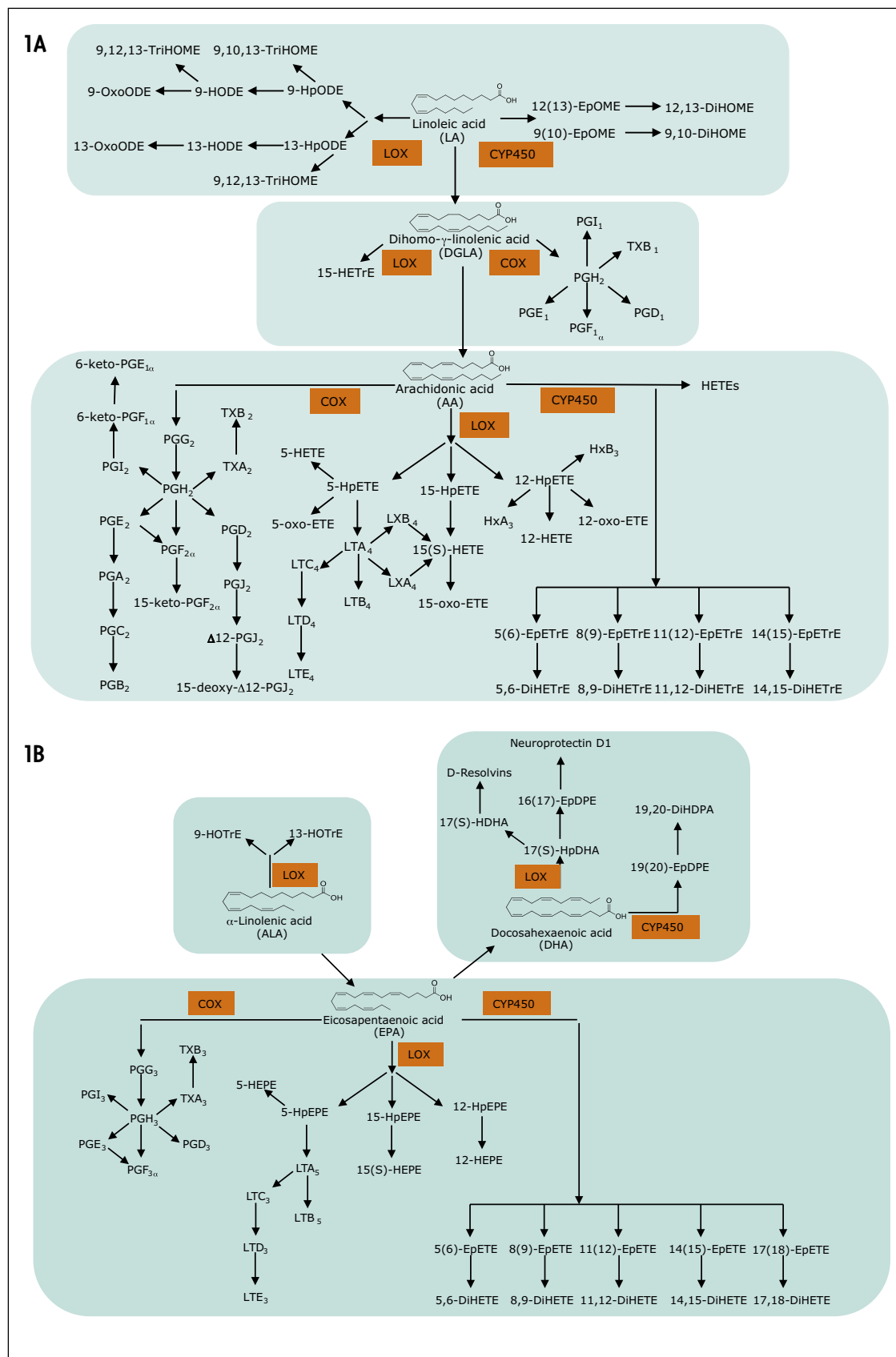


Figure 1. A. Schematic outline of the oxylipins of the omega-6 series produced by linoleic acid $C_{18}$:2 (LA), dihomo-γ-linoleic acid C20:3 (DHGLA), and arachidonic acid C20:4 (AA), via the cyclooxygenase (COX), lipoxygenase (LOX), CYP-450, or free radical catalyzed pathways.

B. Schematic outline of the oxylipins of the omega-3 series produced by α-linolenic acid $C_{18}$:3 (ALA), eicosapentaenoic acid C20:5 (EPA), and docosahexaenoic acid C22:6 (DHA), via the COX, LOX, CYP-450, or free radical catalyzed pathways.

Abbreviations: dihydroxyeicosatetraenoic acid (DiHETE), epoxy-octadecenoic acid (EpOME), hydroxy-eicosatrienoic acid (HETrE), hydroxy-eicosatetraenoic acid (HETE), hydroxy-heptadecatrienoic acid (HHTrE), hydroxy-octadecadienoic acid (HODE), hydroxy-eicosapentaenoic acid (HEPE), oxo-eicosatetraenoic acid (KETE), oxo-octadecadienoic acid (KODE), prostaglandin (PG), thromboxane (TX).

| | Compound name | M1 | M2 | RT | I | Precursor | Class | Pathway |
|---|---|---|---|---|---|---|---|---|
| 1 | Tetranor-PGFM | 329.2 | 311.2 | 0.48 | (d4) PGF2α | AA | Prostanoid | COX |
| 2 | Tetranor-PGEM | 327.1 | 309.2 | 0.53 | (d4) PGE2 | AA | Prostanoid | COX |
| 3 | 20-hydroxy PGE2 | 367.2 | 287.2 | 1.01 | (d4) PGE2 | AA | Prostanoid | COX |
| 4 | Δ17-6-keto PGF1α | 367.2 | 163.1 | 1.76 | (d4) 6-keto PGF1α | AA | Prostanoid | COX |
| 5 | 6-keto PGF1α | 369.2 | 163.1 | 2.27 | (d4) 6-keto PGF1α | AA | Prostanoid | COX |
| 6 | 2,3-dinor-11b PGF2α | 325.2 | 145.1 | 2.27 | (d4) PGF2α | AA | Prostanoid | COX |
| 7 | (d4) 6-keto PGF1α | 373.2 | 167.2 | 2.28 | ISTD | | | |
| 8 | 20-carboxy LTB4 | 365.2 | 347.2 | 2.35 | (d4) LTB4 | AA | Leukotriene | LOX |
| 9 | 6-keto PGE1 | 367.2 | 143.1 | 2.37 | (d4) PGE2 | AA | Prostanoid | COX |
| 10 | 20-hydroxy LTB4 | 351.2 | 195.1 | 2.46 | (d4) LTB4 | AA | Leukotriene | LOX |
| 11 | TXB3 | 367.2 | 169.1 | 2.48 | (d4) TXB2 | EPA | Thromboxane | COX |
| 12 | PGF3α | 351.2 | 193.2 | 2.75 | (d4) PGF2α | EPA | Prostanoid | COX |
| 13 | TXB1 | 371.2 | 171.1 | 2.79 | (d4) TXB2 | DGLA | Thromboxane | COX |
| 14 | PGE3 | 349.2 | 269.2 | 2.83 | (d4) PGE2 | EPA | Prostanoid | COX |
| 15 | (d4) TXB2 | 373.2 | 173.1 | 2.86 | ISTD | | | |
| 16 | 8-iso PGF2α | 353.2 | 193.2 | 2.87 | (d4) PGF2α | AA | Isoprostane | non enzymatic |
| 17 | TXB2 | 369.2 | 169.1 | 2.88 | (d4) TXB2 | AA | Thromboxane | COX |
| 18 | PGD3 | 349.2 | 269.2 | 2.92 | (d4) PGD2 | EPA | Prostanoid | COX |
| 19 | 11β-PGF2α | 353.2 | 193.2 | 2.93 | (d4) PGF2α | AA | Prostanoid | COX |
| 20 | (+/-) 5-iPF2α-VI | 353.2 | 115.1 | 3.04 | (d4) PGF2α | AA | Isoprostane | non enzymatic |
| 21 | 9,12,13-TriHOME | 329.2 | 211.2 | 3.07 | (d4) 9(S)-HODE | LA | Triol | LOX |
| 22 | 9,10,13-TriHOME | 329.2 | 171.1 | 3.12 | (d4) 9(S)-HODE | LA | Triol | LOX |
| 23 | (d4) PGF2α | 357.3 | 197.2 | 3.12 | ISTD | | | |
| 24 | PGF2α | 353.2 | 193.2 | 3.14 | (d4) PGF2α | AA | Prostanoid | COX |
| 25 | PGF1α | 355.2 | 293.2 | 3.14 | (d4) PGF2α | DGLA | Prostanoid | COX |
| 26 | (d4) PGE2 | 355.2 | 275.2 | 3.19 | ISTD | | | |
| 27 | PGE2 | 351.2 | 271.2 | 3.2 | (d4) PGE2 | AA | Prostanoid | COX |
| 28 | 11β-PGE2 | 351.2 | 271.2 | 3.25 | (d4) PGE2 | AA | Prostanoid | COX |
| 29 | PGK2 | 349.2 | 205.1 | 3.28 | (d4) PGE2 | AA | Prostanoid | COX |
| 30 | 15-keto PGF2α | 351.2 | 219.1 | 3.28 | (d4) PGF2α | AA | Prostanoid | COX |
| 31 | 5(S),14(R)-Lipoxin B4 | 351.2 | 221.2 | 3.29 | (d4) LTB4 | AA | Lipoxin | LOX |
| 32 | PGE1 | 353.2 | 273.2 | 3.29 | (d4) PGE2 | DGLA | Prostanoid | COX |
| 33 | (d4) PGD2 | 355.2 | 275.2 | 3.31 | ISTD | | | |
| 34 | PGD2 | 351.2 | 271.2 | 3.32 | (d4) PGD2 | AA | Prostanoid | COX |
| 35 | PGD1 | 353.2 | 273.2 | 3.32 | (d4) PGD2 | DGLA | Prostanoid | COX |
| 36 | 11β-13,14-dihydro-15-keto PGF2α | 353.2 | 113.2 | 3.35 | (d4) PGF2α | AA | Prostanoid | COX |
| 37 | 15-keto PGF1α | 353.2 | 221.1 | 3.37 | (d4) 6-keto PGF1α | DGLA | Prostanoid | COX |
| 38 | 13,14-dihydro PGF2α | 355.2 | 275.2 | 3.39 | (d4) PGF2α | AA | Prostanoid | COX |
| 39 | 13,14-dihydro-15-keto PGE2 | 351.2 | 175.2 | 3.54 | (d4) PGE2 | AA | Prostanoid | COX |
| 40 | 13,14-dihydro-15-keto PGF2α | 353.2 | 183.1 | 3.56 | (d4) PGF2α | AA | Prostanoid | COX |
| 41 | 5(S),6(R)-Lipoxin A4 | 351.2 | 115.1 | 3.58 | (d4) LTB4 | AA | Lipoxin | LOX |
| 42 | 5(S),6(S)-Lipoxin A4 | 351.2 | 115.1 | 3.68 | (d4) LTB4 | AA | Lipoxin | LOX |
| 43 | 13,14-dihydro-15-keto PGF1α | 355.2 | 193.2 | 3.72 | (d4) PGF2α | AA | Prostanoid | COX |
| 44 | 13,14-dihydro-15-keto PGD2 | 351.2 | 175.2 | 3.77 | (d4) PGD2 | AA | Prostanoid | COX |

| | Compound name | M1 | M2 | RT | I | Precursor | Class | Pathway |
|---|---|---|---|---|---|---|---|---|
| 45 | 1α,1b-dihomo PGF2α | 381.3 | 337.2 | 3.77 | (d4) PGF2α | ADA | Prostanoid | COX |
| 46 | 14,15-LTE4 | 438.2 | 333.2 | 3.78 | (d3) LTE4 | AA | Leukotriene | LOX |
| 47 | LTD4 | 495.2 | 177.1 | 3.9 | (d3) LTE4 | AA | Leukotriene | LOX |
| 48 | Resolvin D1 | 375.2 | 141 | 3.9 | (d11) 14,15-DiHETrE | DHA | rRsolving | LOX |
| 49 | Resolvin E1 | 349.2 | 195 | 3.9 | (d11) 14,15-DiHETrE | EPA | Resolving | LOX |
| 50 | 13,14-dihydro-15-keto PGD1 | 353.2 | 209.1 | 3.91 | (d4) PGD2 | AA | Prostanoid | COX |
| 51 | PGA2 | 333.2 | 271.2 | 3.91 | (d4) PGE2 | AA | Prostanoid | COX |
| 52 | Δ12-PGJ2 | 333.2 | 233.1 | 3.97 | (d4) 15-deoxy-Δ12,14-PGJ2 | AA | Prostanoid | COX |
| 53 | PGJ2 | 333.2 | 233.1 | 3.97 | (d4) PGD2 | AA | Prostanoid | COX |
| 54 | LTB5 | 333.2 | 195.1 | 4.03 | (d4) LTB4 | EPA | Leukotriene | LOX |
| 55 | 11-trans LTD4 | 495.2 | 177.1 | 4.05 | (d3) LTE4 | AA | Leukotriene | LOX |
| 56 | (d3) LTE4 | 441.2 | 336.2 | 4.12 | ISTD | | | |
| 57 | LTE4 | 438.2 | 333.2 | 4.13 | (d3) LTE4 | AA | Leukotriene | LOX |
| 58 | 8(S),15(S)-DiHETE | 335.2 | 235.2 | 4.23 | (d4) LTB4 | AA | Diol | CYP450 |
| 59 | 12,13-DiHODE | 311.2 | 293 | 4.23 | (d4) 9,10-DiHOME | ALA | Diol | CYP450 |
| 60 | bicyclo-PGE2 | 333.2 | 113.2 | 4.25 | (d4) PGE2 | AA | Prostanoid | CYP450 |
| 61 | 11-trans LTE4 | 438.2 | 333.2 | 4.26 | (d3) LTE4 | AA | Leukotriene | LOX |
| 62 | 10(S),17(S)-DiHDoHE | 359.2 | 153.2 | 4.34 | (d8) 12(S)-HETE | DHA | Protectin | LOX |
| 63 | Neuroprotectin D1 | 359.2 | 206 | 4.34 | (d8) 12(S)-HETE | DHA | Protectin | LOX |
| 64 | 17,18-DiHETE | 335.2 | 247.2 | 4.34 | (d11) 14,15-DiHETrE | EPA | Diol | CYP450 |
| 65 | 5(S),15(S)-DiHETE | 335.2 | 115.2 | 4.37 | (d4) LTB4 | AA | Diol | CYP450 |
| 66 | 6-trans-LTB4 | 335.2 | 195.1 | 4.4 | (d4) LTB4 | AA | Leukotriene | LOX |
| 67 | 14,15-DiHETE | 335.2 | 207.1 | 4.46 | (d11) 14,15-DiHETrE | EPA | Diol | CYP450 |
| 68 | (d4) LTB4 | 339.2 | 197.1 | 4.48 | ISTD | | | |
| 69 | 15-deoxy-Δ12,14-PGD2 | 333.2 | 271.2 | 4.49 | (d4) 15-deoxy-Δ12,14-PGJ2 | AA | Prostanoid | COX |
| 70 | Hepoxilin A3 | 335.2 | 273.2 | 4.5 | (d8) 12(S)-HETE | AA | Hepoxilin | LOX |
| 71 | LTB4 | 335.2 | 195.1 | 4.5 | (d4) LTB4 | AA | Leukotriene | LOX |
| 72 | (d4)(±)12,13-DiHOME | 317.3 | 185.2 | 4.56 | ISTD | | | |
| 73 | 12,13-DiHOME | 313.2 | 183.2 | 4.58 | (d4) 12,13-DiHOME | LA | Diol | CYP450 |
| 74 | (d4)-(±)9,10-DiHOME | 317.3 | 203.2 | 4.69 | ISTD | | | |
| 75 | 9,10-DiHOME | 313.2 | 201.1 | 4.71 | (d4) 9,10-DiHOME | LA | Diol | CYP450 |
| 76 | (d11) 14,15-DiHETrE | 348.3 | 207.1 | 4.77 | ISTD | | | |
| 77 | 19,20-DiHDPA | 361.2 | 273.3 | 4.79 | (d11) 14,15-DiHETrE | DHA | Diol | CYP450 |
| 78 | 14,15-DiHETrE | 337.2 | 207.2 | 4.8 | (d11) 14,15-DiHETrE | AA | Diol | CYP450 |
| 79 | 12S-HHTrE | 279.2 | 179.2 | 4.84 | (d8) 12(S)-HETE | AA | Alcohol | COX |
| 80 | 11,12-DiHETrE | 337.2 | 167.2 | 4.98 | (d11) 14,15-DiHETrE | AA | Diol | CYP450 |
| 81 | 5,6-DiHETrE | 337.2 | 145.1 | 4.99 | (d11) 14,15-DiHETrE | AA | Diol | CYP450 |
| 82 | 9-HOTrE | 293.2 | 171.1 | 5.07 | (d4) 9(S)-HODE | ALA | Alcohol | LOX |
| 83 | 17(18)-EpETE | 317.2 | 259.2 | 5.16 | (d11) 14,15-DiHETrE | EPA | Epoxide | CYP450 |
| 84 | (d4) 15-deoxy-Δ12,14-PGJ2 | 319.2 | 275.3 | 5.2 | ISTD | | | |
| 85 | (d6) 20-HETE | 325.3 | 279.2 | 5.24 | ISTD | | | |
| 86 | 20-HETE | 319.2 | 289.2 | 5.25 | d6-20-HETE | AA | Alcohol | CYP450 |
| 87 | 15(S)-HEPE | 317.2 | 219.2 | 5.25 | (d8) 5(S)-HETE | EPA | Alcohol | LOX |
| 88 | 12(S)-HpETE | 317.1 | 153.0 | 5.34 | (d8) 12(S)-HETE | AA | Hydroxyperoxide | LOX |

| | Compound name | M1 | M2 | RT | I | Precursor | Class | Pathway |
|---|---|---|---|---|---|---|---|---|
| 89 | 8,9-DiHETrE | 337.2 | 127 | 5.35 | (d11) 14,15-DiHETrE | AA | Diol | CYP450 |
| 90 | 5(S),6(S)-DiHETE | 335.2 | 115.1 | 5.35 | (d4) LTB4 | AA | Diol | CYP450 |
| 91 | 12(S)-HEPE | 317.2 | 179.1 | 5.35 | (d8) 12(S)-HETE | EPA | Alcohol | LOX |
| 92 | 13-HODE | 295.2 | 195.2 | 5.5 | (d4) 9(S)-HODE | LA | Alcohol | LOX |
| 93 | 5(S)-HEPE | 317.2 | 115.1 | 5.51 | (d8) 5(S)-HETE | EPA | Alcohol | LOX |
| 94 | (d4) 9(S)-HODE | 299.2 | 172.1 | 5.53 | ISTD | | | |
| 95 | 9-HODE | 295.2 | 171.1 | 5.56 | (d4) 9(S)-HODE | LA | Alcohol | LOX |
| 96 | 15-HETE | 319.2 | 219.2 | 5.62 | (d8) 5(S)-HETE | AA | Alcohol | LOX |
| 97 | 16(17)-EpDPE | 343.2 | 233.2 | 5.62 | (d11) 14,15-DiHETrE | DHA | Epoxide | CYP450 |
| 98 | 13-HpODE | 293.1 | 113.0 | 5.63 | (d4) 9(S)-HODE | LA | Hydroxyperoxide | LOX |
| 99 | 13-KODE | 293.2 | 113.1 | 5.64 | (d4) 9(S)-HODE | LA | Ketone | LOX |
| 100 | 17-HDoHE | 343.2 | 281.3 | 5.67 | (d8) 5(S)-HETE | DHA | Alcohol | LOX |
| 101 | 9-HpODE | 293.1 | 185.0 | 5.68 | (d4) 9(S)-HODE | LA | Hydroxyperoxide | LOX |
| 102 | 15-HpETE | 317. | 113.0 | 5.71 | (d8) 5(S)-HETE | AA | Hydroxyperoxide | LOX |
| 103 | 15-KETE | 317.2 | 113.2 | 5.72 | (d8) 5(S)-HETE | AA | Ketone | LOX |
| 104 | 11-HETE | 319.2 | 167.1 | 5.74 | (d8) 12(S)-HETE | AA | Alcohol | COX |
| 105 | 14(15)-EpETE | 317.2 | 207.1 | 5.74 | (d11) 14,15-DiHETrE | EPA | Epoxide | CYP450 |
| 106 | 9-KODE | 293.2 | 185.2 | 5.77 | (d4) 9(S)-HODE | LA | Ketone | LOX |
| 107 | (d8) 12(S)-HETE | 327.3 | 184.2 | 5.78 | ISTD | | | |
| 108 | 12-HETE | 319.2 | 179.2 | 5.81 | (d8) 12(S)-HETE | AA | Alcohol | LOX |
| 109 | 8-HETE | 319.2 | 155.1 | 5.85 | (d8) 5(S)-HETE | AA | Alcohol | LOX |
| 110 | 15(S)-HETrE | 321.2 | 221.2 | 5.88 | (d8) 5(S)-HETE | DGLA | Alcohol | LOX |
| 111 | 9-HETE | 319.2 | 167.1 | 5.91 | (d8) 12(S)-HETE | AA | Alcohol | non-enzymatic |
| 112 | (d8) 5(S)-HETE | 327.3 | 116.1 | 5.97 | ISTD | | | |
| 113 | 5-HETE | 319.2 | 115.1 | 6.00 | (d8) 5(S)-HETE | AA | Alcohol | LOX |
| 114 | 19(20)-EpDPE | 343.2 | 281.3 | 6.09 | (d11) 14,15-DiHETrE | DHA | Epoxide | CYP450 |
| 115 | 12(13)-EpOME | 295.2 | 195.2 | 6.09 | (d4) 12,13-DiHOME | LA | Epoxide | CYP450 |
| 116 | 14(15)-EpETrE | 319.2 | 219.2 | 6.11 | (d11) 14,15-DiHETrE | AA | Epoxide | CYP450 |
| 117 | 5(S)-HpETE | 317.1 | 203.1 | 6.11 | (d8) 5(S)-HETE | AA | Hydroxyperoxide | LOX |
| 118 | 9(10)-EpOME | 295.2 | 171.2 | 6.15 | (d4) 9,10-DiHOME | LA | Epoxide | CYP450 |
| 119 | 12-KETE | 317.2 | 273.3 | 6.25 | (d8) 12(S)-HETE | AA | Ketone | LOX |
| 120 | 5-KETE | 317.2 | 203.2 | 6.26 | (d8) 5(S)-HETE | AA | Ketone | LOX |
| 121 | 11(12)-EpETrE | 319.2 | 167.1 | 6.27 | (d11) 14,15-DiHETrE | AA | Epoxide | CYP450 |
| 122 | 8(9)-EpETrE | 319.2 | 155.1 | 6.33 | (d11) 14,15-DiHETrE | AA | Epoxide | CYP450 |
| 123 | 5(6)-EpETrE | 319.2 | 191.2 | 6.42 | (d11) 14,15-DiHETrE | AA | Epoxide | CYP450 |

*Table 2. List of MRM transitions (M1=precursor; M2= fragment) and retention times (RT) for oxylipins.*

Oxylipins are present at very low abundance in biological samples, and as such the quality of sample preparation is an important factor for successful analyses. To eliminate non-lipid contaminants and highly abundant species like phospholipids, we used mixed mode solid-phase extraction (SPE) prior to UPLC-MS analysis. Normalization of the extraction efficiency was achieved by adding stable isotope labeled compounds (internal standards), prior to the extraction procedure (Table 1 and 2, and Figure 2).



Plasma sample

Add anti-oxidant / internal standard

Dilute with buffer and Load

Mixed Mode SPE

Wash

Elute

Inject into UPLC-MS/MS
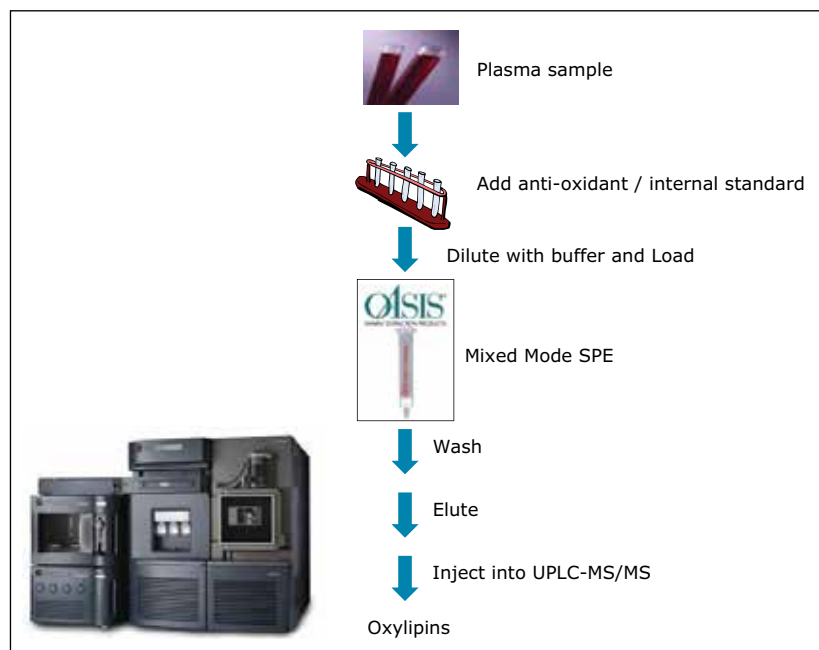
Oxylipins

*Figure 2. Workflow of the sample preparation for the analysis of oxylipins from plasma.*

To optimize the chromatographic separation of our analytes, we used a mixture of a wide chemical variety of commercially available oxylipins. Using reversed-phase UPLC (see Experimental), oxylipins eluted in order of decreasing polarity, numbers of double bonds and increasing acyl chain length, allowing the separation of most isomeric and isobaric species (e.g., PGE2 and PGD2) in less than 10 minutes (Figure 3). Using a Xevo TQ-S in negative ESI-mode, retention times and optimal MRM transitions (compound specific precursor $\Rightarrow$ product ion transitions) were determined for all individual oxylipins (Table 2).

To enhance the sensitivity of detection, these MRM transitions were monitored in defined retention time windows, maximizing dwell times by reducing overlapping transitions. In the case of co-eluting metabolites, compound specific precursor ions and their corresponding fragment ions allowed selective profiling of those compounds. Calibration curves for the majority of the analytes were produced and displayed a linear coefficient (Pearson's correlation, $R^2$) higher than 0.99. (Figure 4). Using this UPLC-MS/MS assay, we rapidly profiled 107 oxylipins in human plasma samples (Figure 5).

With minor modifications in the sample preparation protocol, this assay could be extended to the measure of oxylipins in other biological matrices.
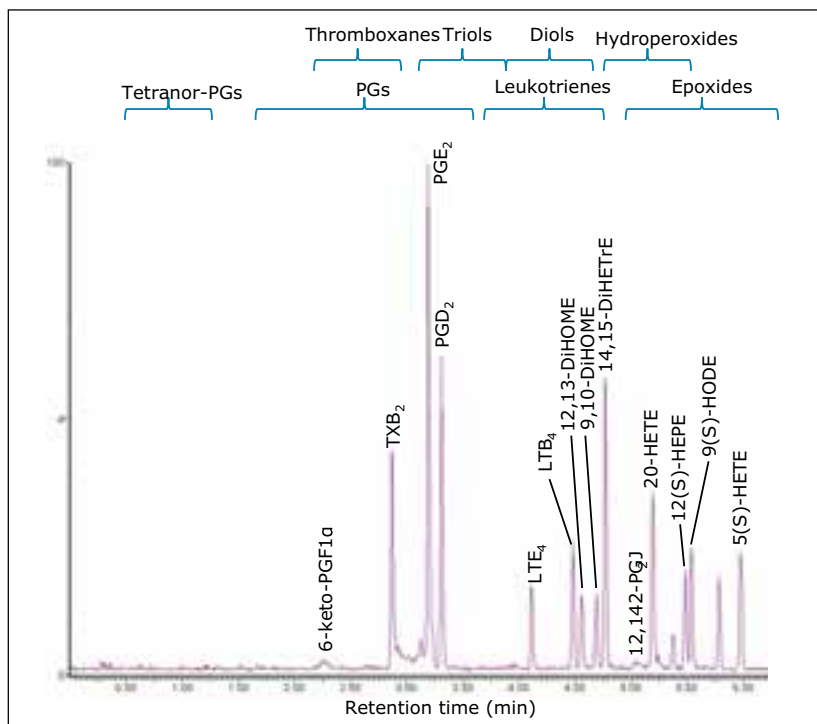
Figure 3. Representative UPLC-MS/MS chromatogram of a wide chemical variety of oxylipin species.
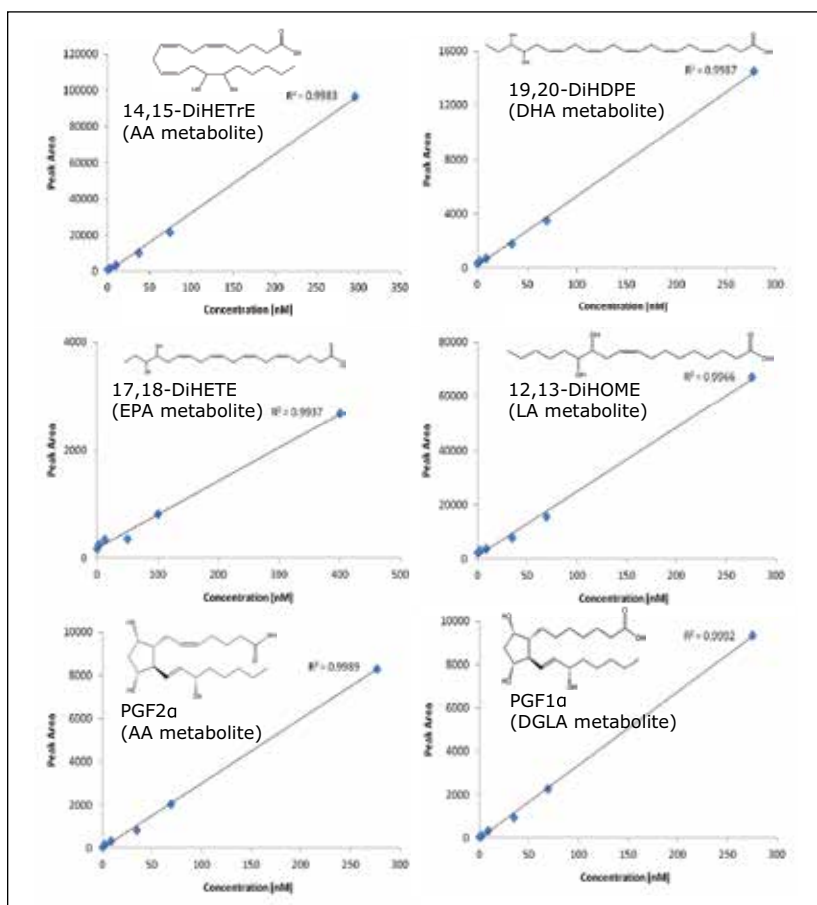


Figure 4. Linearity of response for representative endogenous oxylipin species present in the plasma samples.
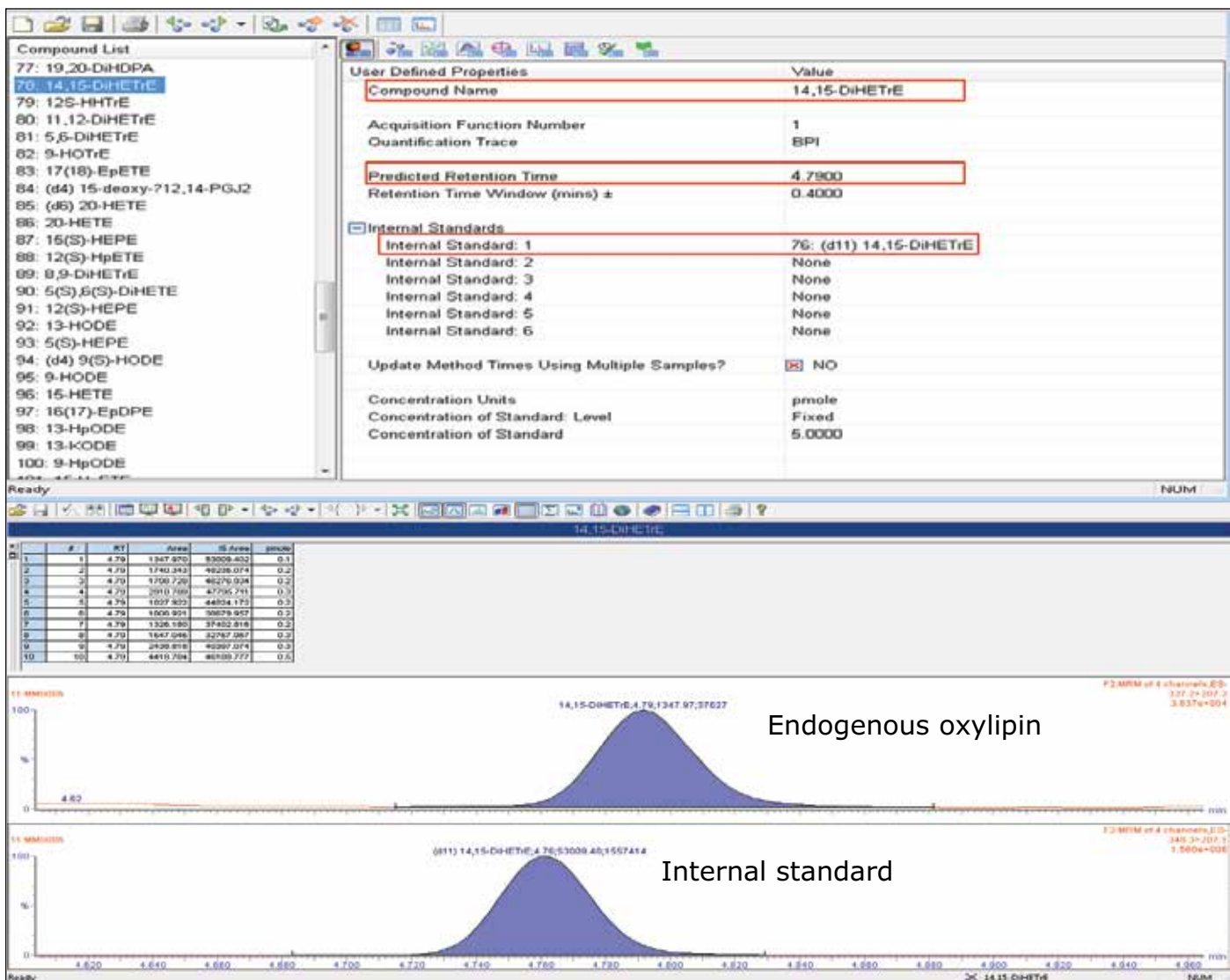
*Figure 5. An example of oxylipin quantification in plasma using TargetLynx, showing the use of a specified retention time, MRM transitions and internal standard for the identification and quantification of a selected oxylipin.*

## CONCLUSIONS

We have presented a routine high-throughput MRM method to profile over 100 oxylipins in plasma. These targets include a wide array of both pro- and anti-inflammatory lipid mediators. This SPE-UPLC-MRM assay could find applications in basic research to facilitate our understanding of the role of these lipid mediators in health and disease, nutritional research, clinical research, and drug discovery and development.

### References

1. Lundstrom SL, Saluja R, Adner M, Haeggstrom JZ, Nilsson GP, Wheelock CE. Lipid mediator metabolic profiling demonstrates differences in eicosanoid patterns in Two phenotypically distinct mast cell populations. *J Lipid Res.* 2012 Oct 3. [Epub ahead of print].

2. Strassburg K, Huijbrechts AM, Kortekaas KA, Lindeman JH, Pedersen TL, Dane A,Berger R, Brenkman A, Hankemeier T, van Duynhoven J, Kalkhoven E, Newman JW, Vreeken RJ. Quantitative profiling of oxylipins through comprehensive LC-MS/MS analysis: application in cardiac surgery. *Anal Bioanal Chem.* 2012 Sep;404(5):1413–26.

3. Sterz K, Scherer G, Ecker J. A simple and robust UPLC-SRM/MS method to quantify urinary eicosanoids. *J Lipid Res.* 2012 May;53(5):1026–36.

4. Nicolaou A, Masoodi M, Mir A. Lipidomic analysis of prostanoids by liquid chromatography-electrospray tandem mass spectrometry. *Methods Mol Biol.* 2009;579:271–86.

5. Astarita G, Kendall AC, Dennis EA, Nicolaou A. Targeted lipidomics strategies for oxygenated metabolites of polyunsaturated fatty acids. *Biochim Biophys Acta.* 2014 Dec 5. pii: S1388-1981(14)00251–0.

# Waters

## THE SCIENCE OF WHAT'S POSSIBLE.®

Waters
THE SCIENCE OF WHAT'S POSSIBLE.®

# Profiling and Quantitation of Metabolomic "Signatures" for Breast Cancer Cell Progression

Henry Shion,[1] Irwin Kurland,[2] Sumanta Goswami,[2,3] David Kusin,[3] Haitao Lu,[2] Bhavapriya Vaitheesvaran,[2] John Shockcor,[1] Alan Millar[1]

[1]Waters Corporation, Milford, MA, USA; [2]Albert Einstein College of Medicine of Yeshiva University, Bronx, NY, USA; [3]Yeshiva University, New York, NY, USA

## APPLICATION BENEFITS

- Quantify known small molecule biomarkers in targeted analysis with Xevo® TQ MS.

- Confirm known – and identify unknown – small molecule biomarkers in untargeted global profinlin analysis with SYNAPT® G2 HDMS.™

- Targeted and untargeted approaches are complementary to each other; new pathways can be discovered using the untargeted approach.

## WATERS SOLUTIONS

SYNAPT G2 HDMS

Xevo TQ MS

ACQUITY UPLC® System

ACQUITY UPLC HSS T3 column

MarkerLynx™ XS Application Manager

MassFragment™ Software

## KEY WORDS

Breast cancer cell analysis, biomarker discovery, metabolomics, small molecule metabolites, glycolysis, TCA cycle, metabolism pathway, exact mass, MS$^E$

## INTRODUCTION

Breast cancer is one of the top five cancers that affect human lives seriously. Therefore, it is of great importance to discover the best ways to study this disease. Metabolic reprogramming is required both during the initial breast cancer transformation process (primary tumor) and during the acquisition of metastatic potential (metastases), shown in Figure 1. The reprogramming process includes altered flux through glycolysis and the pentose phosphate pathway (PPP), resulting in increased fatty acid synthesis needed for proliferation.
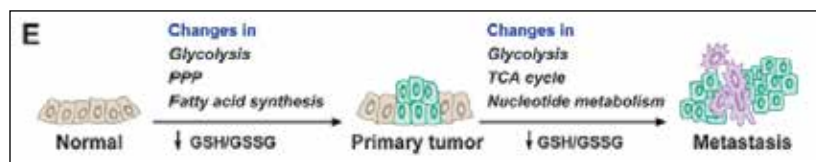


Figure 1. A two-step metabolic progression hypothesis during mammary tumor progression.[1]

Reactive oxygen species produced during tumor progression result in a decreased glutathione GSH (reduced)/GSSG (oxidized) redox pool, which impairs genome stability, tumor suppressor gene function, and control over cell proliferation. Continued GSH/GSSG depletion in the primary tumor may also contribute to general metastatic ability, and includes further changes in glycolysis and tricarboxylic acid cycle (TCA cycle) and increased nucleotide (PPP) flux for replication.

## EXPERIMENTAL

### Cell sample preparation

Two rodent breast cancer cell lines, MTln3 (highly metastatic) and MTC (poorly metastatic), were used and cultured in Eagle's minimal essential medium and supplemented with 5% fetal bovine serum (Invitrogen).

Cells were grown in 10-cm tissue culture dishes, and the media were replaced 24 h and 2 h prior to metabolite extraction. All samples were harvested at subconfluence.

Metabolism was quenched, and metabolites were extracted by aspiration of media and immediate addition of 4 mL of 80:20 methanol/water at 80 °C to simultaneously lyse cells and quench metabolism.

### LC conditions

System:            Waters®
                   ACQUITY UPLC System

Column:            ACQUITY UPLC
                   HSS T3 Column
                   2.1 x 100 mm, 1.8 µm

Column temp.:      40 °C

Flow rate:         300 µL/min

Mobile phase A:    Water, 0.1% Formic acid

Mobile phase B:    Acetonitrile,
                   0.1% Formic acid

Injection vol.:    10 µL

Gradient:

| Time (min) | % A | % B | Curve |
|---|---|---|---|
| Initial | 99 | 1 | Initial |
| 8.0 | 50 | 50 | 6 |
| 8.1 | 1 | 99 | 6 |
| 11.0 | 1 | 99 | 6 |
| 11.1 | 99 | 1 | 6 |
| 15.0 | 99 | 1 | 6 |

Staging of the metabolic reprogramming using metabolomics could pinpoint the metabolic processes that are essential for breast cancer transformation and invasiveness, which may yield biomarkers and new directions for therapeutics. In this application note, we present a metabolomics study that combines targeted and untargeted approaches for breast cancer biomarkers analysis. Figure 2 illustrates the workflow for this study.
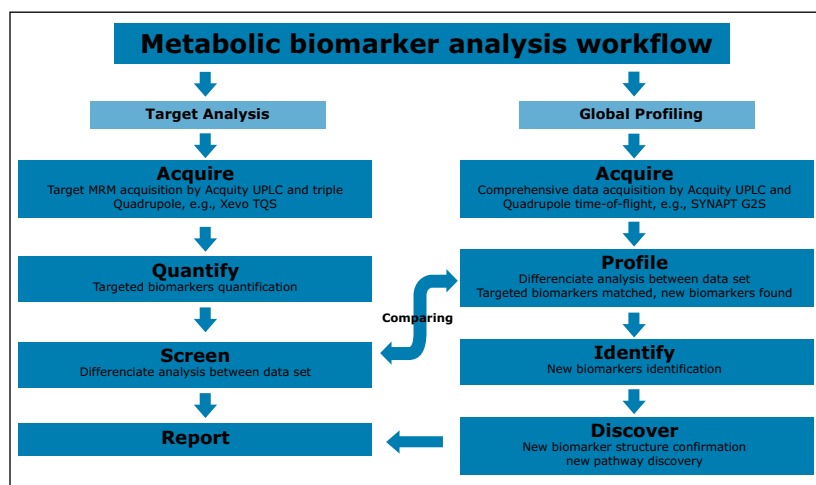


Figure 2. Metabolomics biomarker analysis workflow.

## Mass spectrometry

### SYNAPT G2 HDMS for untargeted global analysis

The SYNAPT G2 HDMS was operated in both positive and negative MS$^E$ modes. The capillary voltage used was 2.0 kV with the source and desolvation temperatures set at 120 °C and 400 °C, respectively.

In the MS$^E$ acquisition mode, the instrument alternates between a low and high collision energy state on alternate scans. This allows for collection of precursor and fragment ion information of all species in an analysis without the sampling bias that is introduced with other common methods, such as DDA where a specific *m/z* must be isolated before fragmentation.
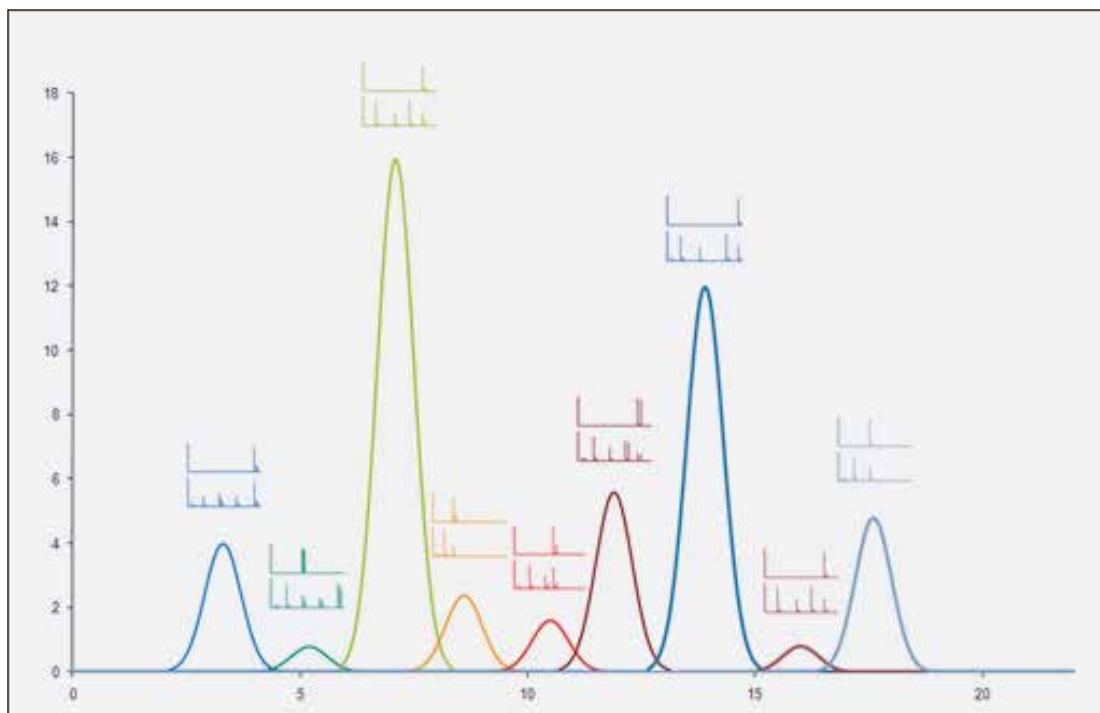
*Figure 3. MS$^E$ enables collection of comprehensive precursor and product ion information for virtually every component of a mixture.*

### Xevo TQ MS for targeted analysis

The Xevo TQ MS was operated in both positive and negative MRM modes. The capillary voltage used was 2.0 kV with the source and desolvation temperatures set at 150 °C and 650 °C, respectively. The desolvation gas flow was set at 1200 L/hr and the collision gas (argon) flow 0.18 mL/min (4 x 10$^{-3}$ mBar), with MS1/MS2 resolution at unit mass.

## RESULTS AND DISCUSSION

Targeted analysis was used to survey known metabolic pathways that are key to cancer aggressiveness, as outlined in Figure 1. Figure 4 shows many of the targeted metabolite markers that are elevated in the MTln3 cells from both the heat map (top) and relative change scale bar plot (bottom). Analysis of experimental data supports a Warburg effect cancer model.[2] For highly aggressive MTln3 cells, high cytosolic NADH is indicated by a glycolytic/TCA cycle signature of an increased malate/aspartate shuttle, shown in Figure 6. High AMP levels for MTln3 cells suggest the elevated malate/aspartate shuttle cannot keep up with cellular energy needs. High levels of amino acids seen in MTln3 cells are necessary for cell growth.
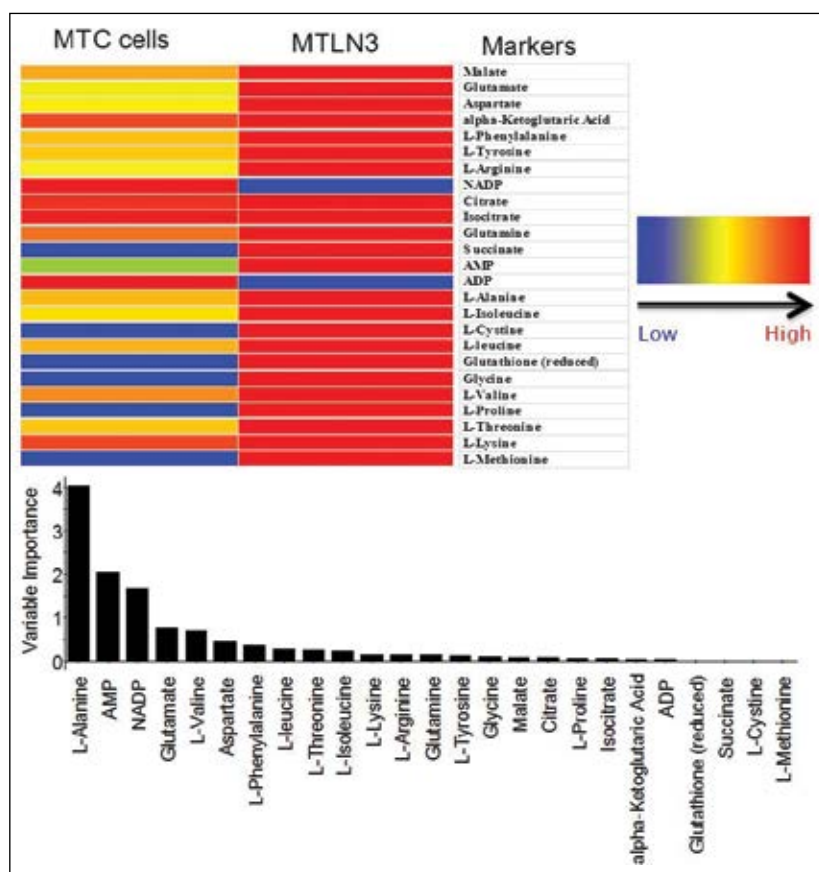


Figure 4. Both the heat map (top) and the relative change scale bar plot (bottom) markers indicate the elevation of the metabolites in the MTLn3 cells.
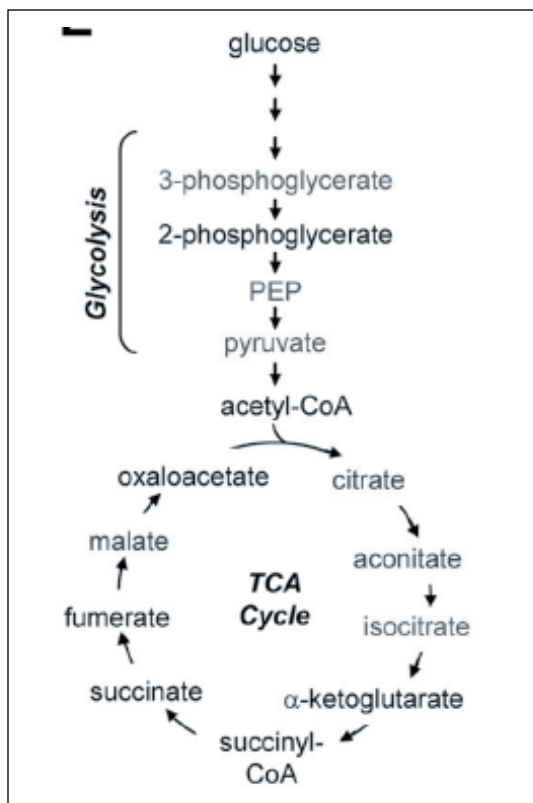
Figure 5. Glycolysis and TCA Cycle.
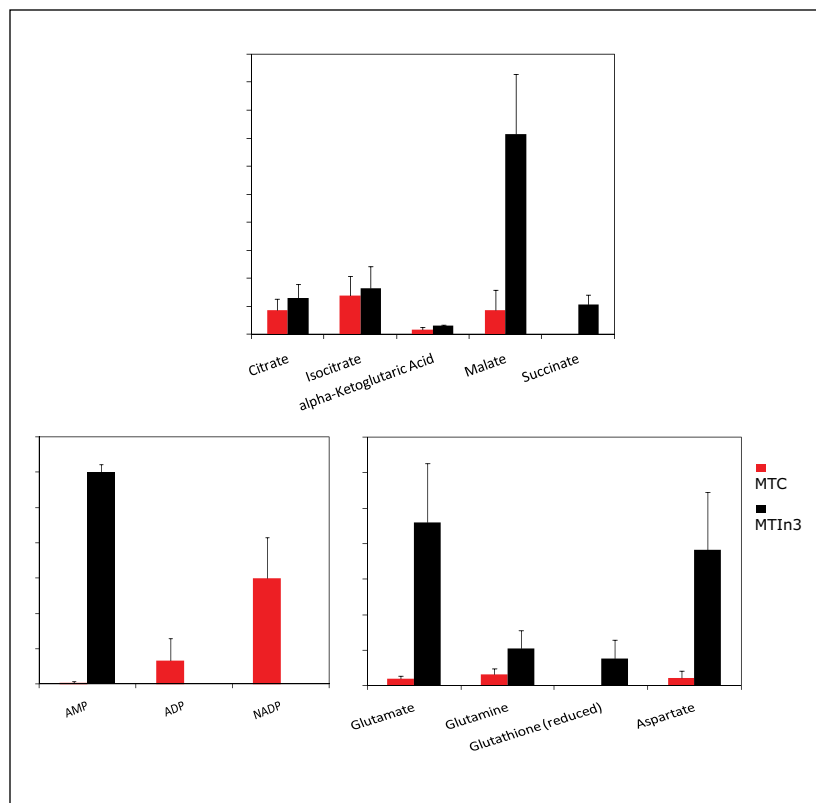


Figure 6. Targeted analysis quantitative bar charts for selected Glycolysis and TCA Cycle metabolites.

As shown in Figure 6, adenosine monophosphate (AMP) is extremely high in concentration. This indicates that the highly aggressive MTln3 cells require a large amount of energy. Even with a high malate/aspartate shuttle, adenosine triphosphate (ATP) production cannot keep pace.

AMP functions as an energy sensor and regulator of metabolism. When ATP production does not keep up with needs, a higher portion of a cell's adenine nucleotide pool is made available in the form of AMP. AMP then stimulates metabolic pathways that produce ATP in the MTln3 cells.

The "signature" of high levels of malate, glutamate, aspartate, and alpha ketoglutarate (as high as 10 fold) means high cytosolic NADH must use these carriers for transport into the mitochondria to turn into ATP. Highly aggressive cancer cells, such as MTln3, have high glycolysis and need the malate/aspartate/glutamate/ alpha-ketogutarate shuttle system to satisfy the ATP needs. This shuttle cannot work fast enough because AMP is still very high.

For untargeted global profiling analysis, all the samples were run in triplicate. A QC sample was made by mixing equal volumes of each sample. 10 QC samples were injected prior to the first sample in the experiment. A QC sample was also injected every 10 sample injections.

For the data analysis, MarkerLynx XS Application Manager[3] was used to integrate and align chemical and biological MS data points and convert them into Exact Mass Retention Time (EMRT) pairs. Those EMRT pairs can then be used for multivariate statistical analysis, such as principle component analysis (PCA-X), partial least-squares to latent structures data analysis (PLS-DA), and orthogonal PLS data analysis (OPLS-DA) to visualize and interpret the information-rich and complex MS data, as shown in both Figures 8 and 9.
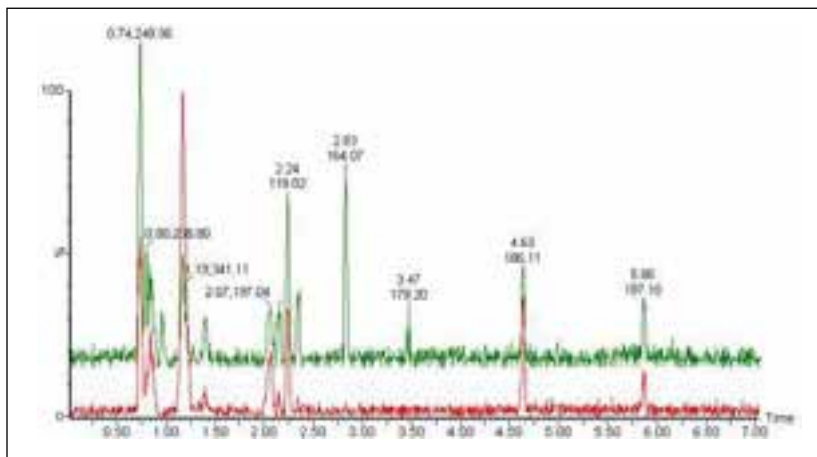


*Figure 7. A comparison of two typical chromatograms from the MTC and MTln3 cells. The figure clearly shows that there is difference between these two samples.*
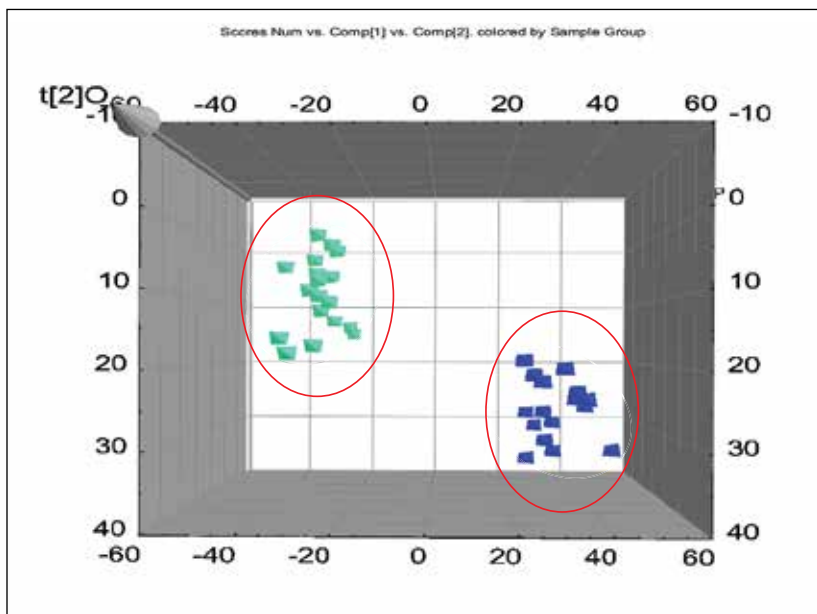


*Figure 8. The difference between the two sets of sample cells further demonstrated in the 3D score plot by multivariate statistical analysis using MarkerLynx XS Application Manager.*
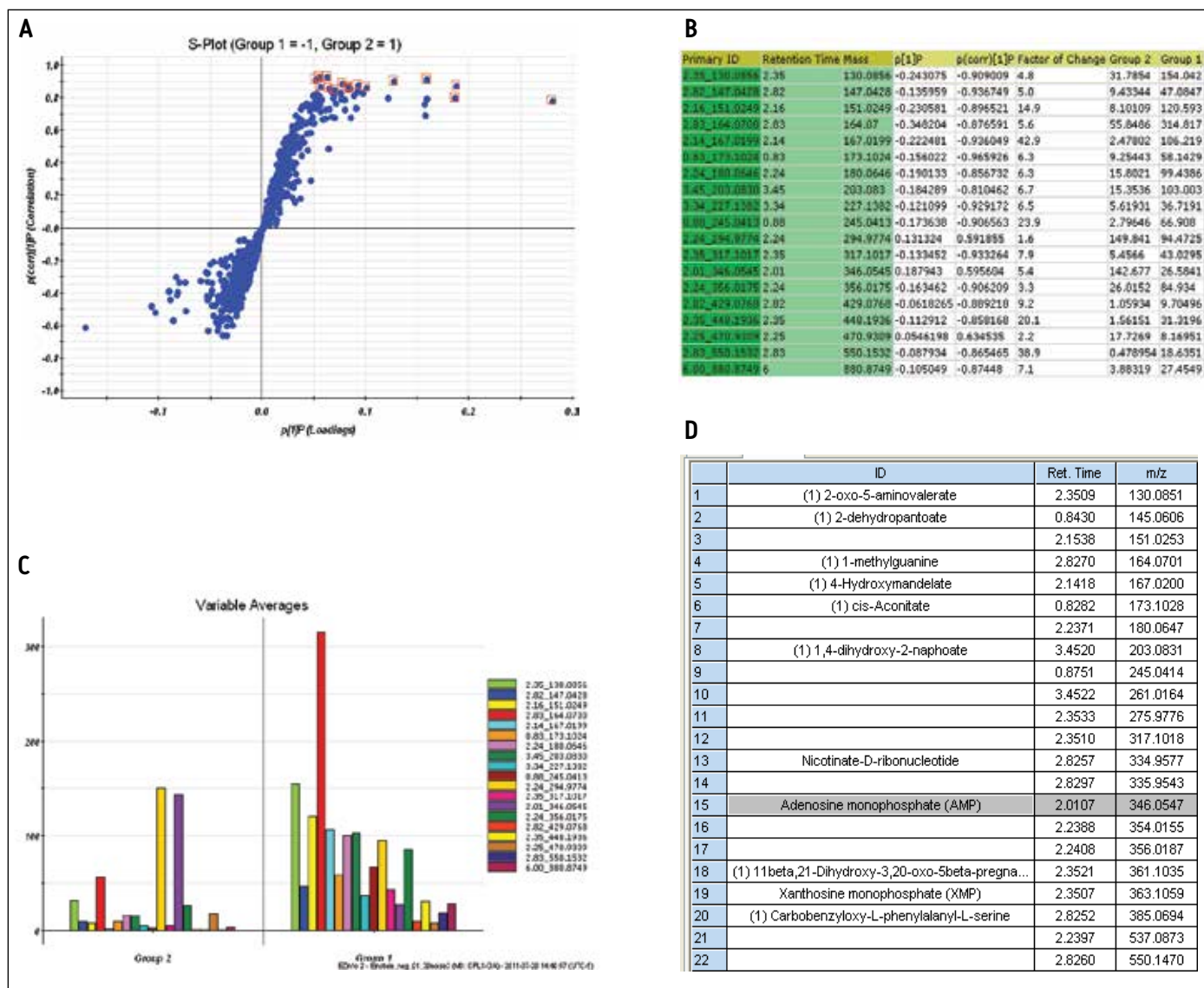
Figure 9. The selected markers from the S-Plot (A) can be transformed into table (B) and bar chart (C) to illustrate their contribution to the differences between the two sample cell lines. The markers can also be used for database searching for identification through in-house or online databases, such as ChemSpider. A couple of new markers, 2-dyhydropantoate and 4-hydroxymandelate were also found from the database. They are indications of increased methyl transferase activity, key to function of biosynthetic pathways. New markers (D) were found from database searching by untargeted analysis.

The markers from MarkerLynx statistical analysis were validated, in part, by identifying hits in pathways complementary to those found in targeted analysis, and builds belief in new untargeted hits found. For example, untargeted analysis, shown in Figures 4 and 6, indicated high AMP and phosphoenelpyruvate (PEP) along with high cis-aconitate in aggressive cells. AMP was identified from targeted analysis; cis-aconitate supports targeted analysis finding for increased flux into the TCA cycle, and PEP for increased glycolysis. Markers/carriers (malate/aspartate shuttle) for high cytosolic NADH from targeted analysis are complementary to untargeted findings of high nicotinamide-D-ribonucleotide, a step in NAD synthesis degradation product of amino acids found to be elevated by targeted analysis. Targeted analysis found high levels of aspartate, isoleucine, tyrosine, arginine, and others. Untargeted analysis showed markers for amino acid degradation with high 2-oxo-5-aminovalerate, a breakdown product of arginine; 1,4 dihyrooxy-2-naphoate, a breakdown product of tyrosine; alpha-hydroxyisovalerate, a marker for branched chain amino acid (isoleucine) breakdown; and homoserine, a breakdown product of aspartate.

Among the new markers found from database searching by untargeted analysis are 2-dehydropantoate and 4-hydroxymandelate, as shown in Figure 9D. They are indications of increased methyl transferase activity, which is key to function of biosynthetic pathways. Our results show that any of these pathways appears to be upregulated in the MTln3 cells.
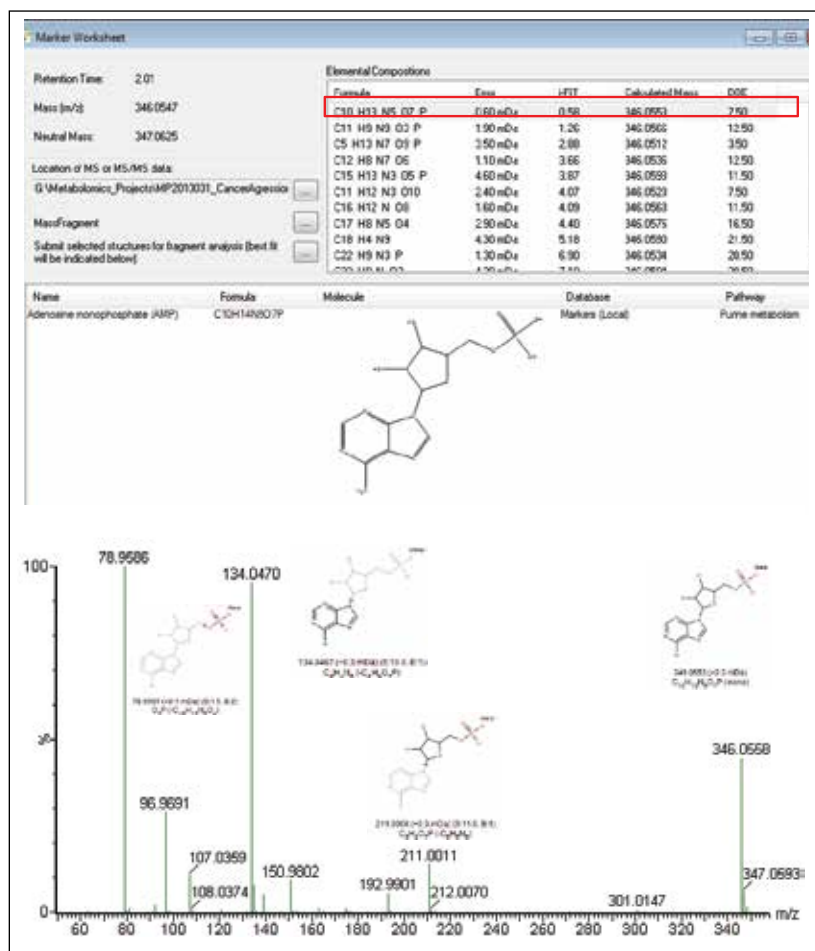


Figure 10. The Chemspider database searching result for AMP indicates a positive identification of the compound (top). The MS/MS spectrum for AMP from the MS$^E$ data acquisition confirms the structure of AMP (bottom). Fragmentation structures were matched using the MassFragment Software.

## CONCLUSIONS

We have successfully demonstrated a metabolomics study workflow that combines targeted and untargeted approaches for breast cancer biomarker analysis.

Aggressive cell MTLn3 and non-aggressive cell MTC show dramatically different concentrations of the biomarkers, such as malate and AMP in glycolysis and TCA cycle, which indicates glycolysis is higher in MTln3 cells.

Known markers of cancer aggressiveness can be analyzed by a targeted approach using Xevo TQ or Xevo TQ-S.

Hits are validated by identifying hits in pathways complementary to those found in targeted analysis using SYNAPT G2; this builds belief in new untargeted hits identified/discovered.

New markers and thereby new pathways can be discovered by untargeted SYNAPT G2 analysis. One example would be 2-dehydropantoate and 4-hydroxymandelate, which are markers for increased methyl transferase activity. Methyl transferase activity is key to the function of biosynthetic pathways.

### References

1. Lu X, Bennet B, Mu E, Rabinowitz J, and Kang Y; JBC, 285, NO. 13, 9317–9321, 2010.

2. Warburg O; "On the Origin of Cancer Cells" Science, 123 (3191): 309–314, 1956.

3. Shion H; "The Metabolomic Analysis of Simvastatin Dosed Rat Plasma by GC/TOF/MS", Waters application note, 720003119en, 2009.

## Waters

### THE SCIENCE OF WHAT'S POSSIBLE.®

**Waters Corporation**
34 Maple Street
Milford, MA 01757 U.S.A.
T: 1 508 478 2000
F: 1 508 872 1990
www.waters.com

Waters
THE SCIENCE OF WHAT'S POSSIBLE.®

# A Definitive Lipidomics Workflow for Human Plasma Utilizing Off-line Enrichment and Class Specific Separation of Phospholipids

Jeremy Netto,[1] Stephen Wong,[1] Federico Torta,[2] Pradeep Narayanaswamy,[2] and Mark Ritchie[1]
[1]Waters Pacific, Singapore
[2]Centre for Life Sciences, National University of Singapore, Singapore

## APPLICATION BENEFITS

Large-scale quantitative and comparative lipidomic studies require the use of simple and high throughput workflows. To answer this need, a tandem quadrupole-based workflow has been developed. The benefits of this targeted lipidomics workflow include the following:

- Simplified extraction of lipids using Ostro™ sample preparation chemistry

- 96-well plate format allows for high throughput extraction with automation technologies

- BEH HILIC chemistry provides well-defined, predictable class-based separation of lipids

- ACQUITY UPLC® System allows shorter run times per sample

- Xevo® TQ-S MS offers highly sensitive detection and quantification of lipids across a large dynamic range

- TargetLynx™ processing method provides rapid, automated, and quantitative data analysis of all the lipids of interest in a large sample batch

## WATERS SOLUTIONS

Ostro Sample Preparation

Xevo TQ-S Mass Spectrometer

ACQUITY UPLC System

ACQUITY UPLC BEH HILIC Columns

TargetLynx Application Manager

## KEY WORDS

Plasma, phospholipid extraction, Ostro, HILIC, TQ-S, TargetLynx

## INTRODUCTION

Lipids play many important roles in maintaining homeostasis of living organisms. Lipidomics analyses could further our understanding of mechanisms of disease, including the identification of biomarkers and potential drug targets.

Biofluids such as plasma are typically complex, with large lipid diversity across many orders of concentration. These, together with the chemical complexity of lipids, present demanding analytical challenges ranging from the sample preparation stage to the analytical techniques used to identify and quantify key lipids. Today, many variations of the Bligh and Dyer method are used for total lipid extraction and purification, with equal amounts used for mass spectrometric analysis.

Recent advances in lipidomics have made use of developments in chemistries and instrumentation, most notably the use of off-line enrichment or solid-phase sample preparation products[1,2] and the coupling of UltraPerformance LC® with mass spectrometry. However, there is little standardization across platforms and workflows for a complete analysis.

Presented here is a tandem quadrupole-based phospholipid analysis workflow from extraction to separation, identification and quantification of the phospholipids from a single vendor. These commercially available products packaged as a complete solution are provided to ease the strains and increase the productivity of laboratories undertaking longitudinal studies spanning hundreds of lipids over thousands of samples.

**WORKFLOW**

**Sample Preparation:**
Extract phospholipids using Ostro Sample Preparation Slides

**Data Acquisition:**
Targeted analysis of lipid classes using a single HILIC-UPLC®/MS/MS methodd with fast polarity switching

**Data Processing and Reporting:**
Identify and quantify detected lipids using TargetLynx
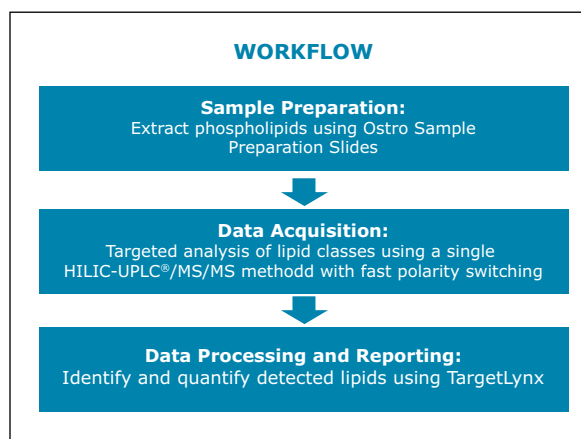
*Figure 1. Workflow for the targeted analysis of phospholipids in human plasma.*

## EXPERIMENTAL

### Method conditions

### LC conditions

| | |
|---|---|
| System: | ACQUITY UPLC |
| Column: | ACQUITY UPLC BEH HILIC 2.1 x 100 mm, 1.7 µm |
| Column temp.: | 30 °C |
| Mobile phase A: | 95:5 acetonitrile/water with 10 mM ammonium acetate, pH 8.0 |
| Mobile phase B: | 50:50 acetonitrile/water with 10 mM ammonium acetate, pH 8.0 |
| Gradient: | 0% to 20% B for 10 min |
| Flow rate: | 500 µL/min |
| Injection volume: | 3.0 µL, partial loop |

### MS conditions

| | |
|---|---|
| Mass spectrometer: | Xevo TQ-S |
| Ionization mode: | ESI, +/- switching |
| Capillary voltage: | 3.8 kV (+) / 1.9 kV (-) |
| Desolvation temp.: | 450 °C |
| Desolvation gas: | 1000 L/h |
| Source temp.: | 150 °C |
| Collision cell pressure: | 3.6 x 10$^{-3}$ mBar |

### Sample description

Human plasma samples were obtained from the Centre for Life Sciences, National University of Singapore. The protocol described here follows a recently published application note.[3]

100 µL of human plasma was loaded into each well of a Waters® Ostro Sample Preparation Plate fitted onto a vacuum manifold. 800 µL of ethanol was added to each well and mixed thoroughly by aspirating the mixture 10x using a micropipette. A vacuum of approximately 15'' Hg was applied to the plate until the solvent was completely drained. This step was repeated with another 800 µL of ethanol with the total fraction collected labelled as the "flow through."

800 µL of elution solvent (4.5:4.5:1.0 chloroform/methanol/triethylamine) was added to each well, and the fraction was collected under 15'' Hg vacuum as the "eluate." This step was repeated, bringing the total fraction volume to approximately 1600 µL.

Both the eluate and flow through fractions were dried down under nitrogen, and reconstituted with 200 µL 1:1 (v/v) chloroform/methanol. 1 µL of the eluate fraction was combined with 99 µL of the flow through fraction to give a 1:100 dilution. This combined sample was then injected into the UPLC/MS system.

| Lipid class | Polarity | MRM time window (min) | No. of species detected | Cone voltage (V) | Collision energy (V) |
|---|---|---|---|---|---|
| Monohexylceramide (MonoHexCer) | + | 0 to 2 | 16 | 20 | 30 |
| Phosphatidylglycerol (PG) | - | 1 to 3 | 19 | 55 | 45 |
| Dihexylceramide (DiHexCer) | + | 2 to 4 | 16 | 20 | 30 |
| Phosphatidylinositol (PI) | - | 3 to 5 | 26 | 48 | 30 |
| Phosphatidylethanolamine (PE) | - | 4 to 6 | 33 | 48 | 40 |
| Phosphatidylcholine (PC) | + | 5 to 7 | 47 | 36 | 30 |
| Lyso-Phosphatidylinositol (LPI) | - | 5 to 7 | 11 | 48 | 30 |
| Lyso-Phosphatidylethanolamine (LPE) | - | 6 to 8 | 11 | 36 | 24 |
| Sphingomyelin (SM) | + | 7 to 9 | 18 | 36 | 24 |
| Lyso-Phosphatidylcholine (LPC) | + | 8 to 10 | 11 | 42 | 26 |

*Table 1. Xevo TQ-S MRM method.*

## RESULTS AND DISCUSSION

### Lipid extraction from Ostro plates using automated liquid handlers

While advancements in instrument technologies such as UPLC have enabled faster analysis of large numbers of samples, sample preparation time has been commonly viewed as the bottleneck.

When performed manually, lipid extraction using the Bligh and Dyer method takes approximately one hour and the Ostro plate method 1.5 hours. As the Ostro plate is available in a standard 96-well plate design, it can be easily adapted to most automated liquid handlers making the process time for one sample or 96 samples approximately the same, for example, 1.5 hours. Whereas, it took almost two days to manually process 96 samples using the Bligh and Dyer method.

| | Manual | Automation |
|---|---|---|
| Lipid Class | Overall %CV | Overall %CV |
| GluCeramides | 13.2 | 9.7 |
| Phosphatidylglycerol (PG) | 10.2 | 7.2 |
| Phosphatidylinositol (PI) | 10.2 | 5.8 |
| Phosphatidylethanolamine (PE) | 16.0 | 6.4 |
| Phosphatidylcholine (PC) | 9.9 | 7.5 |
| Lyso-Phosphatidylinositol (LPI) | 23.0 | 13.0 |
| Lyso-Phosphatidylethanolamine (LPE) | 16.0 | 6.4 |
| Sphingomyelin (SM) | 11.9 | 9.1 |
| Lyso-Phosphatidylcholine (LPC) | 14.4 | 8.4 |

*Table 2. Comparison of well-to-well reproducibility (%CV) of the Ostro plate for manual versus automated sample handling.*

Using an automated liquid handler to process the plasma samples, as shown in Figure 2, the well-to-well reproducibility (%CV) improved compared to manually performing the extraction. This was true for all classes of lipids analyzed, with improvements ranging from 25% (SM) to 60% (PE).

## MRM method setup on Xevo TQ-S

In reversed-phase chromatography of lipids, separation is governed by lipophilicity, alkyl chain length, and degree of saturation for each individual lipid. These result in broad MRM acquisition time windows[4] that, in turn, negatively affect the instrument's duty cycle, thus hindering accurate quantification.

In the HILIC-UPLC/MS method used in this application note, there was a clear and reproducible separation of the various classes of lipids. This was observed very clearly by the difference in retention times of PCs and SMs, which are normally difficult to identify and quantify using reversed-phase methods.[5, 6]
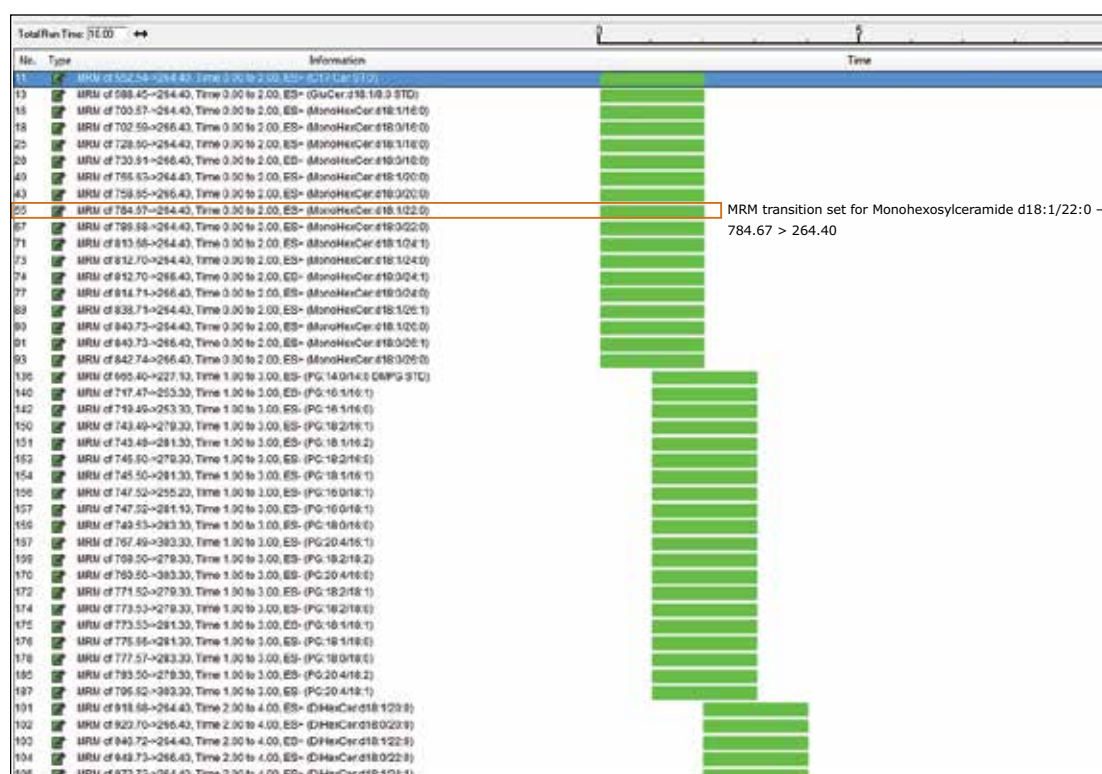


Figure 2. Typical screen shot of the Xevo TQ-S MRM method editor.

By leveraging the reproducible retention times of the lipid classes, MRM acquisition time windows were reduced to two minutes per class, as shown in Table 1. This allowed for the creation of a single MS method to analyze the combined "flow through" and "eluate" fractions in a single run. A total of 215 MRM transitions (+/- polarity) including internal standards were created in this method. Figure 3 shows each lipid transition set up as a single function, for example, monohexosylceramide d18:1/22:0, which will limit the addition or subtraction of lipids to only those of interest to the operator.

## Data processing and reporting
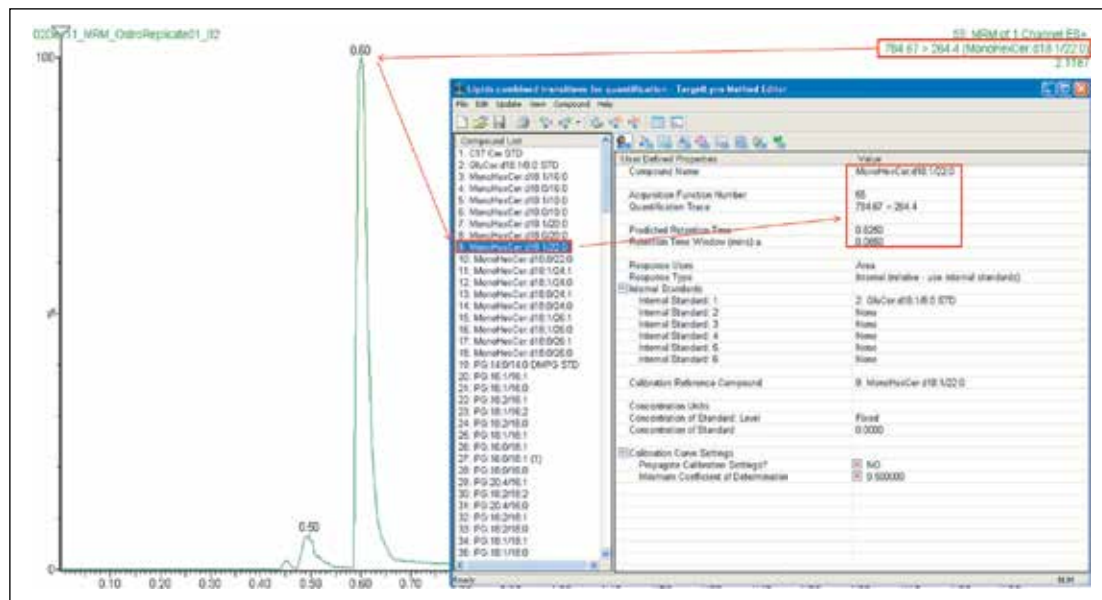


*Figure 3. Typical lipid MRM trace using monohexosylceramide d18:1/22:0 as an example.*

A complementary data processing method was created using the TargetLynx Application Manager, as shown in Figure 4. The insert shows how easily peak information can be "dragged and dropped" into the data processing method.
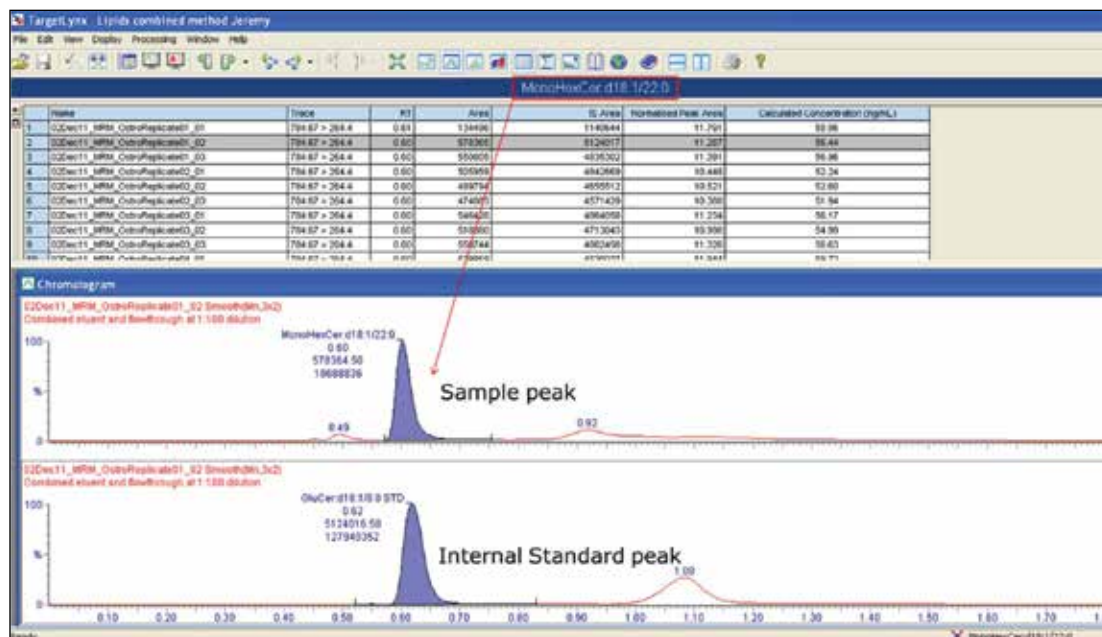


*Figure 4. Quantification of monohexosylceramide d18:1/22:0 MRM trace using TargetLynx. Chromatographic peaks are automatically detected and quantified against a standard for a series of samples.*

Once the processing method had been set with the appropriate transitions and retention times for each lipid, batch processing for any number of samples run under the same conditions described above can be performed. Figure 4 shows a typical TargetLynx results view. Using monohexosylceramide d18:1/22:0 as an example, the application manager automatically integrates both the sample peak and the pre-defined internal standard (IS) peak and calculates the concentration of the lipid in the sample against the known spiked concentration of the IS. A user-defined report can then be printed, or these results can be exported into a number of popular generic formats for further statistical analysis.

## CONCLUSIONS

Consistent, reliable, and rapid identification and quantification of hundreds of lipid species can now be performed in a single run by the application of this workflow. The high throughput nature of the workflow utilizing automation technologies and automated data processing and reporting means that large-scale comparative lipidomic studies can be routinely used by laboratories around the world. In addition, the consistency obtained from this standardized platform means that data can be shared and compared across various sites, thereby enabling a greater understanding of the global lipidome and its associations with diseases.

## References

1. Ferreiro-Vera C *et al.* Comparison of sample preparation approaches for phospholipids profiling in human serum by liquid chromatography-tandem mass spectrometry. *J Chrom A.* 2012;1240: 21-8.

2. Pucci V *et al.* A novel strategy for reducing phospholipids-based matrix effect in LC-ESI-MS bioanalysis by means of Hybrid SPE. *J Pharm Biomed Anal.* 2009;50(5): 867-71.

3. Ritchie M *et al.* Extraction of Phospholipids from Plasma using Ostro Sample Preparation. Waters Application Note 720004201en. 2012.

4. Goh E, Ritchie M. Rapid Lipid Profiling of Serum by Reverse Phase UPLC-Tandem Quadrupole MS. Waters Application Note 720004035en. 2011.

5. Mal M, Wong S. A HILIC-Based UPLC-MS Method for the Separation of Lipid Classes from Plasma. Waters Application Note, 720004048en. 2011.

6. Ritchie M *et al.* UPLC BEH HILIC: The Preferred Separation Chemistry for Targeted Analysis of Phospholipids. Waters Application Note 720004219en. 2012.

## Waters
**THE SCIENCE OF WHAT'S POSSIBLE.®**

**Waters Corporation**
34 Maple Street
Milford, MA 01757 U.S.A.
T: 1 508 478 2000
F: 1 508 872 1990
www.waters.com

Waters
THE SCIENCE OF WHAT'S POSSIBLE.®

# Rapid and Simultaneous Analysis of Plasma Catecholamines and Metanephrines Using Mixed-Mode SPE and Hydrophilic Interaction Chromatography (HILIC) for Clinical Research

Jonathan P. Danaceau, Erin E. Chambers, and Kenneth J. Fountain
Waters Corporation, Milford, MA, USA

## APPLICATION BENEFITS

■ Retention and baseline resolution of monoamine neurotransmitters and metanephrines without the need for ion-pairing reagents

■ Rapid, simultaneous quantification of plasma metanephrines and catecholamines

■ 5x analyte concentration without the need for evaporation and reconstitution

■ Linear, accurate, and precise results down to 10 pg/mL

## WATERS SOLUTIONS

Oasis® WCX 96-well µElution Plate

96-well Sample Collection Plate

ACQUITY UPLC® BEH Amide Column

ACQUITY UPLC System

Xevo® TQ-S Mass Spectrometer

UNIFI® Scientific Information System

## KEY WORDS

Catecholamines, metanephrines, HILIC, SPE, LC-MS/MS, sample preparation

## INTRODUCTION

Clinical researchers are often interested in measuring elevated concentrations of plasma catecholamines and their O-methylated metabolites (metanephrines). However, these compounds (in particular, norepinephrine, epinephrine, and dopamine) can be a challenge to analyze via reversed-phase LC-MS/MS due to their polarity. As a result, many research laboratories still analyze this panel using ion-pairing reagents and electrochemical detection (ECD). While reversed-phase LC-MS/MS has been used successfully, challenges still exist due to ion-suppression from matrix components, insufficient retention, and inadequate separation of normetanephrine and epinephrine.

Hydrophilic interaction chromatography (HILIC) is increasingly becoming a method of choice for the analysis of polar compounds.[1-6] Expanding upon earlier published methods,[6-7] this application note describes the extraction and analysis of monoamine neurotransmitters and metanephrines from plasma. HILIC-based chromatographic separation is achieved using a Waters® ACQUITY UPLC BEH Amide Column. Waters Oasis WCX 96-well µElution Plates are used to extract these compounds from plasma. The use of mixed-mode weak cation exchange solid-phase extraction (SPE) plates, in combination with the amide column for HILIC chromatography and the Waters Xevo TQ-S mass spectrometer, result in a rapid, robust method with excellent linearity, accuracy and precision, as well as minimal matrix effects.

## EXPERIMENTAL

### LC conditions

| | |
|---|---|
| LC system: | ACQUITY UPLC |
| Column: | ACQUITY UPLC BEH Amide, 1.7 μm, 2.1 x 100 mm |
| Column temp.: | 30 °C |
| Sample temp.: | 10 °C |
| Mobile phase A (MPA): | 95:5 Water:ACN containing 30 mM $NH_4HCOO$, pH 3.0 |
| Mobile phase B (MPB): | 15:85 Water:ACN containing 30 mM $NH_4HCOO$, pH 3.0 |
| Needle washes: | Strong and weak needle washes were both placed in MPB |

The gradient ramp is shown in Table 1 and includes an initial hold, followed by a shallow ramp and an increase in flow rate to re-equilibrate the column. The entire cycle time is 4.0 min.

### MS conditions

| | |
|---|---|
| MS system: | Xevo TQ-S |
| Ionization mode: | ESI positive |
| Capillary voltage: | 0.5 kV |
| Cone voltage: | Compound specific (see Table 2) |
| Desolvation gas: | 900 L/hr |
| Cone gas: | 150 L/hr |
| Desolvation temp.: | 550 °C |
| Source temp.: | 150 °C |

Data were acquired and analyzed using UNIFI Software.

| Time (min) | Flow (mL/min) | %A | %B |
|---|---|---|---|
| 0 | 0.6 | 0.0 | 100.0 |
| 1.0 | 0.6 | 0.0 | 100.0 |
| 2.0 | 0.6 | 10.0 | 90.0 |
| 2.1 | 1.0 | 10.0 | 90.0 |
| 2.5 | 1.0 | 30.0 | 70.0 |
| 2.6 | 1.0 | 0.0 | 100.0 |
| 3.9 | 1.0 | 0.0 | 100.0 |
| 4.0 | 0.6 | 0.0 | 100.0 |

*Table 1. Mobile phase gradient. The compositions of MPA and MPB are listed in the methods section.*

Combined stock standards containing 10-μg/mL of dopamine (DA), 3-methoxytyramine, (3-MT) metanephrine (MTN), and normetanephrine (NMT) and 50-μg/mL of norepenephrine (NE) and epinephrine (EP) were prepared in methanol containing 0.1% ascorbic acid to prevent oxidation. A combined internal standard stock solution composed of 10-μg/mL D3-metanephrine, D3-normetanephrine, D4-dopamine, D6-epinephrine, and D6-norepinephrine, was also prepared in methanol containing 0.1% ascorbic acid. Working internal standard solutions were prepared daily in 5% MeOH with 0.1% formic acid at a concentration of 2.5 ng/mL.

Human plasma (sodium heparin) was obtained from Biological Specialty Corporation (Colmar, PA). Pooled plasma (6 lots) was used to prepare calibration and quality control samples.

### Sample preparation

Pooled plasma samples (250 μL) were pre-treated with 250-μL of 50-mM $NH_4CH_3COO$ and 50-μL of an internal standard working solution (2.5 ng/mL). Pre-treated samples were loaded in individual wells of an Oasis WCX 96-well μElution Plate that had been conditioned with 200-μL of MeOH and 200-μL of $H_2O$. After loading the samples, wells were washed with 200-μL of 20-mM $NH_4CH_3COO$ followed by 200-μL of 50:50 ACN:IPA. The 96-well plate was then dried under vacuum for 30 s to remove as much solvent as possible from the sorbent bed. The target compounds were eluted from the plate with 2 x 25-μL aliquots of 85:15 ACN:$H_2O$ containing 2% formic acid into an 700-μL 96-well sample collection plate (p/n 186005837). 15-μL of the eluate was injected onto the UPLC®-MS/MS System.

## RESULTS AND DISCUSSION

The structures of all compounds are shown in Figure 1 along with their individual logP values, demonstrating the highly polar nature of many of these compounds. Table 2 shows the retention times and individualized MS parameters of each compound, including MRM transitions, cone voltage, and collision energy.
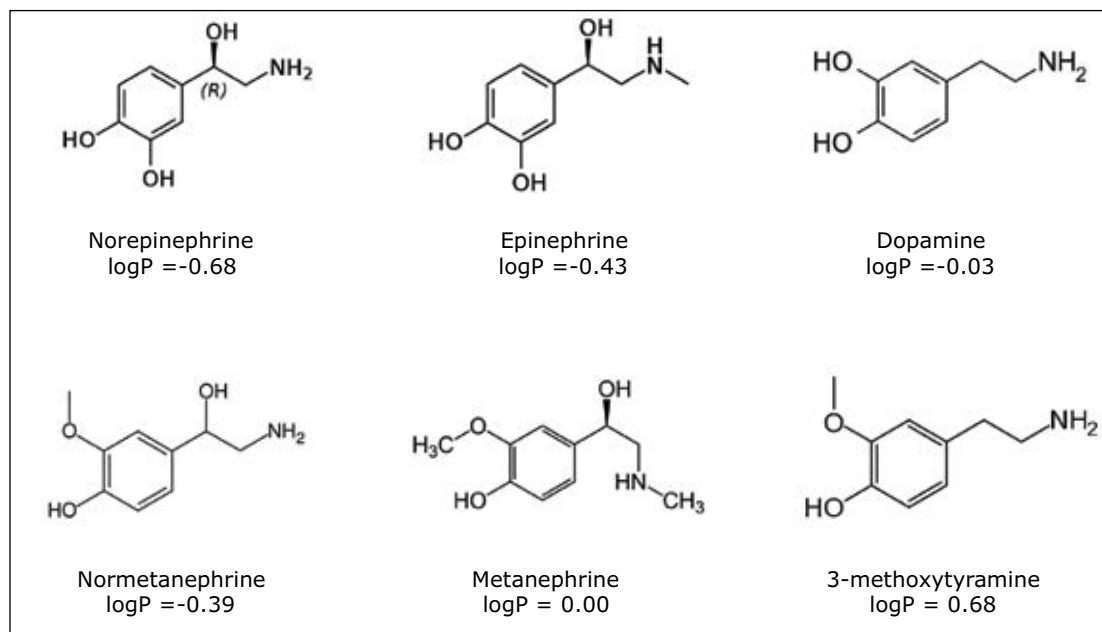


Figure 1. Names, molecular structures, and logP values of catecholamines and metanephrines.

| Analyte | RT (min) | MRM transitions m/z | Cone voltage (V) | Collision energy (eV) |
|---|---|---|---|---|
| 3-Methoxytyramine | 0.84 | 151.1>91.2 | 17 | 22 |
| | | 151.1>119.2 | 17 | 18 |
| Metanephrine | 0.91 | 180>165.1 | 35 | 16 |
| | | 180>148.1 | 35 | 20 |
| Normetanephrine | 1.17 | 166.1>134.1 | 50 | 16 |
| | | 166.1>149.1 | 50 | 10 |
| Dopamine | 1.25 | 137.1>91.1 | 50 | 18 |
| | | 154.1>137.2 | 29 | 10 |
| Epinephrine | 1.40 | 184.1>166.1 | 15 | 8 |
| | | 166.1>107 | 15 | 18 |
| Norepinephrine | 1.98 | 152>135.2 | 46 | 14 |
| | | 152>79.2 | 20 | 20 |

Table 2. Mass spectral parameters used for analysis of catecholamines and metanephrines.

Figure 2A shows the chromatography of all compounds from a 20 pg/mL calibration standard using the ACQUITY UPLC BEH Amide Column. Previous work[6] had shown that 30 mM $NH_4HCOO$ and 15% water in MPB resulted in an ideal balance of ionic strength and solubility, enabling the resolution and peak shape seen in Figure 2A. One important feature of this separation is the resolution between NMT and EP. These two compounds have the same molecular formula and can interfere with each other if not adequately separated. Figure 2A demonstrates the baseline separation of these compounds in HILIC mode, enabling their unambiguous identification and quantification. Figure 2B shows the HILIC chromatography of an unspiked plasma sample, demonstrating the ability to determine endogenous concentrations of 3-MT, MTN, NMT, DA, EP, and NE (7.0, 31.7, 70.6, 0.0, 29.4, and 360.9 pg/mL, respectively).
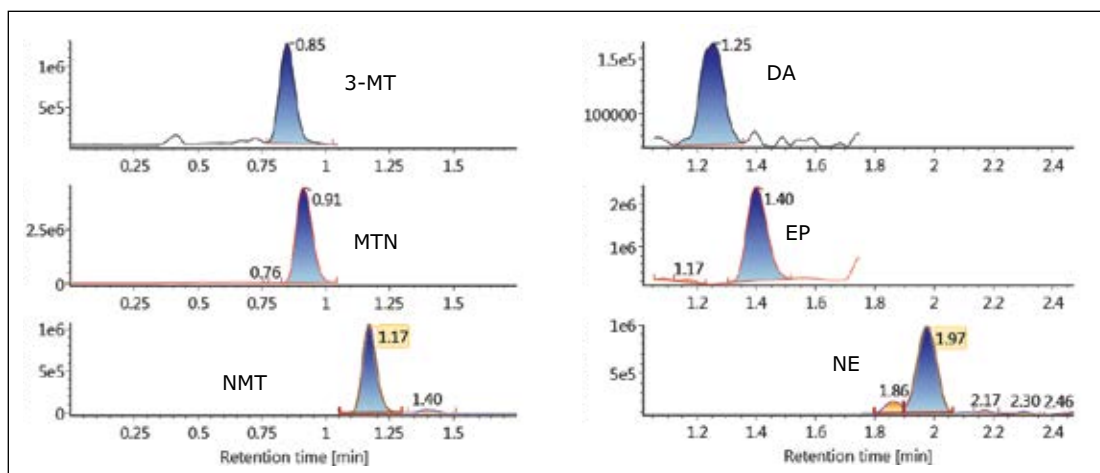


*Figure 2A. Chromatography of catecholamines and metanephrines on the ACQUITY UPLC BEH Amide Column, 1.7 µm, 2.1 x 100 mm. Representative calibration standard spiked at 20 pg/mL (100 pg/mL for EP and NE).*
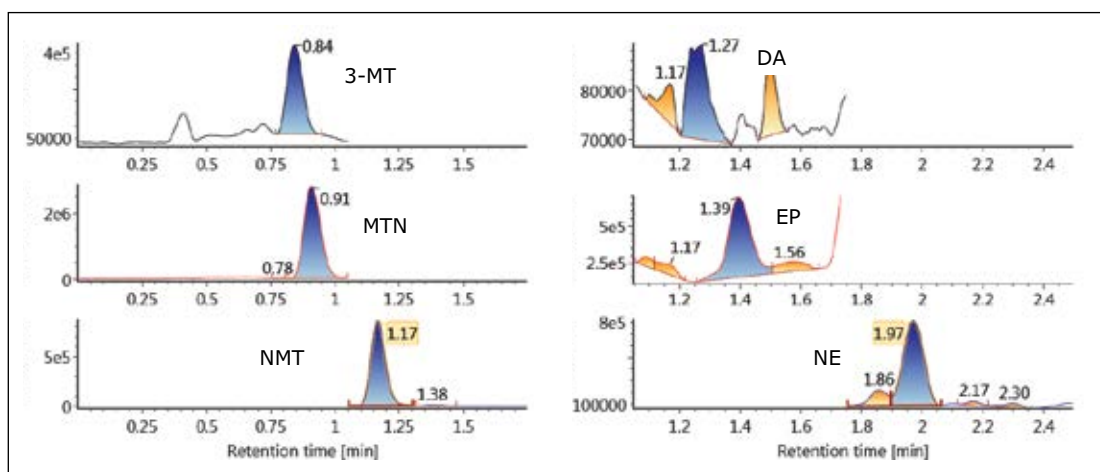


*Figure 2B. Chromatography of catecholamines and metanephrines on the ACQUITY UPLC BEH Amide Column, 1.7 µm, 2.1 x 100 mm. Representative method blank. Endogenous concentrations of all compounds are listed in Table 3.*

## Recovery and matrix effects

Extraction recoveries and matrix effects are shown in Figure 3. Recoveries ranged from 54% for NE to 90% for DA, with an average recovery of 76.4%. Matrix effects averaged -6.9%. The largest matrix effects were -23% and -22% for NE and DA, respectively, but were negligible for all other compounds. These results highlight another advantage of HIILIC chromatography, the ability to minimize matrix effects when analyzing polar compounds.
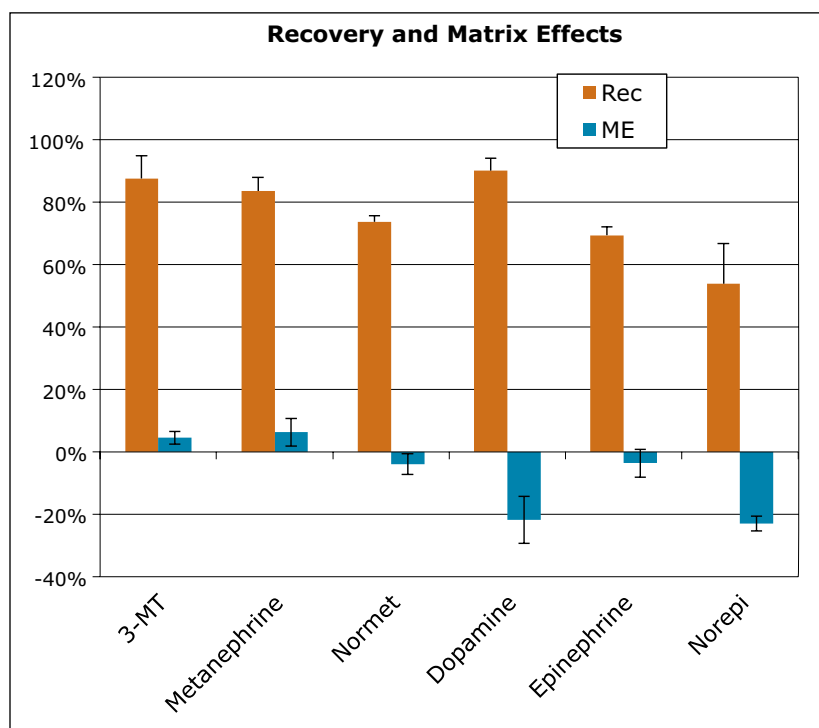


Figure 3. Recovery and matrix effects for catecholamines and metanephrines extracted from urine using Oasis WCX 96-well µElution Plates (N=4). Error bars indicate standard deviations. All compounds were spiked at 100 pg/mL into pooled human plasma.

## Quantitative results

Calibration curves and quality control samples were prepared via the standard addition method by spiking pooled plasma samples with known concentrations of analytes. Two ranges of calibration curves were used, reflecting different expected concentrations of various compounds in plasma. Calibration levels for 3-MT, metanephrine, normetanephrine, and dopamine ranged from 10–2,000 pg/mL. Calibration levels for epinephrine and norepinephrine ranged from 50–10,000 pg/mL. After data processing, the endogenous concentrations were extrapolated from the resulting calibration curves. These data were used to correct the actual calibration concentrations. For example, the plasma sample used for calibration was determined to contain 31.7 pg/mL of metanephrine, so the calibration concentrations were adjusted to 41.7–2031.7 pg/mL. The resulting calibration curves showed excellent linearity, with $R_2$ values of 0.999 or greater for all compounds. Figure 4 shows representative calibration curves for DA and MTN, both of which have $R_2$ values greater than 0.999. Table 3 summarizes the calibration data for all compounds. Mean % deviations from expected calibration values were less than 1% for all analytes. In addition, the maximum % deviations from calibration values are listed and show that with the exception of epinephrine, the maximum % deviation for all calibrators was less than 10%. The calculated endogenous concentration of compounds in the pooled plasma used for calibration is also listed, along with the corrected calibration ranges for each compound.
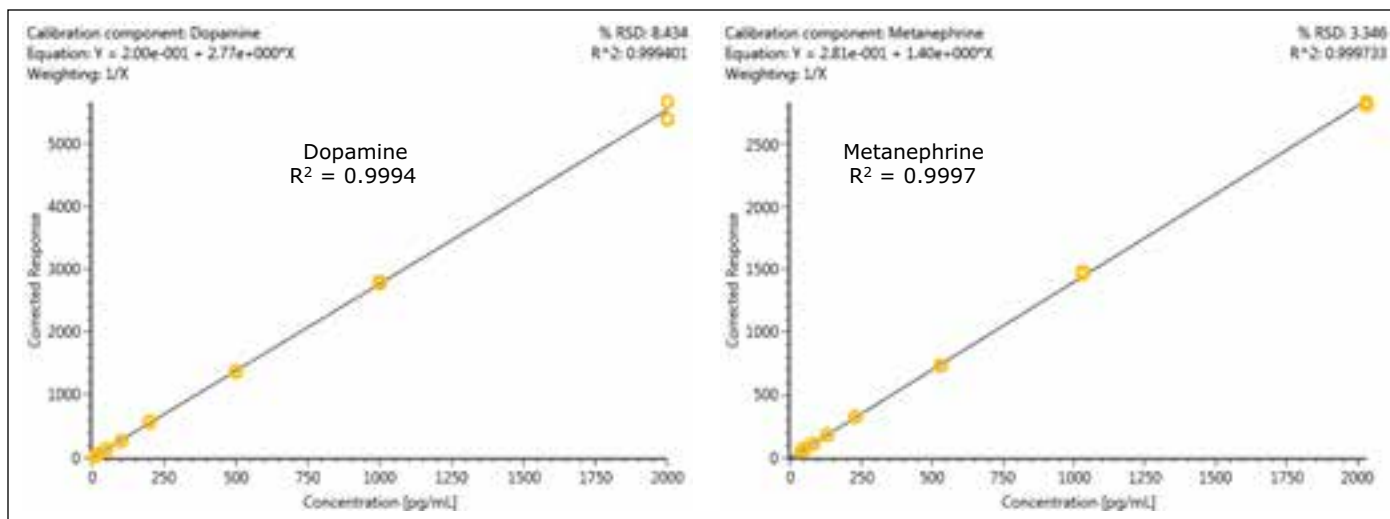
*Figure 4. Representative calibration curves for dopamine (DA) and metanephrine (MTN) extracted from plasma samples. The data were fitted with a 1/x weighted linear fit. Basal concentrations for DA and MTN were 0 and 30 pg/mL, respectively.*

| | $R^2$ | *Mean % Dev.* | Max % Dev. | Endogenous (pg/mL) | Corrected Calibration Range |
|---|---|---|---|---|---|
| 3-MT | 0.9993 | 0.25% | 2.89% | 7 | 17-2007 |
| Metanephrine | 0.9997 | 0.00% | 2.50% | 32 | 42-2042 |
| Normetanephrine | 0.9998 | 0.00% | 1.72% | 71 | 81-2081 |
| Dopamine | 0.9994 | -0.33% | 4.57% | 0 | 10-2000 |
| Epinephrine | 0.9990 | 0.84% | 11.83% | 29 | 79-10079 |
| Norepinephrine | 0.9995 | 0.00% | 2.59% | 361 | 411-10411 |

*Table 3. Summary of calibration data for plasma metanephrines and catecholamines. Mean % deviation indicates the average % deviation of all calibration points from their theoretical concentrations. The max % deviation indicates the maximum deviation over the entire calibration range. The calculated endogenous concentrations are listed and used to correct the calibration range.*

Quality control samples (N=6) were overspiked at 200, 500, 2000, and 4000 pg/mL for EP and NE and at 40, 100, 400, and 800 pg/mL for the remaining compounds. QC results were accurate and precise (see Table 4). All QC values were within 10% of their target values, and most were within 5%. In addition, all coefficients of variation (%CV) were less than 10%. This demonstrates that the method is linear, accurate, and precise over a calibration range that includes the entire scope of expected values for normal and pathologically elevated samples.

| | QC spike concentration | | | | | | | | | | | |
|---|---|---|---|---|---|---|---|---|---|---|---|---|
| | 40 pg/mL | | | 100 pg/mL | | | 400 pg/mL | | | 800 pg/mL | | |
| | Mean | S.D. | %CV | Mean | S.D. | %CV | Mean | S.D. | %CV | Mean | S.D. | %CV |
| 3-MT | 99.9% | 7.4% | 7.4% | 99.2% | 3.0% | 3.1% | 105.9% | 1.8% | 1.7% | 93.9% | 2.6% | 2.8% |
| Metanephrine | 99.9% | 2.0% | 2.0% | 97.6% | 0.8% | 0.8% | 107.3% | 1.2% | 1.1% | 94.6% | 1.7% | 1.7% |
| Normetanephrine | 99.8% | 1.6% | 1.6% | 96.8% | 1.7% | 1.8% | 104.6% | 0.4% | 0.4% | 93.4% | 1.0% | 1.1% |
| Dopamine | 97.0% | 7.2% | 7.4% | 91.2% | 3.4% | 3.7% | 103.7% | 3.1% | 3.0% | 95.6% | 2.7% | 2.8% |
| | 200 pg/mL | | | 500 pg/mL | | | 2000 pg/mL | | | 4000 pg/mL | | |
| | Mean | S.D. | %CV | Mean | S.D. | %CV | Mean | S.D. | %CV | Mean | S.D. | %CV |
| Epinephrine | 97.3% | 4.3% | 4.4% | 98.8% | 2.2% | 2.2% | 100.8% | 1.4% | 1.4% | 97.0% | 2.6% | 2.6% |
| Norepinephrine | 105.1% | 7.7% | 7.4% | 102.6% | 8.2% | 8.0% | 96.7% | 1.3% | 1.3% | 97.1% | 4.2% | 4.3% |

Table 4. Quality control results for plasma catecholamines and metanephrines. Concentrations refer to the spiked concentration. Accuracies were calculated by comparing the result of the sum of the spiked concentration and endogenous calculated values in the plasma sample to the theoretical sum of these concentrations.

## CONCLUSIONS

The extraction and analysis of plasma catecholamines and metanephrines using Oasis WCX µElution Plates and an ACQUITY UPLC BEH Amide Column in HILIC mode is detailed. Extraction using the Oasis WCX µElution Plate resulted in low matrix effects and consistent recoveries for all compounds that translated into excellent analytical accuracy and precision. In addition, the ability to elute the samples in an extremely low volume (50 µL) enabled 5x sample enrichment without the extra time or risk associated with evaporation and reconstitution. The ACQUITY UPLC BEH Amide Column used for HILIC separation resulted in rapid and efficient separation of all compounds, with baseline resolution between normetanephrine (NMT) and epinephrine (EP). It also enabled the analysis of the monoamines, dopamine, norepinephrine and epinephrine. Quantitative results were excellent, with highly linear responses across the entire calibration range and excellent accuracy and analytical precision.

## References

1. Cubbon S, Antonio C, Wilson J, Thomas-Oates J. Metabolomic applications of HILIC-LC-MS. *Mass Spectrom Rev.* 2010 Sep–Oct;29(5):671–84.

2. Jian W, Edom RW, Xu Y, Weng N. Recent advances in application of hydrophilic interaction chromatography for quantitative bioanalysis. *J Sep Sci.* 2010 Mar;33(6-7):681-97.

3. Xu RN, Rieser MJ, El-Shourbagy TA. Bioanalytical hydrophilic interaction chromatography: recent challenges, solutions and applications. *Bioanalysis.* 2009 Apr;1(1):239–53.

4. Jian W, Xu Y, Edom RW, Weng N. Analysis of polar metabolites by hydrophilic interaction chromatography–MS/MS. *Bioanalysis.* 2011 Apr;3(8):899–912.

5. Hemström P, Irgum K. Hydrophilic interaction chromatography. *J Sep Sci.* 2006 Aug;29(12):1784–821.

6. Danaceau JP, Chambers EE, Fountain KJ. Hydrophilic interaction chromatography (HILIC) for LC-MS/MS analysis of monoamine neurotransmitters. *Bioanalysis.* 2012 Apr;4(7):783–94.

7. Peaston RT, Graham KS, Chambers E, van der Molen JC, Ball S. Performance of plasma free metanephrines measured by liquid chromatography-tandem mass spectrometry in the diagnosis of pheochromocytoma. *Clin Chim Acta.* 2010 Apr 2;411(7-8):546–52.

*For Research Use Only. Not for use in diagnostic procedures.*

## Waters

### THE SCIENCE OF WHAT'S POSSIBLE.®

**Waters Corporation**
34 Maple Street
Milford, MA 01757 U.S.A.
T: 1 508 478 2000
F: 1 508 872 1990
www.waters.com

Waters
THE SCIENCE OF WHAT'S POSSIBLE.®

# The Application of UPLC/MS[E] for the Analysis of Bile Acids in Biological Fluids

Elizabeth J. Want,[1] Muireann Coen, Perrine Masson, Hector C. Keun, Jake T.M. Pearce, Michael D. Reily, Donald Robertson, Cynthia M. Rohde, Elaine Holmes, John Lindon, Robert S. Plumb,[2] Stephen McDonald,[2] and Jeremy K Nicholson

[1]Imperial College, London, UK
[2]Waters Corporation, Milford, MA, USA

## APPLICATION BENEFITS

UPLC®/MS[E] can be used to measure bile acids reproducibly and reliably in biological fluids. This method analyzes a wide range of endogenous metabolites to provide both a targeted assay and a global metabolite profiling approach in the same analytical run. Use of this metabolic approach allows for a more comprehensible interpretation of metabolite changes, and it can be easily extended to other sample types and studies.

## WATERS SOLUTIONS

ACQUITY UPLC® Columns

ACQUITY UPLC System

QTof Premier™ Mass Spectrometer

MarkerLynx™ XS Application Manager

## KEY WORDS

Bile acids, endogenous metabolites, liver damage, hepatic and biliary tract disease

## INTRODUCTION

Individual bile acids are endogenous markers of liver cell function and studies of both qualitative and quantitative bile acid changes have been conducted as a result of liver and intestinal diseases. The measurement of serum bile acid concentrations can provide information pertaining to liver damage, as well as hepatic and biliary tract diseases.[1-4] However, traditional chromatographic methods have not typically provided sufficient separation in order to differentiate between structurally similar bile acids. Utilization of the Waters® UltraPerformance LC® (UPLC) Technology high resolution chromatographic system has greatly improved the abillity to separate metabolites from endogenous matrice. UPLC provides superior resolution, sensitivity, and throughput compared with conventional LC approaches. Using UPLC, previously co-eluting metabolites can be separated and matrix effects, such as ESI ion suppression, are minimized. By combining UPLC with oa-TOF mass spectrometry, both high-resolution and exact mass measurements can be achieved, aiding the identification of metabolites. This application note describes a new, sensitive UPLC-MS approach developed to measure bile acid reproducibly and reliably in biological fluids. Over 30 individual bile acids were separated and detected in a 5-minute window using an ACQUITY UPLC HSS T3 2.1 x 100 mm, 1.8 µm Column coupled to a Q-ToF Premier Mass Spectrometer. Bile acids were extracted from serum using methanol and a gradient elution of water and acetonitrile was employed, which also enabled the detection of a wide range of endogenous metabolites, such as lipids. MS[E] data were acquired using a patented acquisition method that collects precursor and product ion information for virtually every detectable species in a mixture. This allowed for characteristic metabolite fragmentation information to be obtained in a single analytical run, easily distinguishing glycine and taurine bile acid conjugates. This assay was applied to the study of the hepatotoxin galactosamine (galN) in rat. Serum bile acid changes were observed after galN treatment, including elevated taurine-conjugated bile acids, which correlated to liver damage severity. This UPLC-MS approach to bile acid analysis offers a sensitive and reproducible tool that will be of great value in exploring both markers and mechanisms of hepatotoxicity.

## EXPERIMENTAL

### UPLC conditions

| | |
|---|---|
| LC System: | ACQUITY UPLC |
| Column: | ACQUITY UPLC HSS T3, 2.1 x 100 mm, 1.8 µm |
| Column temp.: | 40 °C |
| Sample temp.: | 4 °C |
| Mobile phase A: | Water |
| Mobile phase B: | Acetonitrile |
| Flow rate: | 0.5 mL/min |
| Injection volume: | 5 µL |

Gradient:

| Time (min) | % A | Curve |
|---|---|---|
| 0.0 | 0 | 0 |
| 2.0 | 0 | 6 |
| 12.0 | 5 | 6 |
| 17.0 | 5 | 6 |
| 18.0 | 100 | 6 |
| 22.0 | 100 | 6 |
| 22.5 | 5 | 6 |
| 23.0 | 0 | 6 |
| 26.0 | 0 | 6 |

| | |
|---|---|
| Data processing: | MarkerLynx XS Application Manager |

### MS conditions

| | |
|---|---|
| MS system: | Q-ToF Premier Negative electrospray mode |
| Scan range: | 50 to 1000 Da |
| Capillary voltage: | 2.4 Kv |
| Source temp.: | 120 °C |
| Desolvation temp.: | 350 °C |
| Cone voltage: | 35 V |
| Desolvation gas flow: | 900 L/hr |
| Collision energy (CE): | Low CE: 5 eV |
| High CE: | ramp of 10 to 70 eV |

## METHODS

### Animal dosing

Table 1 details the dosing of 40, six-week old male Sprague Dawley rats. The animals were euthanized 24 hrs after galactosamine (galN) or vehicle administration. Serum was isolated from blood samples collected at necropsy from the abdominal vena cava and stored at -40 °C pending analysis.

| Group | Sex | No. of Animals per group | Galactosamine (mg/kg) |
|---|---|---|---|
| 1 | M | 8 | 0* |
| 2 | M | 40 | 415 |

*0.9% saline

Table 1. Animal and treatment details. Control = Group 1 and treated = Group 2.

### Clinical chemistry and histopathology

*Clinical Chemistry Analysis*. Serum alanine aminotransferase (ALT), aspartate aminotransferase (AST), and total bilirubin levels were analyzed using a Vitros 950 analyzer (Ortho-Clinical Diagnostics, Rochester, NY).

*Histological Analysis*. Liver samples were fixed in 10% buffered formalin, embedded in paraffin, sectioned, and stained with hematoxylin and eosin. Liver sections were assigned the following histoscores: 0) absence of hepatocellular necrosis, 1) minimal necrosis, 2) mild necrosis, 3) moderate necrosis, and 4) marked necrosis.

### Sample preparation

Ice-cold methanol (150 µL) was added to 50 µL serum and vortexed for 30 seconds. The samples were then incubated at -20 °C for 20 mins, centrifuged at 13,000 rpm for 10 min, and the supernatant was removed to a clean tube. The supernatant was then dried down in a vacuum evaporator (Savant), reconstituted in 100 µL water, and transferred into 96-well 350 µL plates.

## RESULTS AND DISCUSSION

The UPLC-MS assay developed allowed for the reproducible separation and detection of 24 fully identified bile acids, plus 10 tentatively identified bile acids. All bile acids eluted within a 4 min window (6 to 10 mins) with good separation of individual bile acids, as shown in Figure 1. This method offers shorter analysis time than conventional HPLC methods (data not shown), and therefore allows significantly increased sample throughput.
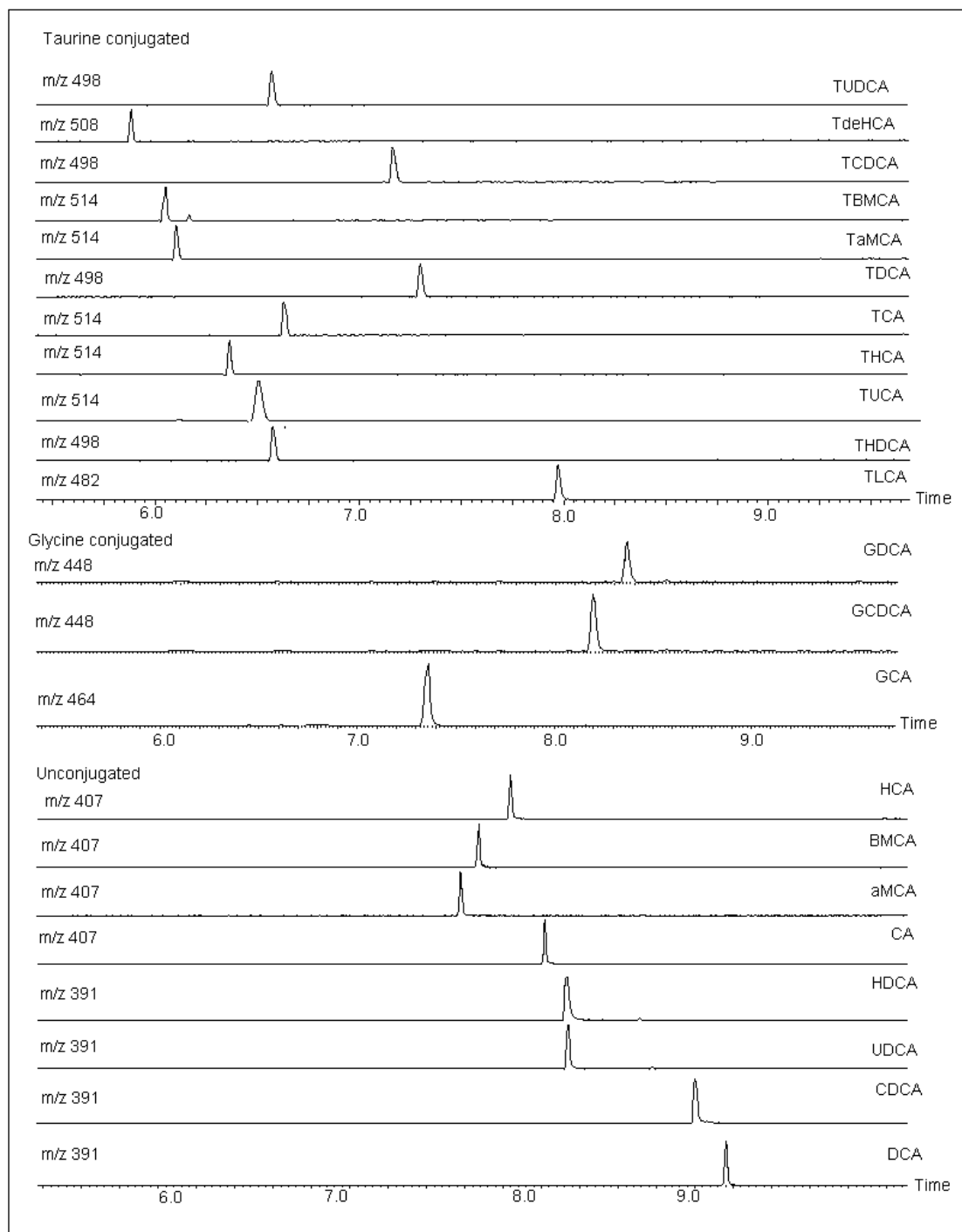


Figure 1. Excellent separation of bile acids using UPLC-MS. 24 bile acids were fully identified, with 10 putative identifications, some of which are illustrated here.

Bile acids ionize strongly using negative mode ESI, producing a prominent precursor [M-H]⁻ ion in the low energy data and informative fragmentation data in the high energy data. This allows conjugates to be easily distinguished by fragment ion analysis. Glycine conjugates give rise to a diagnostic ion at 74 *m/z* and taurine conjugates at 79.9, 106.0, and 124.0 *m/z* respectively, as shown in Figure 2. This information was obtained using MSᴱ, facilitating the determination of the different conjugation classes of bile acids in a single run.

Importantly, in addition to bile acids, this assay allows for the detection of a wide range of endogenous metabolites, providing additional, complementary metabolite information. This is of great utility in metabonomics studies, as sample numbers may be large and it is desirable to obtain maximum information in a single analytical run. This provides reductions in sample volume, throughput time, and solvent consumption.
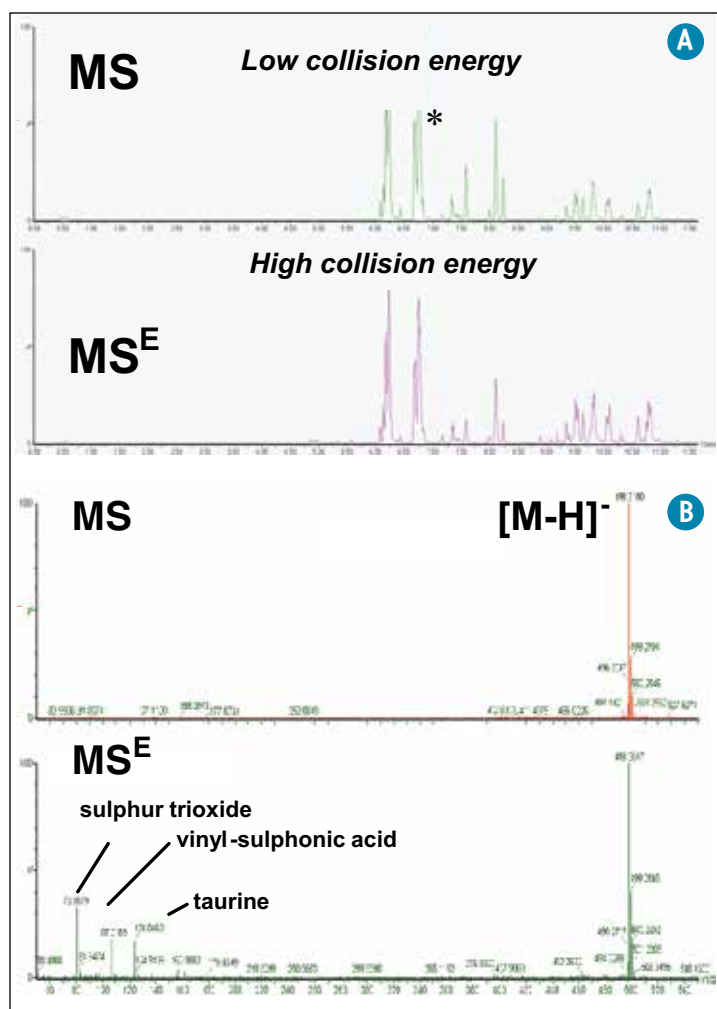


*Figure 2.*
*A) \*Taurodeoxycholic acid (m/z 498) in (top) the low collision energy run and (below) the elevated collision energy total ion chromatograms. B) (top) The corresponding low collision energy and (below) high collision energy spectra, showing characteristic fragment ions. The application of this UPLC-MSᴱ approach allows for the identification of over 30 bile acids in a single analytical run, reducing sample analysis time and the amount of sample required.*

Figure 3 shows representative base peak intensity (BPI) UPLC-MS chromatograms of serum from a control animal and those treated with galactosamine, demonstrating varying degrees of severity of liver damage. Dramatic serum BA changes were visible after galactosamine treatment, as shown in Figure 3, with obvious increases in the taurine-conjugated BAs. These increases correlated with the extent of liver damage (as determined by histoscore) and also the clinical chemistry (AST and ALT).
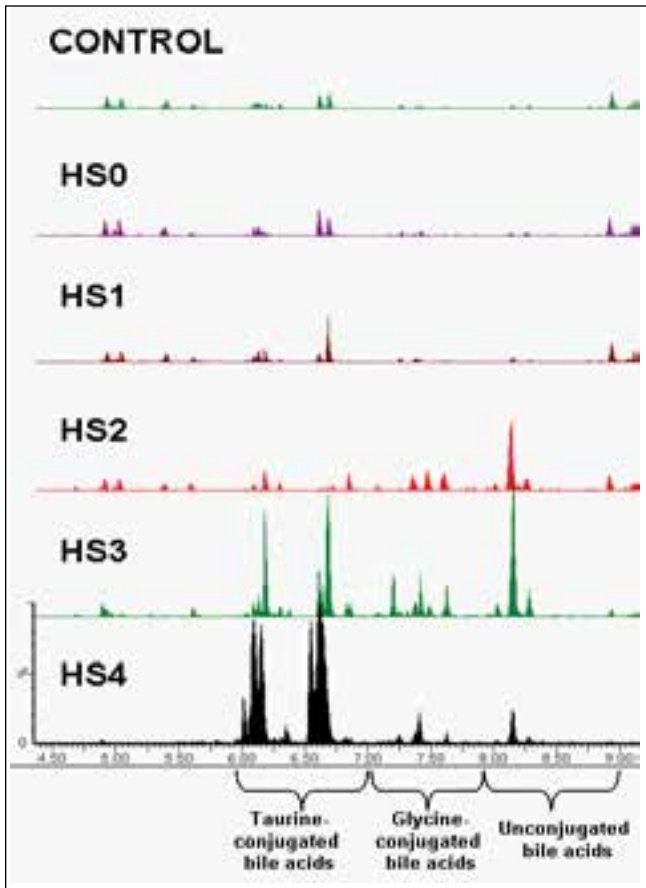


*Figure 3.*
*Selected region of the base peak ion (BPI) chromatograms of animals after galactosamine treatment, graded by histoscore. HS0 denotes no liver damage, whereas animals with a score of HS4 had marked liver damage. Taurine-conjugated bile acids were greatly elevated as liver damage increased; glycine conjugated bile acids showed some elevation whereas conjugated bile acids were unchanged.*

## CONCLUSIONS

UPLC-MS$^E$ offers a reliable and reproducible approach for the analysis of bile acids in biological fluids. This was demonstrated with serum samples applied to a toxicity study, and could easily be extended to other sample types and studies. The employment of a 26-min gradient allowed for the analysis of a wide range of endogenous metabolites, providing both a targeted assay and a global metabolite profiling approach in the same analytical run. This approach enhances the information obtained, leading to a more comprehensive interpretation of metabolite changes.

### References

1. Yousef IM, Bouchard G, Tuchweber B, Plaa GL. *Mechanism Involved in BA-Induced Cholestasis. In Toxicology of the Liver. 2nd edition.* Plaa GL and Hewitt WR, editors. Taylor & Francis, NY. 1988. 347–382.

2. Ostrow J D. *Metabolism of Bile Salts in Cholestasis in Humans. In Hepatic Transport and Bile Secretion: Physiology and Pathophysiology.* N. Tavolini and P. D. Berk, editors. Raven Press, NY. 1993. 673–712.

3. de Caestecker JS, Jazrawi RP, Nisbett JA, Joseph AE, Maxwell JD, Northfield TC. *Direct Assessment of the Mechanism for a Raised Serum Bile Acid Level in Chronic Liver Disease.* Eur J Gastroenterol Hepatol. 1995 7(10):955-61.

4. Hofmann, AF. *The Continuing Importance of Bile Acids in Liver and Intestinal Disease.* Arch Intern Med. 1999 13-27;159(22):2647-58.

# Waters

## THE SCIENCE OF WHAT'S POSSIBLE.®

**Waters Corporation**
34 Maple Street
Milford, MA 01757 U.S.A.
T: 1 508 478 2000
F: 1 508 872 1990
www.waters.com

**Imperial College London**

Waters
THE SCIENCE OF WHAT'S POSSIBLE.®

# Targeted Lipidomics Using the ionKey/MS System

Giuseppe Astarita,[1] Angela Doneanu,[1] Jay Johnson,[1] Jim Murphy,[1] James Langridge[2]
[1] Waters Corporation, Milford, MA, USA
[2] Waters Corporation, Manchester, UK

## APPLICATION BENEFITS

The ionKey/MS™ System allows for fast and robust LC-MS lipidomics analyses with considerable reduction in solvent consumption and increase in sensitivity when compared to 2.1 mm I.D. chromatography. Potential applications include large-scale lipid profiling and low-abundance lipids analyses in biological materials.

## INTRODUCTION

Lipidomics is the comprehensive analysis of hundreds of lipid species in biological samples. Lipids play prominent roles in the physiological regulation of many key biological processes such as inflammation and neurotransmission. Alterations in lipid pathways have been associated with many diseases including cardiovascular diseases, obesity, and neurodegenerative disorders.

The ability to measure the wide array of lipid species in biological samples could help our understanding of their roles in health and disease. The need for a fast, comprehensive and sensitive analysis of the hundreds of lipid species challenges both the chromatographic separation and mass spectrometry.

Here we used the novel ionKey/MS System, which utilizes the iKey™ Separation Device packed with 1.7 µm particles for fast and robust chromatographic separation. By integrating microscale LC components into a single platform design, the device avoids problems associated with capillary connections, including manual variability, leaks, and excessive dead volume. This integrated microfluidic device is suitable for lipidomics analyses with considerable advantages when compared to analytical scale LC-MS analysis.

## WATERS SOLUTIONS

ionKey/MS System

ACQUITY UPLC® M-Class

ionKey™ Source

Xevo® TQ-S

iKey Separation Device CSH™ C18

MassLynx™

## KEY WORDS

Lipidomics, lipid, microfluidics, metabolomics

## EXPERIMENTAL

### LC conditions

| | |
|---|---|
| LC system: | ACQUITY UPLC M-Class |
| Sample loop: | 1 µL |
| Column: | iKey CSH™ $C_{18}$ 130 Å, 1.7 µm, 150 µm x 100 mm |
| Column temp.: | 55 °C |
| Flow rate: | 2 µL/min |
| Mobile phase A: | Acetonitrile/Water (60/40) with 10 mM ammonium formate + 0.1% formic acid |
| Mobile phase B: | Isopropanol/Acetonitrile (90/10) with 10 mM ammonium formate + 0.1% formic acid |
| Volume injected: | 0.2 - 0.5 µL |

Gradient:

| Time (min) | %A | %B | Curve |
|---|---|---|---|
| Initial | 55.0 | 45.0 | Initial |
| 1.00 | 40.0 | 60.0 | 6 |
| 10.00 | 1.0 | 99.0 | 6 |
| 16.00 | 1.0 | 99.0 | 6 |
| 16.01 | 55.0 | 45.0 | 6 |
| 18.00 | 55.0 | 45.0 | 6 |

### MS conditions

| | |
|---|---|
| Mass spectrometer: | Xevo TQ-S |
| Acquisition mode: | MRM |
| Ionization mode: | ESI positive |
| Capillary voltage: | 3.0 KV |
| Source temp.: | 120 °C |

### Materials

Lipid standards were purchased from Avanti Polar Lipids (Alabaster, AL) and Nu-Chek Prep (Elysian, MN). Total lipid extract from bovine brain was purchased from Avanti Polar Lipids. Mouse plasma (10 µL) was extracted with isopropanol (490 µL). The solution was then allowed to stand for 30 min in ice, vortexed and then centrifuged (10,000 x g, at 4 °C for 10 min). The supernatant was collected in a new vial, evaporated to dryness under vacuum and kept at -80 °C until further analysis. Immediately prior to analysis, all lipid extracts were re-suspended in isopropanol/acetonitrile/water (50/25/25, 250 µL).

### RESULTS AND DISCUSSION

For the analysis of lipids, we used the ionKey/MS System, comprised of the Xevo TQ-S Mass Spectrometer, the ACQUITY UPLC M-Class, the ionKey source and the iKey Separation Device. The iKey contains the fluidic connections, electronics, ESI interface, heater, e-cord, and the chemistry, permitting operation at high pressure with sub 2 micron particles, leading to highly efficient LC separations of lipid molecules. By integrating microscale LC components into a single system design, we avoided problems associated with capillary connections, including manual variability, leaks and excessive dead volume. Lipidomics analyses were conducted using small volumes of lipid standards and lipid extracts from typical biological samples including plasma and brain tissues (0.2 µL). We separated lipids at flow rates of 2 µL/min using a ACQUITY UPLC M-Class engineered with 150 µm I.D. x 100 mm ceramic channel packed with CSH™ $C_{18}$ 130 Å 1.7 µm particles size (Fig. 1). The small column diameter (150 µm) of the iKey device allows low injection volumes (0.5 µL) and low flow rates (2 µl/min) increasing up to 10x the sensitivity compared to regular analytical columns (*e.g.*, 2.1 mm I.D.) (Fig.1). Mobile phase consumption was reduced compared to 2.1 mm I.D. chromatography albeit maintaining comparable chromatographic resolution and analysis times (Fig. 2)[1].
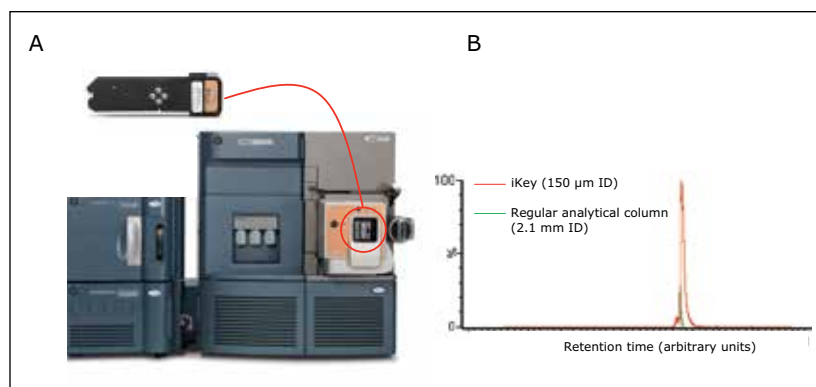


Figure 1. (A) The ionKey/MS System: comprised of the Xevo TQ-S, the ACQUITY UPLC M-Class, the ionKey source and the iKey Separation Device. (B) Representative analysis of phosphatidylcholine (14:0/14:0) using ionKey/MS (red line) as compared to regular UPLC/MS[1] (green line).
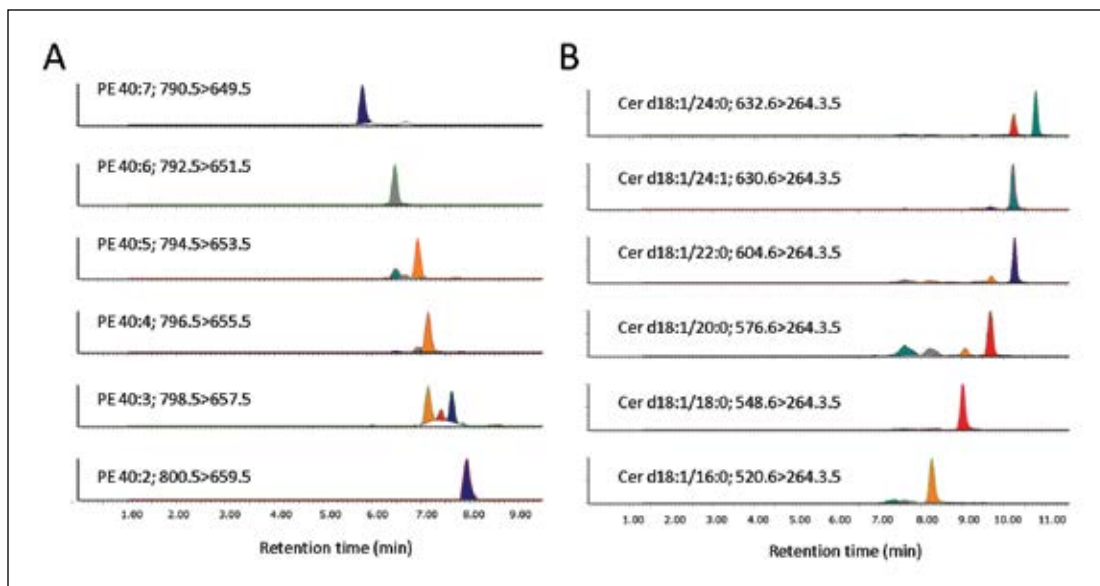
*Figure 2. Representative extracted ion chromatograms of A) glycerophospholipids (e.g., phosphatidyletahnolamines, PE) extracted from bovine brain and B) sphingolipids (e.g., ceramides, Cer) extracted from mouse plasma. Samples were analyzed using the ionKey/MS System.*

We conducted targeted lipidomic analyses using Xevo TQ-S in MRM mode and monitored 215 lipid species belonging to various lipid classes including phosphatidylethanolamines (PE), lyso PE, phosphatidylcholines (PC), lyso PC, ceramides (Cer), sphingomyelins, hexosylceramides, lactosylceramides and cholesterol esters (Table 1). Targeted lipids were measured over approximately five orders of dynamic range (Fig. 3 and 4). Lipids were separated according to acyl chain length and number of double bonds. Quantification was performed using TargetLynx™ Application Manager (Fig. 5). Initial reports in peer reviewed journals showed the advantages of using the ionKey/MS system in real world applications dealing with the analysis of low abundance lipids.[2,3]

| Lipid Class | No. MRMs | Cone voltage | Collision energy |
|---|---|---|---|
| PE | 45 | 26 | 18 |
| Lyso PE | 18 | 26 | 18 |
| PC | 44 | 42 | 26 |
| Lyso PC | 19 | 42 | 26 |
| Ceramide | 19 | 20 | 30 |
| Sphingomyelin | 20 | 36 | 24 |
| HexosylCeramide | 19 | 20 | 26 |
| LactosylCeramide | 16 | 20 | 30 |
| Cholesteryl Ester | 15 | 36 | 24 |

*Table 1. Overview of the MRM method used.*
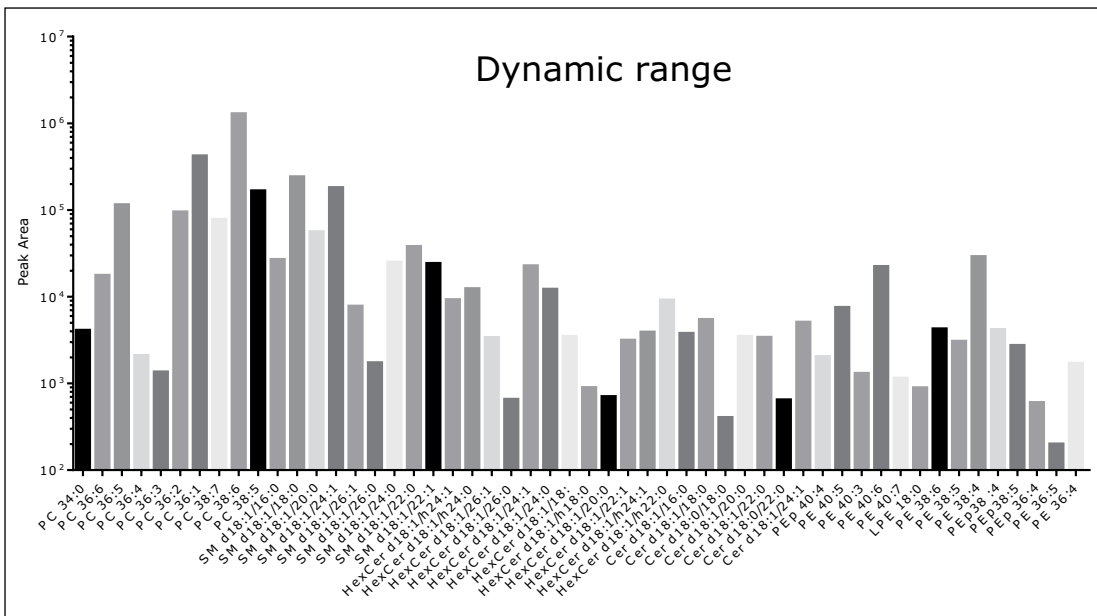
Figure 3. Intensities of selected lipids extracted from bovine brain.
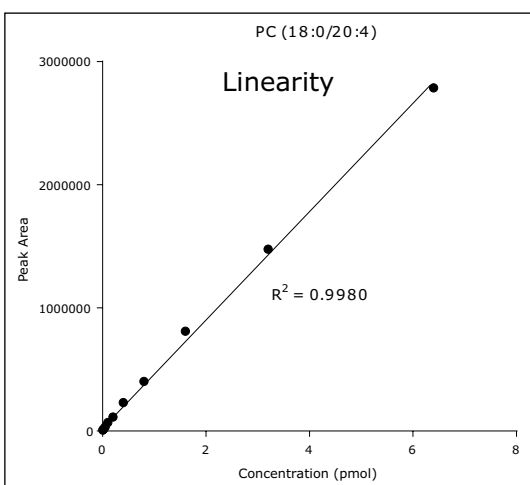


Figure 4. Linearity of response for a selected phosphatidylcholine species (PC).
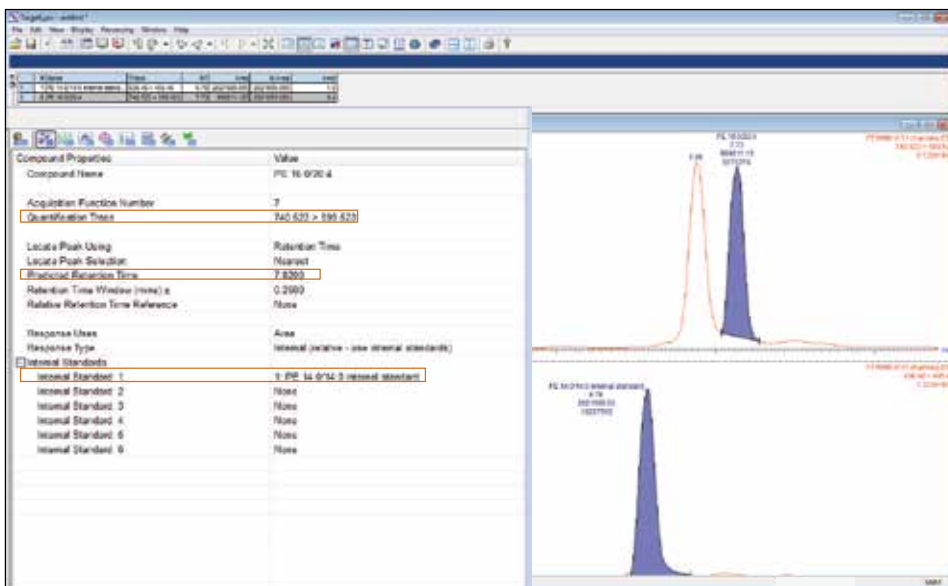


Figure 5. Quantification can be performed using TargetLynx. MRM and retention times are automatically extracted and normalized by comparison to selected internal standard.

## CONCLUSIONS

The ionKey/MS System is a novel microfluidics-MS platform that leads to highly efficient LC separation of lipids with comparable resolution to analytical scale LC-MS analysis.[1] The use of the 150 µm iKey enables the development of low flow MRM methods, bringing three major advantages over standard flow rate analysis[1]:

1. up to 200x decrease in solvent consumption, making it convenient for the large-scale analysis and screenings of hundreds or thousands samples;

2. up to 10x increase in sensitivity, which could facilitate the detection of low abundance metabolites;[2,3]

3. low volumes injection (*e.g.*, 0.2 µL), which makes it ideal when sample limited studies or when multiple injections are required. Potential applications include large-scale lipid profiling and low-abundance lipids analyses in biological materials.[2,3]

### References

1. Isaac G, McDonald S, Astarita G: Lipid separation using UPLC with charged surface hybrid technology. Waters App note (2011);720004107en.

2. Aqai P, Cevik E, Gerssen A, Haasnoot W, Nielen MW: High-throughput bioaffinity mass spectrometry for screening and identification of designer anabolic steroids in dietary supplements. *Anal Chem* (2013);85:3255-3262.

3. Broccardo CJ, Schauer KL, Kohrt WM, Schwartz RS, Murphy JP, Prenni JE: Multiplexed analysis of steroid hormones in human serum using novel microflow tile technology and LC-MS/MS. *J Chromatogr B Analyt Technol Biomed Life Sci* (2013);934:16-21.

## Waters
### THE SCIENCE OF WHAT'S POSSIBLE.®

Waters
THE SCIENCE OF WHAT'S POSSIBLE.®

# Multiplexed Analysis of Steroid Hormones Using ionKey/MS

Carolyn Broccardo,[1] James P. Murphy,[2] Giuseppe Astarita,[2] and Jessica Prenni[1]
[1] Colorado State University, Fort Collins, CO, USA
[2] Waters Corporation, Milford, MA, USA

## APPLICATION BENEFITS

A highly analytically sensitive multiplexed assay was developed for targeted quantitation of five steroids in human serum. The use of the ionKey™ source and the 150 µm iKey™ Separation Device yielded a 100–400 fold increase in on-column sensitivity while at the same time decreasing solvent usage by 150 fold as compared to standard flow methods. The increased on-column analytical sensitivity allowed for simplification of the steroid extraction procedure which in turn streamlined the sample preparation and reduced per/sample assay cost.

## INTRODUCTION

The measurement of steroids in human serum is an important clinical research tool. Traditionally, these assays are performed using a variety of biochemical techniques including radioimmunoassay (RIA), enzyme-linked immunosorbent assay (ELISA), and chemiluminescent immunoassay (CLIA). However, immunoassays suffer from antibody cross-reactivity with structural isomers which has been shown to result in an overestimation of steroid levels. Recently, LC-MS/MS has emerged as a viable alternative for this important assay in the clinical research setting. While providing improved accuracy as compared to antibody based techniques, standard flow LC-MS/MS assays also consume high levels of solvent and often require time-consuming sample extraction procedures such as liquid-liquid or solid phase extraction to adequate analytical sensitivity.

In this application, we report the use of the newly developed 150 µm ionKey/MS System for the multiplexed quantitation of five important steroid compounds in human serum: testosterone, dihydrotestosterone, progesterone, cortisone, and cortisol. The reduced flow method results in a 150 fold decrease in solvent consumption and a 100–400 fold increase in on-column analytical sensitivity.[1]

## WATERS SOLUTIONS

ionKey/MS™ System

nanoACQUITY® UPLC®

ionKey Source

Xevo® TQ-S Mass Spectrometer

iKey Separation Device BEH C18

MassLynx™

## KEY WORDS

Xevo, TQ-S, iKey, ionKey/MS, multiplexed

## EXPERIMENTAL

### Method conditions

### LC conditions

| | |
|---|---|
| LC system: | nanoACQUITY UPLC |
| Sample loop: | 5 µL |
| Column: | iKey BEH C$_{18}$ 130, 1.7 µm, 150 µm x 50 mm |
| Column temp.: | 45 °C |
| Flow rate: | 3.06 µL/min |
| Mobile phase A: | Water + 0.1%formic acid |
| Mobile phase B: | Methanol + 0.1% formic acid |
| Volume injected: | 0.5 µL using partial loop mode |

Gradient:

| Time (min) | %A | %B | Curve |
|---|---|---|---|
| Initial | 90.0 | 10.0 | Initial |
| 0.25 | 90.0 | 10.0 | 6 |
| 1.00 | 45.0 | 55.0 | 6 |
| 7.50 | 5.0 | 95.0 | 6 |
| 8.00 | 55.0 | 10.0 | 6 |
| 12.00 | 55.0 | 10.0 | 6 |

### MS conditions

| | |
|---|---|
| Mass spectrometer: | Xevo TQ-S |
| Acquisition mode: | MRM |
| Ionization mode: | ESI positive |
| Capillary voltage: | 3.2 kV |
| Source temp.: | 100 °C |
| Source offset: | 50 V |
| Collision gas: | argon |
| Dwell times for all compounds: | 0.011 s |

### Sample preparation

Serum samples were precipitated with 3.7 volumes of ice cold methanol containing stable isotope-labeled internal standards for each steroid at a level of 10 ng/mL. Samples were incubated at -80 °C for 30 minutes, centrifuged at 3270 x g for 10 minutes and supernatant was collected. All sample preparation and injections were conducted in 96-well plates. 0.5 µL of extracted serum was injected and separation was performed using a nanoACQUITY UPLC connected to an ionKey source using a 150 µm iKey packed with BEH C$_{18}$ (1.7 µm particles). The column effluent was monitored using a Xevo TQ-S Mass Spectrometer operated in multiple reaction monitoring (MRM) positive ion electrospray mode.

| Compound | MRM time acquisition window (min) | MRM transition | Cone (V) | Collision energy (V) |
|---|---|---|---|---|
| testosterone | 4.1–5.3 | 289.24>97.03 | 50 | 20 |
| dihydrotestosterone | 4.5–5.5 | 291>255 | 46 | 14 |
| d3 testosterone | 4.1–5.3 | 292.2>97.03 | 50 | 20 |
| d3 dihydrotestosterone | 4.5–5.5 | 294.1>258.2 | 46 | 14 |
| progesterone | 4.9–6 | 315>109 | 20 | 26 |
| $^{13}C_3$ progesterone | 4.9–6 | 318.2>112.2 | 20 | 26 |
| cortisone | 3.5–4.6 | 361>163.05 | 25 | 30 |
| cortisol | 3.5–5 | 363>327.14 | 25 | 16 |
| d4 cortisol | 3.5–5 | 367.2>331 | 25 | 22 |
| d7 cortisone | 3.5–4.6 | 368.2>169 | 25 | 22 |

Table 1. MRM transitions and instrument settings for each compound. (Broccardo 2013)

### Data analysis

Quantification was performed using linear regression against a standard curve in MassLynx Software. Peak areas for each compound were normalized to the corresponding internal standard in each sample.

## RESULTS AND DISCUSSION

Chromatographic separation of the five compounds is illustrated in Figure 1. An average peak width of 6s was achieved.
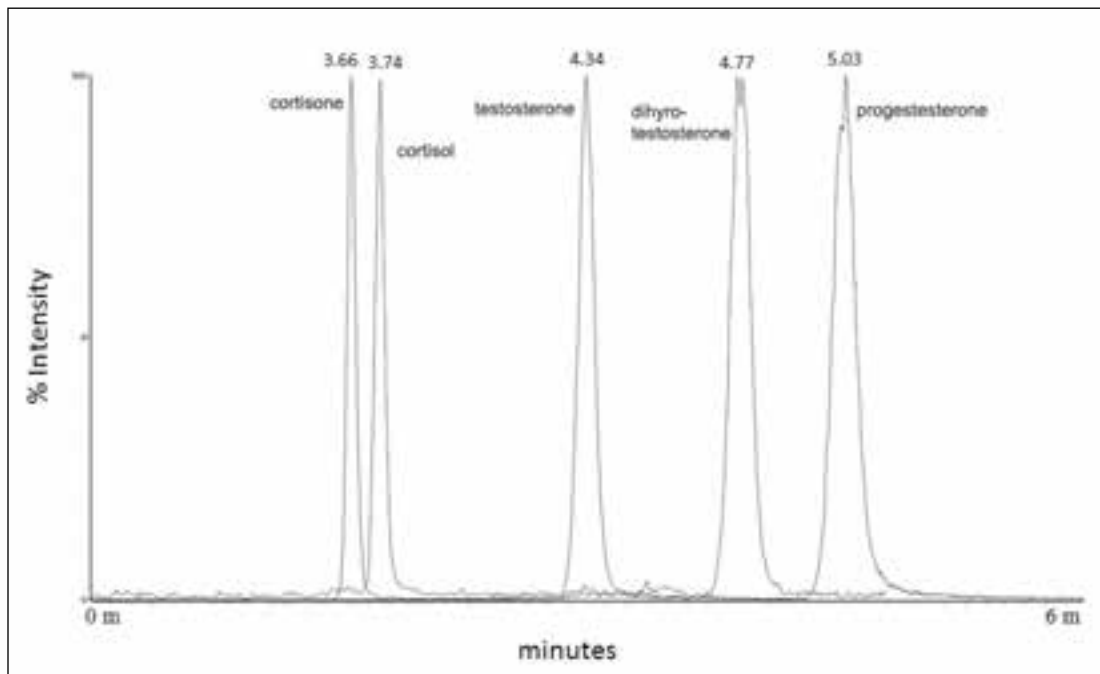


*Figure 1. Chromatographic separation of the five steroid compounds in human serum. (Broccardo 2013)*
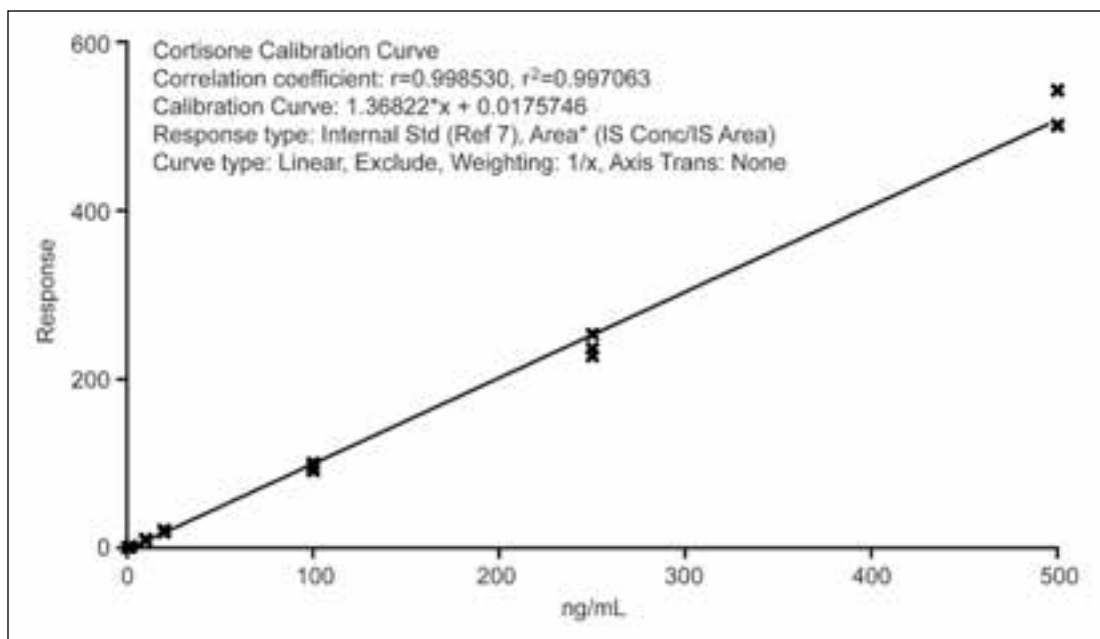


*Figure 2. Calibration curve for cortisone measured in human serum. (Broccardo 2013)*

A typical calibration curve is shown in Figure 2. The correlation coefficients for all compounds were 0.99 or greater.

The lower limit of quantification (LOQ) and lower limit of detection (LOD) for all five compounds is listed in Table 2. These values represent a 100–400 fold increase in on-column analytical sensitivity as compared to published standard flow assays which typically require injection volumes of 50–200 µL of extracted sample;[2,4] only 0.5 µL of extracted sample is used in the assay presented here.

| Analyte | LOD (ng/mL) | LOQ (ng/mL) |
|---|---|---|
| testosterone | 0.12 | 0.41 |
| dihydrotestosterone | 0.42 | 1.40 |
| progesterone | 0.03 | 0.40 |
| cortisone | 0.09 | 0.29 |
| cortisol | 0.57 | 1.90 |

*Table 2. LOD and LOQ values for the five steroids in human serum. (Broccardo 2013)*

## CONCLUSIONS

■ The ionKey/MS System with the Xevo TQ-S and 150 µm iKey enabled the development of a low flow MRM assay of five steroids in human serum for clinical research.

■ The low flow regime resulted in an increase in on-column analytical sensitivity and a 150 fold decrease in solvent consumption, as compared to standard flow multi-use methods in the literature.

**For Research Use Only. Not for use in diagnostic procedures.**

## References

1. C. J. Broccardo, K. L. Schauer, W.M. Kohrt, R.S. Schwartz, J.P. Murphy, J.E. Prenni, *J Chromatogr B Analyt Technol Biomed Life Sci* (2013) 16.

2. N. Janzen, S. Sander, M. Terhardt, M. Peter, J. Sander, *J Chromatogr B Analyt Technol Biomed Life Sci* 861 (2008) 117.

3. M.M. Kushnir, A.L. Rockwood, W.L. Roberts, B. Yue, J. Bergquist, A.W. Meikle, *Clin Biochem* 44 (2011) 77.

4. I.A. Ionita, D.M. Fast, F. Akhlaghi, *J Chromatogr B Analyt Technol Biomed Life Sci* 877 (2009) 765.

## Waters
### THE SCIENCE OF WHAT'S POSSIBLE.®

**Waters Corporation**
34 Maple Street
Milford, MA 01757 U.S.A.
T: 1 508 478 2000
F: 1 508 872 1990
www.waters.com

Waters
THE SCIENCE OF WHAT'S POSSIBLE.®

# Fast and Simple Free Fatty Acids Analysis Using UPC²/MS

Giorgis Isaac,[1] Michael D. Jones,[1] Besnik Bajrami,[1] Wassim Obeid,[2] James Langridge,[3] Patrick Hatcher[2]
[1]Waters Corporation, Milford, MA, USA
[2]Old Dominion University, Norfolk, VA, USA
[3]Waters Corporation, Manchester, UK

## APPLICATION BENEFITS

■ Demonstrates the separation of free fatty acid (FFA) species based on chain length and number of double bonds

■ No derivatization is required, which results in easier and fast sample preparation and eliminates artifact formation

■ Organic phase lipid extract can be directly injected onto the system, saving time and reducing cost per analysis

■ Less than three-minute chromatographic separation is up to 10X faster compared to GC/MS

■ Unlike GC/MS, low volatile and very long chain fatty acids (>24 carbon atoms) can be easily analyzed with UPC²®

## WATERS SOLUTIONS

ACQUITY UPC²® System

TransOmics™ Informatics

Xevo® G2 QTof Mass Spectrometer

ACQUITY UPC² HSS Column

## KEY WORDS

Free fatty acids, UltraPerformance Convergence Chromatography™, UPC², TransOmics, time-of-flight mass spectrometry, UPC²/MS/MS

## INTRODUCTION

Fatty acids, both free and as part of complex lipids, play a number of key roles in metabolism – as major metabolic fuel (storage and transport of energy), as essential components of all membranes, and as gene regulators. In addition, dietary lipids provide polyunsaturated fatty acids that are precursors of powerful locally acting metabolites, e.g., eicosanoids.

The common fatty acids of animal and plant origin have even-numbered chains of 16 to 24 carbon atoms with 0 to 6 double bonds. Nature provides countless exceptions, however, and odd- and even-numbered fatty acids with up to nearly 100 carbon atoms exist. In addition, double bonds can be of the *cis* (Z) and *trans* (E) configuration and there can be innumerable other structural features, including branch points, rings, oxygenated functions, and many more.

Fatty acid chains may contain one or more double bonds at specific positions (unsaturated and poly unsaturated with *cis* (Z) or *trans* (E) configuration) or they may be fully saturated. The LIPIDMAPS systematic nomenclature for fatty acids indicates the location of double bonds with reference to the carboxyl group with "Δ".[1] Fatty acid structures also contain a methyl group at one end of the molecule (designated omega, ω) and a carboxyl group at the other end. The carbon atom next to the carboxyl group is called α carbon and the subsequent one the β carbon. The letter "n" is also often used instead of ω to indicate the position of the double bond closest to the methyl end.[2] Figure 1 outlines the structures of different straight chain fatty acids.

The isolation of free fatty acids (FFA) from biological materials is a complex task and precautions should be taken at all times to prevent or minimize the effects of hydrolyzing enzymes. After isolation, the typical chromatographic methods for analyzing fatty acids include gas chromatography/mass spectroscopy (GC/MS) and liquid chromatography-tandem mass spectrometry (LC/MS/MS). However, there are shortcomings associated with each of these methods.

For example, GC methods require derivatization of the fatty acids to hydrolyze and convert to methyl esters, which is time-consuming and risks re-arrangement of the fatty acids during derivatization, leaving doubt as to whether the esters formed are from FFA or intact complex lipids. Moreover, the GC/MS analysis of low volatile, very-long-chain fatty acids with high molecular weight (>C24) is a problem even after fatty acid methyl ester (FAME) derivatization.
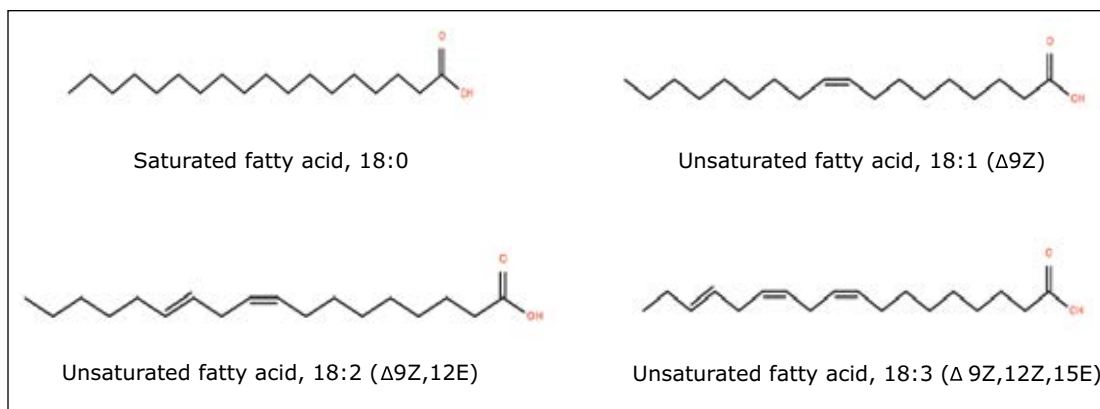
Figure 1. Structure and nomenclature of different straight chain fatty acids with a methyl and a carboxyl (acidic) end. Fatty acids may be named according to systematic or trivial nomenclature. One systematic way to describe the position of double bonds is in relation to the acidic end of the fatty acids; symbolized as Δ (Greek delta) followed with numbers. All unsaturated fatty acids are shown with cis (Z) or trans (E) configuration of the double bonds.

In LC/MS methods, although no sample derivatization is required, the runs typically involve labor-intensive and time-consuming sample preparation, and utilize toxic organic solvents, which are expensive to purchase and dispose. In a typical reversed phase (RP) LC/MS analysis, the organic extracts containing all the lipids have to be evaporated and re-constituted in a more compatible injection solvent.

Thus, it would be beneficial to have streamlined methods for the separation and determination of fatty acids. Here, we present a rapid, high-throughput and efficient method for the separation and analysis of FFA using UltraPerformance Convergence Chromatography (UPCC, or UPC$^2$) with mass spectrometry.

UPC$^2$ is a complementary, orthogonal separation technology that is taking its place alongside LC and GC. While all three use a stationary phase to interact with compounds of interest and a mobile phase to move compounds through the stationary phase and achieve separation, the techniques differ mainly by the mobile phases used.

GC is defined by using a gas as its mobile phase, LC is defined by using liquids as its mobile phase, and CC is defined by using both gas and liquids. It is this convergence of mobile phases in combination with a far greater choice of stationary phases that makes CC a powerful additional choice for laboratory scientists. Because UPC$^2$ can receive samples in organic solvents such as hexane and chloroform, it significantly simplifies the requirements for sample preparation, while maintaining all the advantages of RPLC.

Here, the analysis of fatty acids in the free form instead of FAME derivatives results in easier and faster sample preparation. The organic phase extract containing all the FFA can be injected directly into the system, which results in significant savings in sample preparation and analysis time, solvent costs, and solvent waste disposal. Additionally, artifact formation that can result from a derivatization procedure is eliminated.

## EXPERIMENTAL

### Method conditions

### UPC$^2$ conditions

| | |
|---|---|
| System: | ACQUITY UPC$^2$ |
| Columns: | ACQUITY UPC$^2$ HSS C$_{18}$ SB 1.8 µm, 2.1 x 150 mm |
| Column temp.: | 50 °C |
| Sample vial: | Total Recovery Vial (p/n 186000385C) |
| Sample temp.: | 10 °C |
| Injection volume: | 0.5 µL |
| Flow rate: | 0.6 mL/min |
| Mobile phase A: | CO$_2$ |
| Mobile phase B: | Methanol in 0.1% formic acid |
| Make up: | Methanol in 0.1% NH$_4$OH (0.2 mL/min) |
| Splitter: | Upchurch cross 1/16 PEEK |

### Gradient

| Time (min) | %A (CO$_2$) | %B | Curve |
|---|---|---|---|
| 0.0 | 95 | 5 | Initial |
| 5.0 | 75 | 25 | 6 |
| 5.1 | 50 | 50 | 1 |
| 6.0 | 50 | 50 | 11 |
| 8.0 | 95 | 5 | 1 |

### MS conditions

| | |
|---|---|
| Mass spectrometer: | Xevo G2 QTof |
| Ionization mode: | ESI negative |
| Capillary voltage: | 1.0 kV |
| Cone voltage: | 30 V |
| Source temp.: | 100 °C |
| Desolvation temp.: | 500 °C |
| Cone gas flow: | 10 L/h |
| Desolvation gas flow: | 600 L/h |
| Acquisition range: | 50 to 600 $m/z$ |

### Sample preparation

#### FFA standard mixtures

Individual saturated FFA standards containing even carbon number C$_8$ to C$_{24}$ were purchased from Sigma. A complex model mixture of different FFA standards (GLC-85 in FFA form) was purchased from Nu-Chek Prep (Elysian, MN, USA). The list of FFA standards analyzed and other detailed information is provided in Table 1. A 1 mg/mL stock solution was prepared in chloroform, and 0.1 mg/mL working lipid mixtures were prepared in chloroform, then injected onto the UPC$^2$/MS system.

#### Algae and algaenan produced oils

Oil produced from hydrous pyrolysis of algae and algaenan at low and high pyrolysis temperature were provided from Old Dominion University (Norfolk, VA, USA). Algae 1 and algaenan 1 were treated at a pyrolysis temperature of (310 °C); and Algae 2 and algaenan 2 were treated at a pyrolysis temperature of (360 °C).

Extraction of algaenan was performed by a modified extraction procedure. Briefly, lipids were removed from the algae by Soxhlet extraction with 1:1 (v/v) benzene/methanol solvent mixture for 24 hours. The residue was treated with 2N sodium hydroxide at 60 °C for two hours. The remaining residue was then washed excessively with deionized water, followed by treatment with Dowex 50W-x8 cation exchange resin to exchange any residual sodium. Finally, the solid was rinsed with deionized water. The oil samples were diluted 10 times in dichloromethane, and 1 µL was injected onto the UPC$^2$/MS system.

#### Data acquisition and processing

When using multivariate data analysis for sample comparison, it is crucial that each sample is randomized and injected a minimum of three times to ensure that the data analysis is statistically valid. For this study, five replicates of each algae and algaenan oil extracts were acquired in MS$^E$ mode, an unbiased Tof acquisition method in which the mass spectrometer switches between low and elevated collision energy on alternate scans. Data analysis and FFA identification were performed using TransOmics Informatics for Metabolomics and Lipidomics (TOIML).

| Compound | Formula | Neutral mass | [M-H]⁻ | Retention time (min) | Common name | Description |
|----------|---------|-------------|--------|---------------------|-------------|-------------|
| 1 | $C_4H_8O_2$ | 88.052429 | 87.045153 | 0.89 | Butyric acid | C4:0 |
| 2 | $C_6H_{12}O_2$ | 116.083730 | 115.076453 | 0.96 | Caproic acid | C6:0 |
| 3 | $C_8H_{16}O_2$ | 144.115030 | 143.107753 | 1.06 | Caprylic acid | C8:0 |
| 4 | $C_{10}H_{20}O_2$ | 172.146330 | 171.139053 | 1.17 | Capric acid | C10:0 |
| 5 | $C_{11}H_{22}O_2$ | 186.161980 | 185.154704 | 1.23 | Undecylic acid | C11:0 |
| 6 | $C_{12}H_{24}O_2$ | 200.177630 | 199.170354 | 1.31 | Lauric acid | C12:0 |
| 7 | $C_{13}H_{26}O_2$ | 214.193280 | 213.186004 | 1.41 | Tridecylic acid | C13:0 |
| 8 | $C_{14}H_{28}O_2$ | 228.208930 | 227.201654 | 1.54 | Myrislc acid | C14:0 |
| 9 | $C_{15}H_{30}O_2$ | 242.224580 | 241.217304 | 1.67 | Pentadecylic acid | C15:0 |
| 10 | $C_{16}H_{32}O_2$ | 256.240230 | 255.232954 | 1.80 | Palmilc acid | C16:0 |
| 11 | $C_{17}H_{34}O_2$ | 270.255880 | 269.248604 | 1.97 | Margaric acid | C17:0 |
| 12 | $C_{18}H_{36}O_2$ | 284.271530 | 283.264254 | 2.11 | Stearic acid | C18:0 |
| 13 | $C_{20}H_{40}O_2$ | 312.302831 | 311.295554 | 2.41 | Arachidic acid | C20:0 |
| 14 | $C_{22}H_{44}O_2$ | 340.334131 | 339.326854 | 2.70 | Behenic acid | C22:0 |
| 15 | $C_{14}H_{26}O_2$ | 226.193280 | 225.186004 | 1.45 | Physeteric acid | C14:1 |
| 16 | $C_{15}H_{28}O_2$ | 240.208930 | 239.201654 | 1.57 | | C15:1 |
| 17 | $C_{16}H_{30}O_2$ | 254.224580 | 253.217304 | 1.67 | Palmitoleic acid | 16:1 |
| 18 | $C_{17}H_{32}O_2$ | 268.240230 | 267.232954 | 1.81 | 10-HEPTADECENOIC Acid | C17:1 (Δ10) |
| 19 | $C_{18}H_{30}O_2$ | 278.224580 | 277.217304 | 1.76 | Gamma Linolenic Acid | C18:3 (Δ6,9,12) |
| 20 | $C_{18}H_{30}O_2$ | 278.224580 | 277.217304 | 1.86 | Linolenic Acid | C18:3(Δ9,12,15) |
| 21 | $C_{18}H_{30}O_2$ | 280.240230 | 279.232954 | 1.88 | Linoleic Acid | C18:2 |
| 22 | $C_{18}H_{34}O_2$ | 282.255880 | 281.248604 | 1.98 | Oleic Acid | C18:1 |
| 23 | $C_{18}H_{34}O_2$ | 282.255880 | 281.248604 | 1.98 | Elaidic Acid | C18:1T |
| 24 | $C_{20}H_{32}O_2$ | 304.240230 | 303.232954 | 1.93 | Arachidonic acid | C20:4 |
| 25 | $C_{20}H_{34}O_2$ | 306.255880 | 305.248604 | 2.04 | HOMOGAMMA LINOLENIC Acid | C20:3 (Δ8,11,14) |
| 26 | $C_{20}H_{34}O_2$ | 306.255880 | 305.248604 | 2.14 | 11-14-17-EICOSATRIENOIC Acid | C20:3 (Δ11,14,17) |
| 27 | $C_{20}H_{36}O_2$ | 308.271530 | 307.264254 | 2.17 | 11-14-EICOSADIENOIC Acid | C20:2 (Δ11, 14) |
| 28 | $C_{20}H_{38}O_2$ | 310.287180 | 309.279904 | 2.24 | 11-EICOSENOIC Acid | C20:1 (Δ11) |
| 29 | $C_{22}H_{32}O_2$ | 328.240230 | 327.232954 | 2.09 | Docosahexaenoic Acid | C22:6 |
| 30 | $C_{22}H_{40}O_2$ | 336.302831 | 335.295554 | 2.46 | Docosadienoic Acid | C22:2 |
| 31 | $C_{22}H_{38}O_2$ | 338.318481 | 337.311204 | 2.54 | Erucic Acid | C22:1 |
| 32 | $C_{24}H_{46}O_2$ | 366.349781 | 365.342504 | 2.83 | Nervonic acid | C24:1 |

Table 1. A list of analyzed saturated and unsaturated standard FFA mixtures with corresponding retention time determined from Figure 3A.

## RESULTS AND DISCUSSION

### Analysis of saturated FFA standards

Figure 2 shows the separation of saturated FFA with carbon chain length $C_8$ to $C_{24}$. The ACQUITY UPC$^2$ High Strength Silica (HSS) $C_{18}$ SB 1.8 μm, 2.1 x 150 mm Column provides an RP-like separation that results in effective separation of the different FFA species. The gradient is run under acidic conditions using a small percentage of formic acid (0.1% v/v in methanol) to improve the peak shape and decrease peak tailing.

The ACQUITY UPC$^2$ method is 10X faster (only a three-minute run) than GC/MS and RPLC methods, and uses less toxic and cheaper $CO_2$ as a solvent. A typical lipidomics study involves the analysis of thousands of biological samples, and the additional speed allows for large sample sets to be analyzed efficiently, improving the overall power of the experiment.

The FFA lipid molecular species separation mechanism is mainly based on hydrophobic interaction of the FFA carbon numbers and number of double bonds with the HSS $C_{18}$ SB material. Therefore, the elution order of the FFA species depends on the length and the number of double bonds on the fatty acid chain. Thus, the longer and the more saturated the acyl chain length the longer the retention time.

The co-solvent mobile phase B (methanol in 0.1% formic acid) can be optimized to increase the chromatographic resolution and peak capacity. The higher the percentage of the co-solvent, the shorter the retention time and the narrower the peaks. However, when analyzing a complex biological sample containing saturated and unsaturated FFA species with different carbon chain length, peak capacity is important in order to reduce coeluting lipid species. The co-solvent gradient 5% to 25% methanol in 0.1% formic acid was used for further analysis.
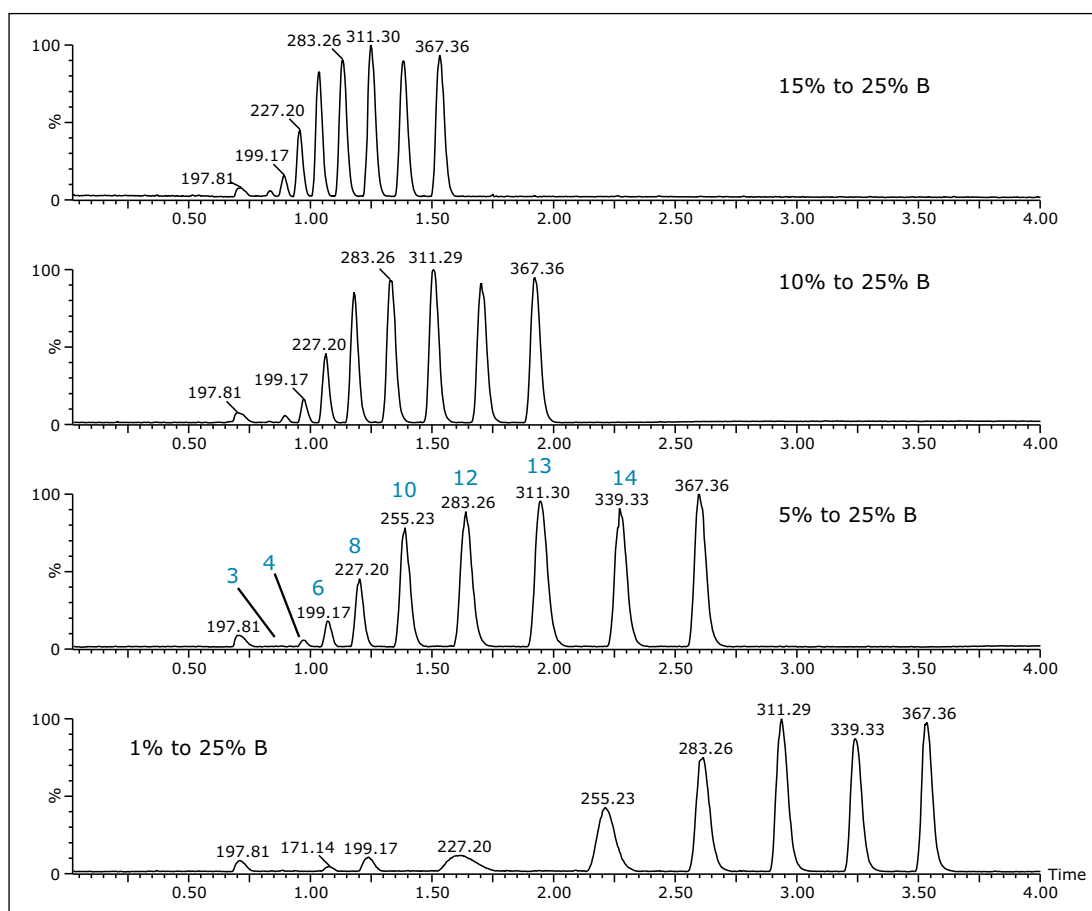


Figure 2. The separation of saturated FFA with carbon chain length C8-C24 with various co-solvent gradient. For the lipid ID, see Table 1.

## Analysis of complex saturated and unsaturated FFA standards GLC-85

Reversed-phase chromatography separates lipids according to both chain-length and degree of unsaturation. The problem lies in the fact that the dual nature of the reversed-phase separation process (a double bond in the fatty acyl chain reduces the retention time and the fatty acyl chain length increases the retention time) can hamper the analysis of real samples; the number of components is often so great that identification becomes difficult due to coelution (Figures 3A and B).

On the other hand, by using the precursor exact mass, corresponding product ion information and ion mobility (separation of lipid ions in the gas phase according to their size and molecular shape), each coeluting peak can be extracted and identified.
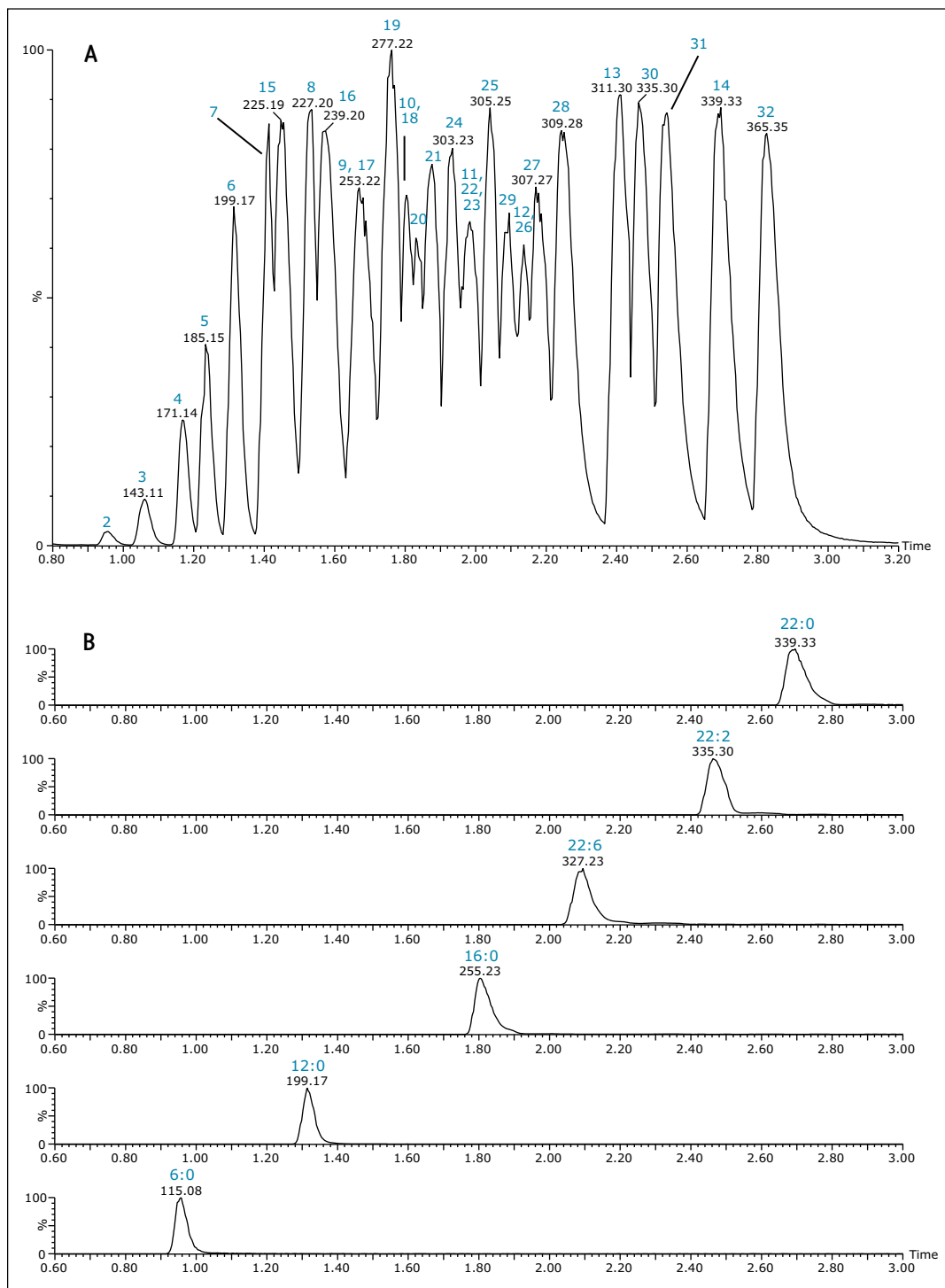


*Figure 3. A) The separation of complex standard mixture that contains saturated, unsaturated, short and long chain 32 different FFA species. B) The separation depends on both chain length and degree of unsaturation. In an RP separation, the fatty acyl chain length increases the retention time and the number of double bonds in the fatty acyl chain decreases the retention time. For the lipid ID, see Table 1.*

Another benefit of the method is the ability to separate between lipid isomers. FFA can have different biological functions based on the double bond position (e.g., omega-3 and omega-6). Figure 4 shows the separation of FFA isomers based on the position of the double bond. The separation of 18:3 (Δ6,9,12) and 18:3 (Δ9,12,15); and 20:3 (Δ8,11,14) and 20:3 (Δ11,14,17) isomers have been observed.
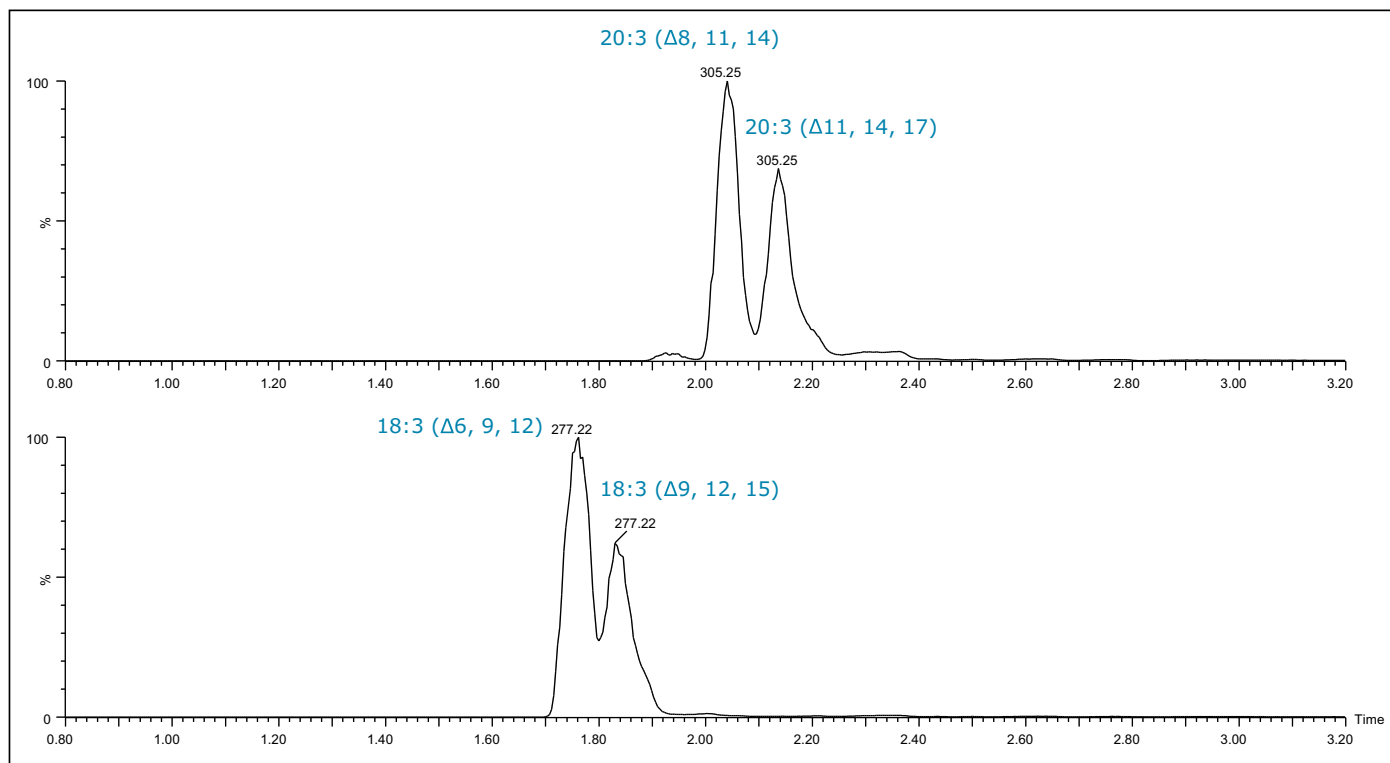


Figure 4. Extracted ion chromatogram (from figure 3) showing the separation of isobaric lipid species based on the position of the double bond.

### Biological application and data analysis using TransOmics

The developed UPC[2]/Xevo G2 QTof MS method was applied with minor modifications for the profile of FFA in algae and algaenan extracts treated at low (310 °C) and high (360 °C) pyrolysis temperatures.

Algaenan is a non-hydrolyzable, insoluble biopolymer in the cell walls of several green freshwater and marine microalgae.[3] Figure 5 shows a representative chromatogram from algaenan 1 with the UPC[2] conditions used for the analysis. For complete analysis of the data, set the gradient 1% to 10% co-solvent mobile phase B (methanol in 0.1% formic acid) in 10 minutes was used.
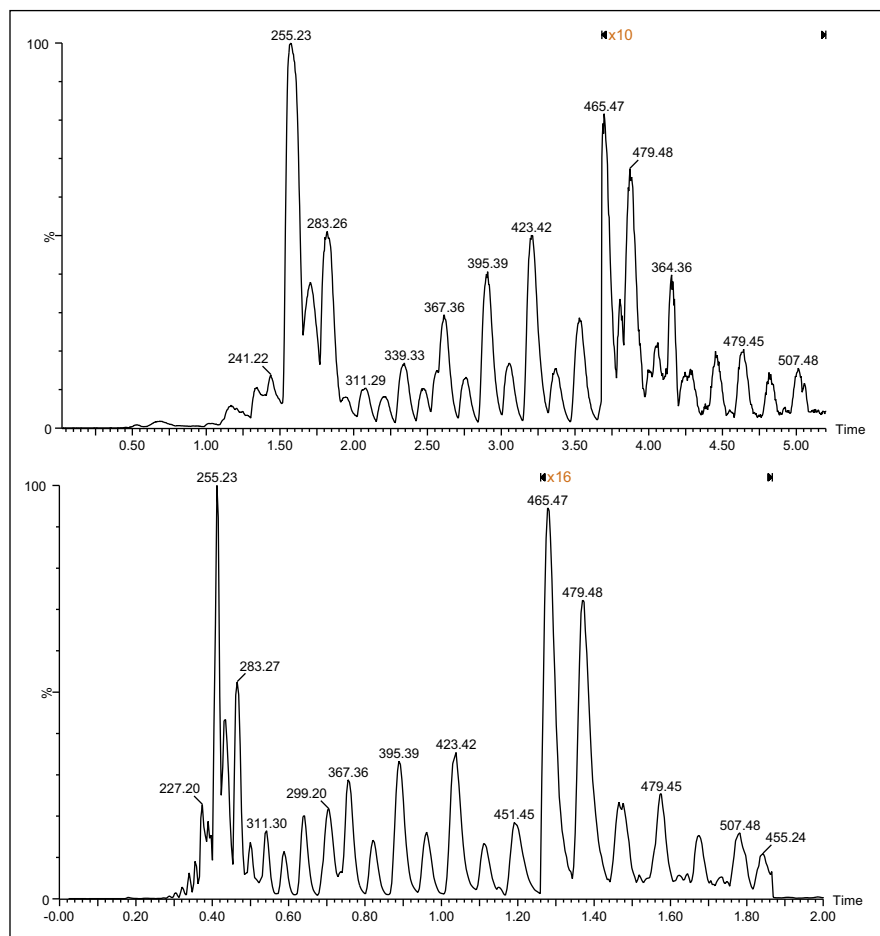


Figure 5. Representative chromatogram from algaenan 1 with various co-solvent gradients (top 1% to 10% methanol in 10 minutes, lower 5% to 20% methanol in 10 minutes). (UPC[2] conditions: HSS $C_{18}$ SB (2.1 x 100 mm), flow rate= 1.5 mL/min. The other UPC[2] conditions are described in the method conditions).

The lipid profiles of the algae and algaenan oil were investigated using TransOmics (TOIML) Software to determine the pattern and composition of FFA at two different pyrolysis temperatures. Differential analysis of results across different treatments can quickly be performed, thereby facilitating identification and quantitation of potential biomarkers. The software adopts an intuitive workflow approach to performing comparative UPC$^2$/Xevo G2 QTof MS metabolomics and lipidomics data analysis.

The workflow starts with UPC$^2$/MS raw data file loading, then retention time alignment and deconvolution, followed by analysis that creates a list of features. The features are then identified with compound searches and explored using multivariate statistical methods.

Principal component analysis (PCA) was used in the first instance to identify the combination of the FFA species that best describe the maximum variance between algae 1, algae 2, algaenan 1, and algaenan 2 oils (Figure 6). The PCA plot showed excellent technical UPC$^2$/MS measurements. The PCA plot effectively displays the inter-sample relationships in multi-dimensional hyperspace, with more similar samples clustering together and dissimilar samples separated.[4]

The clustering in Figure 6 indicates that algae 1 and algaenan 1 are different, but algae 2 and algaenan 2 have more similarity in their FFA compositions after high pyrolysis temperature treatment. Orthogonal projections latent structure discriminant analysis (OPLS-DA) binary comparison can be performed between the different sample groups (algae 1 vs. algae 2, algaenan 1 vs. algaenan 2, algae 1 vs. algaenan 1, and algae 2 vs. algaenan 2) to find out the features that change between the two groups.
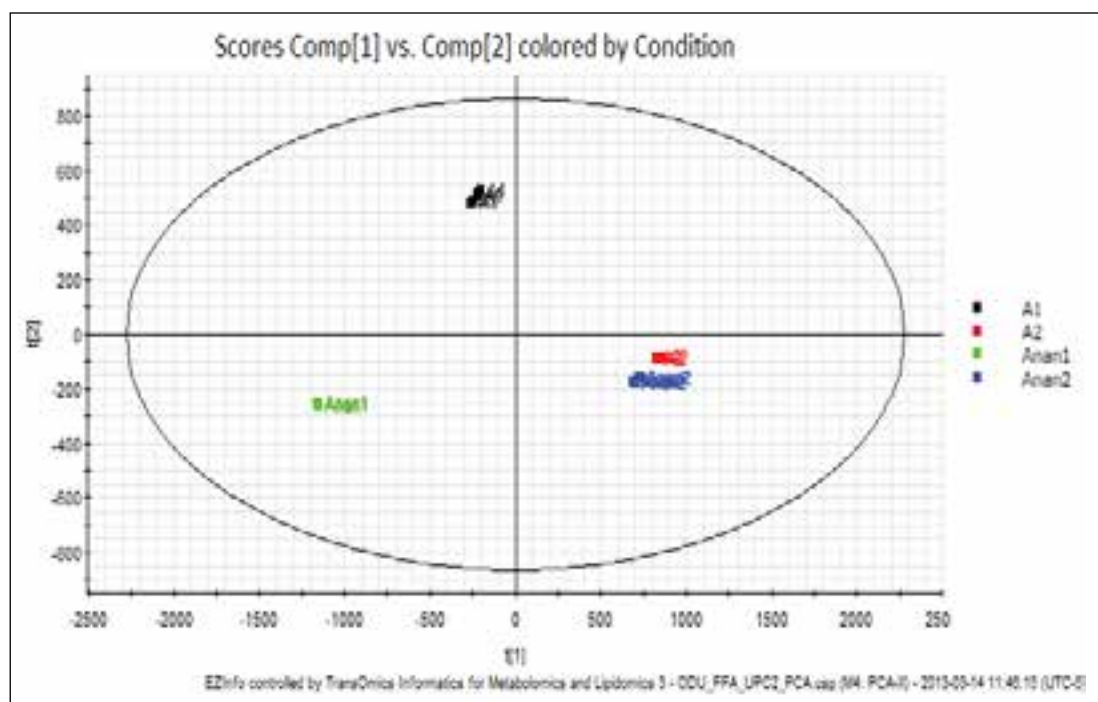


*Figure 6. Principal component analysis of algae and algaenan oil extracts treated at low and high pyrolysis temperature. (A1= algae at low pyrolysis temperature A2= algae at high pyrolysis temperature Anan1= algaenan at low pyrolysis temperature Anan2= algaenan at high pyrolysis temperature).*

As an example, the OPLS-DA binary comparison between algae 1 vs. algae 2 is shown in Figure 7A. As shown in the S-plot, the features that contribute most to the variance between the two groups are those farthest from the origin of the plot, highlighted in red (Figure 7B). These selected features can be exported to TransOmics for further identification. This helps the researcher focus on the features/compounds that change between samples instead of spending time on the whole data set.

Figures 7C and 7D show representative trend plots that change most between algae 1 and algae 2. Figure 8A shows the ion map, mass spectrum, and chromatogram across all the runs for FFA 29:0. This view allows to review compound measurements such as peak picking and alignment to ensure they are valid across all the runs. Figure 8B shows the normalized abundance of FFA 29:0 across all the conditions. FFA 29:0 is elevated in algeanan 1 compared to algae 1, algae 2, and algeanan 2; however, there is no significant difference between algae 2 and algeanan 2. Detailed investigation and comparison between algae 1 and algae 2 showed that algae 1 contains elevated levels of short (C9:0 to C13:0) and long (C31:0 to C37:0) chain FFA, whereas algae 2 contains elevated levels of medium (C14:0-C29:0) chain FFA. Similarly, the comparison between algaenan 1 and algaenan 2 showed that algaenan 1 contains elevated levels of long (C28:0 to C37:0) chain FFA, whereas algaenan 2 contains elevated levels of short and medium (C9:0 to C27:0) chain FFA.
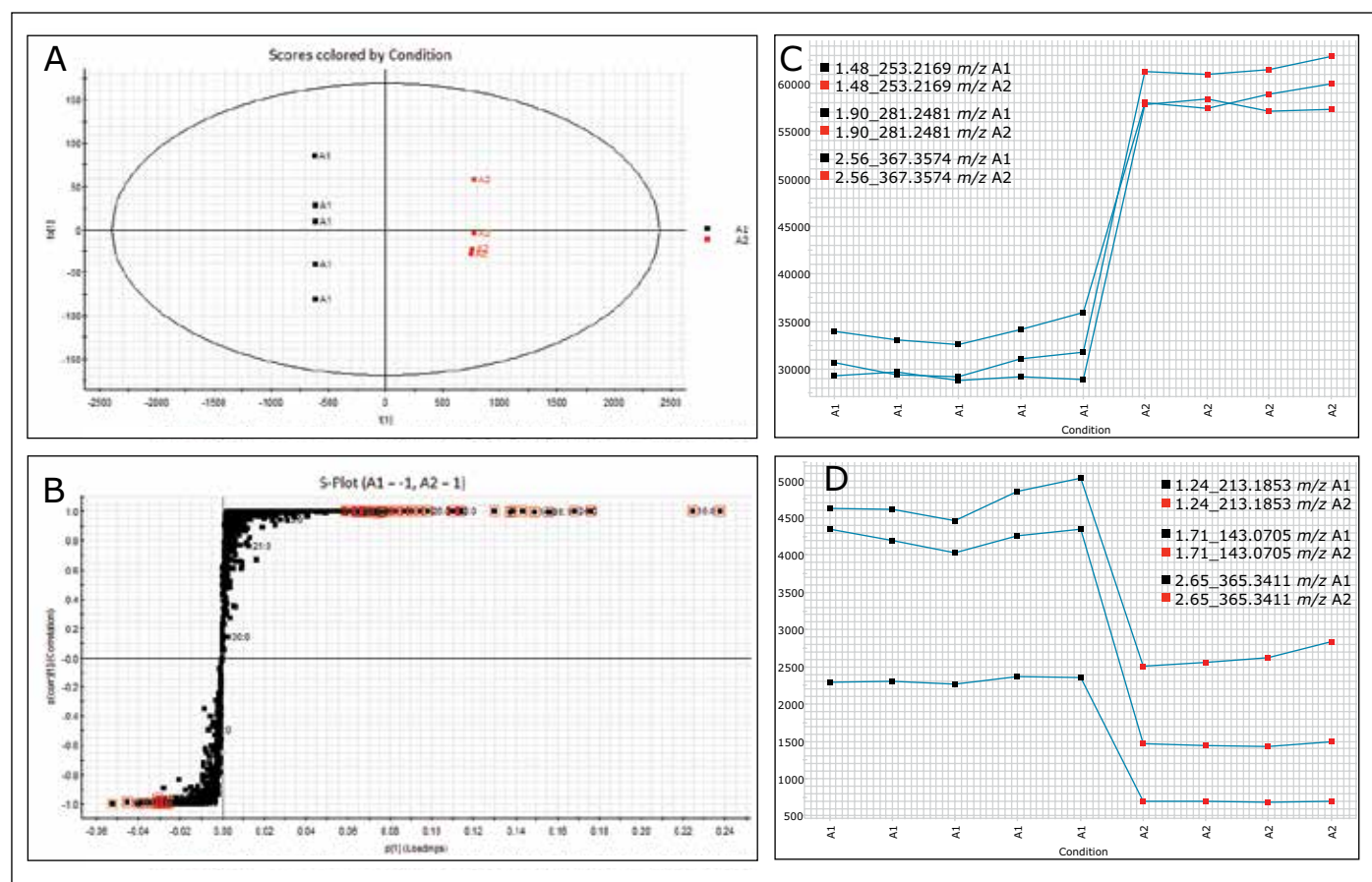


Figure 7. (A) OPLS DA plot between algae 1 and algae 2 group difference. (B) S-plot indicating the major features (highlighted in red) that contribute to the group difference between algae 1 and algae 2. (C) Representative trend plot showing the major up-regulated 16:1, 18:1, and 24:0 FFA in A1 (D) Representative trend plot showing the major up-regulated 8:0, 13:0, and 24:1 FFA in A2. (A1= algae at low pyrolysis temperature A2= algae at high pyrolysis temperature).
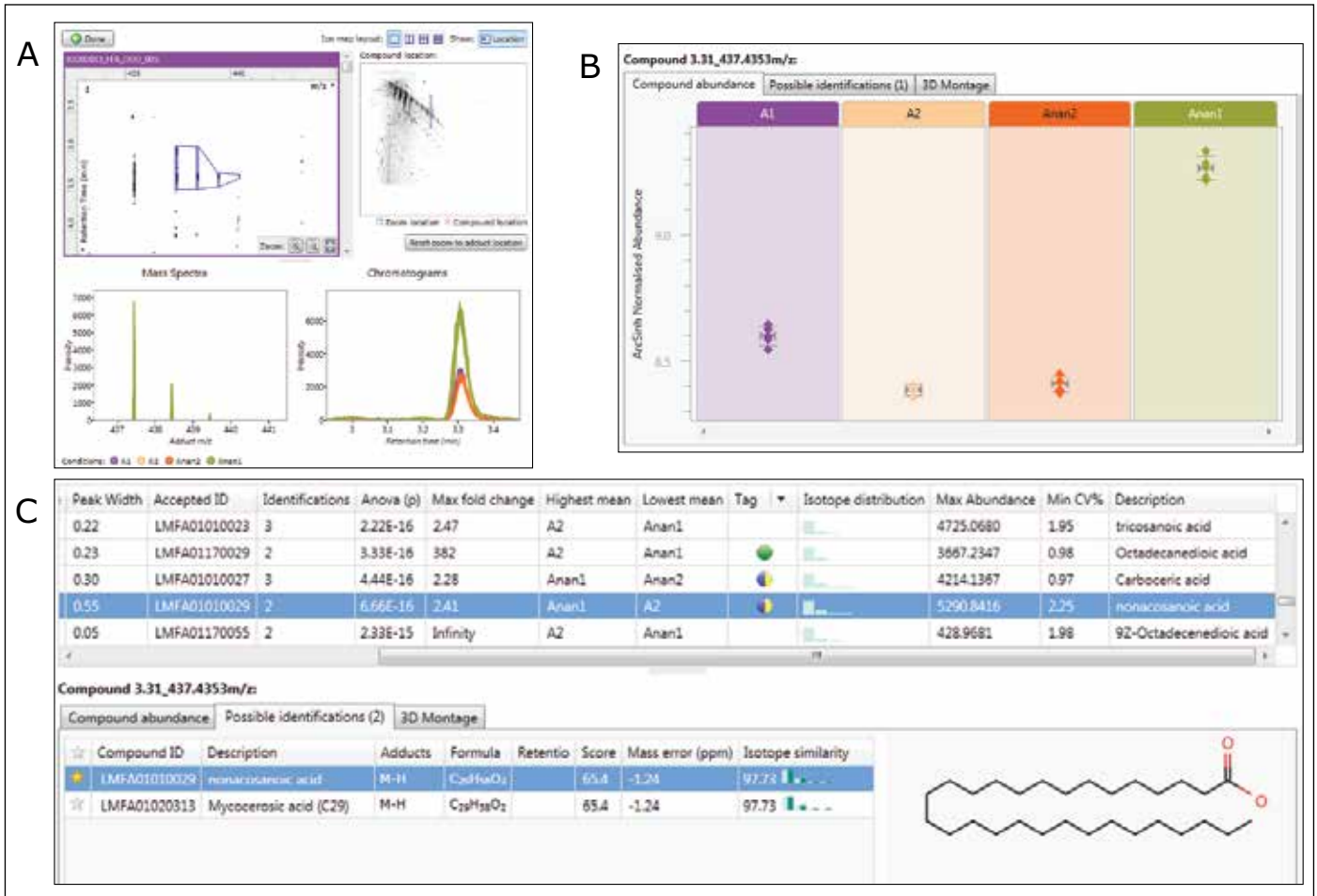
Figure 8. (A) Selected FFA 29:0 showing its ion map, mass spectrum, and chromatogram across all the runs. (B) Normalized abundance of FFA 29:0 across all the conditions. (C) Identification can be performed by means of local or web-based database search. In this example, the feature with retention time and exact mass pair 3.31_437.4353 is identified as nonacosanoic acid (29:0 FFA). (A1= algae at low pyrolysis temperature, A2= algae at high pyrolysis temperature; Anan1= algaenan at low pyrolysis temperature Anan2= algaenan at high pyrolysis temperature).

Identification can be performed by means of local or web-based (such as LIPID MAPS, HMDB, and METLIN) compound searches based on retention time, low energy exact mass, high energy fragment ion, theoretical isotope pattern distribution, and collision cross section area (CCS) (Figure 8C). In this example, the feature with retention time and exact mass 3.31_437.4353 is identified as nonacosanoic acid (29:0 FFA) based on retention time, low energy exact mass, and theoretical isotope pattern distribution. Figure 9 shows the expression and abundance profile of selected features according to their relative similarity between the different groups.
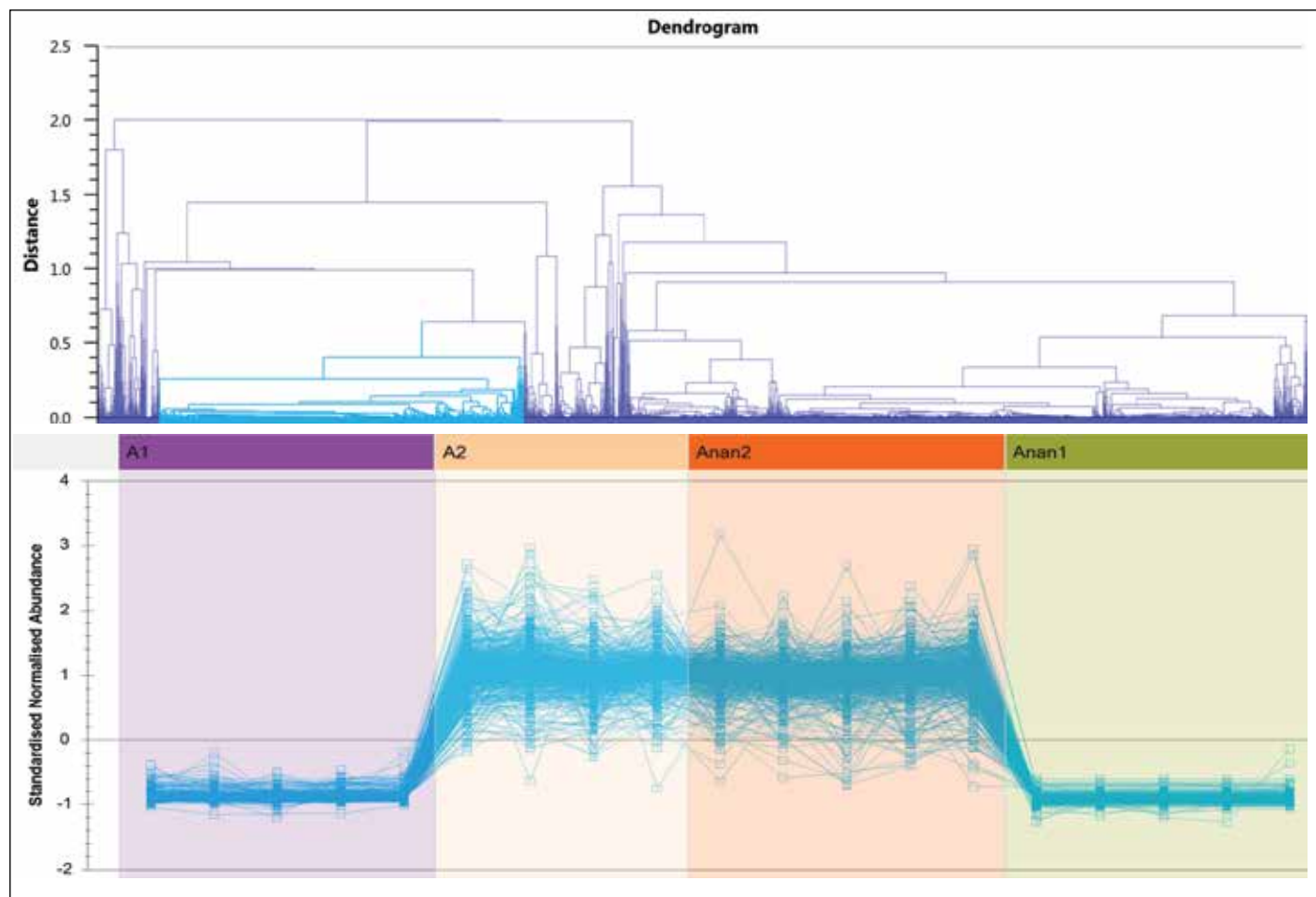


Figure 9. Expression and abundance profile of selected features according to their relative similarity between the different groups.

## CONCLUSIONS

The UPC$^2$/MS FFA analysis described provides a simple and fast method with a significant reduction in analysis time compared to alternative techniques such as GC/MS, which requires FAME derivatization. In addition, the organic layer extract containing the lipids can be injected directly into the system, omitting the need for solvent exchange for compatibility with reversed-phase LC methods.

Saturated and unsaturated FFA containing C$_8$ to C$_{36}$ carbons were separated and determined, including low volatile very long chain fatty acids (>24 carbon atoms) that have challenged GC/MS even after FAME derivatization. Data analysis and FFA identification was facilitated using TransOmics for Metabolomics and Lipidomics Software that adopts an intuitive workflow approach to performing comparative ACQUITY UPC$^2$/Xevo G2 QTof MS metabolomics and lipidomics data analysis.

### References

1. Fahy E et al. Update of the LIPID MAPS comprehensive classification system for lipids. *J Lipid Res.* 2009; 50: S9-S14.

2. Rustan AC, Drevon CA. Fatty Acids: Structures and Properties. eLS. 2005.

3. Allard B, Templier J. Comparison of neutral lipid profile of various trilaminar outer cell wall (TLS)-containing microalgae with emphasis on algaenan occurrence. *Phytochemistry.* 2000; 54: 369-380.

4. Stump CL, Goshawk J. The MarkerLynx Application Manager: Informatics for Mass Spectrometric Metabonomic Discovery. Waters Application Note 720001056en. 2004.

## Waters
### THE SCIENCE OF WHAT'S POSSIBLE.®

**Waters Corporation**
34 Maple Street
Milford, MA 01757 U.S.A.
T: 1 508 478 2000
F: 1 508 872 1990
www.waters.com

# Bile Acid Profiling Using UltraPerformance Convergence Chromatography (UPC²) Coupled to ESI-MS/MS

Kaori Taguchi,[1] Eiichiro Flukusaki,[2] and Takeshi Bamba[2]
[1]Waters Corporation, Milford, MA, USA
[2]Department of Biotechnology, Osaka University, Suita, Japan

## GOAL

Develop a novel method for rapid profiling and quantification of bile acids using UltraPerformance Convergence Chromatography™ (UPC²™).

## BACKGROUND

Bile acids play an important role as the signaling molecules that regulate triglyceride, cholesterol, and glucose metabolism.[1] These signaling pathways have become the source of attractive drug targets for metabolic diseases. Also bile acids are used as biomarkers in serum to interpret liver diseases and the mechanism of bile acid-regulated metabolism.[2–5] Therefore, an analytical method that determines the bile acid profile in the body is beneficial.

The separation of bile acids is complex due to the presence of structural analogues including isomeric forms, and the polarity diversity between unconjugated and conjugated forms. In the past, gas chromatography (GC) and liquid chromatography (LC) have been used to analyze these compounds; however, several limitations have been observed. GC always requires exhaustive derivatization steps which lead to a loss in bile acids at each step. In addition, aliquots of the samples have to be extracted separately to determine the composition or the concentration of conjugated bile acids in GC analysis.

**UltraPerformance Convergence Chromatography combined with ESI-MS/MS enables the simultaneous profiling of 25 bile acids within 13 minutes.**
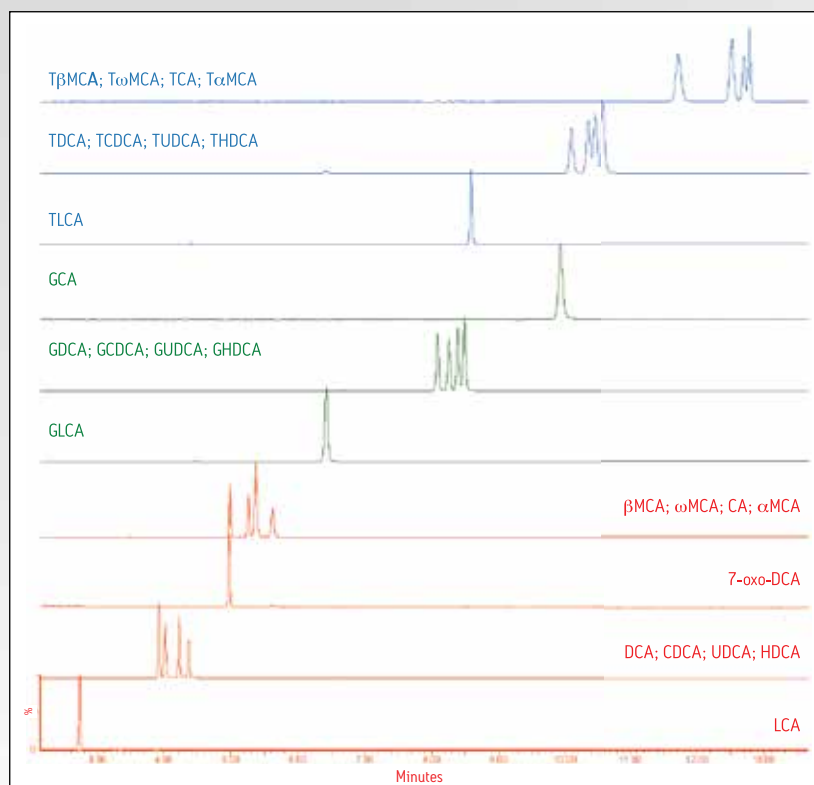


Figure 1. Simultaneous analysis of a 25-bile acids standard mixture including glycine and taurine conjugates was achieved within 13 minutes. The compound name is shown in order of retention time on each MRM chromatogram.
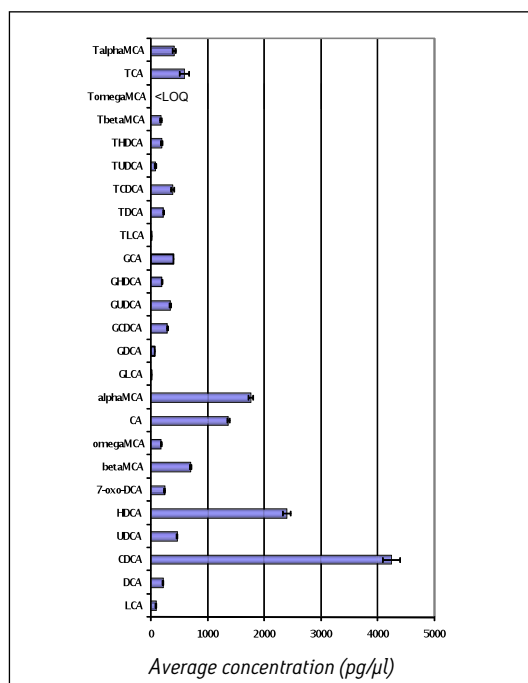
*Figure 2. The quantification of bile acids in rat serum by UPC²/MS (n=6).*

While LC can detect conjugated and unconjugated forms simultaneously, the separation can take up to 30 minutes for a sample. This application note describes a faster UPC²/MS method for bile acid profiling and quantification.

## THE SOLUTION

A method using supercritical carbon dioxide (SCCO$_2$)-based mobile phases was developed on the Waters® ACQUITY UPC²™ System to simultaneously separate 25 different bile acids including their conjugates. The use of SCCO$_2$ as the primary mobile phase allows for faster analyte diffusion and lower back pressure, resulting in faster analysis times. The ACQUITY UPC² System was connected to a Xevo® TQ-S Mass Spectrometer in order to enhance the sensitivity and specificity of the analysis. Separation results for 25 different bile acids (including glycine and taurine

conjugates) are shown in Figure 1. All bile acids were separated within 13 minutes, which is approximately two-fold faster than previous methods of analysis in bile acid profiling. This method was optimized through systematic investigation of different stationary phases, column temperature settings, additives, and pH in the modifier. The detection mode using the Xevo TQ-S was ESI negative. No make-up flow resulted in maximum sensitivity.

The developed method was applied to the quantitation of bile acids and their conjugates in a real biological sample (rat serum). Commercially purchased rat serum was deproteinized using methanol in a ratio of 3:1 methanol/serum, vortexed, and centrifuged. The supernatant was then injected onto UPC²/MS/MS in order to determine the amount of each bile acid and their conjugates present in the serum sample. Figure 2 shows the results, indicating that this method can reproducibly determine the levels of individual bile acids and their conjugates in biological fluids.

## SUMMARY

The use of UltraPerformance Convergence Chromatography (UPC²) in conjunction with ESI-MS/MS enables the simultaneous profiling of 25 bile acids including conjugated forms in biological fluids. The profiling is achieved within 13 minutes by a sub-2-µm particle column on the system with acceptable resolution of the analytes. This application demonstrates that this novel separation method is highly suitable for determining the effects of bile acid levels in triglyceride, cholesterol, and glucose metabolism and has a potential to speed up the development of novel drug targets for metabolic diseases.

### References

1. Houten SM, Watanabe M, Auwerx J. Endocrine functions of bile acids. *The EMBO Journal*. 2006 April; 25(7): 1419-25.

2. Barnes S, Gallo GA, Trash DB, Morris JS. Diagnostic value of serum bile acid estimations in liver disease. *Journal of Clinical Pathology*. 1975; 506-509.

3. Qiao X, Ye M, Xiang C, Bo T, Yang W, Liu C, Miao W, Guo D. Metabolic regulatory effects of licorice: a bile acid metabonomic study by liquid chromatography coupled with tandem mass spectrometry. *Steroids*. 2012 June; 77(7): 745-55.

4. Patti ME, Houten SM, Bianco AC, Bernier R, Larsen PR, Holst JJ, Badman MK, Maratos-Flier E, Mun EC, Pihlajamaki J, Auwerx J, Goldfine AB. Serum bile acids are higher in humans with prior gastric bypass: potential contribution to improved glucose and lipid metabolism. *Obesity* (Silver Spring, MD). 2009 September; 17(9): 1671-7.

5. Ye L, Liu S, Wang M, Shao Y, Ding M. High-performance liquid chromatography-tandem mass spectrometry for the analysis of bile acid profiles in serum of women with intrahepatic cholestasis of pregnancy. *Journal of Chromatography. B, Analytical technologies in the biomedical and life sciences*. 2007 December; 860(1): 10-7.

## Waters

### THE SCIENCE OF WHAT'S POSSIBLE.®

**Waters Corporation**
34 Maple Street
Milford, MA 01757 U.S.A.
T: 1 508 478 2000
F: 1 508 872 1990
www.waters.com

Waters
THE SCIENCE OF WHAT'S POSSIBLE.®

# Method Development for the Analysis of Endogenous Steroids Using Convergence Chromatography with Mass Spectrometric Detection

Christopher J. Hudalla, Stuart Chadwick, Fiona Liddicoat, Andrew Peck, and Kenneth J. Fountain
Waters Corporation, Milford, MA, USA

## APPLICATION BENEFITS

- Analysis of endogenous steroids in approximately two minutes

- Minimal sample prep without requiring sample derivitization

- Ability to separate compounds that are structurally very similar

- 50% to 95% reduction in analysis time relative to GC and LC methods enables high-throughput analysis

- Compatible with UV and mass spectrometric detection

## WATERS SOLUTIONS

ACQUITY UPC$^2$™ System

ACQUITY UPC$^2$ BEH Column

Xevo® TQ Mass Spectrometer

Empower® 3 Software

MassLynx® Software

LCMS Certified Maximum Recovery Vials

## KEY WORDS

Steroid, hormone, metabolic, clinical research, UPC$^2$, method development, convergence chromatography

## INTRODUCTION

Steroid biosynthesis is a complex metabolic pathway utilizing simple precursors to synthesize multiple steroidal forms. This biosynthetic pathway is unique to animals and provides a common target for antibiotics and other anti-infective drugs. Precise and accurate steroid analysis is critical for the development of steroid-based therapeutics. For mass spectrometric analysis of steroids, due to their structural similarity, chromatographic separation of the steroids is essential prior to analysis. Typical research analyses utilize either gas (GC/MS) or liquid (LC/MS) chromatographic methods. GC/MS methods require sample derivitization prior to analysis resulting in analysis times of approximately 40 minutes.[1] For LC/MS methods, typical analysis times are approximately 12 minutes for HPLC, or four to five minutes with the use of more recent UHPLC methods.[2,3]

This study focuses on the application of convergence chromatography (CC), utilizing liquid $CO_2$ as the primary mobile phase, for the rapid chromatographic analysis of endogenous steroids (structures shown in Figure 1).



Androstenedione
MW: 286.4

Testosterone
MW: 288.4

Estrone
MW: 270.4

17α-Hydroxyprogesterone
MW: 330.6

Corticosterone
MW: 346.5

Aldosterone
MW: 360.4

Estradiol
MW: 272.4

11-Deoxycortisol
MW: 346.5

Cortisol
MW: 362.4
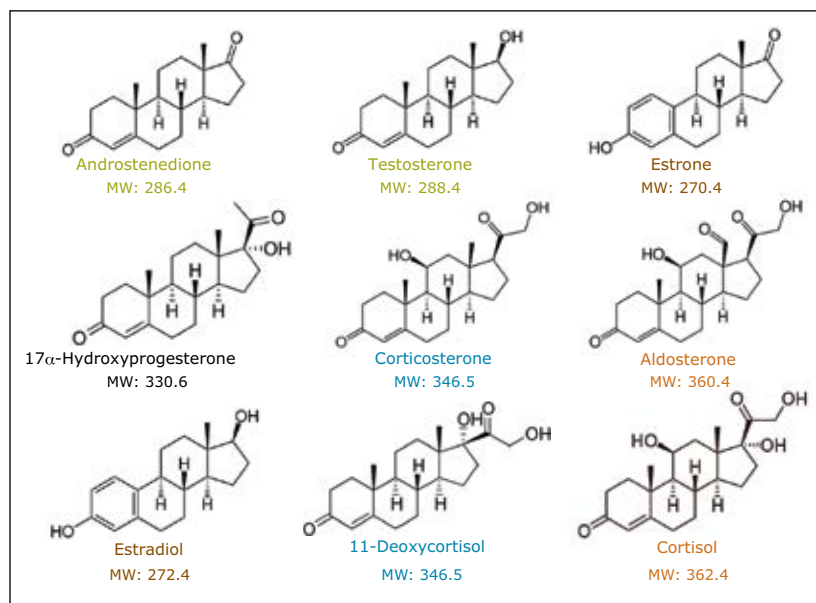
Figure 1. Structures of steroids evaluated. Compounds with the same color font indicate compounds with similar molecular weights that generate similar MS fragments.

## EXPERIMENTAL

### Sample description

Column screening (UV detection): A mixture of nine steroid standards was prepared at 0.2 mg/mL each, using a diluent of 88:12 methanol/ethanol.

Mass spectrometer evaluations: Often times, matrix interferences can limit the applicability of a technique. For this reason, standards were evaluated in a human plasma matrix. However, to insure these evaluations were indicative of technique sensitivity and not affected by recovery issues during sample preparation, the plasma samples were post-spiked after a 3:1 acetonitrile protein crash of the plasma. After centrifugation, the supernatant was collected and spiked with a mixture of the nine steroid standards. Spiking of steroids to various levels was achieved by serial dilution of the sample with additional crashed plasma.

### Method conditions

Screening columns:

ACQUITY UPC$^2$ BEH
1.7 µm, 3.0 x 50 mm
(p/n 186006562)

ACQUITY UPC$^2$ BEH 2-Ethylpyridine
1.7 µm, 3.0 x 50 mm
(p/n 186006580)

ACQUITY UPC$^2$ CSH Fluoro-Phenyl
1.7 µm, 3.0 x 50 mm
(p/n 186006571)

ACQUITY UPC$^2$ HSS C$_{18}$ SB
1.8 µm, 3.0 x 50 mm
(p/n 186006621)

### UPC$^2$ conditions

| | |
|---|---|
| System: | ACQUITY UPC$^2$ with PDA detector |
| Mobile phase A: | CO$_2$ (tank, medical grade) |
| Modifier B: | Methanol (Fisher Optima grade) |
| Column temp.: | 40 °C |
| ABPR: | 1800 psi |
| Gradient: | 2% to 17% modifier B in two minutes, re-equilibration at 2% modifier B for one minute |
| Flow rate: | 3.65 mL/min |
| UV detection: | 220 nm (compensated 380 to 480 nm) [40 pts/s] |
| Injection volume: | 1 µL |
| Needle wash: | 50:50 methanol/2-propanol |
| Seal wash: | Methanol |

### Data management

Empower 3 Software

### Make-up flow pump conditions

| | |
|---|---|
| Solvent: | Methanol with 2.5% water and 0.1% ammonium hydroxide |
| Flow rate: | 0.4 mL/min |

### MS conditions

| | |
|---|---|
| Mass spectrometer: | Xevo TQ |
| Capillary voltage: | 1 kV |
| Desolvation temp.: | 500 °C |
| Desolvation gas flow: | 750 L/h |
| Data management: | MassLynx Software |

Here, we present data collected with the ACQUITY® UltraPerformance Convergence Chromatography™ (UPC²®) System. In combination with stationary phases designed specifically for UPC², based on the bridged ethylene hybrid, BEH Technology,™ this technique results in the analysis of steroids in approximately two minutes. After initial method development using UV detection, the system was coupled to a tandem quadrupole mass spectrometer for analysis of steroid-spiked plasma samples. In addition to the significant reduction in analysis time relative to other techniques, convergence chromatography minimizes the consumption of mobile-phase solvents (e.g., methanol), thereby generating less waste for disposal and significantly reducing the cost of analysis per sample.

## RESULTS AND DISCUSSION

A generic two-minute screening gradient was used to evaluate the separation of the nine-steroid mixture on four different stationary phases to determine which would provide the best separation. The chromatograms in Figure 2 demonstrate the selectivity differences of the ACQUITY UPC² stationary phases, as well as the inherent speed of this chromatographic technique. Based on these results, the ACQUITY UPC² BEH stationary phase was chosen for additional application development with mass spectrometric detection.
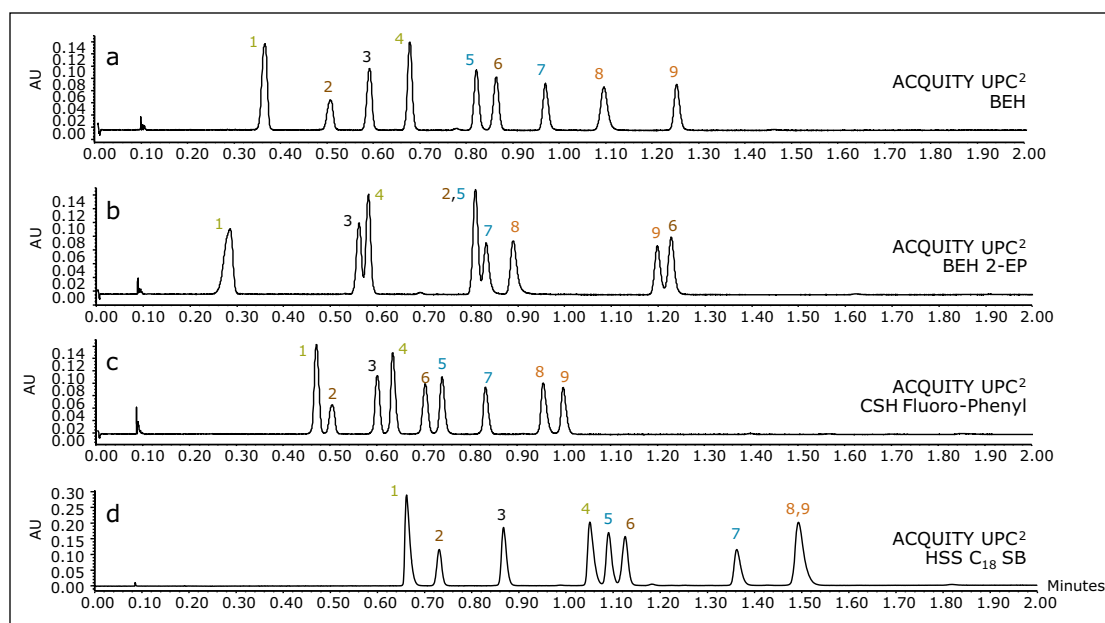


Figure 2. UPC² separations (UV) of steroid standards on ACQUITY UPC² columns including: (a) BEH, (b) BEH 2-EP, (c) CSH™ Fluoro-Phenyl, and (d) HSS C$_{18}$ SB. All columns were 3.0 x 50 mm, 1.7-µm configurations except for the HSS C$_{18}$ SB which is a 1.8-µm particle size. Steroid compounds are the following: (1) androstenedione, (2) estrone, (3) 17a-OHP [17α-hydroxyprogesterone, (4) testosterone, (5) 11-deoxycortisol, (6) estradiol, (7) corticosterone, (8) aldosterone, and (9) cortisol. Colored peak assignments denote compounds with similar molecular weights and m/z fragments.

Individual mass spectrometer (MRM) transitions were optimized by direct infusion of standards into the
Xevo TQ MS using on-board fluidics, without the connectivity of the ACQUITY UPC$^2$ System (Table 1). After
optimization of transitions, the mass spectrometer was coupled to the UPC$^2$ system using a mass spectrometer
splitter, incorporating the addition of a make-up flow pump, to facilitate sample flow into the MS and
subsequent ionization (Figure 3).

| Compound | Precursor | Product | Collision energy | Dwell | Cone voltage | Mode |
|---|---|---|---|---|---|---|
| Estrone | **271.05** | 153.1 | 30 | 0.005 | 25 | ESI + |
|  |  | **253.2** | **15** |  |  |  |
| Androstenedione | **287.05** | 97.15 | 21 | 0.005 | 25 | ESI + |
|  |  | **109.2** | **26** |  |  |  |
| Testosterone | **289.10** | 97.15 | 21 | 0.005 | 25 | ESI + |
|  |  | **109.15** | **26** |  |  |  |
| 17α-Hydroxy progesterone | **331.10** | 97.15 | 21 | 0.005 | 25 | ESI + |
|  |  | **109.1** | **26** |  |  |  |
|  |  | 313.3 | 16 |  |  |  |
| 11-Deoxycortisol | **347.05** | **97.11** | **24** | 0.005 | 26 | ESI + |
|  |  | 109.14 | 26 |  |  |  |
| Corticosterone | **347.05** | 105.1 | 42 | 0.005 | 24 | ESI + |
|  |  | **121.1** | **28** |  |  |  |
| Aldosterone | **361.05** | 97.15 | 35 | 0.005 | 25 | ESI + |
|  |  | 315.2 | 20 |  |  |  |
|  |  | **343.2** | **16** |  |  |  |
| Cortisol | **363.05** | **121.2** | **25** | 0.005 | 25 | ESI + |
|  |  | 309.2 | 20 |  |  |  |
|  |  | 327.2 | 15 |  |  |  |
| Estradiol | **271.00** | **145.1** | **38** | 0.005 | 55 | ESI - |
|  |  | 183.1 | 38 |  |  |  |

*Table 1. Multiple reaction monitoring (MRM) transitions used for the analysis of nine structurally related steroids. MS conditions for the MRM transitions were optimized using IntelliStart™ in infusion mode only (without the UPC$^2$ instrument). MRM transitions in bold are transitions chosen for monitoring.*
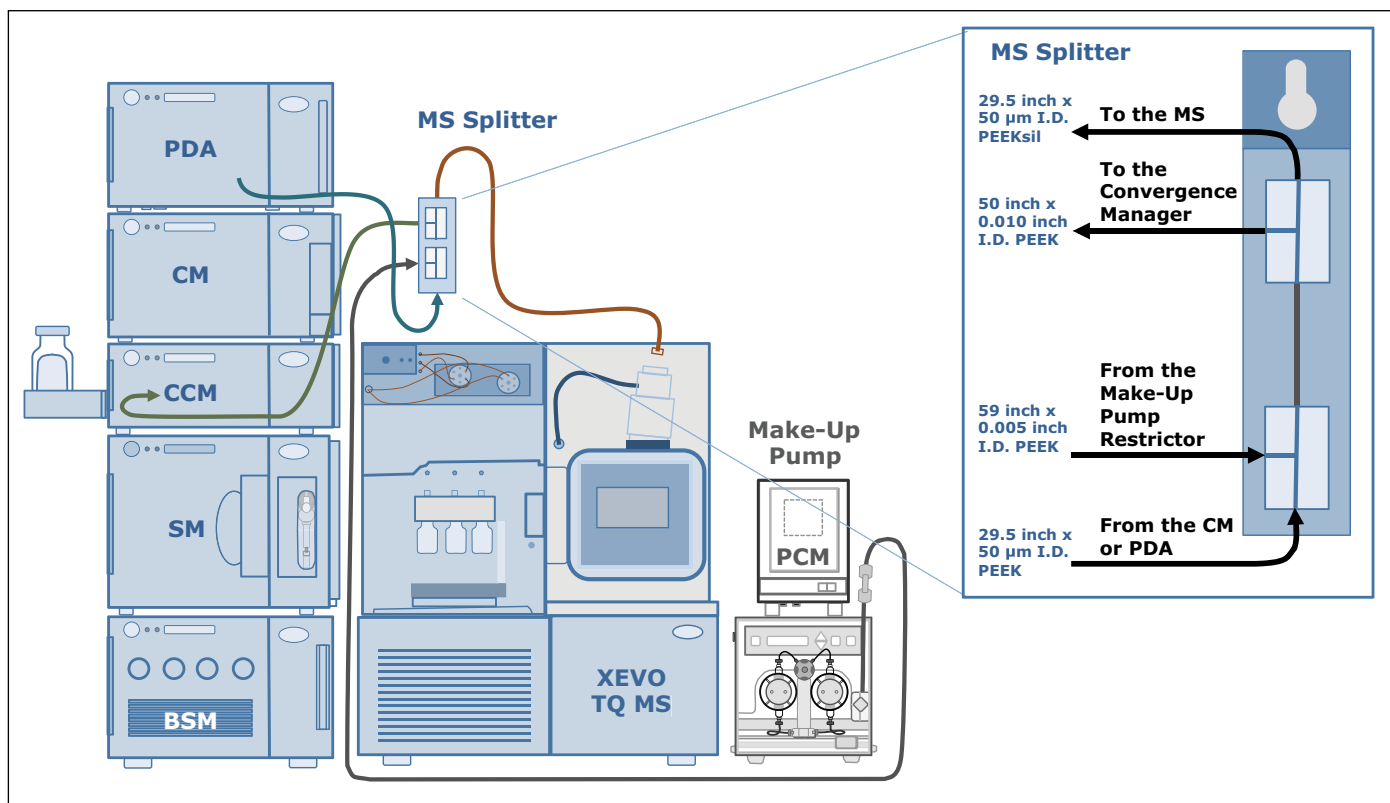
Figure 3. ACQUITY UPC$^2$ System coupled to a Xevo TQ MS, includes a Binary Solvent Manager (BSM), Sample Manager (SM), Convergence Chromatography Manager (CCM), Column Manager (CM), Photodiode Array (PDA) Detector, Make-up Flow Pump with additional Pump Control Module (PCM). The mass spectrometer splitter is used to connect all components together.

## Optimization of make-up flow

The make-up flow introduced through the mass spectrometer splitter has a dual purpose. It facilitates the post-mixer transfer of the sample through the tubing, as the $CO_2$ in the mobile phase starts to decompress as it reaches the mass spectrometer. This is especially important at low concentrations of the organic modifier in the mobile phase, as seen in the early stages of the current gradient profile. In addition, the use of additives in the make-up flow (such as water, ammonium hydroxide ($NH_4OH$), or formic acid (FA)) can assist in ionization of the analytes within the mass spectrometer source, thereby improving sensitivity. To optimize the make-up flow and additional MS conditions, a plasma sample spiked with the nine steroids (at 50 ng/mL) was used to evaluate various conditions including: additive used in make-up flow solvent, capillary voltage, desolvation temperature, and gas flow. The results of those evaluations are shown in Figure 4.
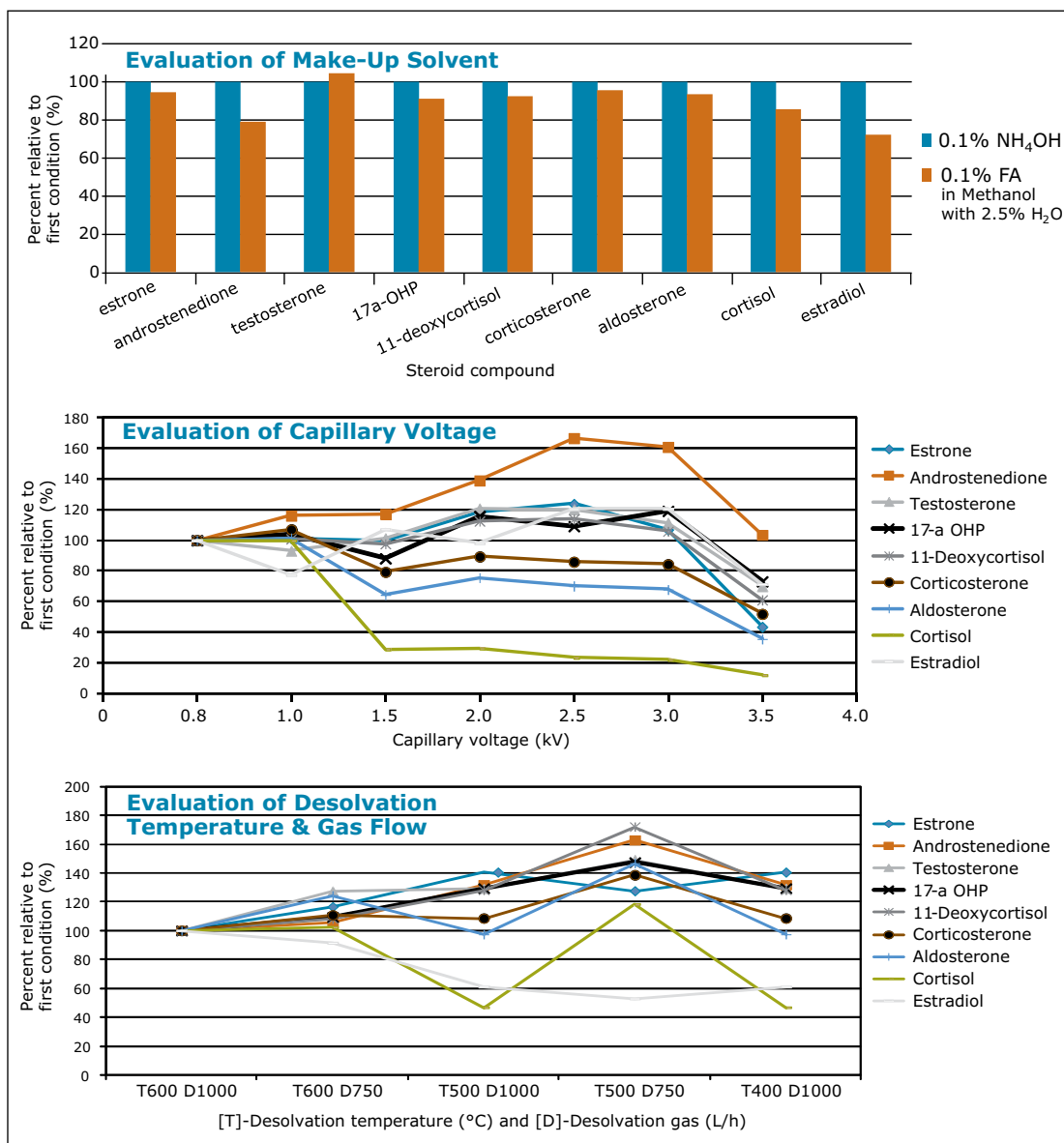


Figure 4. Optimization of make-up flow solvent, capillary voltage (kV), desolvation temperature (°C), and gas flow (L/h). Values reported are in percentages relative to the first conditions evaluated.

Method Development for the Analysis of Endogenous Steroids using Convergence Chromatography

The top panel of Figure 4 shows eight of the nine steroids yielded higher MS signals (better ionization) when using ammonium hydroxide as an additive in the make-up flow. In addition, most of the steroid signals were ambivalent to capillary voltages between 0.8 and 3.0 kV, as shown in the middle panel of Figure 4. However, at voltages higher than 1.0 kV, the signal for cortisol diminished dramatically. Based on these evaluations, the optimum conditions were determined, with the best overall signal obtained for all steroids using a make-up solvent composed of methanol with 2.5% water and 0.1% ammonium hydroxide, and a flow rate of 0.4 mL/min. The optimum results were obtained by MS when using a capillary voltage of 1.0 kV, with a desolvation temperature of 500 °C, and a gas flow of 750 L/h (bottom panel of Figure 4). The resulting chromatography for the nine steroids post-spiked into the human plasma after protein crash is shown in Figure 5.
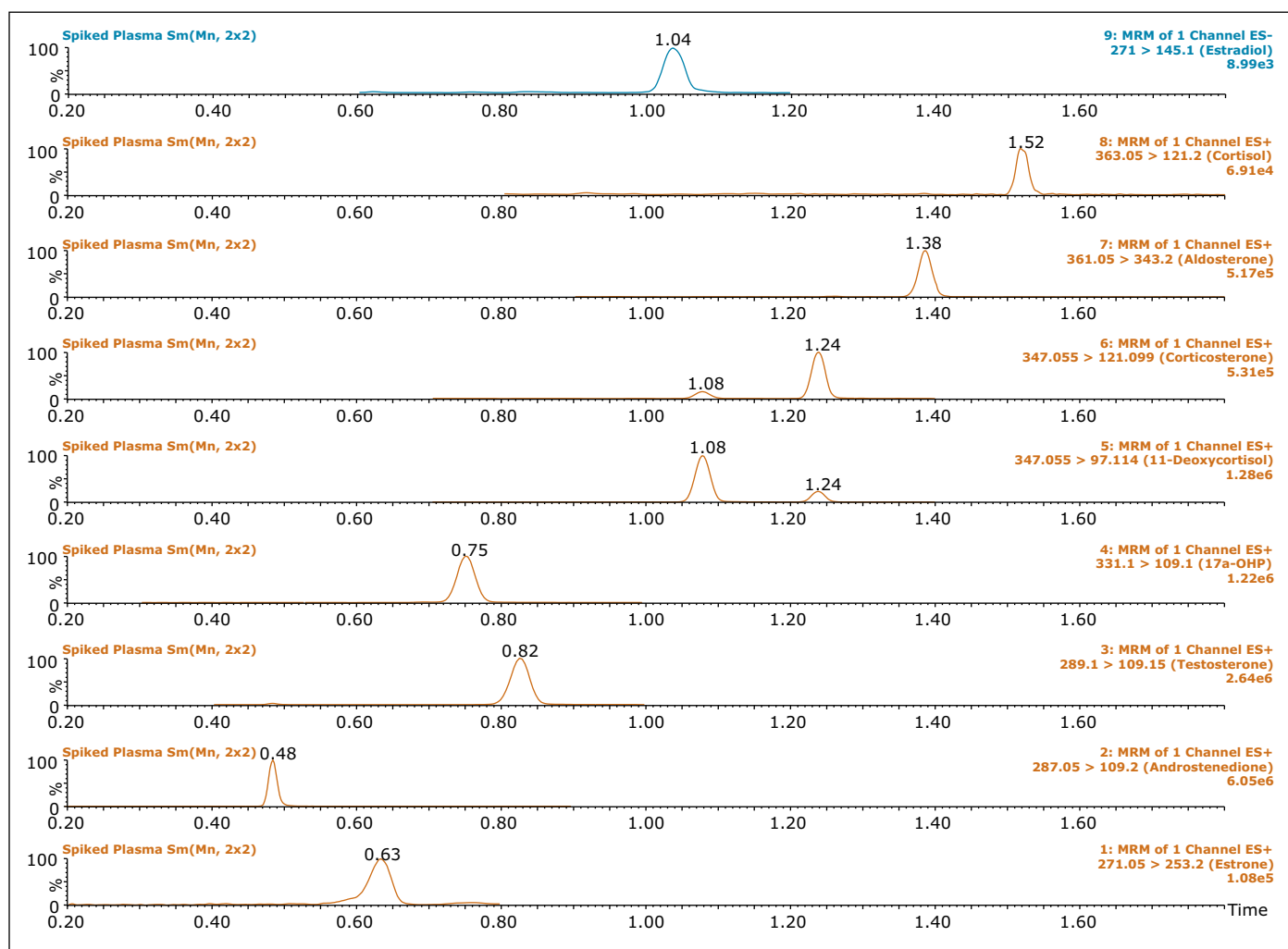


Figure 5. Total ion chromatograms (TIC) of the nine steroids. Standards were post-spiked at a concentration of 50 ng/mL into a 3:1 acetonitrile protein crash of human plasma.

## Reproducibility

As in any method development, the accuracy and reproducibility of the method is critical for success. To evaluate reproducibility of the method, the peak areas for the individual steroids were monitored over the course of 100 injections (using 1-µL injection volumes of 50-ng/mL steroid spiked in plasma). The RSD values for the peak areas ranged from 5.6% to approximately 13.7%. A representative example of the reproducibility results are shown in Figure 6. Similar results were obtained for the other steroids evaluated.
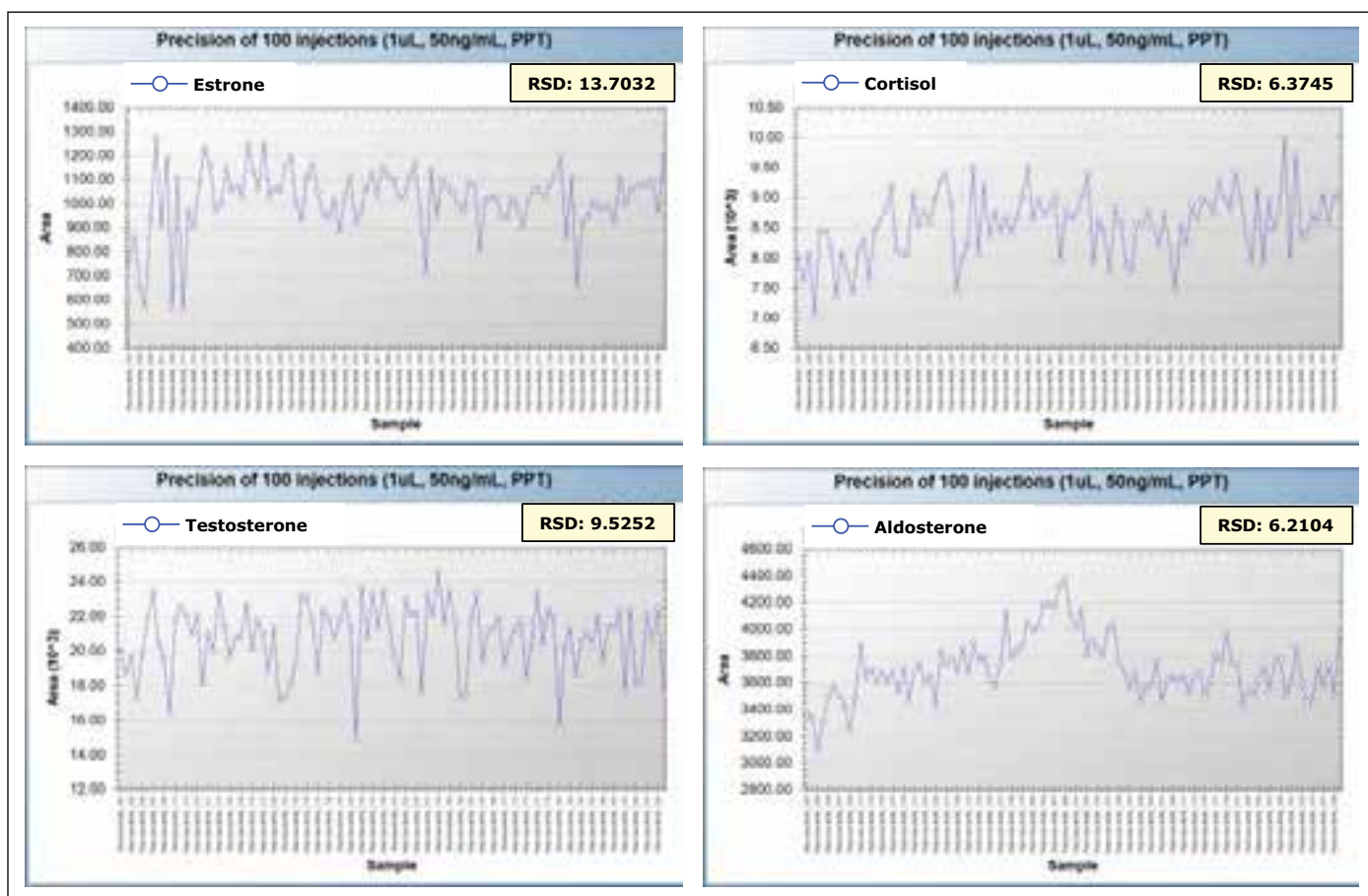


Figure 6. Examples of injection-to-injection reproducibility over 100 injections (1 µL) of steroid-spiked (50 ng/mL) human plasma for estrone (top left), cortisol (top right), testosterone (bottom left), and aldosterone (bottom right). Peak area RSDs range from approximately 5.6% to 13.7%.

To evaluate the linearity of response, calibration curves were generated using 5-µL injections of the spiked steroid plasma samples (after 3:1 acetonitrile protein crash). Concentrations of the steroids ranged from 0.98 to 500 ng/mL. Representative calibration curves are shown in Figure 7, with more complete data for each of the steroids shown in Table 2.

Compound name: **Estradiol**
Correlation coefficient: r = 0.998437, $r^2$ = 0.996876
Calibration curve: 5.88593 * x + -5.10485
Response type: External Std, Area
Curve type: Linear, Origin: Exclude, Weighting: 1/x, Axis trans: None

Compound name: **Estrone**
Correlation coefficient: r = 0.999017, $r^2$ = 0.998035
Calibration curve: 61.6364 * x + 47.9504
Response type: External Std, Area
Curve type: Linear, Origin: Exclude, Weighting: 1/x, Axis trans: None

Compound name: **Cortisol**
Correlation coefficient: r = 0.999389, $r^2$ = 0.998778
Calibration curve: 16.4433 * x + 449.494
Response type: External Std, Area
Curve type: Linear, Origin: Exclude, Weighting: 1/x, Axis trans: None

Compound name: **Corticosterone**
Correlation coefficient: r = 0.996287, $r^2$ = 0.992588
Calibration curve: 190.222 * x + 317.703
Response type: External Std, Area
Curve type: Linear, Origin: Exclude, Weighting: $1/x^2$, Axis trans: None



*Figure 7. Four representative calibration curves demonstrating the response linearity. All are 5-µL injections of 3:1 acetonitrile crashed human plasma spiked from 0.98 to 500 ng/mL with steroid standards.*

| | Conc (ng/mL) | Compound (% Dev) | | | | | | | | |
|---|---|---|---|---|---|---|---|---|---|---|
| | | Estradiol | Cortisol | Aldosterone | Corticosterone | 11-deoxy cortisol | 17a-OHP | Testosterone | Androstene-dione | Estrone |
| Std 0.5 | 1.0 | BLQ | E | 10.8 | -4.2 | 1.7 | 18.7 | E | E | BLQ |
| Std 1 | 2.0 | BLQ | E | (44.5) | 0.8 | -8.8 | -10.2 | E | -15.2 | BLQ |
| Std 2 | 3.9 | BLQ | 16.6 | -15.3 | 11.4 | 3.4 | 8.5 | E | -20.9 | -14.9 |
| Std 3 | 7.8 | 23.1 | -26.2 | -9.2 | 4.7 | 12.6 | -2.6 | -5.3 | 28.3 | 4.4 |
| Std 4 | 15.6 | -2.6 | 9.5 | -6.0 | 9.4 | 6.7 | -3.5 | -12.1 | 11.0 | 18.8 |
| Std 5 | 32.3 | -8.5 | 1.3 | 0.9 | -1.3 | -4.4 | -12.2 | 6.1 | (26.4) | -14.9 |
| Std 6 | 62.5 | -16.0 | -3.7 | 12.7 | -2.7 | -0.2 | -5.6 | -1.8 | -1.9 | 6.4 |
| Std 7 | 125.0 | -0.3 | 3.6 | 4.0 | -6.0 | 8.1 | 5.9 | 15.6 | -1.3 | 0.0 |
| Std 8 | 250.0 | -1.2 | -1.0 | 8.8 | -12.1 | -9.0 | 2.0 | 2.4 | (-40.1) | 1.2 |
| Std 9 | 500.0 | 2.9 | 0.0 | -6.6 | (-24.1) | -10.0 | -1.0 | -4.8 | (-20.6) | -1.0 |

- ▪ %Dev <20%
- ▪ % Dev 20 - 25%
- ▪ %DEV >25%

BLQ — Below limit of quantification
E — Rejected standard due to endogenous levels in the blanks
( ) — Rejected Standard (large deviation)

*Table 2. Percent deviation from the calibration curve for each steroid at each level of spiking.*

## CONCLUSIONS

Convergence chromatography enables fast, accurate analysis of steroids with reduced analysis times relative to current LC and GC methodologies. UPC$^2$ offers scientists a unique workflow, application, and environmental impact benefits, compared to LC and GC platforms, with simplified sample preparation. Samples extracted in organic solvents can be injected without additional steps to exchange solvents for RP-compatible diluents. In addition, with $CO_2$ as the primary mobile phase, the cost of analysis per sample is reduced, using a more environmentally friendly solvent relative to conventional RP methods. This method demonstrates the separation power of convergence chromatography utilizing either UV or MS detection. While the limits of detection and quantification presented here are not compatible with the low levels of steroid concentrations typically found in biological samples (e.g. plasma), additional optimization of MS parameters, with the possibility of additional sample derivitization to improve ionization, may help to reach higher sensitivity levels. This could further enable the application of this method to the analysis of steroids for clinical research.

### References

1. Sellers K. Rapid analysis of steroid hormones by GC/MS using the new Rxi-1ms column. Restek Application Note.

2. Licea-Perez H, Wang S, Szapacs ME, Yang E. Development of a highly sensitive and selective UPLC/MS/MS method for the simultaneous determination of testosterone and 5α-dihydrotestosterone in human serum to support testosterone replacement therapy for hypogonadism. *Steroids*. 2008; 73:601-610.

3. Schwarz E, Liu A, Randall H, Haslip C, Keune F, Murray M, Longo N, Pasquali M. Use of steroid profiling by UPLC-MS/MS as a second tier test in newborn screening for congenital adrenal hyperplasia: The Utah experience. *Pediatric Research.* 2009; 66: 230-235.

## Waters

### THE SCIENCE OF WHAT'S POSSIBLE.®

**Waters Corporation**
34 Maple Street
Milford, MA 01757 U.S.A.
T: 1 508 478 2000
F: 1 508 872 1990
www.waters.com

Waters
THE SCIENCE OF WHAT'S POSSIBLE.®

# Enantiomeric and Diastereomeric Separations of Fragrance and Essential Oil Components using the ACQUITY UPC$^2$ System with ACQUITY UPC$^2$ Trefoil Columns

John P. McCauley and Rui Chen
Waters Corporation, Milford, MA, USA

## APPLICATION BENEFITS

■ Shorter analysis times compared to chiral GC.

■ The 2.5-μm particle chiral stationary phases provide high efficiency enantiomeric separations for fragrance compounds.

■ The low system volume and extra-column volume of the ACQUITY UPC$^2$ System enables superior, faster, and more efficient enantiomeric separations of fragrance compounds compared to traditional SFC.

■ UPC$^2$ solvents are more compatible with mass spectrometry, compared to those used in normal-phase chiral HPLC, enabling superior real time peak identification.

## WATERS SOLUTIONS

ACQUITY UPC2 ® Trefoil™

ACQUITY UPC2 System with ACQUITY UPC2 PDA Detector and ACQUITY® TQ Detector

MassLynx® Software

## KEY WORDS

Enantiomers, chiral stationary phase, fragrance, essential oils, UltraPerformance Convergence Chromatography (UPC$^2$), convergence chromatography (CC), Trefoil

## INTRODUCTION

Perception of aroma occurs at the olfactory membrane. This membrane is comprised in part of proteins and carbohydrates, which are chiral in nature. This makes it possible for the olfactory receptors to distinguish between enantiomers. Many enantiomers of fragrance molecules are perceived differently by our sense of smell.[1] For example, carvone is a chiral terpenoid where the R enantiomer smells like spearmint while the S enantiomer has the distinct odor of caraway seed.[2]

Chiral composition of fragrance molecules is important for many industries, including food, cosmetics, and consumer products, in controlling the olfactory perception of products.[1] In addition, chiral analyses are routinely performed to authenticate the natural sources of essential oils. Since naturally chiral sources of essential oils are generally more costly and have a greater perceived health benefit than their synthetic counterparts, rapid chiral analysis allows manufacturers to quickly exclude adulterated products containing inexpensive racemic synthetic materials at the time of purchase.[3]

Historically, chiral separations of fragrance compounds have primarily been carried out using chiral stationary phases (CSPs) in capillary gas chromatography (GC).[2,3,4] The analysis time often ranges from 15 to 50 minutes.[3] More recently, supercritical fluid chromatography (SFC) with CSPs has been applied to these separations, often resulting in comparable resolution and reduced run time.[5,6] Despite the great success in chiral separation by SFC, the associated instrumentation and CSPs have been slow to tap into the technology advancements that have taken place in the HPLC field. For example, one of most significant breakthroughs in HPLC in the past decade is the advent of Waters® UPLC® Technology, which utilizes sub-2-μm particles. ACQUITY UPLC® Systems retain the practicality and principles of HPLC while increasing the overall interlaced attributes of speed, sensitivity, and resolution. Until very recently, the standard particle size for commercially available CSPs has remained 5 μm.

Convergence chromatography is the next evolution in SFC. The Waters ACQUITY UPC$^2$ System is a holistically designed system that has similar selectivity to normal-phase chromatography and is built upon proven UPLC technology.

## EXPERIMENTAL

### Instrumentation

All experiments were performed on an ACQUITY UPC$^2$ System equipped with an ACQUITY UPC$^2$ PDA Detector and an ACQUITY TQ Detector. The system is controlled by MassLynx Software.

### Samples

The standard samples used in this study were purchased from TCI Americas, with their structures shown in Figure 1. Essential oils were purchased from various commercial sources. All samples were dissolved in tert-butyl methyl ether (TBME) for the analyses.

### UPC$^2$ conditions

Column:         ACQUITY UPC$^2$  Trefoil AMY1 or CEL1 (2.5 µm, 3.0 x 150 mm)

Backpressure:   1740 psi

Temperature:    40 °C

Mobile phase A: $CO_2$

Mobile phase B: Isopropanol

MS:             APCI positive mode

Other key parameters are listed in their respective figure captions.

UltraPerformance Convergence Chromatography™ (UPC$^2$®) offers minimized system and dwell volume, enabling users to leverage the superior separation power inherent to smaller particle sizes.

We present herein the enantiomeric and diastereomeric separations of four fragrance compounds using Waters ACQUITY UPC$^2$ Trefoil AMY1 and CEL1 Columns on an ACQUITY UPC$^2$ System. Compared to the traditional method of analysis by GC, UPC$^2$ offered similarly high resolution with significantly shorter run times, resulting in improved productivity.
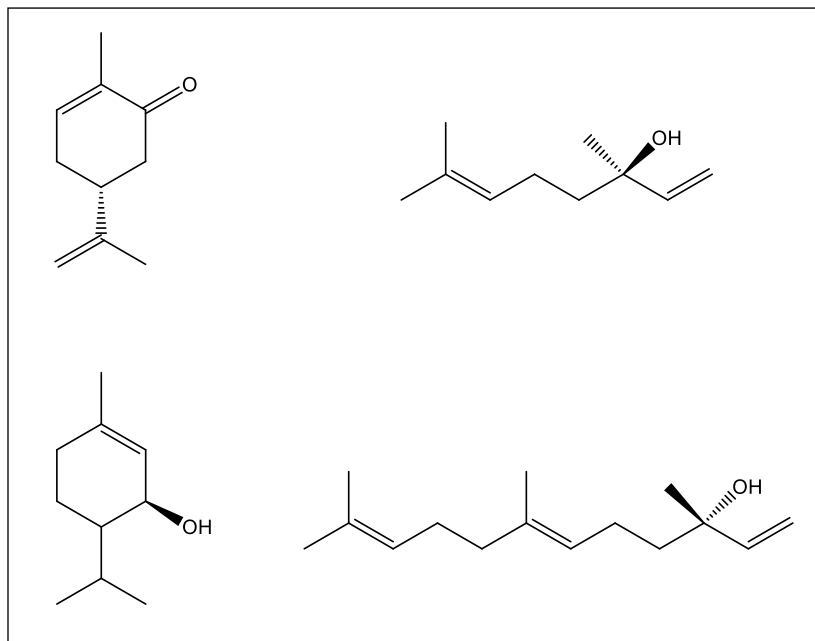


Figure 1. Structures of the four fragrance compounds presented in this study.

## RESULTS AND DISCUSSION

Figure 2 shows the UPC$^2$-UV chromatogram of carvone enantiomers on an ACQUITY UPC$^2$ Trefoil CEL1 Column. The enantiomeric pair was baseline resolved in less than 2.5 min (Figure 2C). The peak widths at half-height are 2-3 s. It is also interesting to note that there are detectable antipodes present in both single enantiomer standards (Figures 2A and 2B). In both cases, the minor peaks account for approximately 1% of the main peaks, resulting in a 98% enantiomeric excess (e. e.). This example clearly demonstrates a high efficiency chiral separation enabled by a 2.5-µm CSP on an ACQUITY UPC$^2$ System, resulting in short analysis time, sharp peaks, and improved detection sensitivity.
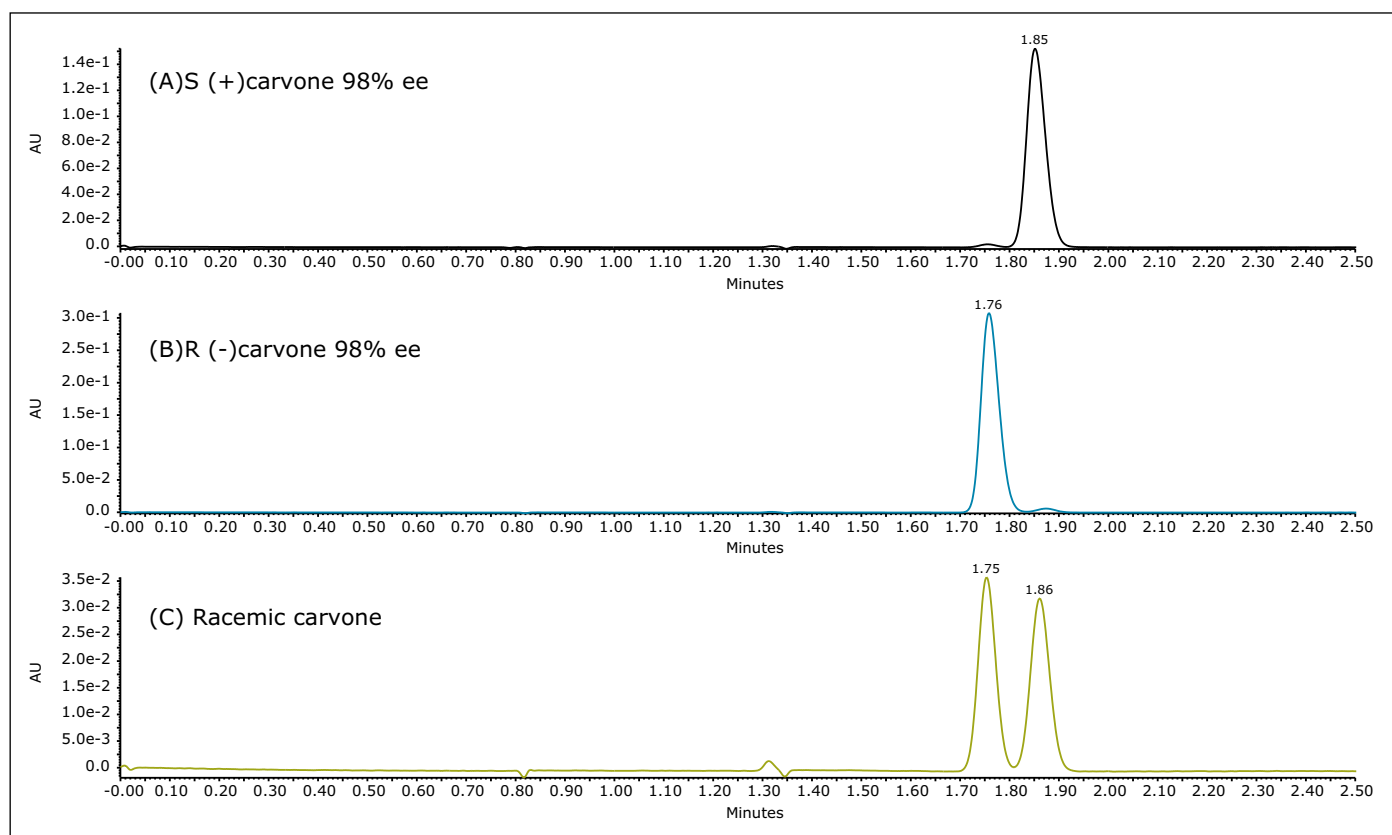


Figure 2. UPC$^2$-UV chromatograms of the enantiomeric separation of carvone on an ACQUITY UPC$^2$ Trefoil CEL1 Column: (A) S (+) carvone; (B) R (-) carvone; and (C) racemic carvone. An isocratic method with 4% isopropanol was used. The flow rate was 0.9 mL/min.

Linalool is a terpene alcohol with a soft floral odor, and can be found in different plant extracts. Figure 3A shows the enantiomeric resolution of the linalool standard on an ACQUITY UPC$^2$ Trefoil AMY1 Column. It is noted that the linalool standard was non-racemic (Figure 3A), suggesting the standard was derived from a natural source. The e. e. was estimated to be 40% in favor of the late eluting isomer. Figure 3B is the UPC$^2$-UV chromatogram of a commercially available lavender essential oil obtained under the same condition. The two linalool enantiomers were identified by both retention time and corresponding mass spectra (results not shown). It is noted that MS plays a critical role for the positive identification of the target analytes in a complex matrix. While bearing a similar selectivity to normal-phase LC, UPC$^2$ is inherently advantageous in incorporating MS detection due to its MS-friendly mobile phase. The linalool in this lavender essential oil exhibited a 92% e. e. in favor of the later eluting peak at 2.07 min.



| Time | Area | Area% |
|------|------|-------|
| 1.775 | 636.49 | 4.02 |
| 2.068 | 15189.31 | 95.98 |
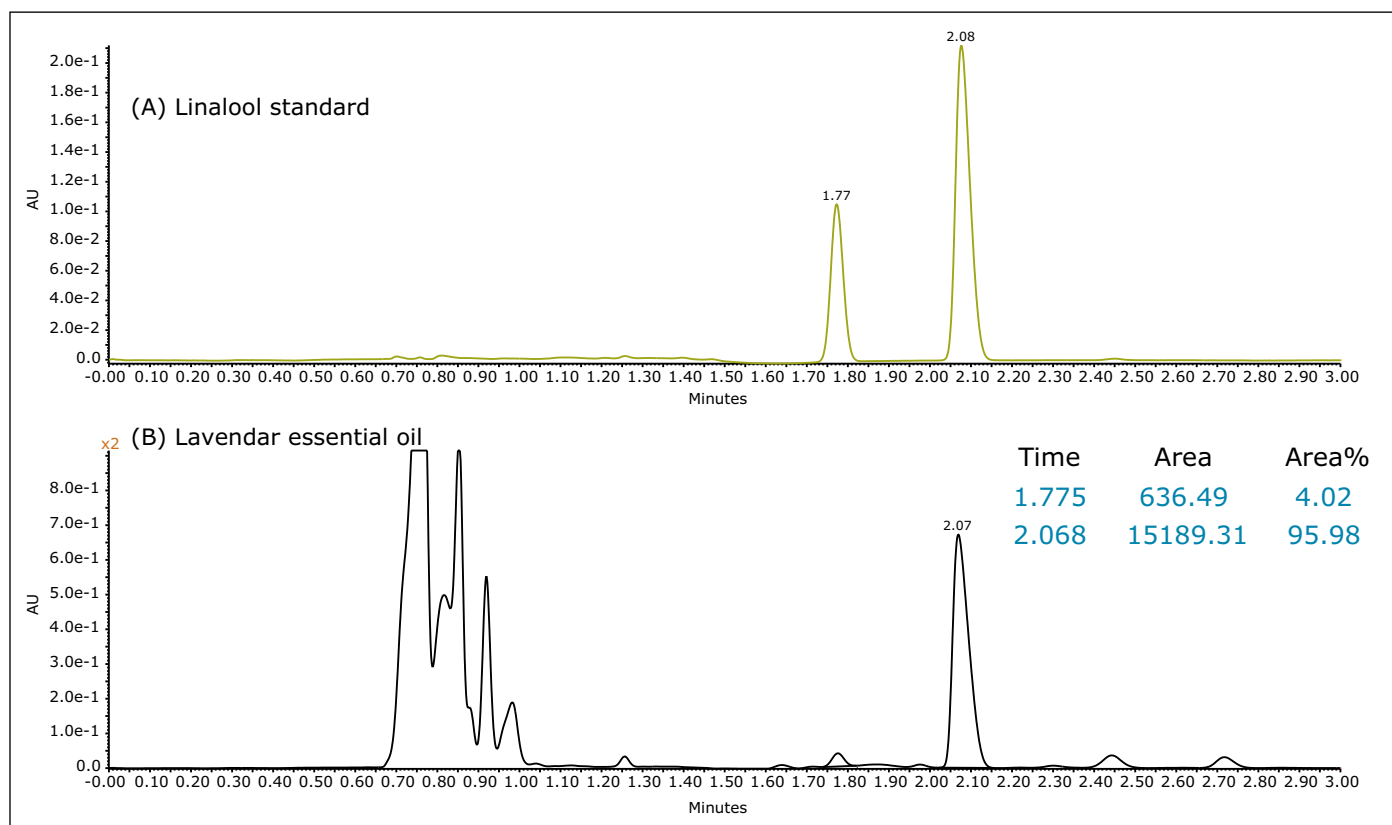
Figure 3. UPC$^2$-UV chromatograms of (A) linalool standard (B) lavender essential oil on an ACQUITY UPC$^2$ Trefoil AMY1 Column. An isocratic method with 3% isopropanol was used for linalool. The flow rate was 1.0 mL/min.

Similarly, terpinen-4-ol is a terpene with a pleasant conifer odor, and is a major constituent of tea tree oil. Figure 4A shows the enantiomeric resolution of the two isomers of a terpinen-4-ol standard on an ACQUITY UPC$^2$ Trefoil™ AMY1 Column. The terpinen-4-ol standard was nearly racemic (Figure 4A), suggesting its synthetic origin. Examination of a tea tree essential oil (Figure 4B) revealed that the terpinen-4-ol exhibited a 37% e. e. in favor of the early eluting isomer at 1.95 min.
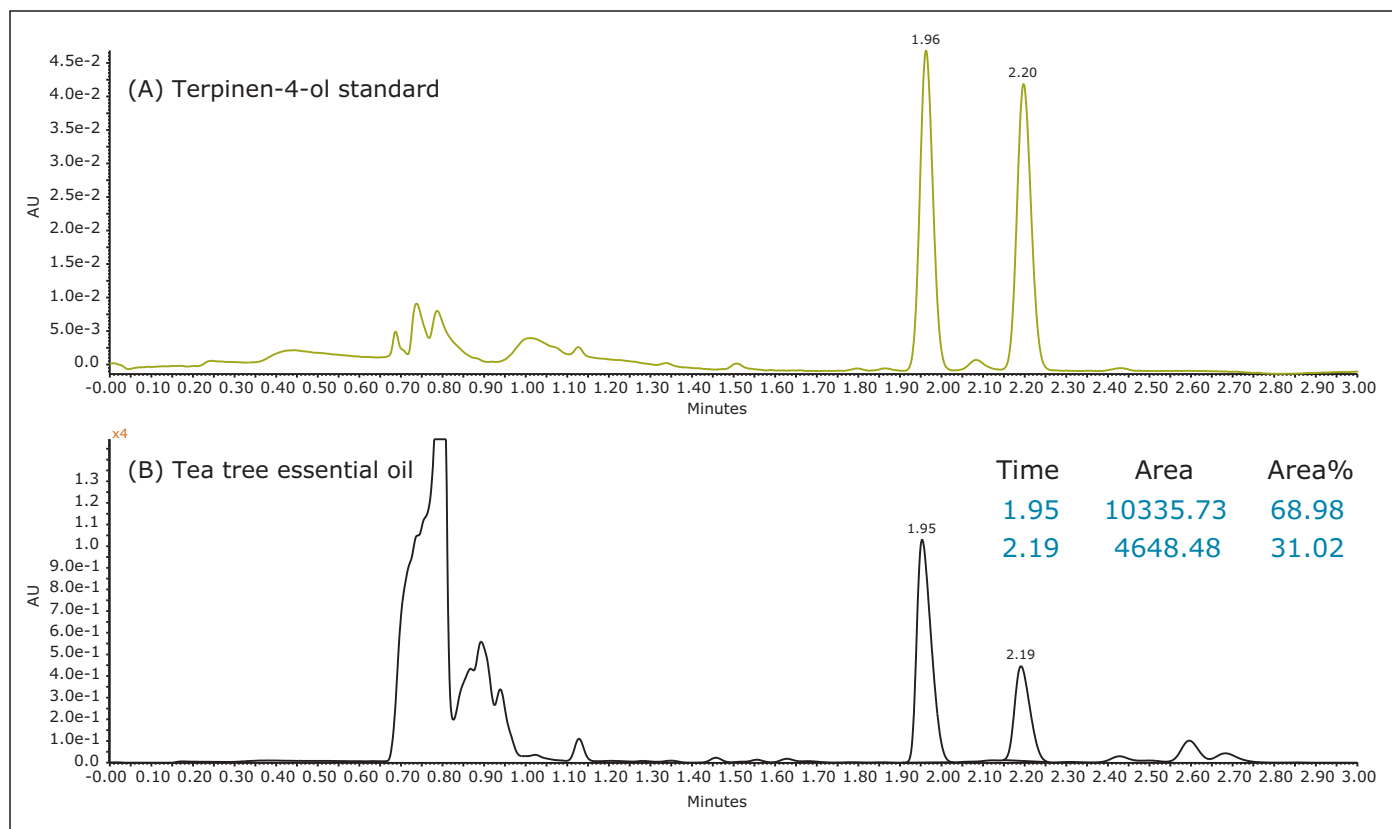


*Figure 4. UPC$^2$-UV chromatograms of (A) Terpinen-4-ol standard and (B) Tea Tree essential oil on an ACQUITY UPC$^2$ Trefoil AMY1 column. An isocratic method with 5% isopropanol was used. The flow rate was 1.0 mL/min.*

Nerolidol, which can be found in the neroli essential oil derived from the bitter orange plant, is a sesquiterpene with a pleasant woody odor reminiscent of fresh bark. The nerolidol molecule (Figure 1) contains a chiral center and a double bond generating cis/trans isomerism, resulting in four possible stereoisomers in a mixture. Figure 5 shows the simultaneous separation of all four nerolidol isomers on an ACQUITY UPC$^2$ Trefoil AMY1 column in less than 3 min. Figure 5B is the selected ion recording (SIR) for the isomeric mixture at *m/z* 205.2, corresponding to the [(M+H)-H$_2$O]$^+$ of nerolidol. The observation of the base peak of nerolidol resulting from the loss of water is consistent with other reports.[7]
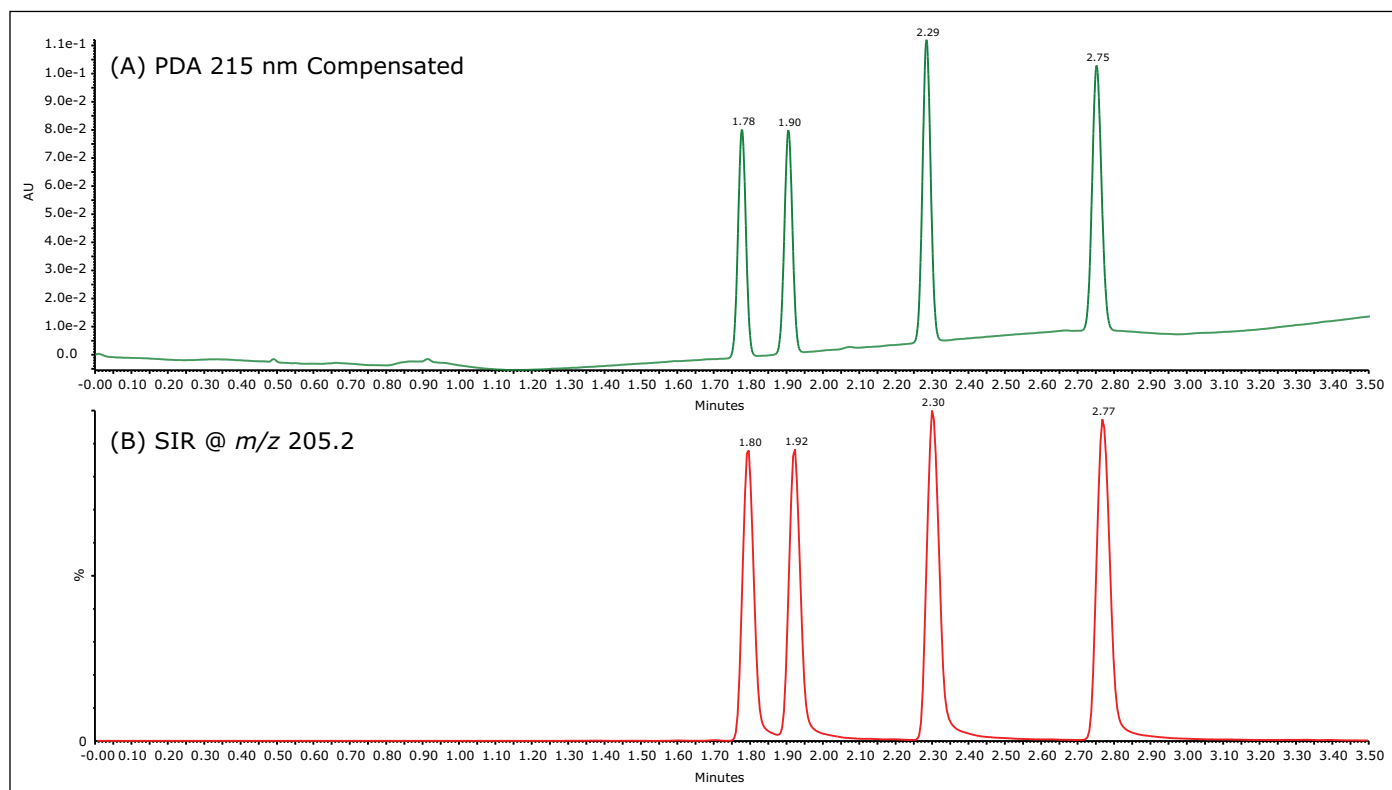


*Figure 5. UPC$^2$ chromatograms of a nerolidol standard separated on an ACQUITY UPC$^2$ Trefoil AMY1 Column: (A) UV at 215 nm with a compensation wavelength of 260-310 nm; and (B) SIR at m/z 205.2. The flow rate was 1.5 mL/min. A gradient of 2-7% isopropanol in 3.5 min was used.*

## CONCLUSIONS

In this application note, we have demonstrated the successful chiral separations of fragrance compounds on ACQUITY UPC$^2$ Trefoil AMY1 and CEL1 Columns using an ACQUITY UPC$^2$ System. The low system volume and extra-column volume of the UPC$^2$, combined with the reduced particle size of the ACQUITY UPC$^2$ Trefoil AMY1 and CEL1 Columns, enable superior, faster, and more efficient separations compared with traditional SFC and GC. The demonstrated analysis times range from 2 to 3 minutes, significantly shorter than the 15-50 minute analysis time typical for chiral GC,[3] allows for a fast authentication of the natural sources of essential oils. In all cases, the closely eluting isomers were baseline resolved. For the essential oil analysis, the oil samples were diluted and directly injected onto an ACQUITY UPC$^2$ System without tedious sample preparation. Furthermore, the inherent compatibility between UPC$^2$ and MS offered an unambiguous identification of the target analytes in a complex sample matrix. The high efficiency, short analysis time, and simple sample workup demonstrated in this study should be welcomed by industries where chiral analyses of fragrance compounds are routinely performed.

## References

1. Leffingwell J, Leffingwell D. Chiral chemistry in flavours and fragrances. *Specialty Chemicals Magazine* 2010 March; 30-33.

2. Ravid U, Putievsky E, Katzir I, Weinstein V, Ikan R. Chiral GC analysis of (S)(+)- and (R)-carvone with high enantiomeric purity in caraway, dill and spearmint oils. *Flavour and Fragrance Journal* 1992; 7, 5, 289-292.

3. Konig W, Hochmuth D. Enantioselective Gas Chromatography in Flavor and Fragrance Analysis: Strategies for the Identification of Plant Volatiles. *Journal of Chromatographic Science* 2004; 44, 423-429.

4. Uzi R, Putievsky E, Katzir I, Raphael I. Determination of the enantiomeric composition of terpinen-4-ol in essential oils using a permethylated β-cyclodextrin coated chiral capillary column. *Flavour and Fragance Journal* 1992; 7, 1, 49-52.

5. Yaguchi, Y. Enantiomer separation of fragrance compounds by supercritical fluid chromatography. Seibutsu Kogaku Kaishi 2010; 88, 10 520-524.

6. Sugimoto D, Yaguchi Y, Kasuga H, Okajima S, Emura M. Preparation of chiral flavor chemicals using enatioselective supercritical fluid carbon dioxide chromatography. Recent Highlights in Flavor Chemistry and Biology, Proceedings of the 8th Wartburg Symposium on Flavor Chemistry and Biology. Eisenach, Germany, February 27-March 2, 2007, 340-344.

7. Martin D, Gershenzon J, Bohlmann J. Induction of volatile terpene biosynthesis and diurnal emission by methyl jasmonate. *Plant Physiology* 2003; 132, 3, 1586-1589.

## Waters

THE SCIENCE OF WHAT'S POSSIBLE.®

# CHAPTER 4
### MS IMAGING AND AMBIENT IONIZATION-MS FOR METABOLOMICS & LIPIDOMICS
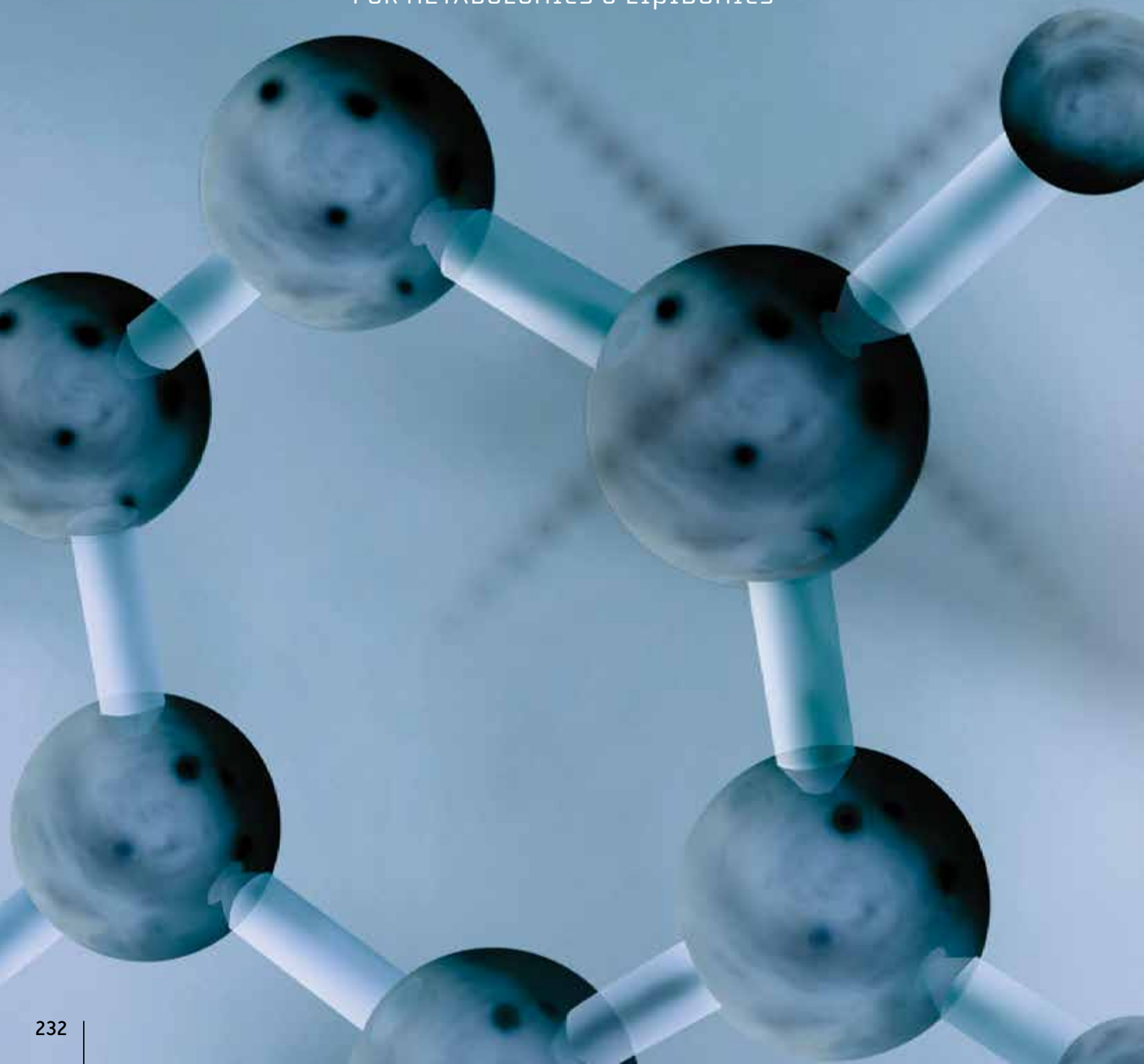
# MS IMAGING AND AMBIENT IONIZATION-MS FOR METABOLOMICS AND LIPIDOMICS

There is a growing interest in applying surface-based desorption ionization (DI) techniques for metabolomics and lipidomics. In DI, the ionization process begins by irradiating a defined spot on the solid-state sample using a focused, excitatory beam such as a laser or charged solvent droplets. Upon impact, the sample's surface releases a vapor of ionized molecules that can be directed into a mass spectrometer. Alternatively, acoustic or thermal desorption could initiate the ionization process. The combined use of ion mobility after DI offers the unique opportunity to separate most of the mass interferences deriving from matrix, peptides and isobaric species, thus improving the overall sensitivity, signal-to-noise, and specificity of analysis. The two main DI-MS approaches for metabolomics and lipidomics are MS imaging and ambient ionization MS.

MS Imaging can provide information about the spatial distribution of metabolites and lipids on a sample (e.g., animal and plant tissues, entire insect body, etc.), generating topographic maps of the molecular composition. This level of information is often missed during traditional sample-preparation and extraction protocols for metabolomics and lipidomics. Various DI technologies, combined with ion mobility-MS, have been used for MS imaging in metabolomics and lipidomics, including matrix-assisted laser DI (MALDI) and desorption electrospray ionization (DESI).

Ambient ionization MS allows for real-time, rapid, in situ screening of analytes in biological samples. The main DI technologies that can be applied to real-time-MS metabolomics and lipidomics are rapid evaporative ionization mass spectrometry (REIMS), atmospheric solids analysis probe (ASAP), and direct-analysis in real time (DART).

- Spatial localization of metabolites and lipids with ion mobility-MS coupled with MALDI or DESI
- Unique capabilities for post-ionization separation of isobaric species and matrix interferences using ion mobility-MS (HDMS)
- High Performance, accurate Mass MALDI MS-MS
- Real-time, rapid, in situ screening of metabolites and lipids from biological samples

Waters
THE SCIENCE OF WHAT'S POSSIBLE.®
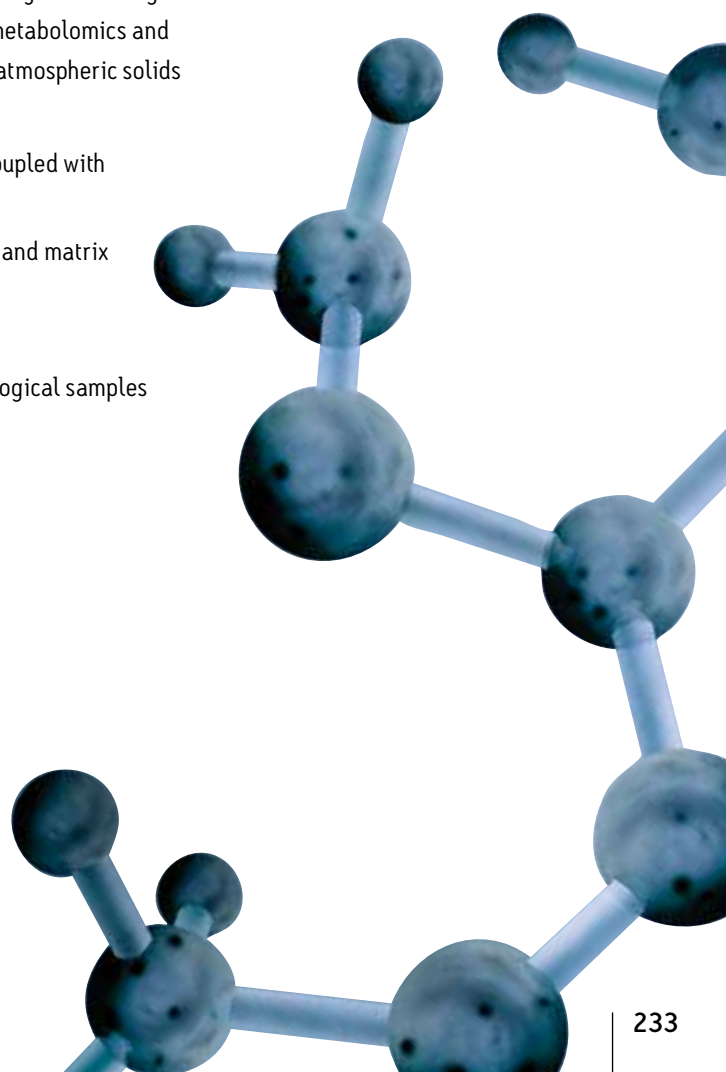
# Biomarker Discovery Directly from Tissue Xenograph Using High Definition Imaging MALDI Combined with Multivariate Analysis

Emmanuelle Claude and Mark Towers
Waters Corporation, Manchester, UK

## APPLICATION BENEFITS

New features have been implemented into Waters High Definition Imaging (HDI) 1.2 Software to allow multivariate data analysis, such as principal component analysis (PCA) and partial least squares discriminant (PLS-DA). These capabilities, integrated to the workflow, reduce the dimensionality of data and ease the comparison of multiple datasets. In this work, we demonstrate their use with MALDI imaging in studying the changes over time in the proteome on xenograph tissues sections after administration of an anti-cancer drug.

## WATERS SOLUTIONS

MALDI SYNAPT® G2 HDMS™

High Definition Imaging (HDI) 1.2 Software

MassLynx® Software

## KEY WORDS

Proteomics, multivariate analysis, principal component analysis (PCA), partial least squares discriminant (PLS-DA), MALDI imaging

## INTRODUCTION

In biomedical research, proteomics has become an indispensable tool for the discovery of candidate biomarkers and drugs. Moreover, mass spectrometry imaging (MSI) enables researchers to determine the spatial distribution of proteins and peptides directly from a tissue section, without radioisotope labeling or tagging.

However, a MALDI imaging experiment can readily generate a vast amount of data, depending on tissue size and acquisition mass range. Both of these factors relate to the number of ion detections, number of pixels recorded, and the possible addition of ion mobility separation to improve the specificity of the analysis. Moreover, in the case of comparing multiple samples, such as different states of a disease or drug time-course experiment, data review complexity is multiplied, amounting in tedious and time-consuming data review to identify molecular species changes.
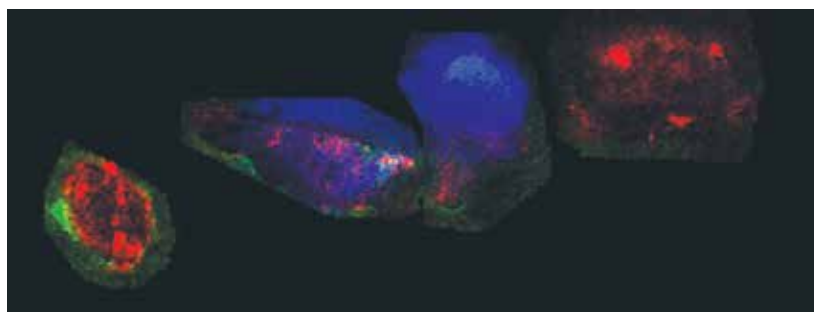


Figure 1. Overlay of three tryptic peptide ion images from xenograph tissue sections.

## EXPERIMENTAL

### Conditions

#### Data acquisition

| | |
|---|---|
| System: | MALDI SYNAPT G2 HDMS, positive mode |
| Mass range: | 600-3,000 Da |
| Laser: | 1 KHz solid state Nd:YAG laser (λ = 355 nm) |
| Spatial resolution: | 150 μm (lateral) |

#### Data management

The obtained data were processed and visualised using HDI MALDI 1.2 Software. Regions of interest (ROIs) information were analysed using EZInfo (Umetrics Software). MassLynx Software was also utilized.

### Sample description

Four rats were injected subcutaneously with a cancer cell line to allow the growth of tumor mass, called a xenograph. The animals were administrated with the anti-cancer drug Dasanitib at a concentration of 30 mg/kg and scarified at different time points (control, 1, 3, and 6 hours). After tumour excision, frozen tissue sections from each animal were thaw-mounted onto a single glass slide. Tissue samples were washed with different baths of cold ethanol and chloroform. *In situ* trypsin digestion was performed by spraying a solution of trypsin directly onto the tissue and incubating overnight in a humidity chamber at 37 °C.

Post-digestion, several layers of matrix, α-cyano-4-hydroxicinnamic acid (CHCA) containing aniline in acetonitrile/water/TFA (1:1:0,1), were also sprayed directly onto the tissue samples. A single jpeg image of the four tissue sections mounted on the glass slide was taken using a flatbed scanner. Using High Definition Imaging (HDI) MALDI software, the visual image was co-registered, and areas to be imaged by MSI were defined. This allowed the overlay of the MS information and the visual image later in the analysis (Figure 2A).

## RESULTS AND DISCUSSION

Figure 2A represents the processed data loaded in the Analysis tab of HDI Software. It is possible to define one or several regions of interest (ROIs) on the four tissue sections as shown in Figure 2B. The ROIs can be drawn using the free draw tool, eclipse (or round), and rectangle (square) options.

By clicking on the Umetrics icon as shown in Figure 2B, the intensities for each entry (*m/z*, dt) present in the processed data are averaged and TIC normalized across the pixels present within each defined ROI. The output is reported in a csv file (Figure 2C). EZInfo can be launched directly from MassLynx Software by clicking on the Extended Statistics icon (Figure 2D). The output txt file is loaded in EZinfo where the different groups can be specified, as seen in Figure 2D).
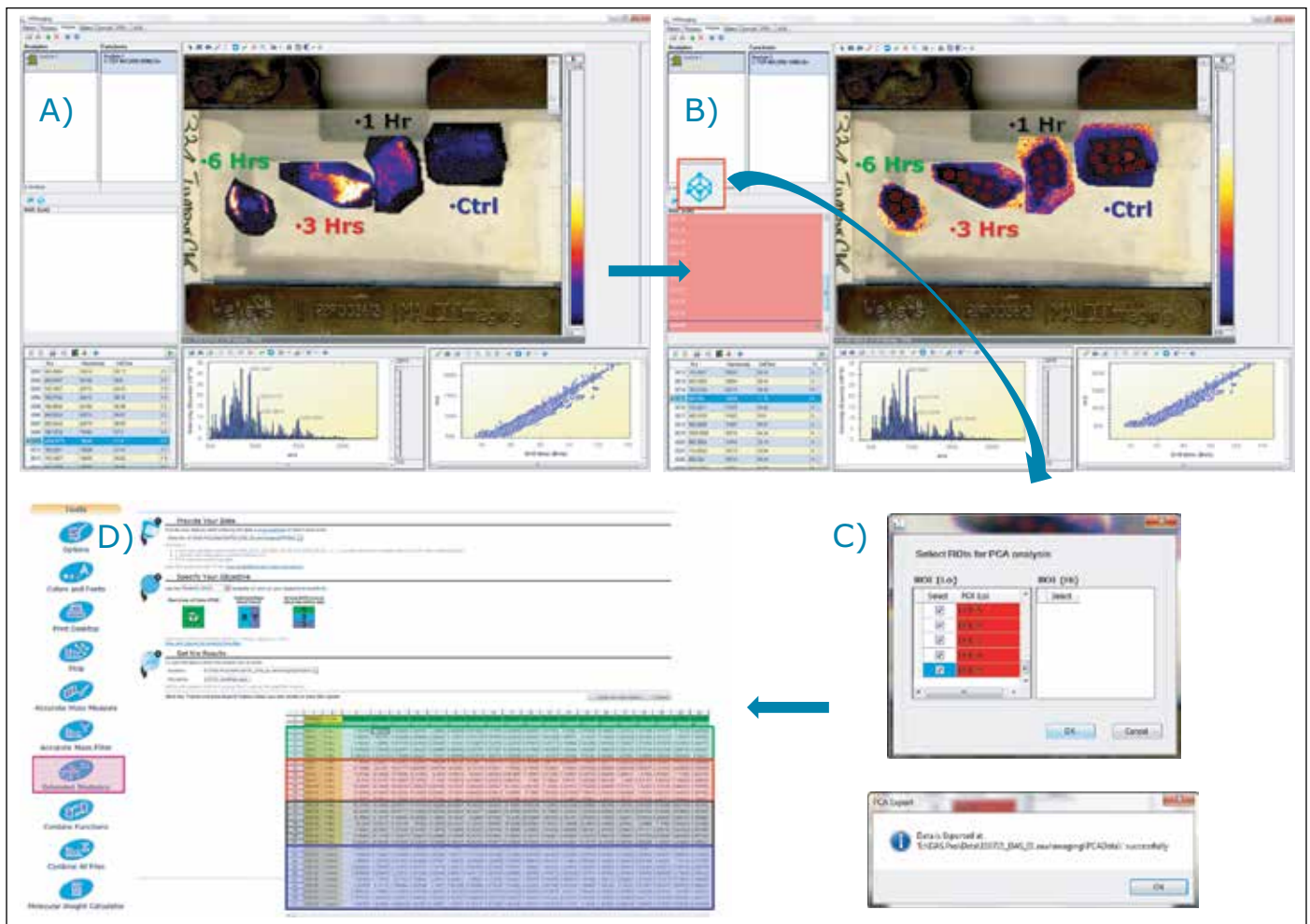


Figure 2. Workflow with A) MALDI imaging processed data loaded in HDI; B) Multiple ROIs drawn for each tissue section; C) Average normalized intensities calculated; D) View of the csv matrix where intensities are reported for each entry (m/z, dt) and ROI - EZinfo is launched directly from MassLynx Software.

## Principal component analysis (PCA) of the MALDI imaging data

Following on from the data matrix loaded in EZInfo, as shown in Figure 2D, PCA is performed and the result scores plot displayed in Figure 3A. Each dot represents an ROI observation, which has been color coded to one of the four groups (*i.e.*, one of the tissue section). Scores values for each group clustered well together.

A second data processing step was performed within EZInfo to obtain the loadings data for the analysis as demonstrated in Figure 3B. Each loading dot, representing a (*m/z*, dt) entry, can be selected and a list can be generated comprising peak IDs of each of the selected variables with its associated PCA coordinates (Figure 3C). This list can be imported back into the HDI Software following the route shown in Figure 3D. The loadings plot is recreated in HDI Software (Figure 3E) and the dataset queried to highlight ion images associated with variables from the loadings distribution.
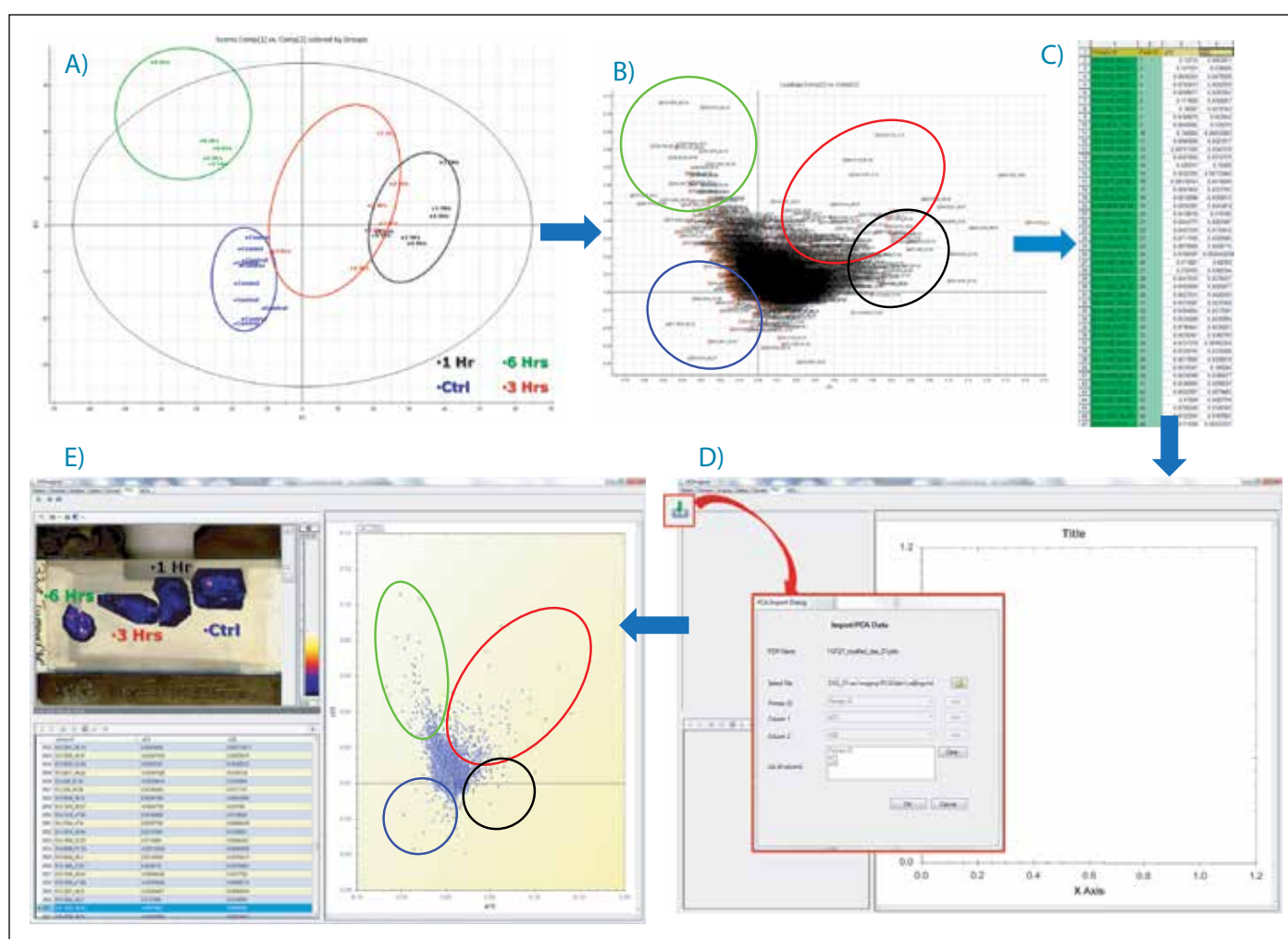


Figure 3. Workflow where A) PCA scores distribution is shown, and B) the resultant loadings distribution is displayed and the all variables are selected to generate the table in C). D) Route where the table is imported back in HDI Software. E) Loadings plot loaded in HDI Software with corresponded ion images displayed.

The latter is illustrated in Figure 4, where ion images of specific tryptic peptides are likely to distinguish the different conditions from the PCA experiments. Figure 4A shows the selection in the loadings distribution of variable (*m/z*_dt) 871.5_62, which is dominant in the control condition compared to the other tissue section images. Figure 4B shows the selection of (*m/z*_dt) 1144.6_74 that is more abundant in the 1 hour condition. Figure 4C shows the selection of (*m/z*_dt) 1033.6_72 that is more abundant in the 3 hours condition and Figure 4D shows the selection of (*m/z*_dt) 1027.54_70 that is more abundant in the 6 hours condition.
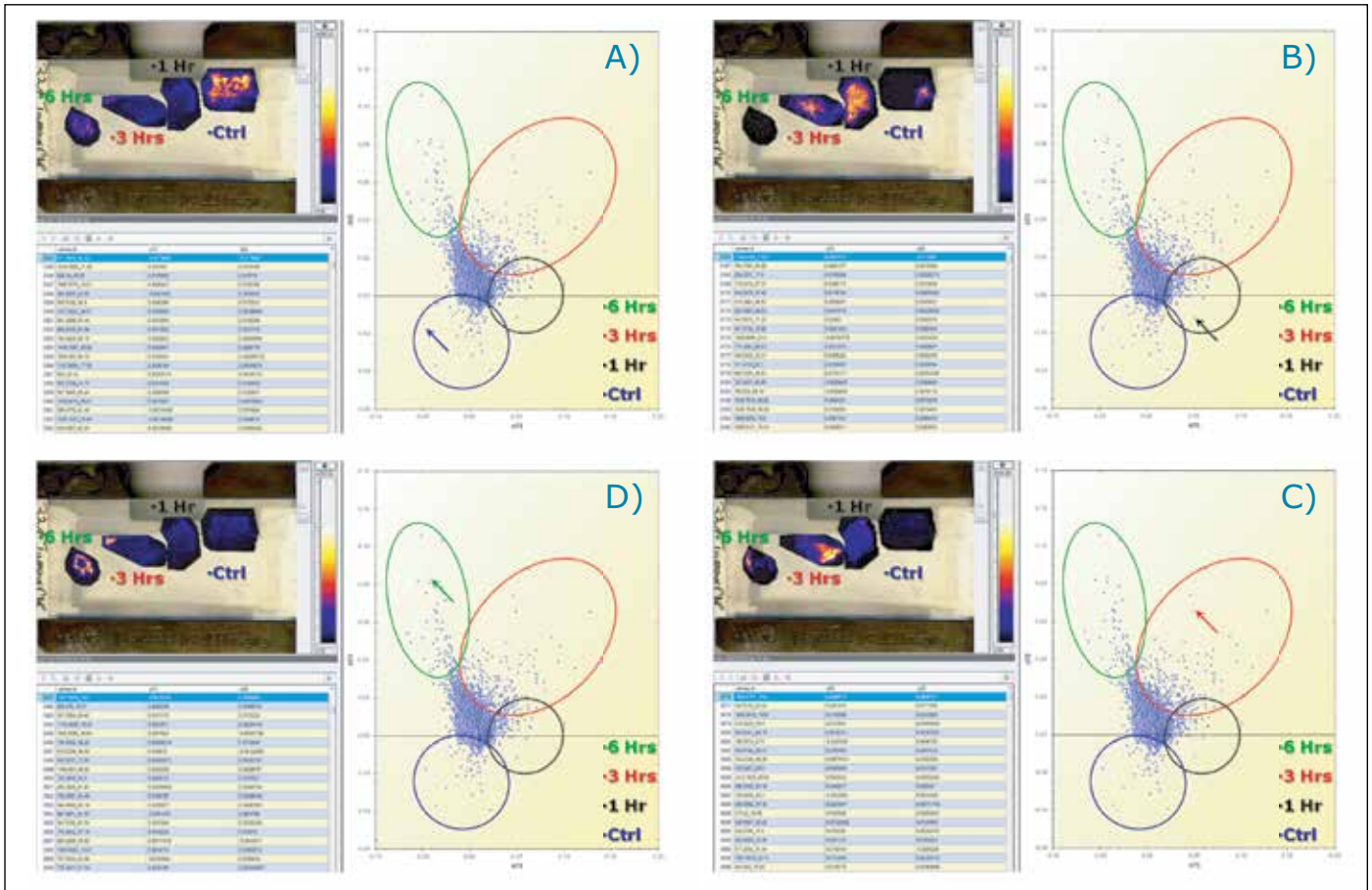


Figure 4. Querying of the PCA loadings distributions to display ion images of the analytes that differentiate the groups. Selection of tryptic peptides A) (m/z_dt) 871.5_62 for the control condition; B) (m/z_dt) 1144.6_74 for the 1 hr condition; C) (m/z_dt) 1033.6_72 for the 3 hrs; and D) (m/z_dt) 1027.54_70 for the 6 hrs condition.

## OPLS/OPLS-DA of the MALDI imaging data

From the data matrix of ($m/z$_dt) analyte values, intensities, and group definitions shown in Figure 2D, it is possible to select only two groups, such as group 1 and 3 hours (Figure 5A), which were the two groups that were the least clearly differentiated in the unsupervised analysis.

An OPLS/OPLS-DA distribution was generated (Figure 5B) with its S-plot (Figure 5C) that illustrates confidence of change on the Y-axis and magnitude of change on the X-axis. As for the unsupervised analysis, the loadings data can be imported back into the HDI Software where analyte/ion images associations can be viewed (Figure 5D) and queried (Figure 6).
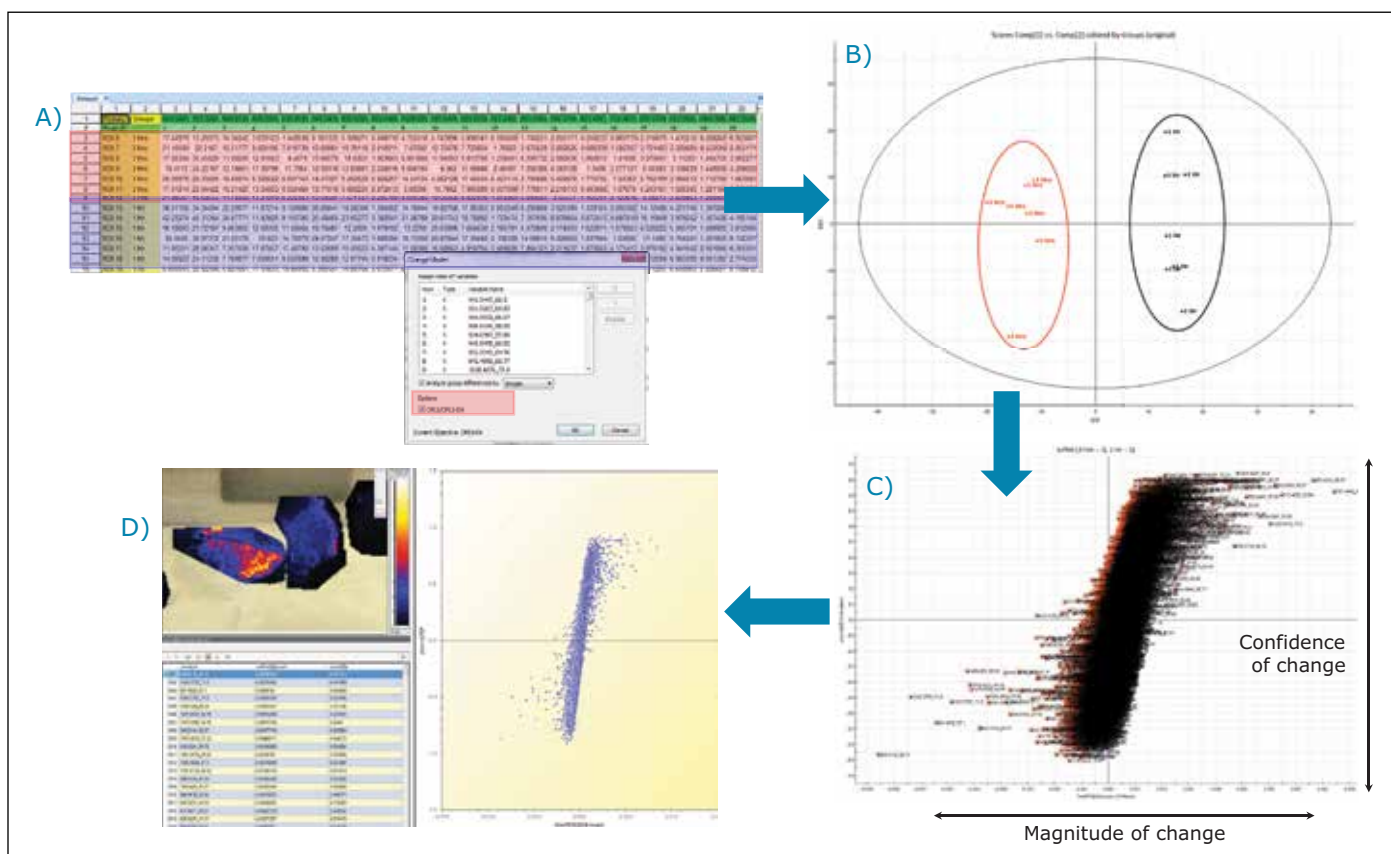


*Figure 5. Workflow where A) Amended data matrix with two groups defined; B) OPLS/OPLS-DA scores plot is shown; C) the resultant S-plot is displayed and the all variables are selected to generated the table; D) Loadings plot loaded in HDI Software with corresponded ion images displayed.*
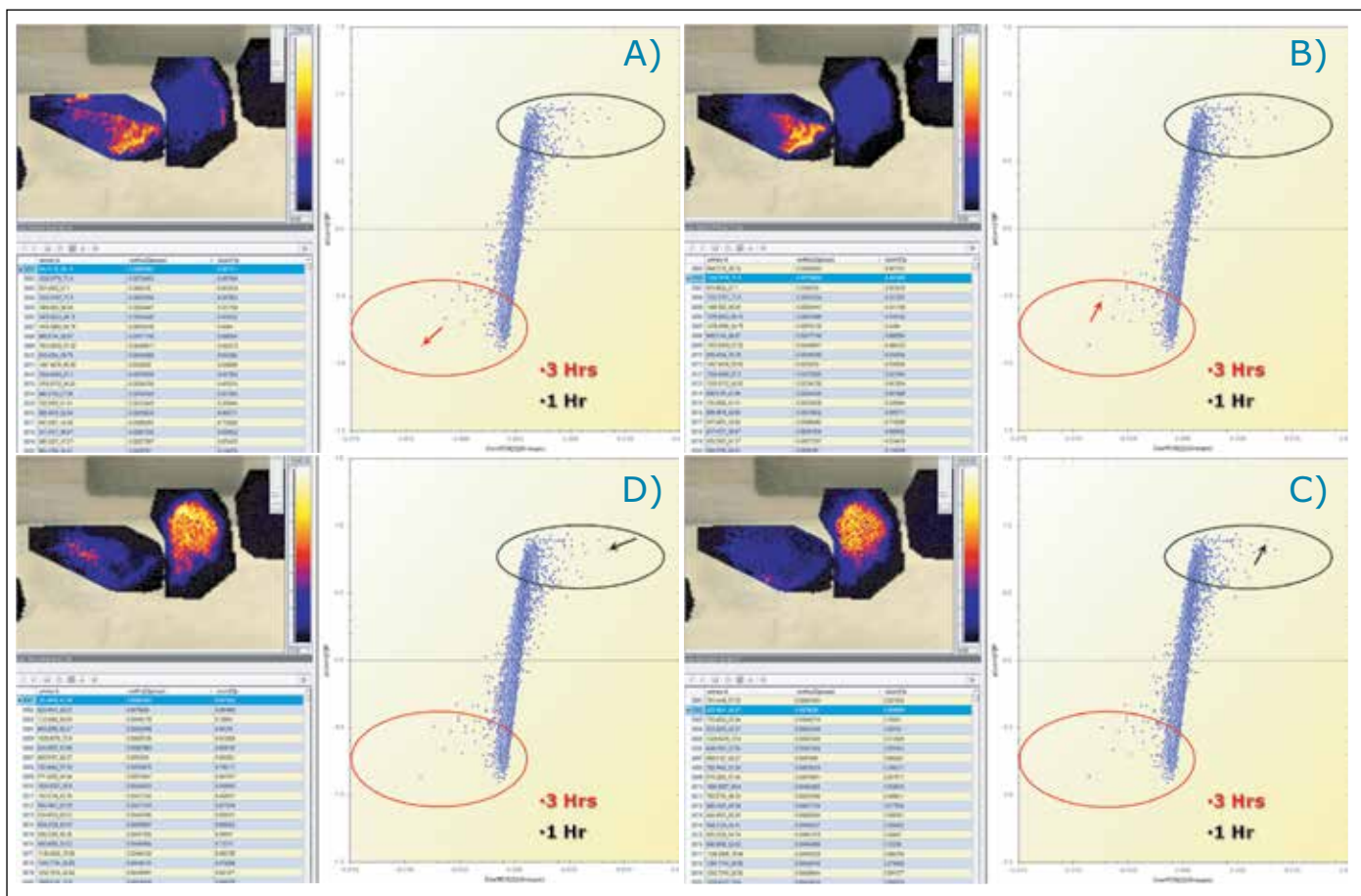
Figure 6. Querying of the OPLS/OPLS-DA S-plot to display ion images of the analytes that differentiate the groups. Selection of tryptic peptides more expressed in the 3 hr tissue section A) (m/z_dt) 944.51_68 and B) (m/z_dt) 1032.58_72. Selection of tryptic peptides more expressed in the 1 hr tissue section C) (m/z_dt) 823.45_60 and D) (m/z_dt) 781.45_57.

## CONCLUSIONS

- High Definition Imaging (HDI) Software allows supervised and unsupervised multivarariant analysis on complex multidimensional imaging datasets.

- Multiple statistical analyses can be carried out on the same dataset, including PCA, PLS-DA, and OPLS/OPLS-DA.

- Full integration of the multivarariant analysis results in the HDI Software linked to ions images.

- The interrogation of the data is therefore greatly speeded up and simplified compared to manual mining of the data.

## Waters
### THE SCIENCE OF WHAT'S POSSIBLE.®

**Waters Corporation**
34 Maple Street
Milford, MA 01757 U.S.A.
T: 1 508 478 2000
F: 1 508 872 1990
www.waters.com

# Improved MALDI Imaging Quality and Speed Using the MALDI SYNAPT G2-S*i* HDMS

## SUMMARY

A new laser with an improved laser focus profile has been incorporated into the MALDI SYNAPT® G2-S*i* HDMS™ System, resulting in enhanced ion imaging quality and higher sensitivity for imaging with sub-50-micron pixel sizes. The instrument control has also been optimized so that, combined with the higher laser repetition rates, data is acquired faster.

## BACKGROUND

The use of solid-state lasers such as diode-pumped ND:YAG lasers has been critical in the development of MALDI imaging applications, providing higher repetition rates than could be achieved with nitrogen lasers. The MALDI SYNAPT G2-S*i* laser provides higher repetition rates, up to 2.5 kHz, increasing analytical speed. It also has a longer laser life-span, of typically several billion shots.

For high spatial resolution imaging, the main limitation is defined by the diameter of the laser focus, although oversampling can partially overcome this constraint. The improved beam profile of the MALDI SYNAPT G2-S*i* laser allows a tight focus to be produced.

**With a new laser, the MALDI SYNAPT G2-S*i* HDMS offers improved MALDI imaging capabilities, with faster analysis of tissue sections and higher data quality for high spatial resolution experiments.**
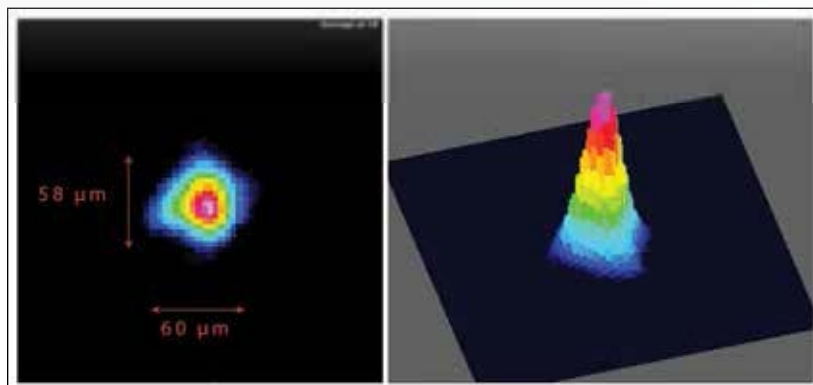


*Figure 1. The focused laser beam profile of the new MALDI SYNAPT G2-Si laser.*

## THE SOLUTION

The MALDI SYNAPT G2-S*i* HDMS Mass Spectrometer introduces a new laser system that offers several enhancements, including:

- Faster maximum laser repetition rate, maximizing analytical speed

- Variable laser repetition rate control, from 100 Hz to 2.5 kHz

- Sharper and rounder beam profile with low eccentricity

- Increase in data quality for high spatially resolved MALDI imaging experiments

- Improved synchronization between the laser firing and the stage movement results in significantly shorter acquisition times

Waters
THE SCIENCE OF WHAT'S POSSIBLE.®

Figure 1 illustrates the focus profile of the laser included with the MALDI SYNAPT G2-S*i* HDMS. It is circle-shaped with a minimal degree of eccentricity. The profile has an approximate diameter of 30 microns at FWHM, which is significantly smaller than the previous laser. The laser fluence, which also affects the ion desorption area, can be controlled using the built-in variable neutral density filter.

MALDI imaging experiments were carried out using a rat whole body tissue section comparing the quality of the data obtained using the previous laser system and the new laser system (same sample, sample preparation, and mass spectrometer).

The sample target plate was programmed to move in 15, 20, and 50 micron pixel sizes (pitches) while maintaining the minimum laser focus diameter possible for both lasers. The total image summed spectra for each experiment are displayed in Figure 2. In all three cases, the background noise is clearly less abundant, while the lipid peak intensities are higher with the MALDI SYNAPT G2-S*i* laser, especially for the 15 and 20 micron pixel sizes.

Figure 3 shows the overlay of three lipid species that are distributed in very specific anatomical regions of the cerebellum rat brain. The red ion image represents a lipid that is more concentrated in the grey matter of the cerebellum, whereas the blue ion image shows localization of the sample lipid, as an example, in the white matter. The green ion image represents a lipid more specific to the pia matter. It is noticeable that the white matter layer and the pia matter layer are distinguished although their cross sections are less than 100-200 microns.
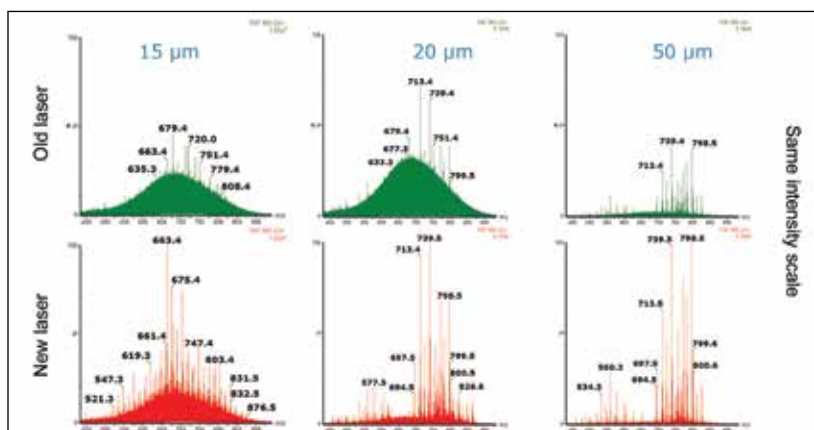


Figure 2. Comparing the summed spectra quality obtained for MALDI imaging experiments carried out with pixel sizes of 15, 20, and 50 microns. Overall, the background noise is lower, and the intensity of lipid species peaks higher with the MALDI SYNAPT G2-Si laser, particularly at spatial resolution sub-50-microns.
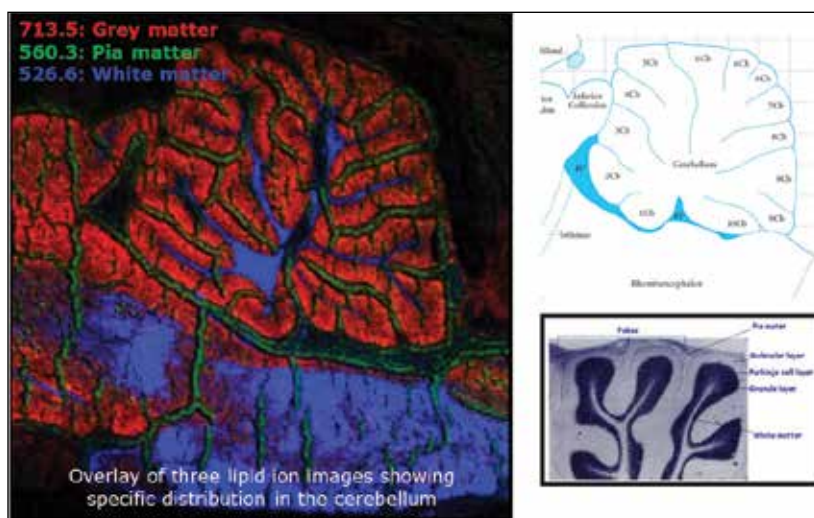


Figure 3. Overlay of three lipid ion images that are distributed to very explicit parts of rat cerebellum. Lipid m/z 713.5 is specific to the grey matter, lipid m/z 560.3 to the pia and lipid m/z 526.6 to the white matter.

## SUMMARY

For high spatial resolution MALDI imaging experiments, the MALDI SYNAPT G2-S*i* HDMS can acquire both faster and with greater signal to noise. The enhancements are directly attributed to the improved laser focusing and pulse synchronization.

## Waters
### THE SCIENCE OF WHAT'S POSSIBLE.®

**Waters Corporation**
34 Maple Street
Milford, MA 01757 U.S.A.
T: 1 508 478 2000
F: 1 508 872 1990
www.waters.com

Waters
THE SCIENCE OF WHAT'S POSSIBLE.®

# Data Independent MALDI Imaging HDMS$^E$ for Visualization and Identification of Lipids Directly from a Single Tissue Section

Emmanuelle Claude, Mark Towers, and Kieran Neeson
Waters Corporation, Manchester, UK

## APPLICATION BENEFITS

■ Identification of lipids based on high mass accuracy, fragment ion information, and spatial correlation — all obtained from a single experiment.

■ Parallel fragmentation approach for a MALDI imaging experiment allowing structural identification of all detectable lipid species within the tissue section sample.

■ Information obtained from valuable tissue sections is maximized.

■ Simple and generic acquisition methodology reduces the need for designing targeted MS/MS experiments.

■ Untargeted data sets provide an information-rich, digital archive of the sample to enable detection and identification of new species in the future, that is, acquire data first and ask (biological) relevant questions regarding the data later.

## WATERS SOLUTIONS

MALDI Imaging HDMSE

MALDI SYNAPT™ G2-S HDMS™

## KEY WORDS

MALDI imaging, high definition imaging, HDI, identification, lipids, HDMS$^E$

## INTRODUCTION

Recent advances in mass spectrometry (MS) have enabled the simultaneous analysis of a wide range of chemically similar lipids as well as structurally diverse lipid classes, contributing to an increased interest in lipidomics research. However, the spatial localization of lipids within tissue micro-structures is often lost during the process of lipid extraction, as applied in more traditional analysis approaches, resulting in the loss of valuable information pertaining to origin and biological function.

Mass spectrometry imaging (MSI) visualizes the location of lipid species in entire tissue sections. The first step is typically an untargeted MS analysis experiment that enables large numbers of species to be detected and localized simultaneously. Structural identification of the detected lipid species is the next step; however, this can be time-consuming since it consists of manually conducting a series of MS/MS acquisitions on selected components, using either single or consecutive tissue sections.

A data independent MALDI imaging acquisition method called MALDI Imaging High Definition MS$^E$ (HDMS$^E$), presented here, enables detection and identification of lipid species in a single analytical run. This unique methodology provides MS and MS/MS information from detectable ion species within the same experiment, without the need for precursor selection. Post acquisition, precursors and fragments are correlated on the basis of ion mobility (drift time) and spatial distribution to provide highly informative results for every detectable molecular component.

## EXPERIMENTAL

### Sample description

A 30-µm-thick rat whole-body sagittal tissue section was mounted on invisible mending tape that was cut using a scalpel to fit a Waters® MALDI target with double-sided tape. A solution of α-cyano-4-hydroxycinnamic acid (CHCA) matrix at 5 mg/mL was applied evenly to the sample in several coats using a SunCollect (SunChrom GmbH) nebulising spray device.

### Method conditions

### MS conditions

| | |
|---|---|
| Mass spectrometer: | MALDI SYNAPT G2 HDMS |
| Mode: | Positive |
| Mass range: | 100 to 1000 Da |
| Transfer collision voltage: | Low energy function: 4 eV |
| | Elevated energy function: 50 eV |
| Laser: | 1 KHz solid state Nd: YAG laser ( λ = 355 nm) |
| Spatial resolution: | 200 µm (lateral) |

### Data management

The raw data obtained were subsequently processed using High Definition Imaging (HDI) MALDI Software, whereby the low energy and elevated functions were processed and combined in a .txt output file. Only a limited drift time range, specific for lipids, from 100 to 160 mobility bins was considered.

Identification based on mass accuracy and fragmentation information was carried out using SimLipid 3 (PremierBioSoft, US) Software and LipidMaps MS tools (http://www.lipidmaps.org/tools/index.html).

## RESULTS AND DISCUSSION

Ions are generated in the source of the mass spectrometer and passed through the quadrupole (with no precursor selection) in the Triwave® region, as shown in Figure 1. The ions are rapidly separated (in 20 to 50 msec) based on their size, shape, and charge (i.e. ion mobility, or IM) to better enable detection of isobaric and isomeric components.[1] Following IM separation, ions pass through the TRANSFER T-Wave™ collision cell, where, in the first low energy function precursor ion spectra are recorded (intact lipid information), and in the second elevated energy function energy product ion spectra are recorded (lipid fragment information). The two functions can be acquired on the same pixel (to maximize spatial resolution) or consecutive pixels (to maximize sensitivity). The low energy precursors can be associated with the relevant elevated energy fragments since they share similar drift time values from the IM separation, as shown in Figure 1. The datasets are subsequently processed, using the High Definition Imaging (HDI) MALDI Software, where the data from both the low and elevated energy functions are peak detected, aligned, and a two-step correlation based on drift time and position between precursor and fragment ions is performed.
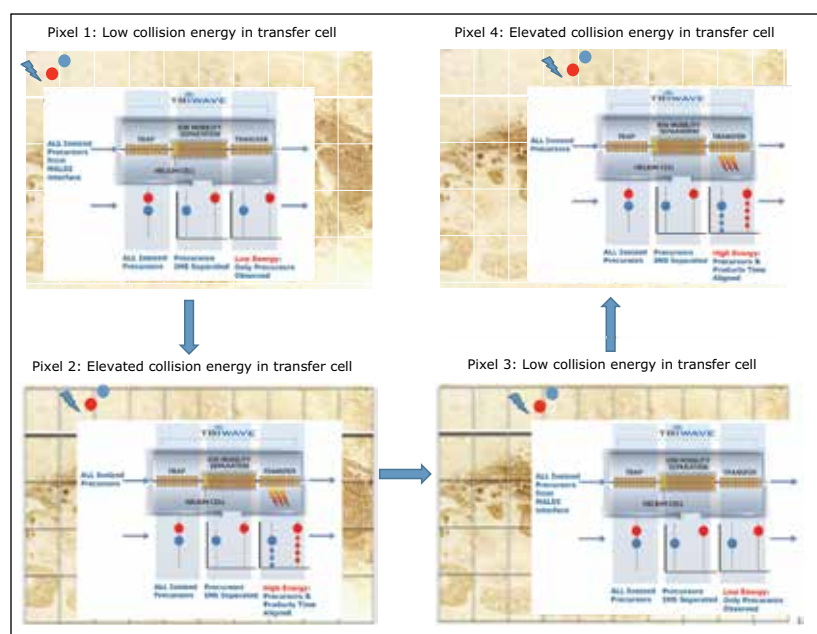


Figure 1. Schematic of a MALDI Imaging HDMS$^E$ experiment.

The user interface of HDI Software and the display of the processed data are shown in Figure 2. In this view, the peak lists, mass spectra, and ion images from the two functions are integrated in an interactive manner. A two-dimensional plot of drift time versus *m/z* plot is also included, to enhance visualization and peak selection (blue dots represent the low energy information and green dots the elevated peak detected ions).
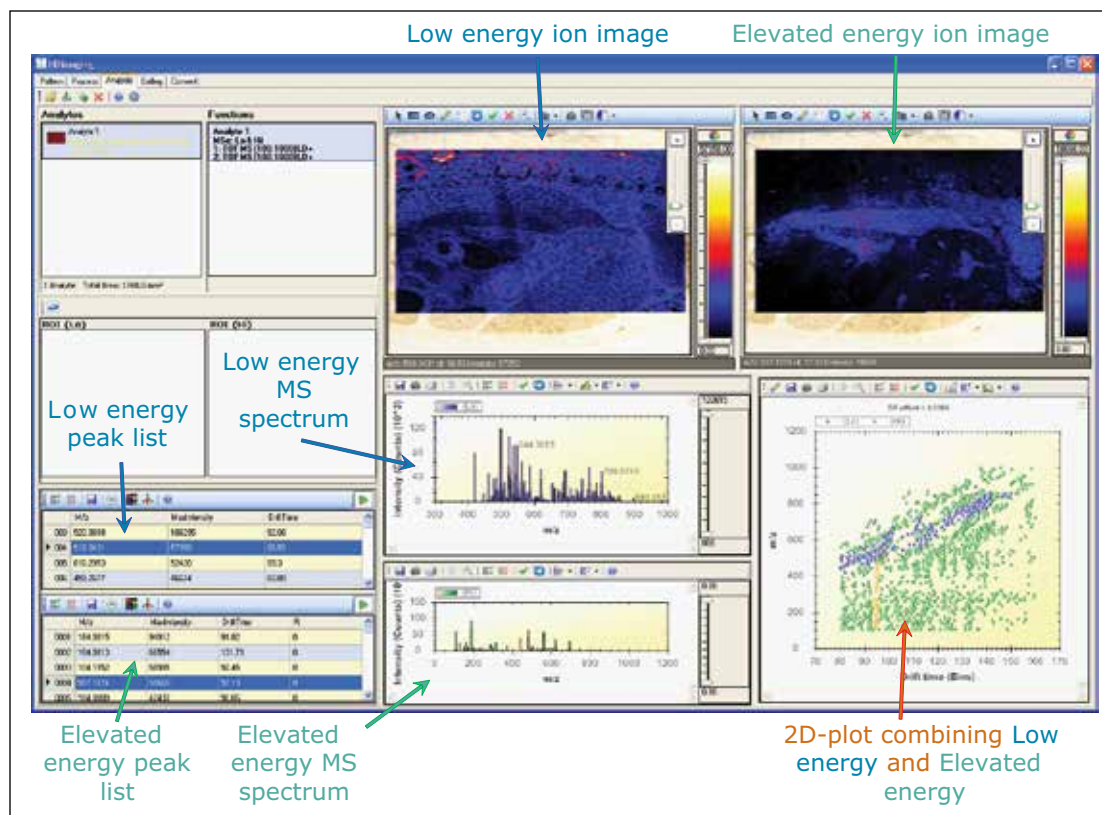


*Figure 2. MALDI Imaging HDMS$^E$ view of the processed data with High Definition Imaging DHI Software.*

The main, distinct advantage of MALDI imaging HDMS$^E$ is its ability to generate precursor ion and fragment ion information for every detectable molecular ion. Initial correlation is achieved on drift time similarity, which is realized within the IM cell. However, one particular challenge with lipid samples is the high number of species within a limited mass and drift range. Fragments that do not belong to the correct precursor can sometimes be assigned incorrectly, but this situation is strongly improved using a second correlation step based on spatial distribution similarity of fragment ions and their precursors.

The workflow of the two-step correlation process for fine association of fragment ions to their originating precursors is illustrated in Figure 3. For example, precursor lipid ion *m/z* 760.6 was selected in the top HDI window. In the *m/z* versus dt plot, the drift time associated fragment ions are displayed as orange dots. After accepting the drift time correlation results, 108 potential fragments were drift time associated to this particular lipid precursor ion, as displayed in the middle window. The next step was the spatial correlation. When a correlation factor from 0.3 to 1.0 was applied, the number of potential fragment ions was reduced to 39, as can be seen in the bottom window.

Drift time correlation

Spatial correlation
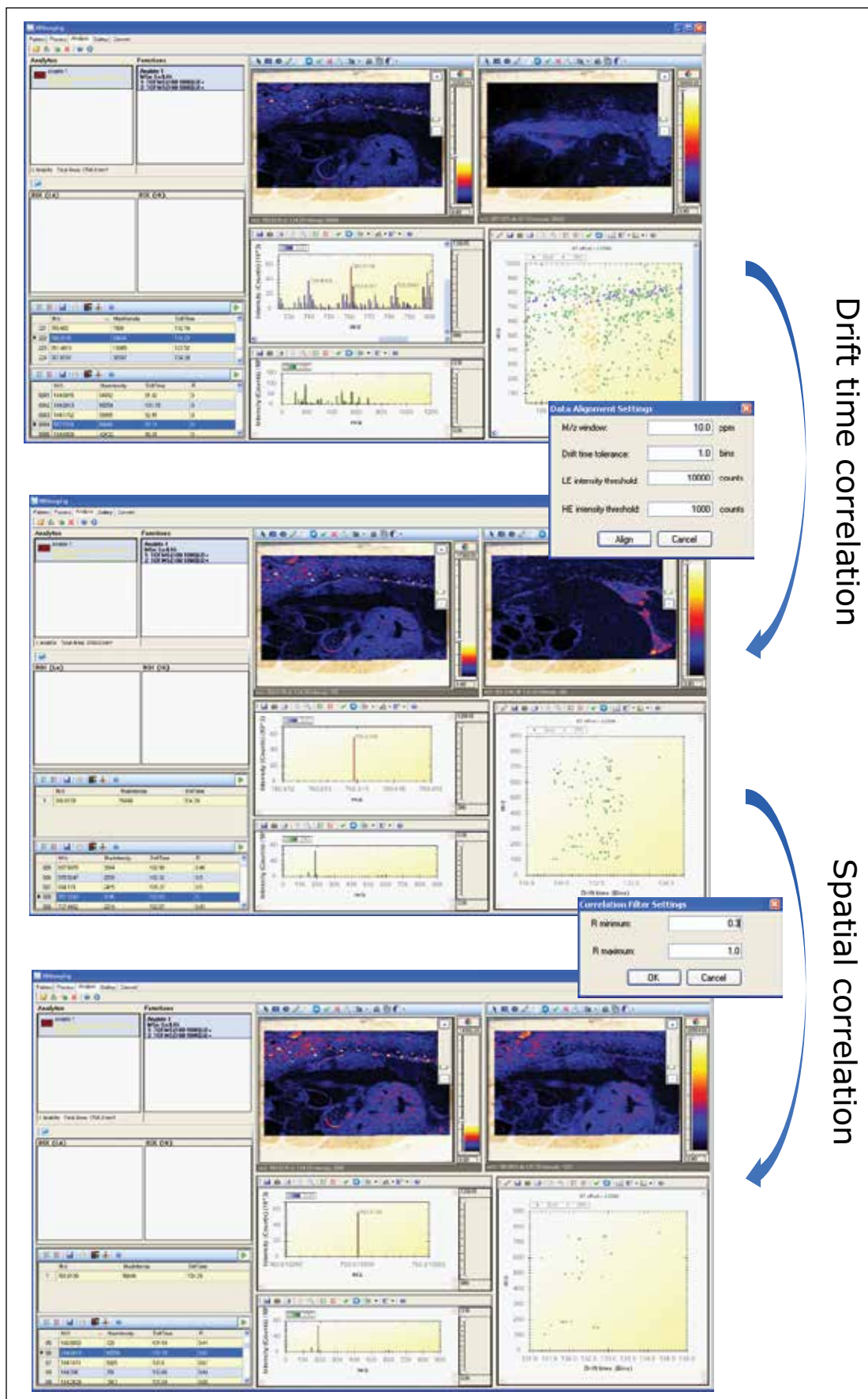
Figure 3. Workflow of the two-step correlation. The top image shows all processed data that were drift time associated with precursor ion m/z 760.0. The middle image shows only fragment ions that were drift time associated to precursor ion m/z 760.6. In the bottom image, spatial correlated fragment ions are displayed (correlation factor 0.5 to 1.0).

The results from the two-step correlation process were imported into SimLipid 3 for lipid identification. Here, parent $m/z$ values were internally lockmass-corrected after identification of lipid $m/z$ 798.5. In this instance, lipid $m/z$ 760.5859 was identified as either PC (16:0/18:1) H$^+$ or PC (18:1/16:0)H$^+$ with fragment ions $m/z$ 478.3301 (M-18:1-H$_2$O) and 496.3404 (M-18:1). The annotated MS/MS spectrum is shown in Figure 4.
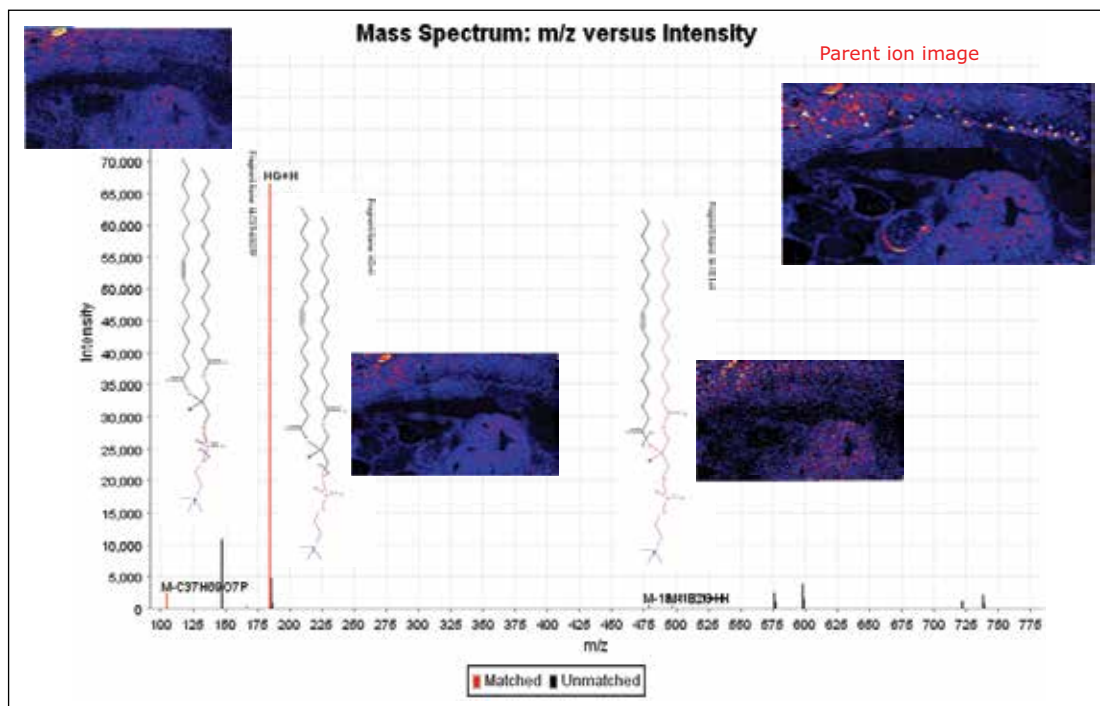


Figure 4. MS/MS spectrum generated from SimLipid 3 with lipid fragment structures and ion images displayed.

Using the information from the two-step correlation and mass accuracy, over 20 lipid species were identified from the single MALDI imaging HDMS[E] experiment and are summarized in Table 1.

| Experimental *m/z* | Theoretical *m/z* | Systematic name | | ppm |
|---|---|---|---|---|
| 713.4543 | 713.4524 | PA (14:0/20:1) or PA(20:1/14:0) | K+ | 2.7 |
| 721.4794 | 721.4803 | PA (20:4/18:2) or PA(18:2/20:4) | H+ | -1.2 |
| 721.4794 | 721.4803 | PA (18:2/18:1) or PA(18:1/18:2) | Na+ | -1.2 |
| 723.4948 | 723.4941 | PA (18:1/18:1) | Na+ | 1.0 |
| 725.5581 | 725.5573 | SM (d34:1) | Na+ | 1.1 |
| 734.571 | 734.57 | PC (13:0/19:0) or PC (19:0/13:0) | H+ | 1.4 |
| 737.4536 | 737.4524 | PA (14:1/22:2) or PA (22:2/14:1) | K+ | 1.6 |
| 739.4694 | 739.4674 | PA (36:2) | K+ | 2.7 |
| 741.483 | 741.4831 | PA (36:1) | K+ | -0.1 |
| 741.5323 | 741.5313 | SM (d18:1/16:0) | K+ | 1.3 |
| 745.4788 | 745.4786 | PG (P-16:0/16:0) | K+ | 0.3 |
| 756.4964 | 756.4946 | PE (12:0/22:1) or PE (22:1/12:0) | K+ | 2.4 |
| 756.4964 | 756.4946 | PC (19:1/12:0) or PC (12:0/19:1) | K+ | 2.4 |
| 758.5706 | 758.57 | PC 34:2 | H+ | 0.8 |
| 760.5859 | 760.5856 | PC (16:0/18:1) or PC (18:1/16:0) | H+ | 0.4 |
| 780.5527 | 780.5543 | PC (16:0/20:5) or PC (20:5/16:0) | H+ | -2.0 |
| 782.5695 | 782.5694 | PE (19:0/20:4) or PE (20:4/19:0) | H+ | 0.1 |
| 796.5285 | 796.5259 | PE-Nme (18:1/18:1) | K+ | 3.3 |
| 798.5415 | 798.5415 | PC (14:0/20:1) or PC (20:1/14:0) | K+ | 0.0 |
| 820.528 | 820.5259 | PE (17:2/22:2) or PE (22:2/17:2) | K+ | 2.6 |
| 824.5598 | 824.5572 | PC:36:2 | K+ | 3.2 |
| 826.573 | 826.5727 | PE (P-20:0/22:6) | Na+ | 0.4 |
| 832.5842 | 832.5832 | PE (20:4/21:0) or PE (21:0/20:4) | Na+ | 1.2 |
| 835.6686 | 835.6669 | SM (d18:1/24:1) or SM (d24:1/18:1) | Na+ | 2.0 |

*Table 1. Lipid identification summary from the MALDI Imaging HDMS[E] experiment following the two-step correlation workflow.*

## CONCLUSIONS

■ A novel, untargeted MALDI imaging experiment called MALDI Imaging HDMS$^E$ is described, which allows precursor and fragment ion information to be collected from a single tissue section MALDI imaging experiment.

■ Association of product ions with its precursor is confidently achieved with a high level of specificity by the described two-step correlation based on drift time and spatial distribution.

■ Lipid species were identified directly from a single, untargeted MALDI imaging experiment while structural identification was made possible from the untargeted dataset using the high mass accuracy of the spectral data and the two-step (drift time and spatial location) correlation process.

### Reference

1. Triwave – More Complete Characterization of Mixtures and Molecules. Waters Corporation. 2012; 720004176en.

## Waters
### THE SCIENCE OF WHAT'S POSSIBLE.®

# Distribution of Biomarkers of Interest in Rat Brain Tissues Using High Definition MALDI Imaging

## GOAL

To illustrate a complete MALDI imaging biomarker discovery workflow through visualization of the effects of various diets on the distribution of Biomarkers of Interest (BOIs) in the rat brain.

## BACKGROUND

MALDI is one of several ionization methods that enables mass spectral analysis directly from the sample surface of fresh, unfixed tissues that are difficult to access. The use of MALDI to image tissue sections is gaining popularity, which promises to deliver a complete and accurate structural picture of the tissue for putative biomarker characterization and drug development. Not only does this technique allow determination of BOIs, but it also shows their localization with no anatomical distortion. With very little tissue manipulation and disruption, MALDI provides an important advantages for drug development and for the understanding of (metabolic) diseases. Undoubtedly, this technique will become very useful for the demonstration of central nervous system effects of diet, cognition, obesity, gut-brain interactions; metabolic diseases such as diabetes, hypertension, Alzheimer's; and inflammatory conditions.

Most metabolomics or lipidomics biomarker discovery studies use biofluids (mainly blood and urine) in order to evaluate the biological process that occurs in tissues and organs that are not easily accessible. In this technology brief, we demonstrate how MALDI imaging allows direct analysis of BOIs in tissues; the workflow is shown in Figure 1. This novel approach could lead to a better understanding of the physiological processes and the pathophysiology of diseases because it allows both discovery and localization of biomarkers.

## Gain a better understanding of physiological processes and pathophysiology of diseases with High Definition MALDI Imaging.
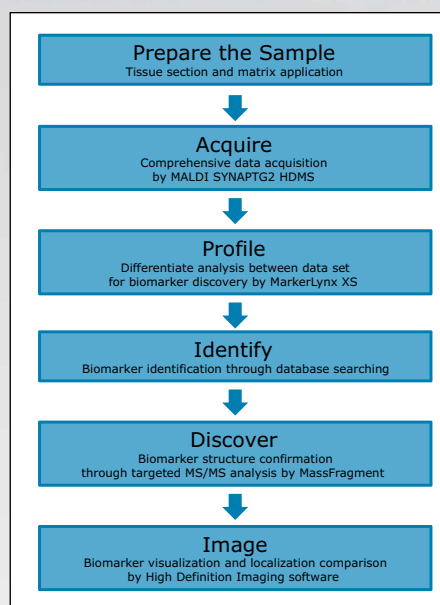


Figure 1. MALDI imaging bioanalysis workflow.

## THE SOLUTION

The left brain hemispheres of two rats kept on different diets were sliced in 10 µm sections using a cryostat. Tissue sections were mounted on microscope slides, frozen, and stored at -80 °C until use. 2,5 dihydroxybenzoic acid (DHB) was used as the matrix and a TM Sprayer was used for the matrix application. MALDI imaging analysis was performed on the Waters® MALDI SYNAPT® G2 HDMS.™ Positive HDMS full scan data were acquired for the mass range of $m/z$ 100 to 1000. The Nd:YAG laser was operated at a firing rate of 200 Hz with a spatial resolution of 75 µm. Waters new High Definition Imaging Software (HDI) was used for the visualization of MALDI imaging data.

Waters
THE SCIENCE OF WHAT'S POSSIBLE.®

After data acquisition, the complex data set was processed by HDI software and analyzed using MarkerLynx™ XS Software. The discovered BOIs were identified by database searching using exact mass molecular ion. The identity of the BOIs was confirmed and validated by performing targeted MS/MS experiments, combined with MassFragment Software to propose assignments for the precursor and fragmentation peaks, and matching them between the data generated from the standards and directly from the tissue sample.

Visualization was performed and compared in HDI using both exact mass and drift time information. Figure 2 shows the MS/MS spectrum of an indentified BIOs, a lipid phosphatidylcholine (PC) (18:1 (9Z)/16:0) or PC (16:0/18:1 (9Z)) observed at $m/z$=760.5859. The structure of the lipid was confirmed by matching the diagnostic fragmentation pattern of the spectrum with the standard one. The average mass error for the six diagnostic ions in the MS/MS spectrum was 0.48 mDa. Figure 3 shows the MALDI image comparison for the same lipid from the brain tissues of the two rats fed by different diets. Very different distributions of the lipid are observed in the two images, indicating that the found lipid biomarker may be of importance.[1] Using this technology, it was possible to highlight several BOIs reflecting the impact of the different diets.



Figure 2. Biomarker structure confirmation through targeted MS/MS analysis. Fragment ions assigned by MassFragment.
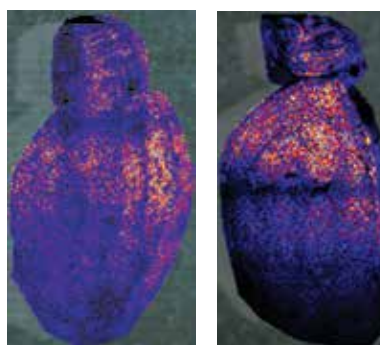


Figure 3. Lipid biomarker MALDI image localization and distribution comparison using High Definition Imaging (HDI) Software.

In high definition MALDI imaging, the combination of MarkerLynx XS and MassFragment software enable discovery, identification, and confirmation of BOIs within tissue samples.

Compared to traditional biomarker discovery analysis (mainly LC-ESI-MS approach), this workflow has the potential to lead to a better understanding of physiological processes, as well as the pathophysiology of diseases, with added information about their spatial distribution in heterogenous, not easily accessible tissue sample.

This approach may be applicable to biomarker discovery and distribution analysis in areas including metabolomics, lipidomics, and proteomics in various application fields such as: metabolic diseases, aging, gut-brain interactions, cognition, and inflammatory diseases associated to the health benefits linked to adequate nutritional interventions.

## SUMMARY

This technology brief demonstrates a complete MALDI imaging biomarker discovery workflow for use in rat brain tissues and its modification by dietary components.

Waters High Definition Imaging (HDI) Software integrates pattern generation, HDMS data processing, and visualization in a single interface.

1. Koizumi S, et al. Imaging Mass Spectrometry Revealed the Production of Lysophosphatidylcholine in the Injured Ischemic Rat Brain, Neuroscience 168 (1):219-25(2010).

## Waters

### THE SCIENCE OF WHAT'S POSSIBLE.®

**Waters Corporation**
34 Maple Street
Milford, MA 01757 U.S.A.
T: 1 508 478 2000
F: 1 508 872 1990
www.waters.com

Waters
THE SCIENCE OF WHAT'S POSSIBLE.®

# Tissue Imaging of Pharmaceuticals by Ion Mobility Mass Spectrometry

Stacey R. Oppenheimer[1], Emmanuelle Claude[2], and Tasneem Bahrainwala[3]
[1]Groton, USA; [2]Waters Corporation, Manchester, UK; [3]Waters Corporation, Beverly, MA, USA

Cyclosporin (CsA) is a drug commonly used as an immunosuppressant that functions as a signal transduction kinase inhibitor; however, CsA has been shown to induce kidney injuries in humans[1]. The objective of this study was to examine the distribution of CsA within renal tissues at varying known doses to induce a certain degree of toxicity.

The traditional approach for MALDI imaging of small molecules, e.g. drug compounds in tissue, utilizes a targeted MS/MS approach followed by mass analysis. This selective strategy provides confirmation of the identity of the drug and enables the molecules to be differentiated from endogenous signals of the same molecular weight. However, some small molecules do not produce satisfactory fragmentation and must therefore be monitored by their intact mass in the MS mode.

Cyclosporin (Figure 1), does not produce intense fragment ions in MS/MS mode and conventional MALDI-TOF MS alone was unable to provide the selectivity required for the analysis.

In this application note, High Definition Mass Spectrometry™ (HDMS™) was used as an alternative approach for imaging CsA distribution. HDMS is based on travelling wave (T-Wave™) technology[2] incorporated into the mass spectrometer. Triwave™ consists of three T-Wave devices, as shown in Figure 2. The first T-Wave (Trap) is used to trap ions during the period when an ion mobility separation (IMS) is being performed in the second T-Wave, thus greatly enhancing the efficiency of the IMS process. The final T-Wave (Transfer) transports the separated ions to the TOF analyzer.
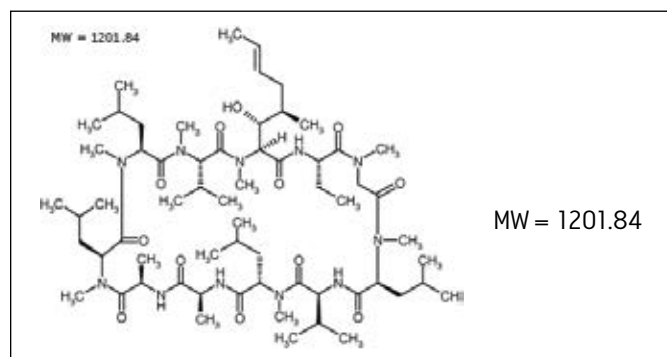


Figure 1. Chemical structure of Cyclosporin (CsA).

MW = 1201.84

## EXPERIMENTAL

Mouse kidneys (control, 20 mg/kg, and 80 mg/kg, frozen subcutaneously for seven days) were sectioned at 20 μm thickness and thaw-mounted onto MALDI target plates. Subsequent sections were acquired for histology staining and anatomical visualization. Matrix [30 mg/mL of 2,5-dihydroxybenzoic acid (DHB) in 50.0/50.0/0.1 (v/v/v) water/methanol/trifluoroacetic acid] was deposited with a nebulizing spray device (manual nebulizer or ImagePrep (Bruker Daltonics, Bremen, Germany).
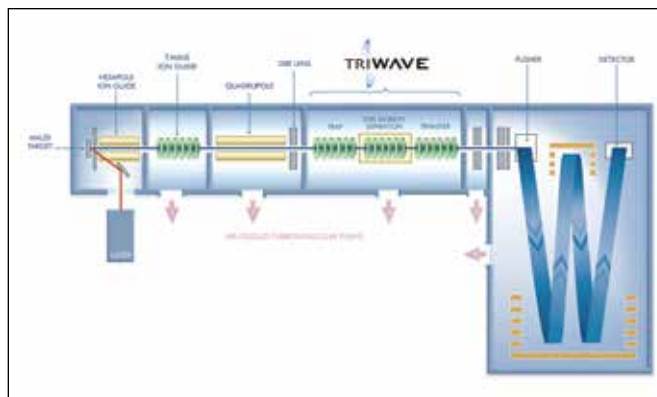


Figure 2. Schematic of the MALDI SYNAPT HDMS.

The image area was selected using MALDI Imaging Pattern Creator (Waters Corporation, Manchester, UK). Data were acquired using Waters® MALDI SYNAPT™ HDMS System in HDMS positive ion mode over the m/z range 100 to 1,500 at an image resolution of 150 x 150 μm and a laser speed of 200 Hz; Figure 2 shows a schematic view. Post acquisition, the ion mobility dimension of the data was evaluated using DriftScope™ Software. Image reconstruction was performed using BioMap (Novartis, Basel, Switzerland).

## RESULTS

In the mass range of the drug compound, the background ions from the tissue and matrix were intense. Here, the most abundant ion species was the [M+K]+ signal at *m/z* 1240.84; without the selectivity of the ion mobility separation, it was difficult to distinguish drug-related ions.

Figure 3 shows a comparison of the DriftScope 2D plots obtained from the control kidney and the 80-mg/kg-dosed kidney, zoomed around the [M+K]+ ion. The red circle indicates the position of the ion species from CsA in the dosed kidney data. In addition, the drift time of the ion was different from the drift time of the interfering background ions to enable specific selection of CsA. Therefore, it is possible to extract very specifically the CsA [M+K]+ ion species from the DriftScope 2D plot and recreate the ion-image.

Figure 4 shows the mobilogram (drift time versus intensity plot) of ion *m/z* 1240.8 in the dosed tissue, again showing the presence of two species at the same *m/z* value, each with different mobility.

The mass spectrum for each species can be extracted and the mass spectrum on the left-hand side represents the interference species, whereas the mass spectrum on the right-hand side corresponds to the Cyclosporin drug.
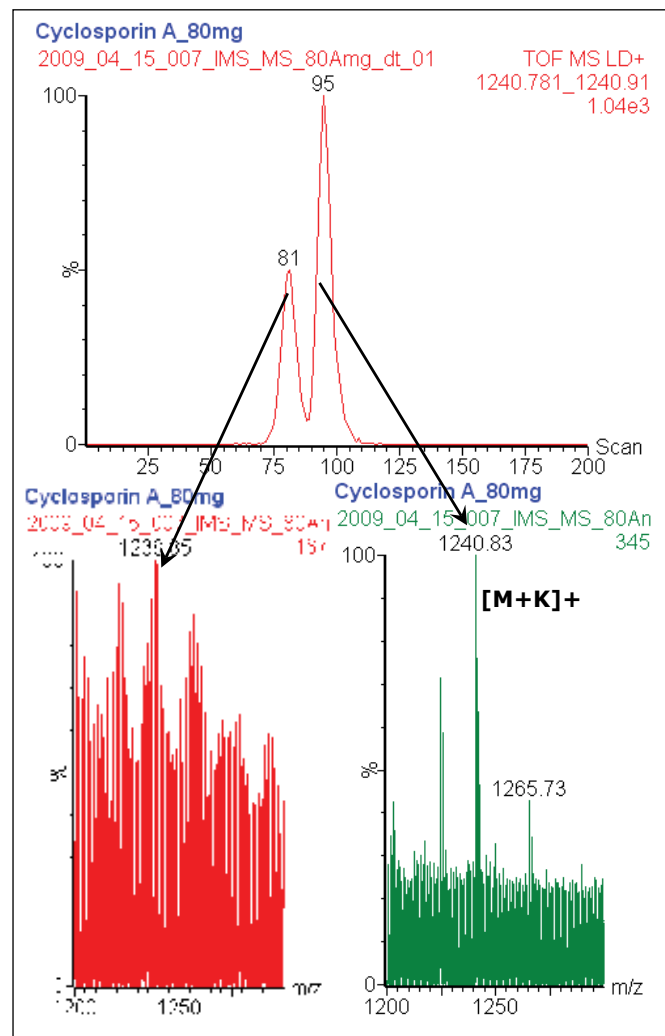


*Figure 4. Top: Mobilogram of m/z 1240.8. Bottom: Extracted MS spectra with specific drift time from each species.*



*Figure 3. DriftScope 2D plots of the control and 80-mg/kg-dosed tissue sections.*
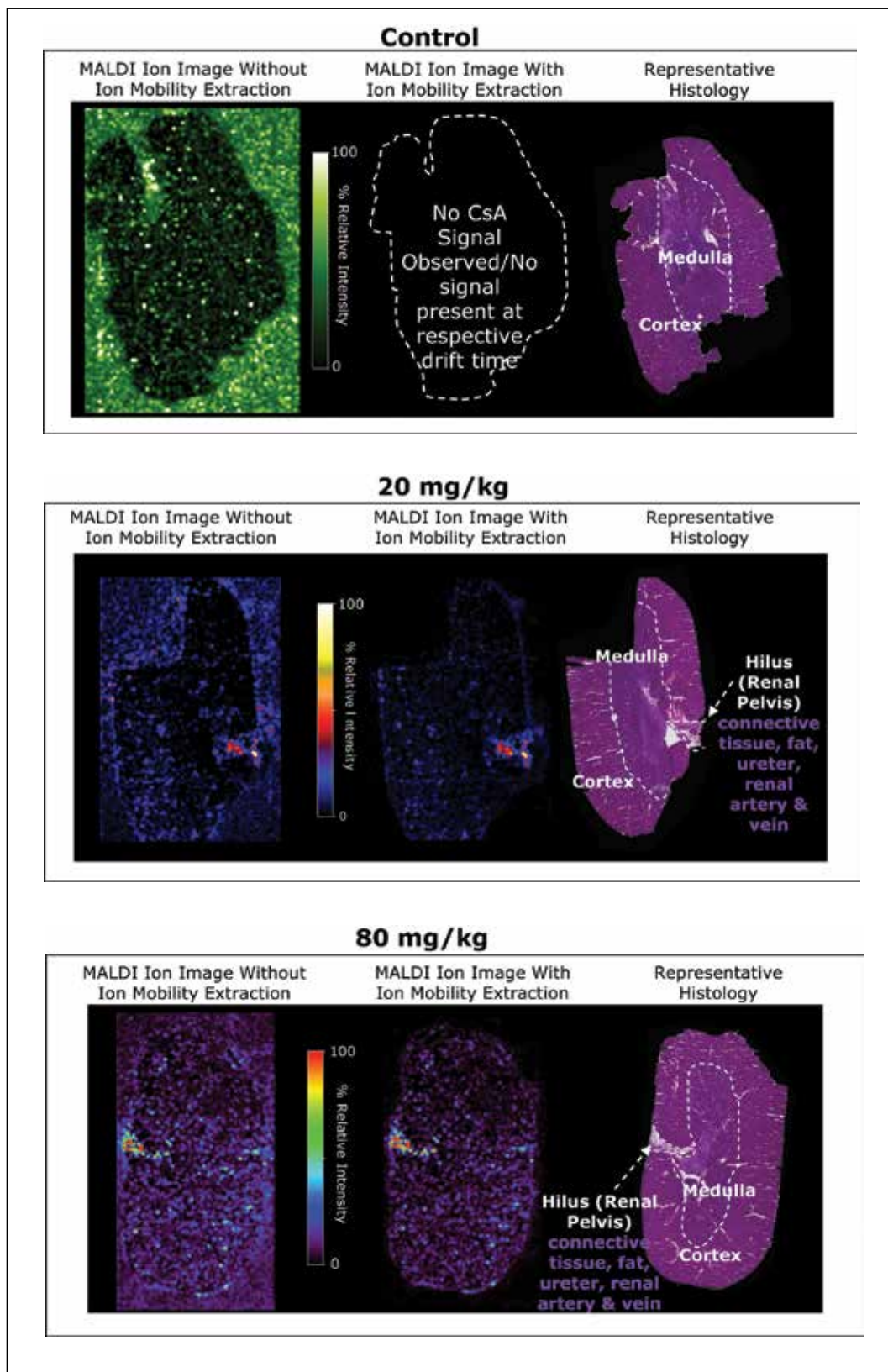
*Figure 5. CsA ion reconstituted images of control, 20 mg/kg, and 80 mg/kg-dosed kidney, with and without ion mobility separation, compared to the histology image.*

Figure 5 illustrates the effect of ion mobility on the MALDI ion images. Images of control, low, and high CsA-dosed renal tissues are shown. Each panel contains the ion image prior to and after drift time selective extraction of the CsA signal from the DriftScope data, together with the corresponding histology image. For each reconstructed image, the same *m/z* range was selected. The matrix ion was used for normalization purposes.

The ion mobility 2D plot from the control sample confirms that no signal corresponding to CsA is present endogenously in renal tissues, but the image reconstructed from the *m/z* value (without incorporating drift data) corresponding to CsA reveals the distribution of the background ions present at that *m/z* value. The ion images shown from dosed tissue, before and after the use of DriftScope to isolate the analyte, demonstrate the added selectivity provided by ion-mobility separation. The 20-mg/kg dose was near the lower limit of detection for CsA.

## BIOLOGICAL DISCUSSION

Images from the 80-mg/kg and the 20-mg/kg CsA-dosed samples illustrate CsA's distribution to the renal medulla, cortex, papilla, and hilus. Less drug is present in the 20-mg/kg sample, but shows a similar distribution pattern to the 80-mg/kg sample.

The drug was more highly concentrated in the hilus region than in the cortex or the medulla. The hilus region contains the renal pelvis where concentrated urine, containing the drug to be excreted, accumulates prior to its passage to the bladder. The renal artery within the hilus region may also contribute to the higher drug concentrations. The renal artery carries blood into the kidney where it is filtered and then exits through the renal vein.

## CONCLUSIONS

- The advantage of applying IMS as a first-dimension separation of ions prior to time-of-flight (TOF) mass analysis for imaging pharmaceuticals in tissues was demonstrated in this study.

- In the case of pharmaceutical compounds that do not give satisfactory MS/MS fragmentation, the selectivity of the traditional approach, where only mass analysis is taken into account, can be poor. In the case of CsA, the drug was confounded by unresolved background ions. The control image highlights the amount of interfering signal at the same m/z as CsA.

- Incorporation of ion mobility separation prior to TOF mass analysis in an imaging experiment enabled the true visualization of CsA distribution in the renal tissues, without interfering signal obstruction.

### References

1. Kahah BD. Transplantation Proceedings, 2009; 41: 1423-1437.

2. Giles K, Pringle S, Worthington K, Little D, Wildgoose J, Bateman R. Rapid Commun. Mass Spectrom., 2004; 18: 2401-2414.

# Waters

## THE SCIENCE OF WHAT'S POSSIBLE.®

**Waters Corporation**
34 Maple Street
Milford, MA 01757 U.S.A.
T: 1 508 478 2000
F: 1 508 872 1990
www.waters.com

# A Novel High Definition Imaging (HDI) Informatics Platform

## GOAL

A brief overview of the new Waters® High Definition Imaging (HDI™) Software solution that allows the maximum information to be obtained from imaging experiments that combine ion mobility with mass spectrometry.

## BACKGROUND

Imaging using mass spectrometry is a rapidly expanding area that has extensively used MALDI ionization. Waters has pioneered the use of ion mobility spectrometry with MALDI imaging experiments. Ion mobility allows ions to be separated in the gas phase by their size and shape prior to MS, allowing differentiation of isobaric species. This is directly integrated in all High Definition Mass Spectrometry (HDMS™) systems fitted with a MALDI source, and has been extensively used during the analysis of molecules directly ionized from tissue samples.

To access the detailed spatial information contained within the data, dedicated software is required. Waters MALDI SYNAPT® G1 and G2 raw data have previously been converted into an ANALYZE 7.5 format to be visualized using BioMAP (Novartis, Switzerland). However, this software approach is not integrated; therefore, it is not designed for incorporating the ion mobility dimension.

Waters has recently developed a proprietary software solution, designed for MS imaging, that provides a seamless workflow and makes full use of the ion mobility MS data.



Five types of MS experiments

TOF-MS

TOF-MS/MS

HD-MS

HD-MS/MS

HD-MS$^E$

Unique to MALDI SYNAPT HDMS

Figure 1. Experiments supported using Waters HDI Imaging Software.
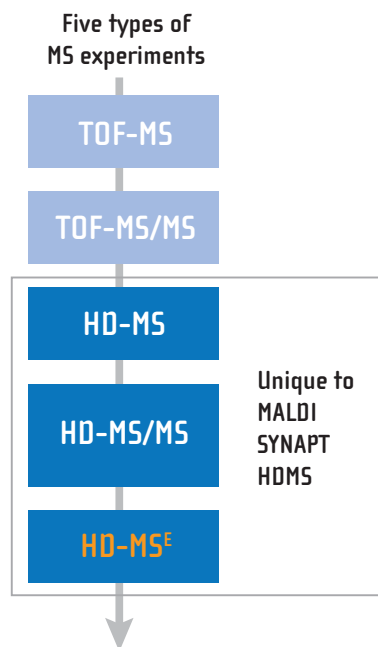
**HDI Imaging Software enables users to easily acquire and visualize MALDI HDMS$^E$ data for fully incorporated ion mobility information.**

## THE SOLUTION

Waters' new HDI Imaging Software is designed to simplify and streamline the imaging workflow allowing the user to fully integrate all of the steps in an MS imaging experiment for MALDI SYNAPT Mass Spectrometers using a single intuitive interface. An outline of the workflow is shown in Figure 1, which details the different experiments that are supported.

HDMS$^E$ is a patented method of data acquisition that records the exact mass precursor and fragment ion information for every detectable component in a sample. HDMS$^E$ rapidly alternates between two functions: the first acquires low-energy precursor ion spectra and the second acquires elevated-energy (CID) fragment ion data. Precursor and fragment ions are deconvoluted and reconstructed by alignment of their ion mobility drift-times. This drift-time aligned data can subsequently be visualized in Waters HDI Software.

Waters
THE SCIENCE OF WHAT'S POSSIBLE.®

## Workflow of the HDI Software

The initial step is to use the pattern definition tool to assign reference points to the photographic image, in order to select the area of interest for HD imaging.

The processing experiment file is created directly from the HDI Software and loaded into a MassLynx™ Software sample list. Processing of the data using the algorithm Apex 3D to create a peak list with *m/z* and drift time information occurs automatically after acquisition.

The resulting raw data are processed in the Analysis Section of the software, where all types of experiments described in Figure 1 are supported. Analysis of the acquired imaging data sets fully incorporates the ion mobility information, which is integrated into the data processing and visualization, as shown in Figure 2. This allows the distribution of molecules such as drugs, lipids, or peptides to be determined without the interference of background ions or isobaric species.

Smooth interactions between the available visualizations – including the peak list table, mass spectrum, drift time versus *m/z* plot – and the ion images allow scientists to analyze their data in a powerful, user-friendly fashion.

Following fully automated HDI data acquisition and processing, the results can be exported as raw data for statistical treatment using MarkerLynx™ XS Application Manager, or directly into other MassLynx applications for further processing, such as the elemental composition tool, or MassFragment.™

The user-defined grid gallery allows the comparison of a series of ion images of interest by using the Red/Green/Blue (RGB) overlay capability.
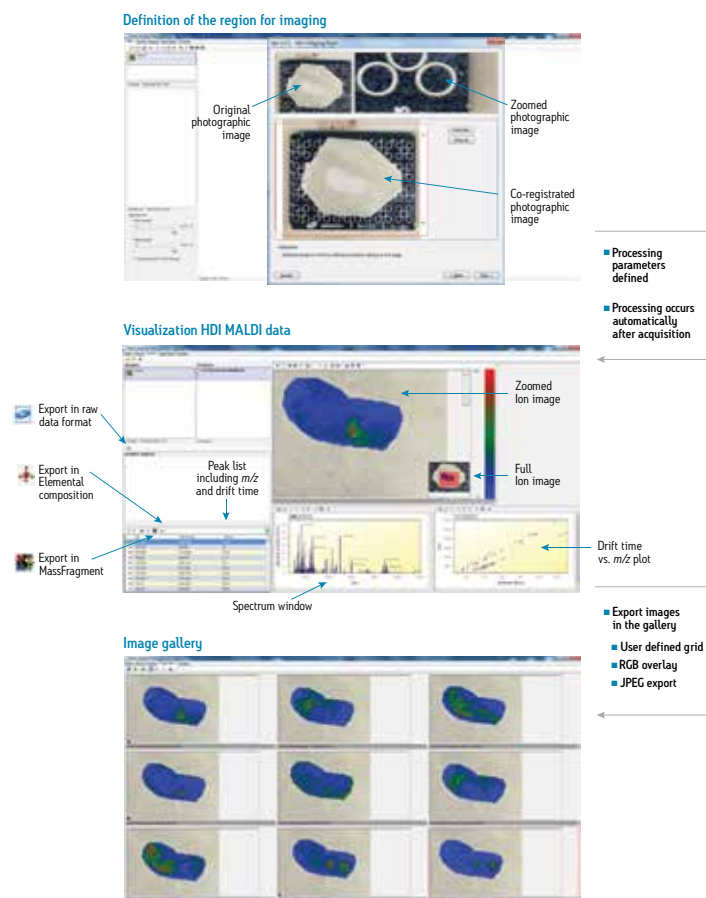


Figure 2. Acquired imaging data sets fully incorporate the ion mobility information that is integrated into the data processing and visualization tool.

## SUMMARY

- Waters' High Definition Imaging Software is a new, fully integrated software suite for MALDI imaging experiments.

- Integration of HDI data acquisition processing and visualization is performed in a single interface.

- For the first time, MALDI imaging ion mobility information is fully incorporated and used within the imaging software.

- MALDI HDMS$^E$ data can be acquired and easily visualized.

- Flexible export options are available for calculating elemental composition, statistical analysis using MarkerLynx XS Application Manager, or analysis with MassFragment.

## Waters

### THE SCIENCE OF WHAT'S POSSIBLE.®

**Waters Corporation**
34 Maple Street
Milford, MA 01757 U.S.A.
T: 1 508 478 2000
F: 1 508 872 1990
www.waters.com

# Collision Cross-Section Determination of Lipids on the MALDI SYNAPT G2 HDMS System

## GOAL

To determine the collision cross-sections of singly charged lipid ions analyzed by MALDI mass spectrometry.

## BACKGROUND

Lipidomics is a rapidly expanding field of research, where mass spectrometry plays a key role. Moreover, visualizing the localization of lipids within a tissue section is challenging since there are no antibodies specific to lipids. However, imaging by MALDI mass spectrometry allows the location of different classes of lipids directly from tissue sections to be visualized, thereby enhancing lipid studies.

The use of ion mobility to evaluate the size and shape of ions in the gas phase is a technique which is rapidly gaining recognition. Initial studies were carried out on proteins; however, it has now been demonstrated that it is possible to use ion mobility to measure the collision cross-section of other types of molecules, like lipids.

The MALDI SYNAPT® G2 HDMS™ System (schematic shown in Figure 1) provides an ideal platform to conduct these imaging studies, and in addition, allows the collision cross-sections to be calculated during the same experiment. Furthermore, data is acquired at high resolution, enabling exact mass measurements to be made on both precursor and fragment ions, coupled to the ability to separate target analytes from isobaric background interferences using gas-phase ion mobility separations.

**The MALDI SYNAPT® G2 HDMS™ System provides an ideal platform to conduct lipid imaging studies, and in addition, allows the collision cross-sections to be calculated during the same experiment.**
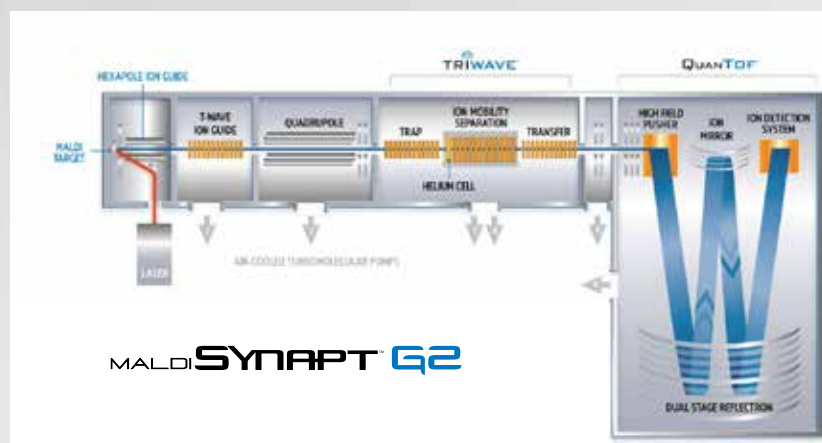


Figure 1. Schematic of the MALDI SYNAPT G2 HDMS System.

## THE SOLUTION

First, we calibrated the IMS T-Wave®[1] using polyalanine, with previously determined collision cross-section values (from http://www.indiana.edu/~clemmer). The calibration curve was generated with DriftScope™ Software using a power trend line where R=0.9995.

Waters
THE SCIENCE OF WHAT'S POSSIBLE.®

To calculate the collision cross-sections of each lipid standard, PC (16:0/16:0), PS (18:1/18:1), and PG (16:0/18:1) (Avanti Polar Lipids) were mixed individually with α-cyano-4-hydroxycinnamic acid (CHCA) matrix, spotted onto a MALDI stainless steel target, and analyzed under identical conditions to those used for the polyalanine standard. The analysis was performed using a 1 kHz Nd:YAG laser system on a MALDI SYNAPT G2 operated in HDMS mode. CCS calculations were also determined for the sodiated and potassiated species, when present.

Figure 2 shows that the collision cross-section, which was calculated to be 214.9 Å$^2$ for MH$^+$ of PC (16:0/16:0). This is in accordance with previously published results[2] by Ridenour et. al., where their CCS calculation of these lipids on a MALDI SYNAPT (G1) HDMS instrument were found to be 215.3 Å2 +/- 3.6.
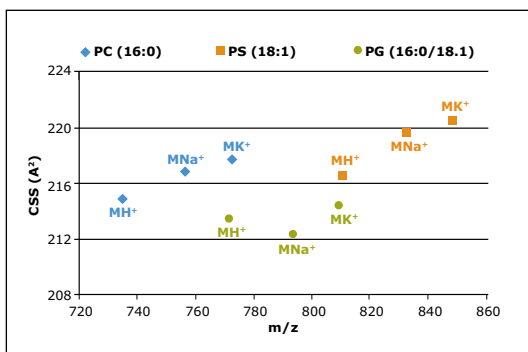


*Figure 2. Collision cross-section calculation for lipid standards.*

The collision cross-section of the Na$^+$ and K$^+$ species of the PC and PS standards indicate a more open configuration in the gas phase relative to the MH$^+$ species when compared to the PG lipid standard. Here the Na$^+$ and K$^+$ of the PG ion appear to be more compact in the gas phase versus their MH+, which could indicate that the lipid may be folded around the salt.

Further analysis was carried out on a rat tissue section, under the same IMS conditions and the CCS of lipids calculated directly from tissue section, as shown in Figure 3. As lipids tend to have similar mass defects for each class, the data was colored following the first decimal of the m/z. Here, the trend lines can be observed in the data following the mass defect.
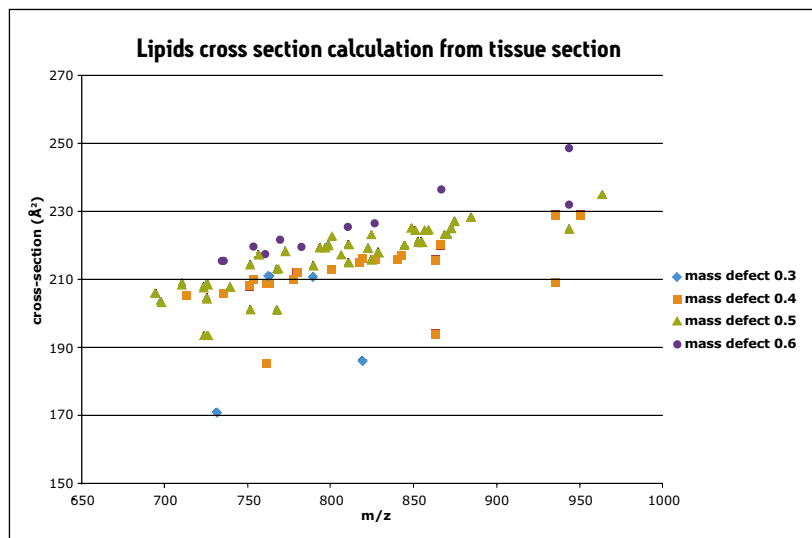


*Figure 3. Collision cross-section calculation for lipids analyzed directly from a tissue section. Data is colored by mass defect of the lipids.*

## SUMMARY

The MALDI SYNAPT G2 HDMS System enables the calculation of collision cross-sections of lipid standards. Here we have observed that the sodiated PG lipid standard had a more compact configuration in the gas phase compared to its counterpart MH+.

This type of analysis can also be carried out for endogenous species analyzed directly from tissue sections. In a single experiment, it is possible to calculate collision cross-sections for endogenous species and carry out a MALDI imaging experiment to observe their location throughout the tissue.

### References

1. The travelling wave device described here is similar to that described by Kirchner in US Patent 5,206,506 (1993).

2. Structural characterization of phospholipids and peptides directly from tissue sections by MALDI traveling-wave ion mobility-mass spectrometry. Ridenour WB, Kliman M, McLean JA, Caprioli RM. Anal Chem. 2010 Mar 1;82(5):1881-9.

## Waters
### THE SCIENCE OF WHAT'S POSSIBLE.®

**Waters Corporation**
34 Maple Street
Milford, MA 01757 U.S.A.
T: 1 508 478 2000
F: 1 508 872 1990
www.waters.com

# Utility of Desorption Electrospray Ionization (DESI) for Mass Spectrometry Imaging

Emmanuelle Claude and Emrys Jones

## GOAL

To describe the DESI imaging technique as applied to mass spectrometry imaging using time-of-flight (TOF) mass spectrometers, such as the SYNAPT® G2-S*i* or the Xevo® G2-XS.

## BACKGROUND

In the past few years, mass spectrometry imaging (MSI) has seen a rapid increase in interest and utilization in areas such as proteomics, biomarker discovery and validation, drug distribution, and clinical research. MSI was originally developed using a matrix assisted laser desorption ionization (MALDI) mass spectrometer, where the sample is prepared by first coating it with an ionizable matrix. Then, the sample is placed under vacuum and a rastering laser is used to ioninze molecules in the sample for analysis by a TOF mass spectrometer.

More recently, an ambient ionization technique called desorption electrospray ionization (DESI) was introduced and applied to MSI to allow for the direct analysis of surfaces at atmospheric pressure. DESI imaging uses a charged jet of solvent to deposit micro-droplets onto a surface where analytes are extracted and desorbed into the gas phase at ambient pressure and temperature. Subsequently, they are drawn into the MS inlet where they can be analyzed using a TOF-MS. This technique is compatible with Waters® SYNAPT G2-S*i* or Xevo G2-XS Mass Spectrometers.

**DESI imaging provides effective and meaningful molecular spatial localization within a variety of samples with minimum sample preparation.**
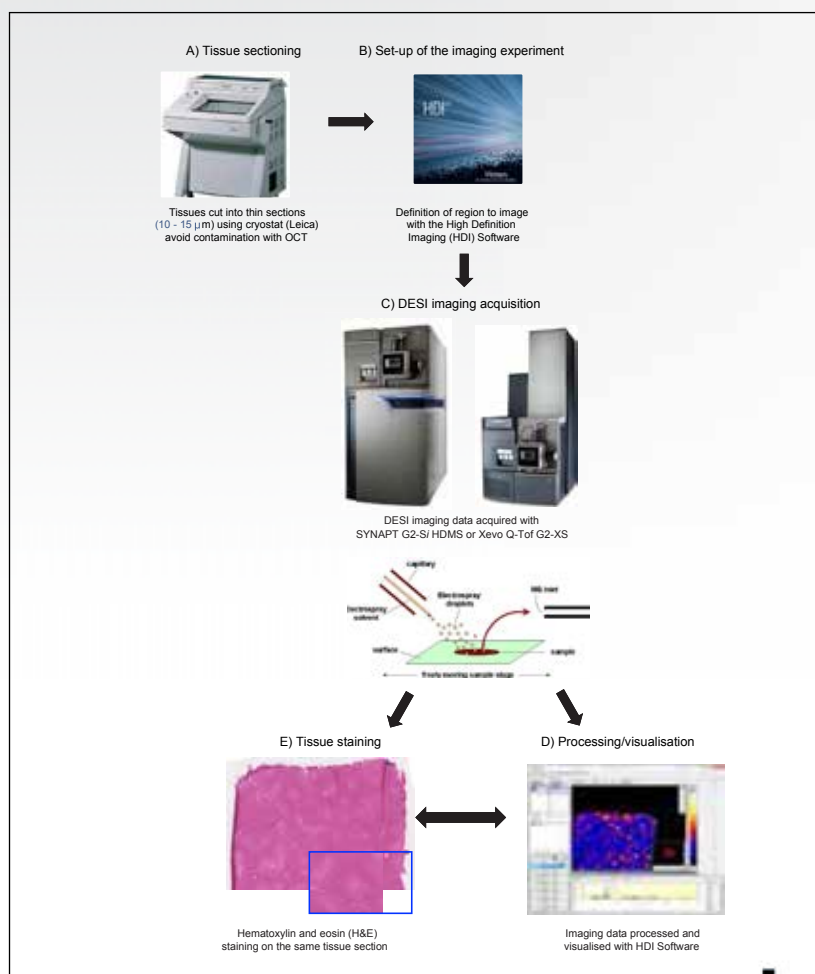


Figure 1. Workflow of a DESI imaging experiment.

THE SCIENCE OF WHAT'S POSSIBLE.®
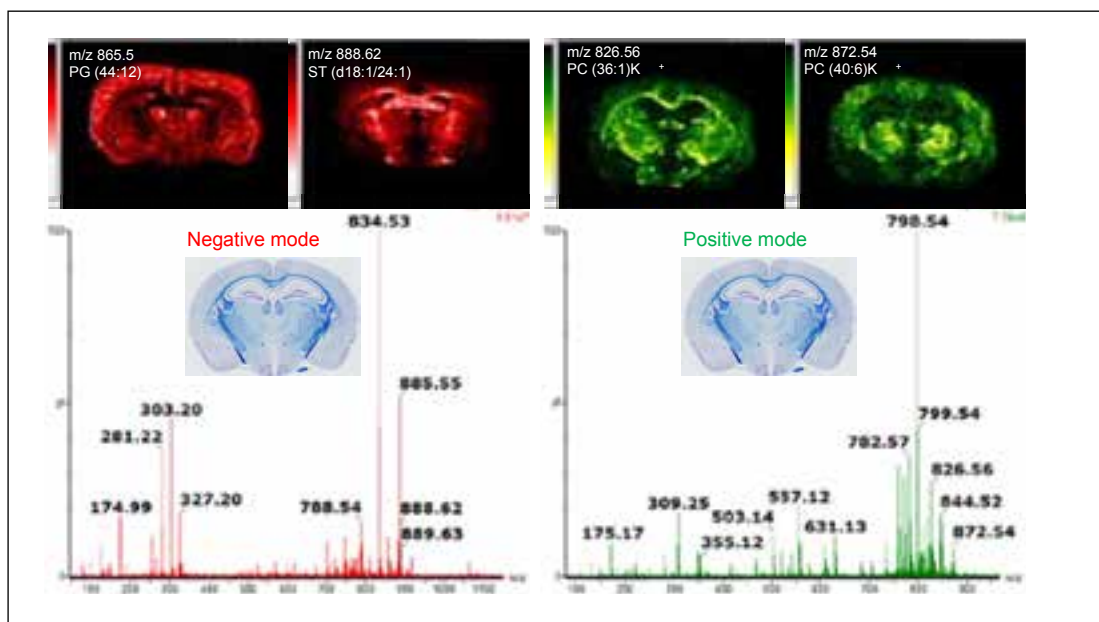
*Figure 2. Multimodal imaging from a single sample. DESI imaging experiments on mouse brain tissue sections[1] with the full combined MS spectra in positive (green) and negative (red) ion modes.*

## THE SOLUTION

To perform a DESI imaging experiment, a fresh frozen thin tissue section is mounted onto a glass slide directly from the cryostat or freezer. The slide is placed onto the 2D linear moving stage of the DESI source without any other pre-treatment. An optical image is taken and co-registered with the High Definition Imaging (HDI®) Software (Figure 1B). This optical image is then used to define the rectangular area to be imaged. The surface of the tissue section is rastered line-by-line using the DESI sprayer with a mass spectrum collected at predefined X,Y coordinates. The pixel size in the X-direction is defined by the speed of the stage movement and acquisition rate of mass spectra. The pixel size in Y-direction is defined by the distance between two lines of acquisition. Typically, DESI imaging experiments are acquired with pixel sizes of 50 μm or more.

Raw imaging data is subsequently processed and visualized within the HDI Software (Figure 1D). When using optimized DESI imaging conditions, the sample is preserved to such an extent that the tissue section can be haemotoxylin and eosin (H&E) stained directly after MS acquisition (Figure 1E). This allows the H&E stained optical image to be overlaid with the DESI molecular images from the same tissue section.

Figure 2 displays ion images of lipids species from consecutive mouse brain sections;[1] one acquired in positive (green) ionization mode and one acquired in negative (red) ionization mode, using a solvent of 90:10 methanol: water, at a pixel size of 100 μm. Both polarities provide DESI MS spectra very rich in small molecules and phospholipid species that localize into specific features within the mouse brain.

### DESI Imaging Versatility

DESI imaging, being a surface analysis technique, can be applied to numerous types of samples, varying from animal and human tissue samples, to plant material, pharmaceutical tablets, and even isolated bacterial colonies on agar. Figure 3 shows a selection of ion images from a variety of samples acquired using a range of pixel sizes from 100 to 200 μm, measured either in positive or negative ionization mode. Figure 3A is an ion image of oleic acid in porcine liver, highly concentrated in the center of the liver lobules co-localized with the central vein. Figure 3B shows the potential to apply DESI imaging to forensic trace evidence

analysis by capturing molecular images from a fingerprint. Figure 3C displays the overlay of two small molecules, differentially distributed within a bacterial colony grown on agar.[1] Figure 3D illustrates the analysis of a human tissue sample[2] that contains both normal tissue and a secondary tumor tissue. The distribution of two lipids $m/z$ 698.51 (PE (O-34:3)) and $m/z$ 773.53 (PG (36:2)) specifically correlates to the identity of the tissue type. In this example PE (O-34:3) is specifically localized within the tumor region.
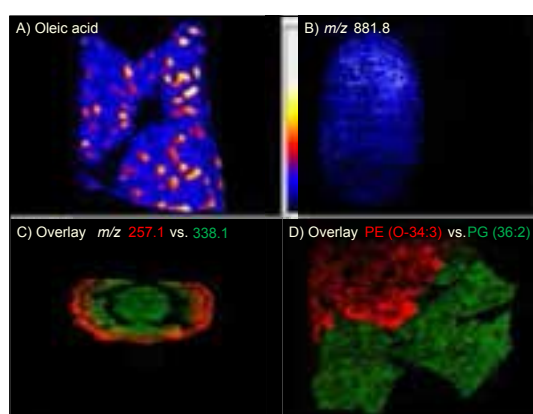


Figure 3. Application flexibility with DESI imaging. A) ion image of oleic acid in porcine liver, B) m/z 881.8 ion image of a human fingerprint, C) overlay of m/z 257.1 (red) and 338.1 (green) from a bacterial colony,[1] and D) overlay of ion images m/z 698.51 (PE (O-34:3) (red) and m/z 773.53 (PG (36:2)) (green) from human liver sample.[2]

## SUMMARY

DESI imaging represents a significant enhancement in the capabilities of mass spectrometers to analyze and determine spatial localization and molecular distribution of target molecules within a variety of samples. Use of DESI imaging has the advantages of requiring minimal sample preparation to collect a wealth of molecular information. When optimized, the technique allows for either multiple analyses of a single sample (with different MS polarities if desired) or enables additional visualization techniques (i.e. staining) to be performed on the sample after DESI imaging is complete. As seen is these examples, DESI imaging has been shown to be very effective in analyzing small molecules such as lipids or other small molecule cellular metabolites.

The advantages of DESI imaging include:

■ Accommodation of multimodal imaging analyses on a single sample (i.e., DESI and MALDI; positive and negative ion mode analysis)

■ Minimum sample preparation

■ Non destructive, multimodal image analysis to maximize information from precious samples

■ Compatibility with additional analysis techniques after DESI imaging (i.e., staining)

■ Excellent sensitivity for a variety of small molecule analytes (i.e., lipids and small molecules)

■ Flexibility to analyze a wide variety of sample types and analytes

### Acknowledgements

## Waters
THE SCIENCE OF WHAT'S POSSIBLE.®

**Waters Corporation**
34 Maple Street
Milford, MA 01757 U.S.A.
T: 1 508 478 2000
F: 1 508 872 1990
www.waters.com

# Generation of Multiple Images from a Single Tissue Section with Dual Polarity Desorption Electrospray Ionization Mass Spectrometry

Emmanuelle Claude and Emrys Jones
Waters Corporation, Wilmslow, UK

## GOAL

To demonstrate the flexibility of desorption electrospray ionization (DESI) imaging, showing that the same tissue can repeatedly be imaged at the molecular level in positive and negative ion mode, to maximize information about molecular distribution in tissue.

## BACKGROUND

DESI imaging, a surface analysis technique incorporating an electrospray probe, can be utilized as an imaging technique by rastering a surface under an ionizing solvent sprayer using a high precision X,Y stage. As the droplets impact upon the surface, chemical constituents are desorbed and carried towards the atmospheric inlet of the mass spectrometer. Ionization of the desorbed molecules occurs via the charge imparted onto the droplets. In contrast to other ionization techniques often used for tissue imaging (i.e., MALDI), no special sample preparation, such as coating of the tissue section with a specialized solvent/ionizable matrix mixture, is required. In this study, gas and solvent flow rates as well as ionization voltages are optimized to allow DESI imaging experiments that preserve the tissue sample being analyzed. These less destructive DESI ionization conditions provide an opportunity for a single tissue section to be analyzed multiple times with the same or different experimental conditions or techniques.

**Sequential analysis of a single tissue section for comprehensive molecular profiling is made possible with dual-polarity DESI imaging.**
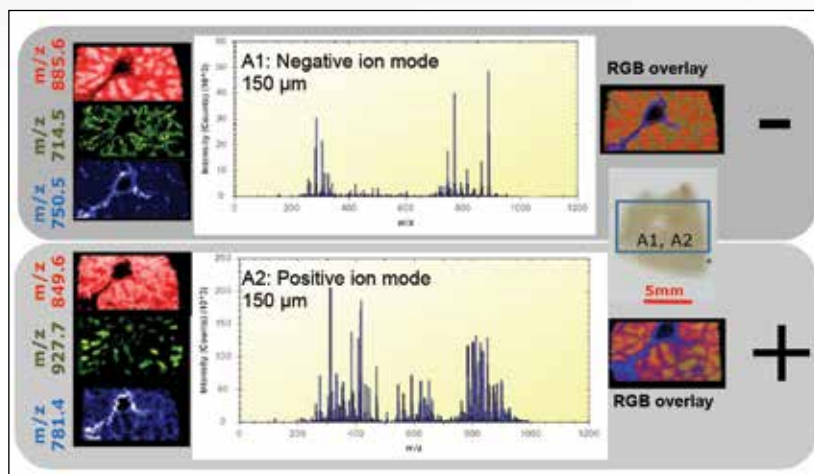


Figure 1. Two successive DESI imaging analyses of the same region of a tissue section from porcine liver. A1) First analysis, 150 µm spatial resolution negative ion mode, three color overlay and average spectrum. A2) Second analysis, same raster conditions— 150 µm spatial resolution positive ion mode, three color overlay and average spectrum.

## THE SOLUTION

Here we demonstrate that by optimizing DESI conditions, a wealth of molecular information can be accessed from a single tissue section, without the need to substantially alter the analysis conditions.

Mass spec imaging of tissue sections was accomplished by using a SYNAPT® G2-S*i* HDMS Mass Spectrometer equipped with a 2D-DESI source. Data was generated and analyzed using HDI Software v1.3.

Fresh frozen tissues of porcine and human liver were sectioned on a cryo-microtome to 15 μm thickness and thaw-mounted onto conventional glass slides. When required, the samples were stored at -80 °C. Immediately prior to analysis, the samples were brought to room temperature and placed directly onto the stage of the DESI source. No further sample preparation was required.

A 2D-DESI source was mounted onto a SYNAPT G2-S*i* HDMS Mass Spectrometer. Spray conditions were set as follows: flow rate of 1.5 μL/min, with a 90:10 MeOH:water mixture at 100psi $N_2$ gas pressure, and a voltage of 5kV for both polarities. To conduct the imaging experiment, a raster pattern was defined over the tissue region of interest and the scan speed and line spacing were selected appropriately for the target pixel dimensions. For 150 μm resolution images, the stage was scanned at 0.15 mm per second on the X-axis; and stepped 0.15 mm in the Y-axis between each DESI line scan. In all instances, the MS scan time was 1 second.

As the flow rates used are sufficiently low and the desorption was considered a soft event, the same tissue section can be analyzed more than once without modification or exhaustion of the surface molecules- allowing dual polarity analysis on the exact same section for increased information depth.

Initially, imaging experiments on porcine liver were performed with the MS operating in negative mode, subsequently followed by imaging the same tissue section in positive mode (Figure 1). In both modes of ionization, plentiful lipids and endogenous metabolites were detected, giving intense peaks for analysis by the mass spectrometer.

A second experiment was designed to evaluate whether the repeated imaging of the same tissue sample alters the chemical information obtained. Figure 2 compares the spectrum from a single DESI imaging experiment in positive mode (top), with the positive mode spectrum (bottom) generated from a consecutive tissue section, after first analyzing it in negative mode. Identical peaks were observed in both spectra with very similar relative intensities.
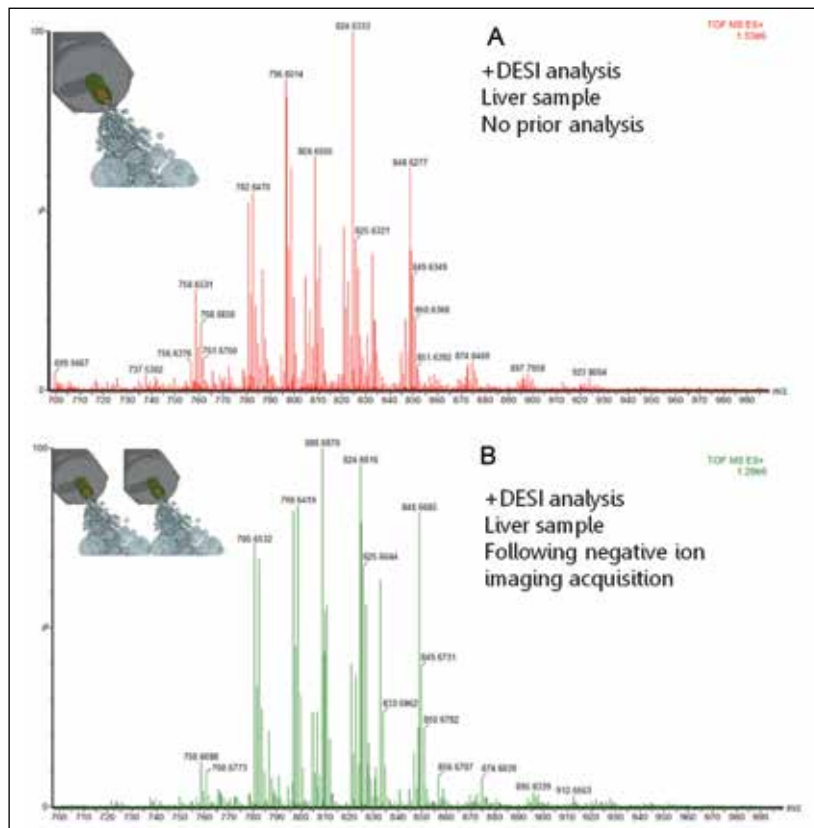


Figure 2. Combined positive mode mass spectra from similar regions of serial porcine liver sections: A) on a pristine surface B) on an altered surface where a full negative ion DESI imaging experiment was previously carried out.
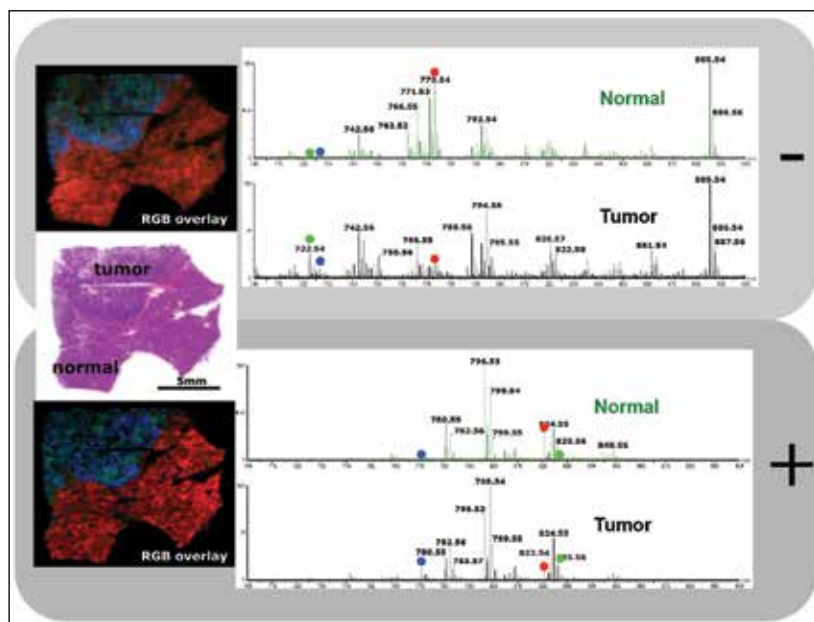


Figure 3. A single tissue section from a block of liver containing both normal tissue and a secondary tumor was analyzed in negative; then again in positive ion mode, where many lipid species in both polarities were discriminatory and more abundant in one tissue type than the other. This created a signature chemical fingerprint defining the tissue morphology and type.

The ability to revisit the same section to increase the amount of information could be of great importance when samples are precious, for example with a human liver sample. Figure 3 shows one such example where the same section was analyzed by MS imaging in both polarities. Lipid species specific to tumor tissue and healthy tissue were identified in positive and negative ion mode. This would seem to indicate that the tissue has not been significantly affected by the DESI imaging technique and is still relatively intact. By not perturbing the tissue with DESI imaging, subsequent additional surface analysis or staining techniques (i.e., H&E staining) could be utilized on the same tissue sample for further, more comprehensive characterization.

## SUMMARY

DESI imaging provides metabolite and lipid molecular information directly from a tissue section with no tissue sample pre-treatment. With low flow rates, the tissue section can be analyzed multiple times without significant degradation of signal or modification of the chemical signature obtained from the tissue. Using the same analytical MS instrument setup, information rich spectra in both positive and negative ion mode can be generated without the need to change solvent or analysis conditions. Therefore, positive and negative ion mode DESI data can be obtained from the same tissue and combined for extended chemical coverage and sample differentiation.

Here we demonstrate that by optimizing DESI imaging conditions, a wealth of molecular information can be accessed from a single tissue section. Multiple images containing unique information can be collected from a tissue sample without the need for the analysis of a number of serial sections.

The advantages of DESI imaging include:

■ Optimization of DESI conditions allows multiple imaging experiments to be performed on the same tissue sample without altering the architecture or composition of the tissue

■ Both positive and negative ion mode DESI imaging data can be collected from a single tissue section

■ Using optimized DESI conditions enables subsequent analysis of tissue sections by other visualization techniques (i.e. H&E staining)

### Acknowledgments

## Waters

### THE SCIENCE OF WHAT'S POSSIBLE.®

**Waters Corporation**
34 Maple Street
Milford, MA 01757 U.S.A.
T: 1 508 478 2000
F: 1 508 872 1990
www.waters.com

# Multiple, Sequential DESI Images from a Single Tissue Section at Different Spatial Resolution

Emmanuelle Claude and Emrys Jones
Waters Corporation, Wilmslow, UK

## GOAL

To demonstrate that desorption electrospray ionization (DESI) imaging can be utilized as a non-destructive imaging technique, which allows multiple analyses in rapid succession on the same tissue section at different spatial resolution.

## BACKGROUND

DESI, a surface analysis technique incorporating an electrospray probe, can be utilized as an imaging technique for a broad range of samples. Imaging of a sample is accomplished by rastering a surface under a spray of ionized solvent using a high precision X,Y stage. As the electrospray droplets impact the sample surface, chemical constituents are desorbed and carried towards the atmospheric inlet of a mass spectrometer for analysis. Ionization of various analytes is provided by the charge imparted onto the droplets. Unlike other mass spectrometry based imaging techniques, such as matrix assisted laser desorption ionization (MALDI), no sample preparation (i.e., matrix addition) is required for imaging a sample.

When collecting images from a sample using DESI imaging, the characteristics of the ionized solvent spray used to desorb analyte molecules from the sample affects the spatial resolution of the imaging experiment. The spatial resolution of the image collected can be manipulated to allow for higher or lower levels of spatial resolution as desired by the researcher.

## DESI imaging allows multiple analyses of a single tissue section at different spatial resolutions.
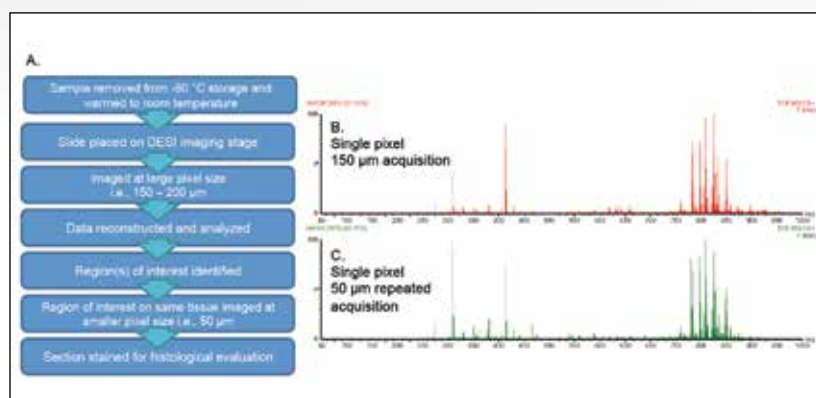


*Figure 1. A: Workflow for acquiring multiple DESI images with different spatial resolutions. B: MS spectrum from a single pixel of 150 µm resolution on a pristine porcine liver section. C: MS spectrum from a single pixel of 50 µm resolution on a previously DESI imaged porcine liver section.*

Moreover, by modifying the conditions used with the DESI technique, the amount of sample surface disruption can be tightly controlled such that the sample is not destroyed when obtaining an image.

This ability to control and manipulate many of the parameters utilized for DESI imaging allows a single sample to be analyzed multiple times with different experimental conditions or techniques (i.e., one experiment at low spatial resolution, followed with a higher spatially resolved experiment to further characterize a region of interest). This experimental flexibility also allows a DESI imaging study to be followed with hematoxylin and eosin (H&E) or the use of another staining or imaging technique on the same sample.

Waters
THE SCIENCE OF WHAT'S POSSIBLE.®

## THE SOLUTION

In this study, a SYNAPT® G2-S*i* Mass Spectrometer equipped with an enhanced DESI imaging source was used to analyze a number of tissue samples. Data collection and image analysis were performed using MassLynx® and HDI® v1.3 Software.

Snap frozen tissues of porcine and human liver were sectioned on a cryo-microtome to 15 µm thickness and thaw mounted onto conventional glass slides. The samples were stored at -80 °C prior to analysis if needed. Immediately prior to analysis, the samples were brought to room temperature and placed onto the stage, without any further sample preparation. The enhanced DESI source was mounted onto a SYNAPT G2-S*i* HDMS. DESI spray conditions were set at 1.5 µL/min, 90:10 MeOH:water at 100psi $N_2$ gas pressure and a voltage of 5 kV for both polarities. The pixel size was determined in the X-direction by the speed of the stage movement and acquisition rate of mass spectra. The Y-direction was defined by the distance between two lines of acquisition.

In the first DESI imaging experiment, a raster pattern was defined over the whole tissue sections, with a pixel size of 150 µm for the porcine liver, and 200 µm for the human liver sample. The second experiment was carried out using a specific region of the same tissues, both at 50 µm. The workflow for these experiments is described in Figure 1A.

Figure 1B and 1C display mass spectra with plentiful lipid and endogenous metabolite signals observed from the DESI analysis of the tissue sections. Each spectrum was obtained from a single pixel acquired on the porcine tissue section at different spatial resolution (150 µm followed by 50 µm) from the same tissue. The relative intensities of the lipid signals are comparable at either spatial resolution.

Examples of images produced from the tissue samples can be seen in Figure 2. Figures 2A and 2B show the ion images of a phosphotidyl glyercerol (PG) containing lipid at *m/z* 927.7 with A) being a pixelated ion image at a 150 µm spatial resolution from a pristine surface, and B) an image of the same tissue section, measured at 50 µm spatial resolution immediately after the 150 µm imaging experiment.
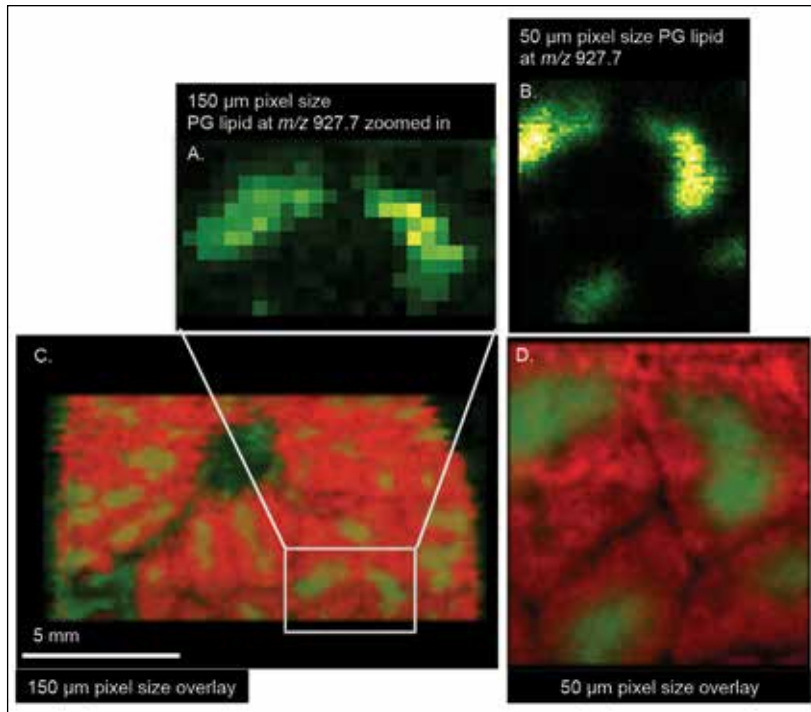


*Figure 2. DESI imaging analyses of the porcine liver in positive ion mode A and B: ion images of m/z 927.7 with A: at 150 µm spatial resolution on pristine surface and B: at 50 µm spatial resolution on previously imaged surface. C and D: RG overlay of m/z 848.55 (PC (38:4) K⁺) (red) and m/z 927.7 (green) in interpolate mode with C: at 150 µm spatial resolution on pristine surface and D: at 50 µm spatial resolution on previously imaged surface.*
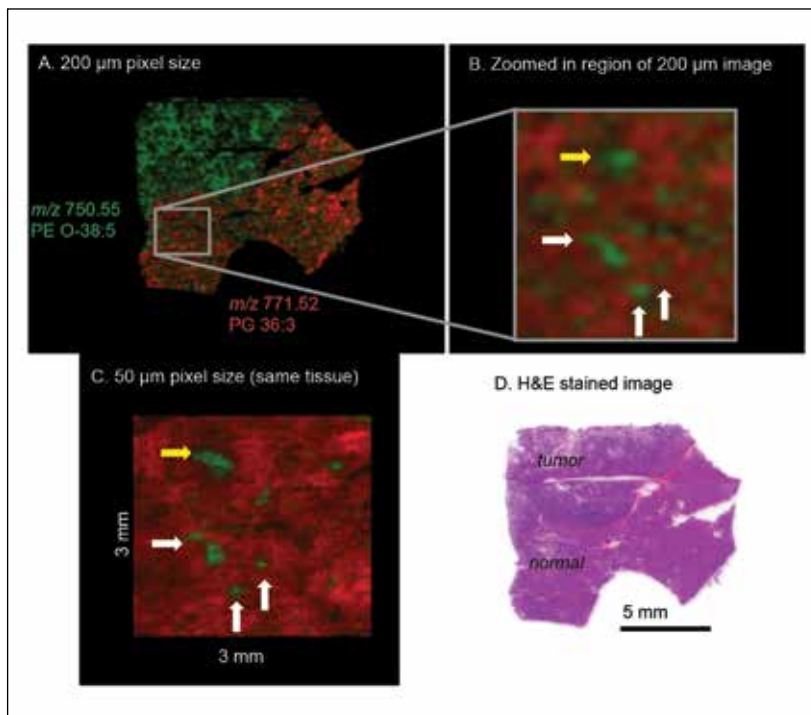


*Figure 3. DESI imaging analyses of human liver sample in negative ion mode A: RG overlay of m/z 771.52 (PG (36:3)- (red ion image)) and m/z 750.55 (PE (O-38:5)- (green ion image)) at 200 µm resolution from a pristine surface. B: zoomed-in view of the "normal" tissue section. C: RG overlay of the same ion species from the 50 µm resolution previously imaged tissue section. D: H&E staining of the tissue section after the two DESI experiments.*

As expected, the image quality noticeably improves at higher spatial resolution. But it is also noteworthy to see that there is no noticeable delocalization of ions from one imaging experiment to the next on the same tissue section. Delocalization can be a problem with other imaging techniques requiring the application of solvents or matrix to a sample for imaging (i.e., MALDI).

Figures 2C and 2D are a Red/Green (RG) overlay of ion images from a $m/z$ 848.55 phosphotidyl choline (PC) containing lipid (38:4)K$^+$ (red ion image) with a PG containing lipid at $m/z$ 927.7 (green ion image). This figure also shows the ion images of the same lipid species acquired during the second sequential imaging experiment acquired at 50 μm resolution.

A similar imaging study was carried out on a human liver biopsy tissue sample that contains both healthy cells and a secondary tumor (Figure 3). The entire tissue section was first imaged at 200 μm resolution. In this experiment, PG containing lipids of $m/z$ 771.52 (36:3)- (red ion image) and phospotidyl ethanolamine (PE) containing lipids of $m/z$ 750.55 (O-38:5)- (green ion image) were found to be specifically localized to either healthy or tumor tissue, and could be utilized to distinguish tissue type in the sample section (Figure 3A). A second imaging experiment on the same human liver tissue section focused on the region of the section that was identified as healthy. This sequential imaging experiment was performed at 50 μm spatial resolution and concentrated on the margin between healthy and cancerous tissue (Figure 3B and 3C). Looking closely at the images obtained at this level of resolution indicates that some tumor cells have begun invasively migrating through the intercellular spaces of the healthy liver tissue.

Finally, once DESI imaging experiments were completed, the tissue section was subsequently H&E stained for accurate correlation of DESI imaging observations with cell and tissue morphology (Figure 3D).

## SUMMARY

DESI imaging has been shown to provide important information about tissue samples especially regarding the distribution of lipids and small molecules throughout a variety of tissues. Here, we have shown that the potential of using DESI imaging to gather information from samples can be enhanced by optimizing the conditions on various tissue sections. Specifically, controlling the gas and solvent flow rates, as well as the voltages applied to the instrument allows for effective DESI imaging at different spatial resolution (i.e., 50 and 200 μm).

This capability of DESI imaging allows for a relatively fast initial scan of a tissue sample, followed by a more high resolution, detailed imaging study of regions of interest identified by the initial experiment. Additionally, after DESI imaging is complete, the tissue section can be directly H&E stained for further morphological analysis.

The advantages of DESI imaging include:

- Sequential image analysis of a single tissue section at one or more levels of spatial resolution.

- Fast scan imaging and subsequent imaging of selected regions on the same tissue sample.

- Identification of tissue discriminating or tissue identifying marker compounds.

- Performance of imaging studies with little sample preparation.

- Capability to combine DESI image analysis of a tissue sample followed by subsequent H&E staining for morphological analysis.

- No potential for analyte relocalization during imaging.

### Acknowledgments

## Waters
### THE SCIENCE OF WHAT'S POSSIBLE.®

**Waters Corporation**
34 Maple Street
Milford, MA 01757 U.S.A.
T: 1 508 478 2000
F: 1 508 872 1990
www.waters.com

Waters
THE SCIENCE OF WHAT'S POSSIBLE.®

# Real Time Lipidomic Profiling Using Desorption Ionization with Ion Mobility MS

Jordan Krechmer,[1] Kieran J. Neeson,[2] Giorgis Isaac,[3] Joseph Tice,[1] Marc V. Gorenstein,[3] Alan Millar,[3] Michael P. Balogh,[3] James Langridge,[2] Giuseppe Astarita[3]
[1] IonSense, Saugus, MA, USA
[2] Waters Corporation, Manchester, UK
[3] Waters Corporation, Milford, MA, USA

## APPLICATION BENEFITS

The combination of real time desorption ionization and ion mobility MS offers a convenient solution for phenotypic identification and comparative lipidomic analysis.

## INTRODUCTION

Lipids are major constituents of food and biological tissues. Among lipid key properties are those to determine the caloric content, texture, and taste of food. Besides their importance in food and nutrition, lipid composition affects the physiology of living cells. Alterations in lipid profiles have been implicated in a wide range of pathologies in many types of organisms including plants and humans. Therefore, assessing lipid profiles and ratios between various lipid species can be indicative of the quality of food or health status of living organisms, as shown in Figure 1.
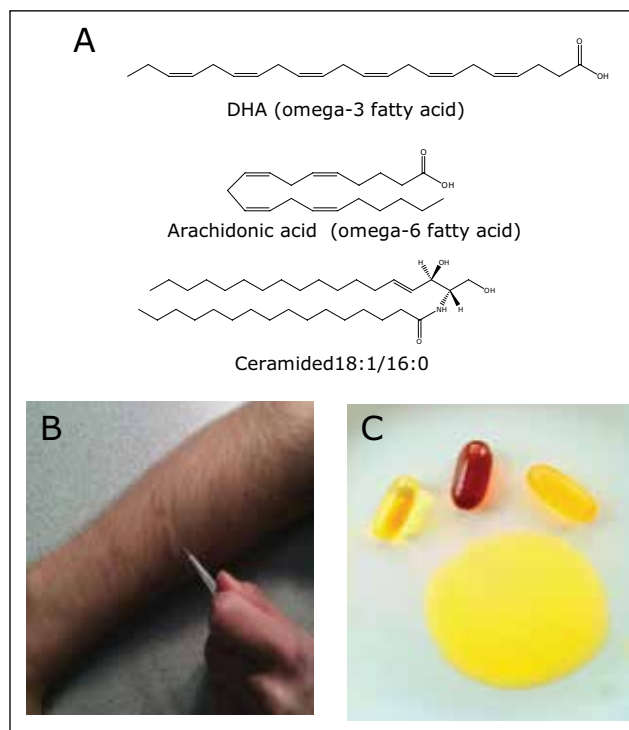


Figure 1. Representative lipid structures analyzed in the study (panel A). Lipids contained in human sebum from skin (panel B) and edible oils (panel C) have been used as representative samples for the DART-IMS-MS analyses.

## WATERS SOLUTIONS

SYNAPT® G2 HDMS™ System

HDMS Compare Software

## KEY WORDS

Lipid, metabolomics, lipidomics, DART, ion mobility, T-Wave™

## EXPERIMENTAL

### Sample description

No sample preparation is required. Samples were swiped on glass capillaries, which were held in the in metastable gas beam between the Direct Analysis in Real Time (DART, IonSense, MA, USA) ion source and SYNAPT G2 HDMS.

Lipid standards and extracts were purchased from Avanti Polar Lipids (AL, USA). Edible oils were purchased at the local grocery store and blindly analyzed.

### MS conditions

Chromatographic separation is not required. Analyses were conducted using a DART source coupled with a Waters® SYNAPT G2 HDMS instrument. DART sources are designed to fit the Waters Xevo® MS family of instruments. Acquisition time was 5 to 10 seconds.

| | |
|---|---|
| Mass spectrometer: | SYNAPT G2 HDMS |
| Ionization: | DART +ve and −ve |
| Cone voltage: | 20 V |
| Source temp.: | 120 °C |
| DART temp.: | 50 to 450 °C |
| Cone gas: | 30 L/h |
| Desolvation gas: | 800 L/h (Nitrogen) |
| IMS gas: | 90 mL/min (Nitrogen) |
| IMS T-Wave velocity: | 833 m/s |
| IMS T-Wave height: | 40 V |
| Acquisition range: | 50 to 1200 |

The analysis of lipid composition often requires very laborious and time-consuming procedures. Furthermore, the detailed spatial distribution of lipid species on a surface is often missed using traditional sample preparation and lipid extraction protocols for large-scale lipid analysis (lipidomic analysis).

The use of desorption ionization (DI) techniques in lipidomics could provide a new level of description beyond the pure measure of lipid concentration. DI-MS techniques are useful for real-time, rapid, in-situ screening of various materials including food, plant, and animal tissue.[1] In particular, DI-MS spectra of biological samples feature ions corresponding mainly to lipids. By molar quantities, the most abundant ionic molecular species in biological tissue, lipids ionize well under DI conditions.

The *in-situ* generation of a particular profile of lipid ions has been proposed for real-time molecular fingerprinting and diagnosis. Here, a rapid (few seconds), real-time method using DI in combination with post-ionization ion mobility separation to analyze lipidomic profiles in food and biological samples is presented.

## RESULTS AND DISCUSSION

For a rapid lipidomic analysis, we combined two emerging technologies: DART and ion mobility separation[2] to analyze lipids extracted from biological samples.

Belonging to the DI techniques, DART is an atmospheric pressure ion source that instantaneously ionizes samples in open air under ambient conditions. DART employs an electrical discharge to create a plasma that produces helium metastables, which react with ambient water, oxygen, or other atmospheric components to produce charged water clusters. Protons are then transferred to the analytes.

Samples were swiped on glass capillaries, held in the in metastable gas beam between the DART ion source and SYNAPT G2 HDMS. Without the need for chromatographic separation, lipids were ionized by DART and guided into the mass spectrometer, where they traveled to the Ion Mobility Separation (IMS) cell. A T-Wave mobility separator used a repeating train of DC pulses to propel lipid ions through a nitrogen-filled IMS cell in a mobility dependent manner. Lipids migrated with characteristic mobility times (drift times) according to their size and shape before TOF detection, as shown in Figure 2.
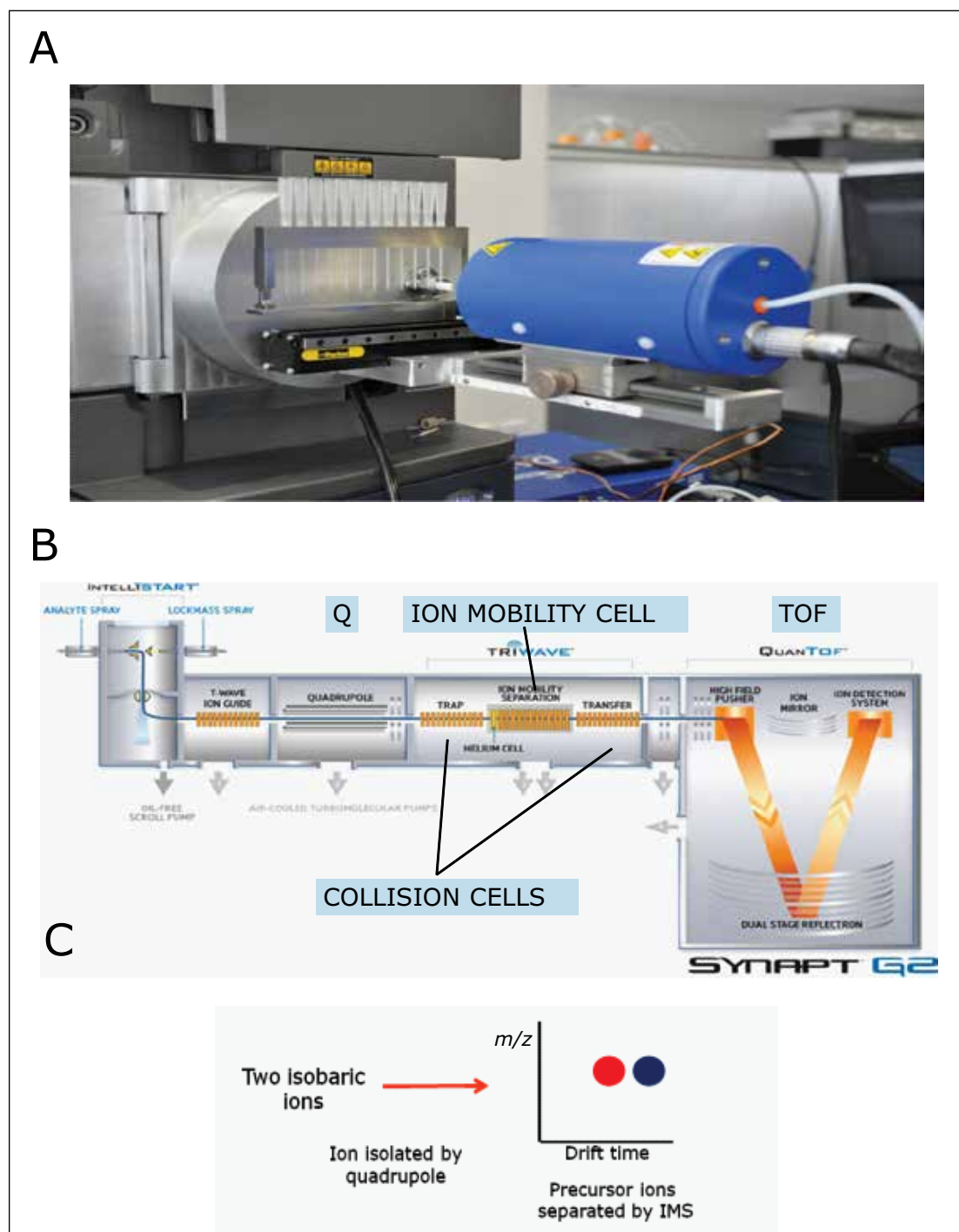


*Figure 2. The DART ion source can be installed on Waters instruments (panel A). The ability to couple DART with a SYNAPT HDMS instrument (schematic in panel B) eliminates sample preparation and chromatographic steps because of the post-ionization separation by ion mobility (C).*

As an example of the power of such an approach, lipid profiles of edible oils (fish oil and olive oil), and lipids extracted from biological samples and human sebum, which is the oily matter that lubricates and waterproofs human skin, were analyzed, as shown in Figure 1. Lipid molecules with different acyl chain length or number of double bonds resulted in characteristic drift times. This enabled the separation and detection of key lipids, such as fatty acids and ceramides, on the millisecond time-scale without the need for prior derivatization or chromatography, as shown in Figures 1, 3, and 4. Ion mobility enabled the separation of the entire lipid profile of a sample on the millisecond time-scale, and a complete DART-IMS-TOF analysis required just a few seconds (0.1 min), as shown in Figures 3 and 4.

Data processing allowed the generation of 3D molecular maps based on drift time, exact mass, and intensity of the signal relative to the various analytes present in the oils. Such representation highlighted the capacity of ion mobility to separate isobaric lipid species (species with the same mass) without the need for prior chromatography, as shown in Figure 3.
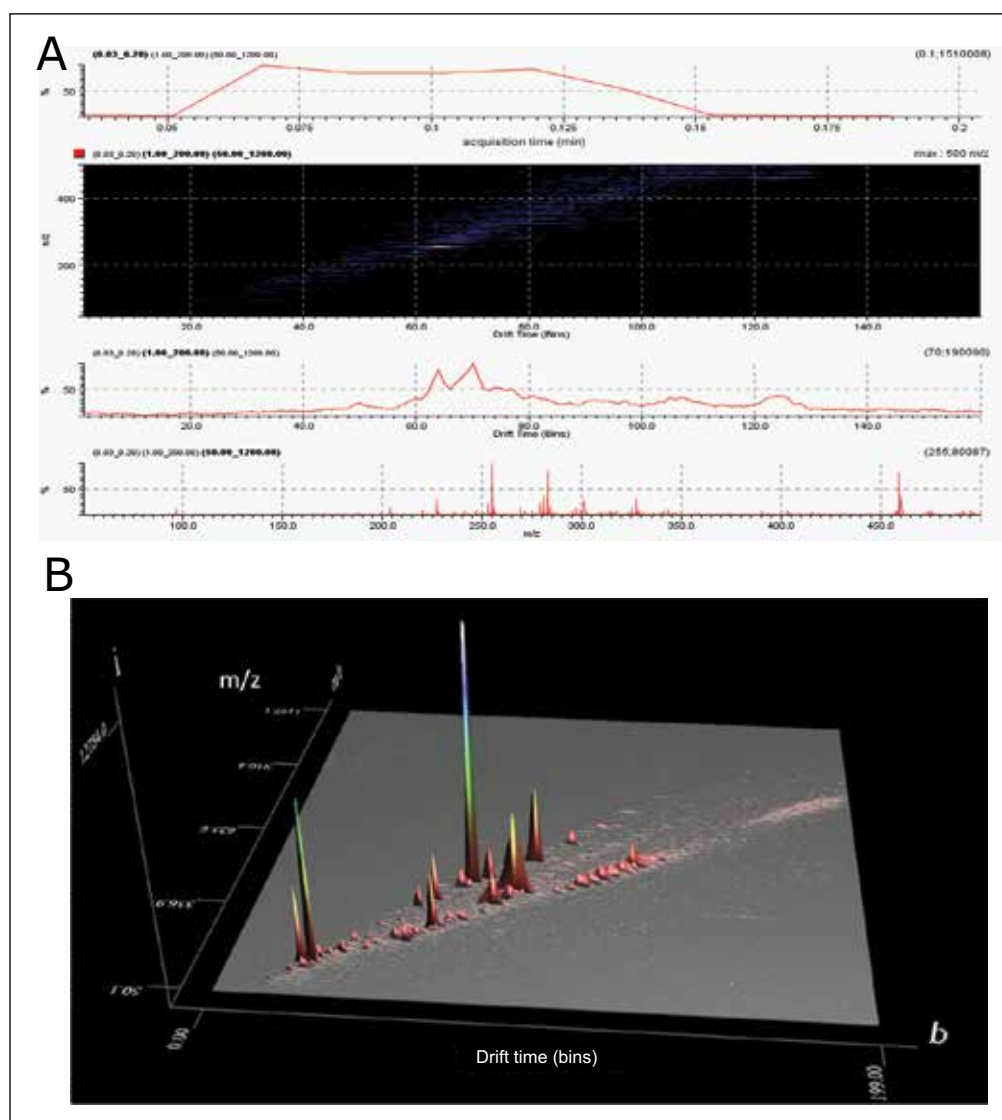


Figure 3. The entire DART-IMS-TOF analysis requires just a few seconds (0.1 min). Lipids are separated by ion mobility on the millisecond time-scale (panel A). Software processing of the data allows the generation of 3D molecular maps based on drift time, exact mass, and intensity of the signal relative to the various analytes present in the oils. Isobaric species are separated by ion mobility.
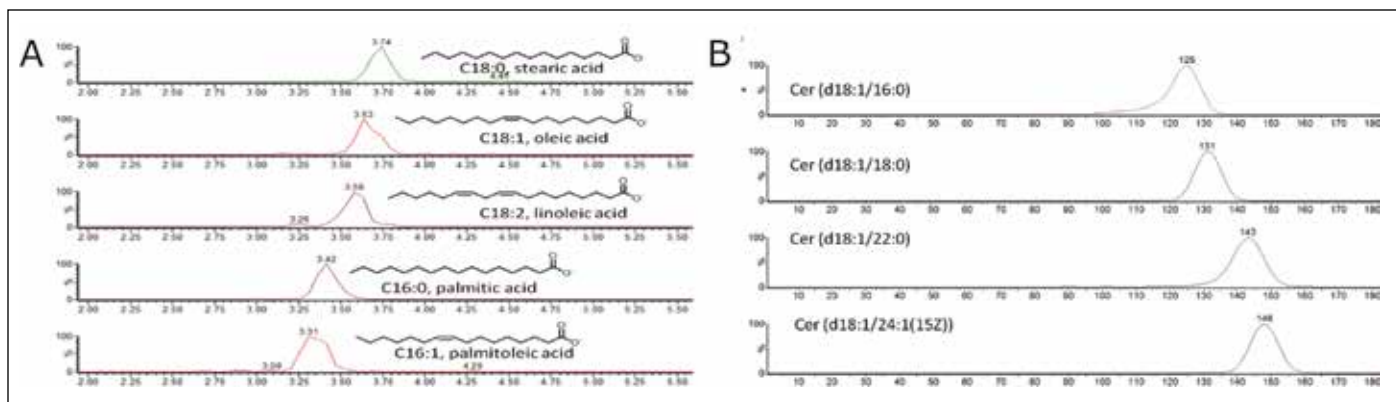
Figure 4. Ion mobility separation of fatty acids from olive oil (panel A), and ceramides from human sebum (panel B) after rapid DART ionization in negative and positive ion mode, respectively. Differences in the acyl chain length or number of double bonds affect the shape and size of lipid molecules, resulting in characteristic drift times.

A comparison of lipid profiles of human sebum, shown in Figure 5, and edible oils shown in Figure 6 was done based on the separation capabilities of IMS-TOF/MS. HDMS Compare Software was used for a rapid binary comparison of different driftograms (masses versus drift time matrices). The drift time and spectral information associated with the components responsible for the differentiation can be extracted from the dataset and analyzed to better understand the underlying reasons for the observed differences.
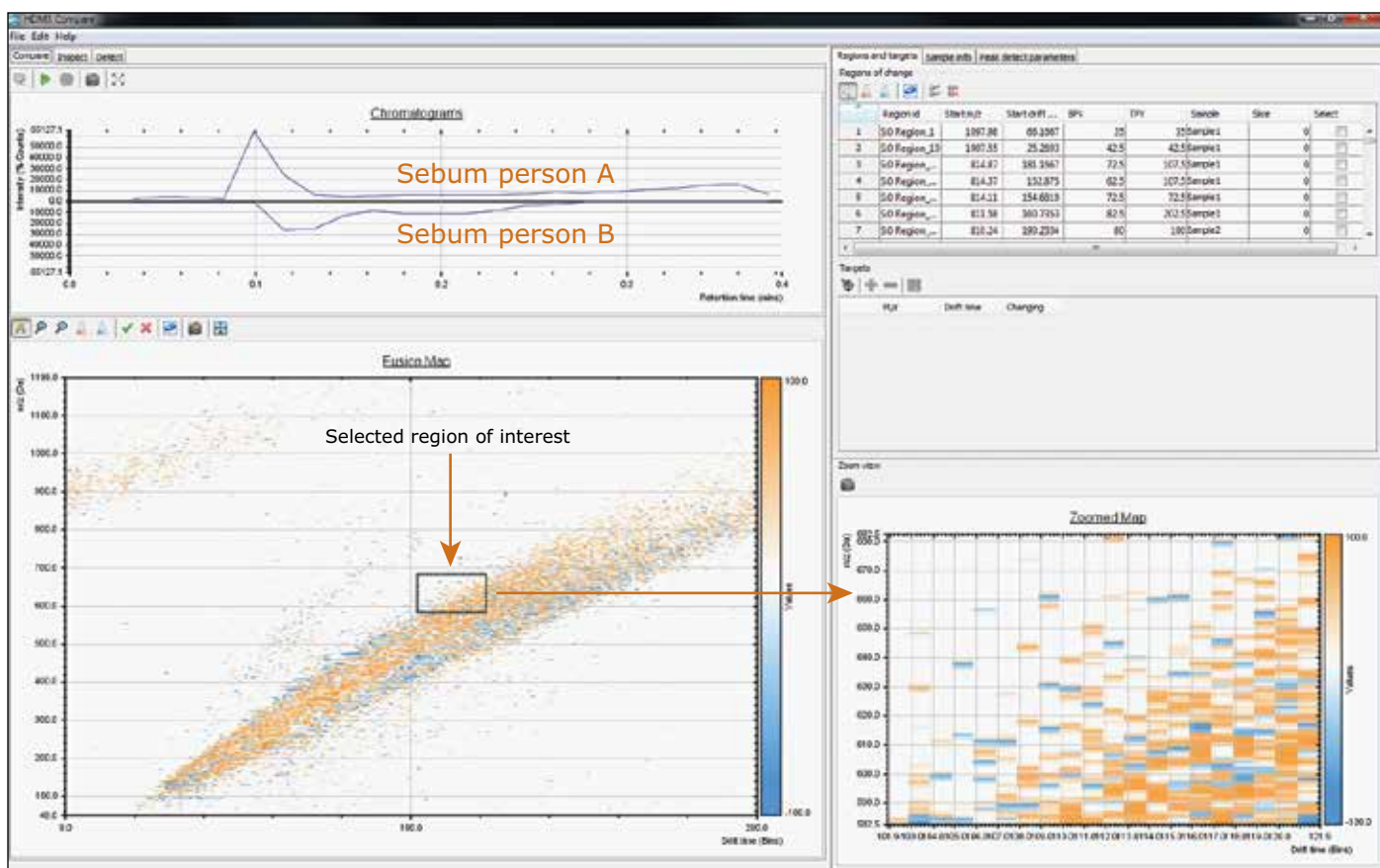


Figure 5. Comparison of sebum skin oils from two human subjects. Overlaying individual molecular maps clearly show areas where the samples are significantly different. Ion mobility data analysis and processing was done using HDMS Compare Software. Key areas of significant differences between two samples were clearly visualized and identified with two different colors. Regions of interest were easily selected and expanded in Zoomed Map view for further interrogation of important sample differences.

HDMS Compare Software also allows importing a list of target ions (mass and drift time) and reporting changes
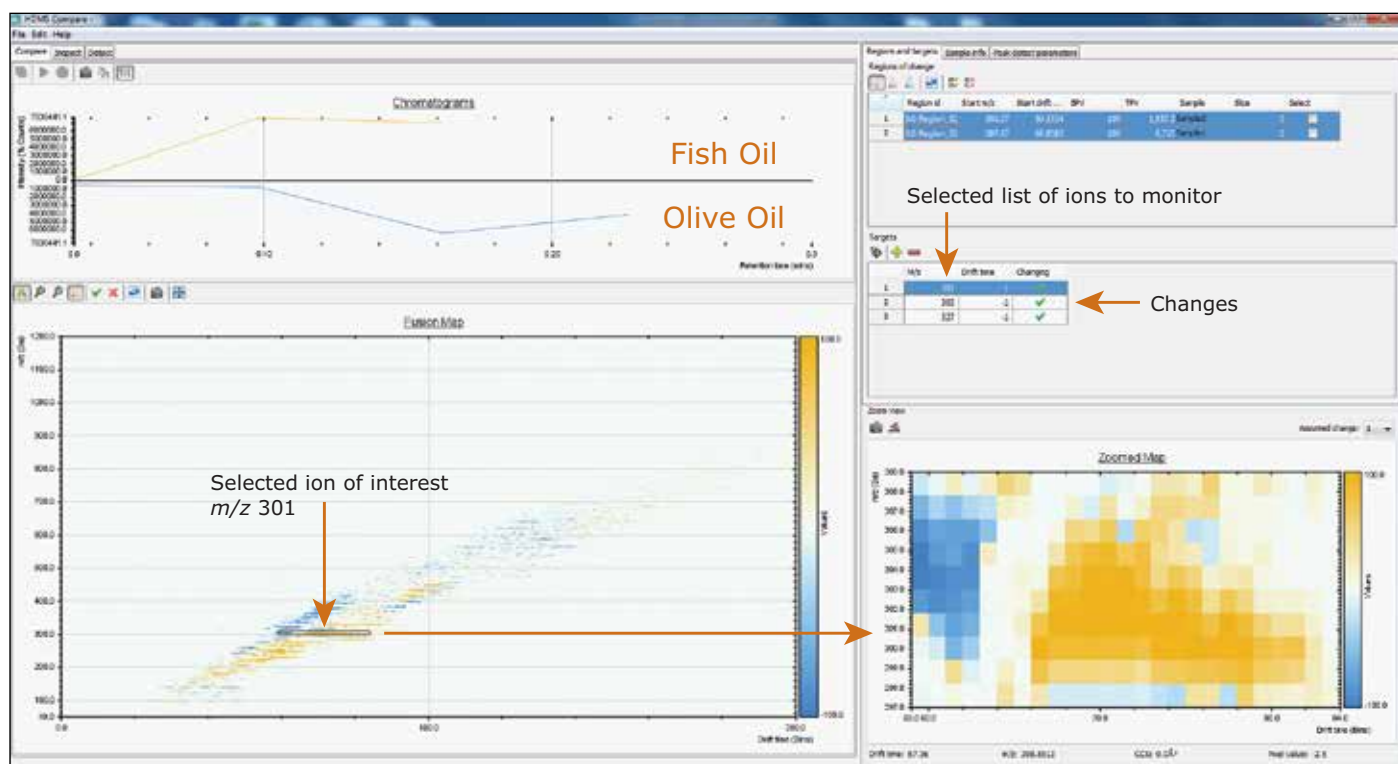in the levels of these targets, as shown in Figure 6.



Figure 6. Comparison of edible oils. HDMS Compare Software was used to determine molecular difference in fish oil versus olive oil. The software automatically
identified significant differences between the two oils in the levels of a selected list of ions, including m/z 301 (eicosapentanoic acid; EPA), 303 (arachidonic acid),
and 327(docosahexaenoic acid; DHA).

## CONCLUSIONS

- The combination of a desorption ionization technique such as DART with ion mobility-TOF offers a convenient solution for lipidomic profiling.

- Post-ionization separation by ion mobility allows resolution of complex mixtures of lipids.

- Software solutions provide overlay driftograms (plots of masses versus drift time) to compare different samples.

- More generally, these results suggest that the combination of desorption ionization techniques and the ion mobility approach is suitable for the rapid screening of bioactive lipids, including fatty acids and ceramides.

- Potential applications include phenotypic fingerprinting and comparative lipidomics in the areas of personalized medicine, disease diagnostics, food analysis, and traditional medicines.

### References

1. Yew JY, Cody RB, Kravitz EA. Cuticular hydrocarbon analysis of an awake behaving fly using direct analysis in real-time time-of-flight mass spectrometry. *Proc Natl Acad Sci* U S A. 2008 May 20;105(20):7135-40. Epub 2008 May 12.

2. Dear GJ, Munoz-Muriedas J, Beaumont C, Roberts A, Kirk J, Williams JP, Campuzano I. Sites of metabolic substitution: investigating metabolite structures utilising ion mobility and molecular modelling. *Rapid Commun Mass Spectrom*. 2010 Nov 15;24(21):3157-62.
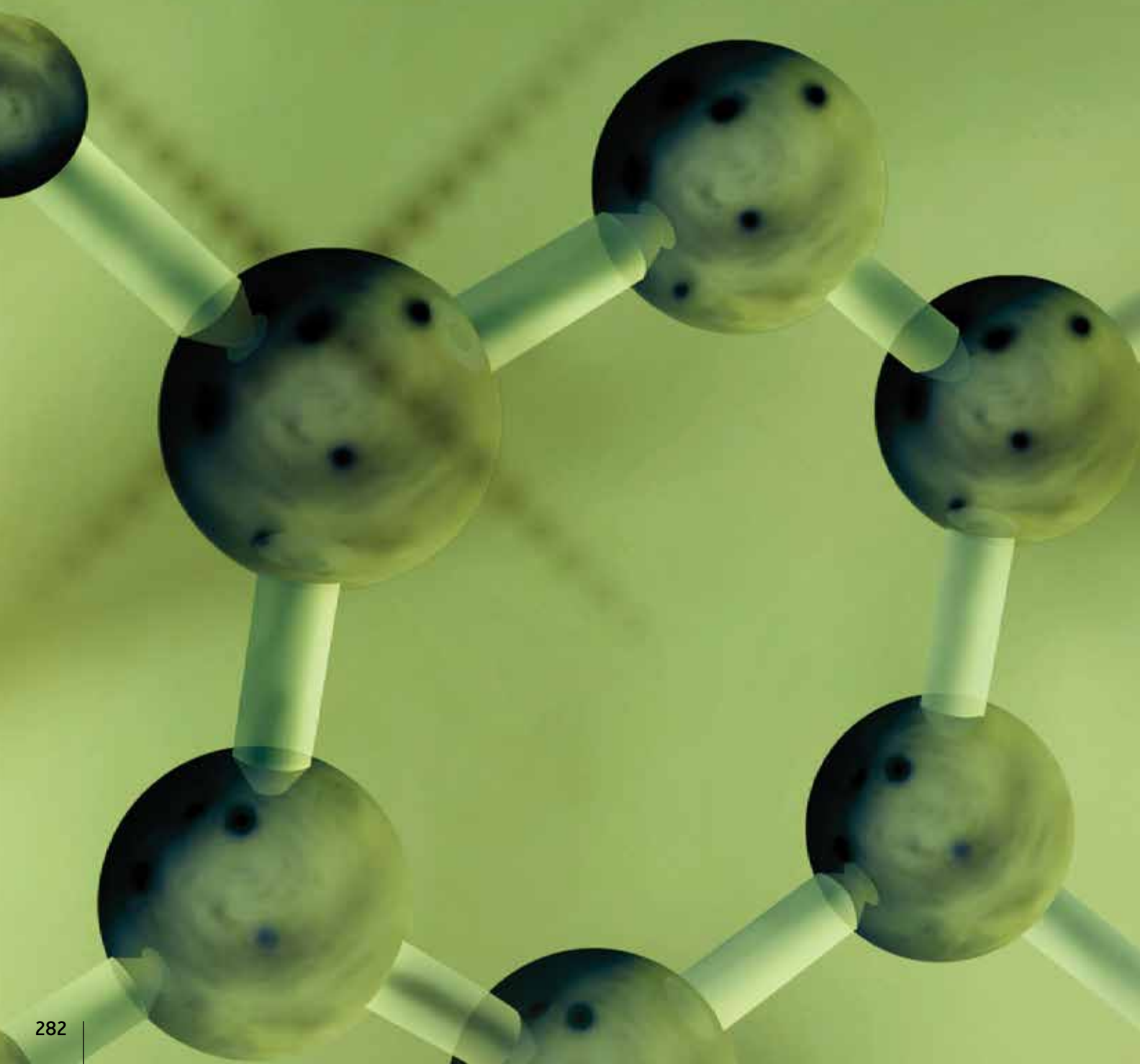
## Waters

### THE SCIENCE OF WHAT'S POSSIBLE.®

# CHAPTER 5 SELECTED PEER-REVIEWED PUBLICATIONS

# peer reviewed publications

## untargeted

1.  Paglia G, Angel P, Williams JP, Richardson K, Olivos HJ, Thompson JW, Menikarachchi L, Lai S, Walsh C, Moseley A, Plumb RS, Grant DF, Palsson BO, Langridge J, Geromanos S, Astarita G. Ion Mobility-Derived Collision Cross Section As an Additional Measure for Lipid Fingerprinting and Identification. *Anal Chem.* 2014 Dec 29. [Epub ahead of print].

2.  Laiakis EC, et al. Metabolic Phenotyping Reveals a Lipid Mediator Response to Ionizing Radiation. *J Proteome Res.* 2014 Sep 5;13(9):4143-54. doi: 10.1021/pr5005295.

3.  Jones MD, Rainville PD, Isaac G, Wilson ID, Smith NW, Plumb RS. Ultra high resolution SFC-MS as a high throughput platform for metabolic phenotyping: application to metabolic profiling of rat and dog bile. *J Chromatogr B Analyt Technol Biomed Life Sci.* 2014 Sep 1;966:200-7. doi: 0.1016/j.jchromb.2014.04.017.

4.  Sedic M, Gethings LA, Vissers JP, Shockcor JP, McDonald S, Vasieva O, Lemac M, Langridge JI, Batini D, Paveli SK. Label-free mass spectrometric profiling of urinary proteins and metabolites from pediatric idiopathic nephrotic syndrome. *Biochem Biophys Res Commun.* 2014 Sep 12;452(1):21-6. doi: 10.1016/j.bbrc.2014.08.016.

5.  Astarita G, et al. A Protective Lipidomic Biosignature Associated with a Balanced Omega-6/Omega-3 Ratio in fat-1 Transgenic Mice. *PLoS One.* 2014 Apr 23;9(4):e96221. doi: 10.1371/journal.pone.0096221.

6.  Sarafian MH, et al. An Objective Set of Criteria for Optimization of Sample Preparation Procedures for Ultra-High Throughput Untargeted Blood Plasma Lipid Profiling by UPLC-MS. *Anal Chem.* 2014 Jun 17;86(12):5766-74. doi: 10.1021/ac500317c.

7.  Zhao YY, Lin RC. UPLC-MS(E) application in disease biomarker discovery: the discoveries in proteomics to metabolomics. *Chem Biol Interact.* 2014 May 25;215:7-16. doi: 10.1016/j.cbi.2014.02.014.

8.  Zhou Q, et al. Chemical profiling of triacylglycerols and diacylglycerols in cow milk fat by ultra-performance convergence chromatography combined with a quadrupole time-of-flight mass spectrometry. *Food Chem.* 2014 Jan 15;143:199-204. doi: 10.1016/j.foodchem.2013.07.114

9.  Paglia G, et al. Ion Mobility Derived Collision Cross Sections to Support Metabolomics Applications. *Anal Chem.* 2014 Apr 15;86(8):3985-93. doi: 10.1021/ac500405x.

10. Shah V, et al. Enhanced data-independent analysis of lipids using ion mobility-TOFMSE to unravel quantitative and qualitative information in human plasma. *Rapid Commun Mass Spectrom.* 2013 Oct 15;27(19):2195-200. doi: 10.1002/rcm.6675.

11. Astarita G, Langridge J. An emerging role for metabolomics in nutrition science. *J Nutrigenet Nutrigenomics.* 2013;6(4-5):181-200. doi: 10.1159/000354403.

12. Glauser G, et al. Ultra-high pressure liquid chromatography–mass spectrometry for plant metabolomics: A systematic comparison of high-resolution quadrupole-time-of-flight and single stage Orbitrap mass spectrometers. *J Chromatogr A.* 2013 May 31;1292:151-9. doi: 10.1016/j.chroma.2012.12.009.

13. Want EJ, Masson P, Michopoulos F, Wilson ID, Theodoridis G, Plumb RS, Shockcor J, Loftus N, Holmes E, Nicholson JK. Global metabolic profiling of animal and human tissues via UPLC-MS. *Nat Protoc.* 2013 Jan;8(1):17-32. doi: 10.1038/nprot.2012.135.

14. Spagou K, Wilson ID, Masson P, Theodoridis G, Raikos N, Coen M, Holmes E, Lindon JC, Plumb RS, Nicholson JK, Want EJ. HILIC-UPLC-MS for exploratory urinary metabolic profiling in toxicological studies. *Anal Chem.* 2011 Jan 1;83(1):382-90. doi: 10.1021/ac102523q.

15. Want EJ, Wilson ID, Gika H, Theodoridis G, Plumb RS, Shockcor J, Holmes E, Nicholson JK. Global metabolic profiling procedures for urine using UPLC-MS. *Nat Protoc.* 2010 Jun;5(6):1005-18. doi: 10.1038/nprot.2010.50.

16. Castro-Perez JM, et al. Comprehensive LC   MSE lipidomic analysis using a shotgun approach and its application to biomarker detection and identification in osteoarthritis patients. *J Proteome Res.* 2010 May 7;9(5):2377-89. doi: 10.1021/pr901094j.

17. Plumb RS, Johnson KA, Rainville P, Smith BW, Wilson ID, Castro-Perez JM, Nicholson JK. UPLC/MS(E); a new approach for generating molecular fragment information for biomarker structure elucidation. *Rapid Commun Mass Spectrom.* 2006;20(13):1989-94. Erratum in: Rapid Commun Mass Spectrom. 2006;20(14):2234.

## STRUCTURAL ELUCIDATION

1. Damen CW, et al. Enhanced lipid isomer separation in human plasma using reversed-phase UPLC with ion-mobility/high-resolution MS detection. *J Lipid Res.* 2014 Jun 2;55(8):1772-1783.

2. Paglia G, et al. Ion Mobility Derived Collision Cross Sections to Support Metabolomics Applications. *Anal Chem.* 2014 Apr 15;86(8):3985-93. doi: 10.1021/ac500405x.

3. Shah V, et al. Enhanced data-independent analysis of lipids using ion mobility-TOFMSE to unravel quantitative and qualitative information in human plasma. *Rapid Commun Mass Spectrom.* 2013 Oct 15;27(19):2195-200. doi: 10.1002/rcm.6675.

4. Garmón-Lobato S, Abad-García B, Sánchez-Ilárduya MB, Romera-Fernández M, Berrueta LA, Gallo B, Vicente F. Improvement using chemometrics in ion mobility coupled to mass spectrometry as a tool for mass spectrometry fragmentation studies: flavonoid aglycone cases. *Anal Chim Acta.* 2013 Apr 10;771:56-64. doi: 10.1016/j.aca.2013.01.065.

5. Castro-Perez J, et al. Localization of fatty acyl and double bond positions in phosphatidylcholines using a dual stage CID fragmentation coupled with ion mobility mass spectrometry. *J Am Soc Mass Spectrom.* 2011 Sep;22(9):1552-67. doi: 10.1007/s13361-011-0172-2.
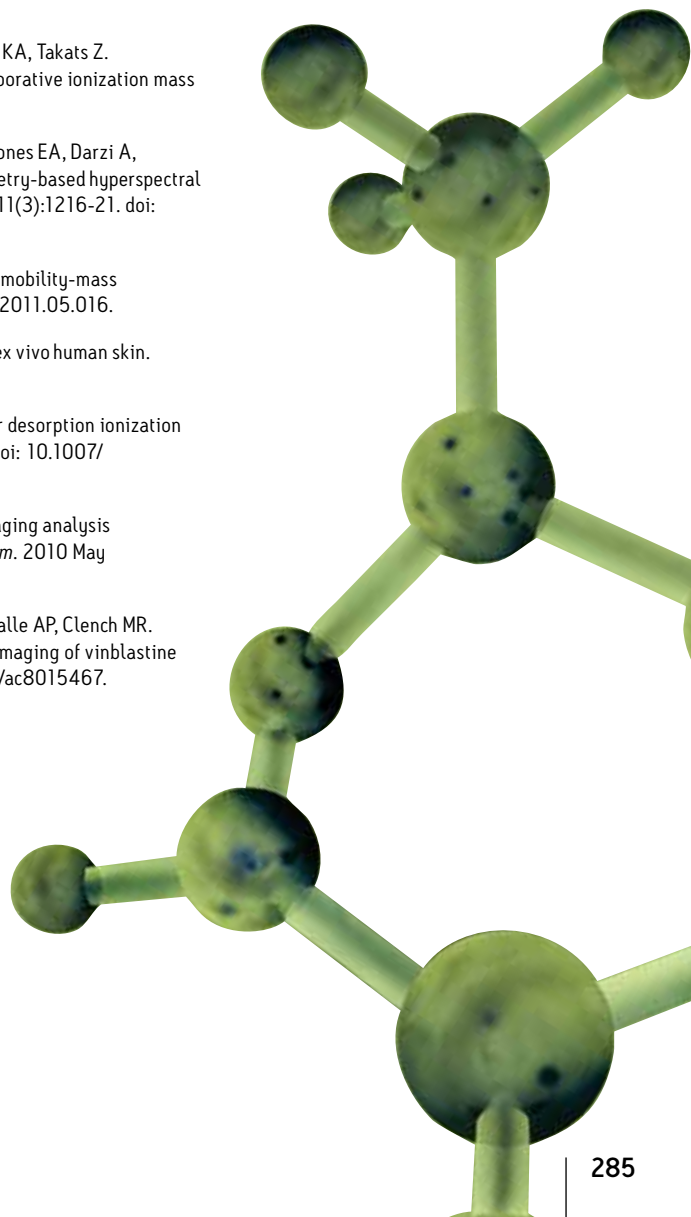
## TARGETED

1. Astarita G, Kendall AC, Dennis EA, Nicolaou A. Targeted lipidomics strategies for oxygenated metabolites of polyunsaturated fatty acids. *Biochim Biophys Acta.* 2014 Dec 5. pii: S1388-1981(14)00251-0. doi: 10.1016/j.bbalip.2014.11.012.

2. Ahonen L, Maire FB, Savolainen M, Kopra J, Vreeken RJ, Hankemeier T, Myöhänen T, Kylli P, Kostiainen R. Analysis of oxysterols and vitamin D metabolites in mouse brain and cell line samples by ultra-high-performance liquid chromatography-atmospheric pressure photoionization-mass spectrometry. *J Chromatogr A.* 2014 Oct 17;1364:214-22. doi: 10.1016/j.chroma.2014.08.088.

3. Laourdakis CD, Merino EF, Neilson AP, Cassera MB. Comprehensive quantitative analysis of purines and pyrimidines in the human malaria parasite using ion-pairing ultra-performance liquid chromatography-mass spectrometry. *J Chromatogr B Analyt Technol Biomed Life Sci.* 2014 Sep 15;967:127-33. doi: 10.1016/j.jchromb.2014.07.012.

4. Mapstone M, et al. Plasma phospholipids identify antecedent memory impairment in older adults. *Nat Med.* 2014 Apr;20(4):415-8. doi: 10.1038/nm.3466.

5. Broccardo CJ, et al. Multiplexed analysis of steroid hormones in human serum using novel microflow tile technology and LC–MS/MS. *J Chromatogr B Analyt Technol Biomed Life Sci.* 2013 Sep 1;934:16-21. doi: 10.1016/j.jchromb.2013.06.031.

6. Gaikwad NW. Ultra performance liquid chromatography-tandem mass spectrometry method for profiling of steroid metabolome in human tissue. *Anal Chem.* 2013 May 21;85(10):4951-60. doi: 10.1021/ac400016e.

7. Aqai P, et al. High-throughput bioaffinity mass spectrometry for screening and identification of designer anabolic steroids in dietary supplements. *Anal Chem.* 2013 Mar 19;85(6):3255-62. doi: 10.1021/ac3036052.
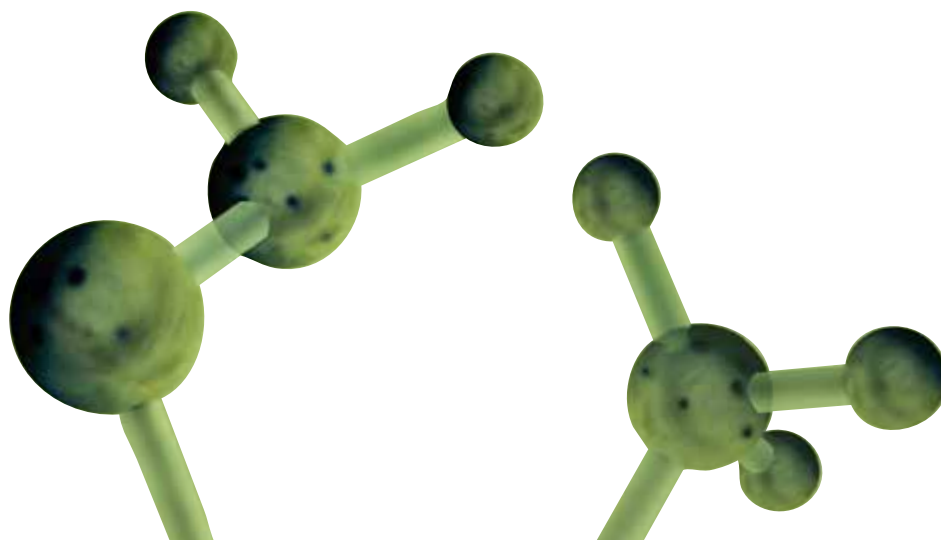
# MS IMAGING AND AMBIENT IONIZATION MS

1.  Castro-Perez J, Hatcher N, Kofi Karikari N, Wang SP, Mendoza V, Shion H, Millar A, Shockcor J, Towers M, McLaren D, Shah V, Previs S, Akinsanya K, Cleary M, Roddy TP, Johns DG. In vivo isotopically labeled atherosclerotic aorta plaques in ApoE KO mice and molecular profiling by matrix-assisted laser desorption/ionization mass spectrometric imaging. *Rapid Commun Mass Spectrom.* 2014 Nov 30;28(22):2471-9. doi: 10.1002/rcm.7039.

2.  Niehoff AC, Kettling H, Pirkl A, Chiang YN, Dreisewerd K, Yew JY. Analysis of Drosophila lipids by matrix-assisted laser desorption/ionization mass spectrometric imaging. *Anal Chem.* 2014 Nov 18;86(22):11086-92. doi: 10.1021/ac503171f.

3.  Räsänen RM, Dwivedi P, Fernández FM, Kauppila TJ. Desorption atmospheric pressure photoionization and direct analysis in real time coupled with travelling wave ion mobility mass spectrometry. *Rapid Commun Mass Spectrom.* 2014 Nov 15;28(21):2325-36. doi: 10.1002/rcm.7028.

4.  Stopka SA, Shrestha B, Maréchal E, Falconet D, Vertes A. Metabolic transformation of microalgae due to light acclimation and genetic modifications followed by laser ablation electrospray ionization mass spectrometry with ion mobility separation. *Analyst.* 2014 Oct 15;139(22):5945-53. doi: 10.1039/c4an01368a.

5.  Rocha B, Cillero-Pastor B, Eijkel G, Bruinen AL, Ruiz-Romero C, Heeren RM, Blanco FJ. Characterization of lipidic markers of chondrogenic differentiation using mass spectrometry imaging. *Proteomics.* 2014 Oct 27. doi: 10.1002/pmic.201400260.

6.  Kettling H, Vens-Cappell S, Soltwisch J, Pirkl A, Haier J, Müthing J, Dreisewerd K. MALDI mass spectrometry imaging of bioactive lipids in mouse brain with a Synapt G2-S mass spectrometer operated at elevated pressure: improving the analytical sensitivity and the lateral resolution to ten micrometers. *Anal Chem.* 2014 Aug 5;86(15):7798-805. doi: 10.1021/ac5017248.

7.  Strittmatter N, Rebec M, Jones EA, Golf O, Abdolrasouli A, Balog J, Behrends V, Veselkov KA, Takats Z. Characterization and identification of clinically relevant microorganisms using rapid evaporative ionization mass spectrometry. *Anal Chem.* 2014 Jul 1;86(13):6555-62. doi: 10.1021/ac501075f.

8.  Veselkov KA, Mirnezami R, Strittmatter N, Goldin RD, Kinross J, Speller AV, Abramov T, Jones EA, Darzi A, Holmes E, Nicholson JK, Takats Z. Chemo-informatic strategy for imaging mass spectrometry-based hyperspectral profiling of lipid signatures in colorectal cancer. *Proc Natl Acad Sci U S A.* 2014 Jan 21;111(3):1216-21. doi: 10.1073/pnas.1310524111.

9.  Kliman M, May JC, McLean JA. Lipid analysis and lipidomics by structurally selective ion mobility-mass spectrometry. *Biochim Biophys Acta.* 2011 Nov;1811(11):935-45. doi: 10.1016/j.bbalip.2011.05.016.

10. Hart PJ, Francese S, Claude E, Woodroofe MN, Clench MR. MALDI-MS imaging of lipids in ex vivo human skin. *Anal Bioanal Chem.* 2011 Jul;401(1):115-25. doi: 10.1007/s00216-011-5090-4.

11. Fernández JA, Ochoa B, Fresnedo O, Giralt MT, Rodríguez-Puertas R. Matrix-assisted laser desorption ionization imaging mass spectrometry in lipidomics. *Anal Bioanal Chem.* 2011 Jul;401(1):29-51. doi: 10.1007/s00216-011-4696-x.

12. Snel MF, Fuller M. High-spatial resolution matrix-assisted laser desorption ionization imaging analysis of glucosylceramide in spleen sections from a mouse model of Gaucher disease. *Anal Chem.* 2010 May 1;82(9):3664-70. doi: 10.1021/ac902939k.

13. Trim PJ, Henson CM, Avery JL, McEwen A, Snel MF, Claude E, Marshall PS, West A, Princivalle AP, Clench MR. Matrix-assisted laser desorption/ionization-ion mobility separation-mass spectrometry imaging of vinblastine in whole body tissue sections. *Anal Chem.* 2008 Nov 15;80(22):8628-34. doi: 10.1021/ac8015467.

## Waters

### THE SCIENCE OF WHAT'S POSSIBLE.®